

Seismic Enhancement of Reinforced Concrete Columns with Lap Splices using External  
Steel Collars



A Dissertation Submitted in Partial Fulfillment of the Requirements  
for the Degree of Doctor of Philosophy in Civil Engineering

Department of Civil Engineering

Faculty of Engineering

Chulalongkorn University

Academic Year 2019

Copyright of Chulalongkorn University

การเสริมกำลังเสาคอนกรีตเสริมเหล็กที่มีการต่อทาบด้วยปลอกเหล็กภายนอก



วิทยานิพนธ์นี้เป็นส่วนหนึ่งของการศึกษาตามหลักสูตรปริญญาวิศวกรรมศาสตรดุษฎีบัณฑิต

สาขาวิชาวิศวกรรมโยธา ภาควิชาวิศวกรรมโยธา

คณะวิศวกรรมศาสตร์ จุฬาลงกรณ์มหาวิทยาลัย

ปีการศึกษา 2562

ลิขสิทธิ์ของจุฬาลงกรณ์มหาวิทยาลัย



พชร เครือวิทย์ : การเสริมกำลังเสาคอนกรีตเสริมเหล็กที่มีการต่อทาบด้วยปลอกเหล็ก  
ภายนอก. ( Seismic Enhancement of Reinforced Concrete Columns with Lap  
Splices using External Steel Collars) อ.ที่ปรึกษาหลัก : รศ. ดร.อาณัติ เรืองวัศมี

งานวิจัยนี้ศึกษาพฤติกรรมเสาสะพานคอนกรีตเสริมเหล็กที่มีการต่อทาบเหล็กและใช้  
ข้อต่อเชิงกล โดยวิธีทดสอบขนาดเท่าโครงสร้างจริงและวิเคราะห์ทำนายความสามารถรับแรง  
ด้านข้างของตัวอย่างทดสอบโดยใช้แบบจำลองเชิงตัวเลข ถูกทดสอบในลักษณะแบบเสถียรรับ  
แรงกระทำทางด้านข้างแบบวัฏจักรร่วมกับน้ำหนักบรรทุกเนื่องจากแรงโน้มถ่วงขนาดคงที่  
ตัวอย่างทดสอบประกอบด้วยเสาที่ไม่มีการต่อทาบเหล็กเสริม เสาที่มีการทาบเหล็กเสริมด้วยวิธี  
ต่อทาบและใช้ข้อต่อเชิงกล รวมถึงเสาที่ต่อทาบเหล็กเสริมและทำการเสริมกำลังด้วยปลอก  
เหล็กภายนอก โดยพิจารณาตัวแปรในการทดสอบคือการจัดเรียงข้อต่อเชิงกล และนำเสนอ  
หลักการวิเคราะห์หน้าตัดแบบไฟเบอร์เพื่อทำนายความสัมพันธ์ระหว่างแรงและการเคลื่อนที่  
ของตัวอย่างทดสอบ รวมถึงอัตราส่วนเชิงปริมาตรของปลอกเหล็กภายนอกที่ใช้เสริมกำลัง จาก  
การทดสอบพบว่า การต่อทาบเหล็กเสริมด้วยข้อต่อเชิงกลให้กำลังต้านทานน้ำหนักบรรทุก  
ด้านข้างได้ใกล้เคียงกับค่าดังกล่าวของตัวอย่างทดสอบในกรณีที่ไม่มีการต่อทาบเหล็กเสริม การ  
จัดเรียงข้อต่อเชิงกลไม่ส่งผลต่อกำลังต้านทานน้ำหนักบรรทุกทุกด้านข้างของตัวอย่างทดสอบอย่าง  
มีนัยสำคัญ อีกทั้งแบบจำลองเชิงตัวเลขสามารถประมาณความสามารถรับแรงด้านข้างสูงสุด  
ของตัวอย่างทดสอบได้สอดคล้องกับค่าที่ได้จากผลการทดสอบ สำหรับวิธีเสริมกำลังด้วยปลอก  
เหล็กภายนอกโดยการเพิ่มค่าอัตราส่วนเชิงปริมาตร ส่งผลให้พฤติกรรมการวิบัติของเสาที่ต่อ  
ทาบเหล็กเสริมมีความเหนียวและความสามารถในการรับแรงด้านข้างเพิ่มขึ้น

สาขาวิชา วิศวกรรมโยธา

ลายมือชื่อนิสิต

.....

ปี 2562

ลายมือชื่อ อ.ที่ปรึกษาหลัก

การศึกษา

.....

# # 5671473821 : MAJOR CIVIL ENGINEERING

KEYWORD: coupler, mechanical splice, strengthening, ductility, lap splice,  
confinement, steel collars, OpenSEES

Pochara Kruavit : Seismic Enhancement of Reinforced Concrete Columns  
with Lap Splices using External Steel Collars. Advisor: Assoc. Prof. Anat  
Ruangrassamee, Ph.D.

This research investigated the behavior of reinforced concrete (RC) columns with lap splices and mechanical splices. The study conducted the full-scale test and predicted a lateral load capacity using the proposed numerical model. The test configuration was a cantilever column subjected to a cyclic lateral loading and a constant gravity load. The tested specimens consisted of the RC column without lap splices, RC columns with spliced reinforcement including lap splices and mechanical splices, and RC column with lap splices strengthened by external steel collars. The experimental result indicated that the lateral load capacity of the RC column with mechanical splices was closed to that of the control specimen (column without lap splices). The numerical model using the fiber section analysis was used to predict the lateral load vs displacement relation of the columns with mechanical splices. The numerical model could provide the lateral load capacity in a good agreement with the tested specimens. The strengthening technique by using external steel collars can enhance the ductility and lateral load capacity of RC columns with lap splices significantly.

Field of Study: Civil Engineering

Student's Signature

.....

Academic 2019

Advisor's Signature

Year:

.....

## ACKNOWLEDGEMENTS

I would like to dedicate my greatest gratitude to my thesis advisor Assoc. Prof. Anat Ruangrassame. This research effort would not be possible without his enthusiastic guidance, valuable suggestions, constructive criticisms, friendly discussions, persistent supervision and financial support which are indispensable for the completion of this thesis work.

I would like to extend my gratitude to Dr. Qudeer Hussain who also gives me suggestions and attention in my research. Special thanks to all friends, especially Sornprasit Lumpha, Apichat Wongdee and Tosporn Prasertsri for all the time and experiences we shared together, being such good friends, and unforgettable ones. Then I am really grateful to Sompong Kamchang from the structural lab who help me warmly throughout my experimental.

Sincere appreciation is also due to all committee members of my thesis defense, Assoc. Prof. Tospol Pinkawe, Asst. Prof. Chatpan Chintanapakdee for their thoughtful comments and suggestions and serving as members of the examination committee. I sincerely appreciate lectures and professors of Chulalongkorn University for providing the necessary engineering knowledge.

Last, but not least I would like to show my gratitude towards my parents for making this unforgettable journey at Chulalongkorn University possible and for their constant support, prayers and encouragement.

Pochara Kruavit

## TABLE OF CONTENTS

	Page
.....	iii
ABSTRACT (THAI).....	iii
.....	iv
ABSTRACT (ENGLISH) .....	iv
ACKNOWLEDGEMENTS.....	v
TABLE OF CONTENTS.....	vi
LIST OF FIGURES .....	xii
LIST OF TABLES.....	xxiii
CHAPTER 1 INTRODUCTION .....	1
1.1 Background and Problem Statements .....	1
1.2 Significance of research.....	5
1.3 Objectives of the research .....	5
1.4 Scope of the research .....	5
CHAPTER 2 LITERATURE REVIEW.....	6
2.1 Test on columns without lap splices .....	6
2.2 Test on columns with lap splices .....	9
2.3 Test on the column with mechanical splices .....	16
2.4 Test on the previous research of strengthening columns.....	22
2.4.1 Steel jacketing methods.....	22
2.4.2 Angle and batten jacketing methods.....	31
2.4.3 Steel collar jacketing methods.....	41

2.4.4 Summary .....	47
2.5 Modeling strategies of RC columns .....	48
2.5.1 Material Constitutive Relationships .....	48
2.5.1.1 Unconfined concrete .....	49
2.5.1.2 Confined concrete: .....	50
2.5.1.3 Longitudinal reinforcement model: .....	55
2.5.2 Structural elements .....	57
2.5.2.1 Fiber elements .....	57
2.5.2.2 Fiber section .....	57
2.5.2.3 Elastic elements: .....	58
CHAPTER 3 BEHAVIOR OF COLUMN WITH SPLICED REINFORCEMENT .....	59
3.1 Introduction .....	59
3.2 Experimental program and test configurations .....	59
3.2.1 Specimen details .....	59
3.2.2 Prepare of specimens .....	61
3.2.3 Material Properties of Specimens .....	66
3.2.3.1 Concrete .....	66
3.2.3.2 Reinforcing steel .....	67
3.2.4 Instrumentation .....	69
3.2.4.1 Strain gauge .....	69
3.2.4.2 Displacement transducers .....	71
3.2.4.3 Testing setup .....	74
3.2.5 Test procedures .....	75



3.3 Experimental Result and discussion .....	76
3.3.1 Experimental result of specimen NS.....	77
3.3.1.1 Progressive damage of specimen NS.....	77
3.3.1.2 Appearance failure of specimen NS .....	79
3.3.1.3 Strain in Reinforcing steels of specimen NS .....	82
3.3.2 Experimental result of specimen LS [46].....	83
3.3.2.1 Progressive damage of specimen LS .....	83
3.3.2.2 Appearance failure of specimen LS .....	85
3.3.2.3 Strain in Reinforcing steels of specimen LS.....	88
3.3.3 Experimental result of specimen MS1 [46].....	89
3.3.3.1 Progressive damage of specimen MS1 .....	89
3.3.3.2 Appearance failure of specimen MS1 .....	91
3.3.3.3 Strain in Reinforcing steels of specimen NS .....	94
3.3.4 Experimental result of specimen MS2 .....	95
3.3.4.1 Progressive damage of specimen MS2 .....	95
3.3.4.2 Appearance failure of specimen MS2 .....	97
3.3.4.3 Strain in Reinforcing steels of specimen MS2.....	100
3.3.5 Comparison between column with and without splices reinforcement.....	101
3.3.5.1 Moment-curvature distribution.....	105
3.3.5.2 Distribution of column section rotation .....	107
3.3.5.3 Energy dissipation .....	109
3.4 Discussion of the column with and without splice reinforcements .....	112
CHAPTER 4 NUMERICAL MODELLING OF REINFORCEMENT CONCRETE COLUMNS .....	113

4.1 Cyclic behavior of reinforcing bar and mechanical splice .....	113
4.1.1 Mechanical splice system.....	113
4.1.2 Study on mechanical splice behavior [46] .....	114
4.1.2.1 Test Setup and loading protocols .....	115
4.1.2.2 Test results and discussions .....	116
4.1.2.2.1 Effect of thread mechanical splice under tension test....	117
4.1.2.2.2 Effect of unsupported length under compression test....	118
4.1.3 Propose unsupported length of the bar with couplers .....	122
4.1.3.1 Experimental Verification of Numerical Model .....	125
4.2 Modeling of reinforced concrete column .....	127
4.2.1 Uniaxial material.....	128
4.2.1.1 Reinforcing steel uniaxial material model.....	128
4.2.1.2 Unconfined concrete uniaxial material model.....	131
4.2.1.3 Confined concrete uniaxial material model.....	132
4.2.2 Plastic hinge length.....	133
4.2.3 Elastic elements .....	133
4.2.4 Force-based fiber beam-column element .....	134
4.2.5 Structural Elements .....	135
4.3 Numerical result and discussion .....	137
4.3.1 Numerical result of specimen NS .....	137
4.3.2 Numerical result of specimen MS1 .....	140
4.3.3 Numerical result of specimen MS2 .....	143
4.3.4 Numerical result of specimen LS.....	146

4.4 Discussion of the numerical model .....	149
CHAPTER 5 STRENGTHENING OF REINFORCED CONCRETE COLUMN USING STEEL COLLARS .....	
5.1 Introduction.....	150
5.2 Concept of steel collar.....	150
5.3 Experimental program and test configuration.....	160
5.3.1 Specimen details.....	160
5.3.2 Instrumentation of strain gage on steel collars.....	161
5.3.3 Testing setup and strengthening method.....	163
5.4 Experimental Result and discussion .....	166
5.4.1 Experimental result of specimen SC1.....	166
5.4.1.1 Progressive damage of specimen SC1.....	166
5.4.1.2 Appearance failure of specimen SC1 .....	168
5.4.1.3 Strain in Reinforcing steels of specimen SC1 .....	171
5.4.2 Experimental result of specimen SC2.....	172
5.4.2.1 Progressive damage of specimen SC2.....	172
5.4.2.2 Appearance failure of specimen SC2 .....	174
5.4.2.3 Strain in Reinforcing steels of specimen SC2 .....	177
5.4.3 Experimental result of specimen SC3.....	178
5.4.3.1 Progressive damage of specimen SC3.....	178
5.4.3.2 Appearance failure of specimen SC3 .....	180
5.4.3.3 Strain in Reinforcing steels of specimen SC3 .....	183
5.5 Comparison between column with and without strengthening of steel collars .....	184

5.5.1 Displacement ductility.....	184
5.5.2 Moment-curvature distribution.....	187
5.5.3 Distribution of column section rotation.....	189
5.5.4 Energy dissipation.....	192
5.6 Discussion of the column with and without external steel collars.....	194
CHAPTER 6 CONCLUSION.....	195
6.1 Behavior of RC columns with spliced reinforcement.....	195
6.2 Effect of external steel collars on the behavior of lap-spliced columns.....	195
6.3 Numerical modeling for RC columns with spliced reinforcement.....	196
REFERENCES.....	197
APPENDIX A Bridge parameter.....	203
APPENDIX B Cyclic behavior of NS column specimen.....	205
APPENDIX C Cyclic behavior of LS column specimen.....	220
APPENDIX D Cyclic behavior of MS1 column specimen.....	234
APPENDIX E Cyclic behavior of MS2 column specimen.....	250
APPENDIX F Cyclic behavior of SC1 column specimen.....	266
APPENDIX G Cyclic behavior of SC2 column specimen.....	282
APPENDIX H Cyclic behavior of SC3 column specimen.....	297
APPENDIX C Strain in steel reinforcement.....	312
VITA.....	345

## LIST OF FIGURES

Figure 1.1 (a,b) Failure of reinforced concrete structure (c) Lap splice failure column (d) shear failure columns (Earthquake in May 2014, Chiangrai province) .....	3
Figure 1.2 (a) Construction practices directly steel bar of columns to footings or cap beams (b) Bridge pier structure with a 10 meters span of the Department of rural roads (DRR), Thailand .....	3
Figure 1.3 (a) Construction practices in the building structures in Thailand (b) The longitudinal reinforcement for lap splice steel bars to the next floor.....	4
Figure 1.4 (a) Strengthening of bridge column (b) Less interruptive of strengthening building column .....	4
Figure 2.1 Typical column test specimen [15].....	7
Figure 2.2 Failure of the specimen under gravitation and lateral cyclic loading [15].....	7
Figure 2.3 Tie shape by same as transverse reinforcement ratio and Envelop curve of test result [18].....	9
Figure 2.4 Cantilever column test setup (a) and Reinforcing details (b) [2] .....	10
Figure 2.5 Lateral load and displacement relationship. [2] .....	11
Figure 2.6 Details of longitudinal steel splice specimens [3].....	12
Figure 2.7 Moment-lateral displacement hysteresis curves [3] .....	13
Figure 2.8 Tri-linear stress-strain model for steel bars [21].....	15
Figure 2.9 Bond stress–slip model by [20] .....	16
Figure 2.10 Sample of Mechanical Bar Splices [22] .....	17
Figure 2.11 Repaired Column with Threaded Bar Couplers [10].....	17
Figure 2.12 Force-Displacement Hysteresis of Repaired Column with Threaded Bar Couplers [10].....	18

Figure 2.13 Column with Threaded Bar Couplers [23].....	18
Figure 2.14 Force-Displacement Envelope for Threaded Coupler Columns [23].....	19
Figure 2.15 Cast-in-Place Columns with Threaded Couplers [24].....	20
Figure 2.16 Force-Displacement Envelope for Threaded Coupler Columns [24].....	20
Figure 2.17 Cast-in-Place Column with Threaded Couplers [25].....	21
Figure 2.18 Location of SMA Bar Fracture in Threaded Coupler Column [25] .....	21
Figure 2.19 Steel jacket circular bridge column and the hysteresis response of as-built and retrofitted circular columns [26].....	23
Figure 2.20 Detail of test specimen and steel jacketing schemes [27] .....	24
Figure 2.21 Axial force and strain relationship of steel-jacketed columns [27] .....	24
Figure 2.22 (a) Specimen detail and test set up (b) Jacket details (c) lateral load-deformation of as build specimen (d) Lateral load deformation of retrofitted specimens [28].....	25
Figure 2.23 Jacketing procedures and cross-section of the column (a) As build column (b) Apply external pressure on steel jacket (c) Weld overlap line and (d) Weld lateral strip bands [29] .....	26
Figure 2.24 Load displacement response of the columns [29].....	27
Figure 2.25 Detail of reinforcement of specimens [30] .....	28
Figure 2.26 Load displacement relationship of two specimens [30] .....	29
Figure 2.27 Details of steel jacket [13] .....	30
Figure 2.28 Unretrofitted column and retrofitted column [13] .....	30
Figure 2.29 Envelopes of cyclic response of test columns [13].....	31
Figure 2.30 Theoretical design mode of steel cages (a) original model (b) refined model [32].....	32

Figure 2.31 Detail of test specimens [31] .....	32
Figure 2.32 Hysteresis response of the tested specimens [31] .....	33
Figure 2.33 Energy dissipation capacity of the tested specimens [31] .....	34
Figure 2.34 Specimen dimension and steel jacket configuration [33] .....	34
Figure 2.35 Load displacement relationship for all specimens [33] .....	35
Figure 2.36 Detail of some strengthened specimens [34] .....	36
Figure 2.37 Axial load and axial shortening of Group 1 and Group 2 [34] .....	37
Figure 2.38 Design detail of specimens with and without steel jacketing [35] .....	38
Figure 2.39 Test set up (a) axial compressive test (b) eccentric compressive test [35] 38	
Figure 2.40 Result of axial compressive test for retrofitted and unretrofitted specimens [35].....	39
Figure 2.41 Result of eccentric compressive test for retrofitted and unretrofitted specimens [35].....	39
Figure 2.42 Strengthened and unstrengthened specimens models [36] .....	40
Figure 2.43 Axial load and displacement curves of the test specimens [36] .....	41
Figure 2.44 Bolted collar and welded collar [37].....	41
Figure 2.45 Column reinforcement details and typical test specimen [37] .....	42
Figure 2.46 Load displacement relationship of the test columns [37] .....	43
Figure 2.47 Specimen reinforcement details [38].....	44
Figure 2.48 Fabrication and assembled view of the steel collars [38].....	44
Figure 2.49 Test set up of typical retrofitted specimen [38].....	44
Figure 2.50 Force displacement envelopes for retrofitted test specimens [38] .....	45
Figure 2.51 Detail of the column specimens [39].....	46
Figure 2.52 Detail of the retrofitted specimens [39] .....	47

Figure 2.53 Stress-strain relation of unconfined concrete [40] .....	49
Figure 2.54:Stress-strain relation of confined concrete [40] .....	50
Figure 2.55: Stress-strain relation of confined and unconfined concrete under monotonic loading [41] .....	52
Figure 2.56: Effectively confined to the concrete core [41] .....	53
Figure 2.57: Stress-strain model of confined concrete [42] .....	54
Figure 2.58: Stress-strain relation of reinforcement [43] .....	55
Figure 2.59: Nonlinear beam-column element with fiber section [45].....	57
Figure 3.1 Details of longitudinal steel splice in column specimens.....	60
Figure 3.2 Column detailing of (a) NS, (b) LS, (c) MS1 and (d) MS2 (All dimensions in meters).....	61
Figure 3.3 Prepare ground level and grid line for construction.....	62
Figure 3.4 Rigid footing reinforcement detailing.....	62
Figure 3.5 Tie hoops were placed orderly way along the column and vertical alignment was adjusted .....	62
Figure 3.6 lap splice slope bending ratio 1:6 of lap splice column (LS) [46] .....	63
Figure 3.7 Initial torque of the threaded collars of approximately 200 N-m.....	64
Figure 3.8 Splice reinforcement detailing (a) NS:Non-splice, (b) LS:Lap splice, (c) MS1 and (d) MS2 : Mechanical splice. ....	64
Figure 3.9 Splice reinforcement detailing (a) NS:Non-splice, (b) LS:Lap splice, (c) MS1 and (d) MS2 : Mechanical splice. ....	65
Figure 3.10 Strains measurement of reinforcing steel and mechanical splice .....	65
Figure 3.11 (a) Setup steel formwork of footing, (b) Footing cast and setup steel formwork for the column (c) Complete preparing specimen. ....	66



Figure 3.12 Detailing of strain gauge on reinforcements of NS column .....	69
Figure 3.13 Detailing of strain gauge on reinforcements of LS column .....	70
Figure 3.14 Detailing of strain gauge on reinforcements of MS1 column .....	70
Figure 3.15 Detailing of strain gauge on reinforcements of MS2 column .....	71
Figure 3.16 Sling type of displacement transducers measured at the lateral displacement. ....	72
Figure 3.17 Installation displacement transducer to measuring the curvature .....	72
Figure 3.18 Installation displacement transducer to measure the rotation and footing of the test specimen .....	72
Figure 3.19 (a) The rotation of the foundation, (b) Sliding of the foundation and (c) The displacement of the reaction wall .....	73
Figure 3.20 Experimental setup .....	74
Figure 3.21 Full-scale laboratory at Chulalongkorn University .....	75
Figure 3.22 Data logger acquisition system. ....	76
Figure 3.23 Displacement history for the tested specimen .....	76
Figure 3.24 Hysteresis of NS specimen.....	78
Figure 3.25 Envelop curve of NS specimen .....	78
Figure 3.26 Buckling failure of non-splice column specimen NS.....	79
Figure 3.27 Strain in the longitudinal reinforcement of NS at level 1 and 2 .....	82
Figure 3.28 Hysteresis of LS specimen .....	84
Figure 3.29 Envelop curve of LS specimen .....	84
Figure 3.30 Bond slip failure of lap-splice column specimen LS .....	85
Figure 3.31 Strain in the longitudinal reinforcement of LS at level 2 .....	88
Figure 3.32 Hysteresis of MS1 specimen .....	90

Figure 3.33 Envelop curve of MS1 specimen .....	90
Figure 3.34 Buckling failure of mechanical-splice column specimen MS1 .....	91
Figure 3.35 Strain in the longitudinal reinforcement of MS1 at level 2 .....	94
Figure 3.36 Hysteresis of MS1 specimen .....	96
Figure 3.37 Envelop curve of MS2 specimen .....	96
Figure 3.38 Buckling failure of mechanical-splice column specimen MS2 .....	97
Figure 3.39 Strain in the longitudinal reinforcement of MS2 at level 2 and the coupler level 4 .....	100
Figure 3.40 Section ductility factors element (Sheikh et al., 1994) .....	101
Figure 3.41 Envelop curve of all specimen.....	102
Figure 3.42 Hysteresis of all specimen .....	102
Figure 3.43 Damage state at 2.0% drift. ....	103
Figure 3.44 Damage state at 4.0% drift. ....	103
Figure 3.45 Damage state at failure.....	103
Figure 3.46 Envelop curve of (a) NS, (b) LS, (c) MS1 and (d) MS2 .....	104
Figure 3.47 Curvature distribution on the specimen NS.....	105
Figure 3.48 Curvature distribution on the specimen LS .....	106
Figure 3.49 Curvature distribution on the specimen MS1 .....	106
Figure 3.50 Curvature distribution on the specimen MS2 .....	106
Figure 3.51 Curvature distribution on the specimen NS.....	107
Figure 3.52 Curvature distribution on the specimen LS .....	108
Figure 3.53 Curvature distribution on the specimen MS1 .....	108
Figure 3.54 Curvature distribution on the specimen MS2 .....	108

Figure 3.55 Loop for energy dissipation .....	109
Figure 3.56 Cumulative energy dissipation of all specimens .....	110
Figure 4.1 Schematic of parallel-threaded mechanical splicing system .....	114
Figure 4.2 Uniaxial test setup.....	116
Figure 4.3 Tension failure of deform bar and coupler. ....	117
Figure 4.4 Stress-strain relationship (Tension) of deform bar and coupler specimens (a) DB20 vs MS20, (b) DB25 vs MS25, (c) DB32 vs MS32.....	118
Figure 4.5 Buckling shape of deform bar and coupler under monotonic compression test. ....	120
Figure 4.6 Stress-strain relationship (Compression) of deform bar and coupler specimens(a) DB20 vs MS20, (b) DB25 vs MS25, (c) DB32 vs MS32] .....	120
Figure 4.7 Normalize Stress - normalize strain relationship (Compression) of (a) deform bar and (b) coupler specimens .....	120
Figure 4.8 Relationship of strain energy and L/D ratios of deform bar and coupler specimens .....	122
Figure 4.9 Plastic mechanism of buckling in (a) deform bar and (b) coupler, (c) Numerical modeling of reinforcing bar with and with out mechanical splice .....	124
Figure 4.10. Comparison of numerical predictions and experimental results .....	126
Figure 4.11 Lumped plasticity column model.....	128
Figure 4.12 [43] steel material model .....	129
Figure 4.13 General form of proposed stress-strain curve for lap- spliced bar. [53]...	129
Figure 4.14 Tension stresses induced by force transfer in lap- splices [51] (a) Between bars and (b) Between bar and core.....	130
Figure 4.15 Stress-strain relationship of unconfined concrete [40] .....	131
Figure 4.16 Stress strain relationship for confined concrete [41] .....	132

Figure 4.17 Model of fiber section of RC column (a) Unconfined concrete fiber model and (b) Confined concrete fiber model .....	134
Figure 4.18 Three node element .....	134
Figure 4.19 Reinforcing steel with a coupler in fiber section of specimen MS1, MS2 ...	135
Figure 4.20 The location of a coupler in specimen MS1, MS2 .....	135
Figure 4.21 Plastic hinge length of NS column equal to 450 mm .....	136
Figure 4.22 Plastic hinge length of MS1 column equal to 650 mm .....	136
Figure 4.23 Plastic hinge length of MS2 column equal to 450 mm .....	136
Figure 4.24 Plastic hinge length of LS column equal to 700 mm .....	137
Figure 4.25 Comparison of load-displacement relationship NS(Hysteresis) .....	138
Figure 4.26 Comparison of moment-curvature relationship NS .....	138
Figure 4.27 Stress strain relationship of material model of NS (a) Confined concrete, (b) Unconfined concrete and (c) Reinforcing steel.....	139
Figure 4.28 Comparison of load-displacement relationship MS1 (Hysteresis).....	141
Figure 4.29 Comparison of moment-curvature relationship MS1.....	141
Figure 4.30 Stress strain relationship of the material model of MS1 (a) Confined concrete,(b) Unconfined concrete and (c) Reinforcing steel (d) mechanical splice ....	143
Figure 4.31 Comparison of load-displacement relationship MS2 (Hysteresis).....	144
Figure 4.32 Comparison of moment-curvature relationship MS2.....	144
Figure 4.33 Stress strain relationship of the material model of MS2 (a) Confined concrete, (b) Unconfined concrete and (c) Reinforcing steel (d) Mechanical splice ...	146
Figure 4.34 Comparison of load-displacement relationship LS (Hysteresis).....	147
Figure 4.35 Comparison of moment-curvature relationship MS2.....	147

Figure 4.36 Stress strain relationship of the material model of LS (a) Confined concrete, (b) Unconfined concrete and (c) Reinforcing steel. ....	148
Figure 5.1 Progressive of vertical cracks which along with the lap-splice location of lap-splice column LS.....	151
Figure 5.2 Lateral pressure in square column (a) Lateral pressure buildup in square column, and (b) Pressure distribution resulting from different reinforcement arrangements [56].....	151
Figure 5.3 Reinforcement detailing of lap splice column specimen LS.....	152
Figure 5.4 Modulus of section by weight of steel section.....	155
Figure 5.5 Confinement height of steel section .....	155
Figure 5.6 Distributions of lateral pressure (a) distribution of lateral pressure along member length. And (b) Actual, average, and equivalent lateral pressure .....	156
Figure 5.7 Concrete under multiaxial stresses .....	157
Figure 5.8 Section analysis by using SAP2000 .....	158
Figure 5.9 External steel collar detailing .....	159
Figure 5.10 External steel collar.....	159
Figure 5.11 Lap splice column strengthen by using steel collars.....	161
Figure 5.12 Strain gauge location on steel collars .....	162
Figure 5.13 Epoxy use to fill the gap between collars and column edge .....	163
Figure 5.14 Arrange and adjust leveling the steel collars into column SC1 .....	164
Figure 5.15 Gap-fill between column and steel collars by using epoxy .....	164
Figure 5.16 Completely strength by using steel collars .....	165
Figure 5.17 Strengthen column SC1 .....	165
Figure 5.18 Hysteresis of SC1 specimen.....	167

Figure 5.19 Envelop curve of SC1 specimen .....	167
Figure 5.20 Flexural joint failure of strengthening lap-splice column SC1 .....	168
Figure 5.21 Strain in the longitudinal reinforcement of SC1 at level 2 and steel collars .....	171
Figure 5.22 Hysteresis of SC2 specimen.....	173
Figure 5.23 Envelop curve of SC2 specimen .....	173
Figure 5.24 Flexural joint failure of strengthening lap-splice column SC2.....	174
Figure 5.25 Strain in the longitudinal reinforcement of SC2 at level 1 and level 2.....	177
Figure 5.26 Hysteresis of SC3 specimen.....	179
Figure 5.27 Envelop curve of SC3 specimen .....	179
Figure 5.28 Flexural joint failure of strengthening lap-splice column SC3.....	180
Figure 5.29 Strain in the longitudinal reinforcement of NS at level 1 and level 2.....	183
Figure 5.30 Envelop curve of all specimen.....	184
Figure 5.31 Hysteresis of all specimen .....	184
Figure 5.32 Damage state at 2.0% drift. ....	185
Figure 5.33 Damage state at 4.0% drift. ....	185
Figure 5.34 Damage state at failure.....	185
Figure 5.35 Envelop curve of (a) NS, (b) LS, (c) SC1, (d) SC2 and (e) SC3 .....	186
Figure 5.36 Curvature distribution on the specimen NS.....	187
Figure 5.37 Curvature distribution on the specimen LS .....	188
Figure 5.38 Curvature distribution on the specimen SC1.....	188
Figure 5.39 Curvature distribution on the specimen SC2.....	188
Figure 5.40 Curvature distribution on the specimen SC3.....	189

Figure 5.41 Curvature distribution on the specimen NS.....	190
Figure 5.42 Curvature distribution on the specimen LS .....	190
Figure 5.43 Curvature distribution on the specimen SC1.....	190
Figure 5.44 Curvature distribution on the specimen SC2.....	191
Figure 5.45 Curvature distribution on the specimen SC3.....	191
Figure 5.46 Energy dissipation all specimen.....	192



## LIST OF TABLES

Table 2.1 Specimens detail [15] .....	7
Table 2.2 Specimens detail [18] .....	8
Table 2.3 Test specimens parameter [2] .....	10
Table 2.4 Test result [2].....	11
Table 2.5 Test specimens parameter [19].....	14
Table 3.1 Compressive strength of concrete in this research.....	67
Table 3.2 Tensile strength of transverse reinforcement .....	68
Table 3.3 Tensile strength of longitudinal reinforcement.....	68
Table 3.4 Summary of specimen parameters.....	68
Table 3.5 Experimental results of specimen NS.....	77
Table 3.6 Experimental results specimen LS.....	83
Table 3.7 Experimental results of specimen MS1.....	89
Table 3.8 Experimental results of specimen MS2.....	95
Table 3.9 Experimental results of lateral load capacity and displacement ductility of all specimen .....	104
Table 3.10 Cumulative energy dissipation of all specimens .....	111
Table 4.1 Parametric of experimental. ....	115
Table 4.2 Tensile and compressive properties of deform bar and coupler specimens. .....	116
Table 4.3 Compression test result of deform bar and coupler specimens.....	122
Table 4.4 Propose unsupported length of mechanical splice.....	124
Table 4.5 ReinforcingSteel material properties.....	128



Table 4.6 Lap splice material properties .....	131
Table 4.7 Concrete material properties .....	132
Table 4.8 Numerical results of specimen NS.....	137
Table 4.9 Numerical results of specimen MS1 .....	140
Table 4.10 Numerical results of specimen MS2 .....	143
Table 4.11 Numerical results of specimen LS .....	146
Table 5.1 Volumetric ratio of external steel jacket from previous researchers.....	154
Table 5.2 Steel Section : Rectangular Hollow section : 50x50x2.3 .....	158
Table 5.3 Volumetric of external steel collars of column specimen .....	160
Table 5.4 Experimental results specimen SC1 .....	166
Table 5.5 Experimental results specimen SC2 .....	172
Table 5.6 Experimental results specimen SC3.....	178
Table 5.7 Experimental results of lateral load capacity and displacement ductility of all specimen .....	186
Table 5.8 Cumulative energy dissipation of all specimens .....	193

# CHAPTER 1

## INTRODUCTION

### 1.1 Background and Problem Statements

Many reinforced concrete frame structures were designed only for gravity and wind loads. Compression-only reinforcing details used in the columns of these structures are often associated with non-ductile behaviors. Lateral load resisting elements are a significant concern to evaluate the performance of deficient buildings. The progressive collapse of buildings can be triggered by the failure of columns, which are primary components in the structure.

During the recent earthquake in May 2014, Chiangrai province in the northern part of Thailand, several existing buildings severely damaged because of non-seismic reinforcement detailing. That shows the failure of non-seismic reinforcement detailing clearly by buckling of reinforcement, shear failure, lap-splice failure according to the existing building [1]. The significant detailing deficiencies typically found in such columns are the use of lap splices in the potential plastic hinge area, which are adequate development length, reinforcing bars with deformation patterns that do not conform to current specifications.

Lap splicing is widely used in the construction practice, which requires the overlapping of two parallel bars. The load transfer mechanism takes advantage of the bond between the steel and the concrete to transfer the load. The load in one bar is transferred to the concrete, and then from the concrete to the bar, bearing load at the bar end. The effect of lap splice deficiencies has been examined in the literature such as the tests [2], [3], and [4].

Several types of new splices are available, The researchers studied seismic performance of column test incorporating with up-set headed coupler [5], grouted sleeve couplers [6], shear screw couplers [7] [8], headed bar couplers, swaged couplers [9] and threaded coupler [10].

The primary deficiencies of columns with lap splices for longitudinal reinforcement are non-ductile characteristics. To improve their failure mechanism by changing from brittle to ductile modes can be done by strengthening using various methods. One such technique is steel jacketing. Several researchers investigated the strengthening of RC columns using steel jackets. [11], [12], [13], which helps to improve the global seismic behavior of the structure by increasing lateral strength, ductility and shear capacity of structural members [14].

The research involved the experimental and analytical investigation on seismic behavior of reinforced concrete bridge column with splice reinforcement by using lap splice and mechanical splice. This study proposed the strengthening method by external steel collars to strengthen lap splice columns. The external steel collars can provide the extra-confinement effect of the column that can enhance the ductility of the column with poor lap-splice detailing.

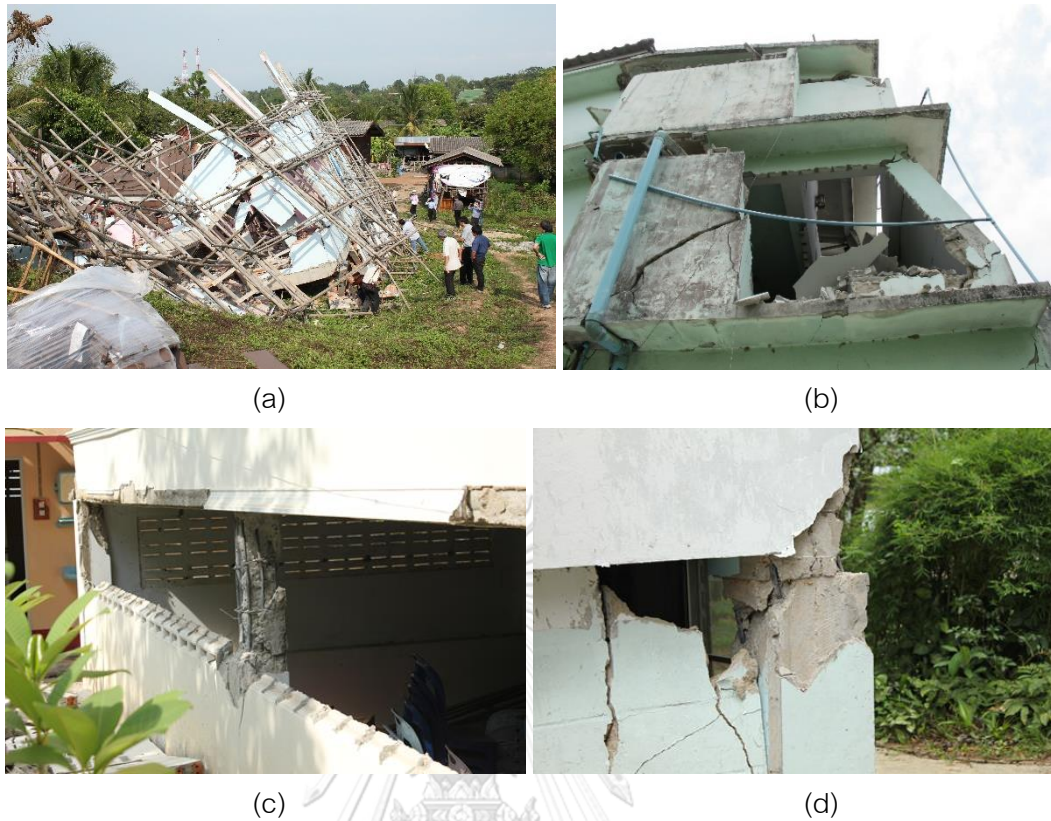


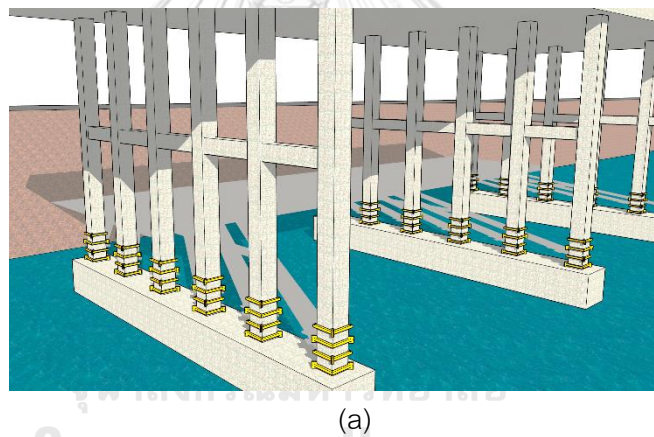
Figure 1.1 (a,b) Failure of reinforced concrete structure (c) Lap splice failure column  
(d) shear failure columns (Earthquake in May 2014, Chiangrai province)



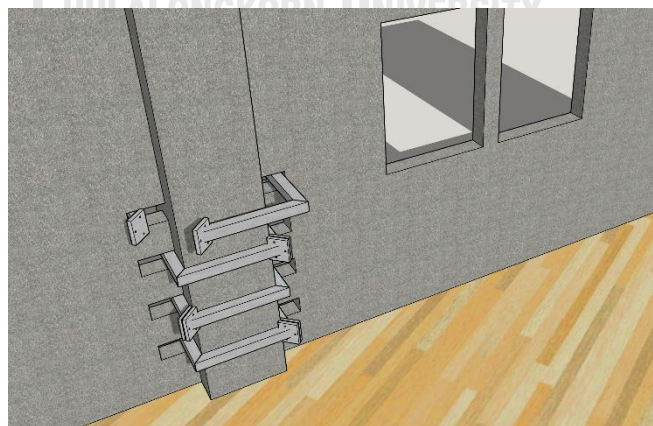
Figure 1.2 (a) Construction practices directly steel bar of columns to footings or  
cap beams (b) Bridge pier structure with a 10 meters span of the  
Department of rural roads (DRR), Thailand



Figure 1.3 (a) Construction practices in the building structures in Thailand  
 (b) The longitudinal reinforcement for lap splice steel bars to the next floor.



(a)



(b)

Figure 1.4 (a) Strengthening of bridge column  
 (b) Less interruptive of strengthening building column

## 1.2 Significance of research

Spliced reinforcement has been used in structures and it can lead to premature failure of structural members. This study clarifies the effect of spliced reinforcement and proposes the strengthening method using external steel collars.

## 1.3 Objectives of the research

The main objectives of the research are;

1. To study the behavior of the column with spliced reinforcement by using the lap splice and mechanical splice
2. To investigate the effectiveness of external steel collars which provides confinement for lap spliced columns.
3. To perform the numerical analysis of reinforced concrete columns with and without spliced reinforcement.

## 1.4 Scope of the research

The scopes of the research are as follows:

1. Seven square reinforced concrete columns were tested: one non-spliced column (control column), one lap spliced columns, two columns with couplers, and three strengthened columns.
2. Spliced reinforcement by the lap splice and mechanical splice were at the plastic hinge region.
3. Specimens were subjected to lateral cyclic loading and constant axial load during the test.
4. Analytical study of the tested specimens was accomplished using the OpenSees program.

## CHAPTER 2

### LITERATURE REVIEW

Many researchers have studied the behavior of non-ductile columns and the strengthening of column. Include mathematical model which was the key to prediction of structural behavior. This chapter gives background information on topics relevant to this research work. In literature provides an overview of previous researches that focuses on corresponding points for the development and achieves the objectives of current work. The first part covers the experimental program that investigated the behavior of reinforced concrete columns with lap splice and mechanical splice. The second part collects the recent studies of strengthening method by external confining of reinforced concrete column with lap splice and evaluates of strengthening system affect to concrete confinement property. Finally, the last section collected the theory on the nonlinear behavior to propose the development of the design of column.

#### 2.1 Test on columns without lap splices

Sezen and Moehle [15] Tested four specimens under different axial load. The study of Sezen concludes that column behavior depends upon the magnitude and history of axial and cyclic loads. Columns with low axial load failed in shear after flexure yielding, whereas column with high axial load failed in brittle shear compression mode. This study pointed out the need for consideration for magnitude axial load while evaluating such non-ductile columns for the seismic response.

Table 2.1 Specimens detail [15]

Specimen	Concrete strength (MPa)	Axial Load (kN)	Axial Force Ratio (P/fc'Ag)	Longitudinal Reinforcement		Transverse Reinforcement		Displacement history
				$\rho_l$	$f_y$ (MPa)	$\rho_s$	$f_{sh}$ (MPa)	
1	21.1	667	0.16	0.025	438	0.0017	476	Standard
2	21.1	2670	0.63					Standard
3	20.9	2670	0.636					Standard
4	21.8	667	0.152					Monotonic

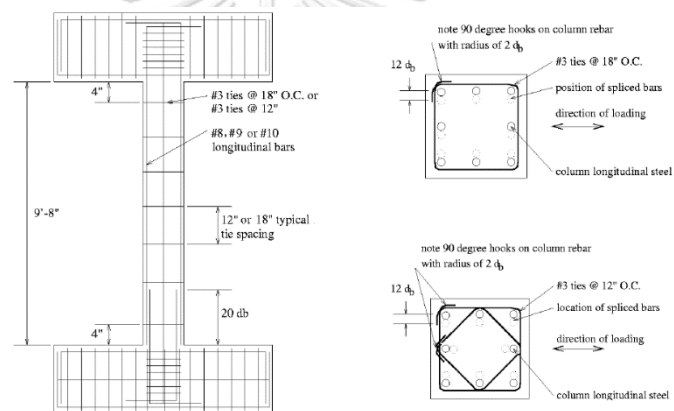


Figure 2.1 Typical column test specimen [15]

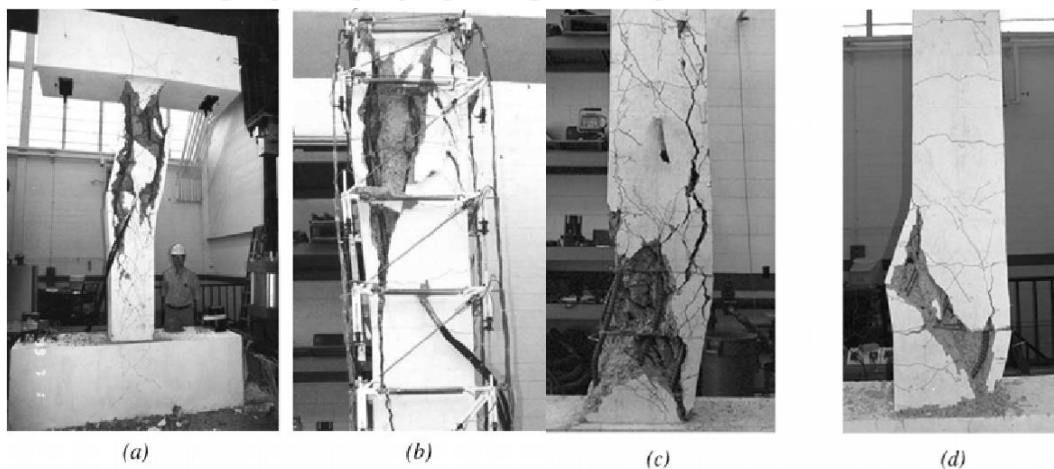


Figure 2.2 Failure of the specimen under gravitation and lateral cyclic loading [15]





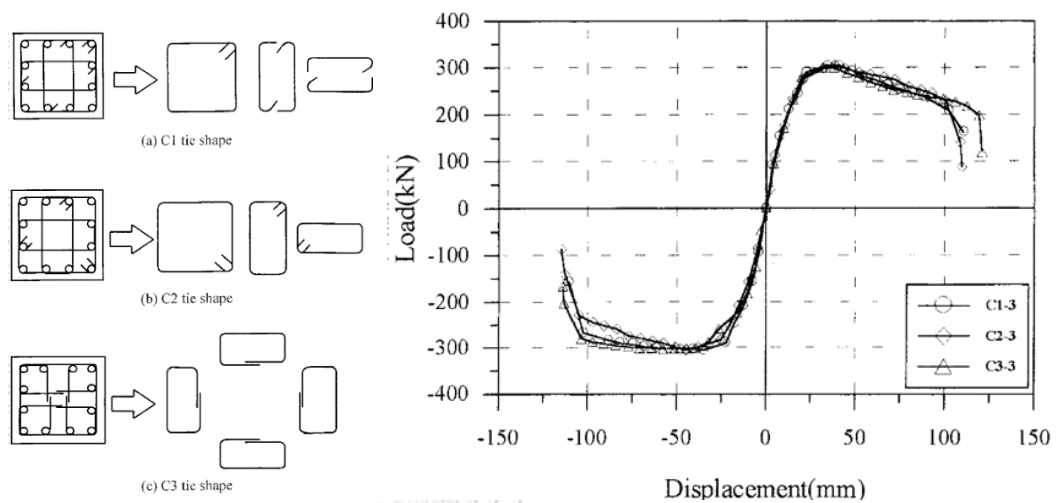


Figure 2.3 Tie shape by same as transverse reinforcement ratio and Envelop curve of test result [18]

## 2.2 Test on columns with lap splices

Lap splices provided in the old reinforced concrete building usually designed as compression splices with the splice length in the order of  $20d_b$  to  $25d_b$  are very common in these buildings. Surveys of post-earthquake studies have depicted that these compression lap splices possess a permanent threat to these buildings; the situation becomes worse if lap splices located in plastic hinge regions slip. During an event of an earthquake, columns undergo a significant moment due to which longitudinal reinforcement experience the high tensile stresses. These tensile stresses require a greater length of splices. In the absence of necessary development length due to high tensile stresses, slip occurred along the splice length. This slip can occur at much lower load levels that otherwise required to develop the nominal moment capacity of the member. This behavior is not well understood; also, very less research has been carried out to study the rate of strength degradation of such columns.

Observations the deficient of lap splice length were conducted by Melek and Wallace [2] investigate the behavior of short lap splices by six rectangular column splices of the provided lap splice length ( $20d_b$ ). The study influenced by axial load level, the column shear demand and the applied displacement history (the standard cyclic lateral load history and near-fault lateral displacement history).

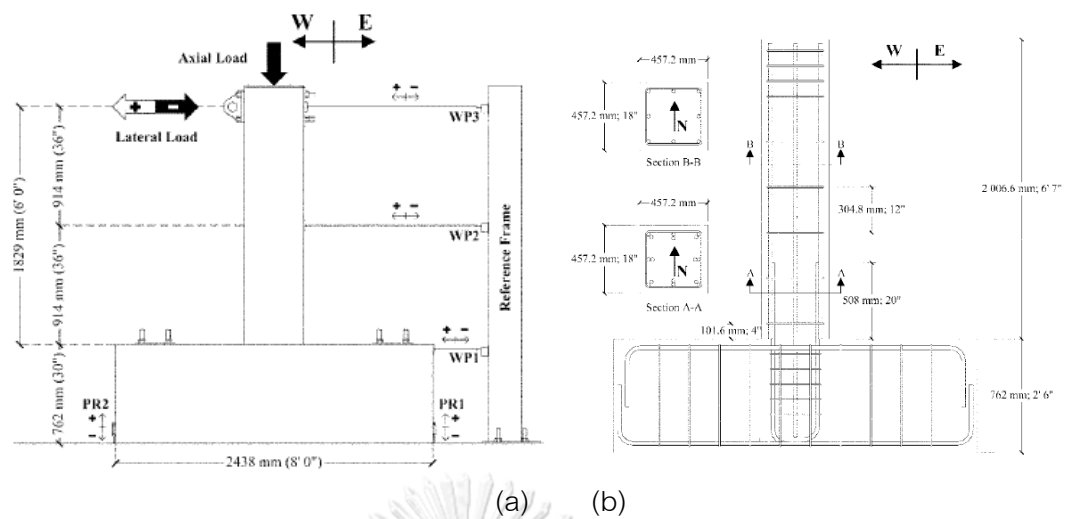


Figure 2.4 Cantilever column test setup (a) and Reinforcing details (b) [2]

Table 2.3 Test specimens parameter [2]

specimens	$\% A_g f'_c$	$\frac{I_{s \text{ provided}}}{I_{s \text{ required}}}$	$V_c$ (kN)	$V_n$ (kN)	$\frac{V_u @ M_{EXP}}{V_n}$	Column height (mm)	Displacement history
2S10M	10	0.65	212	301	0.67	1829	STD
2S20M	20	0.65	245	334	0.70	1829	STD
2S30M	30	0.65	278	367	0.78	1829	STD
2S20H	20	0.64	242	331	0.81	1676	STD
2S20HN	20	0.64	242	331	0.81	1676	Near fault
2S30X	30	0.64	275	363	0.93	1524	STD

They concluded that specimens with  $20d_b$  lap-splice length and poorly confined cross-section behaved unsatisfactorily under cyclic lateral loading. The lateral strength of specimens started degrading at lateral drift levels of 1.0%–1.5%. They have also found that the slippage of splices played an important role in the rotational response of the specimens. 1.5% lateral drift ratio, 80%–85% of the measured rotation was due to the slippage of splices, which lead to higher rate of lateral strength degradation.

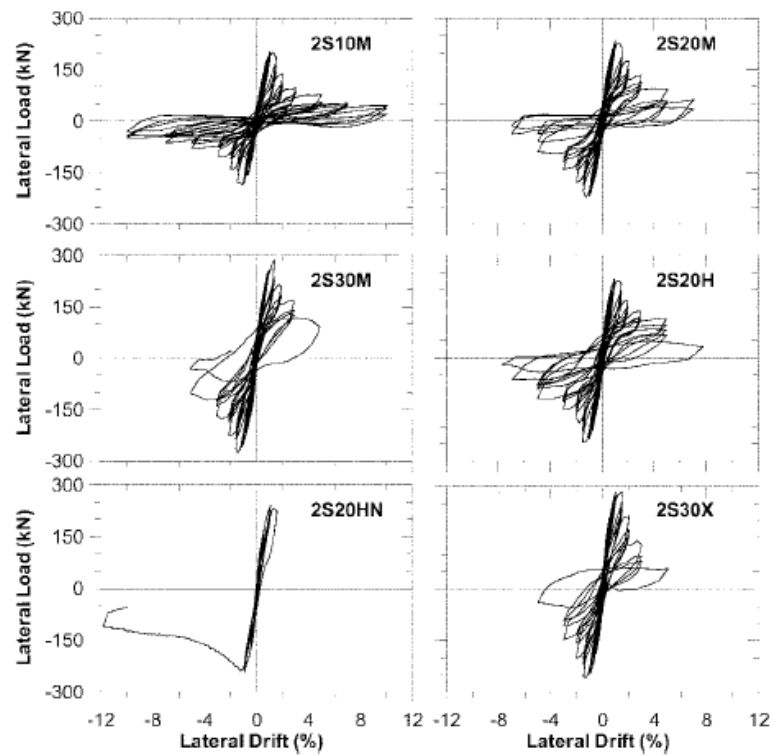


Figure 2.5 Lateral load and displacement relationship. [2]

Table 2.4 Test result [2]

specimens	Maximum Lateral load		Normal – lized lateral load kN	Analyti – cal yield moment kN – m	Maximum base moment $M_{EXP}$ , kN – m	$M_{EXP} / M_y$
	kN	% drift				
2S10M	202.7	1.50	202.7	381.3	370.7	0.97
2S20M	233.5	1.28	233.5	450.4	427.0	0.95
2S30M	285.3	1.45	285.3	509.0	521.8	1.03
2S20H	269.5	1.33	247.0	441.5	451.8	1.02
2S20HN	267.4	1.00	245.1	441.5	448.3	1.02
2S30X	340.7	1.50	283.9	499.5	519.2	1.04

However, the study of lap splice locations is studied by Pam and Ho [3], effects on strength and ductility of reinforced concrete columns. Four columns were the test, lap splices of longitudinal reinforcement place above the beam-column interface that is critical region and moves away from the beam-column interface under inelastic deformation. The lap length of longitudinal steel splice was calculated according to the Hong Kong Code (BD 2004). The test result shows the location of lap splice of longitudinal steel does not have any effect on the tensile cracking nor spalling of concrete cover because they are only dependent on the stress-strain of the unconfined concrete.

For the flexural ductility, the specimen that has lap splices in the critical region had the lowest ultimate flexural ductility because the inelastic damaged region has moved further from the beam-column interface, the specimen with lap splices staggered evenly as well as alternately within and outside the critical region due to the same reason. For the specimen with lap splices place outside the critical region, the damaged region was closer to the beam-column interface and its ultimate flexural ductility was close with the specimen without lap splices.

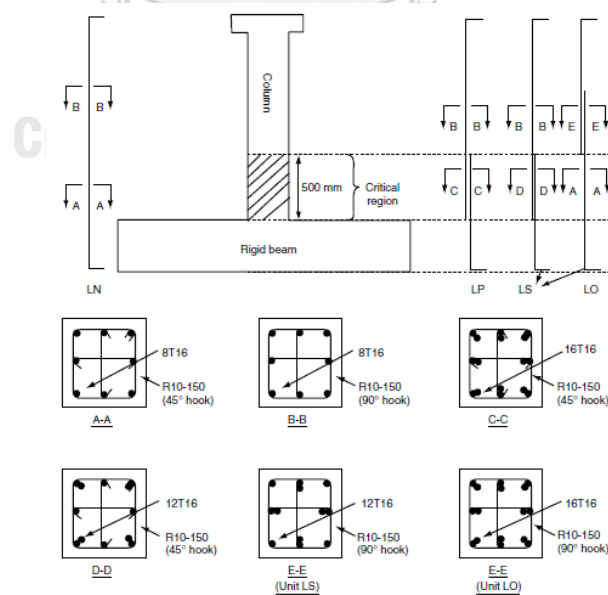


Figure 2.6 Details of longitudinal steel splice specimens [3]

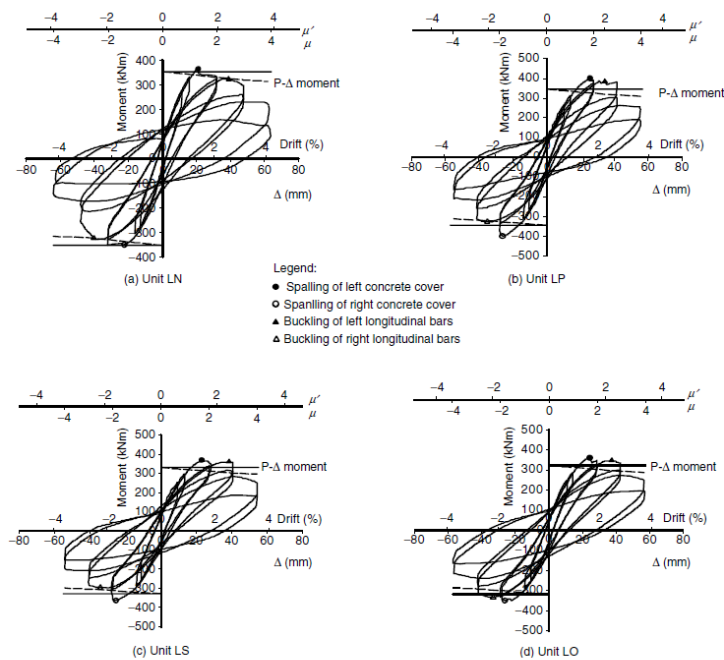


Figure 7. Moment-lateral displacement hysteresis curves of column specimens

Figure 2.7 Moment-lateral displacement hysteresis curves [3]

Lynn, et [19] Tested 8 columns with and without lap splices. The specimen's details are provided in Table 2.5. Specimens were subjected to cyclic loading with varying the axial load. It was found that the response of specimen with low axial load ratio is ductile, whereas the column provided with a high axial load ratio shows brittle failure. Although specimens were able to produce yield stress in the splices bar, the rate of strength degradation was high due to cracking along the splices.

Table 2.5 Test specimens parameter [19]

Specimen	Longitudinal reinforcement	Axial load	Ties	Hoop spacing (mm)	Splice length ( $d_b$ )
3CLH18	8 - #10	$0.12A_{gr}f'_c$	Hoop	457.2 (18)	No splice
2CLH18	8 - #8	$0.12A_{gr}f'_c$	Hoop	457.2 (18)	No splice
3SLH18	8 - #10	$0.12A_{gr}f'_c$	Hoop	457.2 (18)	25
2SLH18	8 - #8	$0.12A_{gr}f'_c$	Hoop	457.2 (18)	20
1CMH18	8 - #8	$0.35A_{gr}f'_c$	Hoop	457.2 (18)	No splice
3CMH18	8 - #10	$0.35A_{gr}f'_c$	Hoop	457.2 (18)	No splice
3CMD12	8 - #10	$0.35A_{gr}f'_c$	Diamond	304.8 (12)	No splice
3SMD12	8 - #10	$0.35A_{gr}f'_c$	Diamond	304.8 (12)	25

During the last few decades, several Lap splice models have been proposed and used for the evaluation of reinforced concrete columns with lap splice. According to most models Harajli [20] presents, the uniaxial stress-strain relationship of confined concrete is an important factor that affects the lap splice strength. A uniaxial stress-strain model for concrete confined with either FRP or transverse reinforcement is adopted to calculate the compressive strength of the confined concrete. A tri-linear stress-strain model is adopted from Park and Paulay [21] The experimental stress-strain curve for steel grades 40, 60, and 75. Figure 2.8 shows the idealized tri-linear stress-strain model. The steel stress-strain relationship is described by

$$f_s = E_s \epsilon_s \quad \text{If } \epsilon_s \leq \epsilon_y = f_y / E_s$$

$$f_s = f_y \quad \text{If } \epsilon_y \leq \epsilon_s \leq \epsilon_{sh}$$

$$f_s = f_y + rE_s(\epsilon_s - \epsilon_{sh}) \quad \text{If } \epsilon_{sh} \leq \epsilon_s \leq \epsilon_{su}$$

where  $f_s$ ;  $\epsilon_s$  are the bar stress and strain,  $E_s$  is the modulus of elasticity or Young modulus of steel,  $f_y$ ;  $\epsilon_y$  are the yield stress and yield strain of steel,  $\epsilon_{sh}$  is the bar strain at the start of the strain hardening, and  $\epsilon_{su}$  is the strain at the steel fracture.

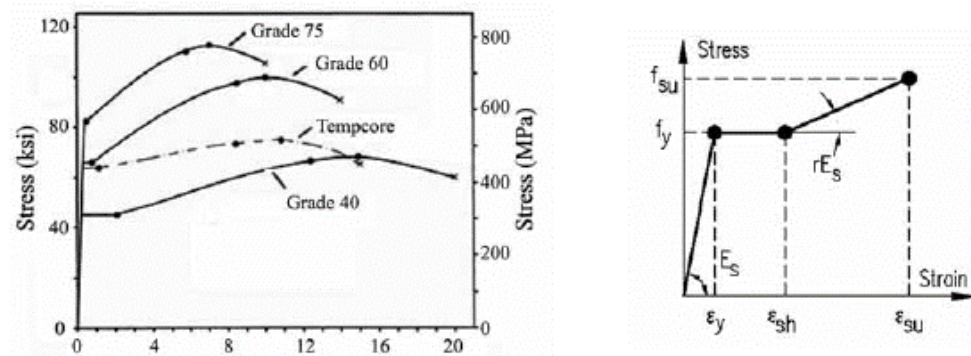


Figure 2.8 Tri-linear stress-strain model for steel bars [21]

Tri-uniform Bond Stress Model presents the column with longitudinal bars spliced with the starter bars at the base of the column. When the load is applied to the column, a crack opens at the interface between the column base and footing. Consider the outermost bar on the tension side; the developed bar stress  $f_s \geq f_y$  at the starting point of lap splice zone (point O) must be in equilibrium with the bond stress on the bar surface along the lap splice zone. The bond stress distribution along the lap splice length  $L_s$  depends on many factors such as the pull-out force  $A_s f_s$ , the length of lap splice  $L_s$ , the confinement condition, and so on. An example of bond stress distribution before lap splice failure state, in which  $u_y$  and  $u_e$ , are bond stresses acting on the yielding part and elastic part, respectively. In the post-yield critical state of splitting failure, the bond stress distribution along the lap splice length is assumed to follow the tri-uniform stress model. In the model, the lap splice length is divided into 3 parts, namely, yielding part (OA), post-splitting part (AB), and splitting part (BC), with bond stresses acting in each part denoted as  $u_y$ ,  $u_r$ , and  $u_{sp}$  respectively. The lengths of the yielding part, post-splitting part, and splitting part are  $L_y$ ,  $L_r$  and  $L_{sp}$  respectively. The length of these 3 parts must be summed to the lap splice length

$$L_s = L_y + L_r + L_{sp}$$



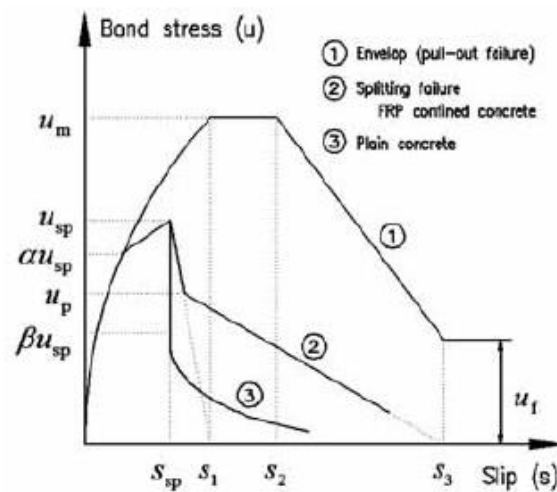


Figure 2.9 Bond stress–slip model by [20]

### 2.3 Test on the column with mechanical splices

Tazarv and Saiidi [22] Some of the mechanical reinforcing bar splices commercially available in the United States are shown in Figure 2.10. Bridge and building design codes use acceptance criteria such as the International Code Council (ICC) AC1332 and ASTM A1034/A1034M3 to quantify the ability of a splice to transfer load, withstand load reversals, and resist slip. Furthermore, some state departments of transportation (DOTs) have developed their own acceptance criteria. After evaluation, mechanical splices are given a performance classification compatible with the corresponding code provision of interest, which is used to restrict placement in a structural member or limit stress/strain demands on spliced bars. In the United States, there is one significant difference between bridge and building code requirements for mechanical splices. ACI 318-025 allows Type 2 mechanical splices, which must be able to develop the full tensile strength of the spliced bars to be placed at any location within a member regardless of local inelastic demands. On the other hand, bridge design codes such as the AASHTO Bridge Design Specifications<sup>6</sup> and Caltrans Seismic Design Criteria (SDC)<sup>7</sup> prohibit all mechanical splices from being placed in plastic hinge regions, which are subjected to high inelastic demands. Such provisions have prevented the use of mechanical splices in plastic hinges of bridge columns and have been a barrier to newer and more innovative bridge columns in earthquake-prone areas.

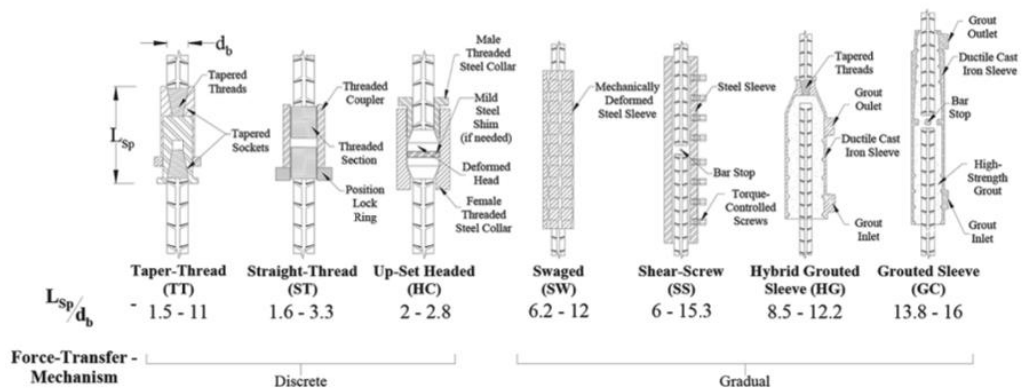


Figure 2.10 Sample of Mechanical Bar Splices [22]

Lehman, et [10] Repaired a severely damaged column using threaded couplers then tested under cyclic loads. The column concrete in the plastic hinge area, as well as a partial depth of footing concrete, were removed and new reinforcement was connected to the column and footing existing bars using threaded couplers (Figure 2.11). Force- displacement hysteretic curves for the original and the repaired column is shown in Figure 2.12. It can be seen that the lateral strength in the repaired column was higher, and the displacement capacity was improved compared to the original column. The higher displacement capacity of the repaired column was because of 2 in. (51 mm) extra clear cover which increased the column longitudinal bar resistance against buckling and fracture.

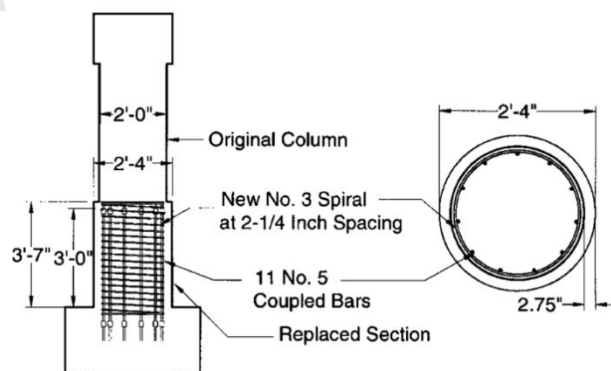


Figure 2.11 Repaired Column with Threaded Bar Couplers

[10]

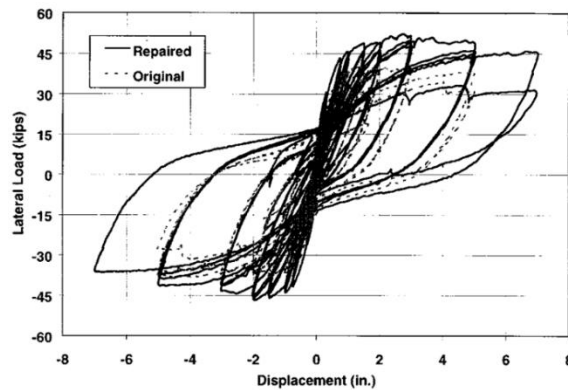


Figure 2.12 Force-Displacement Hysteresis of Repaired Column with Threaded Bar Couplers [10]

Saiidi and Wang [23] Utilized threaded couplers in a quarter-scale bridge column to connect reinforcing SMA bars to reinforcing steel bars in the plastic hinge region. The column was tested on a shake table under 11 runs (Run 11 was 300% of the design level earthquake), during which the drift ratio was 4.8%. The test was stopped after Run 11 to prevent SMA bar failure. The column was then repaired by replacing the conventional concrete of the plastic hinge with ECC. The repaired column was tested under 15 runs (Run 15 was 400% of the design level earthquake), in which a drift capacity of 5.7% was reported. Figure 2.14 shows the force-displacement envelope of the two columns. The test was stopped because the selected motion was not able to impose more deformation on the column. Minor damage of ECC and no SMA bar fracture was observed in these tests. The threaded couplers performed well by allowing the column to deform freely and by transferring the stresses to adjoining bars.



Figure 2.13 Column with Threaded Bar Couplers [23]

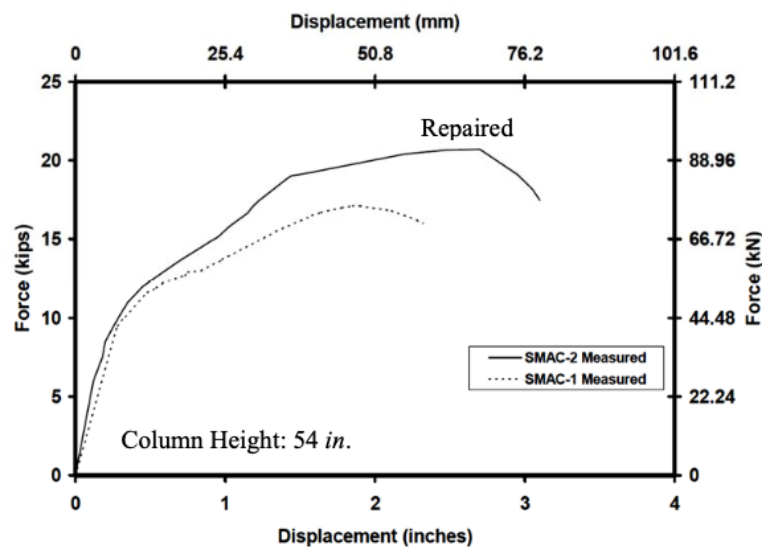


Figure 2.14 Force-Displacement Envelope for Threaded Coupler Columns [23]

Saiidi, et [24] Tested two cast-in-place columns in which threaded couplers were incorporated in the plastic hinge region of these columns to link SMA bars to steel bars (Figure 2.15). Conventional concrete was utilized in one of the SMA columns (RNC), and ECC was used in the plastic hinge of another SMA column (RNE). A reference column with conventional concrete and reinforcing steel bars was also tested (RSC). These columns were tested under cyclic loading to failure. Figure 2.16 shows the measured force-drift envelope for the columns. The columns with threaded couplers showed equal or improved drift capacity compared to the reference column confirming the suitability of the application of threaded couplers in the plastic hinge of columns located in high seismic regions. No bar fracture was reported up to 10% drift ratio cycles. The test was continued for RNE to 14% drift ratio cycles in which one of the SMA bars fractured at the thread inside one of the bottom couplers.

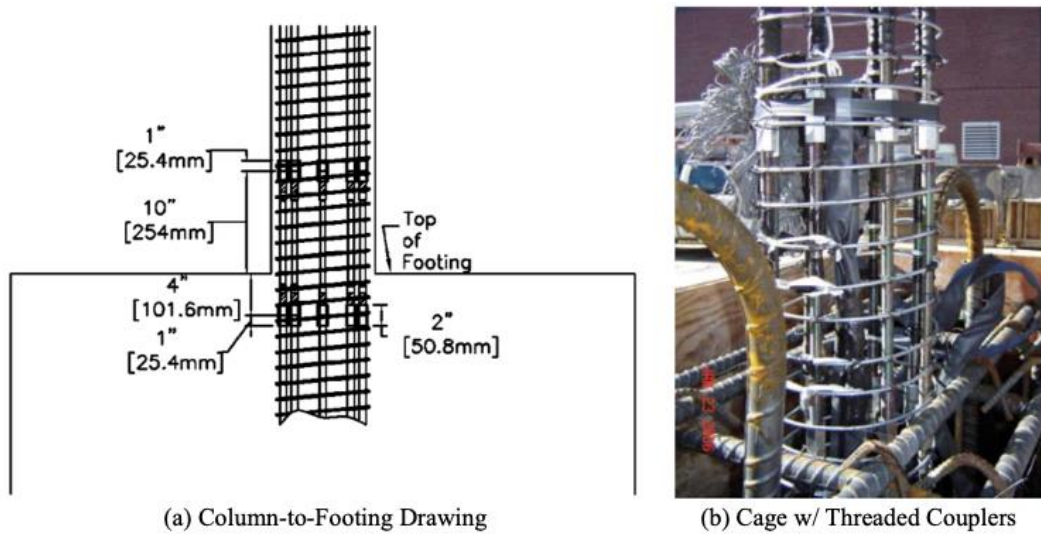


Figure 2.15 Cast-in-Place Columns with Threaded Couplers [24]

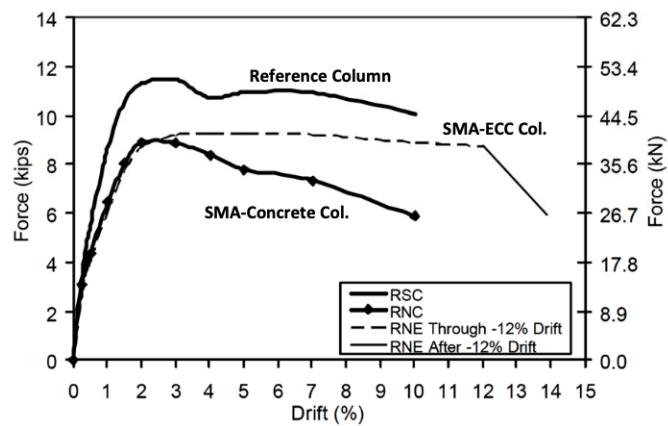


Figure 2.16 Force-Displacement Envelope for Threaded Coupler Columns [24]

A quarter-scale bridge column was tested by Varela and Saiidi [25] in which threaded couplers were utilized to link reinforcing Copper-based SMA bars to reinforcing steel bars (Figure 2.17). The column was tested on a shake table up to 350% of the design level earthquake. The column withstood a drift ratio of 11.8% in which two SMA bars fractured in a ductile manner. The ECC in the column plastic hinge was removed after testing to locate the bar fracture. It was found that both SMA bars fractured away from the threaded couplers, as shown in Figure 2.18. The authors also used threaded couplers in the plastic hinge of six deconstructible bridge columns and a three, two-column bent bridge model. The threaded couplers maintained the integrity of the connections in these tests and allowed the columns to deform freely (NSF-PFI Project, 2014).

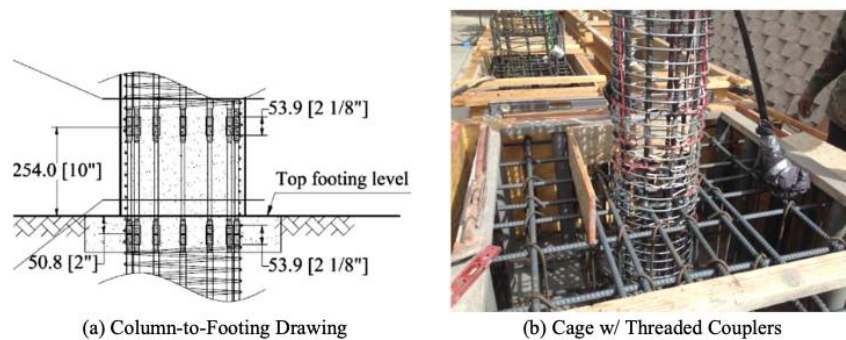


Figure 2.17 Cast-in-Place Column with Threaded Couplers [25]

### จุฬาลงกรณ์มหาวิทยาลัย

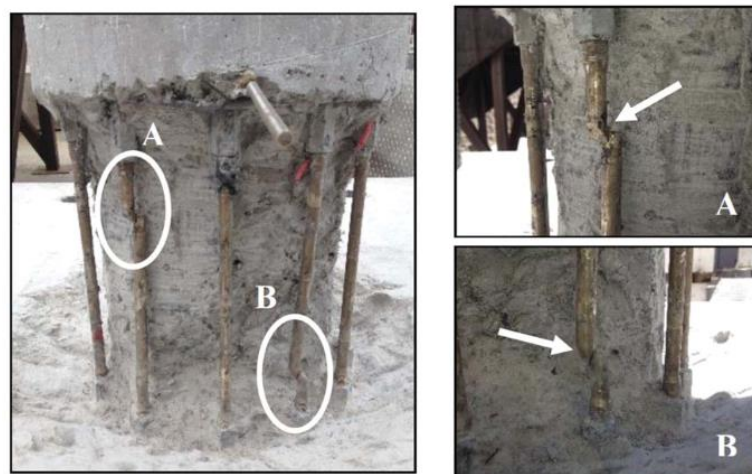


Figure 2.18 Location of SMA Bar Fracture in Threaded Coupler Column [25]

## 2.4 Test on the previous research of strengthening columns

Reinforced concrete jacketing is a traditional and one of the most common methods to retrofit and/or repair reinforced concrete columns. The additional cross-section area helps the column transfer more load while providing additional confinement. Reinforced concrete jackets can have multiple interface mechanisms to facilitate the transfer of loads from the original column to the jacket. According to the previous research and background, various types of steel jacketing methods are addressed. Generally, types of steel jacketing methods found in the literature are steel plate jacketing method, angle and batten jacketing methods, precambered steel plating method, corrugated steel jacketing method, rectified steel jacketing method, and steel collar jacketing method.

### 2.4.1 Steel jacketing methods

Many experimental research programs are needed to study the effect of the strengthening methods, and especially the steel jacketing method, to the reinforced concrete columns. To fulfill these requirements, Chai, et [26] studied the analytical model for steel jacketed RC circular bridge columns that were tested in 1991. In testing the columns, the authors focused on the flexural performance of bridge columns by encasing the plastic hinge region with a steel jacket. One of the reference specimens had lap splice and the other had continuous reinforcement in the plastic hinge region. While experimental testing has demonstrated, in the case of a flexural retrofit, the steel jacket needs not to be extended to the full height of the column. Figure 2.19 shows the steel jacket circular bridge column and the hysteresis response of as-built and retrofitted circular columns containing base lap-splices.

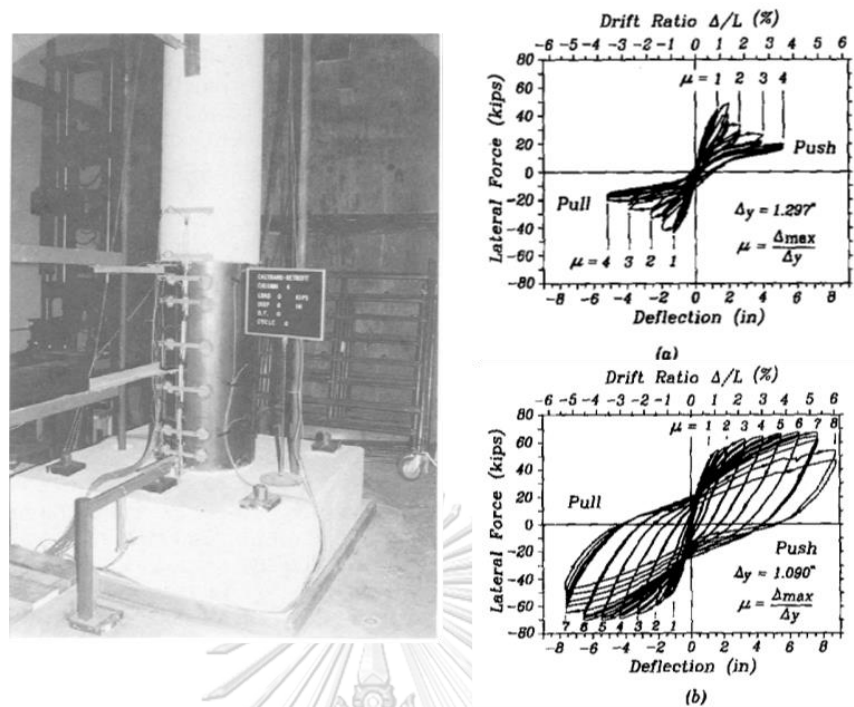


Figure 2.19 Steel jacket circular bridge column and the hysteresis response of as-built and retrofitted circular columns [26]

According to the test result, the columns retrofitted with a steel jacket showed a significantly improved hysteresis behavior. On the other hand, the bond failure that might develop in as-built circular columns detailed with inadequately lapped longitudinal reinforcement was also prevented by steel jacketing.

Tsai and Lin [27] Performed the axial compression test of the square RC columns with various kinds of the jacketing scheme such as circular or octagonal or rectangular shapes, as shown in Figure 2.20. The jacketing materials vary from steel plate to carbon fiber reinforced polymer composites. Among the retrofitted specimens, the steel-jacketed specimen's exhibit not only greatly enhanced and carry capacity but also excellent ductility performance, as shown in Figure 2.21. In rectangular steel jacketing RS45, its improvements in column axial strength and axial ductility are much less than those of other steel jacketed specimens due to premature outward bulging at a small column axial strain. Specimen CS23 had the highest axial strength and the circular retrofit scheme has an excellent performance in axial strength and ductility.



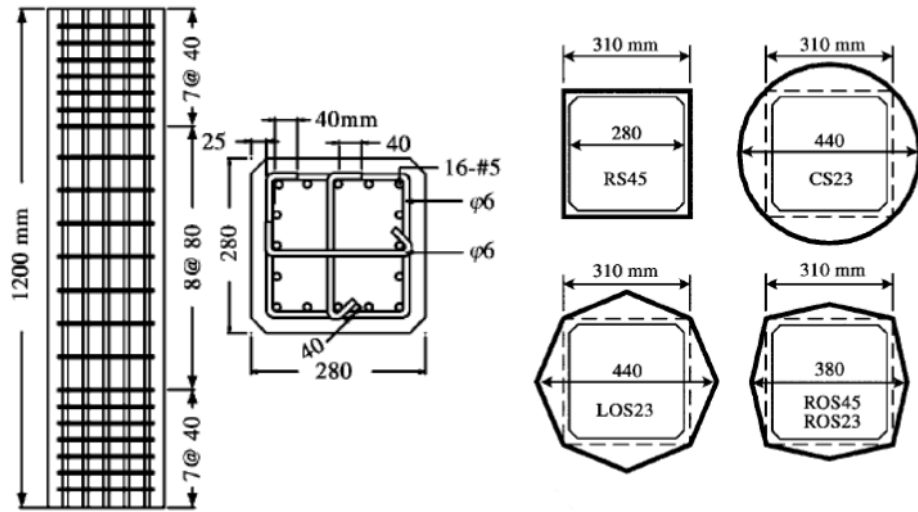


Figure 2.20 Detail of test specimen and steel jacketing schemes [27]

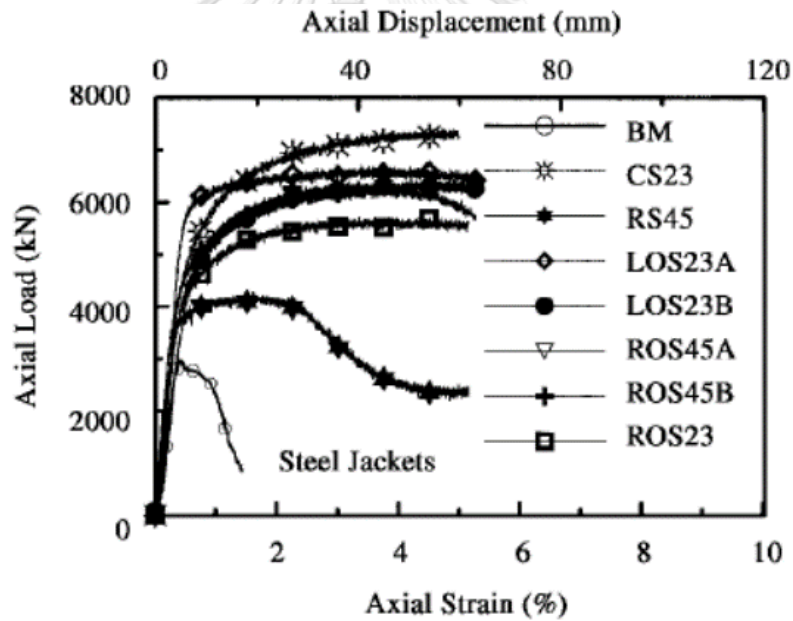


Figure 2.21 Axial force and strain relationship of steel-jacketed columns [27]

As an extension study of previous research of Lin, et [28] investigated the behavior of lap splice deficient column subjected to cyclic lateral loads. One column is as built column, and the other two specimens were retrofitted by steel jackets of the elliptical and octagonal cross-section. The test result reported that the octagonal steel jackets performed a little better than the elliptical steel jackets in terms of energy

dissipation and lateral capacity. As the author expected, the as-built column showed brittle failure, while the retrofitted specimens exhibited ductile performance with the low cycle fatigue failure of longitudinal reinforcement. Figure 2.22 shows the test setup, jacket details and later load deformation of the specimens

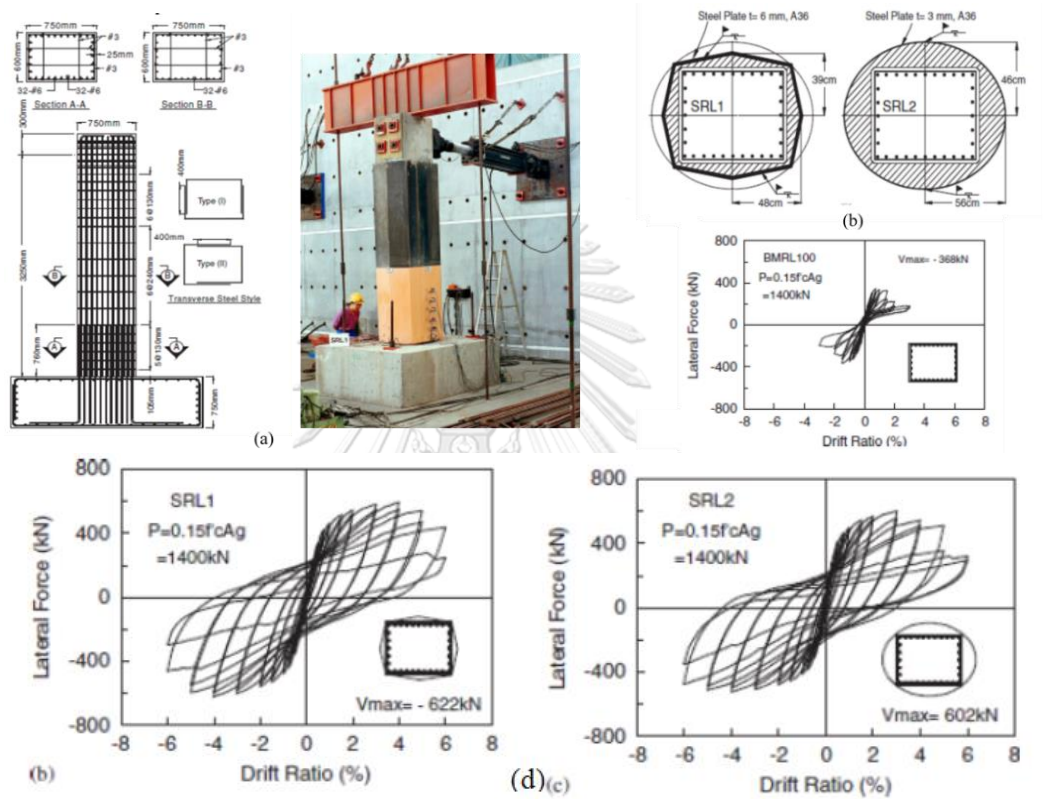


Figure 2.22 (a) Specimen detail and test set up (b) Jacket details

(c) lateral load-deformation of as built specimen

(d) Lateral load deformation of retrofitted specimens [28]

The author concluded that the elliptical or octagonal steel jacket could significantly enhance the seismic performance of the rectangular RC bridge columns. Octagonal steel jackets could be cost-effective and space-saving. Octagonal steel jackets have a smaller cross-section area requirement while slightly improving strength and energy dissipation performance over the elliptical steel jacketing scheme.

As a state of the art new steel jacketing technique, Choi, et [29] proposed a technique wherein steel jackets are installed using the external pressure without the application of grout. Four test columns were subjected to constant axial load and the lateral loading; two of them are un-jacketed columns such as one was with lap splice, and another one was with continuous reinforcement. Another two of them are confined by steel jackets with external pressure; one is a single layer jacket and the other is the double layer jacket. The proposed steel jacketing methods increased the ductility of the lap splices RC columns. Jacketing procedures and cross-section of the column are shown in Figure 2.23. The load displacement response of the column is shown in Figure 2.24.

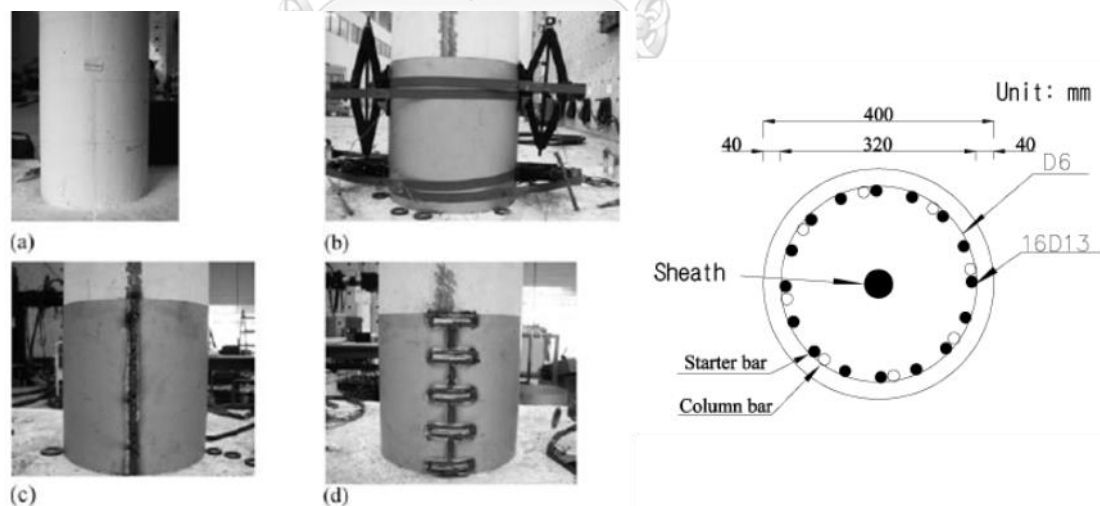


Figure 2.23 Jacketing procedures and cross-section of the column (a) As built column (b) Apply external pressure on steel jacket (c) Weld overlap line and (d) Weld lateral strip bands [29]

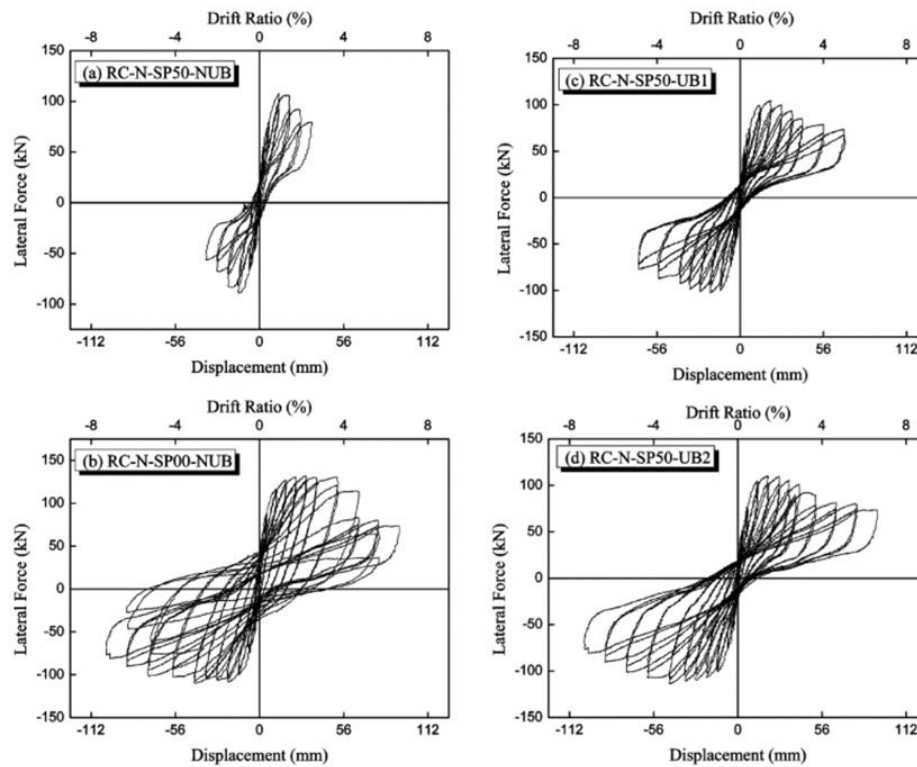


Figure 2.24 Load displacement response of the columns [29]

The author concluded that the new steel jackets enhanced the displacement ductility and energy dissipation capacity of the RC columns with lap splice. The jacket did not increase the flexural strength; this seemed to be from the imperfect installation of the jackets with not enough external pressure. The effective stiffness of the columns did not increase because the jackets did not induce the composite behavior between the jackets and the concrete. However, it was beneficial because it does not disturb the original stiffness of the column. The newly proposed steel-jacketing method can be used to easily install steel jackets at any location (bottom, middle, top). The performance of the double-layered jacket was better than the single-layered jacket.

Ghobarah, et [30] Using corrugated steel jackets, an experimental investigation to provide the confining pressure by passive restraint in the hinge region to the columns designed during the 1960s. The corrugated steel jacket was found to be effective in the rehabilitation of the selected existing structures. Three specimens were tested, but the first specimen and second specimen were detailed to represent the existing reinforced

concrete frame. The specimen S2 was rehabilitated using the corrugated steel jacket around the column to enhance its seismic behavior. Detail of reinforcement of specimen S1 and S2 and rehabilitation system is shown in Figure 2.25

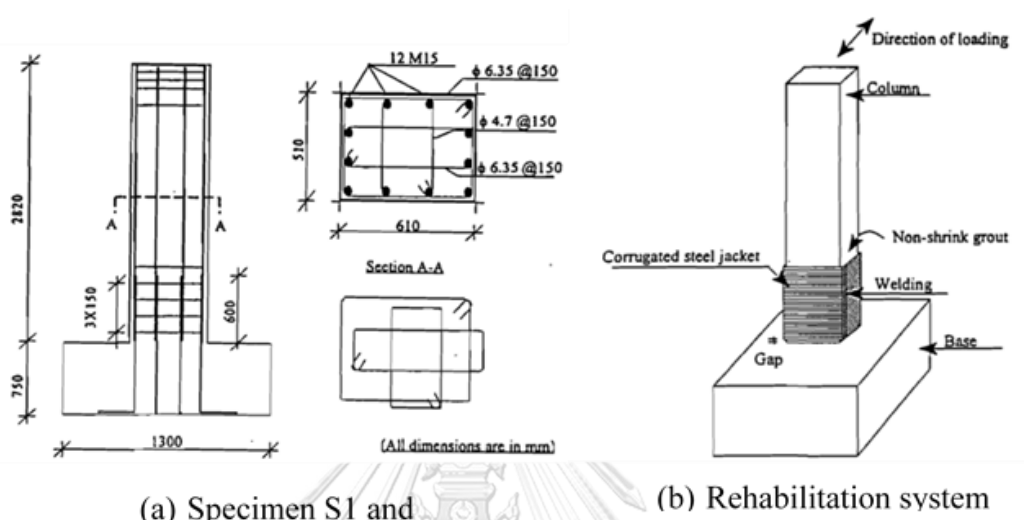


Figure 2.25 Detail of reinforcement of specimens [30]

The results of the tests showed that a corrugated steel jacket rehabilitation system was beneficial in inhibiting the bond-slip failure of lap splices and restraining the buckling of longitudinal steel. Therefore, this method was preferred for lap splice columns. Specimen S2 with corrugated steel jacket improved energy dissipation and slower stiffness degradation. Nevertheless, the jacket dimensions should allow the use of non-shrink ground of a thickness not less than 25 mm for ease of grout pouring. In addition, a 25 to 50 mm gap between the column base and the column jacket was proposed to avoid the unnecessary flexural strength degradation, which may adversely cause excessive moment demands on the foundation. The load displacement relationship of the two specimens is shown in Figure 2.26

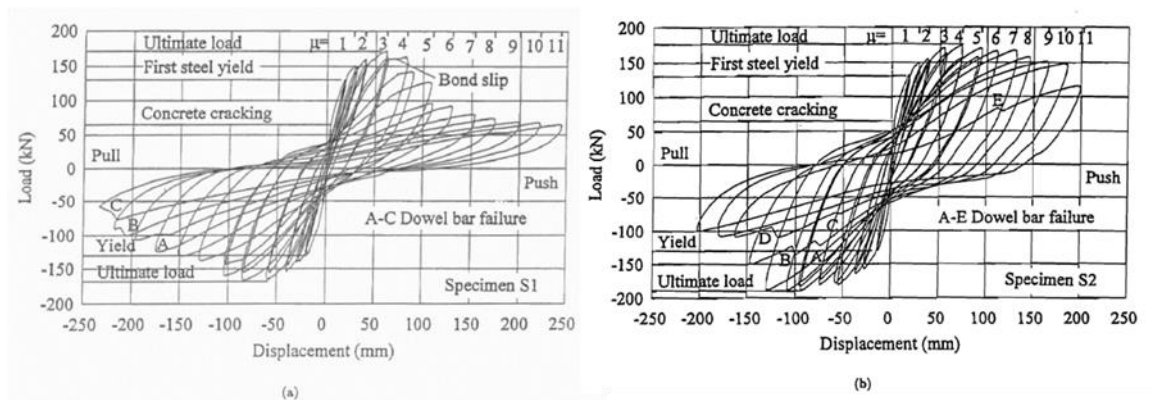


Figure 2.26 Load displacement relationship of two specimens [30]

Aboutaha, et [13] tested rectangular steel jackets on 11 non-ductile reinforced concrete frame columns with inadequate shear strength for seismic retrofit. Different types of steel jackets were tested, including rectangular solid steel jackets and partial steel jackets. Cyclic lateral forces were applied to the half-scale column. The column was cantilevered and framed into a fixed end large footing. For retrofitting of columns with inadequate shear strength, four columns were tested as basic retrofitted specimens. The remaining seven columns were tested after being strengthened with steel jackets. Eight columns were loaded in a weak direction, and three columns were loaded in a strong direction. Details of steel jackets are shown in Figure 2.27 Basic unretrofitted columns and retrofitted column is shown in Figure 2.28. The envelopes of the cyclic response of test columns are shown in Figure 2.29.

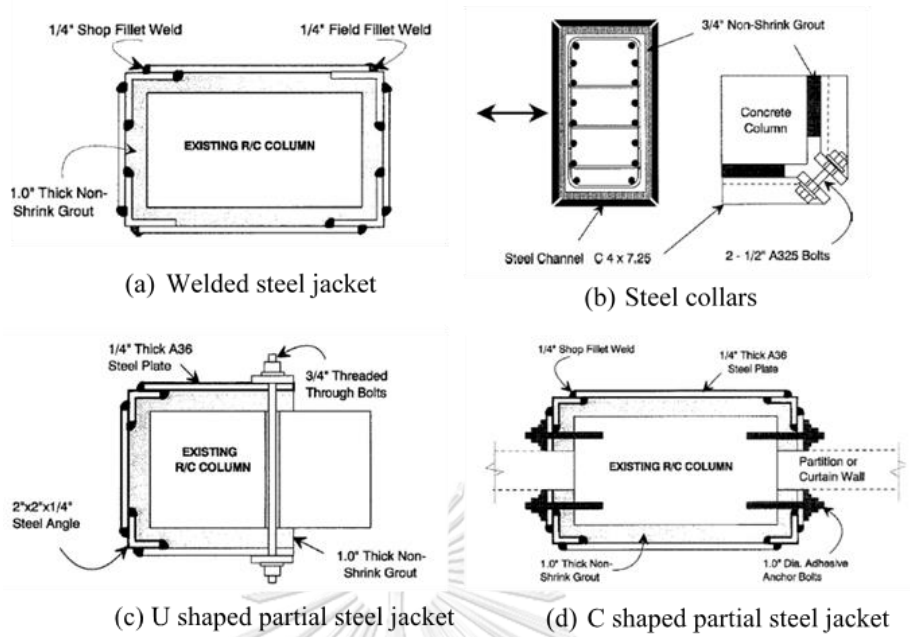


Figure 2.27 Details of steel jacket [13]

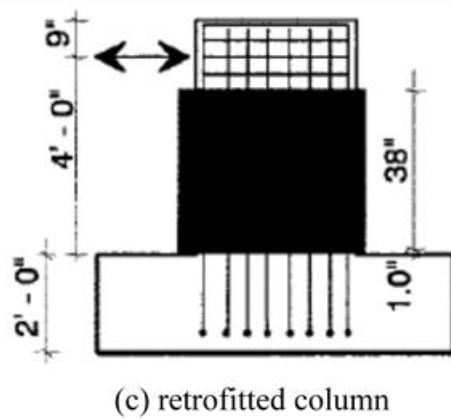
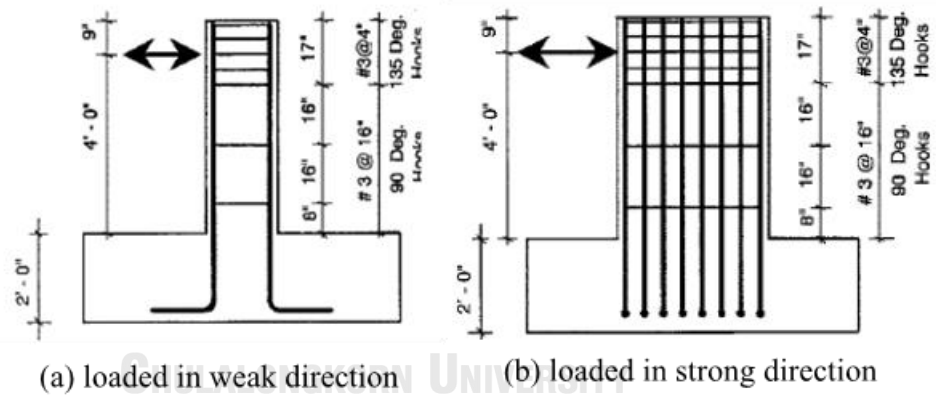


Figure 2.28 Unretrofitted column and retrofitted column [13]

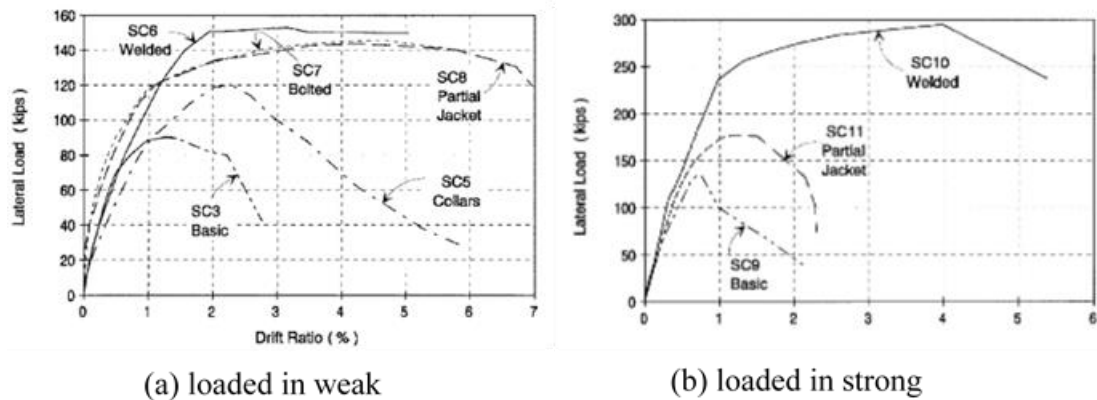


Figure 2.29 Envelopes of cyclic response of test columns [13]

According to the test results, the author concluded that a thin rectangular steel jacket could be highly effective at retrofitting reinforced concrete columns with inadequate shear strength. The steel jackets were effective at improving flexural yield capacity, improving ductility, and having a higher energy dissipation. Despite large lateral displacements, the steel jackets had low maximum strains due to the confinement preventing major shear cracks from opening. Yielding in the steel jacket may reduce stiffness and strength with more crack openings; thus, jacket yielding should be prevented for better performance. Welded or bolted connections at the jacket corners adequately developed the forces in the ties.

จุฬาลงกรณ์มหาวิทยาลัย  
CHULALONGKORN UNIVERSITY

#### 2.4.2 Angle and batten jacketing methods

To avoid the buckling of the steel plate and the increasing of the initial stiffness, Nagaprasad, et [31] investigated the steel caging technique which consisted of steel angles at the corners of RC columns and steel battens along the height of the columns which was the theoretical model of Masri and Goel [32]. The moment capacity of a strengthened RC column was taken as a sum total of moment capacities of the confined RC column section and steel angle sections of the steel cage. That theoretical concept was shown in Figure 2.30. The compressive strength of the confined concrete with steel cage depended on the spacing and size of the battens and number of battens. Wider



battens were placed in the expected plastic hinge region of the steel cage. The method appeared effective in increasing concrete confinement and reducing the likelihood of local buckling of steel angles. Three test specimens were investigated under a constant axial compressive load and gradually increased cyclic lateral displacements. Two specimens were strengthened using longitudinal steel angles and welded transverse battens. Three specimens were designed as RCO, RCS1, and RCS2.

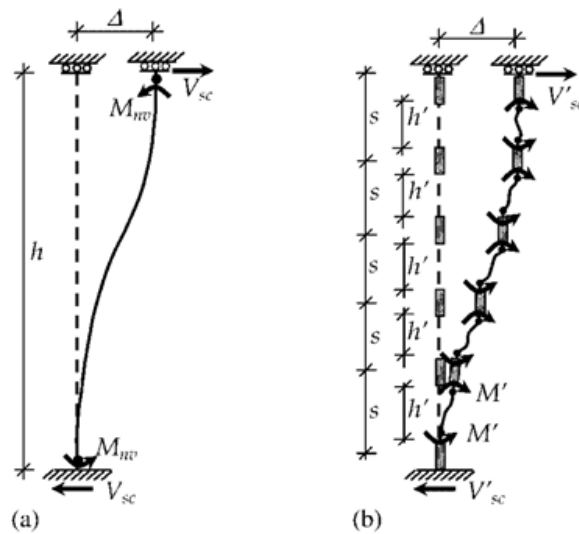


Figure 2.30 Theoretical design mode of steel cages

(a) original model (b) refined model [32]

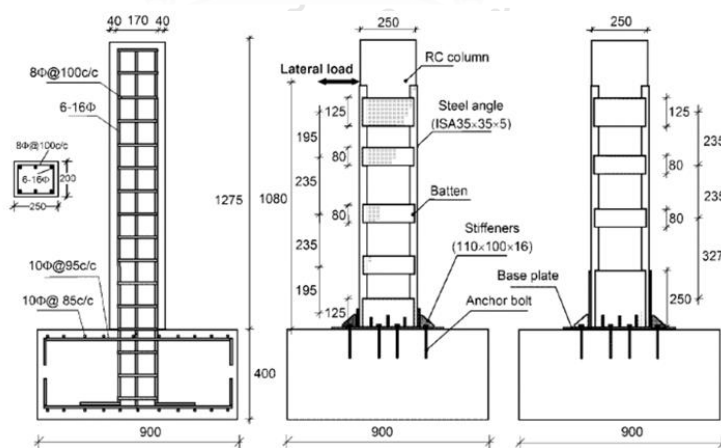


Figure 2.31 Detail of test specimens [31]

This investigation found that detailing the end batten of the steel cages located in the potential plastic hinge region of RC columns plays an important role in improving its overall behavior under lateral loads. The increase in width of end battens of steel cage significantly enhanced the plastic rotational capacity and its resistance to lateral loads; however, it had a minor effect on overall energy dissipation potential. It was concluded that the correct choice of width of end battens depends mostly on the target moment and plastic rotation capacity of the strengthening column. In addition, this method requires an intermediate level of skilled labors since it demands the drilling of holes in the foundation. Damage state and the hysteretic response of the test columns are shown in Figure 2.32. Comparison of energy dissipation capacity is shown in Figure 2.33

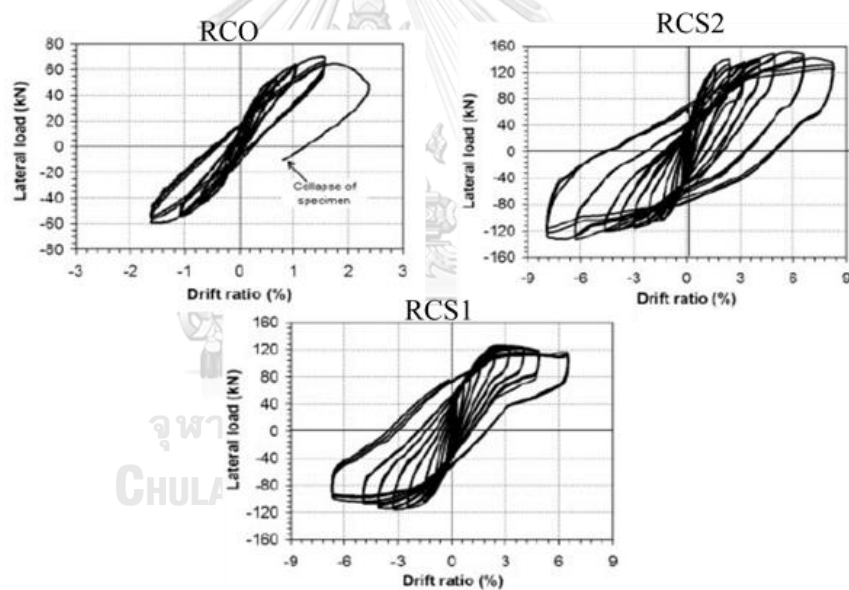


Figure 2.32 Hysteresis response of the tested specimens [31]

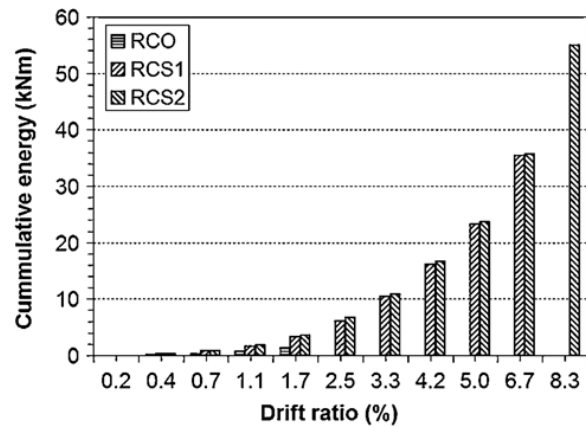


Figure 2.33 Energy dissipation capacity of the tested specimens [31]

Unlike the Nagaprasad, et [31], three variables were considered, such as the shape of strengthening system, size and number of batten plates to study the behavior of strengthened reinforced concrete column by the Belal and Mohamed [33]. Seven specimens; two un-strengthened columns and five strengthened ones with a different steel jacketing configuration, such as the angle with battens, a channel with battens and plates only on four sides. An axial load of 5000 kN was applied to all the tested specimens. Specimen dimension and steel jacket configuration are shown in Figure 2.34.

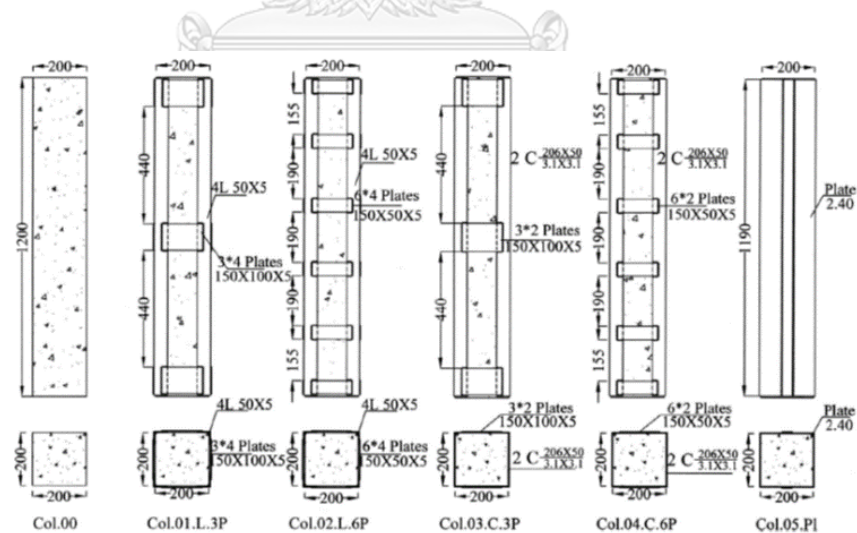


Figure 2.34 Specimen dimension and steel jacket configuration [33]

The beforementioned studies have found that the size of batten had a significant effect on the failure load for specimens strengthened with angles, whereas the number of battens was more effective for specimens strengthened with C-channels. In addition, based on the test results, the author concluded that steel jacketing techniques for strengthening RC columns increased the column capacity to a minimum of 20%. The load displacement relationships are shown for each specimen during testing in Figure 2.35.

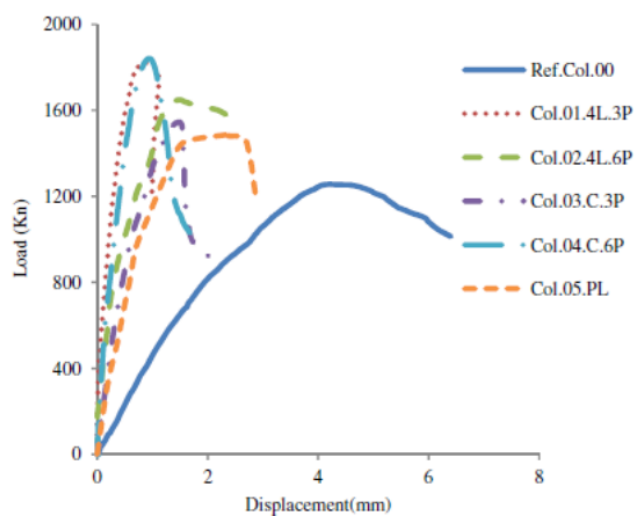


Figure 2.35 Load displacement relationship for all specimens [33]

Different strengthening methods, including angles, channels, and plates only on four sides of columns, have a significant impact on the failure load of columns. The effectiveness of specimens using angles or channels is insignificant. On the other hand, the specimen strengthened with angles or channel sections with battens recorded a higher failure load than that strengthened with plates only. Steel plates had a significantly less capacity due to the thinness of the plates. C sections, with battens or plates only in strengthening concrete columns, need cautions due to buckling consideration of their thin thickness. The simulation results of strengthened columns using the ANSYS program were much closed those measured during experimental testing.

In the situation where it was not feasible to connect the vertical angles to the roof of slabs and beams, steel heads were placed at the ends of the specimens to get the indirectly loaded case. This kind of strengthening technique was investigated by Tarabia and Albakry [34]. Ten square columns were prepared with two different cube strength. The test columns were divided into two groups. The reinforcement detail of the concrete column specimens is shown in Figure 2.36.

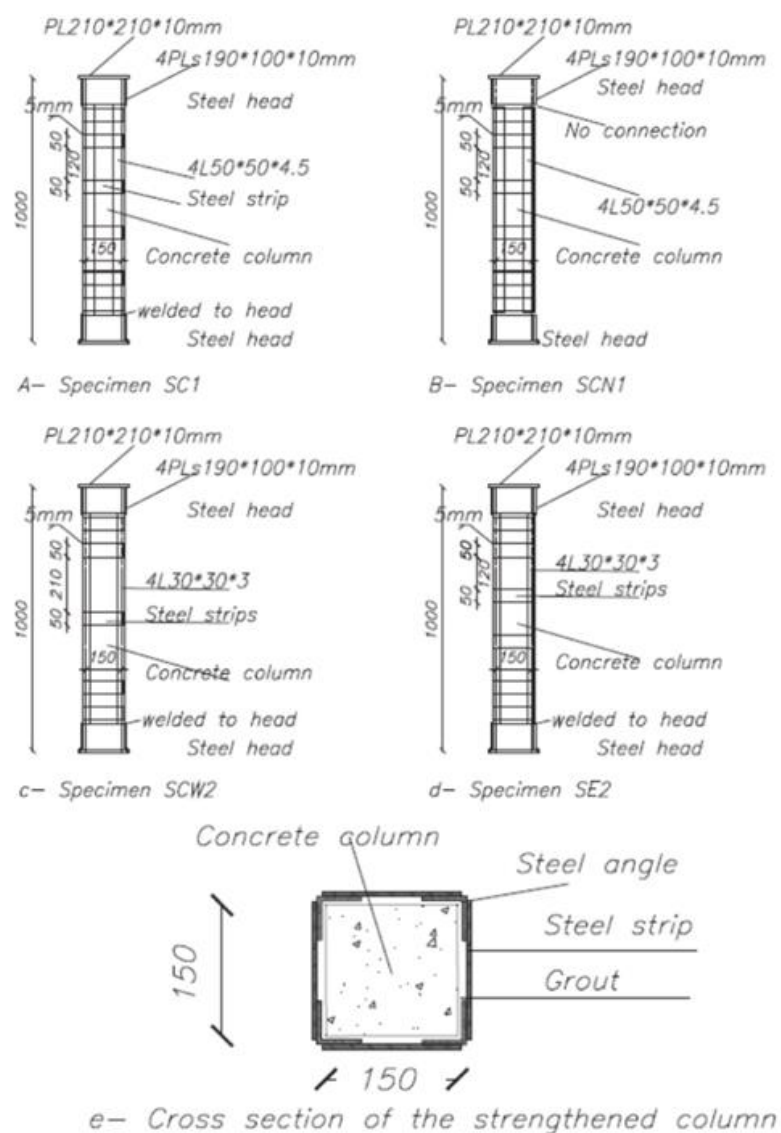


Figure 2.36 Detail of some strengthened specimens [34]

According to the test results, the initial stiffness of the strengthened specimens was higher than that of the reference column of the same group. Generally, all strengthened columns had higher maximum axial shortening than those of the reference columns without axial steel cages. Axial load and axial shortening of Group 1 and Group 2 are shown in Figure 2.37

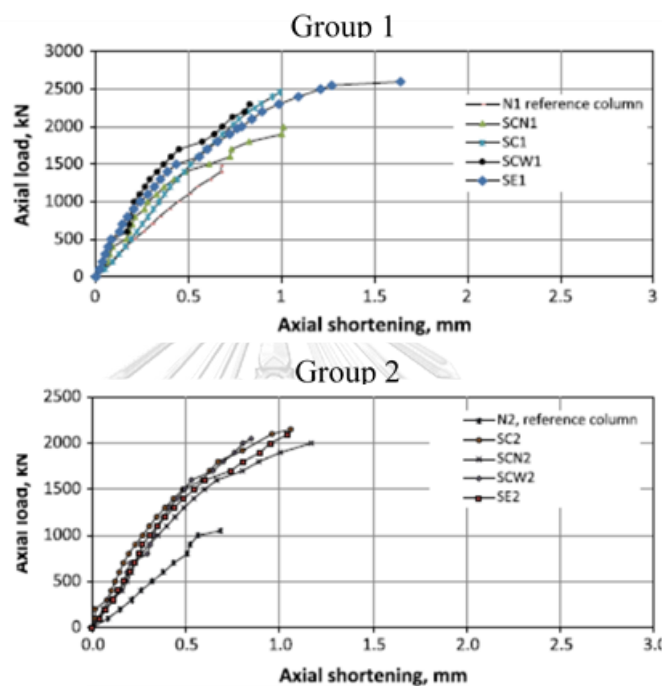


Figure 2.37 Axial load and axial shortening of Group 1 and Group 2 [34]

The author also occurred some facts from the tests, the failure in most of the unstrengthened was due to the buckling of the steel angle after their yielding followed by the crushing of the concrete column. No yielding of the horizontal strip was observed because of the relatively large size of the horizontal strips with respect to the vertical angles. Directly connected vertical angles on the head of the columns showed that all angles yielded before the failure of the strengthening column. On the other hand, in the case of indirectly loaded vertical angles to the head of the columns, the angel did not reach yielding.

For practical reasons, steel angles are arranged, leaving a gap with end beams or slabs in several cases. Despite this disconnection, the angles are still able to carry a portion of the load because of the frictional interaction forces developed long the column angles contact surface. Campione [35] Studied the friction effects in structural behavior of connected angle and battens jacketed RC columns subjected to axial compressive tests and eccentric compressive tests. A total of sixteen specimens was tested. The design detail of the specimen with and without steel jacketing is shown in Figure 2.38. The test set up for a compressive test and the eccentric compressive test is shown in Figure 2.39. Displacement controlled maximum loading capacity of 4,000 kN was applied.

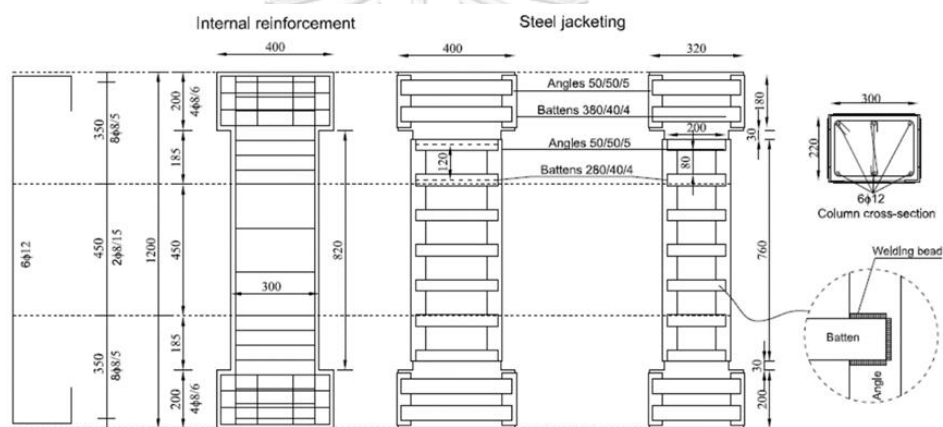


Figure 2.38 Design detail of specimens with and without steel jacketing [35]

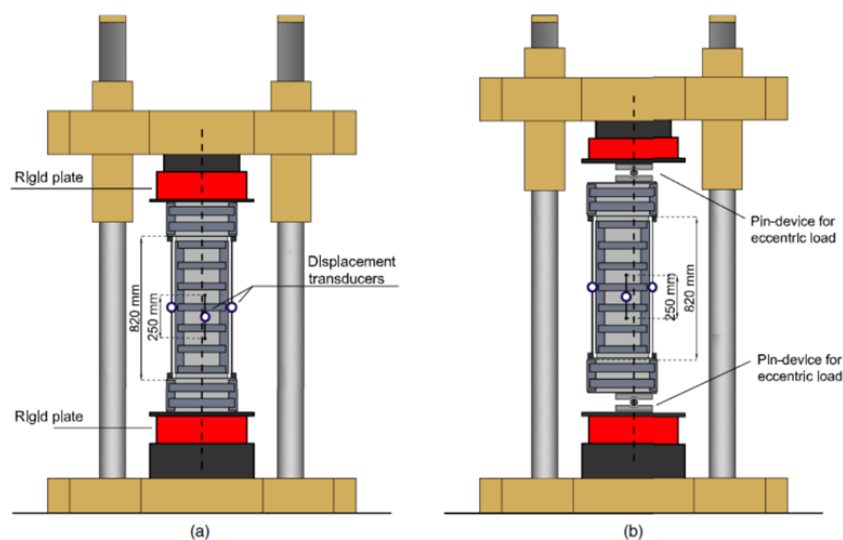


Figure 2.39 Test set up (a) axial compressive test (b) eccentric compressive test [35]

From the results obtained, the author concluded that a significant increase of bearing and deformation capacity was observed for steel jackets in axial compressive tests. Also, for the eccentric compressive tests, a large load increased in steel jacketing columns, even in the case of low strength concrete specimens. For both axial and eccentric compressive tests on the unjacketed specimens, the damage has occurred in the central zones of the columns as well as the large width cracks. Cover spalling and buckling of longitudinal reinforcement also happened. For the jacketed specimens, the damage was less evident and spread out over the entire length of the column. Concrete spalling and buckling of longitudinal reinforcement were escaped by the confinement action. For compressive axial tests, the collapse of the specimens occurred because of the failure of the welding at considerable deformations. The results of the axial compressive test for unretrofitted and retrofitted columns are shown in Figure 2.40. The results of the eccentric compressive test for unretrofitted and retrofitted columns are shown in Figure 2.41.

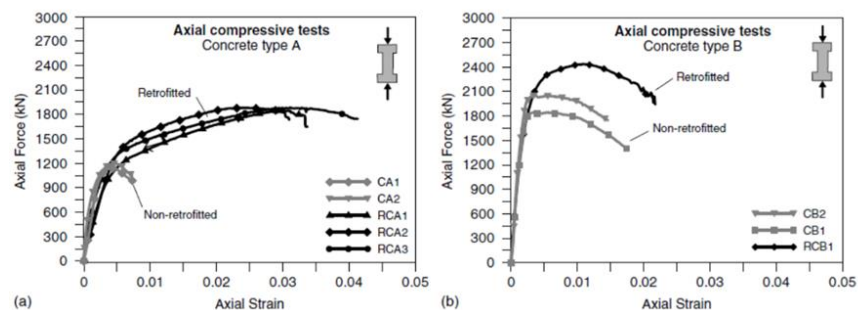


Figure 2.40 Result of axial compressive test for retrofitted and unretrofitted specimens [35]

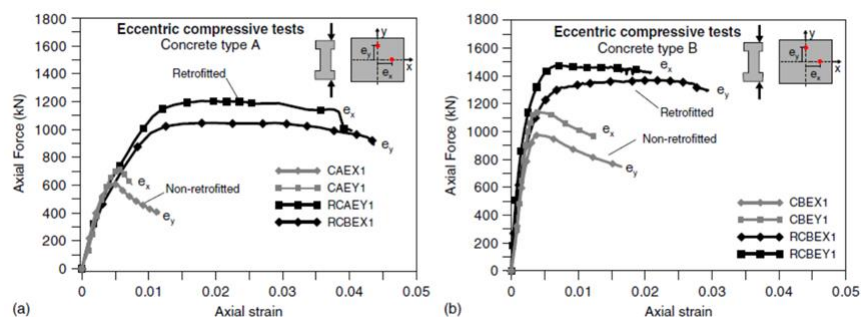


Figure 2.41 Result of eccentric compressive test for retrofitted and unretrofitted specimens [35]



Similar to the Campione [35], the increase in axial capacity and enhancement in ductility of the column between unstrengthened and strengthened specimens under displacement controlled eccentric loading was studied by Montuori and Piluso [36]. Experimental tests had been performed on 13 specimens. A load transmission system made of steel plates and reinforcing and stiffening had been adopted to apply different eccentricities that had been hinged the specimen ends of the testing machine. Strengthened and unstrengthened specimen model is shown in Figure 2.42.

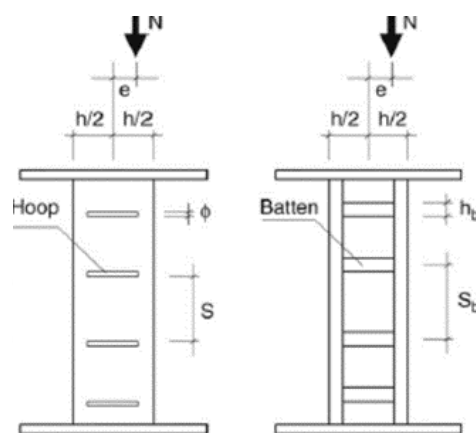


Figure 2.42 Strengthened and unstrengthened specimens models [36]

The results of the test indicated that the strengthened specimens had load capacity, nearly twice that of the unstrengthened specimen, and with higher buckling resistance. Peak axial load with less displacement is exhibited for angles resisting load in both compression and tension, while the highest ductility is obtained for a specimen with angles as confinement elements only. This method provides effective lateral restraint to columns thus preventing buckling of bars. Axial load and load displacement curves resulting from experimental tests are shown in Figure 2.43. The technique is most suitable for a corner column of a building with poor lateral confinement for longitudinal bars.

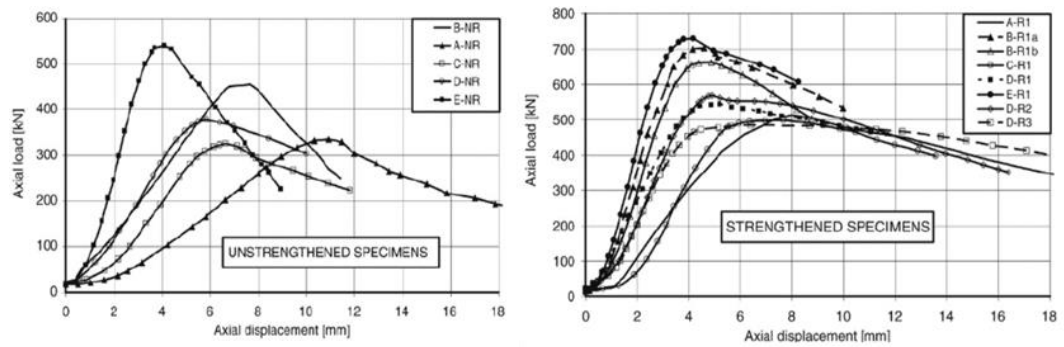


Figure 2.43 Axial load and displacement curves of the test specimens [36]

### 2.4.3 Steel collar jacketing methods

Hussain and Driver [37] Proposed a relatively simple scheme that confines the concrete, externally with hollow structural section (HSS) collars that possess a combination of significant flexural and axial stiffness. These collars do not only provide the benefits of efficient confinement but also inhibit spalling of the outer concrete shell and provide additional shear reinforcement. Typical collars made from HSS sections with bolted or welded corner connections, as shown in Figure 2.44. In the case of the collars with bolted corner connections, 25.4 mm diameter high strength threaded rods were used.

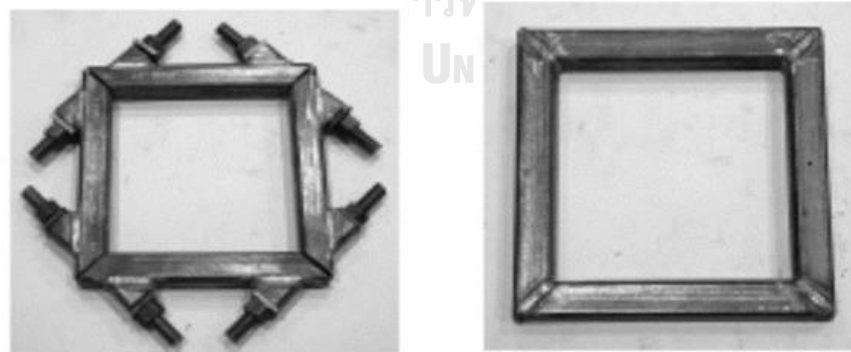


Figure 2.44 Bolted collar and welded collar [37]

In the case of the collar with a welded corner connection, a partial penetration single-V groove weld was deposited all around the corner joints and welded. A total of 11 columns was tested; two columns with conventional reinforcement were control columns, and the remainders had external steel collars. For those columns which had external steel collars, no tie reinforcement was provided in the test region to study the effect of external confinement. Column reinforcement details and typical test specimen with welded collars in the test region is shown in Figure 2.45.

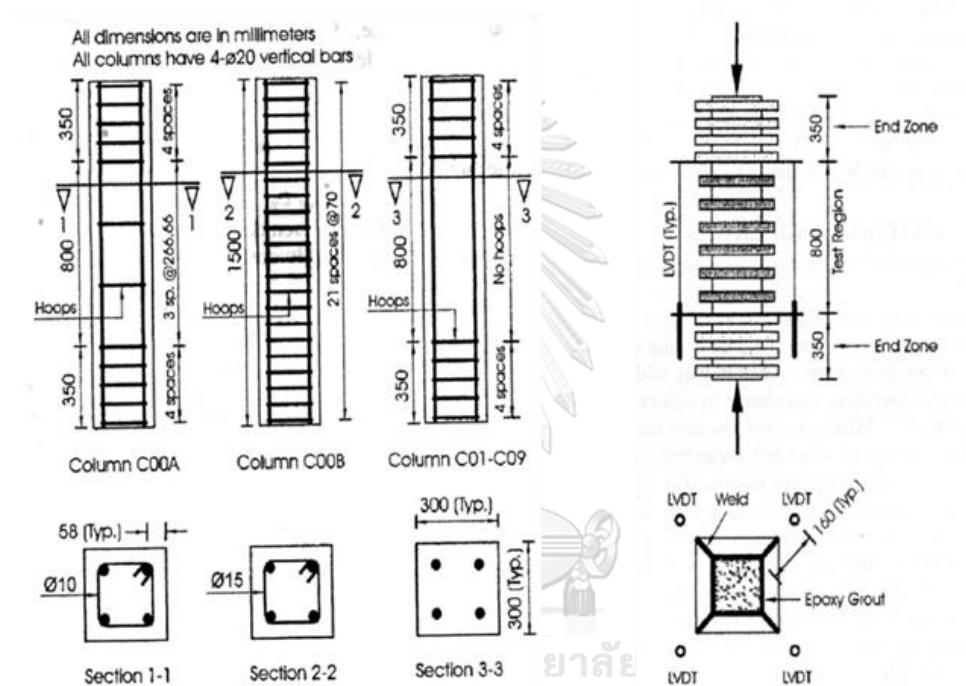


Figure 2.45 Column reinforcement details and typical test specimen [37]

As the author expected, column C00A showed the brittle failure because of the relatively wide spacing of the ties, and the degree of confinement was deficient, and the column behavior was unconfined concrete. Column C00B showed brittle failure because of the closely spaced hoops in the test region. Column C01, C02, C03, C04 with bolted collars showed ductile failure. The ductility of the column C04 was lower because of the large collar spacing. Column C05 was not failed completely, terminated prematurely and the failure strain was not known. Column C06, C07, C08 and C09 with welded collars exhibited brittle failure that had fractured at the corners weld in one or more of the

collars. Generally, the provision of HSS collars results in a considerable enhancement in strength as well as ductile. The effective core area of externally confined is larger than the conventional columns. However, the hollow structural section (HSS) collars were not cost-effective and it may not be easy to install the collars are heavyweight.

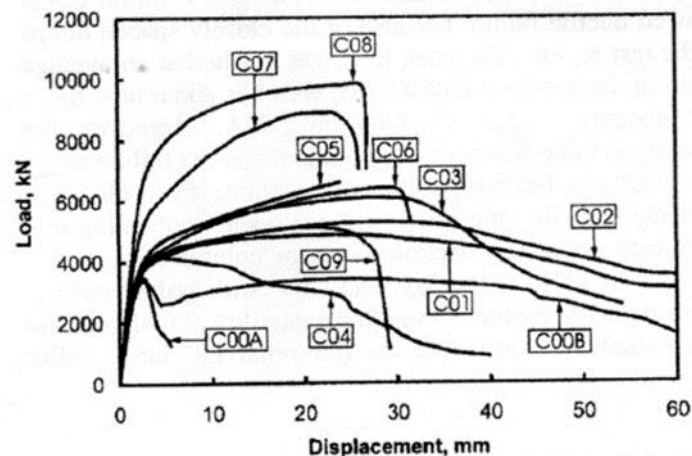


Figure 2.46 Load displacement relationship of the test columns [37]

Similar to Montuori and Piluso [37], Liu [38] investigated reinforced concrete columns strengthened by the steel collar jacketing method. The collars consisted of two L-shaped pieces cut from a 50 mm thick steel plate in a commercial fabrication shop using a conventional computer-controlled Oxy-gas cutting table which is cost effective in comparison to build-up a hollow structural section (HSS) collars. The purpose of this method is to confine the concrete with significant flexural and axial stiffness. Ten cantilever columns including two control columns and eight rehabilitated columns, tested under combined axial load and cyclic load through full-scale experiment. Specimen reinforcement details are shown in Figure 2.47. Fabrication and assembled view of the steel collar are shown in Figure 2.48.

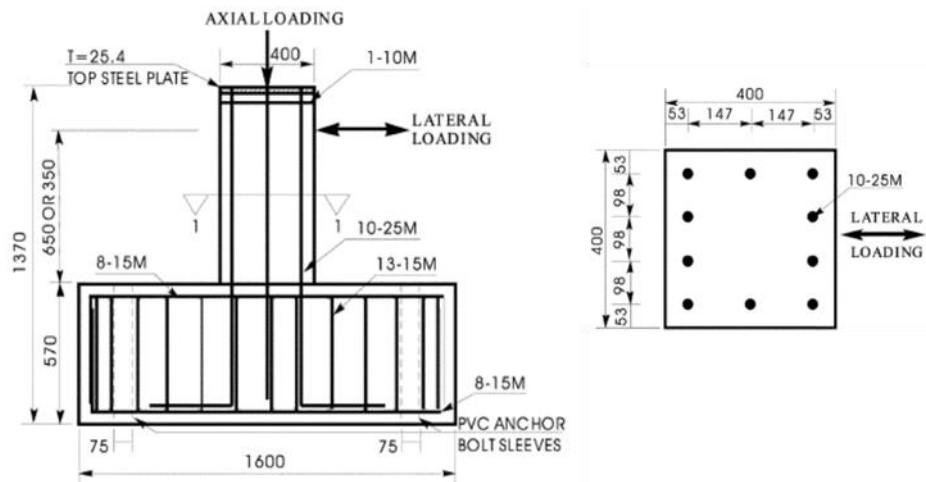


Figure 2.47 Specimen reinforcement details [38]

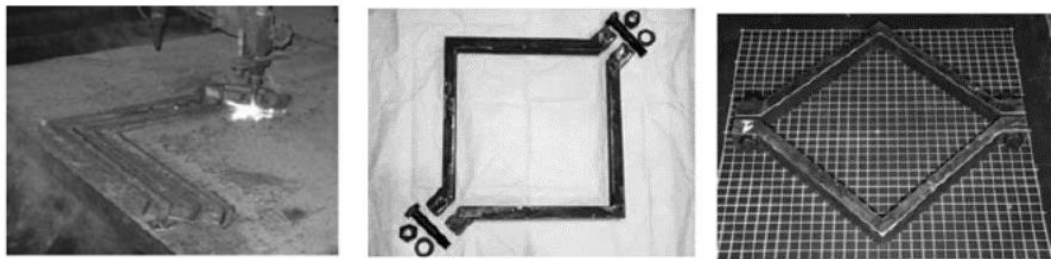


Figure 2.48 Fabrication and assembled view of the steel collars [38]

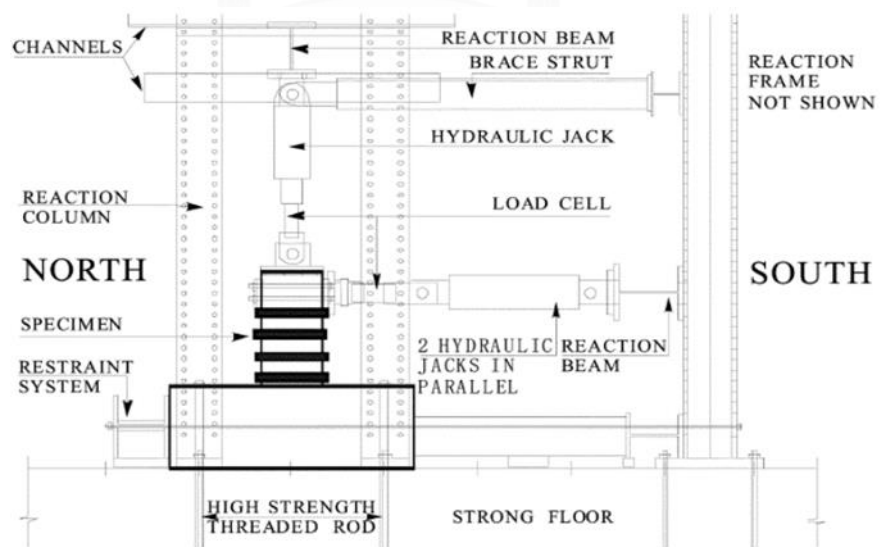


Figure 2.49 Test set up of typical retrofitted specimen [38]

Based on the test results, the author concluded that all columns exhibited flexural failure except the specimen without axial load. Generally, the experimental results showed excellent improvement in ductility, strength, and energy dissipation capacity of the columns due to the presence of the collars. With no slippage of the collars was observed except plastically outward to some degree. No concrete spalling occurred directly under the collars. In general, the steel collars allowed a more general degradation of strength after the peak load, as compared to the control columns without collars. The experiments showed that the collar columns had stable hysteresis behavior. Force displacement envelopes for retrofitted test specimens are shown in Figure 2.50.

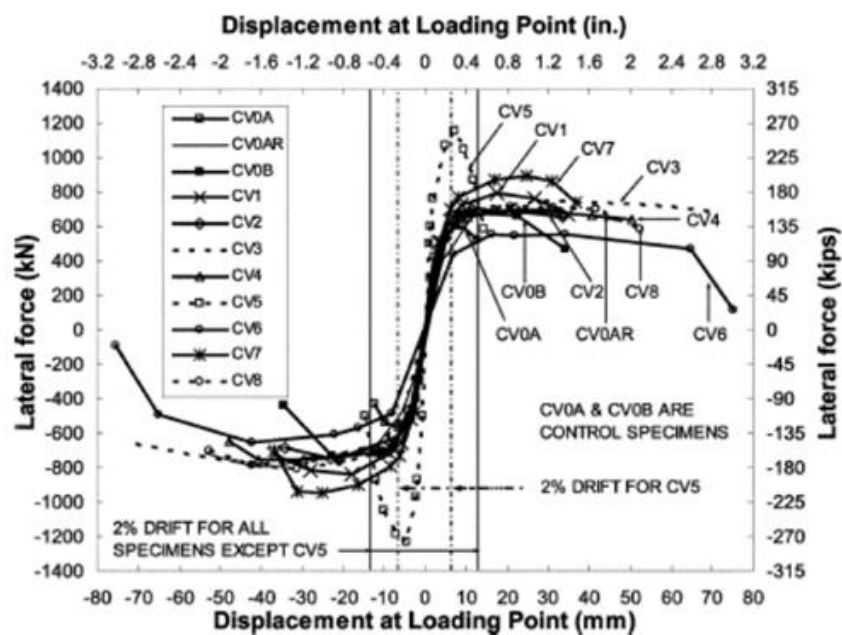


Figure 2.50 Force displacement envelopes for retrofitted test specimens [38]

To avoid the steel plate jacketing buckling in the plastic hinge area, Xiao and Wu [39] proposed the rectified steel jacket technique, which was adding stiffeners in the plastic zones to the steel plate jacketing columns to show the improvement of the stiffeners under the seismic behavior of existing damaged columns. Five rectangular RC columns and a control specimen of 1/3 scale model were tested under constant axial load and cyclic loads. Detail of retrofitted specimens is shown in Figure 2.52

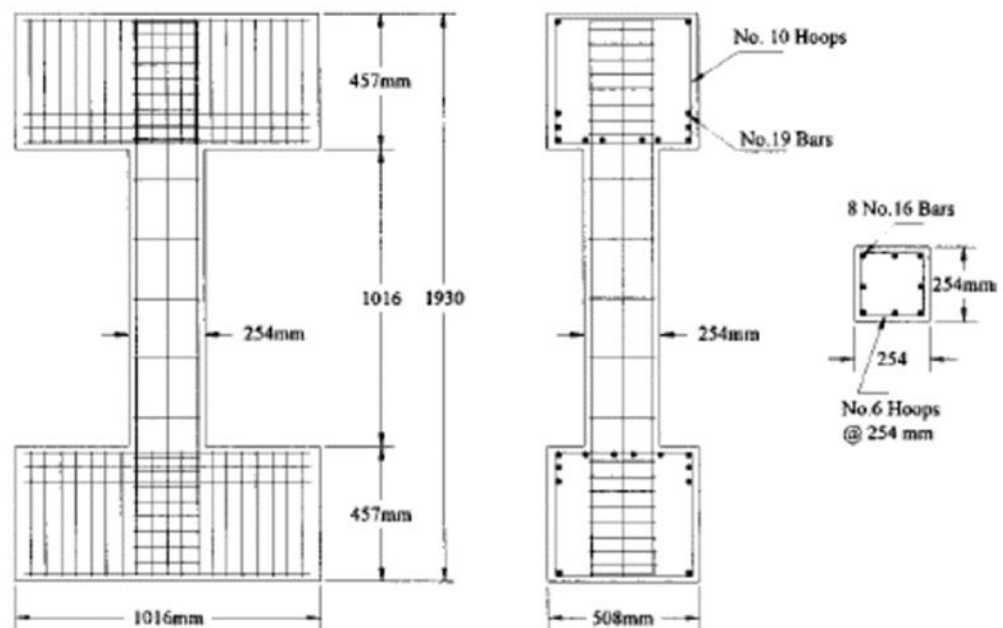


Figure 2.51 Detail of the column specimens [39]

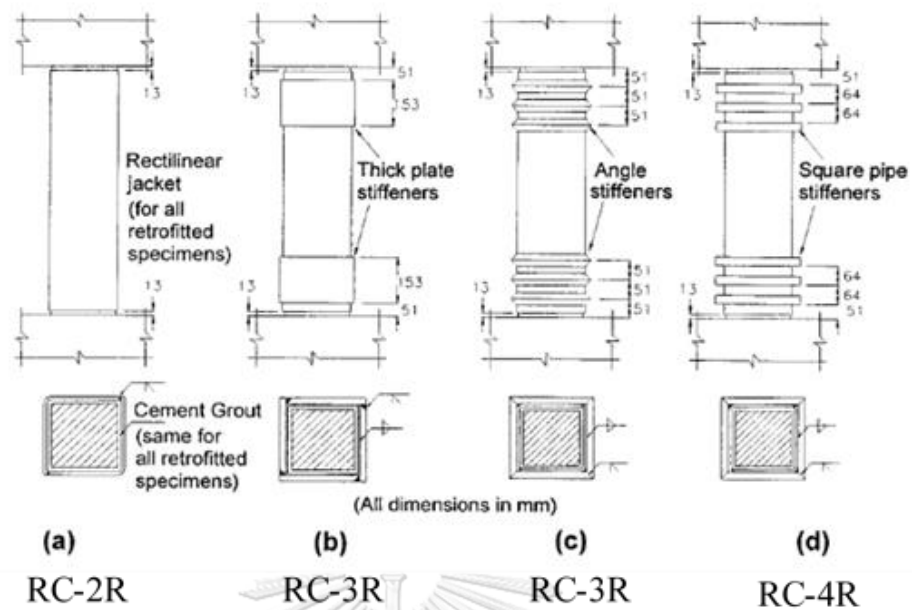


Figure 2.52 Detail of the retrofitted specimens [39]

#### 2.4.4 Summary

The steel collars jacketing methods were able to confine the concrete as confinement effectiveness and gave the excellent improvement in ductility, strength, and energy dissipation capacity of the columns. Due to the presence of the collars, no concrete spalling which was under the collars occurred. However, it can be cost-ineffective if the columns are retrofitted by HSS collars. HSS collars or bolted collars seem to be satisfactory for deficient short reinforced concrete columns.



## 2.5 Modeling strategies of RC columns

The analysis of reinforced concrete (RC) structures requires the accurate constitutive relationships of concrete and reinforcing steel, especially for the fiber elements approach where uniaxial constitutive relations of both constituent materials should be assigned to each element fiber. In the nonlinear analysis, which this research is based on, the nonlinear behavior of the material is needed. The analytical models of materials used in this study are comprised of unconfined concrete for the cover of the RC element, confined concrete for core concrete, and a longitudinal reinforcement model.

### 2.5.1 Material Constitutive Relationships

The analysis of reinforced concrete (RC) structures requires the accurate constitutive relationships of composite materials, reinforced concrete exhibits specific mechanical behaviors due to complex interactions between its concrete and reinforcing steel especially for the fiber elements approach where uniaxial constitutive relationships of both constituent materials should be assigned to each element fiber.

## 2.5.1.1 Unconfined concrete

Kent and Park [40] introduced the stress-strain relation of unconfined concrete, which possesses two separated parts: the first part is when  $\varepsilon_c \leq \varepsilon_0$ , and another is  $\varepsilon_c > \varepsilon_0$ .

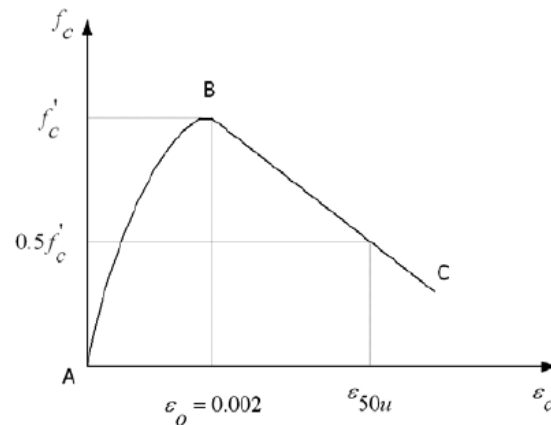


Figure 2.53 Stress-strain relation of unconfined concrete [40]

The stress starts increasing from 0 to reach the maximum stress of the concrete, which is  $f'_c$ . It is clear that at the maximum point of stress (point B), the strain is  $\varepsilon_0 = 0.002$ . After that, the stress begins to decrease assumingly linearly. Both parts were represented by the equations below:

$$f_c = f'_c \left[ \frac{2\varepsilon_c}{\varepsilon_0} - \left( \frac{\varepsilon_c}{\varepsilon_0} \right)^2 \right]$$

$$f_c = f'_c \left[ 1 - z(\varepsilon_c - \varepsilon_0) \right]$$

$$\text{where: } z = \frac{0.5}{\varepsilon_{50u} - 0.002} \text{ and } \varepsilon_{50u} = \frac{3 + 0.002f'_c}{f'_c - 1000}$$

Notation:  $\varepsilon_c$  : longitudinal compressive concrete strain

$\varepsilon_0$  : strain at maximum stress, assumingly 0.002

$f_c$  : longitudinal compressive concrete stress (psi)

$f'_c$  : maximum stress of cylinder specimen (psi)

$\varepsilon_{50u}$  : strain at 50% of maximum stress (obtained from material testing)

### 2.5.1.2 Confined concrete:

There are many researchers related to the model application of confined concrete. Some of the most popular ones are introduced next: Kent and Park [40] gave the stress-strain relation of confined concrete subjected to uniaxial loading.

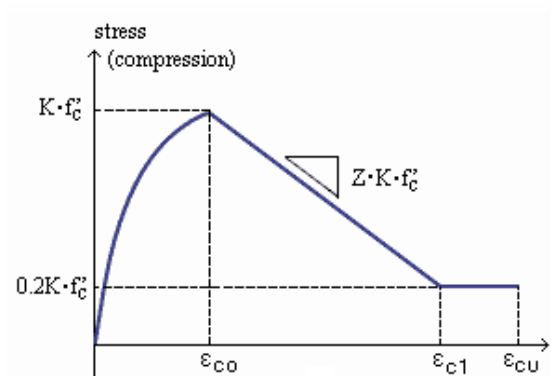


Figure 2.54: Stress-strain relation of confined concrete [40]

The proposed model consists of three different parts:

1. When  $0 \leq \varepsilon_c \leq \varepsilon_0$  the ascending part varies in a parabolic manner with the same equation of the unconfined concrete. The strain at maximum stress point is assumed to be  $\varepsilon_0 = 0.002$ .
2. When  $\varepsilon_0 < \varepsilon_c \leq \varepsilon_{20u}$  the falling part was assumed varying linearly from maximum stress  $f'_c$  to  $0.2f'_c$  where  $\varepsilon_{20u}$  is the strain at 20% of stress point (obtained by experimental result). However, the falling slope  $Z$  is changed and the function was proposed:

$$z = \frac{0.5}{\varepsilon_{50h} + \varepsilon_{50u} - 0.002}$$

where:  $\varepsilon_{50h}$ : additional strain due to the confinement  $\varepsilon_{50h} = \frac{3}{4} \rho'' \sqrt{\frac{b''}{s}}$

$\rho''$ : volumetric ratio (ratio of the volume of transverse reinforcement to the volume of the confined concrete core  $\rho'' = \frac{2(b''+d'')A_s''}{b''d''s}$

$b''$ : the shorter dimension of confined concrete core

$d''$ : the longer dimension of confined concrete core

$A_s''$ : cross-sectional area of the hoop bar

$s$ : center to center of the hoops

3. When  $\varepsilon_c > \varepsilon_{20u}$  this part was called the sustaining branch since it was assumed to be a constant value equal to 0.2 of the maximum stress of cylinder specimen.

The equation was proposed as followed:

$$f_c = 0.2f_c'$$

Mander, et al. [41] also proposed a material model for confined concrete in the form of stress-strain relation, which considered the transverse and longitudinal reinforcement for both rectangular and circular sections. The stress-strain relationship of confined and unconfined concrete under monotonic loading and the constitutional equations were proposed:

$$f_c = \frac{f_{cc}' x^r}{r-1+x^r}$$

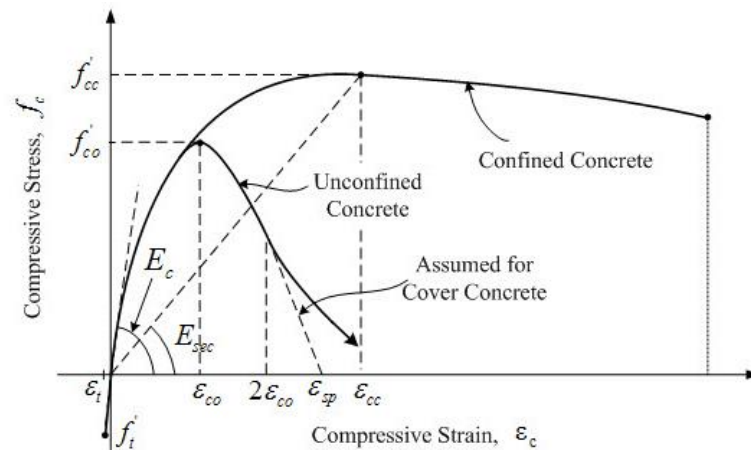


Figure 2.55: Stress-strain relation of confined and unconfined concrete under monotonic loading [41]

where:  $f_c$ : longitudinal compressive concrete stress

$$x = \frac{\varepsilon_c}{\varepsilon_{cc}} \text{ with } \varepsilon_{cc} = \varepsilon_{c0} \left[ 1 + 5 \left( \frac{f'_{cc}}{f'_{co}} - 1 \right) \right] \text{ and } \varepsilon_{c0} = 0.002$$

$f'_{co}$ : unconfined concrete compressive stress calculated by formula

$$f'_{cc} = f'_{co} \left( 2.254 \sqrt{1 + \frac{7.94 f'_l}{f'_{co}}} - 2 \frac{f'_l}{f'_{co}} - 1.254 \right)$$

$\varepsilon_c$ : longitudinal compressive concrete stress

$\varepsilon_{cc}$ : unconfined concrete compressive strain

$$r = \frac{E_c}{E_c - E_{sec}} \text{ with } E_{sec} = \frac{f'_{cc}}{\varepsilon_{cc}}$$

$E_c$ : tangent modulus of elasticity of the concrete  $E_c = 5000 \sqrt{f'_{co}}$

$f'_l$ : effective lateral confining pressure  $f'_l = f_l \cdot k_e$

$f_l$ : lateral confining pressure

$k_e$ : confinement effectiveness coefficient  $k_e = \frac{A_e}{A_{cc}}$

$A_{cc}$ : area of the confined concrete  $A_{cc} = A_c (1 - \rho_{cc})$

$\rho_{cc}$ : the ratio of the area of longitudinal reinforcement to the area of a section

$A_e$ : area of an effective confined concrete core at midway between the levels of the transverse reinforcement

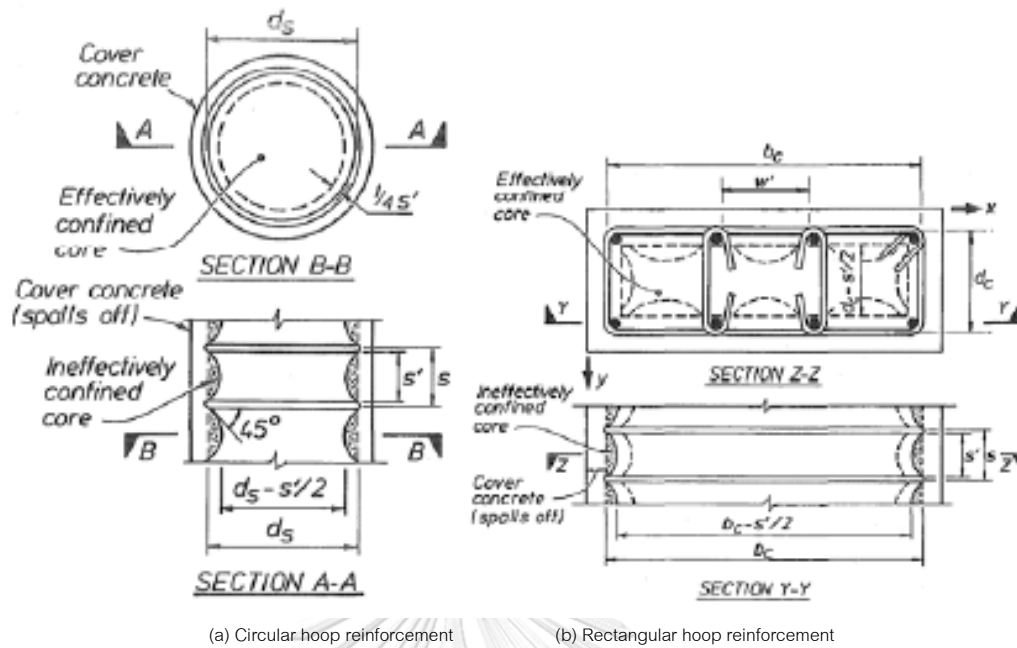


Figure 2.56: Effectively confined to the concrete core [41]

For the circular section, the area of core concrete is defined as  $A_c = \frac{\pi}{4} d_s^2$ .

The effective area of the confined concrete core area was proposed:

$$A_e = \frac{\pi}{4} \left( d_s - \frac{s'}{2} \right)^2 = \frac{\pi}{4} d_s^2 \left( 1 - \frac{s'}{2d_s} \right)^2$$

$$\text{Thus, } k_e = \frac{\left( 1 - \frac{s'}{2d_s} \right)^2}{1 - \rho_{cc}}$$

For the rectangular section, the core concrete section area is  $A_c = b_c d_c$ . The effective confined concrete area of a regular hoop with the initial tangent slope of  $45^\circ$  was proposed in the equation below:

$$A_e = \left( b_c d_c - \sum_{i=1}^n \frac{(w_i')^2}{6} \right) \left( 1 - \frac{s'}{2b_c} \right) \left( 1 - \frac{s'}{2d_c} \right)$$

$$\text{Thus, } k_e = \frac{\left( 1 - \sum_{i=1}^n \frac{(w_i')^2}{6b_c d_c} \right) \left( 1 - \frac{s'}{2b_c} \right) \left( 1 - \frac{s'}{2d_c} \right)}{1 - \rho_{cc}}$$

Hoshikuma, et [42] Introduced the relationship between stress and strain of the confined concrete obtained from the analysis of experimental results for low volumetric ratio ranging from 0.3% to 0.5%. Several parameters including sectional shape, volumetric ratio, hoop spacing, hook configuration and cross tie, were varied and all specimens were tested under uniaxial loading. This model agreed well with the experimental results and it satisfied with boundary conditions at points A, B, and C.

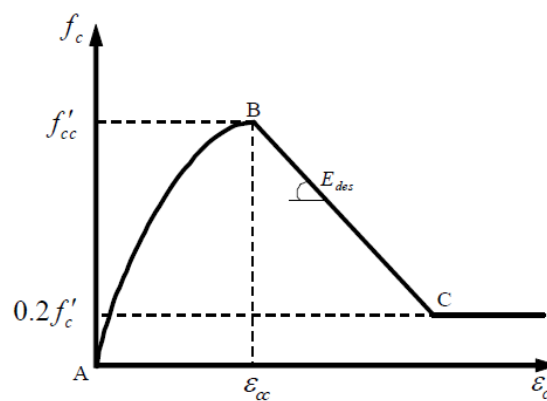


Figure 2.57: Stress-strain model of confined concrete [42]

This model is similar to that of Kent and Park [40] that it consists of three parts: the ascending part, the falling part, and the sustain part. All three equations were proposed respectively as below:

$$f_c = E_c \varepsilon_c \left[ 1 - \frac{1}{n} \left( \frac{\varepsilon_c}{\varepsilon_{cc}} \right)^{n-1} \right]$$

$$f_c = f_{cc} + E_{det} (\varepsilon_c - \varepsilon_{cc})$$

$$f_c = 0.2f'_c$$

Where:

$$n = \frac{E_c \varepsilon_{cc}}{E_c \varepsilon_{cc} - f_{cc}}$$

$\varepsilon_{cu}$ : ultimate strain with the proposed equation  $\varepsilon_{cu} = \varepsilon_{cc} + \frac{f_{cc}}{2E_{det}}$

$f_{cc}$ : maximum longitudinal compressive concrete stress,  $f_{cc} = f_{c0} + 3.8\alpha\rho_s f_{yh}$

$\varepsilon_{cc}$ : longitudinal compressive strain at maximum stress  $\varepsilon_{cc} = 0.002 + 0.033\beta \frac{\rho_s f_{yh}}{f_{co}}$

Where:

$$E_{\text{det}} : \text{deterioration rate with } E_{\text{det}} = 11.2 \frac{f_{co}^2}{\rho_s f_{yh}}$$

$E_c$  : initial stiffness

$f_{co}$  : unconfined concrete compressive stress

$\rho_s$  : volumetric ratio (ratio between the volume of transverse reinforcement and volume of the confined concrete core).

$f_{yh}$  : yield strength of the transverse reinforcement

$\alpha$  and  $\beta$  are modification factors depending on the confined sectional shape

For circular section  $\alpha = 1.0$  and  $\beta = 1.0$

For square section  $\alpha = 0.2$  and  $\beta = 0.4$

### 2.5.1.3 Longitudinal reinforcement model:

Gomes and Appleton [43] Presented the modified nonlinear stress-strain model of longitudinal reinforcement including buckling under cyclic loading from the model proposed by Menegotto and Pinto [44]. This modified model comprised of four different parts: elastic, yielding, hardening and Baushinger effect.

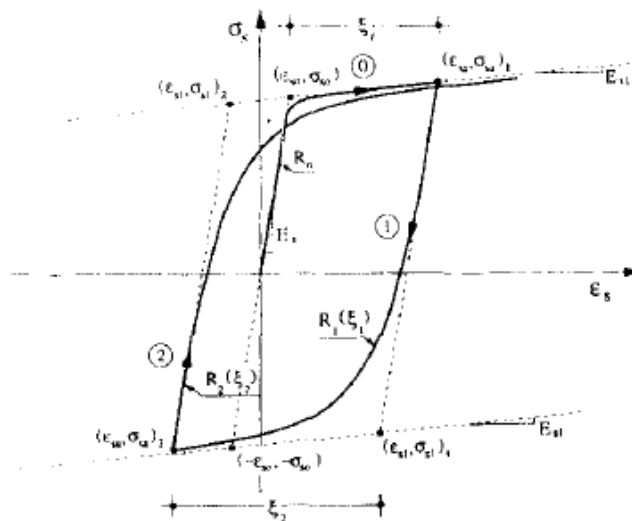


Figure 2.58: Stress-strain relation of reinforcement [43]



The equation of Menegotto and Pinto [44] was modified as follow:

$$\sigma_s^* = \beta \varepsilon_s^* + (1 - \beta) \frac{\varepsilon_s^*}{\left[1 + (\varepsilon_s^*)^R\right]^{1/R}}$$

Where:

$\sigma_s^*$ : normalized stress defined as followed:

$$\text{First load: } \sigma_s^* = \frac{\sigma_s}{\sigma_{s0}}$$

$$\text{First load reverse: } \sigma_s^* = \frac{\sigma_s - \sigma_{sa}}{2\sigma_{s0}}$$

$\varepsilon_s^*$ : normalized strain defined as followed:

$$\text{First load: } \varepsilon_s^* = \frac{\varepsilon_s}{\varepsilon_{s0}}$$

$$\text{First load reverse: } \varepsilon_s^* = \frac{\varepsilon_s - \varepsilon_{sa}}{2\varepsilon_{s0}}$$

$\sigma_{s0}, \varepsilon_{s0}$ : stress and strain respectively at the yield point of the bilinear envelope

$\sigma_{sa}, \varepsilon_{sa}$ : stress and strain respectively at the inversion point

$\beta$ : ratio between the hardening stiffness and the tangent modulus of elasticity at the origin  $\beta = \frac{E_{s1}}{E_s}$

R: constant taking into account the Baushinger effect  $R = R_0 - \frac{a_1 \xi}{a_2 + \xi}$

$R_0, a_1,$  and  $a_2$ : constants of materials equals to 20, 19, 0.3 respectively suggested by [43]

## 2.5.2 Structural elements

### 2.5.2.1 Fiber elements

Fiber elements play an important role in the nonlinear analysis. In OpenSees, the fiber elements are composed of fiber sections and then many sections are combined together to be a fiber element.

### 2.5.2.2 Fiber section

A fiber section has a general geometric configuration formed by sub-regions of simpler, regular shapes, which can be a normal quadrilateral, triangular, or circular region called *patches*. Also, the reinforcement of the elements can be specified to make the section more realistic to the real reinforced concrete section [45].

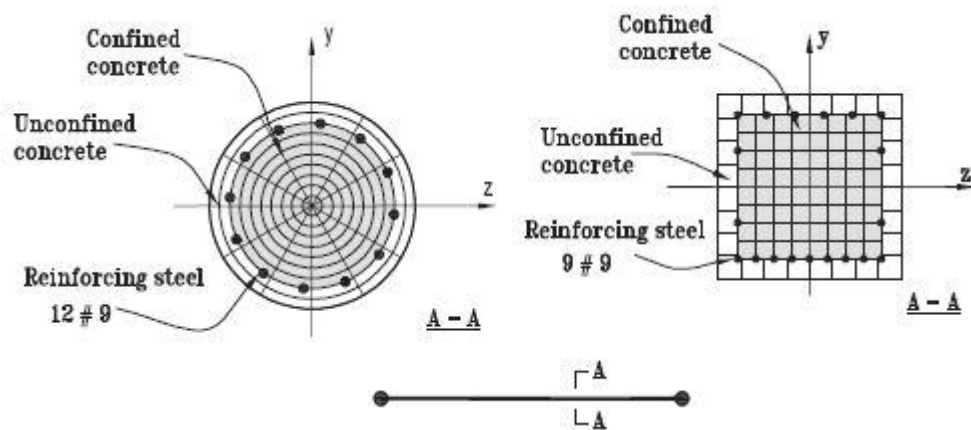


Figure 2.59: Nonlinear beam-column element with fiber section [45]

The section above shows the example of the fiber section in both the circular and rectangular sections. In OpenSees, we can control the number of sub-region to optimize the generation of the result.

### 2.5.2.3 Elastic elements:

In 3D modeling, elastic elements are modeled with more parameters than in the 2D modeling. The basic parameters for elastic elements include:

- A: Area of section
- $I_y, I_z$ : Moment of inertia
- J: Torsional constant

For rectangular section, the formula is followed:

$$J = ab^3 \left( \frac{1}{3} - 0.21 \frac{b}{a} \left( 1 - \frac{b^4}{12a^4} \right) \right)$$

Where:

a: the length of the long side

b: the length of the short side

$E_c$ : Young modulus or Elastic modulus of material (in most cases, the value of Young modulus is from concrete material excluding reinforcement's).

$G_{\text{shear}}$  : shear modulus of the material.

## CHAPTER 3

### BEHAVIOR OF COLUMN WITH SPLICED REINFORCEMENT

#### 3.1 Introduction

The details of an experimental program which was planned to investigate the cyclic response of the reinforced concrete (RC) columns with and without lap splices are presented in this chapter. A total number of four reinforced concrete columns were constructed and tested under lateral loading. In the first column, non-spliced vertical steel bars were provided to serve as a control column. Whereas in the second column, lap spliced vertical steel bars were used. In this column traditional lap splicing i.e., overlapping of steel bars were used. In the last two reinforced concrete columns steel couplers were used to connect vertical steel bars instead of the traditional lap splicing method. The specimens are representative of columns of bridge piers in Thailand. The column properties such as column width-to-depth, aspect ratios, axial load ratios, longitudinal reinforcement ratio, and transverse reinforcement ratio were selected within the guideline and standard drawing of the Department of rural roads (DRR), Thailand, for a small bridge with ten-meter span (as of 2010).

#### 3.2 Experimental program and test configurations

##### 3.2.1 Specimen details

The typical details of test specimens are shown in figures 64 and 65. RC columns were designed as cantilever columns by considering half of the total height of the bridge column. The column section was considered as 400 mm X 400 mm and column height was 2200 mm. The aspect ratio of the test specimen was 5.5. Longitudinal reinforcement is comprised of eight deformed bars of diameter 25 mm. Stirrups were provided using 12 mm deformed steel bars spaced at 200 mm center to center. The ends of the lateral

stirrups were bent at 135 degrees and extended up to a distance equal to four times bar diameter i.e., 48 mm following EIT 1008-38 guidelines.

A total number of four reinforced concrete columns were constructed and tested under lateral loading. In the first column (NS), non-spliced vertical steel bars were provided to serve as control column. Whereas in the second column (LS), lap spliced vertical steel bars were used. In this column traditional lap splicing i.e., overlapping of steel bars was used. In last two reinforced concrete columns (MS1 and MS2) steel couplers were used to connect vertical steel bars instead of traditional lap splicing method. The third specimen (MS1) contained all its mechanical splices in the critical region. The fourth specimen (MS2) had its mechanical splices staggered alternately so that 50% of the mechanical splices were located within the critical region and the rest outside the critical region. A lap splice column (LS) and a mechanical splice column (MS1) had tested by [46]. The summary of these parameters was shown in the following Table 3.4, and Figure 3.1 describes the splice reinforcement condition, and Figure 3.2 describes complete details of all the specimens.

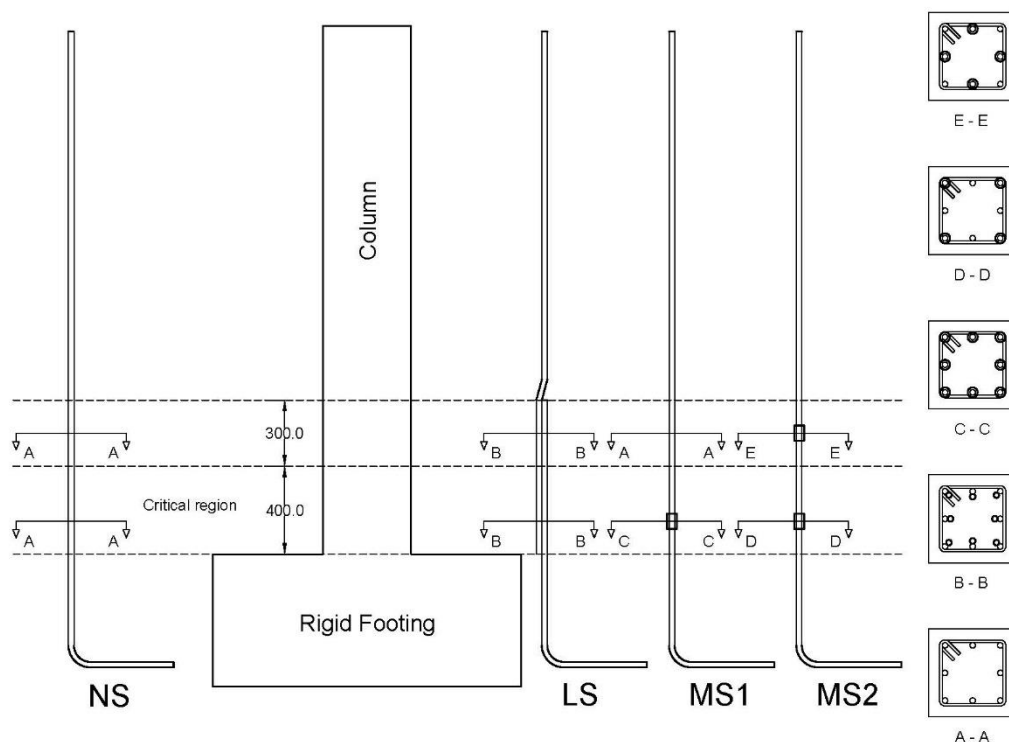


Figure 3.1 Details of longitudinal steel splice in column specimens

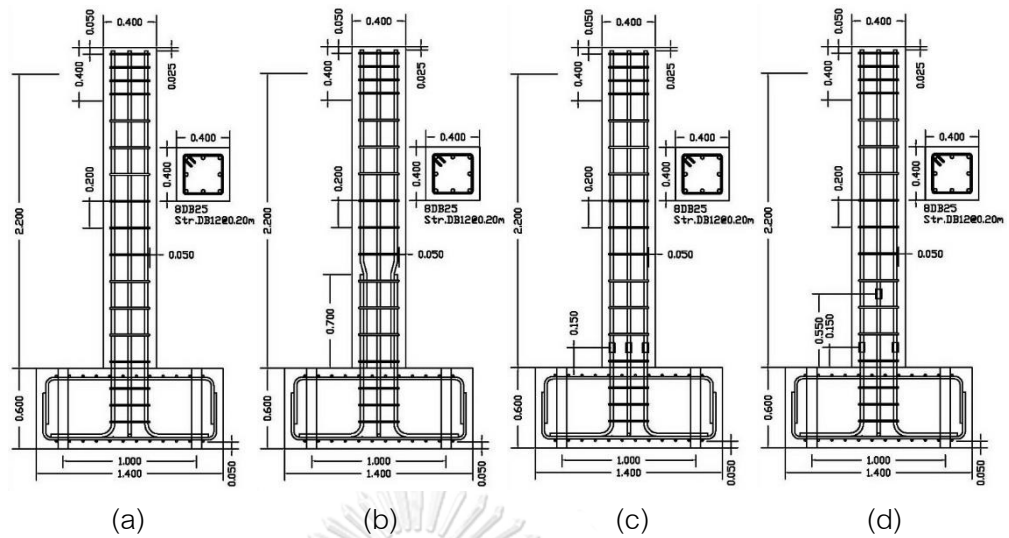


Figure 3.2 Column detailing of (a) NS, (b) LS, (c) MS1 and (d) MS2

(All dimensions in meters)

### 3.2.2 Prepare of specimens

All test specimens were prepared using the same batch of steel bars and concrete to control the quality of specimens. The level of the laboratory floor was leveled and adjusted by using cement grout and level device prior the installation of the steel cage as shown in Figure 3.4. The longitudinal reinforcement was placed at the center of the foundation and lateral stirrups were installed carefully at the specified distance. During the installation of the stirrups, the vertical alignment of the longitudinal steel bars were continuously monitored using level device as shown in Figure 3.5.



Figure 3.3 Prepare ground level and grid line for construction



Figure 3.4 Rigid footing reinforcement detailing

จุฬาลงกรณ์มหาวิทยาลัย



Figure 3.5 Tie hoops were placed orderly way along the column  
and vertical alignment was adjusted

In case of lap sliced RC column (LS), overall lap splice of the steel bar was provided over length of 700 and longitudinal steel bars were bent near the end location of the spliced bar to maintain vertical alignment of the steel bars as shown in Figure 3.6. In third and fourth column, steel couplers (mechanical splices) were used to connect vertical steel bars. Steel coupler is basically comprise of male and female threaded steel collars that join bar segments with deformed heads, which enlarge bar end via a patented cold forging process. The force transferring mechanism of compression the core diameter of the bar is increased to a predetermined diameter. To assemble the threaded mechanical splicing system have to an initial torque of the threaded collars of approximately 200 N-m is needed, as specified by Bartec® Dextra, as shown in Figure 3.7. The Bartec® was in accordance with building design codes ACI 318-02 with type 2 of couplers suitable for seismic areas.

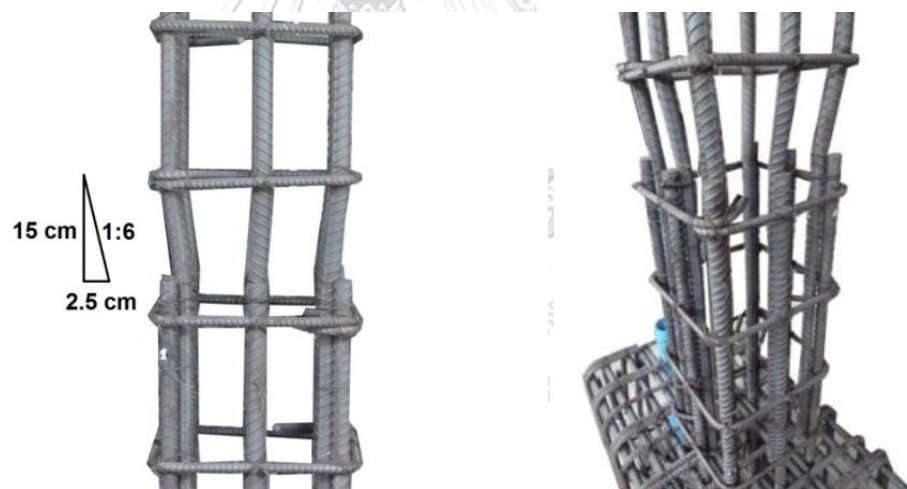


Figure 3.6 lap splice slope bending ratio 1:6 of lap splice column (LS) [46]





Figure 3.7 Initial torque of the threaded collars of approximately 200 N-m.

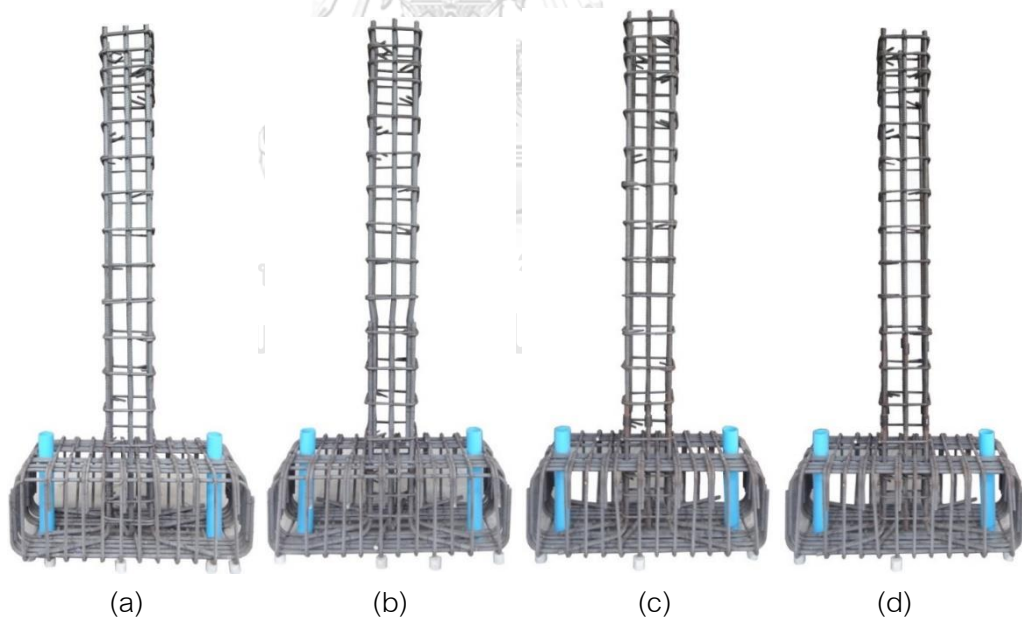


Figure 3.8 Splice reinforcement detailing (a) NS:Non-splice, (b) LS:Lap splice, (c) MS1 and (d) MS2 : Mechanical splice.

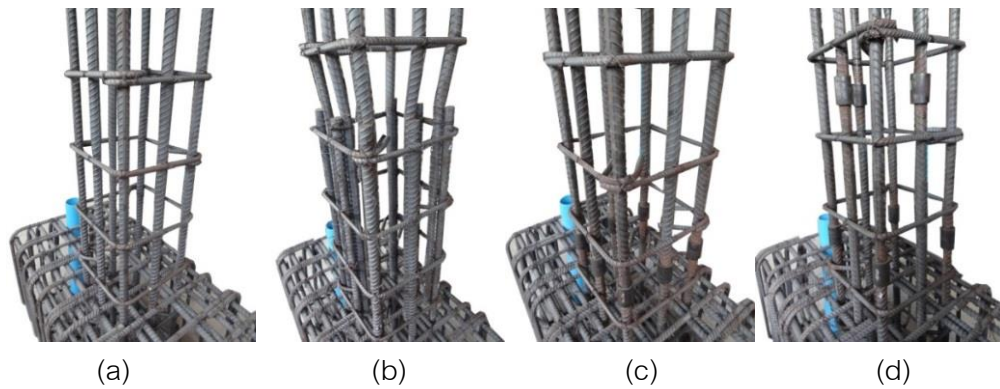
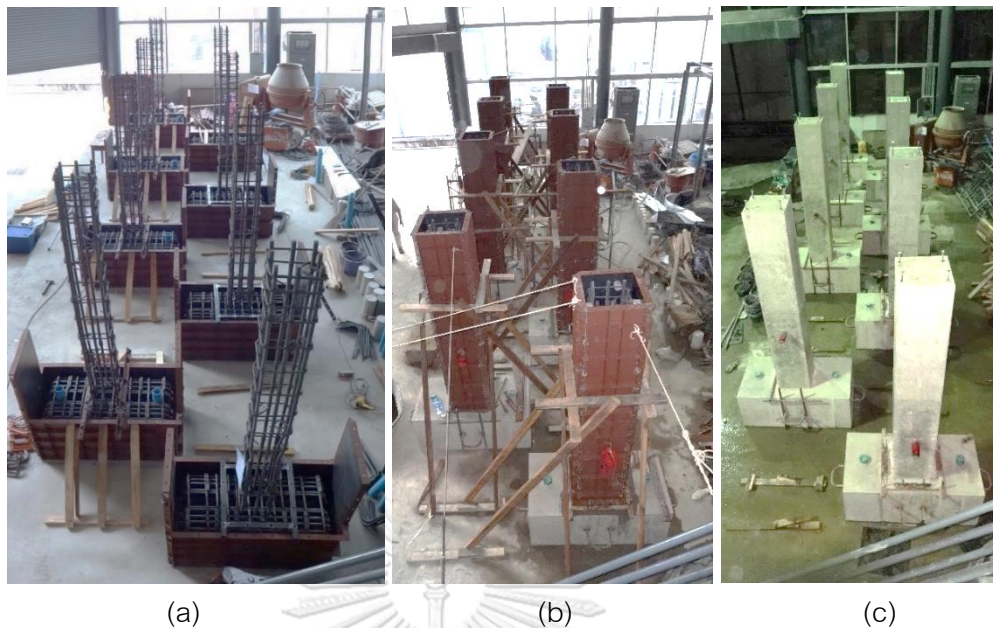


Figure 3.9 Splice reinforcement detailing (a) NS:Non-splice, (b) LS:Lap splice, (c) MS1 and (d) MS2 : Mechanical splice.

Prior to the concrete casting, strain gauges were installed at different locations on the steel bars to record the strain of the steel bars during the test as shown in Figure 3.10. In the first step, base foundations of the RC columns were cast whereas in the second step, RC columns were cast using the same batch of concrete to ensure uniform properties of concrete as shown in Figure 3.11



Figure 3.10 Strains measurement of reinforcing steel and mechanical splice



(a) Setup steel formwork of footing,  
 (b) Footing cast and setup steel formwork for the column  
 (c) Complete preparing specimen.

### 3.2.3 Material Properties of Specimens

#### 3.2.3.1 Concrete

In this study, Type 1 Portland cement as specified in ASTM international was used to prepare concrete. Standard specimens i.e., concrete cylinders of height 300 mm and diameter 150 mm were cast and tested to determine the compressive strength of the concrete. A total number of three cylinder specimens were cast and test. The average of three specimens was considered as a specific strength of the concrete. The material properties of concrete are summarized in Table 3.1

Table 3.1 Compressive strength of concrete in this research

Time	ID	Dimension (mm)		Compressive Load (kN)	$f'_c$ (MPa)	Curing (Day)	Remark
		Diameter	Hight				
1	C1	151	301	383	21.3	8	
	C2	150	301	362	20.2	8	
	C3	149	302	398	22.5	8	
	Average					21.3	
2	C4	150	302	398	22.5	25	
	C5	149	302	-	-	25	Fail
	C6	150	301	401	22.6	25	
	Average					22.5	
3	C7	150	300	447	25.1	28	
	C8	150	300	421	23.7	28	
	C9	151	301	395	22.0	28	
	Average					23.6	

### 3.2.3.2 Reinforcing steel

The experimental program consisted of reinforcing deformed bar with a diameter of 12 and 25 mm and made in accordance with SD40 with Thai Industrial Standards (TIS24-2548(2005)). The average of three tests was used to obtain typical tensile stress for each bar size. The material properties of steel bars are summarized in Table 3.2 and Table 3.3. The average tensile yield strength ( $f_y$ ) of the deformed bar with a diameter of 12 and 25 mm. are 521 MPa and 449 MPa, respectively. Ultimate tensile strength ( $f_u$ ) of steel bars with a diameter of 12 mm and 25 mm are 655 MPa and 628 MPa, respectively. ASTM standard methods were followed for tensile testing of the steel bars.

Table 3.2 Tensile strength of transverse reinforcement

Specimens	Diameter (mm)	$f_y$ (MPa)	$f_{su}$ (MPa)	$E_s$ (GPa)
1	12	526	663	210
2	12	517	649	206
3	12	521	654	208
Average		521	655	208

Table 3.3 Tensile strength of longitudinal reinforcement

Specimens	Diameter (mm)	$f_y$ (MPa)	$f_{su}$ (MPa)	$E_s$ (GPa)
1	25	427	609	203
2	25	431	611	205
3	25	488	664	212
Average		449	628	206

Table 3.4 Summary of specimen parameters

Type of specimens	NS	LS	MS1	MS2
Splice reinforcement	No	Lap splice	Mechanical splice	Mechanical splice
Axial Load ratio $\frac{P}{f'_c \cdot A_g}$	0.075			
Concrete compression strength (MPa)	23.6			
Specimen size	Width	400 m		
	Depth	400 m		
	Length	2200 m		
Steel reinforcement	no of steel/bar size	8-DB25		
	Longitudinal steel (%)	2.45%		
	Yield strength (MPa)	449		
	Ultimate strength (MPa)	621		
Reinforcement according to area	no of steel/spacing	1-DB12@200		
	Transverse steel (%)	0.75%		
	Yield strength (MPa)	521		
	Ultimate strength (MPa)	655		

### 3.2.4 Instrumentation

#### 3.2.4.1 Strain gauge

Strain gauges were used to monitor strains in the longitudinal and transverse steel reinforcements during the test. These strain gauges were installed before concrete casting. The expected critical regions were selected to monitor strains in the reinforcing bars during the test. Typical locations of the strain gauges and corresponding labels are shown in Figure 3.12 to Figure 3.15 for specimen NS, LS, MS1, and MS2, respectively.

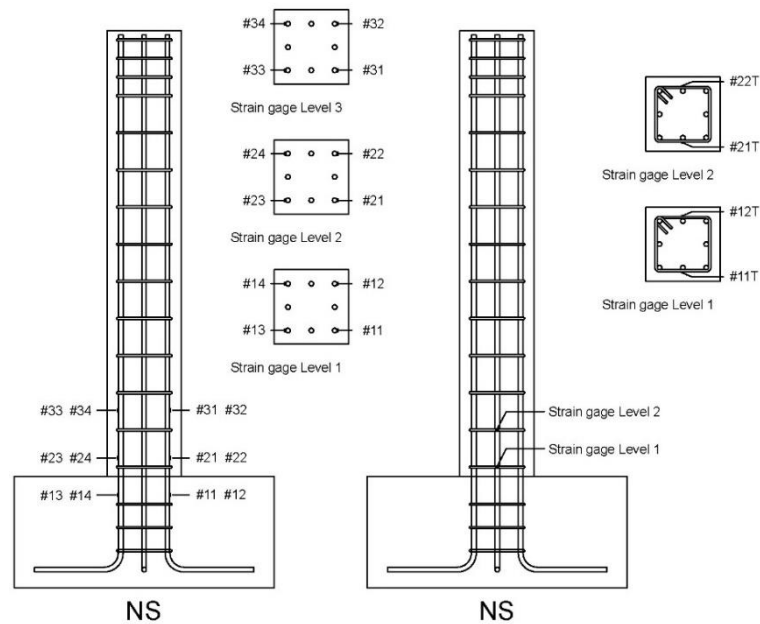


Figure 3.12 Detailing of strain gauge on reinforcements of NS column

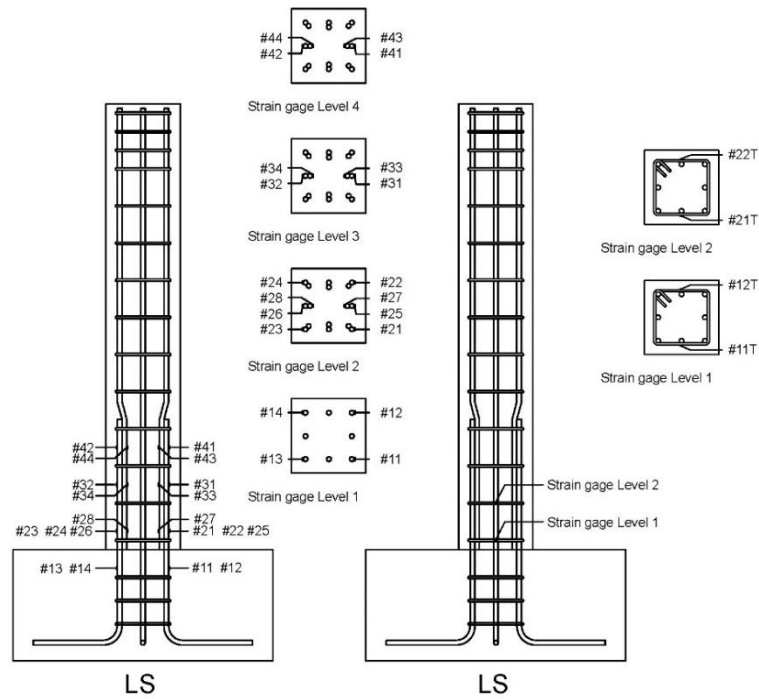


Figure 3.13 Detailing of strain gauge on reinforcements of LS column

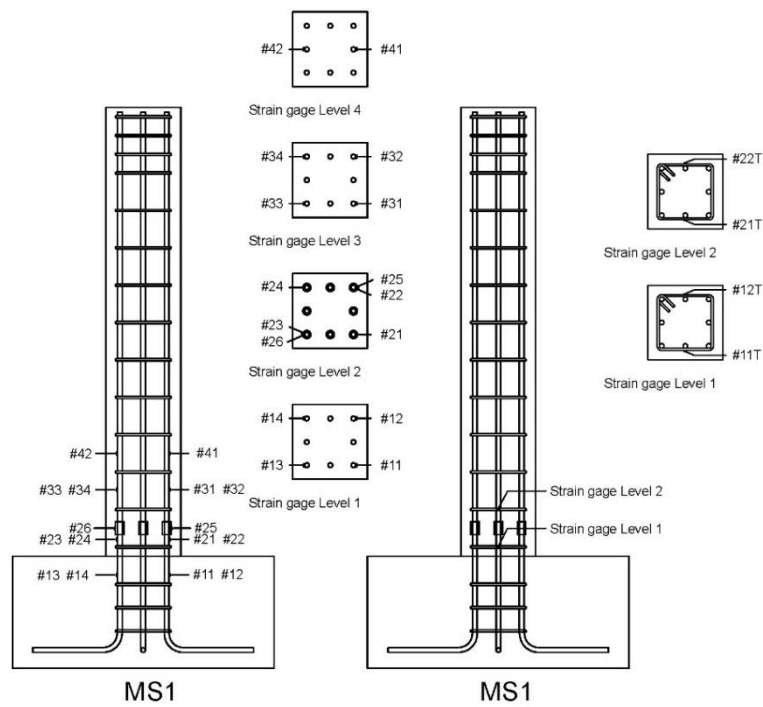


Figure 3.14 Detailing of strain gauge on reinforcements of MS1 column

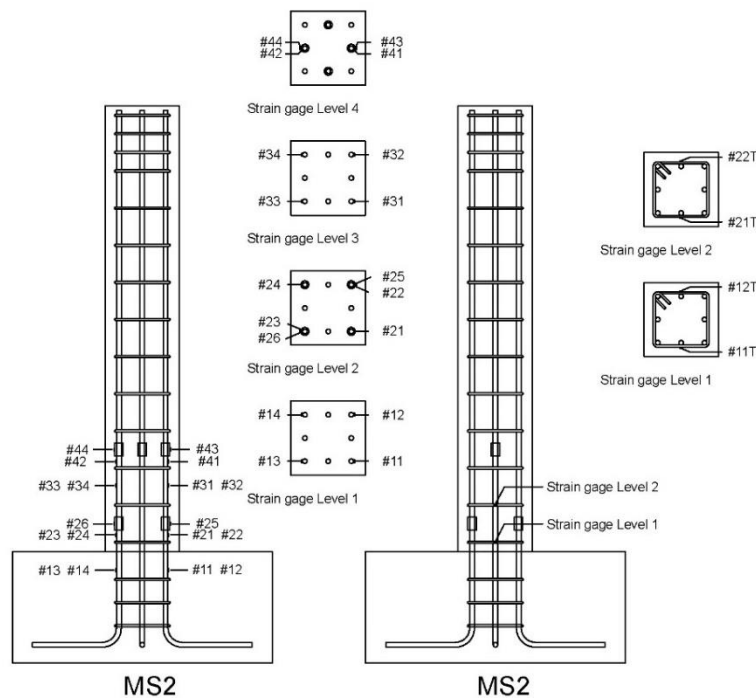


Figure 3.15 Detailing of strain gauge on reinforcements of MS2 column

#### 3.2.4.2 Displacement transducers

A total number of Thirteen displacement transducers were used to measure the deformations of the test specimen. One transducer was installed horizontally at the top of the column to record lateral displacement of the column as shown in Figure 3.16. The expected regions of curvature occur, a critical region of RC columns, were selected to monitor during the test. The location of displacement transducers was used to measure the rotation of the test specimen CL, and CR for level 1-4 were used to measure the bending curvatures of the columns, as shown in Figure 3.17. For resist of a lateral load of the column specimens, were occurred the rotation of footing can measure by FR-L, and FR-R displacement transducers are shown in Figure 3.18 (a), (b). The slip deformation of the footing and reaction wall was measured by FS and WS, respectively Figure 3.18 (c), (d).



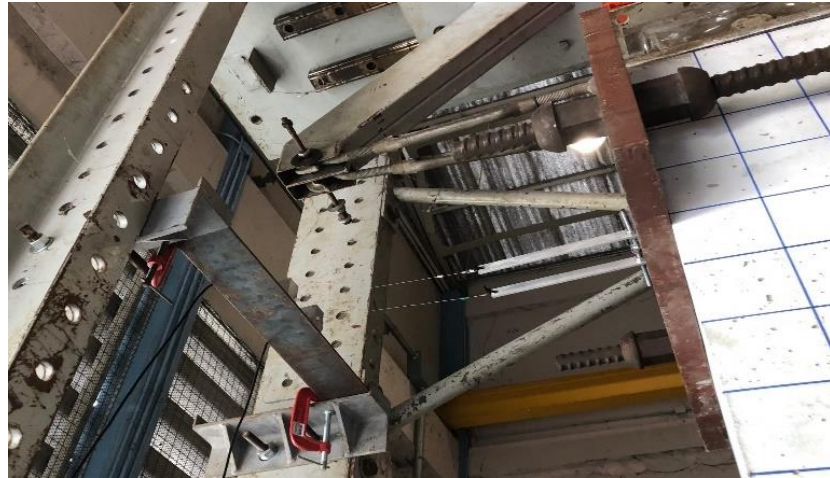


Figure 3.16 Sling type of displacement transducers measured at the lateral displacement.

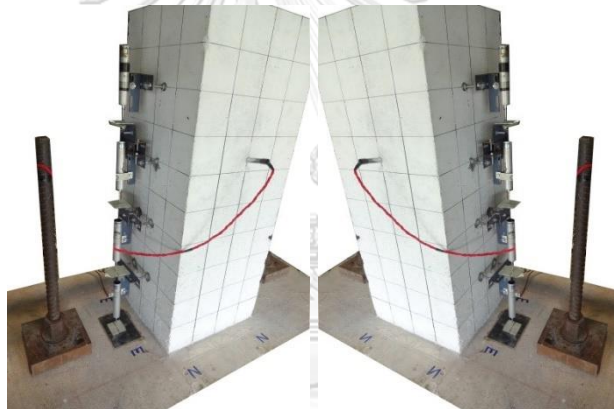
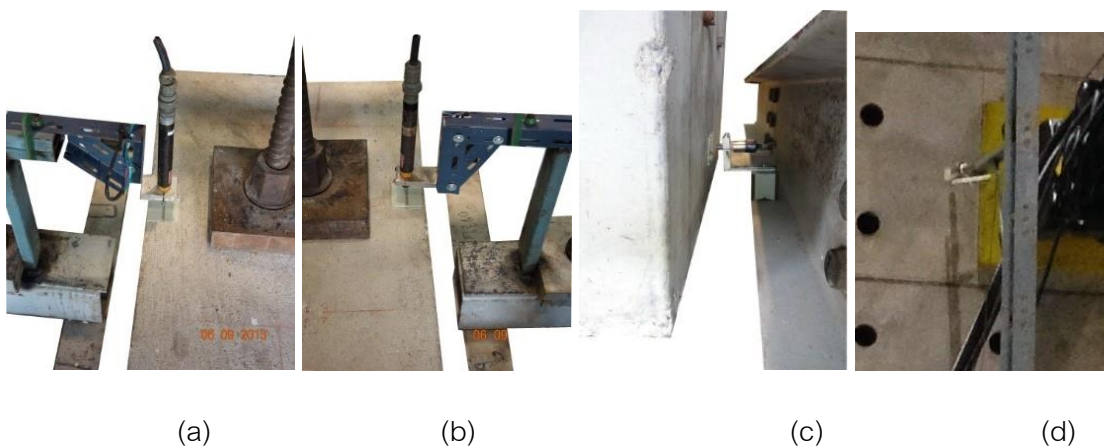


Figure 3.17 Installation displacement transducer to measuring the curvature



(a)

(b)

(c)

(d)

Figure 3.18 Installation displacement transducer to measure the rotation and footing of the test specimen

In experimental results of the hysteretic behavior of each specimen are correction data of displacement. The sliding of the foundation against the strong floor, the rotation of the foundation against the strong floor and the movement of the reaction wall, which is mounted an actuator, are observed as shown in Figure 3.18. Therefore, it is essential to understand how these factors affected experimental results. The data correction of the recorded test results to get usable are necessary. The corrected displacement values are calculated.

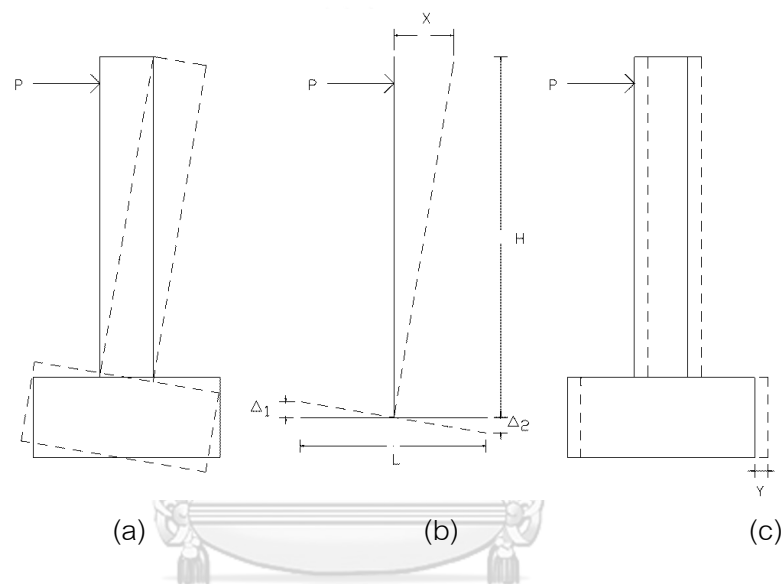


Figure 3.19 (a) The rotation of the foundation, (b) Sliding of the foundation and (c) The displacement of the reaction wall

$$\Delta_{real} = \Delta_{record} - X - Y - Z$$

$$Y = \frac{\Delta_1 + \Delta_2}{L} \cdot H$$

Where;

X = Footing rotation (mm)

Y = Displacement due to sliding (mm)

Z = Displacement of the reaction wall

$\Delta_1$  = Data recorded from LVDT FR-L

$\Delta_2$  = Data recorded from LVDT FR-R

### 3.2.4.3 Testing setup

In this study, lateral Load was applied through a hydraulic actuator of 1000 KN load capacity and 500mm displacement stroke. The actuator bolted at one end with the reaction wall and another end fixed to the column. The axial load applied through a 60-ton hydraulic jack capacity. The axial load was held constant throughout the test. During the test, the axial load was carefully monitored and adjusted to the desired level. Roller support provided at the top of the load cell enables the axial load components to follow the tip displacement of the column. Therefore, the axial load will always be right at the top of the column. Detailing of the test set up is shown in Figure 3.20

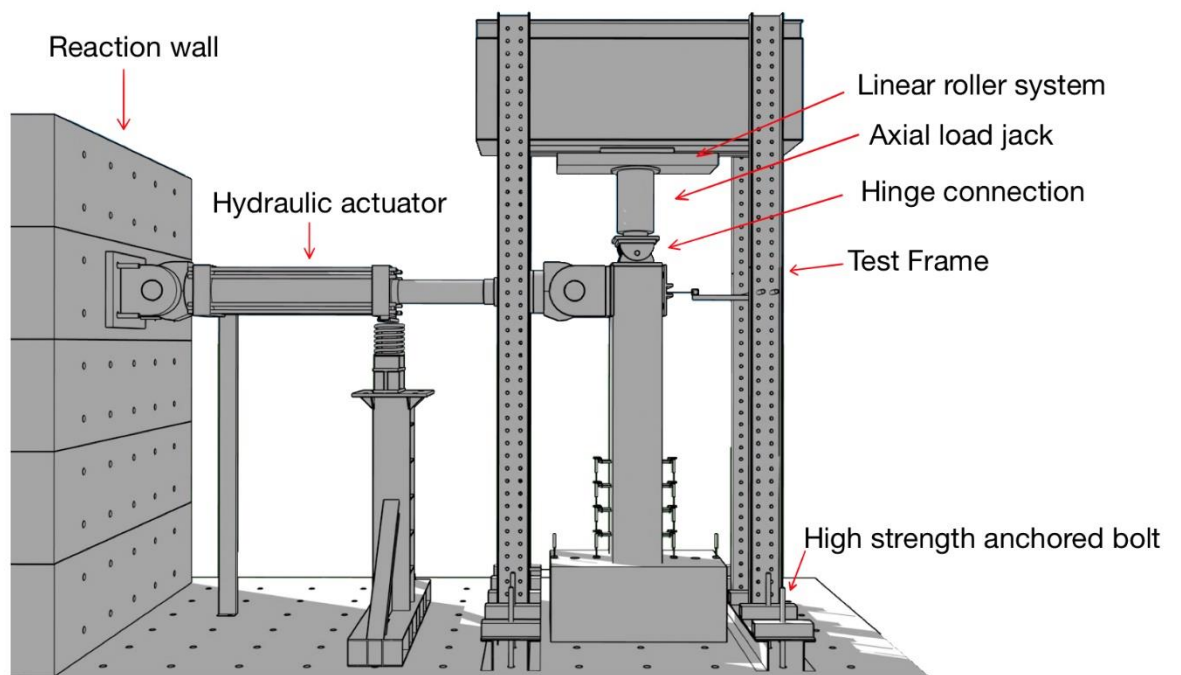


Figure 3.20 Experimental setup



Figure 3.21 Full-scale laboratory at Chulalongkorn University

### 3.2.5 Test procedures

Specimens were recorded the test data by observation to take photo and hand sketch the crack pattern. The measurement by displacement transducer and strain gage including the load and stroke displacement of the actuator, were recorded by using datalogger, as shown in Figure 3.22. Then start the test by subjected to constant axial load to 31 tons and cyclic lateral displacement. Lateral displacement applied through the actuator at the top of the column. The displacement history consists of twice cycles at each lateral drift. The lateral displacement increased monotonically by 0.25%, 0.50%, 0.75%, 1%, 1.5%, 2% until failure as shown in Figure 3.23.

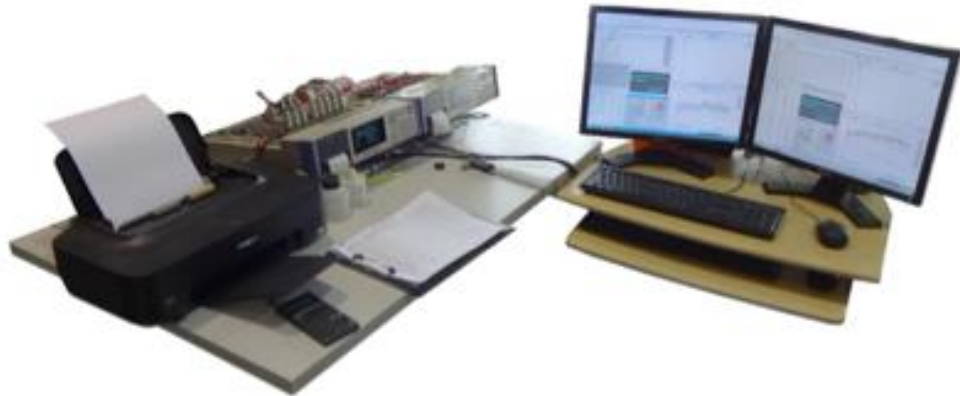


Figure 3.22 Data logger acquisition system.

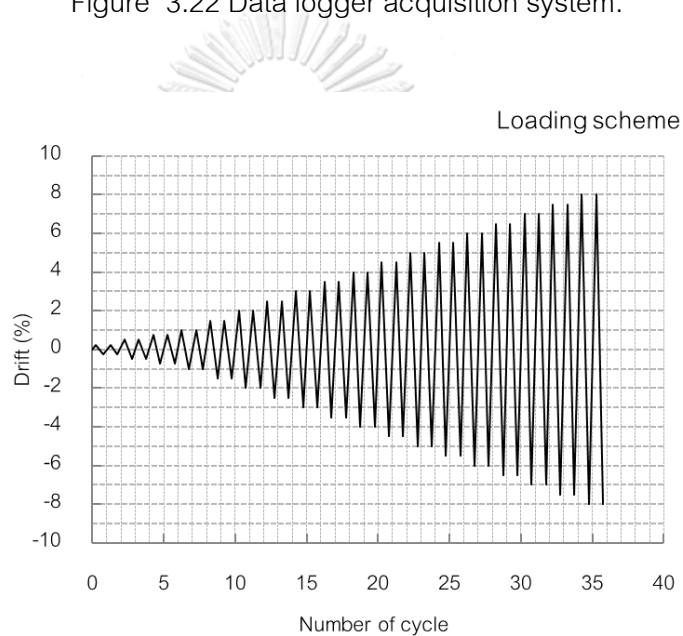


Figure 3.23 Displacement history for the tested specimen

### 3.3 Experimental Result and discussion

In this section, the performance of column with and without splice reinforcement was presented in terms of appearance damage behavior observation and the lateral strength- deformation. The results of strain variation in longitudinal and transverse reinforcement at each stage and curvature variation are discussed. Moreover, a comparison envelopes curve of specimens will also discuss in detail in this chapter.

### 3.3.1 Experimental result of specimen NS

Specimen NS is contained continuous longitudinal steel without any lap splice. Due to it is a long column with a high aspect ratio ( $a/d$ ) of 5.5, a flexure failure was expected. During the test, strength and deformation are shown in hysteresis at cracking. Peak load-displacement ( $\delta_u$ ), and a loss of lateral strength ( $\delta_{0.8u}$ ) were recorded to assess the failure mechanism, as shown in Table 3.5. Including strain in the longitudinal and the transverse reinforcement were discuss.

#### 3.3.1.1 Progressive damage of specimen NS

The sample NS has a small number of cracks during the early experiment state. The first few observable cracks after the movement rate reached 0.5% and have a horizontal direction. After that, the cracks went toward a 45 degree angle, continuing from the horizontal direction with a 1.5% movement rate. When the movement rates reached 2%-5%, the concrete began to crushing at its base. Afterward, the concrete cover began to spall, which the steel buckling and bent to the point that the whole area concrete was pushed out. Finally, when the bar end of transverse reinforcement bent at 135 degrees open, which caused it to collapse. For this sample, the reinforced concrete column has a horizontal displacement at the yield point of 29.5 mm., the highest horizontal movement is 60.7 mm, and the highest lateral force recorded is 143 kN.

Table 3.5 Experimental results of specimen NS

NS	Load (kN)	Displacement (mm)	% Drift
$P_{max}$	143	60.7	2.76%
$0.8 P_{max}$	114	109.0	4.95%

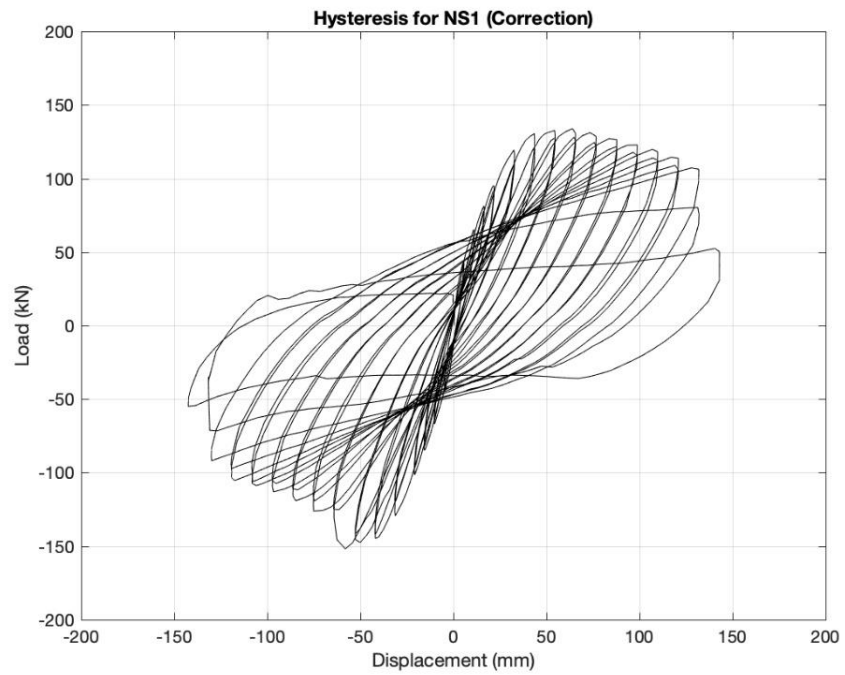


Figure 3.24 Hysteresis of NS specimen

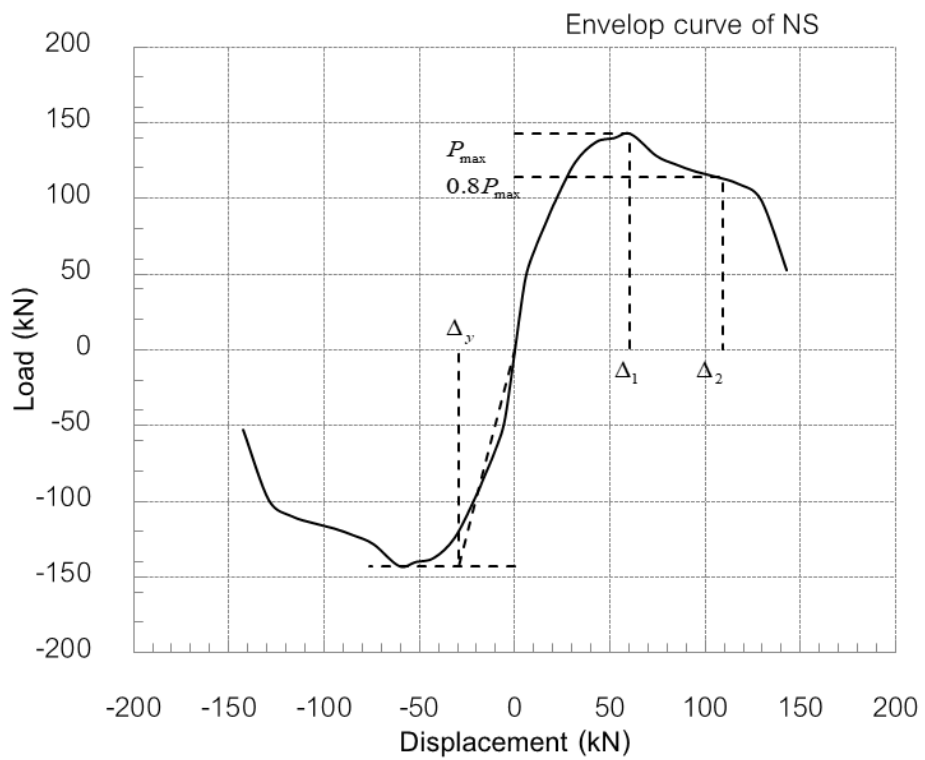


Figure 3.25 Envelop curve of NS specimen

### 3.3.1.2 Appearance failure of specimen NS

The non-splice specimen NS was failed by buckling of longitudinal reinforcing bars. Buckling shape as shown in Figure 3.26 (c) clearly at there height, is 400 mm or 2 of spacing of tie hoops. As a result, the breaking of tie hoop leads to lost lateral load capacity finally.

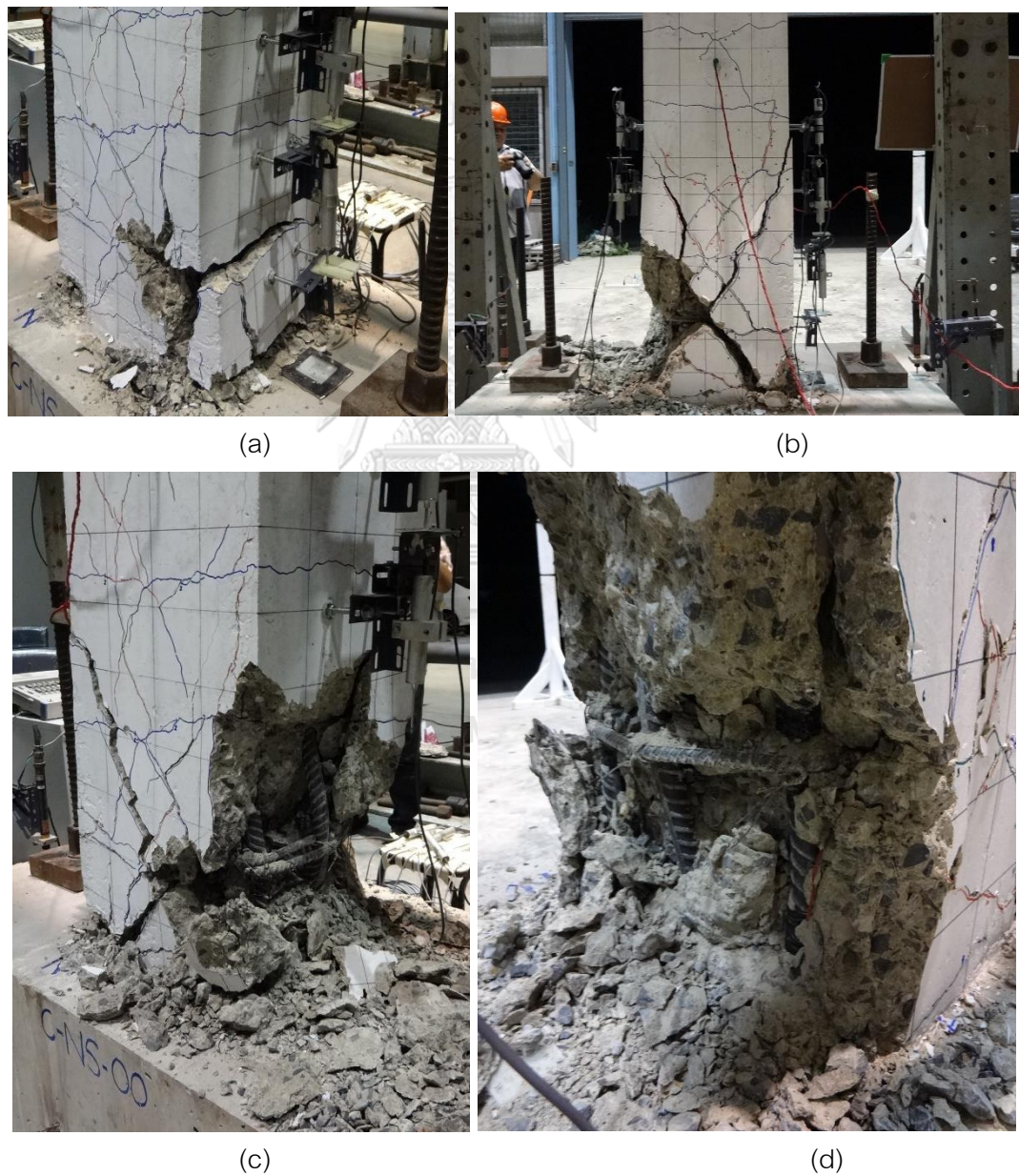
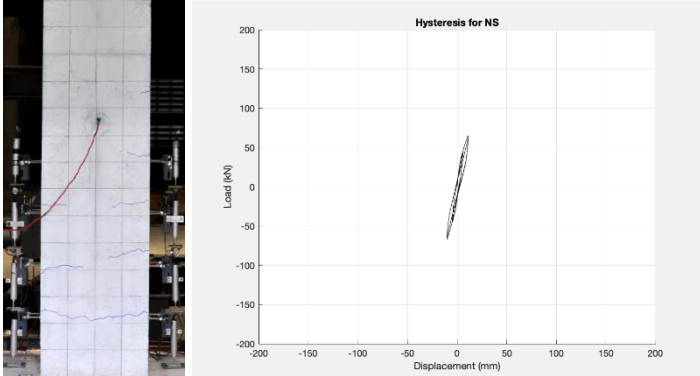
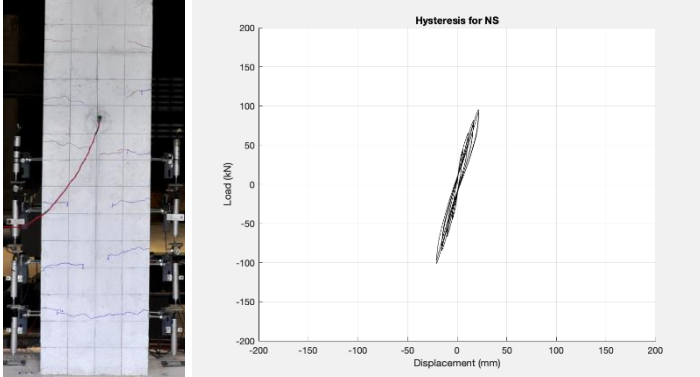
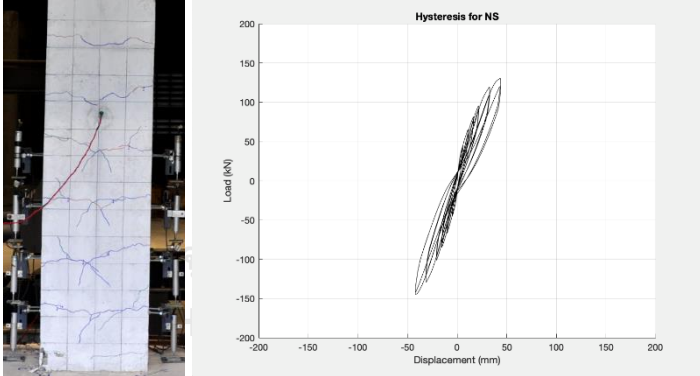
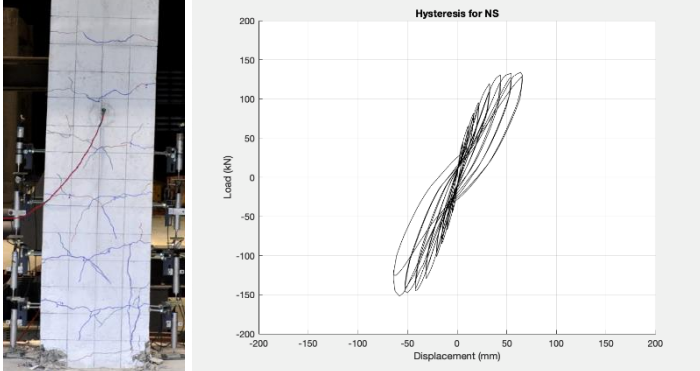
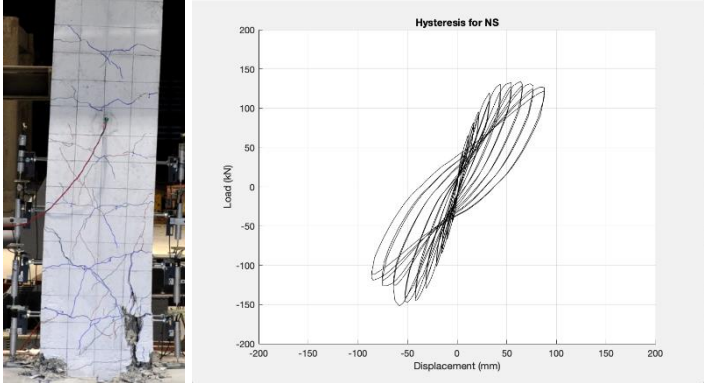
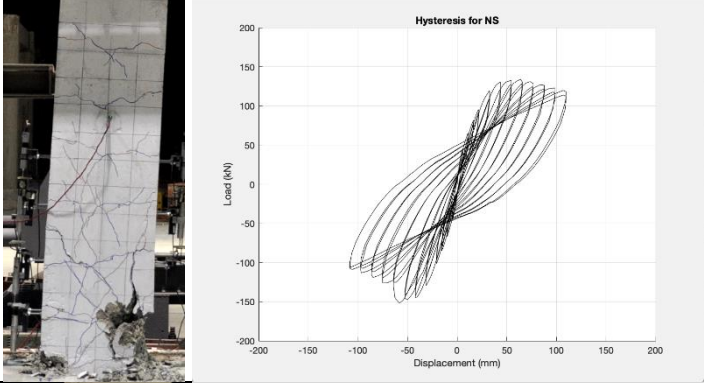
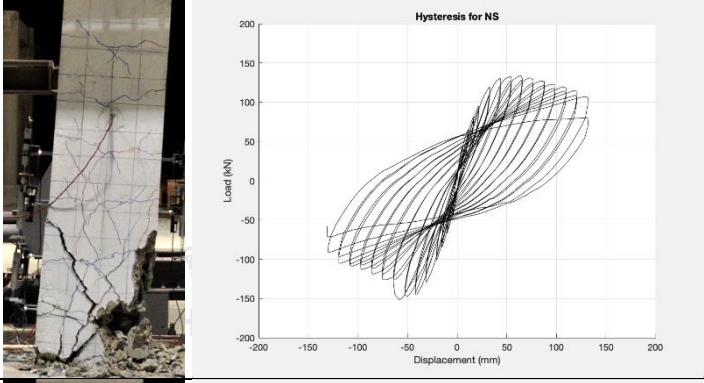
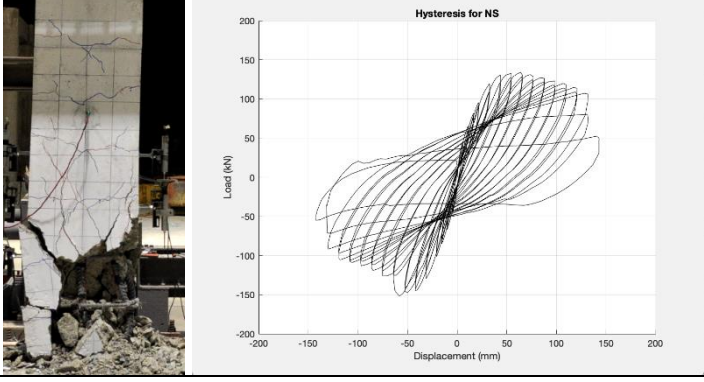


Figure 3.26 Buckling failure of non-splice column specimen NS



%Drift	Crack pattern and lateral load-displacement	Appearance damage
0.5%		<p>a small number of cracks after the movement rate reached 0.5% and has a horizontal direction</p>
1.0%		<p>Increase number of cracks continuing</p>
2.0%		<p>cracks went toward a 45 degree angle, continuing from the horizontal direction</p>
3.0%		<p>Concrete crushing in the corner of column and cracks went toward a vertical, continuing from 45 degree angle</p>

%Drift	Crack pattern and lateral load-displacement	Appearance damage
4.0%		Concrete spalling along vertical crack
5.0%		Buckling occurs in the longitudinal reinforcing bar between two tie hoops
6.0%		Tie hoop failure by the bar end of tie hoop are open cause the column lost the shear strength reasonable to shear crack happen instantly
7.0%		The second tie hoops are break off cause the column lost the shear strength reasonable fail finally

### 3.3.1.3 Strain in Reinforcing steels of specimen NS

Reinforcing steels bar #23 is measured in the longitudinal reinforcing bar above footing for 100 mm on the corner bar is yield at the first cycle of 1.5% drift, and #24 yielded the second cycle of 1% drift, respectively. In contrast, the compression Reinforcing steels bar #21, #22, does not yield. At the time of all longitudinal reinforcement yielded, the lateral load capacity of the NS also closes the peak point. At the end of the loading cycles, all corner longitudinal steel buckled within the plastic hinge region, as shown in Figure 3.27. The #11, #12 are place below rigid footing shows that can develop to yield in both tension and compression.

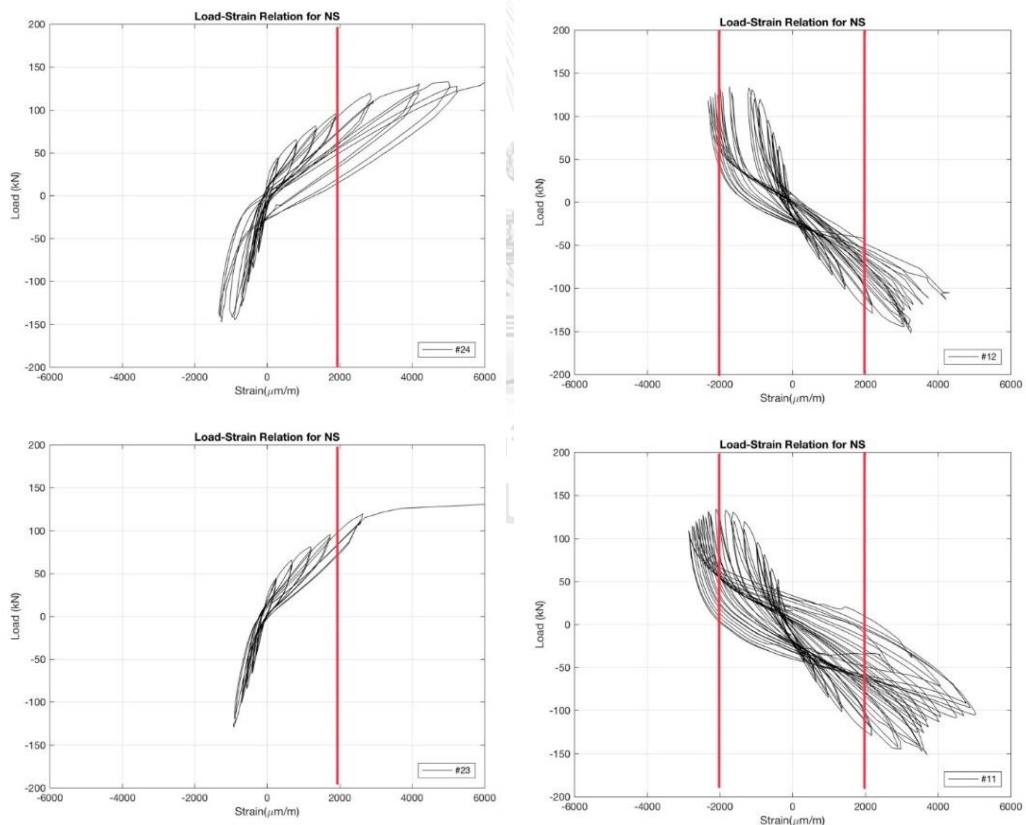


Figure 3.27 Strain in the longitudinal reinforcement of NS at level 1 and 2

### 3.3.2 Experimental result of specimen LS [46]

Specimen LS has contained all its lap splices with 700mm length or 28 times of diameters of longitudinal reinforcement in the critical region.

#### 3.3.2.1 Progressive damage of specimen LS

The sample LS began to crack at the movement rate of 0.25%, the crack was straight crosswise at this rate. At the movement rate of 1%, the crack began to take a 45 degree slope and cracks all over the face surface of the column from the height of 60 cm. Onward. When the force at the movement rate is at 1.5%-2%, the crack began at the reinforcing steel of 700 mm. Height and the concrete began to crush around the base of the column onto the height of 400 mm. Then, the column has more cracks and spalling concrete at the movement rate of 2.5%-3.5% to 700 mm. in height. When the column took repeated force at the movement rate of 4%-5%, the left surface of the column began to crack and more concrete spall until the concrete on all sides of the column peel off to 700 mm. in height. At the same time, the right side of the column has some cracks and peeled off the concrete at the corners to the height of 700 mm., which is a lengthwise extension of reinforced steel. Eventually, all concrete on the column's surface had peeled off and the column lost its hold on the reinforcing steel extension point. At the movement rate of 6%, the column can no longer withstand the horizontal acting force and the column collapsed. For this sample, the lap splice column has a lateral displacement at the yield point of 35.3 mm., the highest horizontal movement is 41.9 mm, and the highest lateral force recorded is 122 kN.

Table 3.6 Experimental results specimen LS

LS	Load (kN)	Displacement (mm)	% Drift
$P_{max}$	122	41.9	1.91%
$0.8 P_{max}$	98	55.9	2.54%

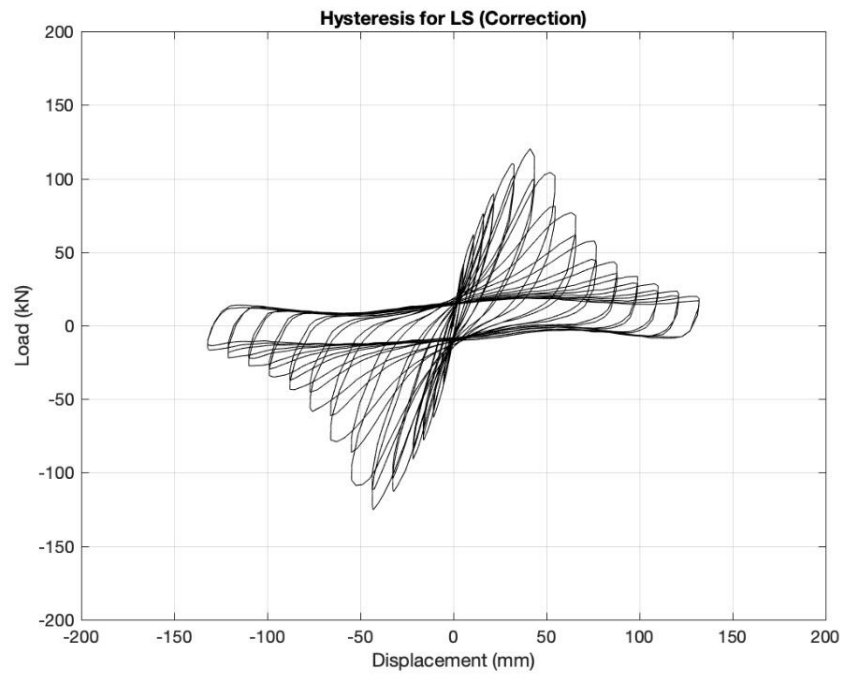


Figure 3.28 Hysteresis of LS specimen

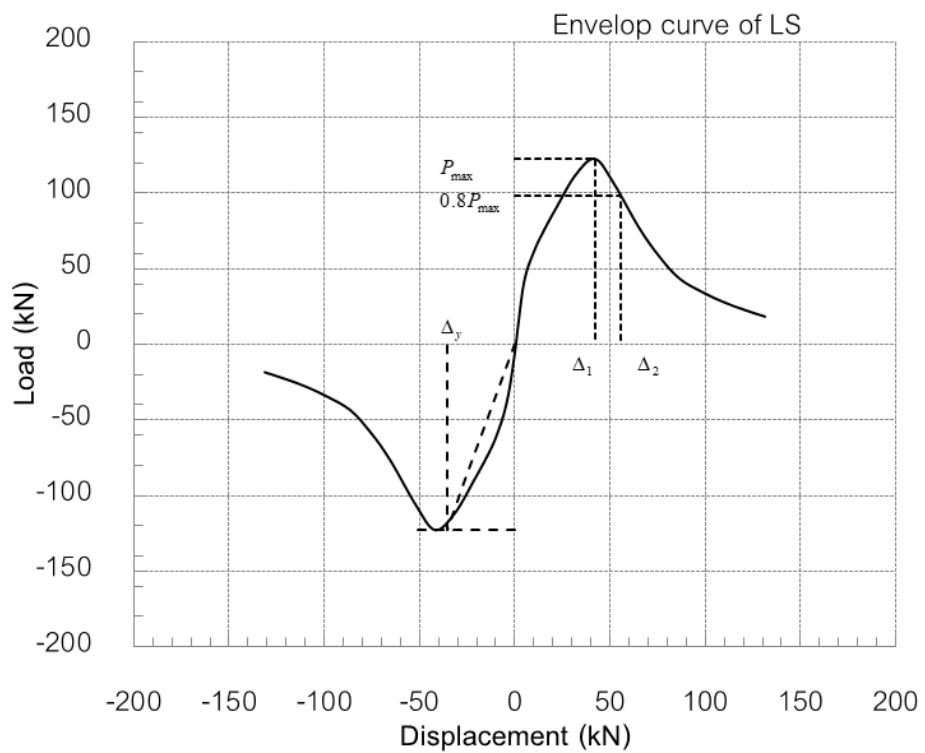


Figure 3.29 Envelop curve of LS specimen

### 3.3.2.2 Appearance failure of specimen LS

The lap-splice specimen LS was failed by bond-slip of lap splice in longitudinal reinforcing bars. The column was spalling of the lap splice plan, as shown in Figure 3.30(b) clearly at there height is 700 mm. As a result, the loss of bond strength leads to the capacity of the lateral load was drop suddenly.

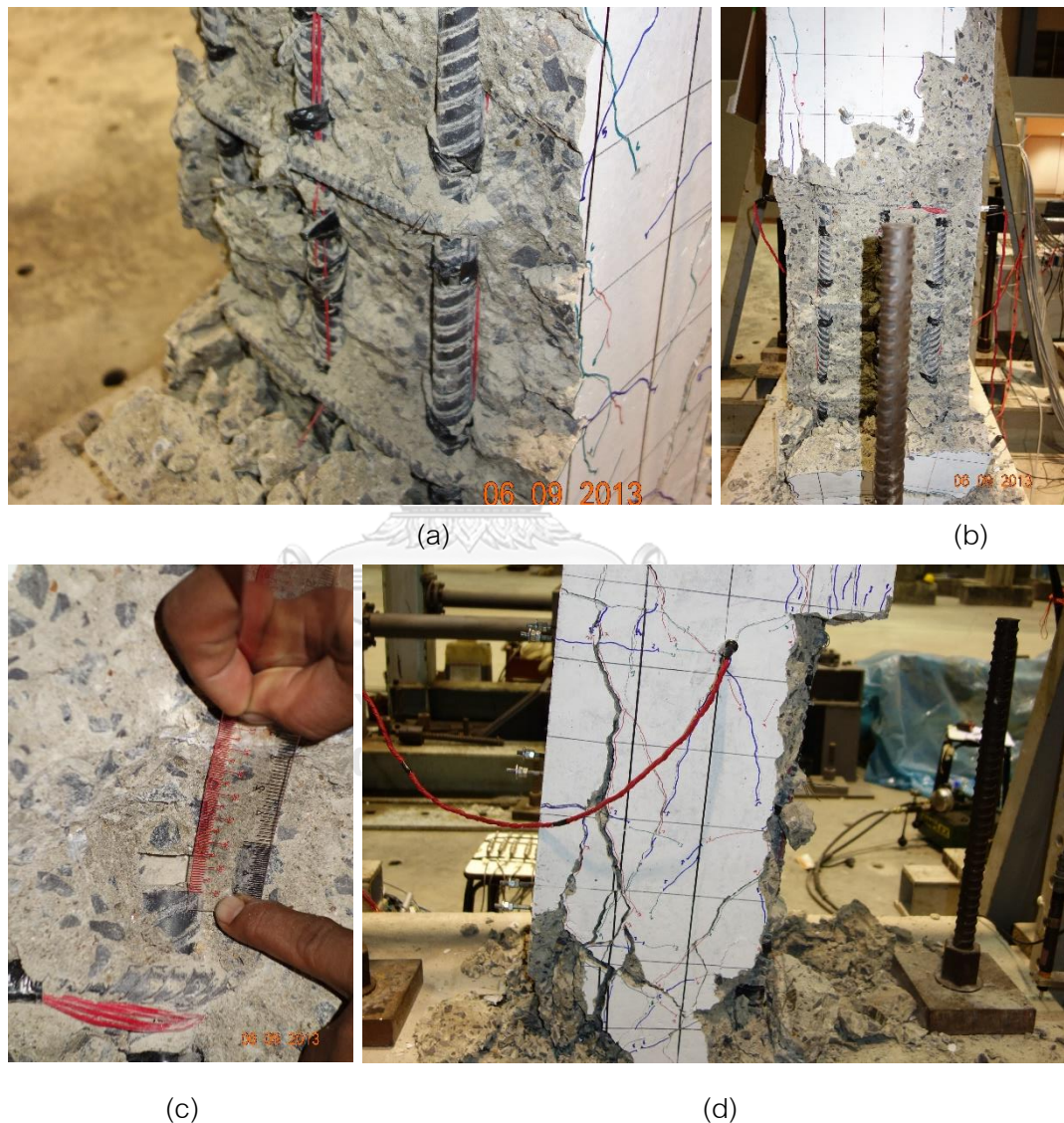
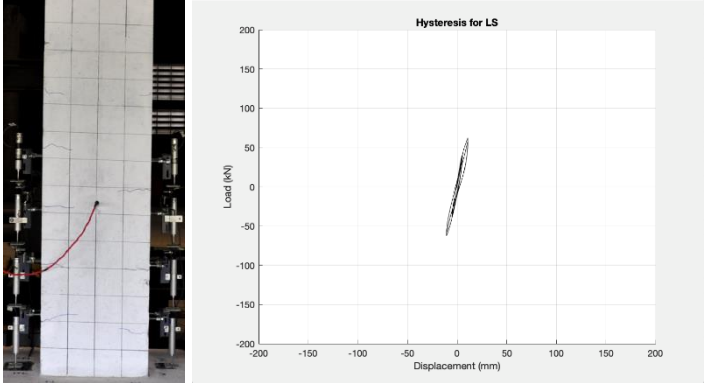
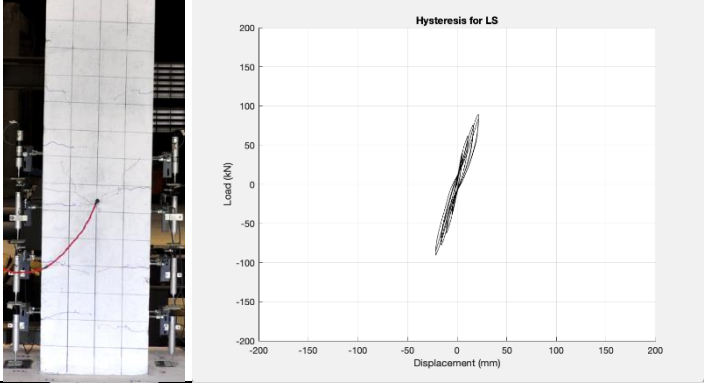
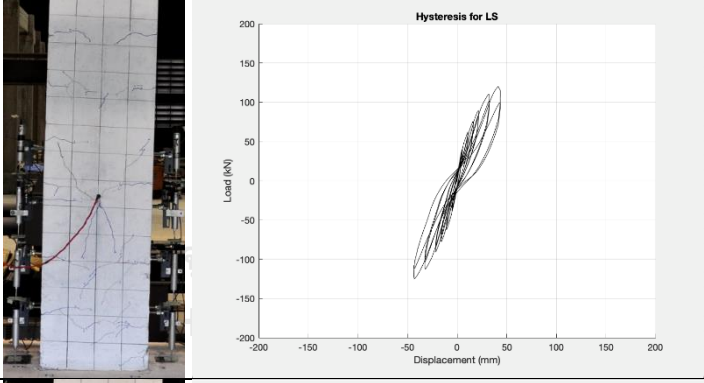
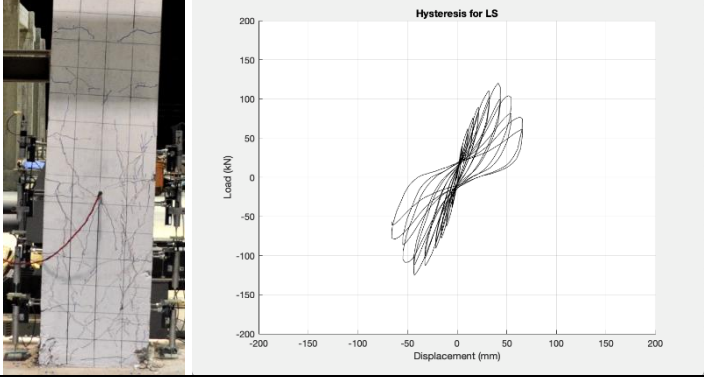
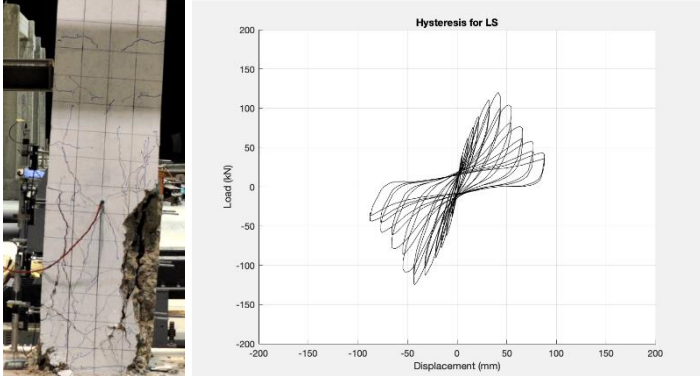
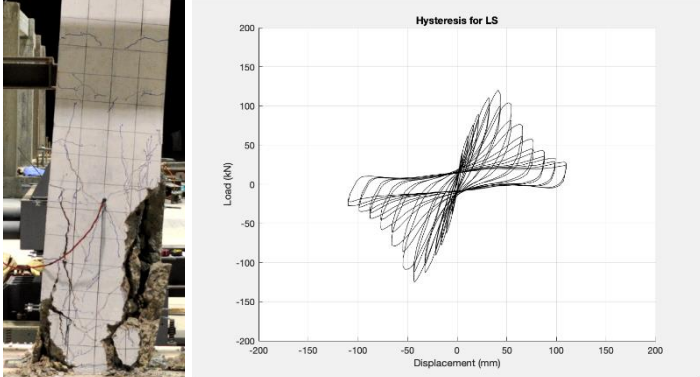
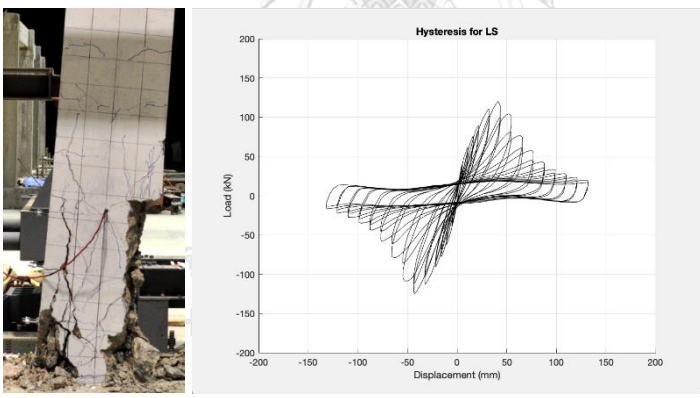


Figure 3.30 Bond slip failure of lap-splice column specimen LS

%Drift	Crack pattern and lateral load-displacement	Appearance damage
0.5%		<p>a small number of cracks on horizontal direction occurs along the column to 1000mm height</p>
1.0%		<p>Increase number of cracks continuing</p>
2.0%		<p>cracks went toward a 45 degree angle, continuing from the horizontal direction</p>
3.0%		<p>Concrete crushing in corner base of column and cracks went toward a vertical, continuing from 45 degree angle along 0-700 mm height</p>

%Drift	Crack pattern and lateral load-displacement	Appearance damage
4.0%		<p>Corner of the column in N-W spalling can see through the longitudinal reinforcing bar with lap splice</p>
5.0%		<p>Westside surface of the column was fell out obviously</p>
6.0%		<p>Column lose the lateral capacity due to lap splice cannot develop strength cause concrete cover are crushing and fell out reasonable to lap splice failure</p>



### 3.3.2.3 Strain in Reinforcing steels of specimen LS

Lap splice of reinforcement with lap splice length 700mm shows the result of developing to yield strength. Strain gage #23 and #24 are measure in longitudinal reinforcing bar anchored into the footing and popped up to overlap with the other bar to column top. Place on the corner bar with 50 mm height above footing, shows develop yield strength at the first cycle of 1.5% drift. As shown in Figure 3.31. The close rebar #25, #26, #27 and #28 are same height 50mm above footing, #25 and #26 measure in longitudinal reinforcing bar anchored into footing and popped up to overlap with the other bar to column top is #27 and #28 show bond stress transfer along lap splice by #25 and #26 shows develop yield strength at the first cycle of 2.5%, Although #27 and #28 cannot develop to yield strength.

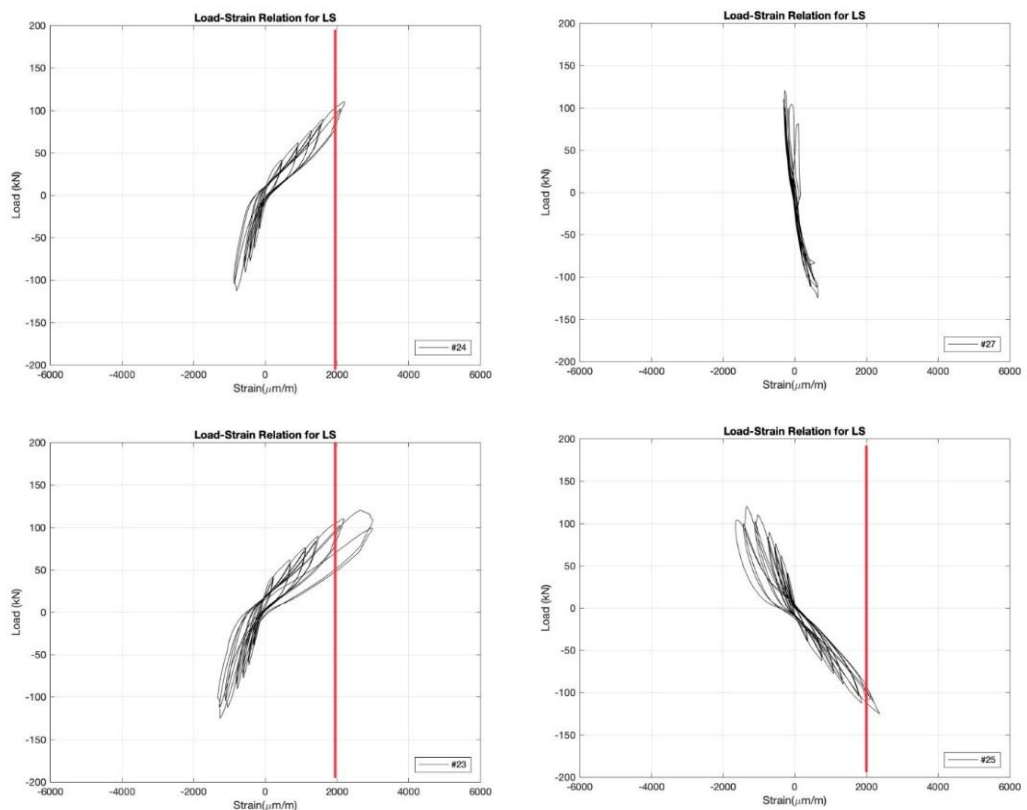


Figure 3.31 Strain in the longitudinal reinforcement of LS at level 2

### 3.3.3 Experimental result of specimen MS1 [46]

Specimen MS1 is contained all longitudinal reinforcement of its mechanical splices in the critical region.

#### 3.3.3.1 Progressive damage of specimen MS1

The sample MS1 did not show any visible cracks at the beginning of the experiment. The column began to crack at the movement rate of 0.5%. The crack was straight crosswise at this rate. Then the crack began to penetrate to the base of the column, and concrete at the corners begin to peel out at the movement rate of 1.5%, which resulted in 45 degree slope cracking direction, which continued from the crack along with the crosswise reinforcing steel at the movement rate of 2.5%. When the force was further increased, so the movement rate is at 3%-5%, damages began to form at the column's base. The concrete peeled off and resulted in the 45 degrees crack getting grow up. When the column received constant force at the movement rate at 7%, concrete peeled off, thus reinforced steel took all the pressure instead of the concrete and the steel became visibly bent. The bend happened in two areas, the first area was from the column's base to the couplers, and the second was the reinforced steel level 2-3, which has no couplers. The reinforced steel without couplers was more visibly bent because there are no couplers to aid the resistant. The said steel also lost its shape lengthwise, which made them flared out at 135 degrees, and the column collapsed. For this sample, the concrete column has a horizontal movement distance at the yield point of 40.9 mm, the highest horizontal movement is 72.9 mm, and the highest lateral force recorded is 145 kN.

Table 3.7 Experimental results of specimen MS1

MS1	Load (kN)	Displacement (mm)	% Drift
$P_{max}$	138	72.9	3.31%
$0.8 P_{max}$	110	121.0	5.50%

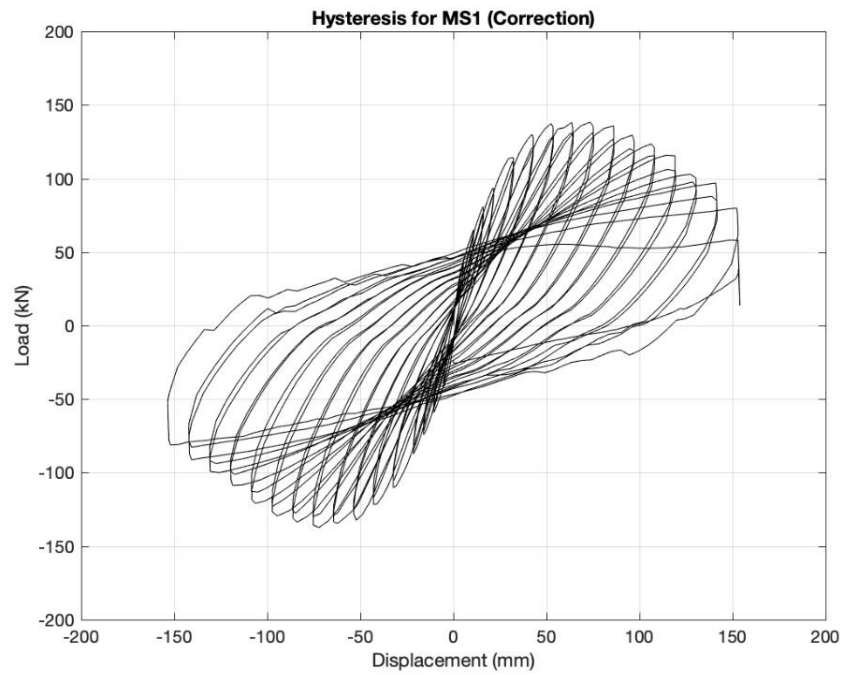


Figure 3.32 Hysteresis of MS1 specimen

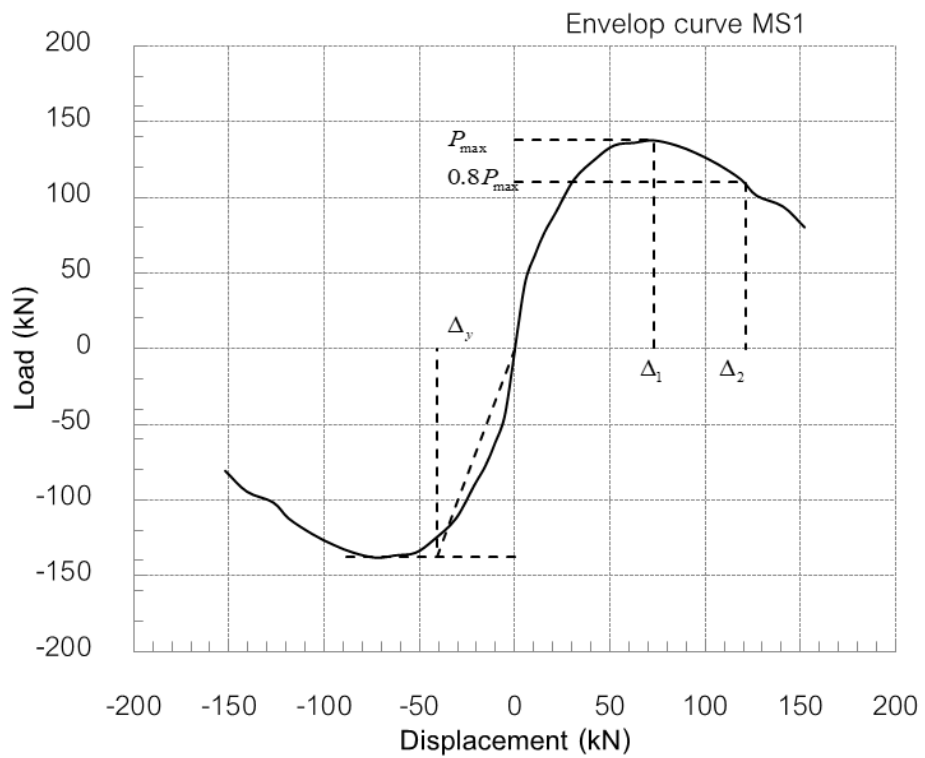


Figure 3.33 Envelop curve of MS1 specimen

### 3.3.3.2 Appearance failure of specimen MS1

The ultimate failure of the column specimen MS1 was mainly due to the buckling of longitudinal steel bars. The buckling mode was different from column specimen NS, as shown in Figure 3.34(c). The buckling of the steel bars was observed at the height of 200 mm. However, the damage in the critical region was observed at the height of 600mm cause shifting of buckling shape into the second level of tie hoop. As a result, the breaking of tie hoop leads to lost lateral load capacity finally.

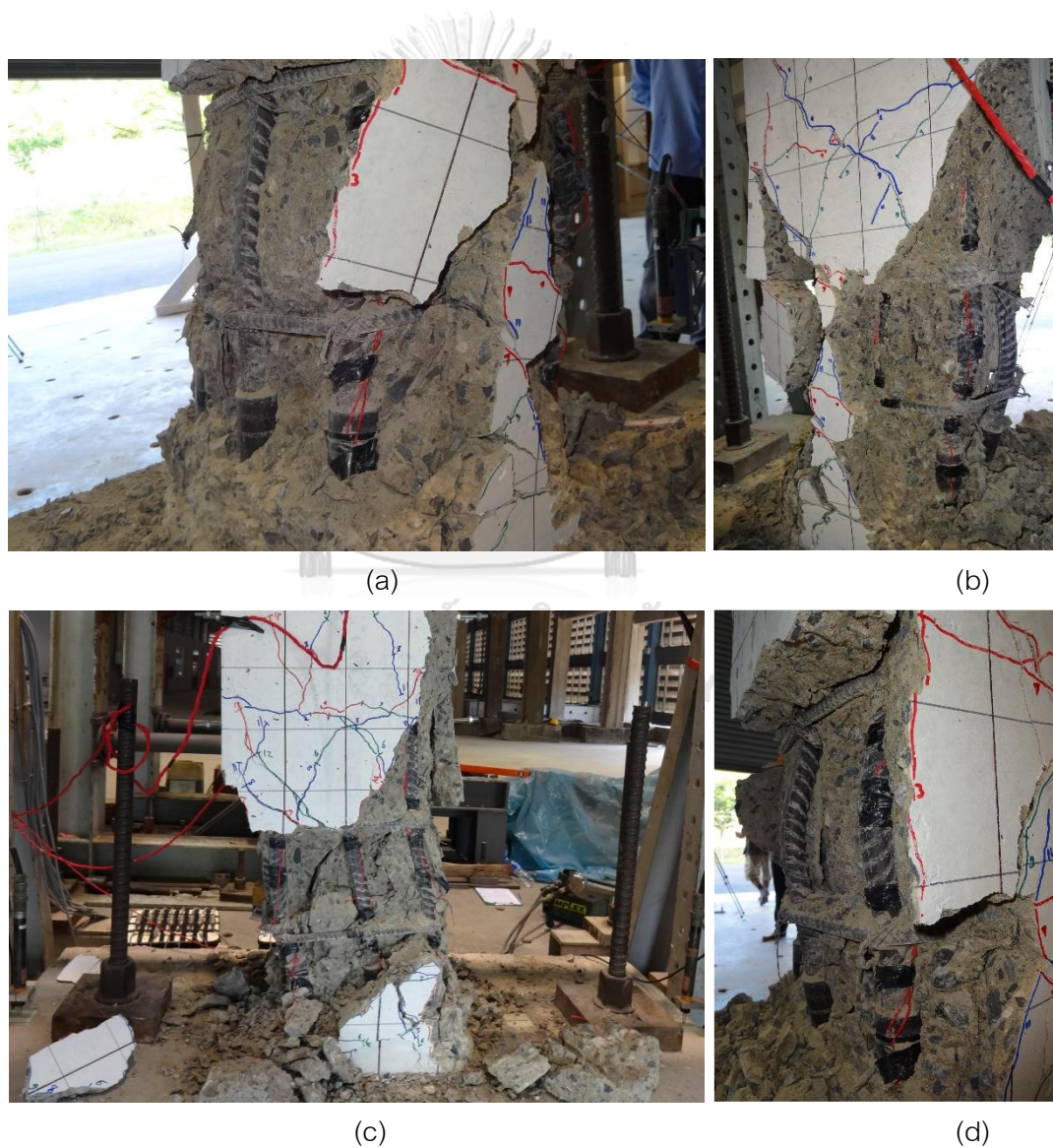
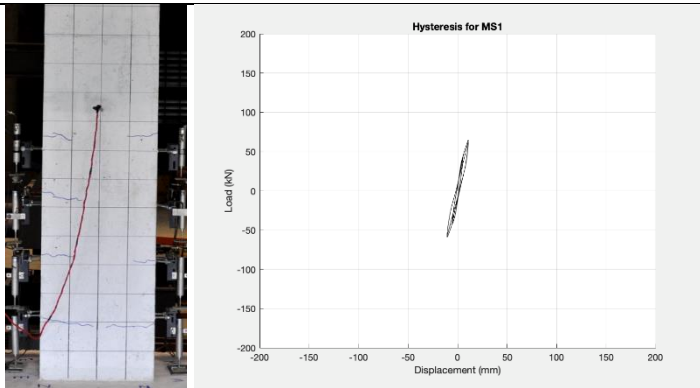
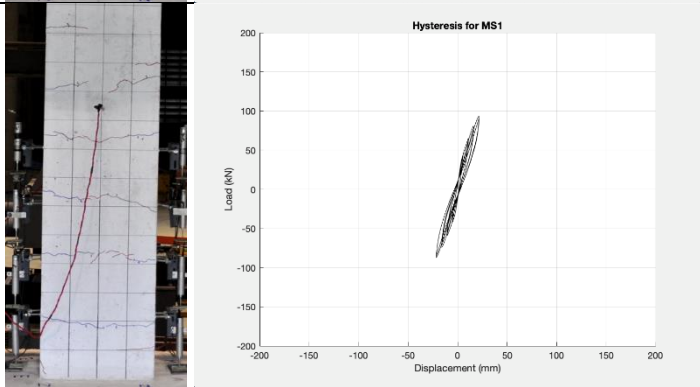
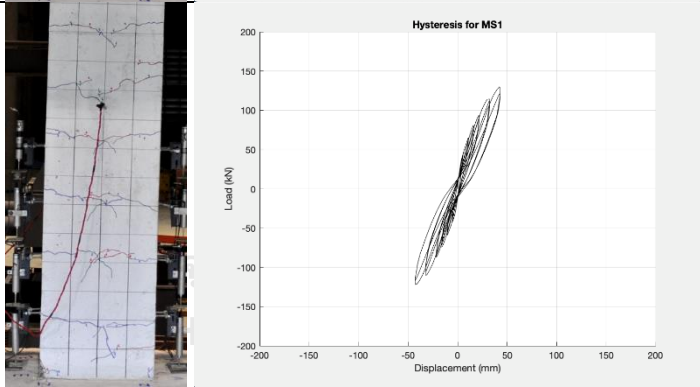
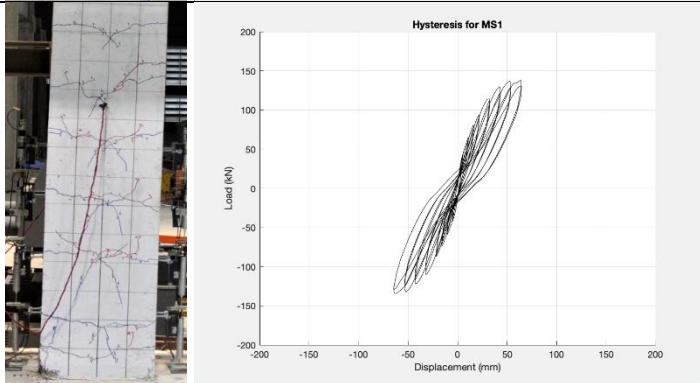
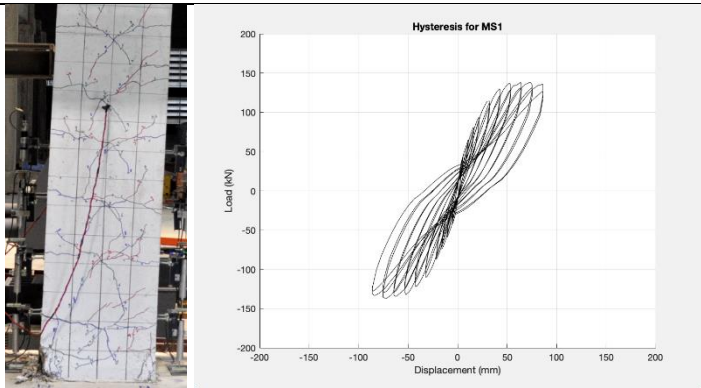
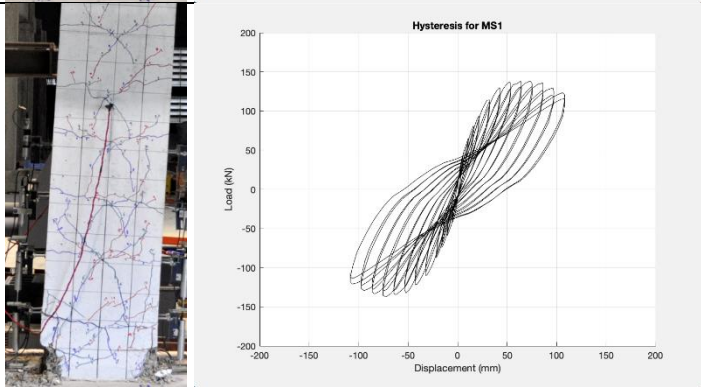
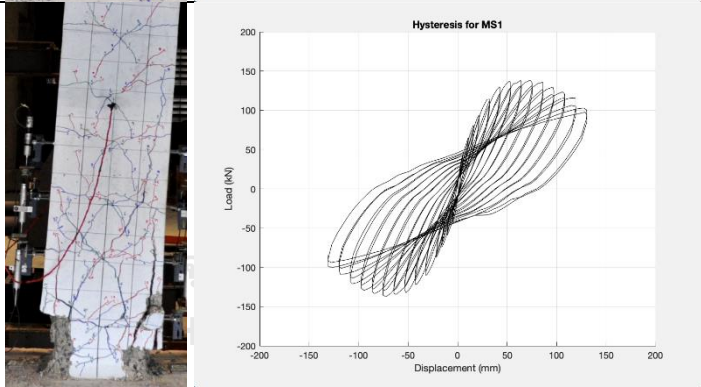
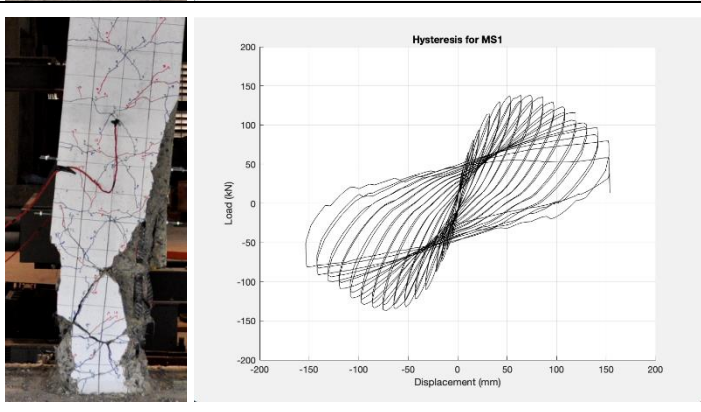


Figure 3.34 Buckling failure of mechanical-splice column specimen MS1

%Drift	Crack pattern and lateral load-displacement	Appearance damage
0.5%		<p>small number of cracks in horizontal direction occur along column with 800 mm height</p>
1.0%		<p>Increase of cracks at 1000, 1200 mm height and crack continuing</p>
2.0%		<p>cracks went toward a 45 degree angle, continuing from the horizontal direction</p>
3.0%		<p>Concrete crushing in corner of column</p>

%Drift	Crack pattern and lateral load-displacement	Appearance damage
4.0%		<p>Concrete more crushing in corner of column</p>
5.0%		<p>cracks went toward a vertical , continuing from 45 degree angle</p>
6.0%		<p>Corner of the column in West spalling can see through the longitudinal reinforcing bar with a mechanical splice</p>
7.0%		<p>Buckling occurs in the longitudinal reinforcing bar between two tie hoops then the concrete spalling in higher along column reasonable to buckling failure</p>

### 3.3.3.3 Strain in Reinforcing steels of specimen NS

Developing to yield strength, shows in strain gage #22 and #23 are measure in the longitudinal reinforcing bar on the corner bar with 50 mm height above footing, shows develop yield strength at the first cycle of 1.5% drift. As shown in In Figure 3.35. The mechanical splices are measured by #25 with above #23 to connecting rebar show coupler sleeve can transfer the force and develop to yield strength at the first cycle of 1.5%.

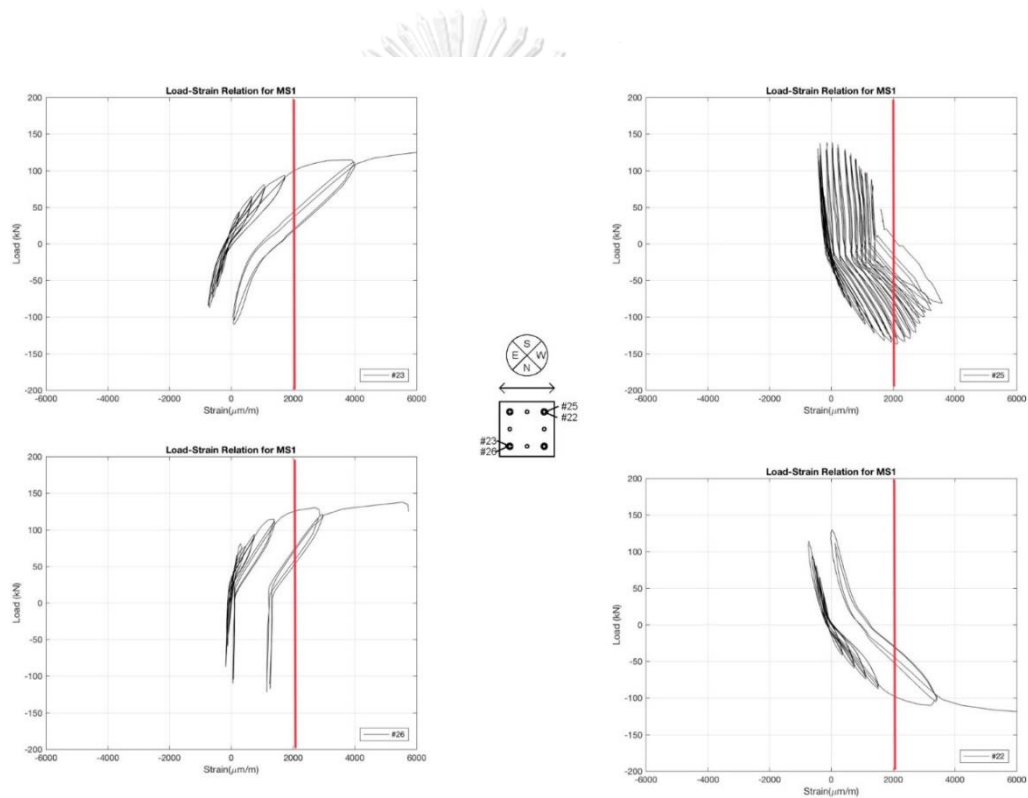


Figure 3.35 Strain in the longitudinal reinforcement of MS1 at level 2

### 3.3.4 Experimental result of specimen MS2

In column specimen MS2, mechanically splices were provided in such a way that that 50% of the mechanical splices were located within the critical region and the rest outside the critical region.

#### 3.3.4.1 Progressive damage of specimen MS2

The column specimen MS2 began to crack at the movement rate of 0.75%, and the crack was straight crosswise at this rate. At the movement rate of 3.5%, the crack began to take a 45 degree slope and the column cracked at the base. The concrete peeled off to the point that both sides of the column were exposed. At 20 cm Height, movement rate of 4%-6%, and horizontal movement force of 6.5%, the column began to show damage at the base. The peeled concrete meant that reinforced steel took all the pressure instead of the concrete and the steel became visibly bent.

Moreover, the concrete began to peel off around the base of the column at the height of 40 cm. The bend started from the base of the column to 40 cm. in height, which resulted in lengthwise reinforced steel bending in two areas. The first area was from the column's base to the couplers and the second was the reinforced steel level 2-3, which has no couplers. The reinforced steel without couplers was more visibly bent because there are no couplers to aid the resistant. However, for the lengthwise reinforced steel extended in the height of 55 cm., the bend only happened in 1 area, which resulted in the secondary steel damaging according to the lengthwise steel's direction. When the steel flared out at 135 degrees, the column collapsed. For this sample, the concrete column has a horizontal movement distance at the yield point of 42.1 mm., the highest horizontal movement is 60.7mm, and the highest lateral force recorded is 145 kN.

Table 3.8 Experimental results of specimen MS2

MS2	Load (kN)	Displacement (mm)	% Drift
$P_{max}$	145	60.7	2.76%
$0.8 P_{max}$	116	119.0	5.41%



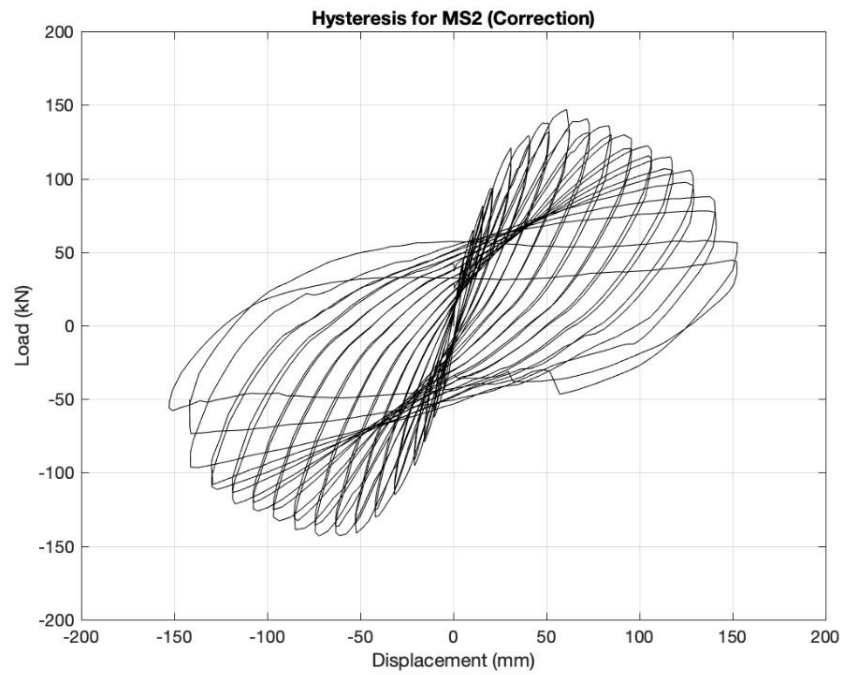


Figure 3.36 Hysteresis of MS1 specimen

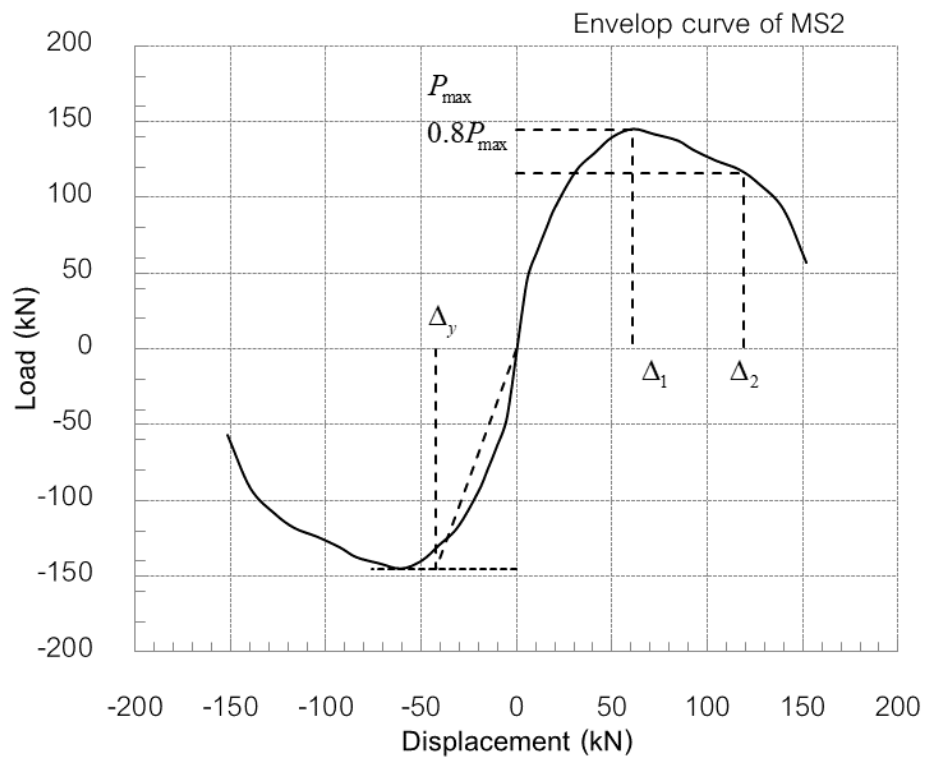


Figure 3.37 Envelop curve of MS2 specimen

### 3.3.4.2 Appearance failure of specimen MS2

The mechanical-splice specimen MS2 was failed by buckling of longitudinal reinforcing bars. The buckling shape was same as NS and MS1, as shown in Figure 3.38(a). The shape of buckling that mechanical splices were located outside the critical region their height, which is 400 mm or 2 of spacing of tie hoops same as NS. For mechanical splices were located within the critical region their height, which is 200 mm or 1 of spacing of tie hoops same as MS1. However, the overall damage in the critical region was damage by 400mm the same as NS. As a result, the breaking of tie hoop leads to lost lateral load capacity finally.

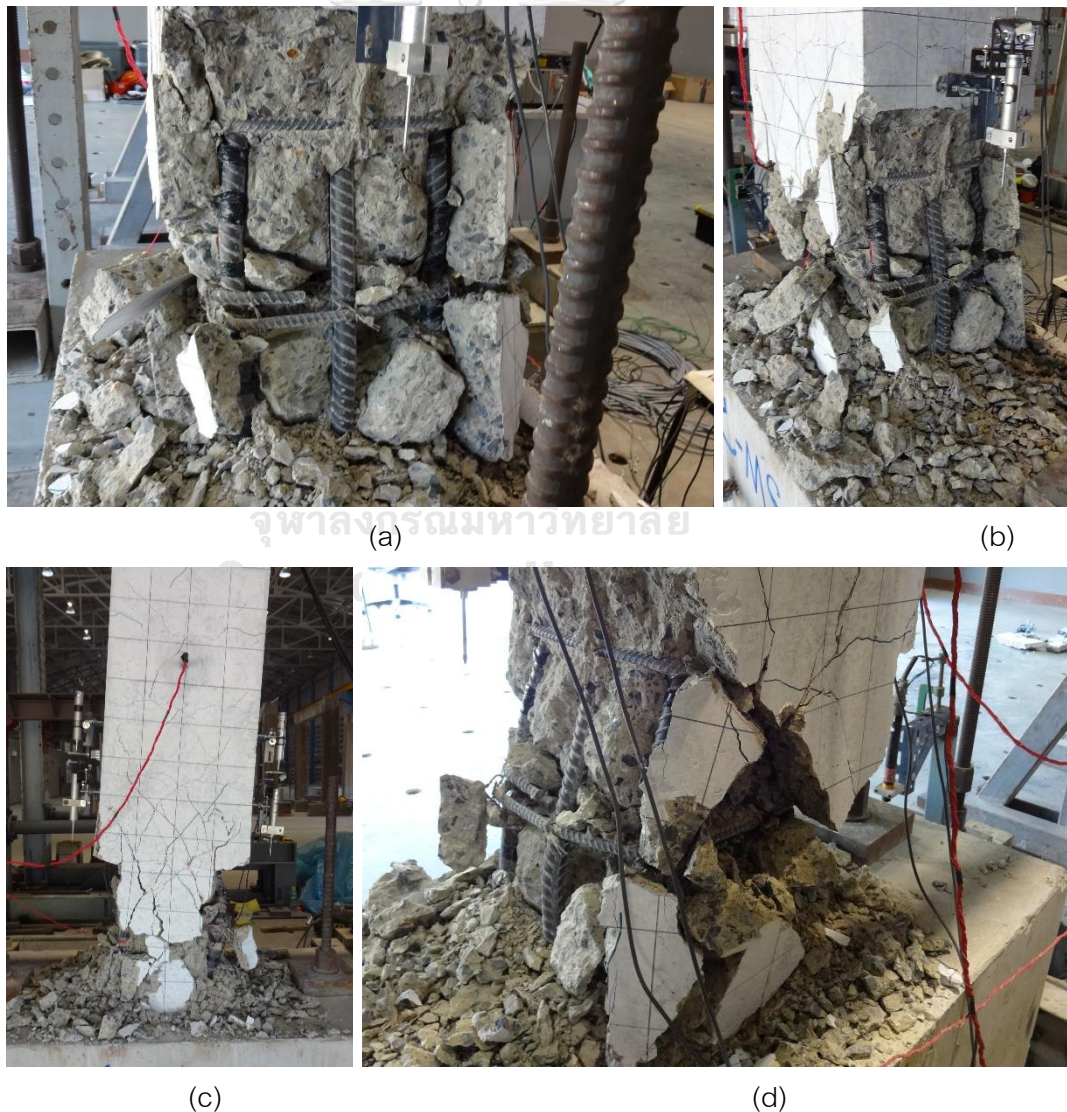
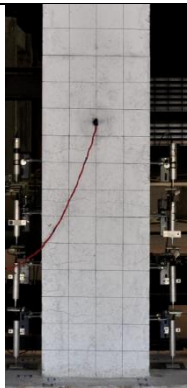
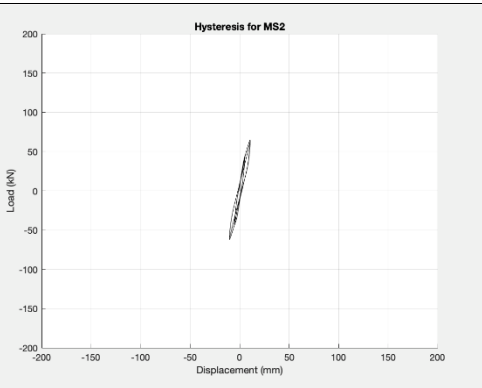
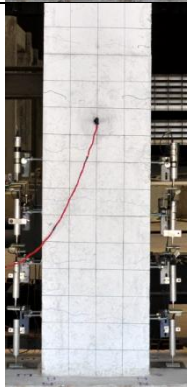
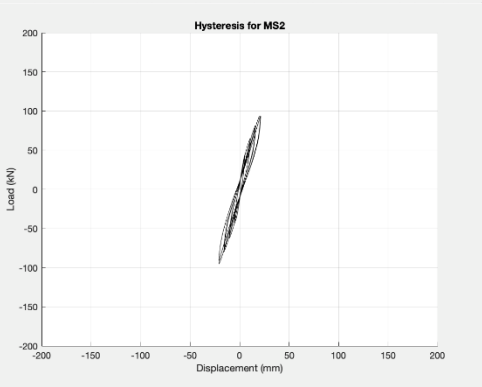
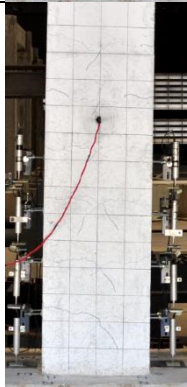
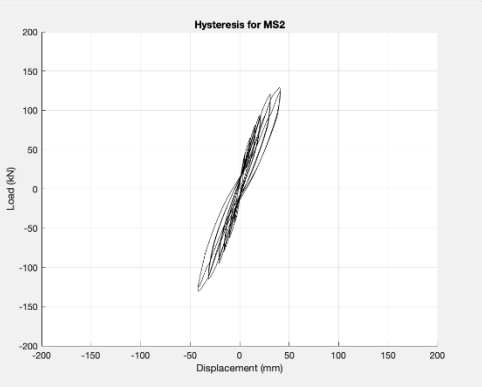
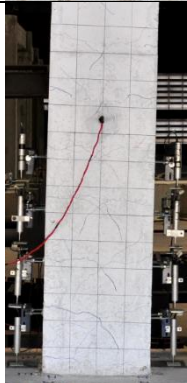
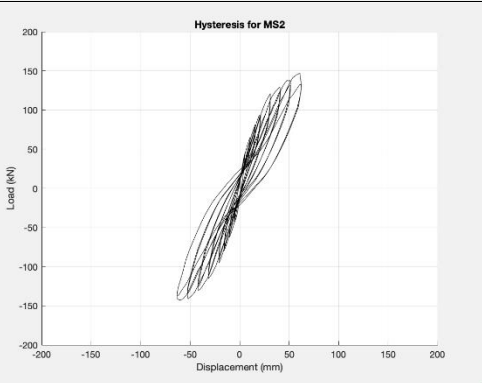
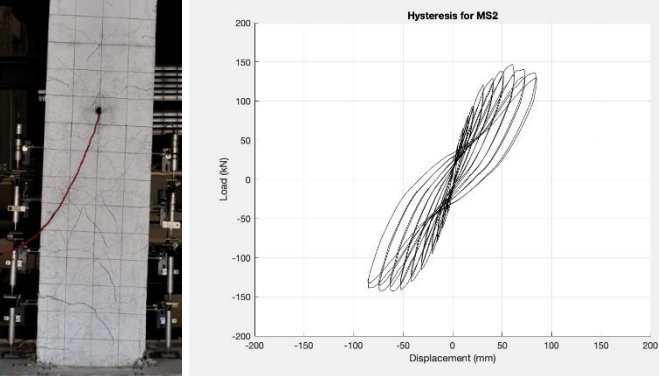
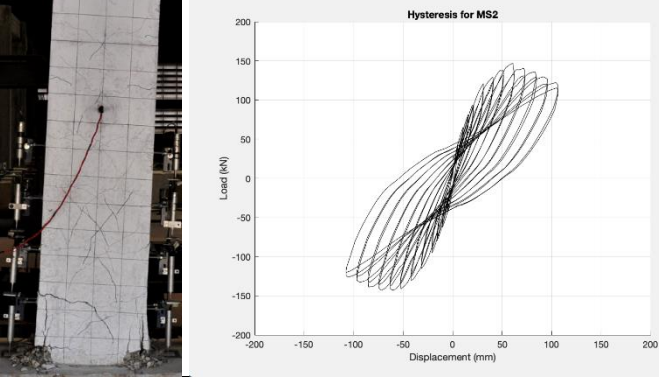
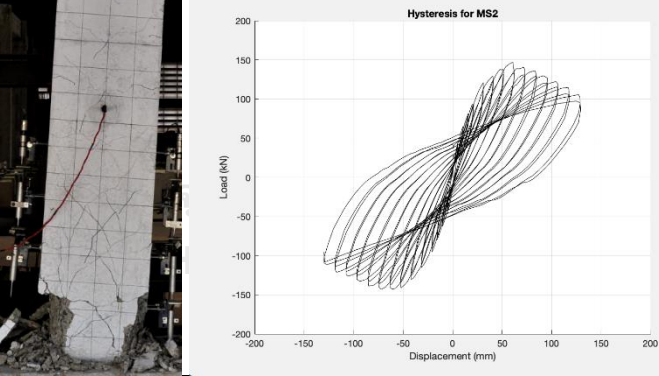
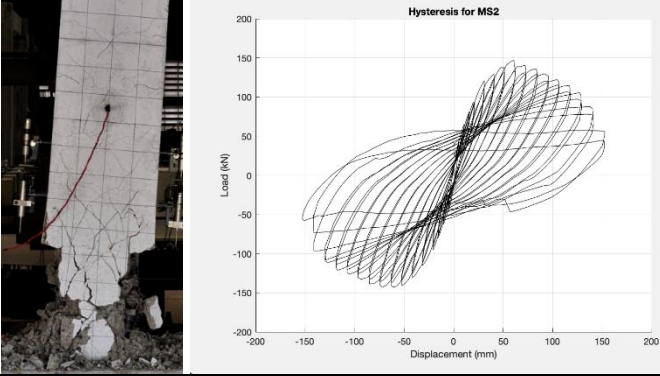


Figure 3.38 Buckling failure of mechanical-splice column specimen MS2

%Drift	Crack pattern and lateral load-displacement	Appearance damage
0.5%	 	<p>small number of cracks after the movement rate reached 0.5% and has a horizontal direction</p>
1.0%	 	<p>Increase number of cracks continuing</p>
2.0%	 	<p>cracks went toward a 45 degree angle, continuing from the horizontal direction</p>
3.0%	 	<p>Concrete crushing in the corner of column and cracks went toward a vertical, continuing from 45 degree angle</p>

%Drift	Crack pattern and lateral load-displacement	Appearance damage
4.0%		Concrete spalling along vertical crack
5.0%		Buckling occurs in the longitudinal reinforcing bar between two tie hoops
6.0%		Tie hoop failure by the bar end of tie hoop are open cause the column lost the shear strength reasonable to shear crack happen instantly
7.0%		The second tie hoop are break off cause the column lost the shear strength reasonable fail finally

### 3.3.4.3 Strain in Reinforcing steels of specimen MS2

Mechanical splice with reinforcement shows the result of developing to yield strength. Strain gage #23 and #24 are measure in longitudinal reinforcing bar anchored into the footing and popped up to overlap with the other bar to column top. Place on the corner bar with 50 mm height above footing, shows develop yield strength at the first cycle of 1.5% drift. As shown in Figure 3.39. The force transfer by coupler to the third level measure by #33, #34 found the rebar yield in at the first cycle of 1.5% drifts same as below level. For coupler outside the critical region was placed in fourth level measure by #42 and #44 on coupler shows behavior to develop yield strength at the first cycle of 1.5% drift.

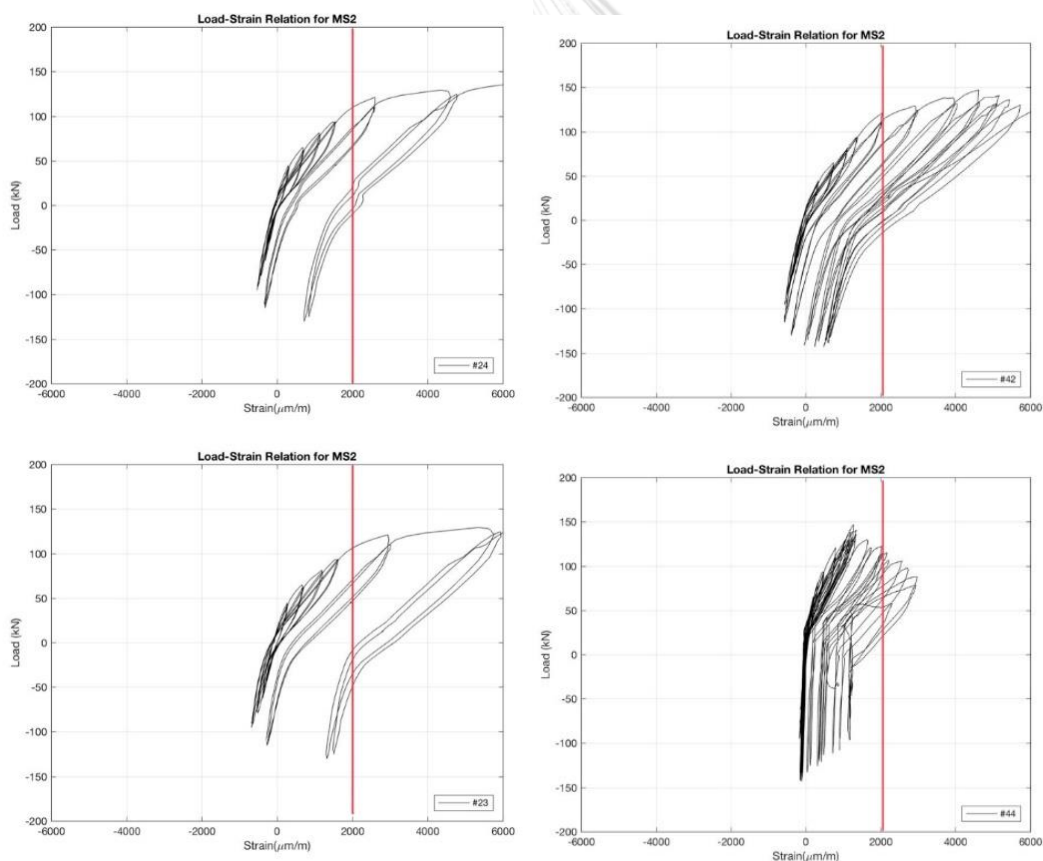


Figure 3.39 Strain in the longitudinal reinforcement of MS2 at level 2 and the coupler level 4

### 3.3.5 Comparison between column with and without splices reinforcement

Experimental results in terms of ductility, average curvature, lateral strength degradation and energy dissipation are briefly discussed and compared in the following sections. .

#### Displacement ductility

Ductility and toughness as defined by Sheikh and Thomas [47] are adopted to evaluate the lateral performance of RC columns. Ductility and toughness can be determined through displacement ductility factor  $\mu_{\Delta}$  which can be calculated as

$$\mu = \frac{\Delta_2}{\Delta_1}$$

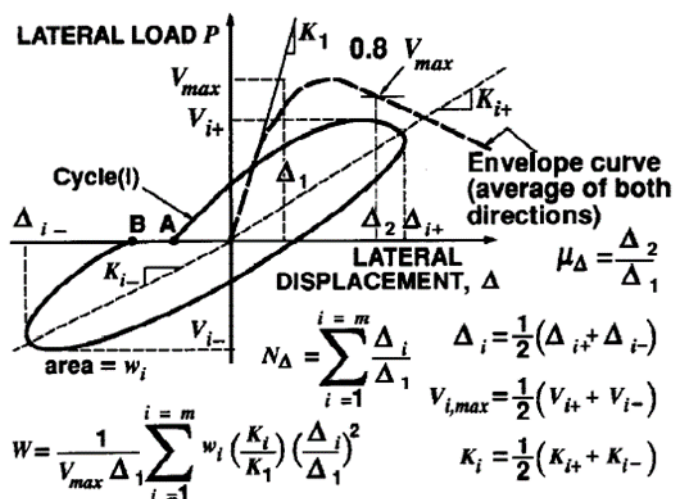


Figure 3.40 Section ductility factors element (Sheikh et al., 1994)

Lateral load versus displacement of columns with and without splices reinforcement were plotted to evaluate the overall response of the specimens in terms of envelope curve, and ductility of the specimens. Lateral load versus displacement curves of the column specimens are shown in Figure 3.41 to Figure 3.42.

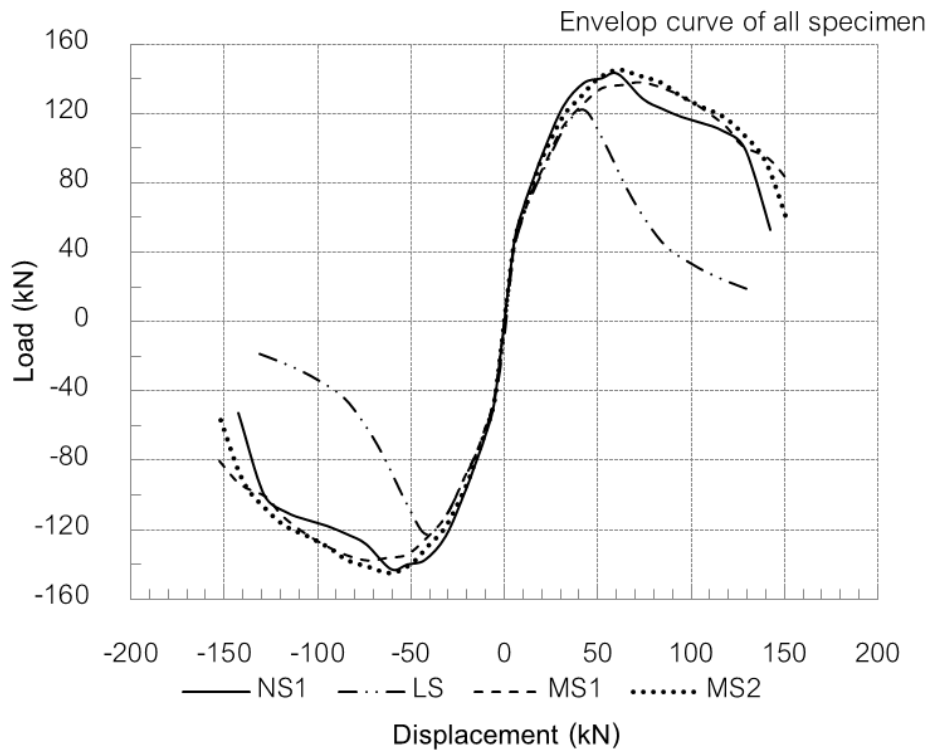


Figure 3.41 Envelop curve of all specimen

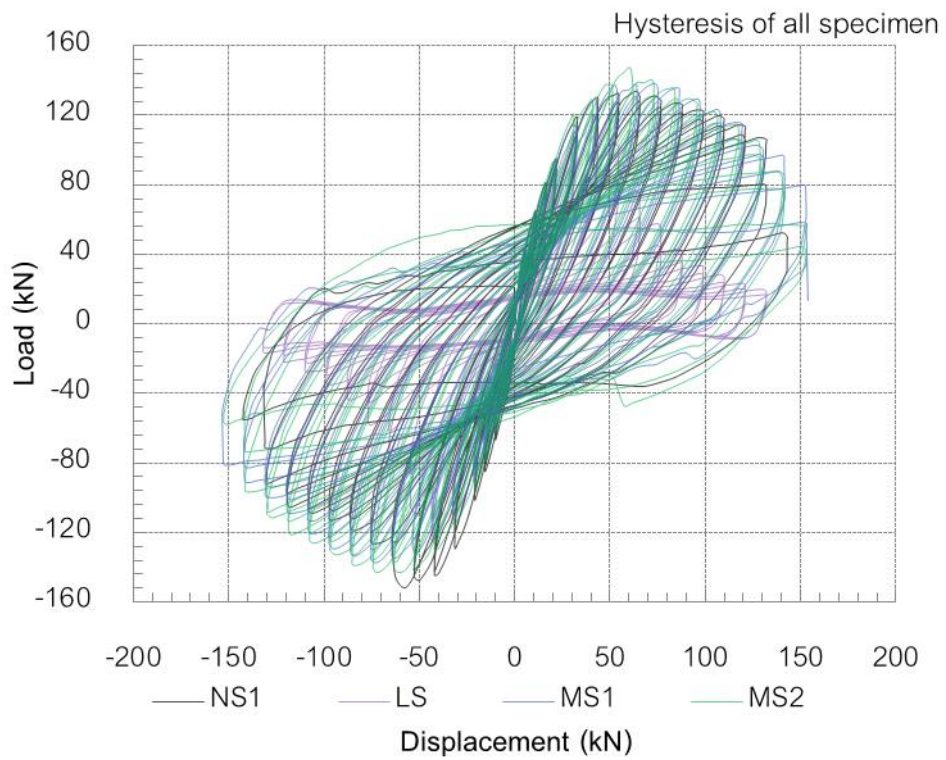


Figure 3.42 Hysteresis of all specimen

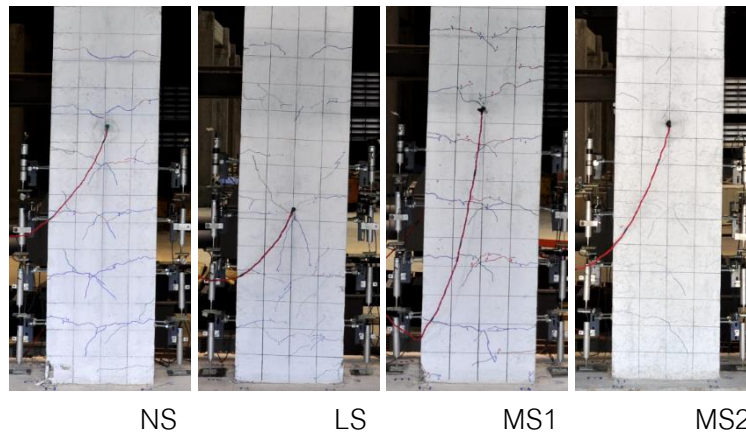


Figure 3.43 Damage state at 2.0% drift.

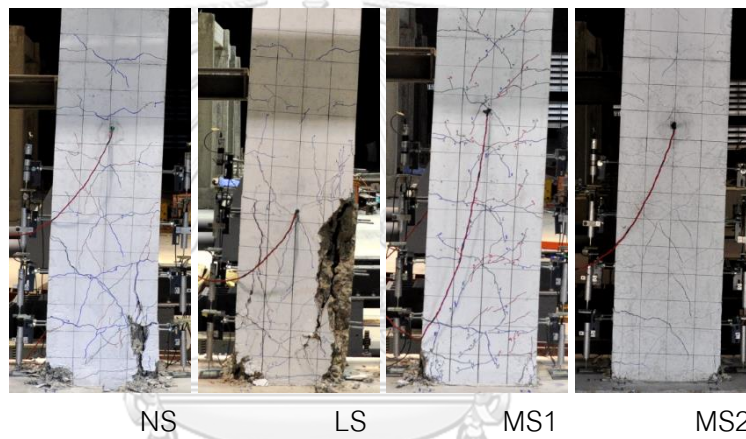


Figure 3.44 Damage state at 4.0% drift.

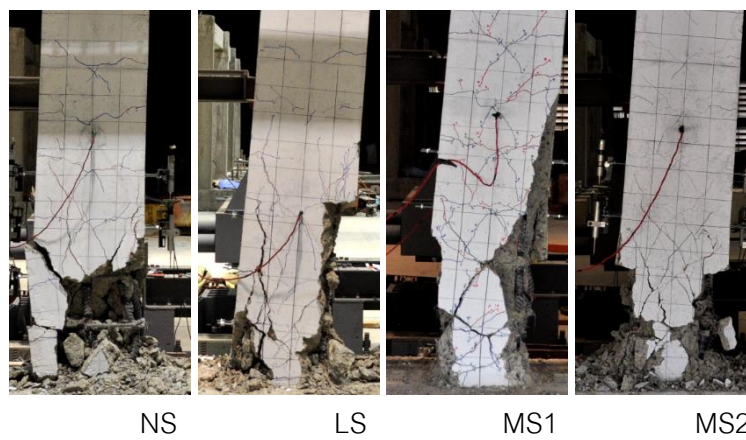


Figure 3.45 Damage state at failure



Table 3.9 Experimental results of lateral load capacity and displacement ductility of all specimen

Specimen	$P_{max}$	Disp@ $P_{max}$	$0.8 P_{max}$	Displ@ $0.8P_{max}$	Disp@75% secant	Ductility	Initial stiffness (kN-mm)
NS	143	60.7	114	109.0	29.5	3.69	8.76
LS	122	41.9	98	55.8	35.3	1.58	6.10
MS1	138	72.9	110	121.0	40.9	2.96	8.37
MS2	145	60.7	116	119.0	42.1	2.83	8.72

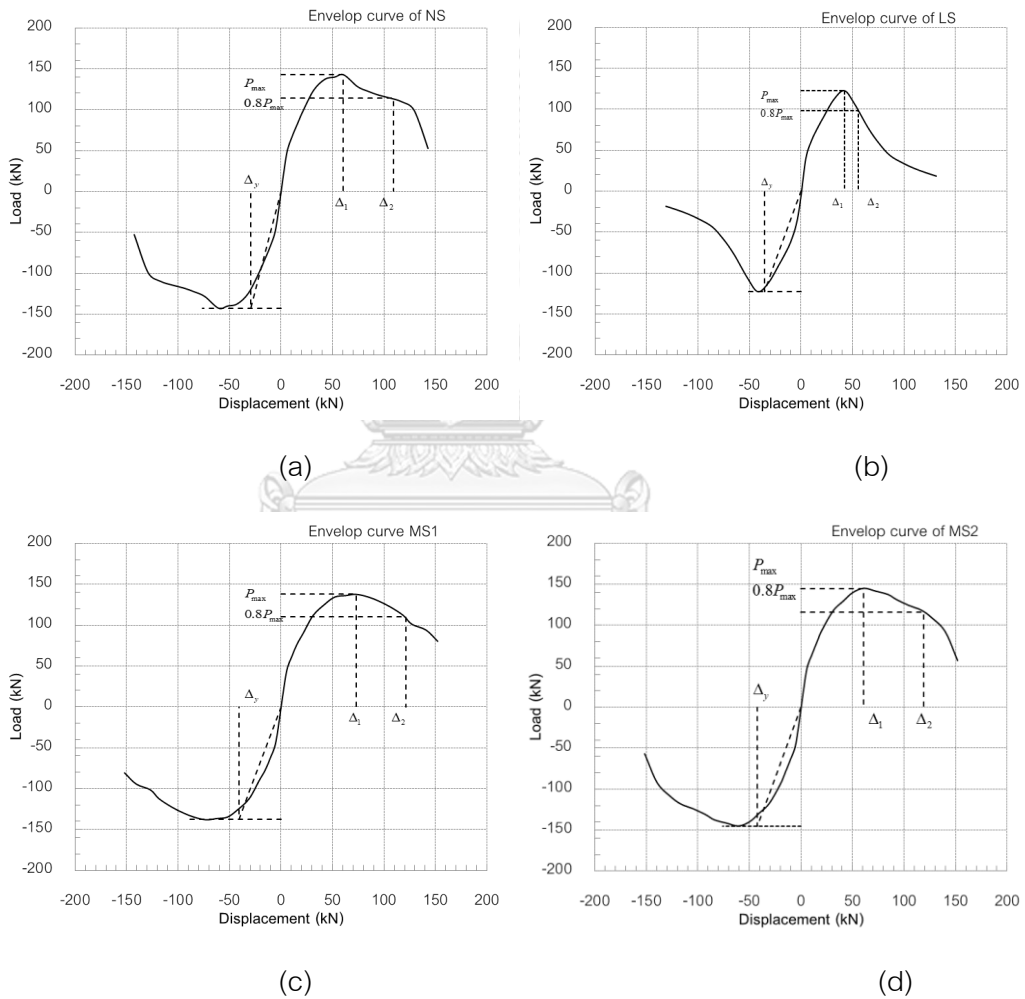


Figure 3.46 Envelop curve of (a) NS, (b) LS, (c) MS1 and (d) MS2

### 3.3.5.1 Moment-curvature distribution

For calculation, the curvature of the column was divided into segments. Curvature between any two segments is calculated as the difference between the measurements of vertical transducers attached on the sides of each segment divided by the product of the horizontal and vertical dimensions of each segment. The reinforcement detailing of all specimens with the curvature measurement levels are shown in Figure 3.47 to Figure 3.50. Moment curvature distribution indicates the bending force distribution to the section of column height. The trend moment curvature distribution is found similar to the trend of energy dissipation. In non-spliced RC column (NS), curvature is concentrated in the region of 400 mm where the maximum moment occurred. For the specimen with mechanical splice moment curvature distribution is found close to column specimen NS. Whereas in case of lap-splices specimen (LS) moment curvature distribution is concentrated in the region 200mm above the base for columns. Maximum curvature is concentrated in the region just above the lap-splices due to the crank portion of longitudinal reinforcement. Also, depicting that rotation at that location is higher than at the base after bond failure.

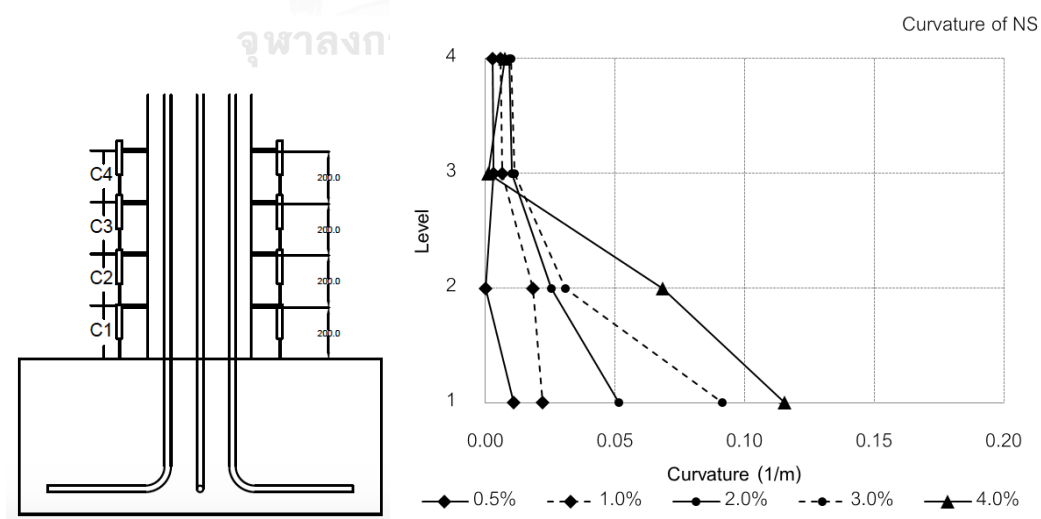


Figure 3.47 Curvature distribution on the specimen NS

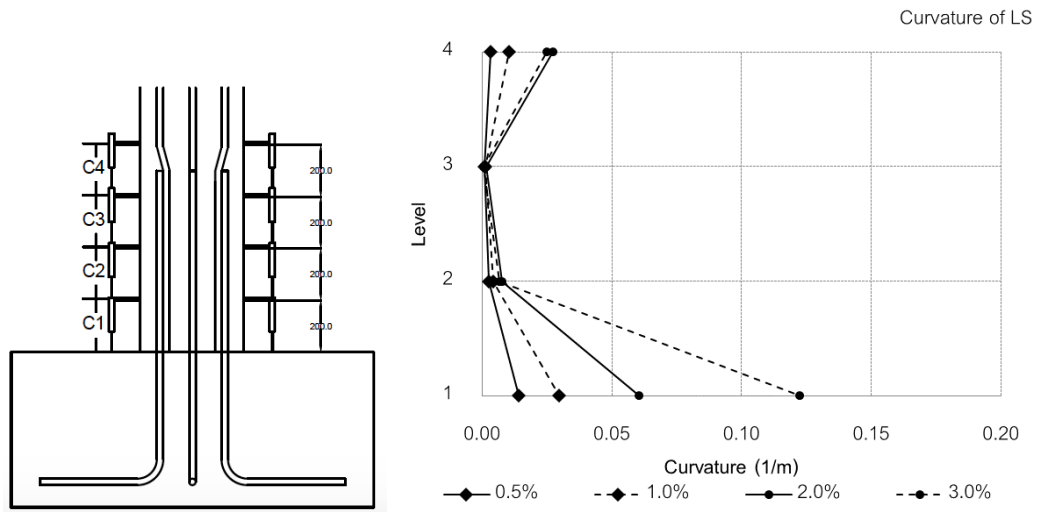


Figure 3.48 Curvature distribution on the specimen LS

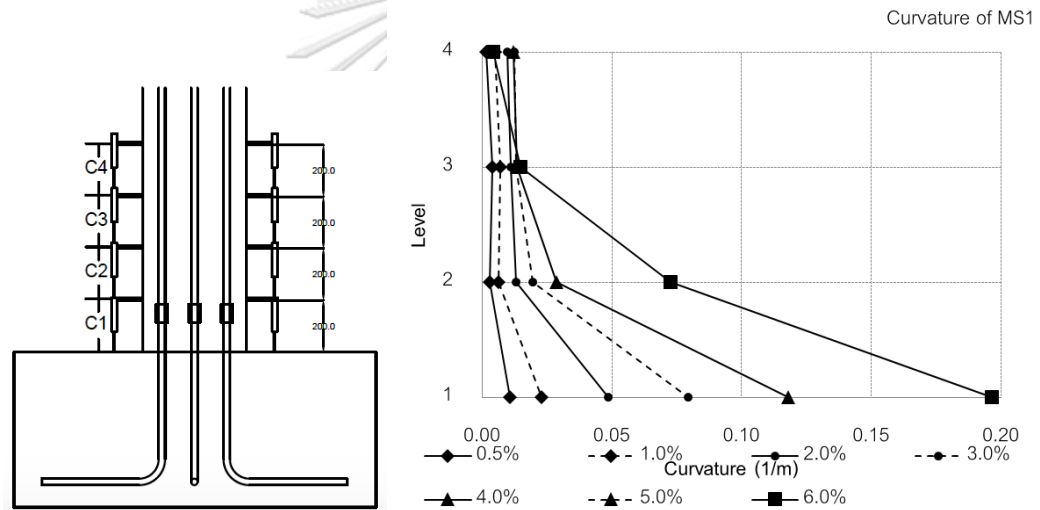


Figure 3.49 Curvature distribution on the specimen MS1

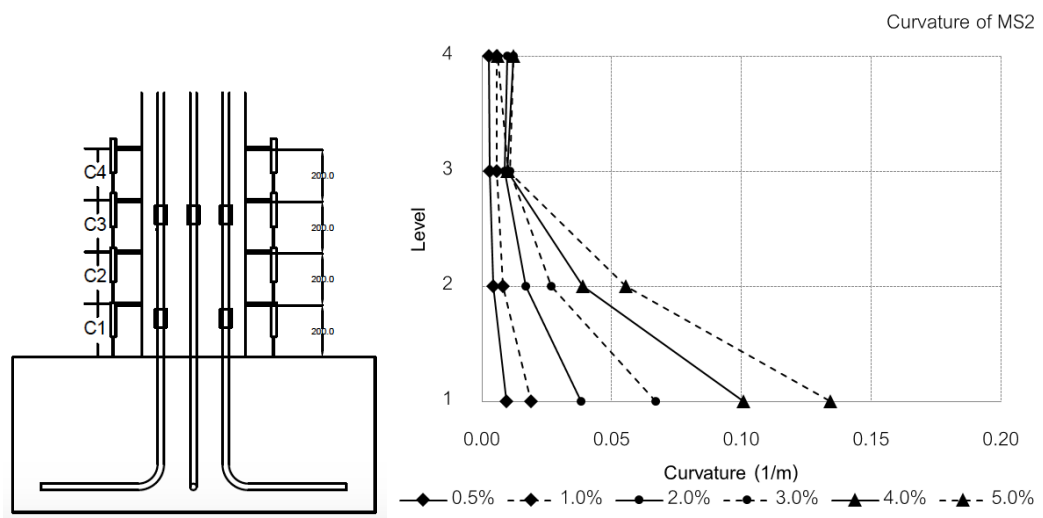


Figure 3.50 Curvature distribution on the specimen MS2

### 3.3.5.2 Distribution of column section rotation

To understand the column deformation deeply. Rotation is a value that indicates the bending force distribution along the column height. As results are in accordance with the result of displacement ductility for all specimens. There is an interesting observation that the rotation of lap-splices specimen (LS) is concentrated in the region 200mm above the base for columns. Maximum rotation is concentrated in the region just above the lap-splices due to the crank portion of longitudinal reinforcement. Further, it is found that rotation at that location is higher than at the base after bond failure. One reason for this behavior is that rotation due to yield penetration of the starter bar is far less than the rotation due to lap-splices. In case of column specimen without lap splices (NS), curvature is concentrated in the region of 400 mm where the maximum moment occurred. For the specimen with mechanical splice, curvature is close to the columns specimen NS.

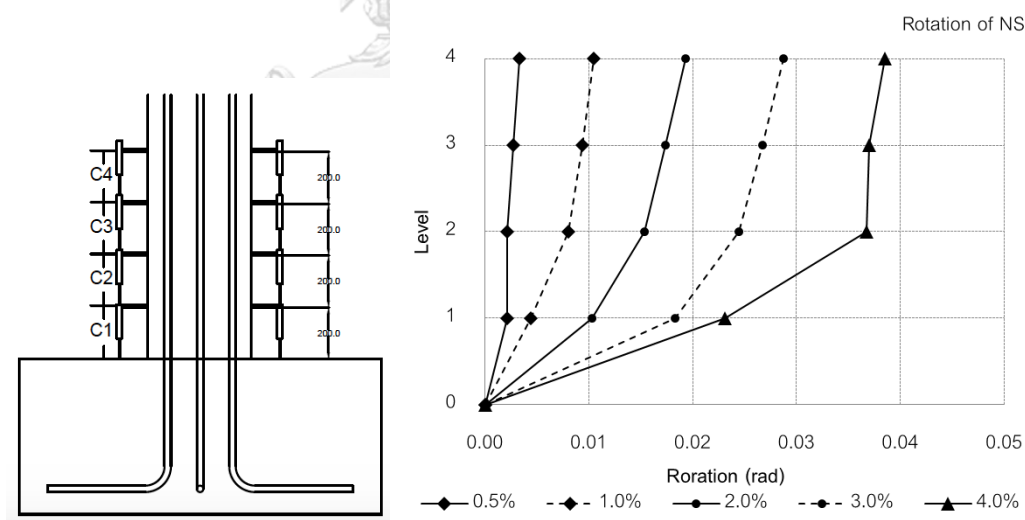


Figure 3.51 Curvature distribution on the specimen NS

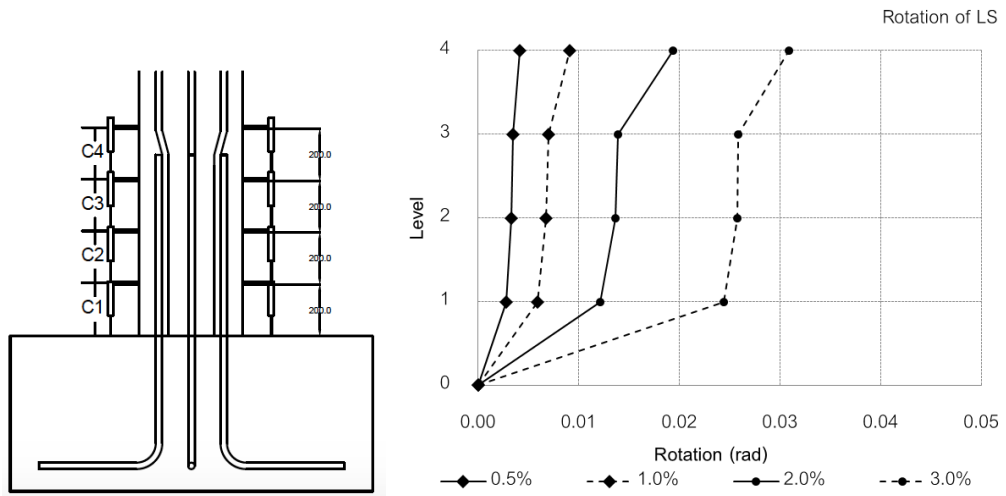


Figure 3.52 Curvature distribution on the specimen LS

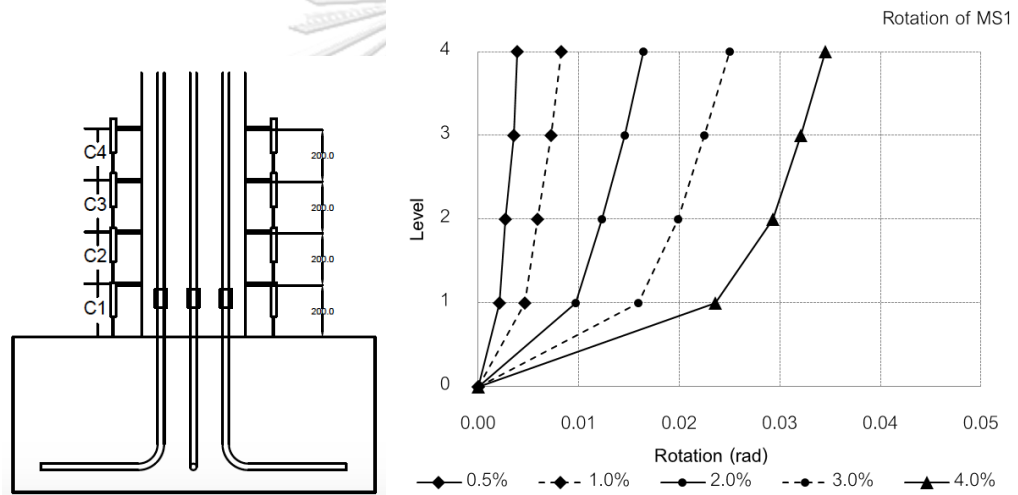


Figure 3.53 Curvature distribution on the specimen MS1

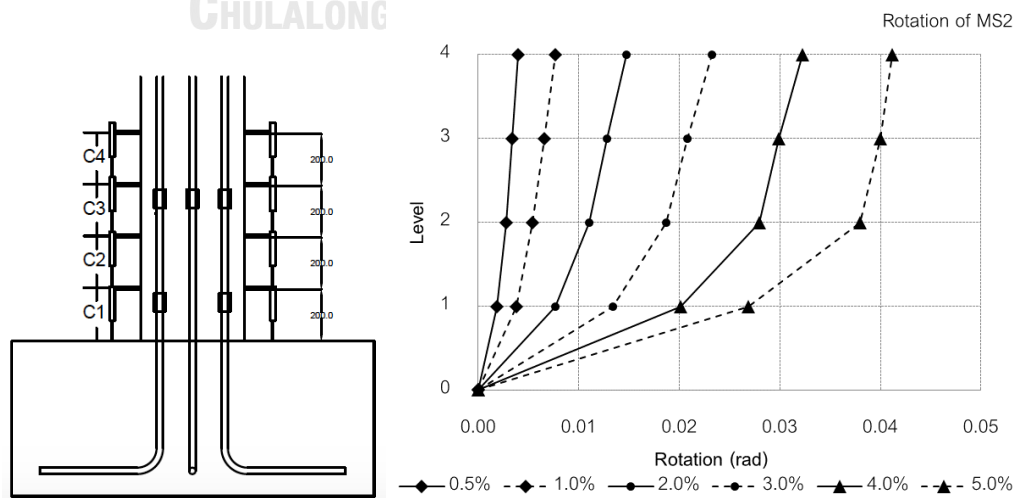


Figure 3.54 Curvature distribution on the specimen MS2

### 3.3.5.3 Energy dissipation

The energy absorbed is the difference between the lost energy. Energy dissipation defined as dissipated in one cycle is the area under the cycle of loading of load-displacement. In this study, energy dissipation was calculated using the numerical method (Trapezoidal rule). The structural components with adequate energy dissipation may perform well during earthquake activity with less or minor damage. The cumulative hysteretic dissipation energy was calculated by using the following expression.

$$Area = \frac{1}{2} \sum_{i=1}^n (y_{i+1} + y_i)(x_{i+1} - x_i) \quad (3.1)$$

$$Energy\ dissipation = \frac{1}{2} Fd \quad (3.2)$$

Where:  $F$  is the lateral force (kN)

$d$  is the displacement of the cycle (mm).

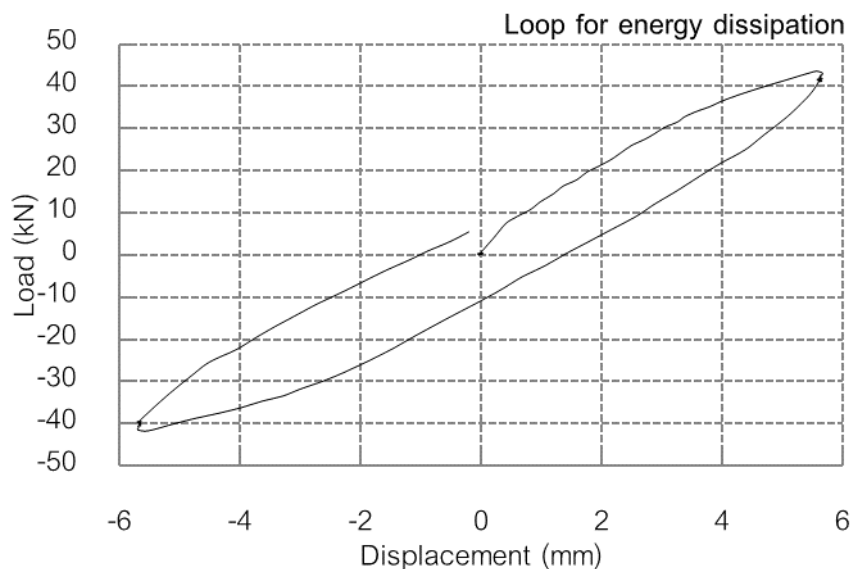


Figure 3.55 Loop for energy dissipation

The energy dissipation of RC columns is compared in this section. As expected, the specimen LS exhibited the lowest energy dissipation. At the 2.0% drift, the LS column reached the maximum lateral load, a vertical crack developed along with lap splice, and the energy dissipation was about 14 kN-m. Until 2.5% drift, the dissipation energy of their specimens was not entirely different. On the other hand, after the 3.0% drift cycle, the energy dissipation trends were different. After a 3.0% drift, the LS cannot dissipate the energy anymore because the specimen failed by laps splice failure. However, the dissipation of the energy capacity of NS, MS1 and MS2 were 34 kN-m, 29 kN-m and 31 kN-m, respectively. The energy dissipation capacity of NS more increased significantly after a 3% drift than MS1 and MS2 columns. The comparison of MS2 had a slightly higher energy dissipation capacity and this can be the effect of a lower amount of mechanical splice in the plastic hinge region. At a 6.0% drift cycle, MS1 reached the 191 kN-m energy dissipation capacities, whereas the ms2 dissipated the energy of about 199 kN-m. On the other hand, the energy dissipation capacity of MS2 was nearly 4% higher than that of MS1. The cumulative dissipated energy for all specimens is compared as shown in Figure 3.56.

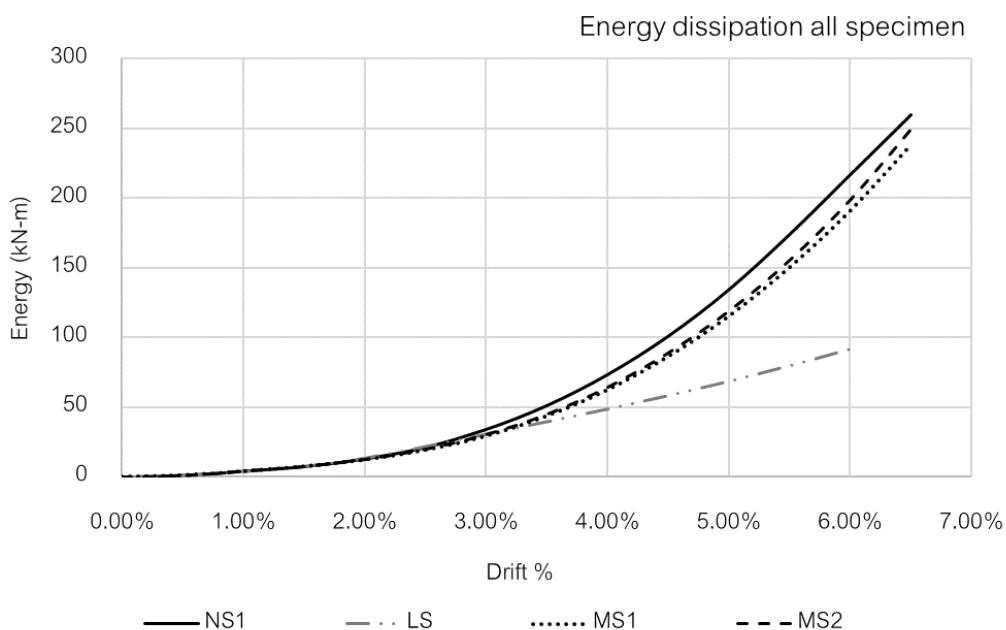


Figure 3.56 Cumulative energy dissipation of all specimens

Table 3.10 Cumulative energy dissipation of all specimens

	NS1	LS	MS1	MS2
Drift %	Cumulative energy dissipation (kN-m)			
0.00%	0	0	0	0
0.25%	0	0	0	0
0.50%	1	1	1	1
0.75%	2	2	2	2
1.00%	4	4	4	4
1.50%	8	8	7	8
2.00%	13	14	12	13
2.50%	21	22	19	20
3.00%	34	31	29	31
3.50%	51	40	43	45
4.00%	74	49	62	64
4.50%	101	58	86	89
5.00%	135	68	115	119
5.50%	174	80	150	156
6.00%	217	92	191	199
6.50%	260		238	250



#### 3.4 Discussion of the column with and without splice reinforcements

- The experimental results indicate different types of failure modes of RC columns. In case of RC column LS in which traditional lap splice was provided, the ultimate failure is mainly observed due to the slip of the bar at the lap-spliced location. Whereas in case of non-spliced RC column NS and mechanically spliced columns, the ultimate failure is observed due to the buckling of the vertical steel bars.
- A comparison of the hysteresis curves of all RC columns indicate that RC column with traditional lap splice resulted in lowest ductility as compared with the Non-spliced and mechanically spliced columns. In case of column LS, there is found a sudden drop in the load carrying capacity after peak strength. The hysteresis curves of non-spliced column and mechanically spliced columns are almost identical. However, initial stiffness and ductility of the mechanically spliced columns is found lower than the non-spliced column.
- Similar to the ductility, the cumulative energy dissipation of the traditionally lap spliced columns is observed very low as compared with the non-spliced and mechanically spliced RC columns. Further, the cumulative energy dissipation of the mechanically spliced RC columns is recorded lower than the non-spliced RC column.

## CHAPTER 4

### NUMERICAL MODELLING OF REINFORCEMENT CONCRETE COLUMNS

This chapter is all about the modelling of reinforced concrete bridge column about introducing all the related parameters for the modeling. Two modeling strategies were applied to the numerical simulation of the splice reinforcement column by using mechanical splice and lap splice. All models were built using the most appropriate computational program OpenSees since it is proved by many researchers to be the most suitable program for nonlinear dynamic analysis. Before analyzing the splice reinforcement column, the analytical model of the non-splice column was a correlation with the experimental results of NS columns that were used to specify in order to make basic model.

#### 4.1 Cyclic behavior of reinforcing bar and mechanical splice

##### 4.1.1 Mechanical splice system

The threaded mechanical splice system consists of male and female threaded steel collars that join bar segments with deformed heads, which enlarge the bar end via a patented cold forging process. The force transferring mechanism of compression the core diameter of bar is increased to a predetermined diameter, then threading mechanically through the threaded bar end as shown in Figure 4.1. The force transferring of compression is transmitted directly through deformed heads and tension through the threaded collars. The threaded mechanical splice system assembles, an initial torque of the threaded collars of approximately 200 N-m is needed, as specified by Bartec® Dextra and in accordance with building design codes ACI 318-02 with type 2 of couplers suitable for seismic areas.

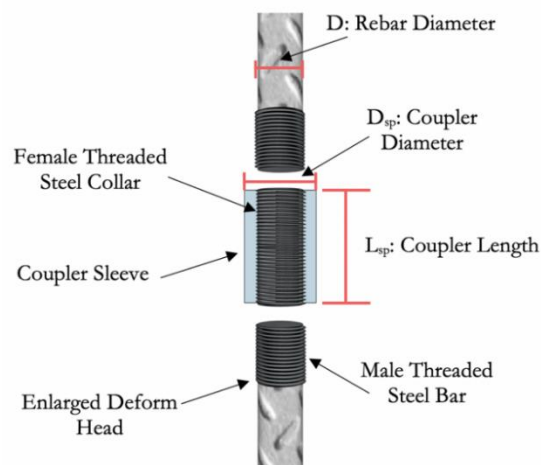


Figure 4.1 Schematic of parallel-threaded mechanical splicing system

#### 4.1.2 Study on mechanical splice behavior [46]

The reinforcing bar with and without threaded mechanical splices was investigated. The experimental program consisted of reinforcing deformed bar with a diameter of 20, 25, and 32 mm are made in accordance with SD40 with Thai Industrial Standards (TIS24-2548(2005)). The average of three tests was used to obtain typical tensile stress for each bar size. The effect of unsupported L/D subjected to compression test were performed at a range of L/D equal to 10, 12, and 16 for cyclic load was performed a range of L/D equal to 10 and 16 and the reinforcing bar diameter of 20, 25, and 32 mm for compression test and 25 and 32 mm for cyclic test, respectively, as shown in Table 4.1

The material properties of bars from the tensile stress–stress curve are summarized in Table 4.2. The average tensile yield strength ( $f_y$ ) of deformed bar with a diameter of 20, 25, and 32 mm are 407, 498, and 473 MPa, respectively. The ultimate tensile strength ( $f_u$ ) is 625, 639, and 622 MPa, respectively. The effect of the diameter in the tensile test result of reinforcing bar is a specific property from factory production.

Table 4.1 Parametric of experimental.

Specimens ID	DB20	MS20	DB25	MS25	DB32	MS32
D: Rebar Diameter (mm)	20	20	25	25	32	32
$D_{sp}$ : Coupler Diameter (mm)	-	32	-	41	-	50
$L_{sp}$ : Coupler Length (mm)	-	54	-	70	-	80
L/D	Compression		10, 12, 16			
L:	L/D = 10	200	250	320		
Unsupported	L/D = 12	240	300	384		
length (mm)	L/D = 16	320	400	512		

\*deformed bar denoted in the following as DB20, DB25, and DB32, coupler denoted in the following as MS20, MS25, and MS32, respectively

#### 4.1.2.1 Test Setup and loading protocols

All specimens were tested in the laboratory of Chulalongkorn University, Thailand, using Instron® 1000kN servo-hydraulic controlled universal testing machine. The loading of monotonic is carried out under displacement-controlled, according to the American Society for Testing and Materials (ASTM A1034). Test setups simulated the longitudinal reinforcing bar with tie hoop to restrain the support, as shown in Figure 4.2. The unsupported length was measured as the distance between the load frame grips of the universal testing machine. The strain was measured directly using a digital extensometer mounted with 200 mm for the gauge length at the mid-height of the specimen. The average strain measured by three linear variable differential transducers were used to measure axial displacements. Strain gauges were not employed due to local strains measured over a gauge length and the absence of actual physical meaning after the initiation of bar buckling.

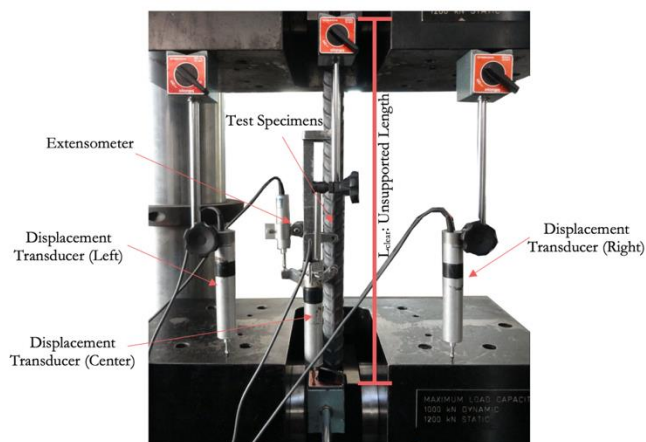


Figure 4.2 Uniaxial test setup

#### 4.1.2.2 Test results and discussions

A summary of test results is provided in Table 4.2, along with the measured material properties for reinforcing bar with and without a mechanical splice. The specimens with a mechanical splice in the compression test lead to a delay postyield softening branch in compression, which strongly influences the cyclic behavior of the bar. The high ratio between of unsupported L/D ratio shows load-carrying capacity dropped rapidly with increasing strains. [48] [49] and [50] reported that the inelastic buckling behavior of a reinforcing bar was very sensitive to unsupported L/D ratio.

Table 4.2 Tensile and compressive properties of deform bar and coupler specimens.

ID	Tensile property					Compressive property					
	Elastic region			Inelastic region		Unsupported length to bar diameter (L/D) ratio					
	Yield strength (MPa)	$\epsilon_y$	E (GPa)	Ultimate strength $f_u$ (MPa)	$\epsilon_{sh}$	10		12		16	
					Stress <sub>max</sub> (MPa)	Strain at Stress <sub>max</sub>	Stress <sub>max</sub> (MPa)	Strain at Stress <sub>max</sub>	Stress <sub>max</sub> (MPa)	Strain at Stress <sub>max</sub>	
DB20	407	0.0020	203	0.0120	625	405	0.0048	413	0.0049	402	0.0031
DB25	498	0.0025	197	0.0075	639	517	0.0051	474	0.0044	490	0.0039
DB32	473	0.0024	193	0.0124	622	472	0.0073	473	0.0043	450	0.0036
MS20	408	0.0032	127	0.0096	653	488	0.0115	405	0.0048	403	0.0068
MS25	501	0.0045	109	0.0075	642	585	0.0201	479	0.0073	467	0.0036
MS32	479	0.0054	87	0.0124	632	553	0.0147	474	0.0058	472	0.0041

#### 4.1.2.2.1 Effect of thread mechanical splice under tension test

The responses of yield strength and ultimate strength obtained from the control bar and coupler specimens were almost identical in all diameters because of the reinforcing bar rupture, which occurred in random locations in the reinforcing bars. No damage to the coupler sleeve was observed, but loosened of threaded in coupler sleeve and threaded bar end were found after the bar rupture shown in Figure 4.3. The stress-strain relationship of deform bar and coupler specimens shows fairly close of yielding and ultimate strength to deform bars. The dominant behavior affecting of tension behavior of coupler is the initial slope. Which is nonlinear and causes property of elastic of modulus to decrease as shown in Figure 4.4. The behavior of hardening mechanisms shows the result is close to the deform bar, including the slope of hardening modulus.

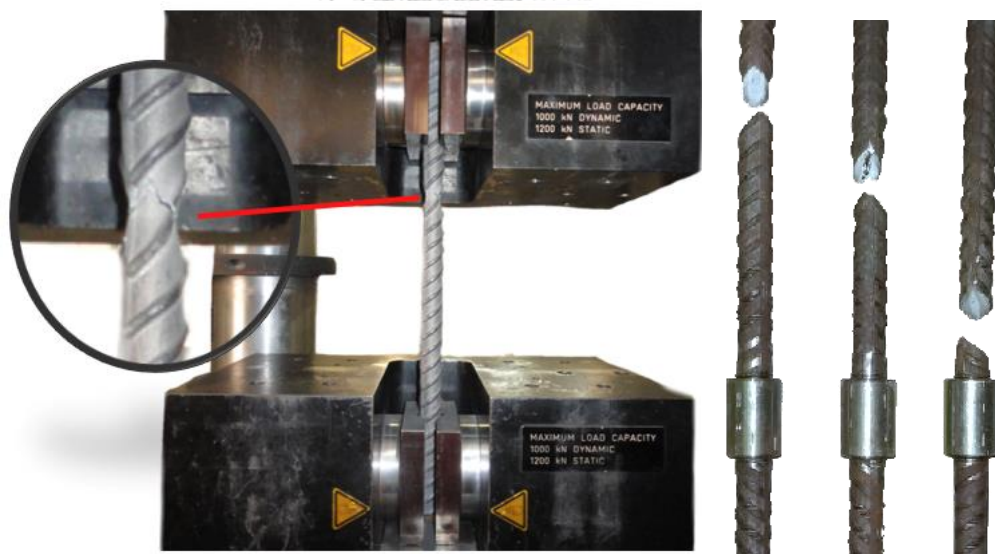


Figure 4.3 Tension failure of deform bar and coupler.

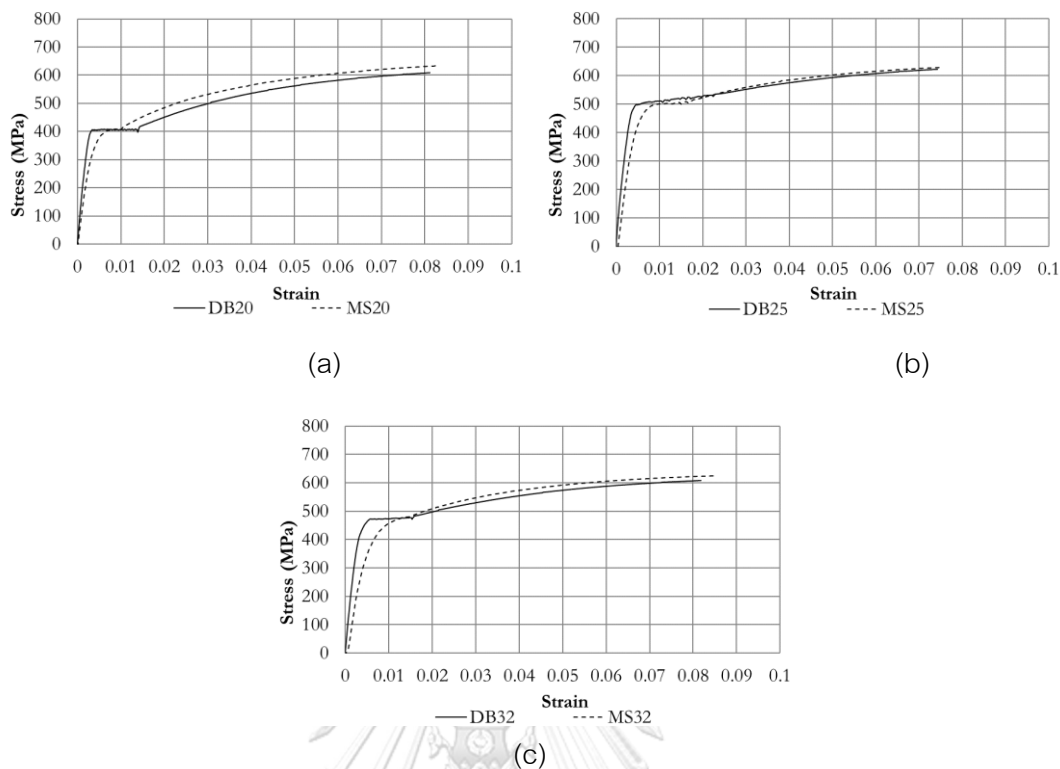


Figure 4.4 Stress-strain relationship (Tension) of deform bar and coupler specimens  
(a) DB20 vs MS20, (b) DB25 vs MS25, (c) DB32 vs MS32

#### 4.1.2.2.2 Effect of unsupported length under compression test

The experiment of the monotonic compressive test, the stress-strain relationship of deform bar and coupler with diameter 20, 25, and 32 mm and L/D ratio equal to 10, 12, and 16 were conducted. The difference of postyield softening branch after buckling results from the unsupported L/D ratios. High L/D ratios for all specimen diameters dropped rapidly of load-carrying capacity with increasing strains. The essential phenomena observed at the buckling shape of the mechanical splice are asymmetric results from coupler sleeve, thus restraining the buckling at the middle, as shown in Figure 4.5

The coupler shows maximum compressive stress in L/D ratios equal to 10 was beyond yield strength by the ratios of maximum compressive stress to yield stress of

coupler specimens with diameter 20, 25, and 32 mm were 1.19, 1.17, and 1.16 respectively (Table 4.2). The highest L/D ratios equal to 16 of deform bar with and without coupler was achieved to yield strength, after buckling the load-carrying capacity dropped rapidly with increasing strains. Moreover, the stress-strain relationship of L/D ratios equal to 12 of the coupler was approximate to the stress-strain relation of the deform bar with L/D ratios equal to 10 for all specimen diameter shown in Fig. 7. The normalized stress-strain relation shown in Figure 4.6 illustrates the slope of post buckling behavior as a result of unsupported L/D ratio for all specimen diameter. Clearly, the coupler sleeve can improve the buckling behavior of reinforcing bar under compression force, and the test results are stable and consistent with the variables studied.

The amount of energy dissipation can confirm the buckling behavior of deform bar and coupler by the relationship between strain energy and unsupported L/D ratios, as shown in Fig. 9. The ratio of strain energy dissipation between the coupler and deform bar is shown in Table. 3. The table shows that the coupler can dissipate strain energy with L/D ratios equal to 12, and 16 with all diameters are approximate to strain energy of deform bar with L/D ratios equal to 10 and 12, respectively. A more significant section of coupler collar that restrains buckling of reinforcing bar affect to dropped gradually of load-carrying capacity. Hence, the coupler with higher compressive strength than the deform bar has an excellent ductility response.

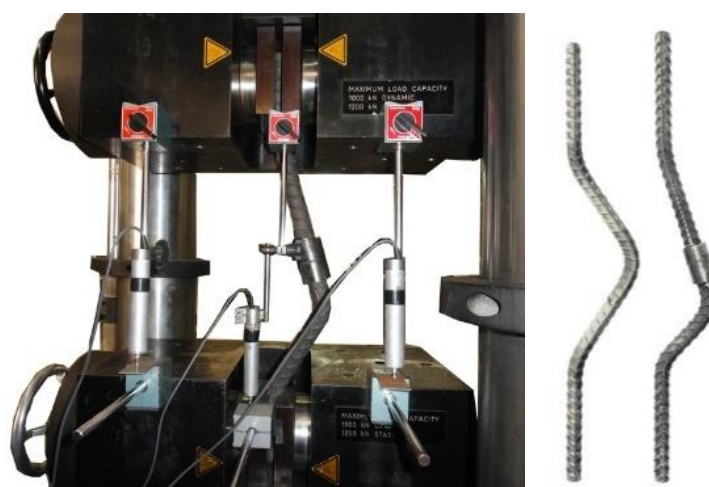
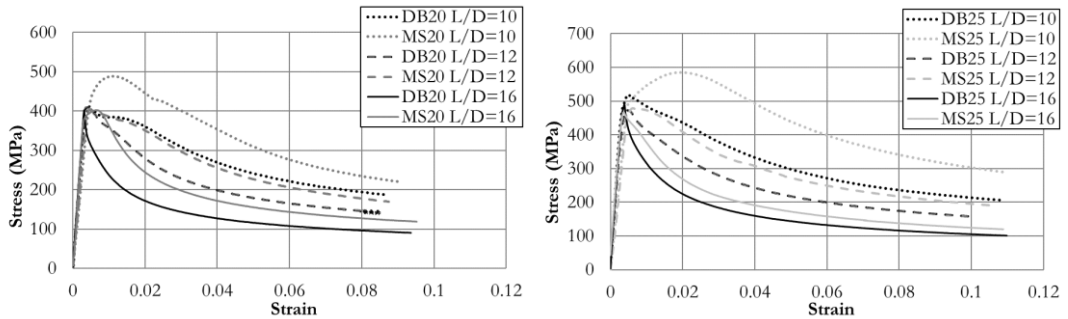


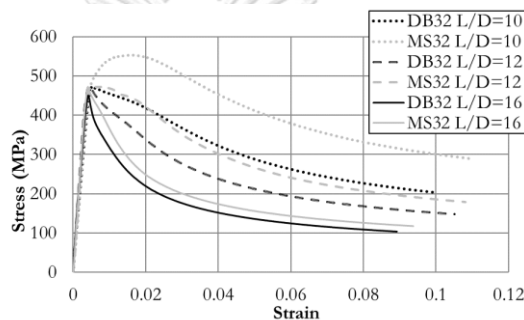


Figure 4.5 Buckling shape of deform bar and coupler under monotonic compression test.



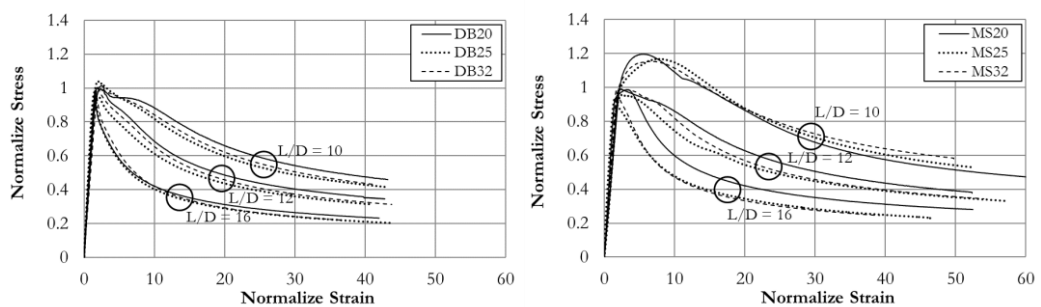
(a)

(b)



(c)

Figure 4.6 Stress-strain relationship (Compression) of deform bar and coupler specimens (a) DB20 vs MS20, (b) DB25 vs MS25, (c) DB32 vs MS32]



(a)

(b)

Figure 4.7 Normalize Stress - normalize strain relationship (Compression) of (a) deform bar and (b) coupler specimens



จุฬาลงกรณ์มหาวิทยาลัย  
**CHULALONGKORN UNIVERSITY**

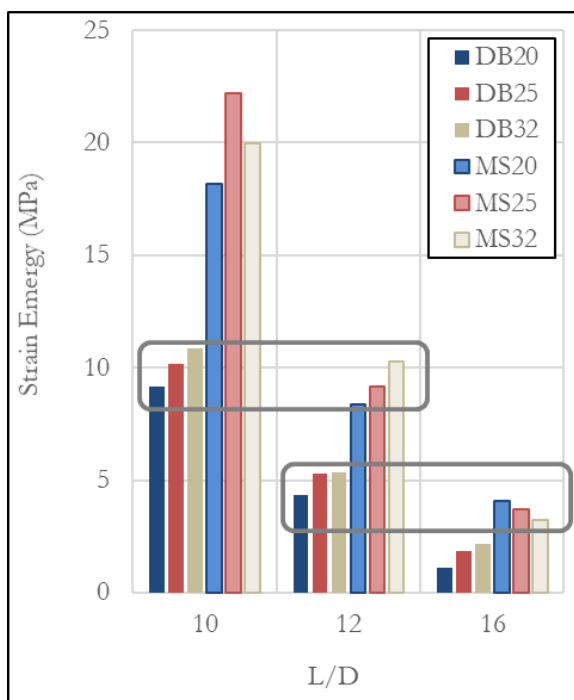


Figure 4.8 Relationship of strain energy and L/D ratios of deform bar and coupler specimens

Table 4.3 Compression test result of deform bar and coupler specimens.

ID	Strain Energy (MPa)			
	L/D	10	12	16
DB20		9.41	4.54	1.16
MS20		18.35	9.24	4.18
DB25		10.52	5.54	1.94
MS25		22.69	9.47	3.83
DB32		11.30	5.65	2.28
MS32		20.68	11.45	3.29

#### 4.1.3 Propose unsupported length of the bar with couplers

Considering the experimental results and the abovementioned thresholds of L/D ratios, the following cases can be defined towards the modeling of the stress-strain relationship of bars. Propose that unsupported length of reinforcing bar with mechanical

splices can be modified by subtracting the length of the mechanical splice, which has characteristics of a rigid element, as shown in Figure 4.9. The numerical model was developed in OpenSees program. The reinforcing bars material properties were defined using available uniaxial material models called "ReinforcingSteel" [43]. The model is the average stress-strain relationship including the buckling of stress-strain relationship. The model established based on the equilibrium of the buckled reinforcing bar limited by two consecutive hoops to simulation for buckling characteristic by a plastic mechanism consisting of three concentrated plastic hinges along the buckled length. The buckling simulations incorporated consist of variations as  $\beta$  is a factor to scale the buckling curve;  $\gamma$  the factor is the positive stress location about which the buckling factor is initiated;  $r$  factor is used to adjust the buckled curve, and  $l_{sr}$  is the unsupported L/D ratio.

To propose that the mechanical splices model concentrates all deformations in three plastic hinges, as shown in Figure 4.9b. The coupler device exhibited an approximately higher compressive stress and dissipating strain energy more than deform bar. The effective unsupported L/D ratios of coupler model can be applied in an individual coupler length with the unsupported length. Hence, the unsupported length can be modified via collar restraint.

Model reinforcing bar with mechanical splice used beam-column element to assign a fiber area section with 10 integrators that define to ReinforcingSteel uniaxial material, as shown in Table 4.4. The parameter of uniaxial material was using the elements in Table 4.2. Axial load was applied by using displacement control with a step of 0.001 strain. The result of stress and strain was recorded from fiber area to compare with the experimental result.

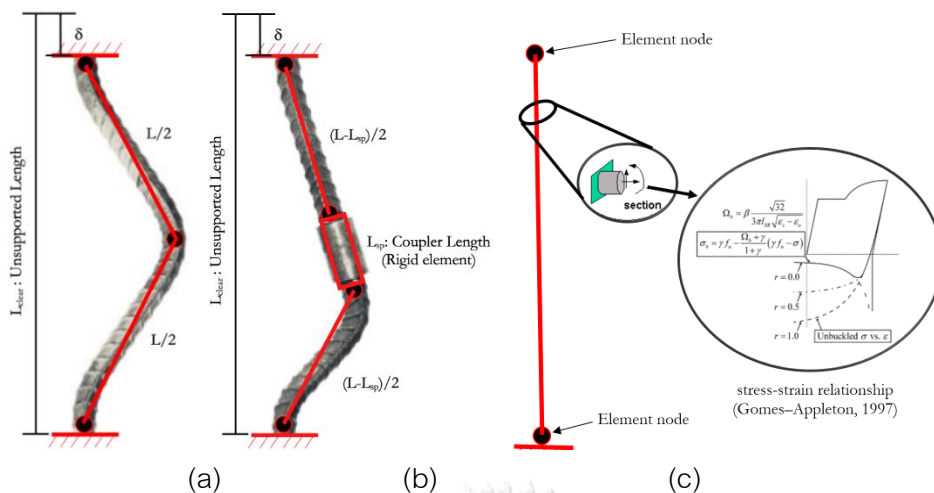


Figure 4.9 Plastic mechanism of buckling in (a) deform bar and (b) coupler, (c) Numerical modeling of reinforcing bar with and with out mechanical splice

Propose modifying unsupported L/D ratio for mechanical splice:  $\frac{L_{clear} - L_{sp}}{D}$

Table 4.4 Propose unsupported length of mechanical splice

$L_{clear}/d$ ( $\beta=1, \gamma=0$ and $r=0.15$ )			
DB20,25,32	10	12	16
$(L_{clear}-L_{sp})/d$ ( $\beta=1, \gamma=0$ and $r=0.15$ )			
MS20	7.3	9.3	13.3
MS25	7.2	9.2	13.2
MS32	7.5	9.5	13.5

#### 4.1.3.1 Experimental Verification of Numerical Model

The proposed model was validated using specimens cyclic test results discussed previously for the threaded mechanical splice. The constitutive model was calibrated using average measured materials properties as in Table 4.2. The numerical model was compared to the test results of specimens in cyclic tests. The theoretical predictions using the [43] model and the proposed modification unsupported length of the mechanical splice, respectively, as shown in Figure 4.10.

Eight steel reinforcing bars with and without mechanical splice under reversed cyclic tests performed a range of  $L/D$  equal to 10 and 16, and the reinforcing bar diameter of 25 and 32 mm are presented verification of the proposed stress-strain model, including buckling effect.

One assumption of the [43] model is that the buckling will immediately cause the plastic stress distribution on the entire reinforcing bar section, which simplifies the buckling stress. A good correlation is observed between unloading and reloading paths of the calculated hysteresis and the measured curve. The solid lines represent the experimental results, whereas dashed lines represent the numerical results

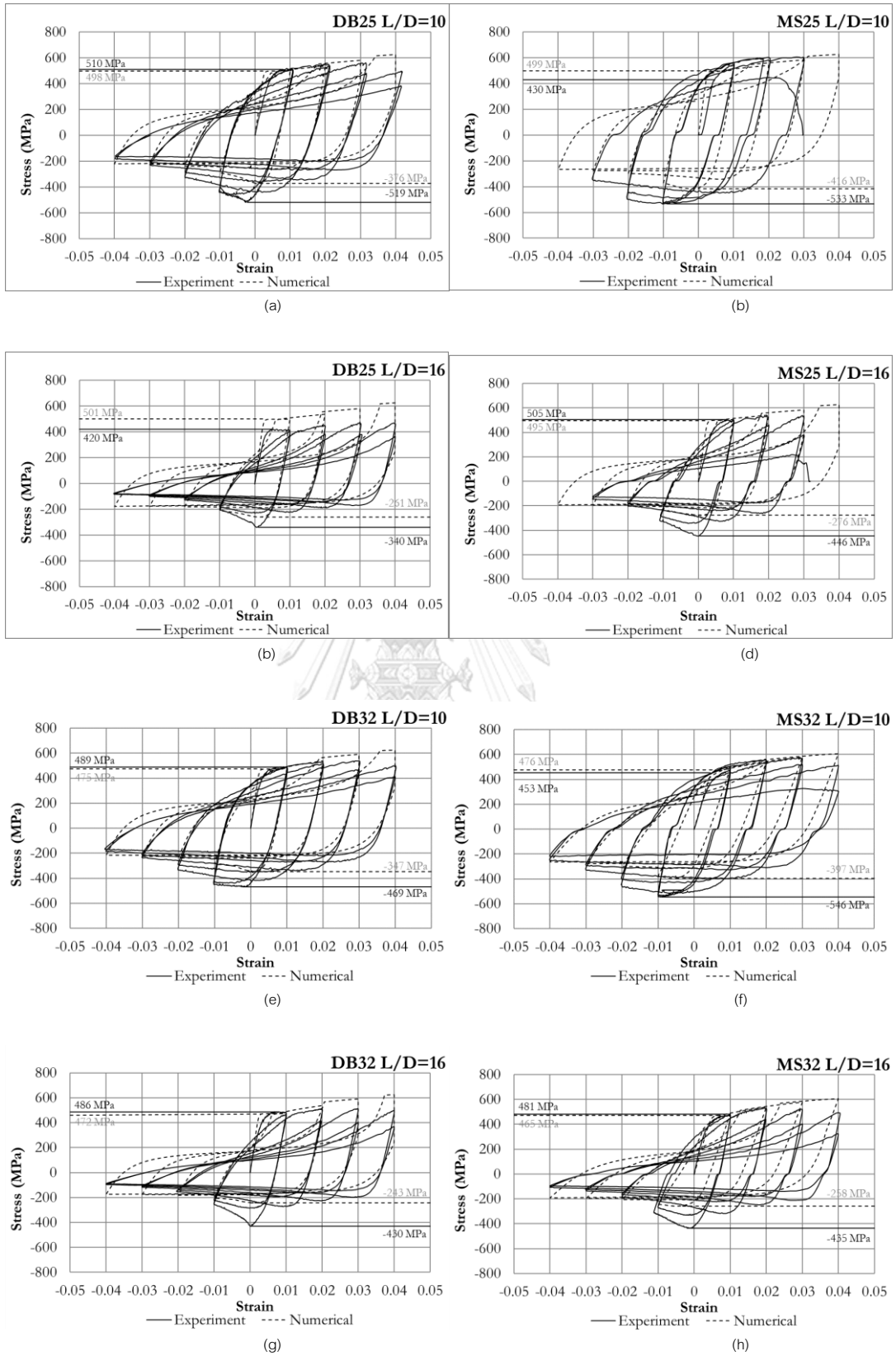


Figure 4.10. Comparison of numerical predictions and experimental results

## 4.2 Modeling of reinforced concrete column

All RC column specimens indicate flexural behavior, therefore, forced based beam-column model with difference reinforcement properties to capture the failure of each column. Two elements, such as a fiber beam-column element, the elastic element, were needed to model the flexural column in OpenSees. Reinforcement was defined by using [43] uniaxial steel material with isotropic strain hardening and established based on the equilibrium of the buckled reinforcing bar as the experimental observation the column NS, MS1, MS2 shows buckling behavior. Moreover, the study of reinforcing bar under monotonic and cyclic loading showed the behavior of a mechanical splice system to propose to uniaxial material properties. Lap splice column was applied in tension stress induce by force transfer in lap splice [51] to a general form of proposed stress-strain curve for lap splice bar.

The reinforced concrete columns were modeled numerically by using the elastic element with the plastic hinge model, as shown in Figure 4.11. Previous researchers show that the numerical analysis of the flexural column with the lumped plasticity column model shows better performance, especially on the initial stiffness which directly or indirectly affect the calculated peak force, absorbed energy as well as the backbone [52]. The test result of NS shows failure mode in flexural behavior, so the shear spring element was not included in the numerical model to capture the shear failure.



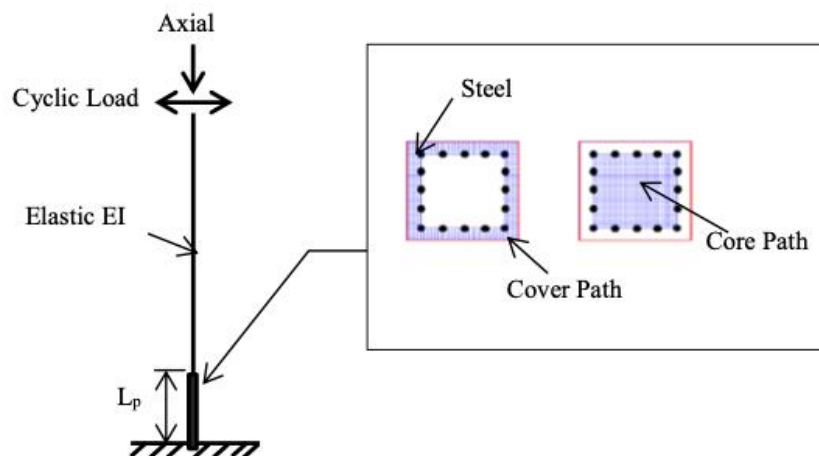


Figure 4.11 Lumped plasticity column model

#### 4.2.1 Uniaxial material

##### 4.2.1.1 Reinforcing steel uniaxial material model

The steel fiber was modeled by as uniaxial [43] steel material with isotropic strain hardening and established based on the equilibrium of the buckled reinforcing bar limited by two consecutive hoops, ReinforcingSteel material model in OpenSees was used to represent. Yield strength of longitudinal steel ( $f_y$ ), initial elastic tangent ( $E_s$ ), Tangent at initial strain hardening ( $E_{sh}$ ), the buckling parameters modified  $\beta$  is an amplification factor that allows the user to scale the buckling curve, and this is useful to adjust the location of the bifurcation point. To adjust the curve between the buckled curve and the unbuckled curve by ( $r$ ). Including the propose that unsupported length of reinforcing bar with mechanical splices can be modified by subtracting the length of the mechanical splice, which has characteristics of a rigid element, as shown in Figure 4.9

Table 4.5 ReinforcingSteel material properties

Specimen	Materials	$f_y$ (Mpa)	$E_s$ (Mpa)	$f_u$ (Mpa)	$l_{sr}$	$\beta$	$\gamma$	$r$
NS	ReinforcingSteel	503	200000	642	8	1	0	0.15
MS1, MS2					7.2			

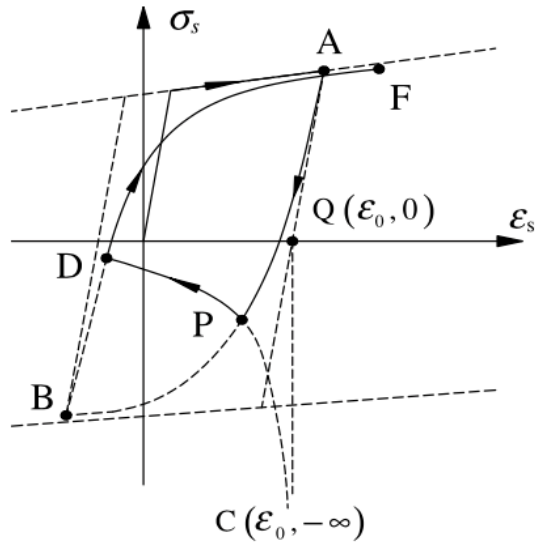


Figure 4.12 [43] steel material model

The longitudinal reinforcement with lap splice is modified the stress-strain relationship by force transfer in lap splice between bar and concrete. Behavior takes into account the damage appearance was observed in experimental. In fiber section were using the reinforcing steel with lap splice by propose stress-strain curve for LS specimens shown in Figure 4.13

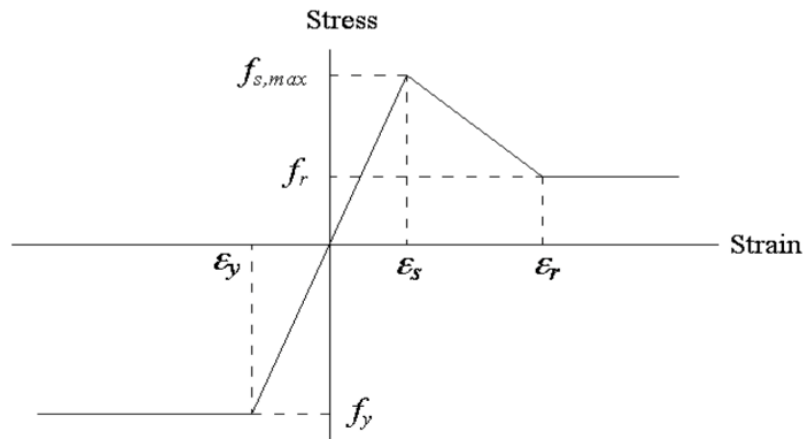


Figure 4.13 General form of proposed stress-strain curve for lap- spliced bar [53]

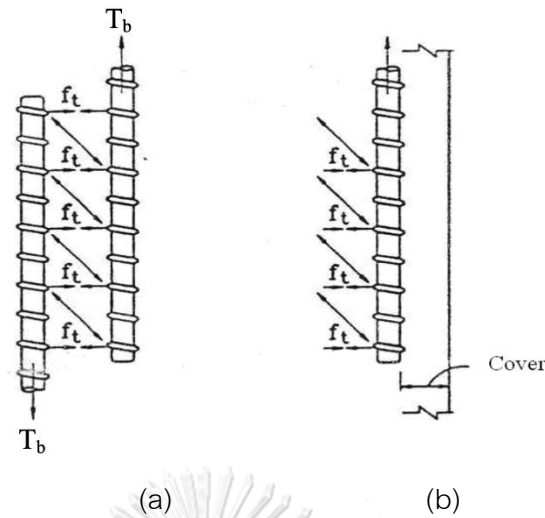


Figure 4.14 Tension stresses induced by force transfer in lap-splices

[51] (a) Between bars and (b) Between bar and core.

$$T_b = A_b f_s = F_t p l_s \quad 4.1$$

Where  $T_b$  is the force developed in lap-spliced bar

$A_b$  is bar cross section,  $f_s$  is bar stress,  $F_t$  is tensile strength of concrete ( $0.33 f'_c$  MPa)

$p$  is perimeter of cylindrical block, and  $l_s$  is lap-splice length.

$$p = \frac{s}{2} + 2(d_b + c) \leq 2\sqrt{2}(c + d_b) \quad 4.2$$

Where  $s$  is average distance between spliced bars.

$$n_t n_i \mu A_h f_h = n A_b f_r \quad 4.3$$

Here  $n_t$  denotes the number of transverse reinforcement legs perpendicular to crack plane,  $n_i$  is number of transverse reinforcements in lap-splice length,  $A_h$  is the area of crack surface,  $f_h$  is yield strength of transverse reinforcement with a maximum of  $0.015 E_s$  where  $E_s$  is bar's modulus of elasticity. In this equation  $n$  is a number of spliced longitudinal bars developed by frictional stress in the crack plane. In the following calculations, the frictional factor,  $\mu$ , is taken equal to 1.4.

Table 4.6 Lap splice material properties

Specimen	Materials	s1p (Mpa)	e1p	s2p (Mpa)	e2p	s1n (Mpa)	e1n	s2n (Mpa)	e2n
LS	Hysteretic	484	0.0038	168	0.014	-503	-0.0025	-642	-0.08

#### 4.2.1.2 Unconfined concrete uniaxial material model

The unconfined concrete fiber was assigned using the constitutive stress-strain relationships proposed by Kent and Park [40]. Concrete material object with degraded linear unloading/reloading stiffness according to the work of Karsan and Jirsa [54] and no tensile strength. The Concrete01 material model in OpenSees was chosen to represent the Kent and Park [40]., material model. In the uniaxial material model in OpenSees, concrete compressive strength at 28 days ( $f'_c$ ), concrete strain at maximum strength ( $\epsilon_{co}$ ), concrete crushing strength ( $f'_{cu}$ ) and concrete strain at crushing strength ( $\epsilon_{cu}$ ) need to be assigned. The ascending branch is represented by and  $\epsilon_{co}$  by 0.002. The concrete crushing strength ( $f'_{cu}$ ) is represented by 20% of the maximum concrete strength and the concrete strain ( $\epsilon_{cu}$ ) is represented by the strain at crushing strength. The consecutive law for Kent and Park unconfined material model is demonstrated in Figure 4.15

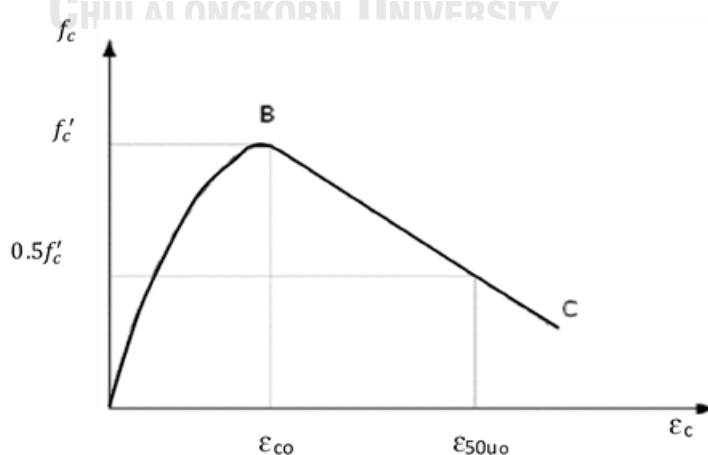


Figure 4.15 Stress-strain relationship of unconfined concrete [40]

#### 4.2.1.3 Confined concrete uniaxial material model

The confined concrete material model proposed by Mander and Priestley [41] was used to represent the confined concrete uniaxial material model. In OpenSees Concrete02 material was used to represent the object with tensile strength and linear tension softening. The effective lateral confining stress for the square column section is calculated. Then the compressive strength of concrete  $f'_{cc}$  and strain at maximum strength  $\epsilon_{cc}$  and crushing strength  $f'_{cu}$ , concrete strain at crushing strength  $\epsilon_{cu}$  are calculated following the Mander and Priestley [41] model. These values are assigned to the Concrete02 material model in OpenSees. The residual stress in the descending branch is considered at 20 %  $f'_{cc}$  defined by Kent and Park [40] in order to relevant the real behavior of the test columns. Mander material model for confined concrete is shown in Figure 4.16

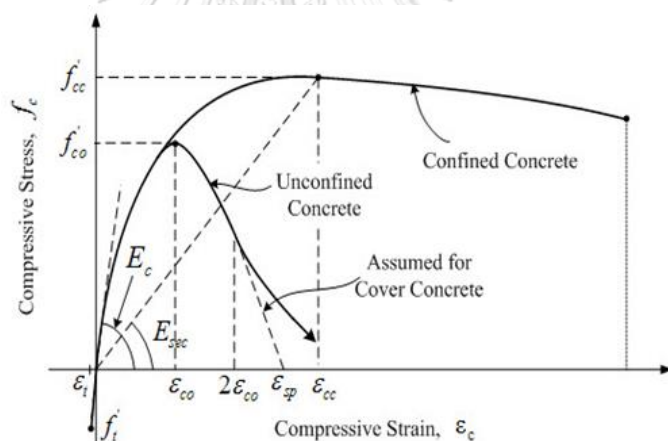


Figure 4.16 Stress strain relationship for confined concrete

[41]

Table 4.7 Concrete material properties

Specimen	Materials	$\sqrt{f'_c}$ (Mpa)	$\epsilon_c$	$f_u$ (Mpa)	$\epsilon_{cu}$	$\lambda$	$E_c$
NS, MS1, MS2, LS	Unconfined Concrete	23.6	0.002	0	0.0064	0.1	$5000\sqrt{f'_c}$
	Confined Concrete	26.08	0.004	5.22	0.0178	0.1	$5000\sqrt{f'_c}$

#### 4.2.2 Plastic hinge length

The length of the plastic hinge is also one of the most important parameters in the nonlinear analysis. Many researchers specified the most appropriate lengths of the plastic hinge which give better analytical results and save time in the analysis. Priestley, et [51]

$$L_p = 0.08L + 0.022d_b f_y$$

where:

L: Column height in meter

$d_b$ : diameter of longitudinal reinforcement in meters.

$f_y$ : yield stress of longitudinal reinforcement in MPa.

So:

$$L_p = 0.08L + 0.022d_b f_y = (0.08 \times 2.2) + (0.022 \times 0.025 \times 449) = 0.423m$$

#### 4.2.3 Elastic elements

In 2D modeling, elastic elements are modeled with basic parameters for elastic elements include:

- $A$  : Area of section
- $I$  : Moment of inertia
- $E_c$  : Young modulus or Elastic modulus of material (in most cases, the value of Young modulus is from concrete material excluding reinforcement's).

#### 4.2.4 Force-based fiber beam-column element

The column element was modeled using the force-based fiber beam-column element. The numerical element consists of a two-dimensional nonlinear beam-column with a fiber section located at the integration points. Each section is subdivided into several fibers where each fiber is under a uniaxial state of stress. In modeling the fiber section of the column, ten integration points were used to compare the global response of the RC columns efficiently. Each section at the integration point was discretized into 60 core fibers and 20 cover fibers in both local  $x$  and  $z$  directions in Figure 4.17. Significant errors are only produced when very crude fiber meshes are used [55]. The NS specimen was modeled as a three-node element and each node has three degrees of freedom. Node 1 was fully fixed and node 3 was a free end. The fiber section of the NS specimen was illustrated in Figure 4.18

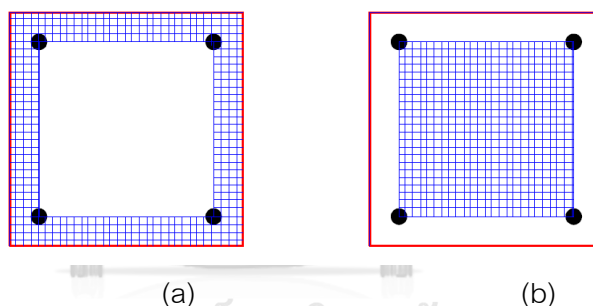


Figure 4.17 Model of fiber section of RC column

(a) Unconfined concrete fiber model and (b) Confined concrete fiber model

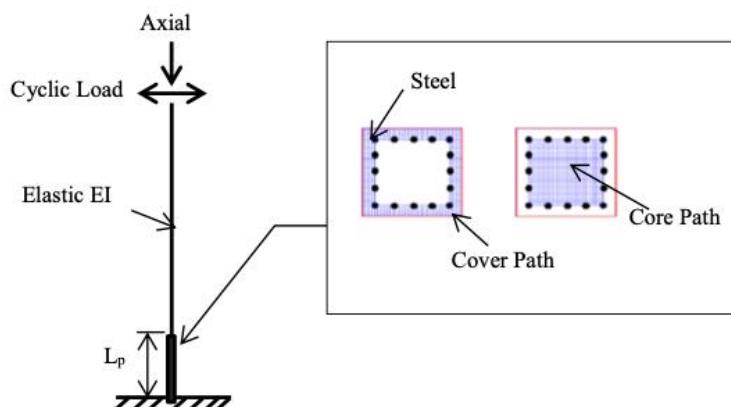


Figure 4.18 Three node element

#### 4.2.5 Structural Elements

The nonlinear behavior of the beam-column element is confined to an assigned plastic hinge with a length  $L_p$ . The curvature distribution is linear above the plastic hinge, and the curvature is calculated within the plastic hinge with moment-curvature analysis of the force-based beam-column element. Plastic rotations are directly related to plastic curvature through the specified plastic hinge lengths.

The experimental results of NS column reveals the damage appearance shows the critical region as shown in Figure 4.21 to Figure 4.24. Which close to previous researchers specified the appropriate of plastic hinge lengths from Priestley, et [51] for column with non-splice. For splice reinforcement column were use the plastic hinge lengths by experimental observcation.

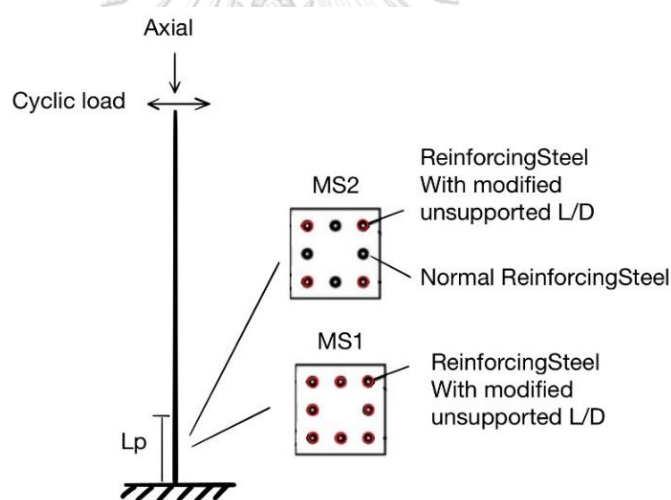


Figure 4.19 Reinforcingsteel with a coupler in fiber section of specimen MS1, MS2

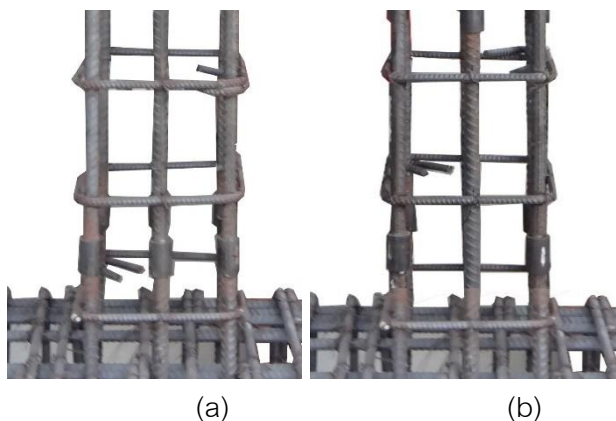


Figure 4.20 The location of a coupler in specimen MS1, MS2



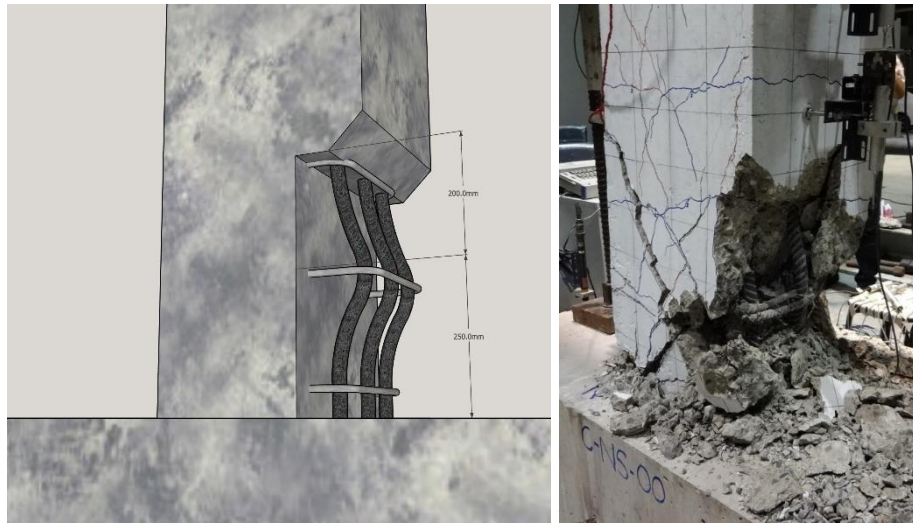


Figure 4.21 Plastic hinge length of NS column equal to 450 mm



Figure 4.22 Plastic hinge length of MS1 column equal to 650 mm



Figure 4.23 Plastic hinge length of MS2 column equal to 450 mm

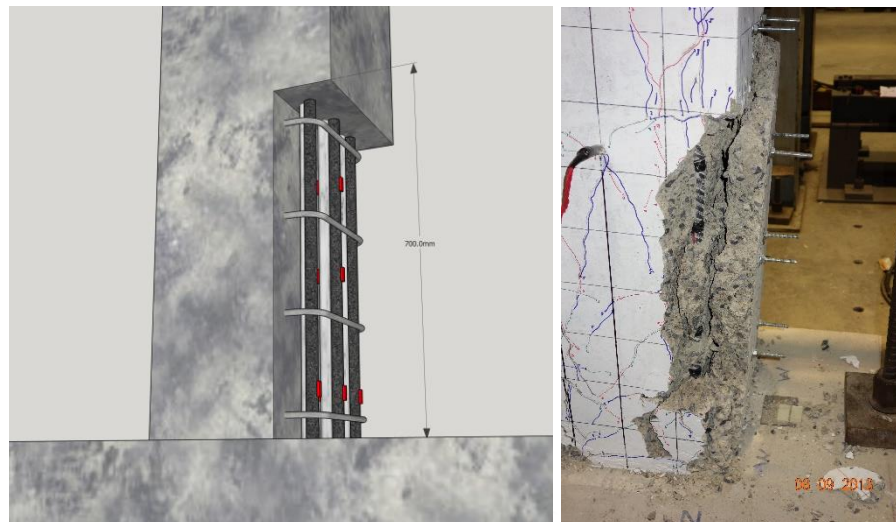


Figure 4.24 Plastic hinge length of LS column equal to 700 mm

#### 4.3 Numerical result and discussion

##### 4.3.1 Numerical result of specimen NS

The NS columns were modeled numerically by using the elastic element with the plastic hinge model. For the specimens which fail in flexure, the load-displacement relation from the analysis matches satisfactorily with that from the experiment. The fiber model can represent the actual behavior of the columns. The longitudinal reinforcement from the fiber section, combined as buckling behavior, takes into account the damage appearance was observed in experimental. The hysteresis loops after the peak load which is mainly governed by steel reinforcement buckling behavior are satisfied between the analysis and experiment. The stress-strain relationship of material model is shown in Figure 4.27. The analysis result of the load-displacement relationship is shown in Figure 4.25

Table 4.8 Numerical results of specimen NS

NS	Peak Load (kN)	Displacement (mm)	% Drift
Experiment	143	60.7	2.76%
Numerical	151	31.9	1.45%

Load-displacement of NS

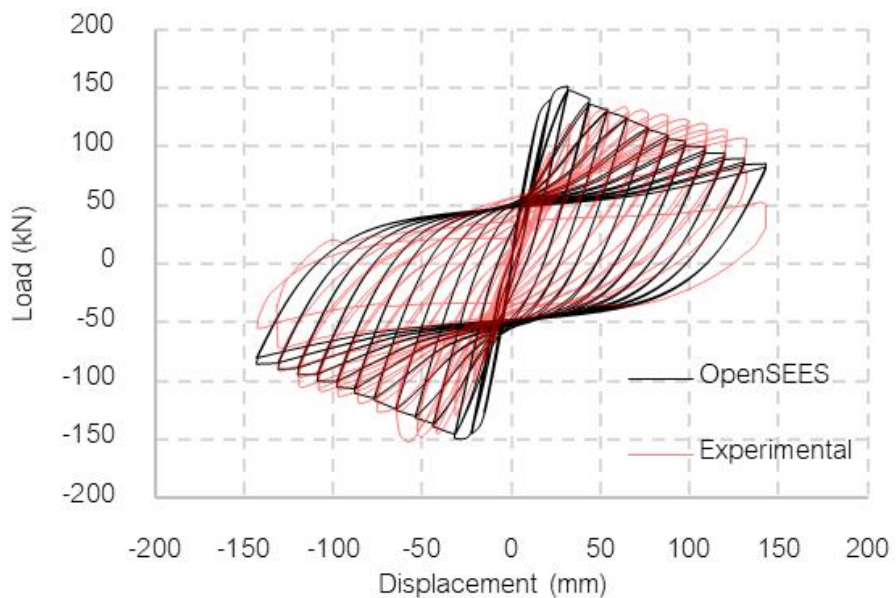


Figure 4.25 Comparison of load-displacement relationship NS(Hysteresis)

Moment-curvature of NS

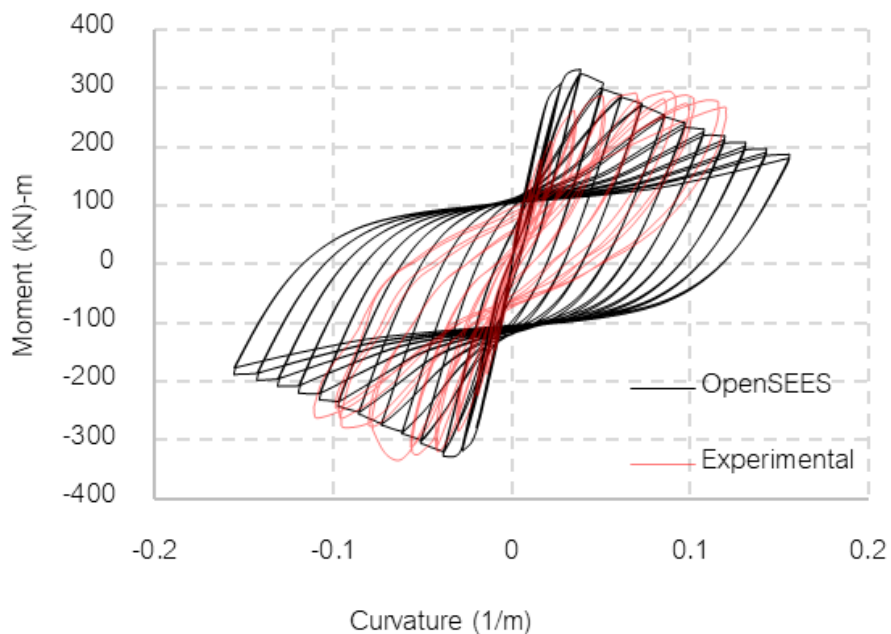


Figure 4.26 Comparison of moment-curvature relationship NS

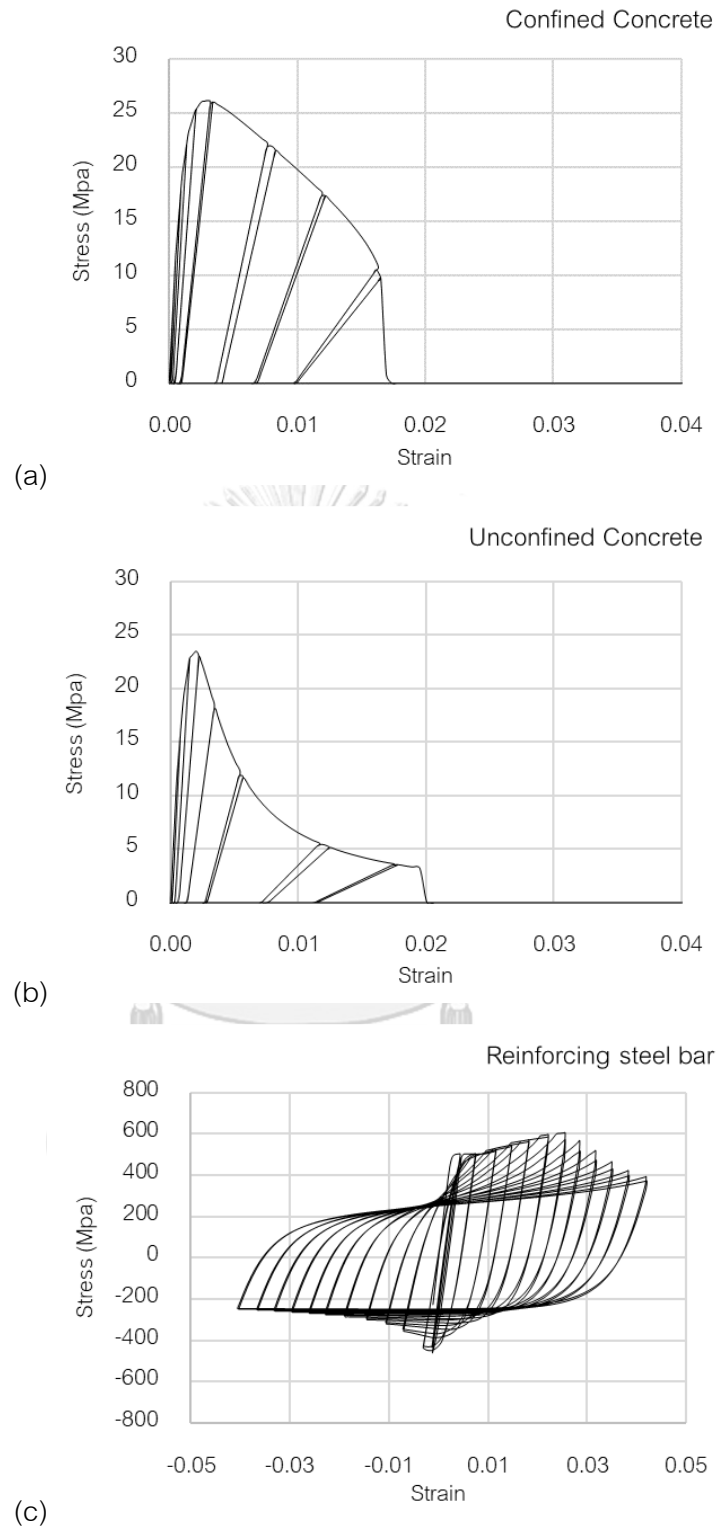


Figure 4.27 Stress strain relationship of material model of NS (a) Confined concrete, (b) Unconfined concrete and (c) Reinforcing steel

The RC columns with mechanical splices were modelled numerically by using the elastic element with a plastic hinge model. For the specimens which fail in flexure, the load-displacement relation from the analysis matches satisfactorily with that from the experiment. The fiber model can represent the actual behavior of the columns. The longitudinal reinforcement with mechanical splice from fiber section is modified unsupported length L/D and combined as buckling behavior take into account the damage appearance was observed in experimental. In fiber section were modify the reinforcing steel with coupler by proposing unsupported length L/D for specimen MS1 and MS1 as shown in Figure 4.19

#### 4.3.2 Numerical result of specimen MS1

Comparison of analytical load displacement and experimental load displacement is shown in Figure 4.28. for specimen MS1. The hysteresis loops after the peak load are found in well agreement with the experimental results. The stress strain relationship of the material model is shown in Figure 4.30.

Table 4.9 Numerical results of specimen MS1

MS1	Peak Load (kN)	Displacement (mm)	% Drift
Experiment	138	72.9	3.31%
Numerical	153	37.5	1.70%

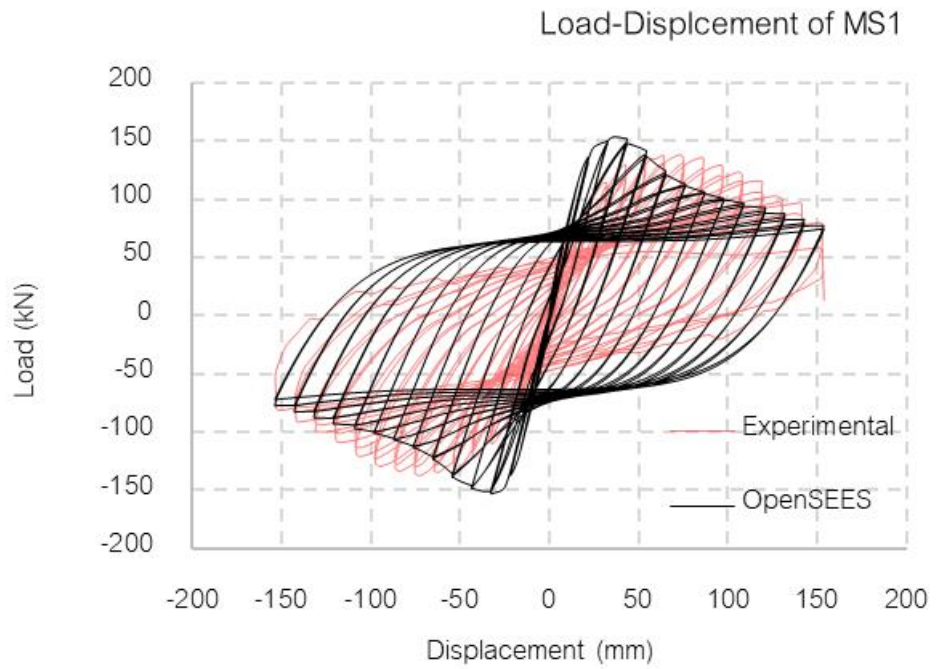


Figure 4.28 Comparison of load-displacement relationship MS1 (Hysteresis)

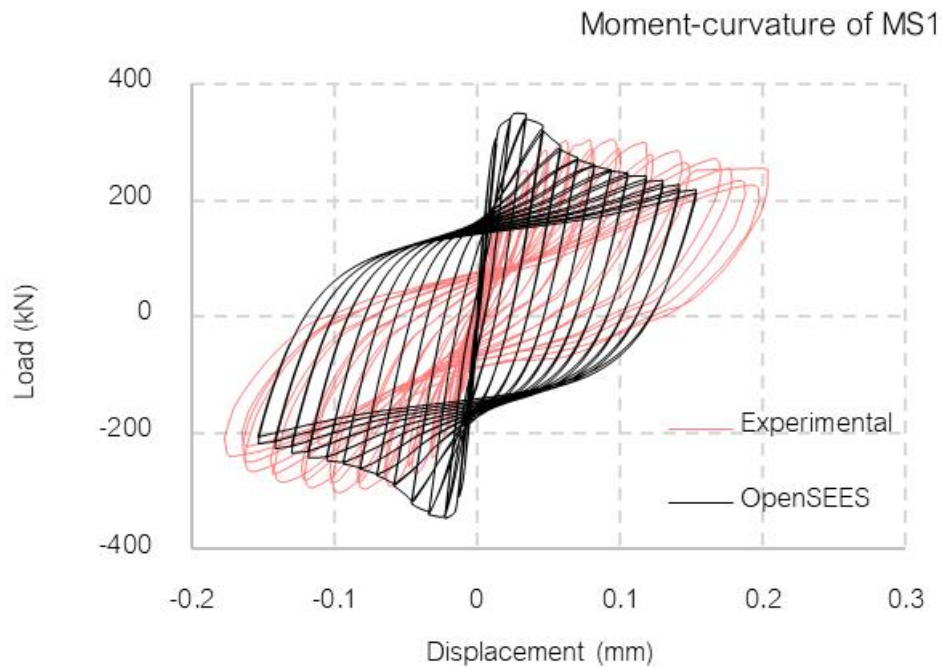
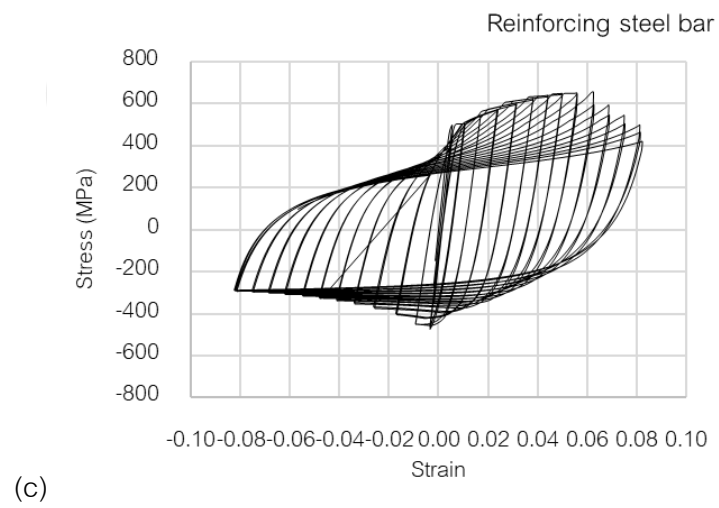
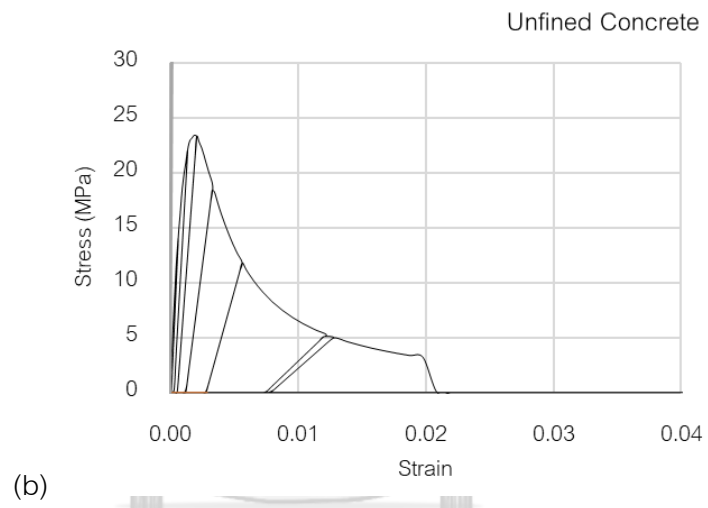
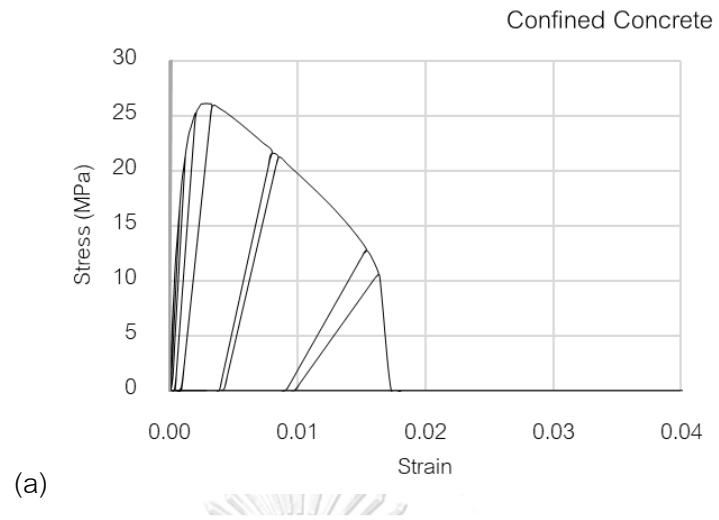


Figure 4.29 Comparison of moment-curvature relationship MS1



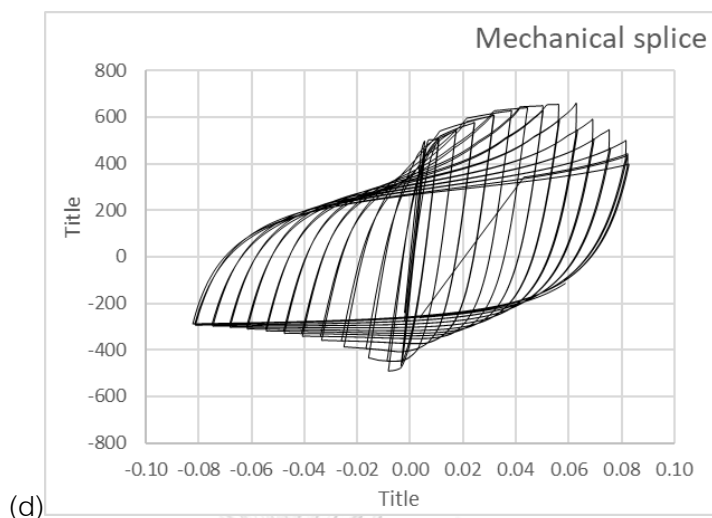


Figure 4.30 Stress strain relationship of the material model of MS1

- (a) Confined concrete, (b) Unconfined concrete and (c) Reinforcing steel  
(d) mechanical splice

#### 4.3.3 Numerical result of specimen MS2

Comparison of analytical load displacement and experimental load displacement is shown in Figure 4.31 for specimen MS2. The hysteresis loops after the peak load are found in well agreement with the experimental results. The stress strain relationship of the material model is shown in Figure 4.33.

Table 4.10 Numerical results of specimen MS2

MS2	Peak Load (kN)	Displacement (mm)	% Drift
Experiment	145	60.7	2.76%
Numerical	156	26.4	1.2%



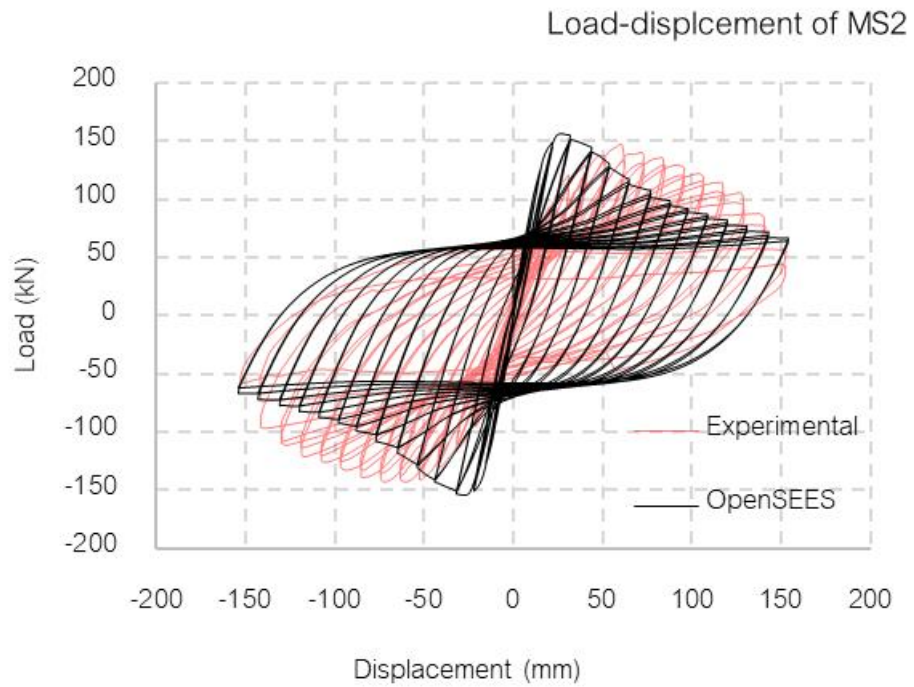


Figure 4.31 Comparison of load-displacement relationship MS2 (Hysteresis)

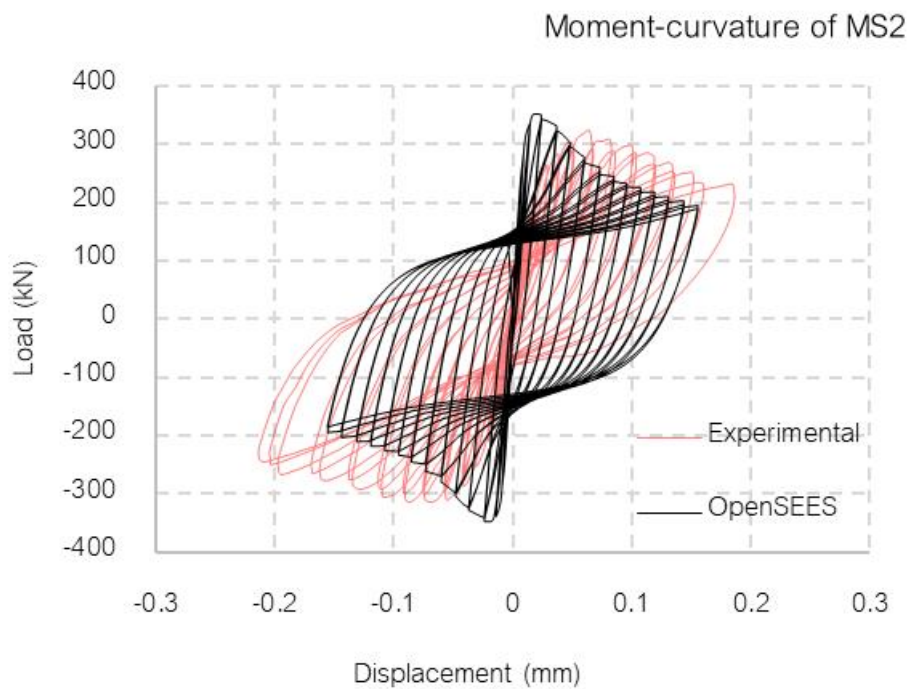
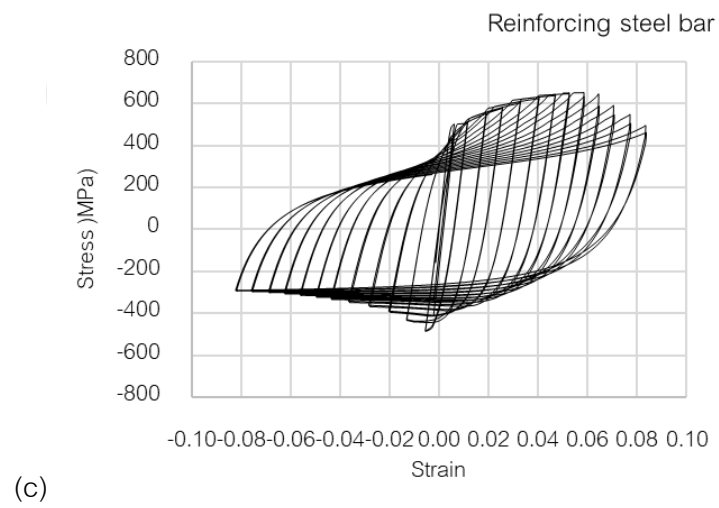
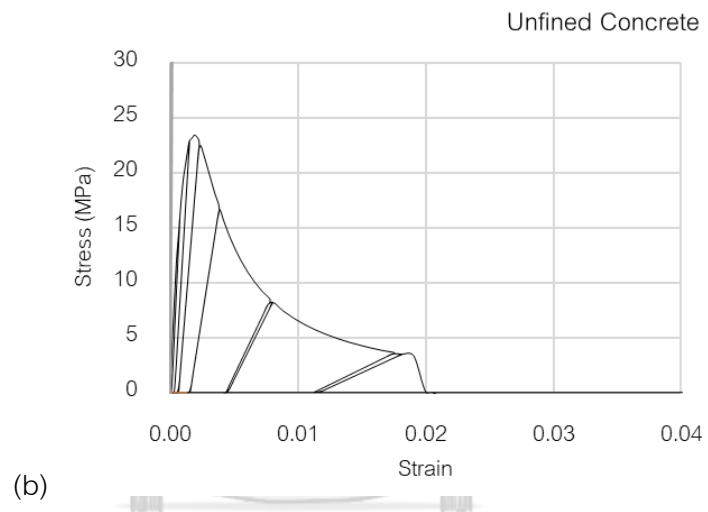
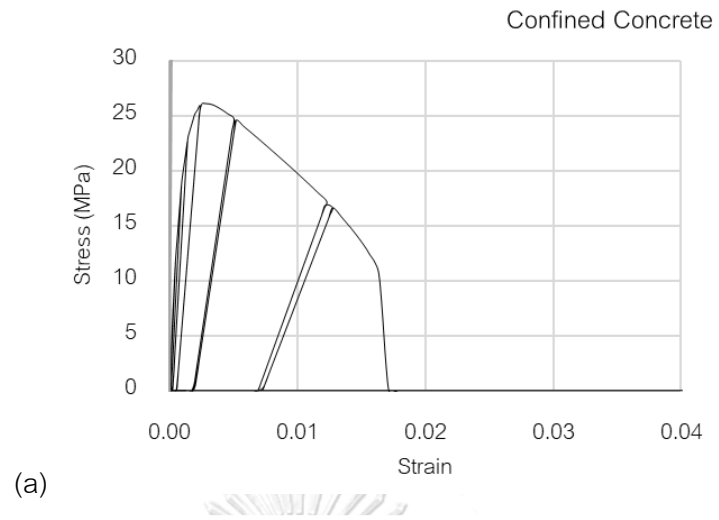


Figure 4.32 Comparison of moment-curvature relationship MS2



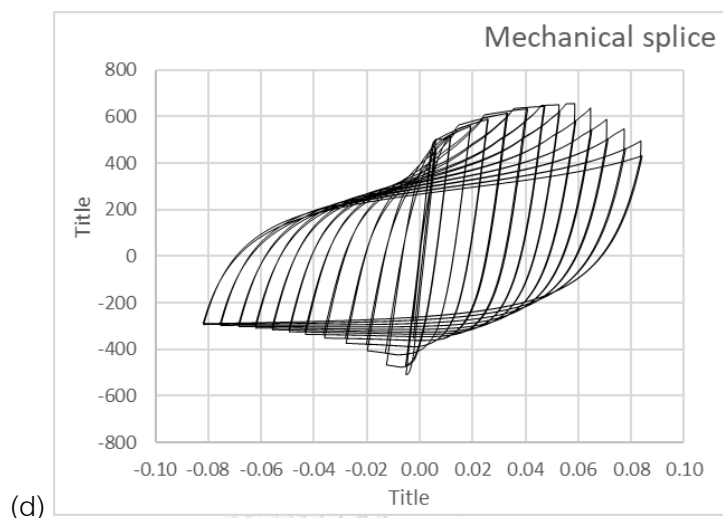


Figure 4.33 Stress strain relationship of the material model of MS2  
 (a) Confined concrete, (b) Unconfined concrete and (c) Reinforcing steel  
 (d) Mechanical splice

#### 4.3.4 Numerical result of specimen LS

Comparison of analytical load displacement and experimental load displacement is shown in Figure 4.34. The hysteresis loops after the peak load are found in good agreement with the experimental results. The stress strain relationship of the material model is also shown in Figure 4.36.

Table 4.11 Numerical results of specimen LS

LS	Peak Load (kN)	Displacement (mm)	% Drift
Experiment	122	41.9	1.91%
Numerical	125	20.9	0.95%

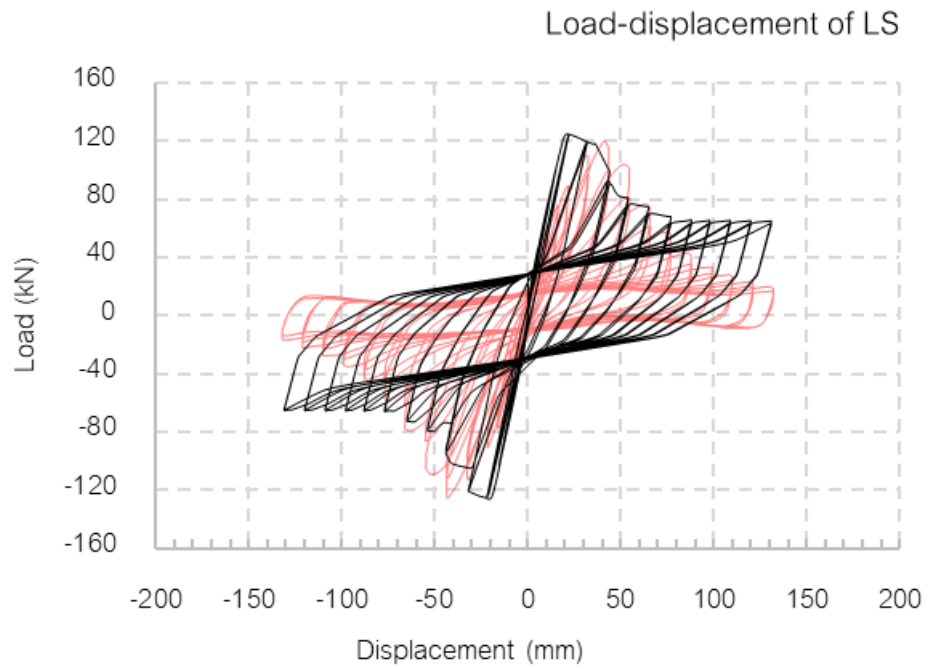


Figure 4.34 Comparison of load-displacement relationship LS (Hysteresis)

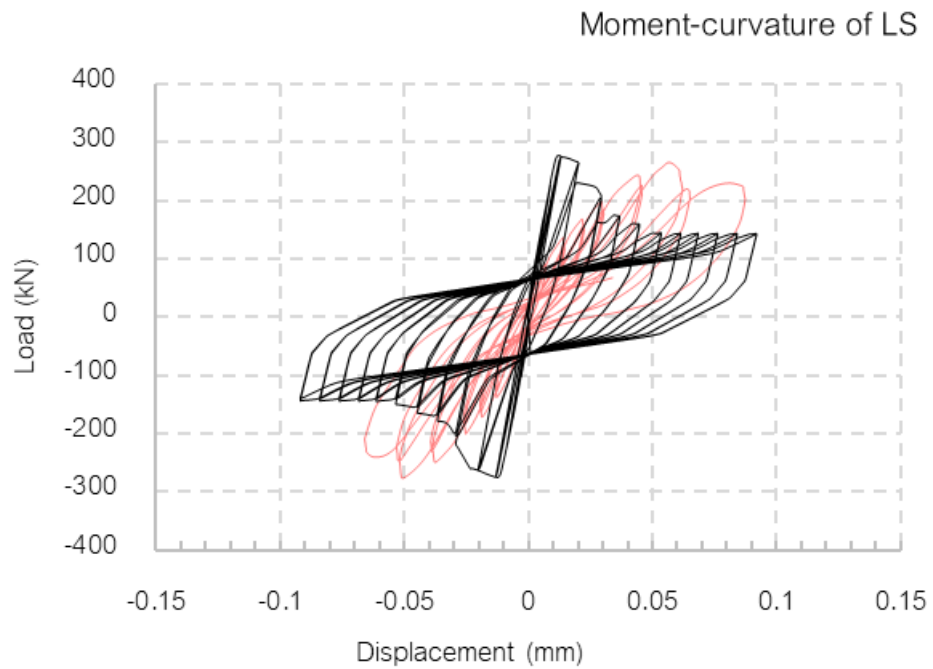


Figure 4.35 Comparison of moment-curvature relationship MS2

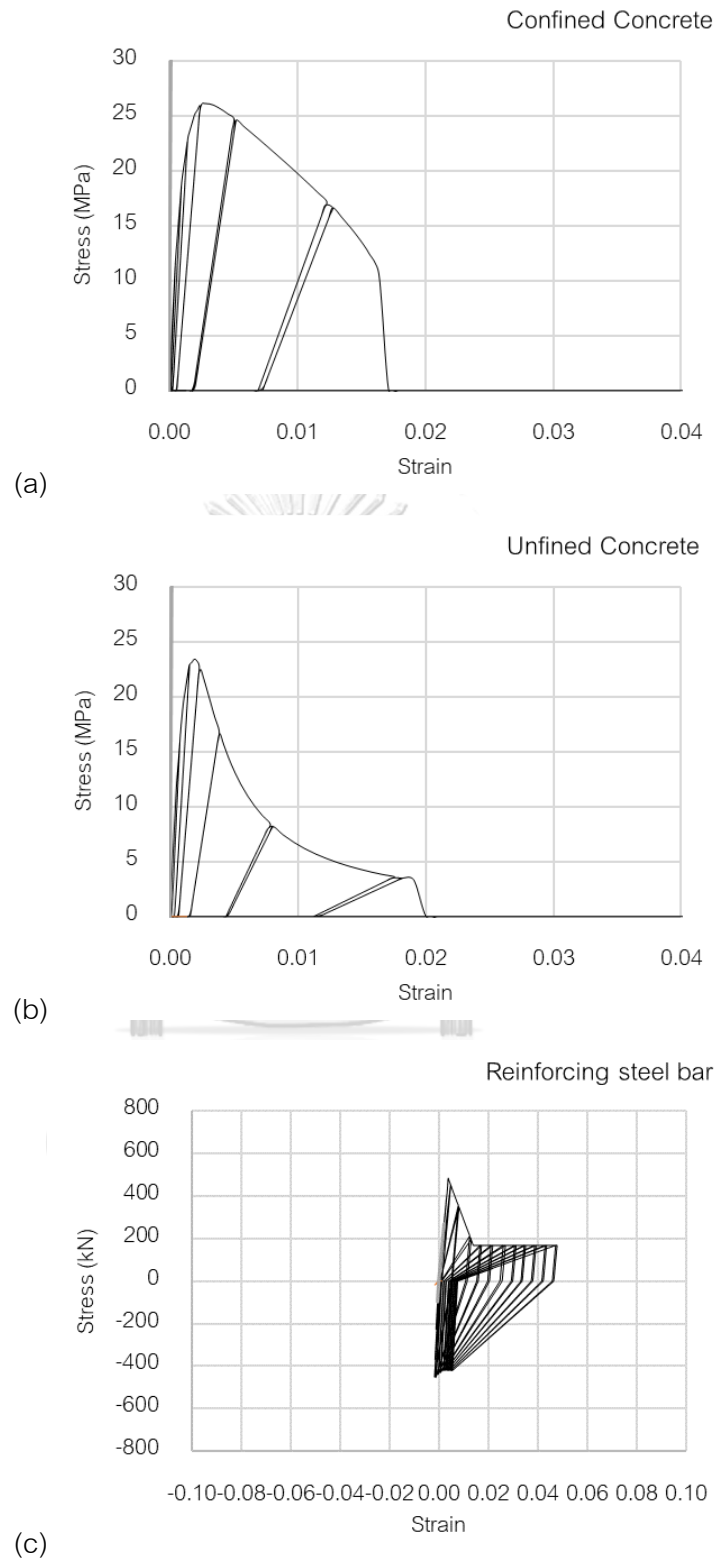


Figure 4.36 Stress strain relationship of the material model of LS  
 (a) Confined concrete, (b) Unconfined concrete and (c) Reinforcing steel.

#### 4.4 Discussion of the numerical model

- Numerical analysis of the control column (Specimen NS) shows that lateral behavior of RC column can be captured well by the analytical model. Analysis indicate slightly different values of initial stiffness as compared with the experimental results.
- Both RC columns with mechanical splices were analyzed using the lumped plasticity fiber model follow to experimental damage appearance in the critical region. The fiber model can represent the actual behavior of the columns by using reinforcing steel material by proposing the unsupported length of the bar with coupler. The initial stiffness, maximum load behaviours are entirely consistent with the test results. Note that the hysteresis loops after the peak load which is mainly governed by steel reinforcement are different between the analysis and experiment.
- The lateral response of lap splice column can represent the actual behavior of the columns by hesteretic material with proposed stress-strain curve for lap-spliced bar. Bond-slip includes using the tension stresses induced by force transfer in lap- splices can be significantly reduced the lateral capacity and finally the specimens fail in bond-slip control.

## CHAPTER 5

### STRENGTHENING OF REINFORCED CONCRETE COLUMN USING STEEL COLLARS

#### 5.1 Introduction

This chapter presents the methods of strengthening the column specimens, which were representative of current constructional practices of non-ductile columns by lap splice were placed in the critical region. The column properties such as column width-to-depth, aspect ratios, axial load ratios, longitudinal reinforcement ratio and transverse reinforcement ratio were identical to column LS as presented in chapter 3. The experimental program was developed to investigate the cyclic force-deformation behavior of three column specimens with strengthening by using steel collars to compare with the non-splice column NS and lap-splice column LS.

#### 5.2 Concept of steel collar

The experimental results in Chapter 3 indicate that the behavior of the column with lap-splice were failed by bond slip. The progressive damage shows the pattern of the cracks toward a vertical, continuing from 45 degree angle along 0-700 mm height, which along with the lap-splice location as shown in Figure 5.1. An additional transverse reinforcement ratio is needed to increase the confinement of the columns to increase the concrete tensile strength to deal with force transfer in lap-splices. In order to fulfill this requirement, the external steel collars were used to create the additional confinement pressure in the columns. The passive confinement of externally developed by the steel collars pressure. [41] [56] The theoretical stress-strain model for confined concrete and confinement effectiveness for the rectangular concrete sections confined by rectangular hoop with cross ties, the same concept was applied to the cross-section of the steel collars. This technique regarded as practical, not only less interruptive, fast and cost-effective but also should result in minimum loss of floor area. To evaluation, the

transverse reinforcement, volumatic ratio of lap-splice column have to compare with guideline code in order to know the demand for supplement.

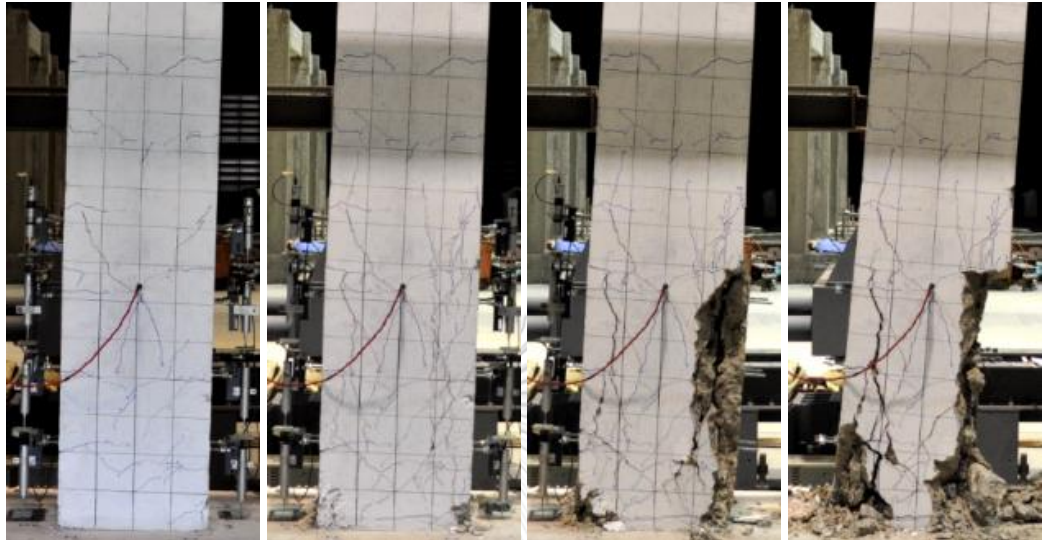


Figure 5.1 Progressive of vertical cracks which along with the lap-splice location of lap -splice column LS

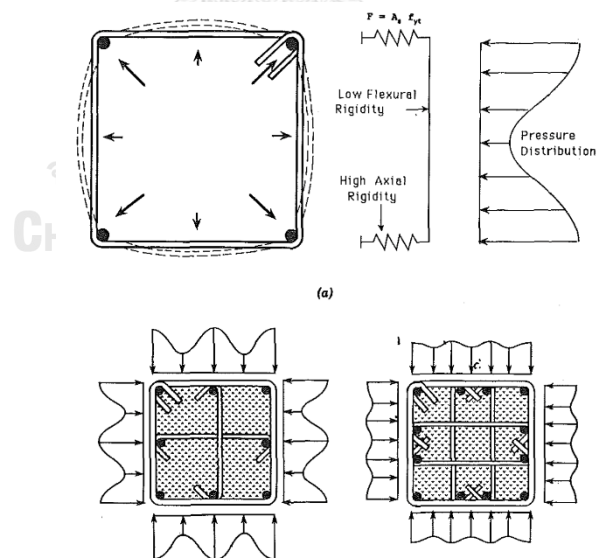


Figure 5.2 Lateral pressure in square column (a) Lateral pressure buildup in square column, and (b) Pressure distribution resulting from different reinforcement arrangements [56]



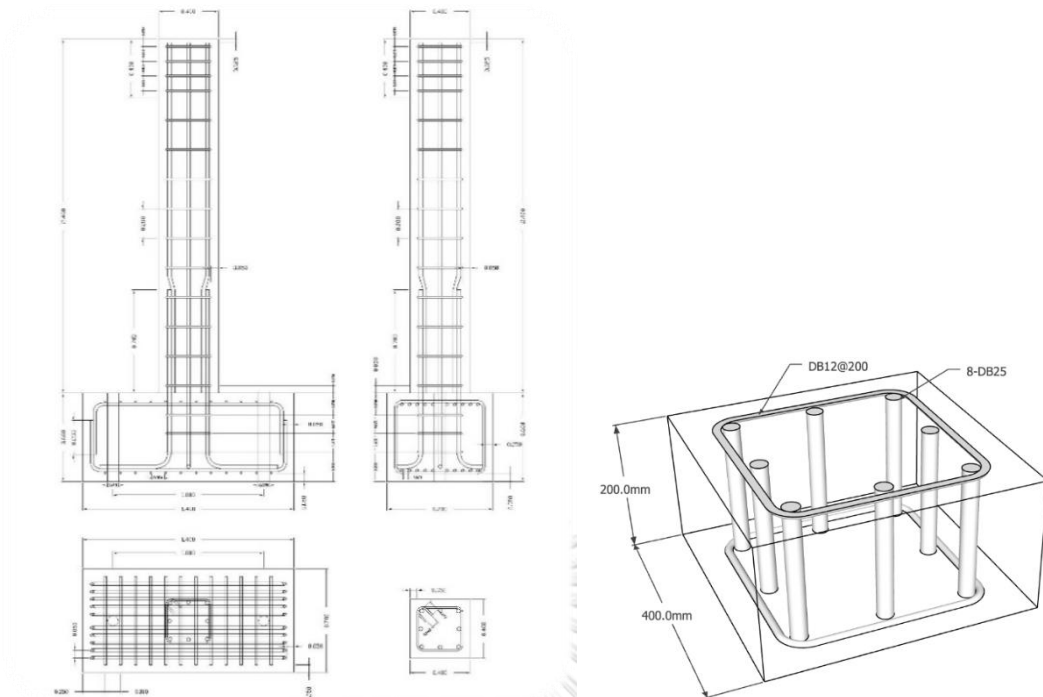


Figure 5.3 Reinforcement detailing of lap splice column specimen LS

The ratio of transverse reinforcement is given by

$$\rho_w = A_{sw} / (s \cdot b_w \cdot \sin \alpha)$$

Where:

- $\rho_w$  is the transverse reinforcement ratio
- $A_{sw}$  is the area of shear reinforcement with in length  $s$
- $s$  is the spacing of the shear reinforcement measured along the longitudinal axis of the member
- $b_w$  is the breadth of web of the member
- $\alpha$  is the angle between shear reinforcement and longitudinal axis

Volume of core concrete =  $200 \times 300 \times 300 = 18 \times 10^6 \text{ mm}^3$

Volume of shear reinforcement =  $(\pi \times 6^2) \times (300 \times 4) = 135,716.8 \text{ mm}^3$

Volumatic of transverse reinforcement ratio is = 0.00754

Shear reinforcement is :

$$A_{sw} = \rho_w (s \cdot b_w \cdot \sin \alpha)$$

$$A_{sw} = 0.00754(200 \cdot 400 \cdot \sin 90)$$

$$A_{sw} = 603.2 \text{ mm}^2$$

From many researchers studied of steel collars can compile the parameter of Volumatic of external steel collars as following:

He, et [57]

External steels are varied by thickness for 1.81 mm., 3.82 mm. and 5.83 mm. can estimate to Volumatic ratio by 1.14%, 2.43% and 3.75% respectively.

Pudjisuryadi and Suprobo, 2015 [58]

External angle 40x40x4 steels are varied by spacing for 180 mm, 120 mm and 90 mm. It can estimate to Volumatic ratio by 4.11%, 6.16% and 8.21% respectively.

Liu, et [38]

External steel collars are varied by spacing and sizing for 95 mm, 150 mm and 200 mm then 30x50 and 50x50. That can estimate to Volumatic ratio by 1.74%, 2.32%, 3.67% and 4.04% respectively.

Hussain and Driver [37]

External steel collars are varied by spacing and sizing. That can estimate to Volumatic ratio by 11.86%, 12.80%, 13.04%, 14.49%, 16.54%, 19.14%, 20.85% and 21.23% respectively.

Pudjisuryadi and Suprobo, 2016 [59]

External angle 40x40x4 steel are vary by spacing for 200 mm, 133 mm, 100mm, 80mm and 67 mm . can estimate to Volumatic ratio by 3.84%, 5.77%, 7.68%, 9.60% and 11.34% respectively.

Table 5.1 Volumatic ratio of external steel jacket from previous researchers

Researchers	Volumatic ratio of external steel jacket	Remark
He, et [57]	1.14%, 2.43% and 3.75%	Plate
Pudjisuryadi and Suprobo, 2016 [59]	.84%, 5.77%, 7.68%, 9.60% and 11.34%	Angle
Pudjisuryadi and Suprobo, 2015 [58]	4.11%, 6.16% and 8.21%	Angle
Liu, et [38]	1.74%, 2.32%, 3.67% and 4.04%	Tube
Hussain and Driver [37]	11.86%, 12.80%, 13.04%, 14.49%, 16.54%, 19.14%, 20.85% and 21.23%	Tube

External steel collars were considered by the variation of lateral pressure along the member length. This is graphically shown in Figure 5.6. It should be noted that the pressure developed at a nodal point, where a lateral tie supports the longitudinal bar is distributed reasonably uniformly along the length of the longitudinal bar. This is because the longitudinal bar in compression, with a short unsupported length between the ties, maintains the restraining action until shortly before it buckles. To strengthen the lateral pressure by using external steel collars were considered by the modulus of a section to action the uniform pressure similar to the variation of lateral pressure.

To selection, the section of steel collars with high modulus of section with a lower weight, mean the cost-effective. Moreover, the detailing of assembly of steel section should be less interruptive as shown in Figure 5.4. The dimension of steel section reasonable to confine area to develop pressure to column, the cost-effective of lower weight was consider with high confine height as shown in Figure 5.5. Finally the rectangular tube was suitable to select to use to external steel collars.

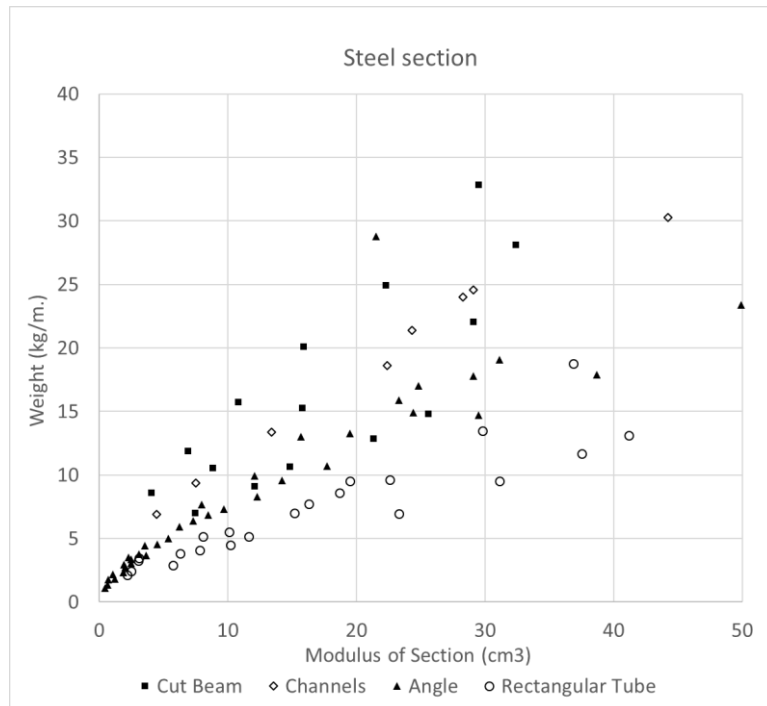


Figure 5.4 Modulus of section by weight of steel section

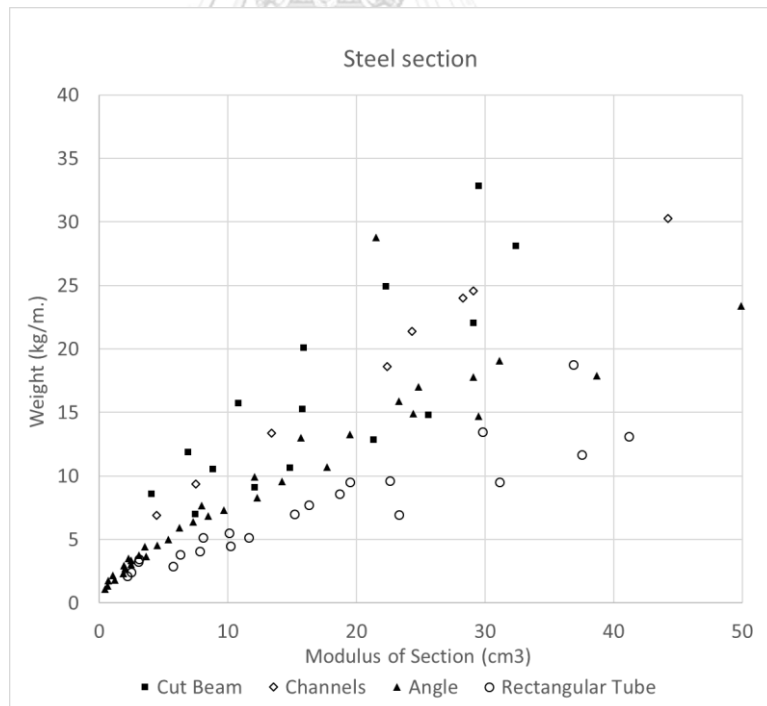


Figure 5.5 Confinement height of steel section

The rectangular tube section was used to strengthen the lap splice column LS that was failed by bond-slip. To increase the compressive strength of concrete to carry out bond-slip by distributions of lateral pressure as shown in Figure 5.6. The concrete under multiaxial stresses model was used to design the section of external steel collars. Overseas experimental research indicates that for axially loaded concrete cylinders, the axial strength will significantly improve if the cylinders are subjected to uniform confining fluid pressure. The increased amplitude is approximately proportional to the confining pressure. When  $\sigma_2$  is not very large, the ultimate compressive strength  $f'_{cc}$  in the direction of  $\sigma_1$  can be expressed as

$$f'_{cc} = f'_{co} + 4.1 \sigma_2$$

5.1

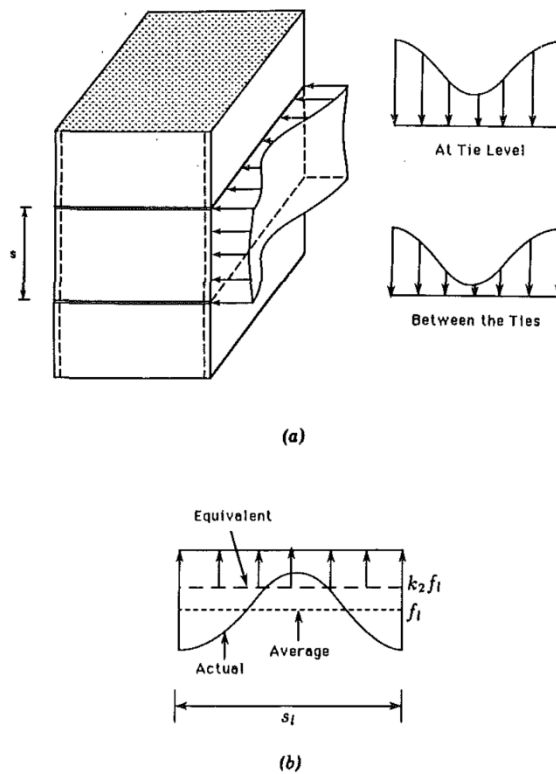


Figure 5.6 Distributions of lateral pressure (a) distribution of lateral pressure along member length. And (b) Actual, average, and equivalent lateral pressure

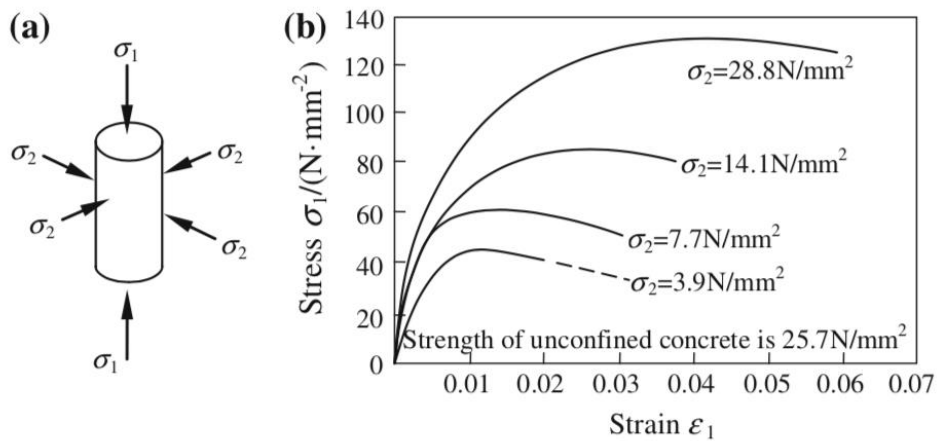


Figure 5.7 Concrete under multiaxial stresses

It was assumed that increasing the strength of concrete by two times can be used to strengthen the bond-slip failure.

Assume increase  $f'_c$  for 2 time to increase bond stress and the rectangular tube section  $50 \times 50 \times 2.3$  were choose with column specimens:  $f'_c = 23.6 \text{ Mpa}$

$$f'_{cc} = f'_{co} + 4.1 \sigma_2$$

$$\text{So : } 23.6 = 4.1 \sigma_2$$

$$\sigma_2 = 5.75 \text{ Mpa}$$

Distribute load to steel collar =  $5.75 \times 50 = 287.5 \text{ N/mm}$

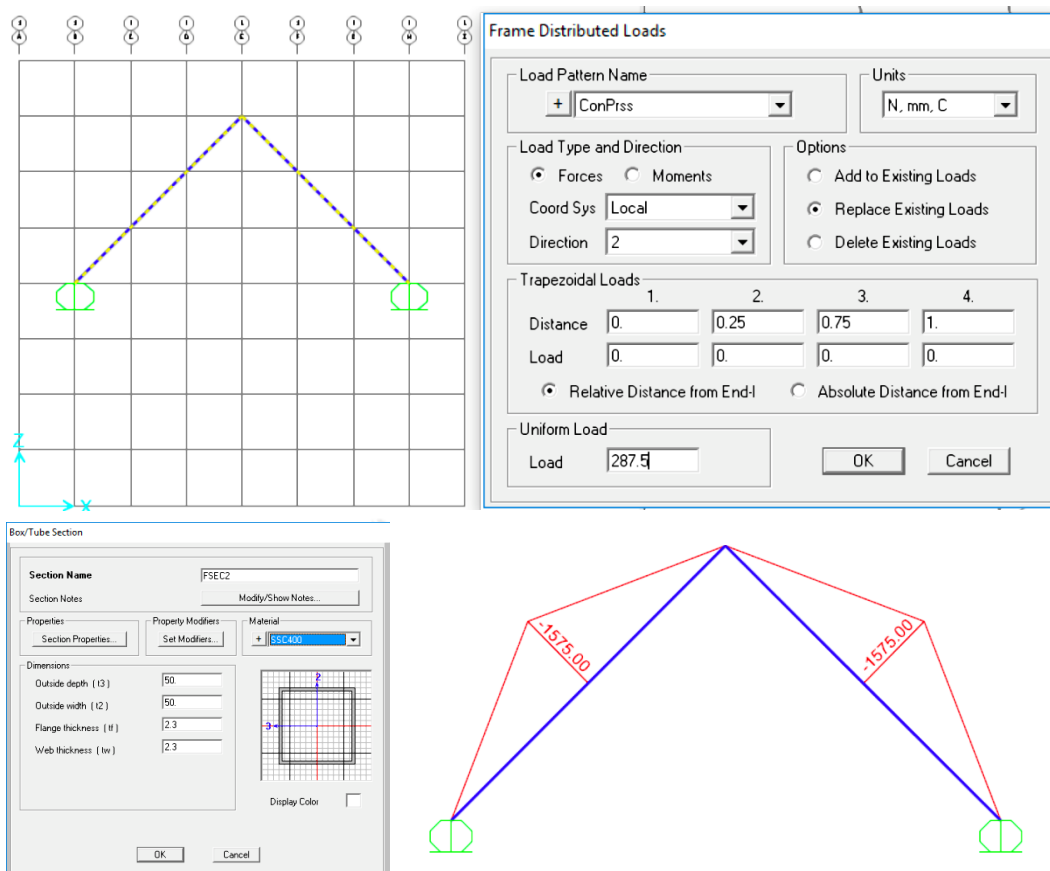


Figure 5.8 Section analysis by using SAP2000

Hollow section 50x50x2.3, Section of modulus =  $6.33 \text{ cm}^3 = 6330 \text{ mm}^3$

Steel SSC400 yeild stress = 245Mpa, Max moment = 1550 kN-mm

Moment occur in member = 6468 kN-mm, Trial Distribute load to member = 70N/mm

Moment occur in member = 1575 kN-mm = Max moment of Hollow section 50x50x2.3

So it can give max confinement pressure = 5.74Mpa

Table 5.2 Steel Section : Rectangular Hollow section : 50x50x2.3

Side length	Thickness (mm)	Weight (kg/m)	Cross section area (cm <sup>2</sup> )	I <sub>x</sub> ,I <sub>y</sub> (mm <sup>4</sup> )	Z <sub>x</sub> ,Z <sub>y</sub> (mm <sup>3</sup> )
50x50	2.3	3.34	4.25	15.82	6.33





### 5.3 Experimental program and test configuration

#### 5.3.1 Specimen details

In order to investigate the seismic response of the columns with lap splice the specimens were designed as LS specimen strengthen with steel collars. The columns were cast in the same batch of columns as in chapter 3. The columns cross section is 400 mm x 400 mm, and the column height is 2200 mm. The lateral load was applied in such a way that giving the aspect ration of 5.5. Eight longitudinal reinforcing bars with a diameter of 25 mm were used. The transverse steel tie diameter is 12 mm with 200 mm spacing. Bar-ends were bent at 135-degree and extended to 48mm (4 times diameters of the transverse reinforcement steel) according to the EIT. 1008-38 guideline.

The variable investigated in the specimens is volumetric of external steel collars as shown in Table 5.3. The specimen (denoted as Unit LS) contained all its lap splices with 700mm length or 28 times of diameters of longitudinal reinforcement in the critical region, same as chapter 3.

Table 5.3 Volumatic of external steel collars of column specimen

ID	Amount of external steel collars	The spacing of external steel collars	Strengthening height	Volumetric of external steel collars
SC1	11	100 mm	1100 m	0.04826
SC2	6	200 mm	1100 m	0.02632
SC3	4	333 mm	1100 m	0.01755

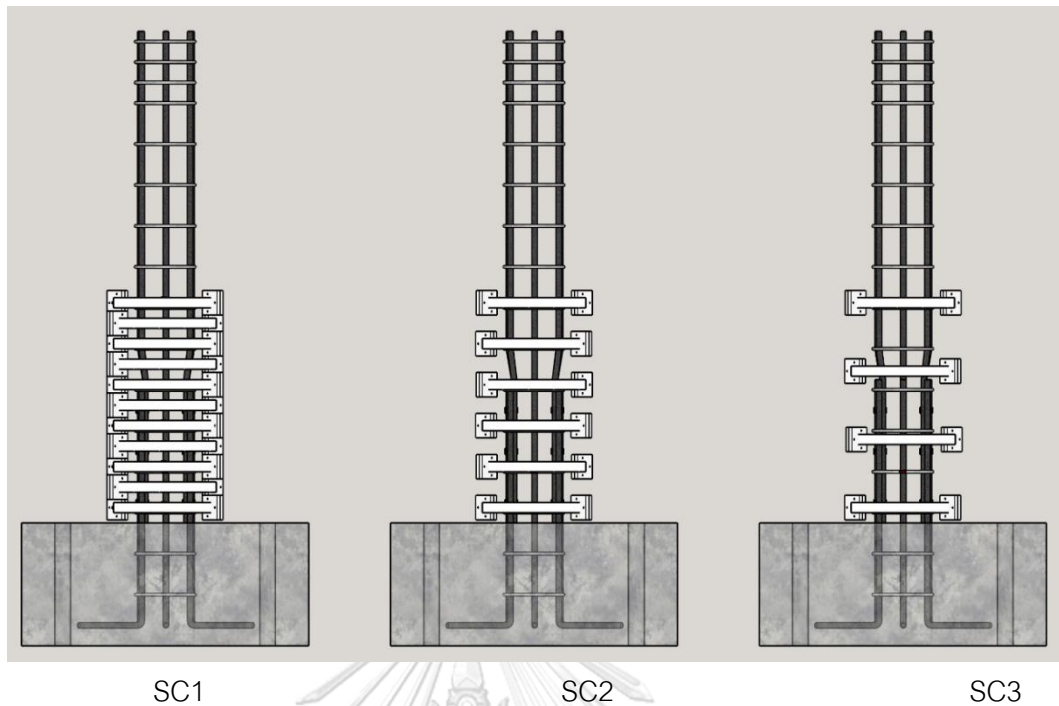
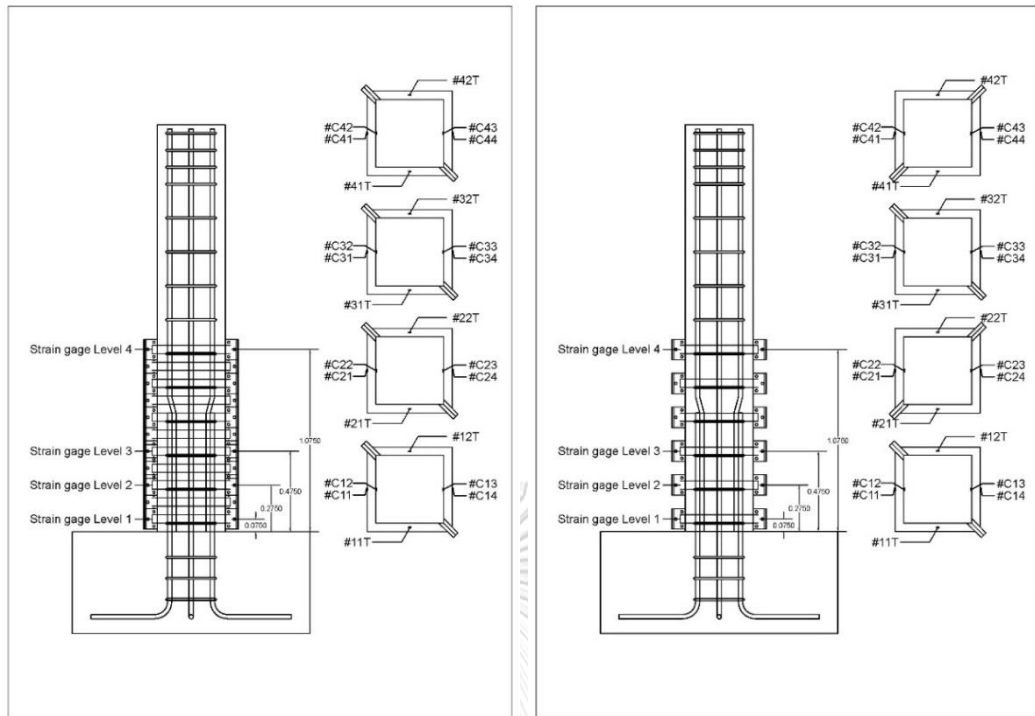


Figure 5.11 Lap splice column strengthened by using steel collars

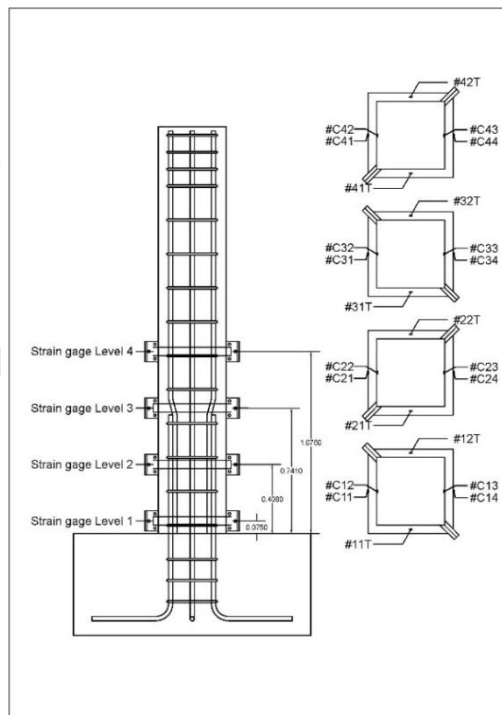
### 5.3.2 Instrumentation of strain gage on steel collars

Strain gages were used to monitor strains in steel collars. These strain gages were installed before strengthening of the columns. The expected internal force was selected to monitor strains in the reinforcing bars during the test. The locations of strain gages and abbreviations are shown in for specimen SC1, SC2 and SC3, respectively. The strain gages were installed on the steel collars to measure the bending and axial force.



SC1

SC2



SC3

Figure 5.12 Strain gage location on steel collars

### 5.3.3 Testing setup and strengthening method

The collars were installed in an alternating orientation sequence by rotating each successive collar 90 degrees about the column longitudinal axis, balancing any possible effect arising from the restraint difference between the rigid and bolted corners. The gap between collars and column edge were filled by Epoxysikadur-42th®. After 24 hours of strength developing of epoxy, the column was testing setup into a test frame. The instrumental and test configuration was setup same as chapter 3.2 as shown in Figure 5.13 to Figure 5.17

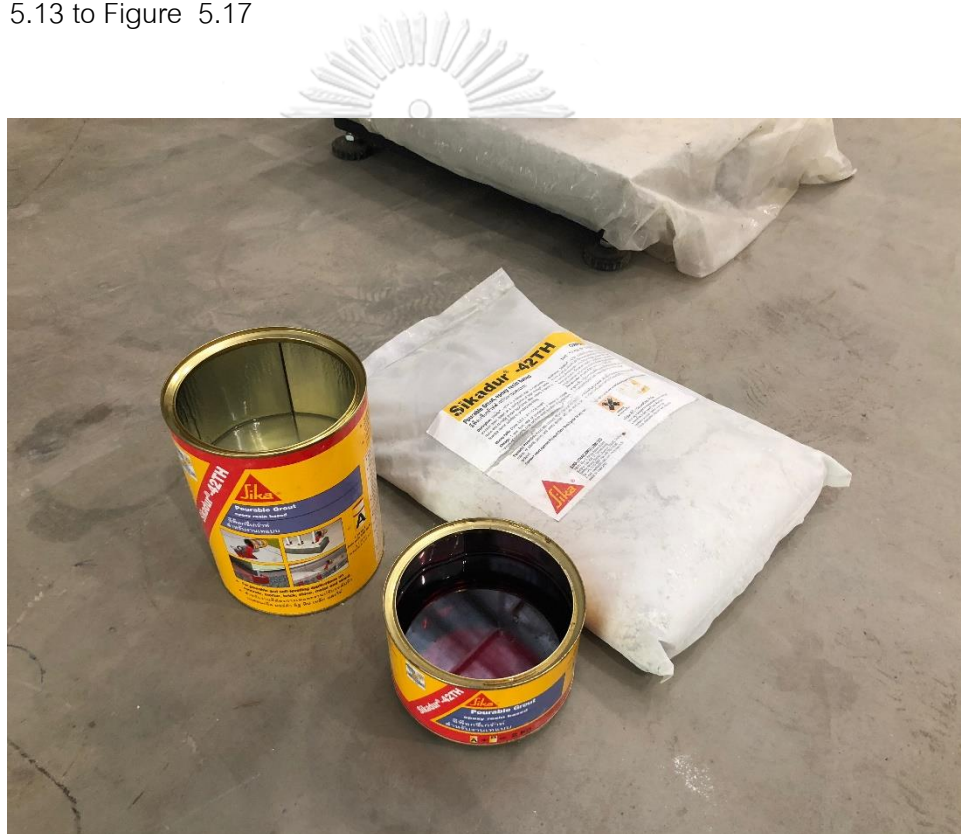


Figure 5.13 Epoxy use to fill the gap between collars and column edge



Figure 5.14 Arrange and adjust leveling the steel collars into column SC1



Figure 5.15 Gap-fill between column and steel collars by using epoxy



Figure 5.16 Completely strength by using steel collars



Figure 5.17 Strengthen column SC1

## 5.4 Experimental Result and discussion

In this section, the performance of lap-splice column specimens strengthen with steel collars is presented in terms of damage behavior and the lateral strength-deformation. The results of curvature variation are also discussed. Moreover, a comparison envelopes curve of specimens will also discuss in detail in this chapter.

### 5.4.1 Experimental result of specimen SC1

Specimen SC1 has contained all its lap splices with 700mm length in the critical region. Strengthening by using steel collars with spacing 100mm along the column 1100 mm height with the external Volumatic ratio is 0.04826.

#### 5.4.1.1 Progressive damage of specimen SC1

The column specimen SC1 has small number of cracks during the early experiment state. The first few observable cracks after the movement rate reached 0.5% and have a horizontal direction, after that the cracks went toward a 45 degree angle, continuing from the horizontal direction with 1.5% movement rate along the column height at 1700 mm. When the movement rates reached 2%-5%, the concrete began to crush at the base. Afterward, the concrete cover began to spall and the concrete being crushed thoroughly. Finally, when the concrete at base are no more shattered, which caused it to collapse. For this sample, the reinforced concrete column has a horizontal displacement at the yield point of 39 mm, the highest horizontal movement is 136.8 mm, and the highest lateral force recorded is 148 kN.

Table 5.4 Experimental results specimen SC1

SC1	Load (kN)	Displacement (mm)	% Drift
$P_{max}$	148	70.3	3.20%
$0.8 P_{max}$	118	136.8	6.22%

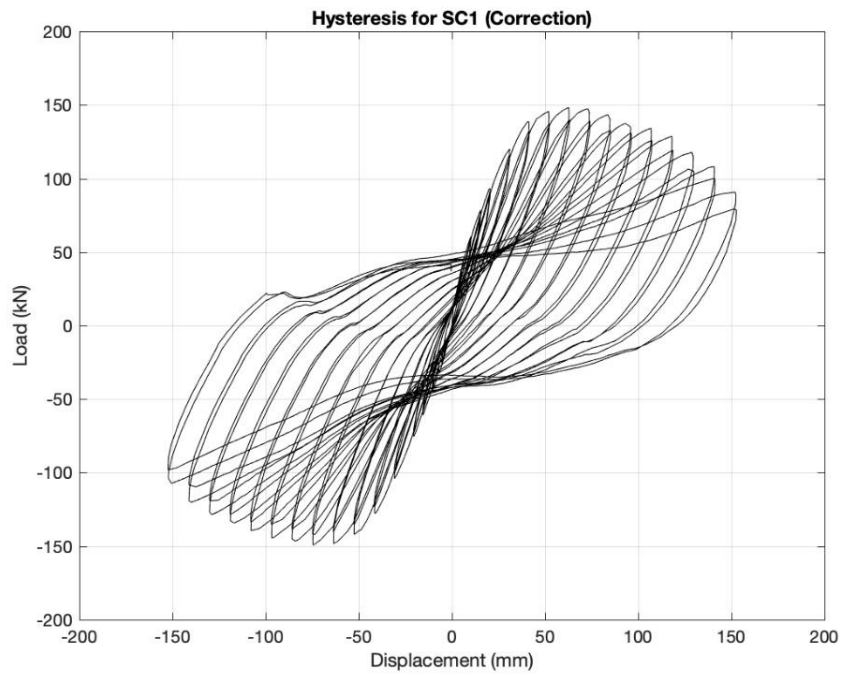


Figure 5.18 Hysteresis of SC1 specimen

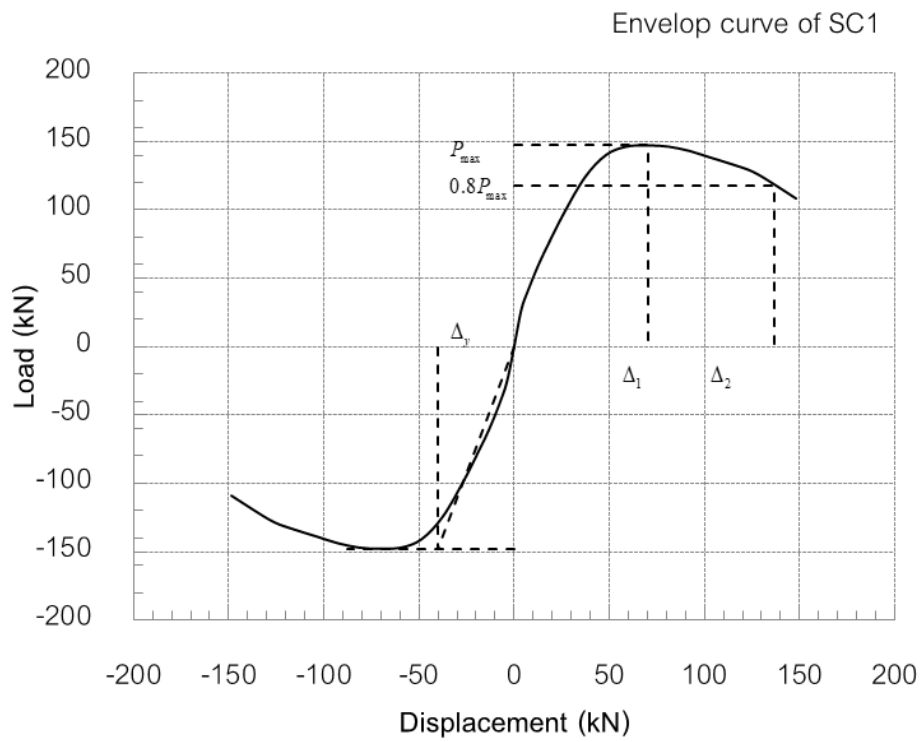


Figure 5.19 Envelop curve of SC1 specimen



#### 5.4.1.2 Appearance failure of specimen SC1

The lap-splice specimen strength by using external steel collars spaced at 100 mm was failed by flexural joint failure. The base between the footing and first collars was crushing, as shown in Figure 5.20. As a result, the loss of concrete to subject compressive stress leads to the capacity of the lateral load was drop to 80% finally.

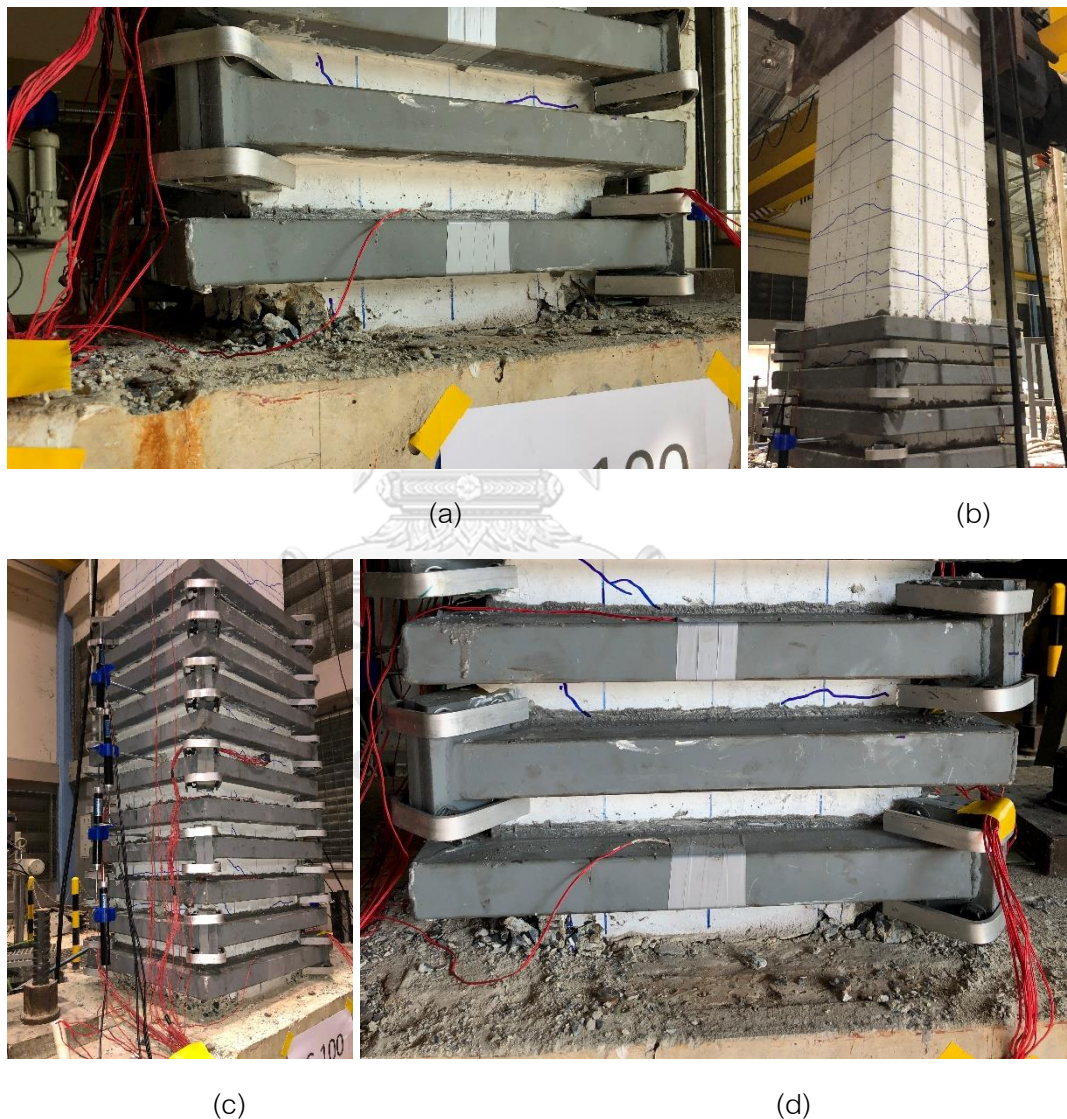
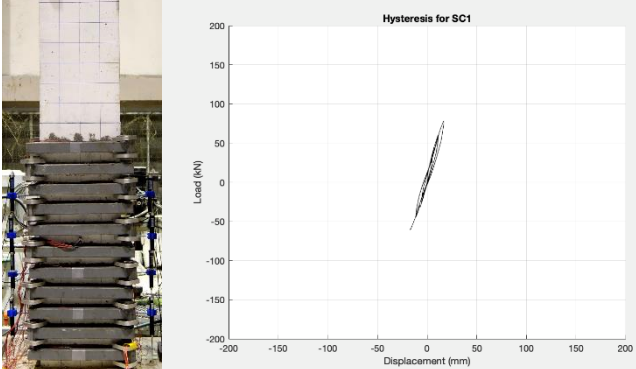
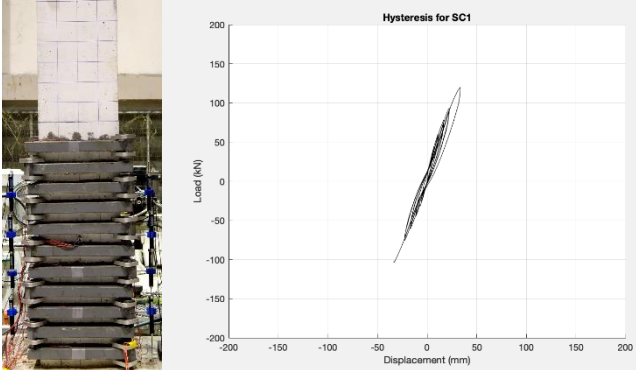
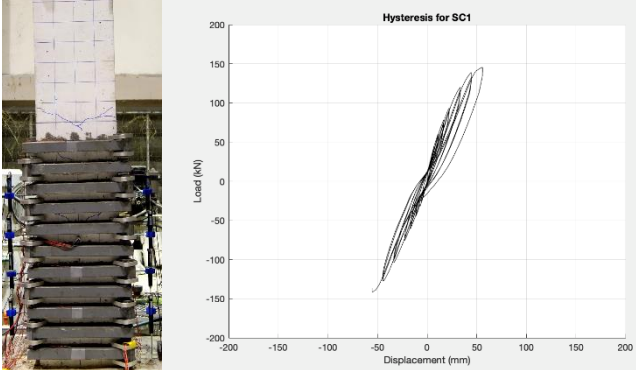
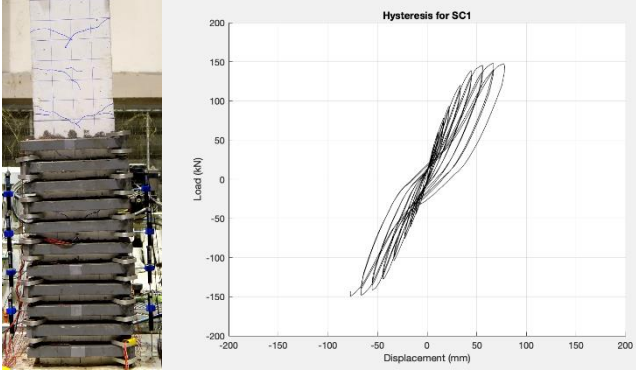
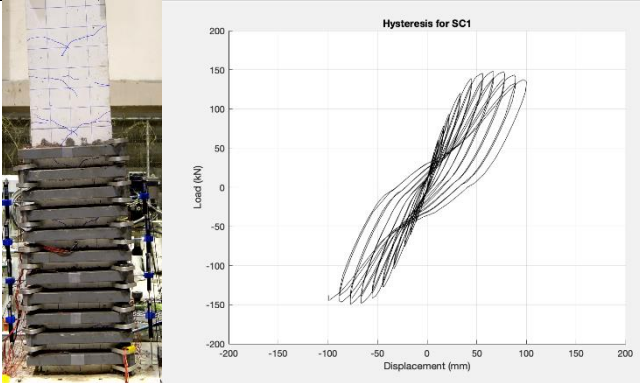
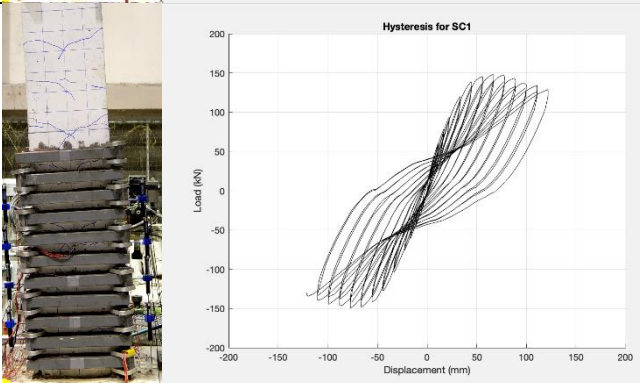
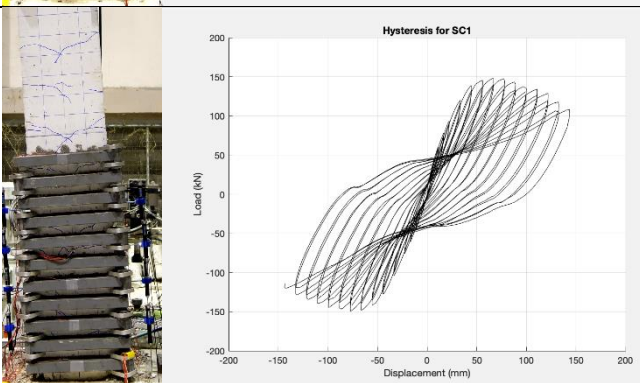
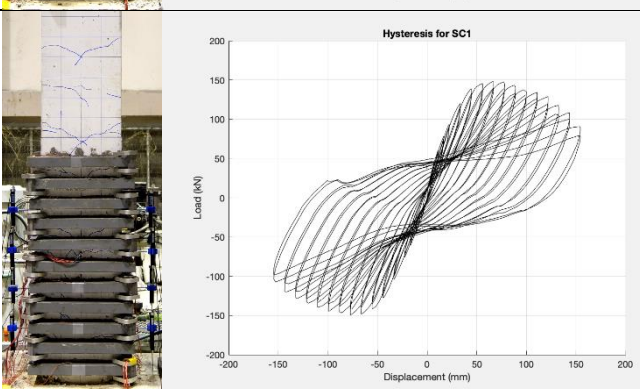


Figure 5.20 Flexural joint failure of strengthening lap-splice column SC1

%Drift	Crack pattern and lateral load-displacement	Appearance damage
0.5%		No crack
1.0%		few cracks in horizontal direction
2.0%		Increase number of cracks continuing went toward a 45 degree angle
3.0%		Concrete crushing in the corner of column and cracks went toward along 1700 mm column height

%Drift	Crack pattern and lateral load-displacement	Appearance damage
4.0%		Concrete crushing at base
5.0%		Concrete being crushed at base
6.0%		Concrete at the base still crushing Increasingly.
7.0%		The column base failed in flexural joint.

### 5.4.1.3 Strain in Reinforcing steels of specimen SC1

Strengthening column with steel collars spaced at 100 mm shows the result of developing to yield strength. Strain gage #23 and #24 are measure in longitudinal reinforcing bar anchored into the footing and popped up to overlap with the other bar to column top. Place on the corner bar with 50 mm height above footing, shows the longitudinal reinforcement can develop yield strength at the first cycle of 1.0% drift. As shown in Figure 5.21. In contrast, the compression steel doesn't yield. Strain gage #C13 and #C14 are measures in steel collars that shows the compression and tension strain, which mean the collars subject the bending to develop the passive confinement to the column.

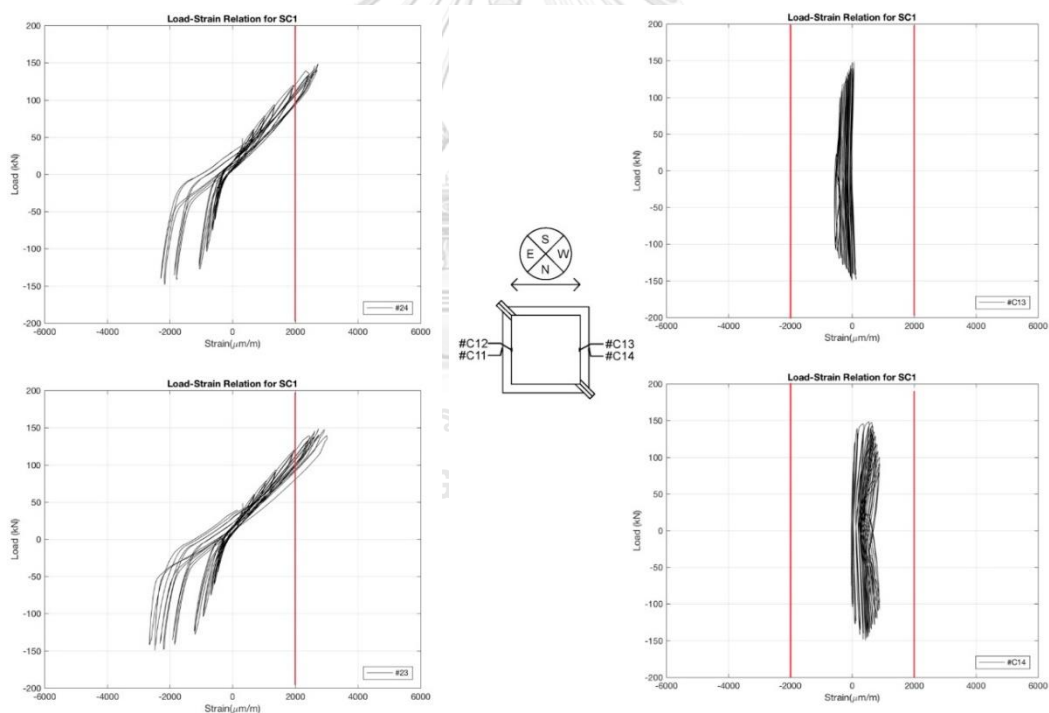


Figure 5.21 Strain in the longitudinal reinforcement of SC1 at level 2 and steel collars

#### 5.4.2 Experimental result of specimen SC2

Specimen SC2 has contained all its lap splices with 700mm length in the critical region. Strengthening by using steel collars with spacing 200mm along the column 1100 mm height with the external Volumatic ratio is 0.02632.

##### 5.4.2.1 Progressive damage of specimen SC2

The sample SC2 has a small number of cracks during the early experiment state. The first few observable cracks after the movement rate reached 0.5% and have a horizontal direction, after that the cracks went toward a 45 degree angle, continuing from the horizontal direction with 1.5% movement rate along the column 1700 mm height. When the movement rates reached 2%-5%, the concrete began to crush at base. Afterward, the concrete cover began to spall, which the concrete being crushed thoroughly. Finally, when the concrete at its base are no more shattered, which caused it to collapse. For this sample, the reinforced concrete column has a horizontal displacement at the yield point of 43.6 mm., the highest horizontal movement is 120.4 mm, and the highest lateral force recorded is 151 kN.

Table 5.5 Experimental results specimen SC2

SC2	Load (kN)	Displacement (mm)	% Drift
$P_{max}$	151	76.3	3.47%
$0.8 P_{max}$	121	120.4	5.47%

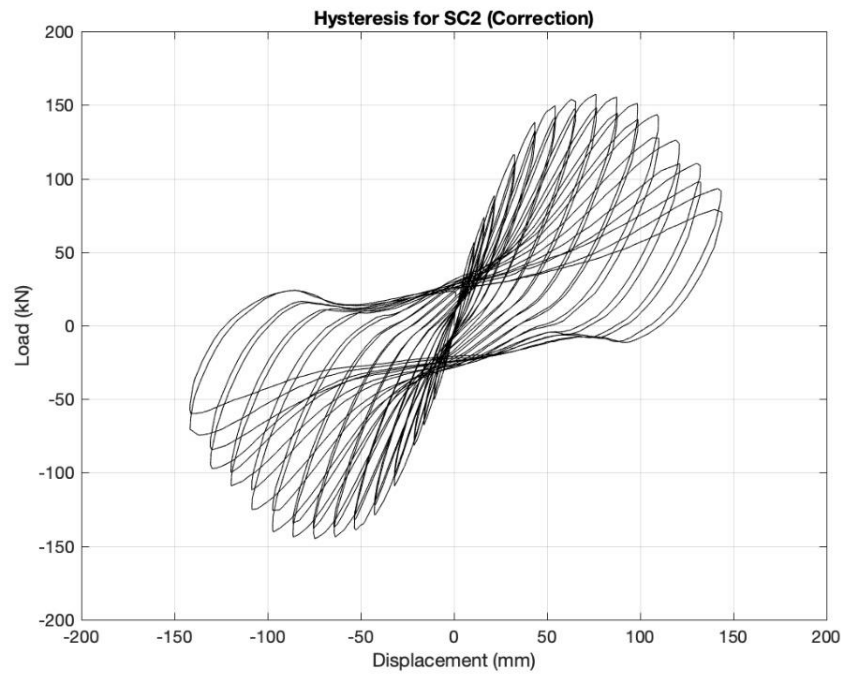


Figure 5.22 Hysteresis of SC2 specimen

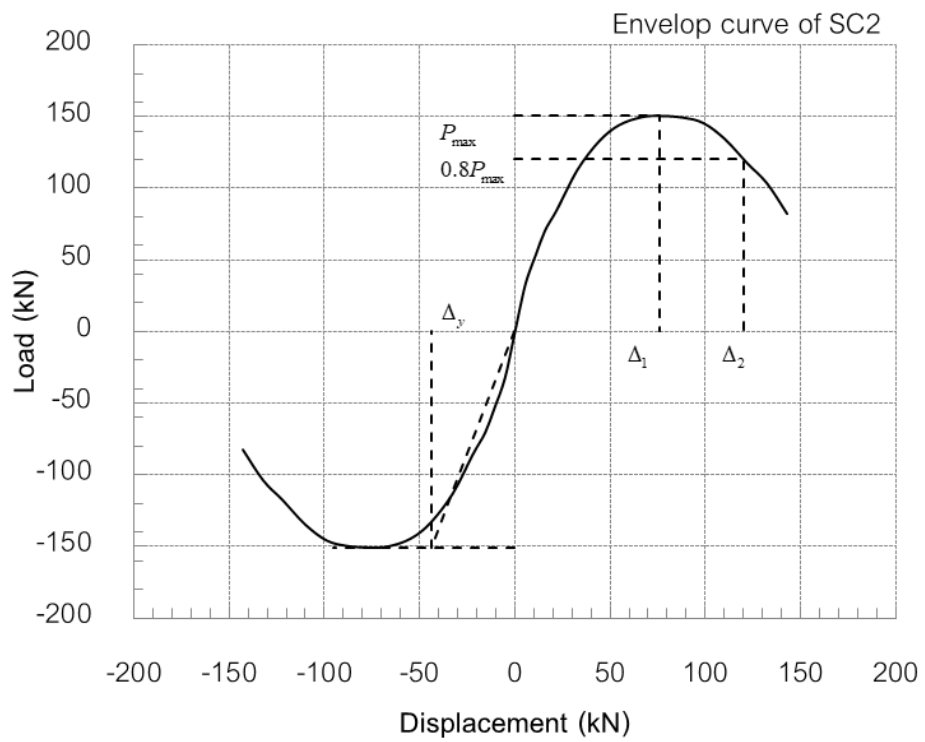


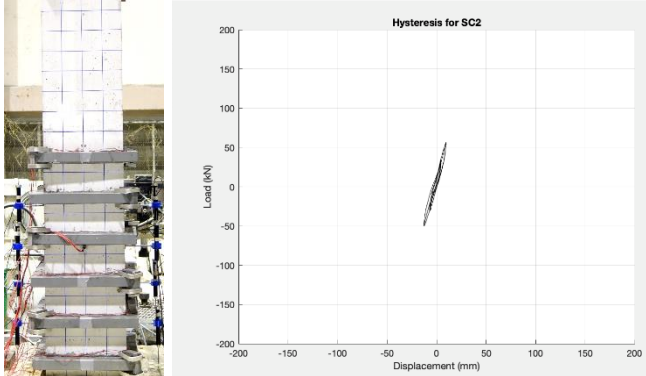
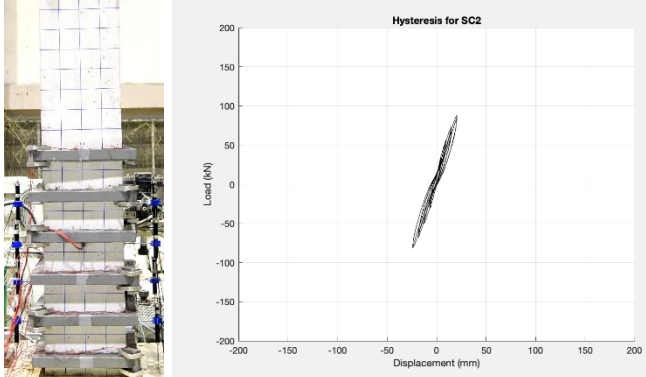
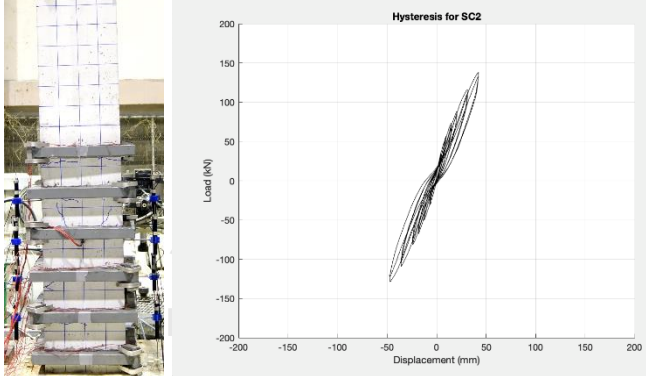
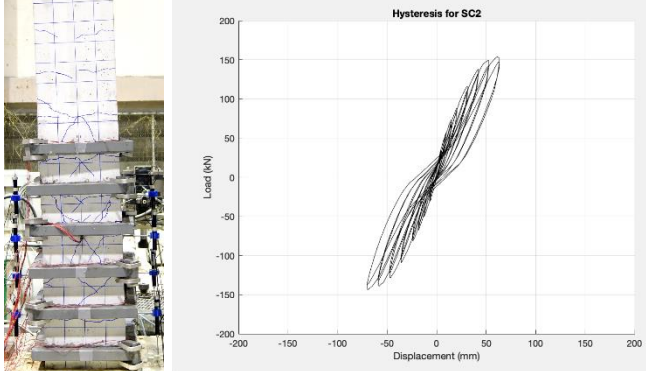
Figure 5.23 Envelop curve of SC2 specimen

#### 5.4.2.2 Appearance failure of specimen SC2

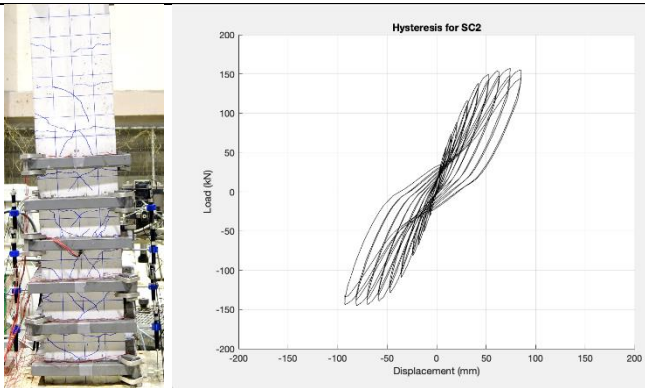
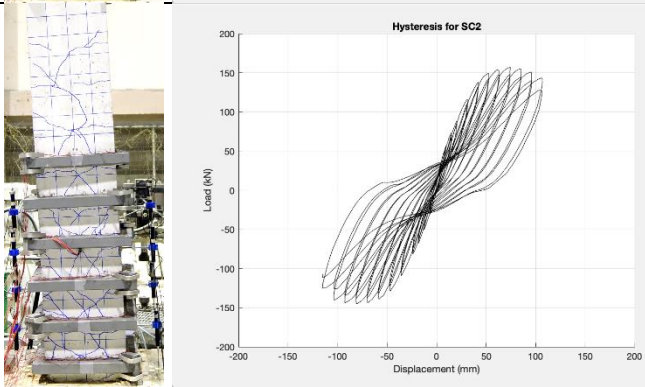
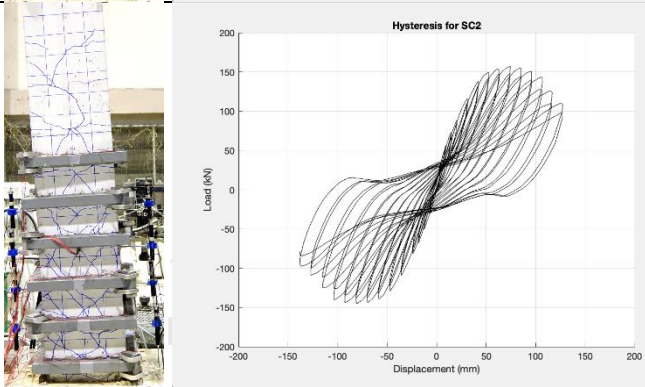
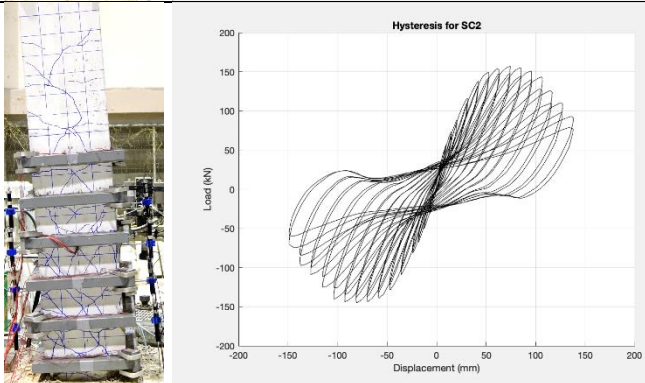
The lap-splice specimen strengthened by using external steel collars spacing 200 mm was failed by flexural joint failure. The crushing of the concrete was observed at the interface of foundation and column as shown in Figure 5.24. As a result, the loss of concrete to subject compressive stress leads to the capacity of the lateral load was drop to 80% finally.



Figure 5.24 Flexural joint failure of strengthening lap-splice column SC2

%Drift	Crack pattern and lateral load-displacement	Appearance damage
0.5%		<p>small number of cracks after the movement rate reached 0.5% and has a horizontal direction</p>
1.0%		<p>Increase number of cracks continuing</p>
2.0%		<p>cracks went toward a 45 degree angle, continuing from the horizontal direction</p>
3.0%		<p>Concrete crushing in the corner of column and cracks went toward along the column 1700 mm height</p>



%Drift	Crack pattern and lateral load-displacement	Appearance damage
4.0%		Concrete spalling along vertical crack
5.0%		crushing occurs at column base between steel collars
6.0%		Further crushing of the concrete
7.0%		The column base failed in flexural joint

### 5.4.2.3 Strain in Reinforcing steels of specimen SC2

The strengthening column with steel collars spaced at 200 mm shows the result of developing to yield strength. Strain gage #23 and #24 are measure in longitudinal reinforcing bar on the corner bar with 50 mm height above footing, shows the longitudinal reinforcement can develop yield strength at the first cycle of 1.0% drift. As shown in Figure 5.21. In contrast, the compression steel doesn't yield. Strain gage #11 and #12 are measures in longitudinal reinforcing bar anchored into the footing below footing surface can develop both of compression and tension to yield strain.

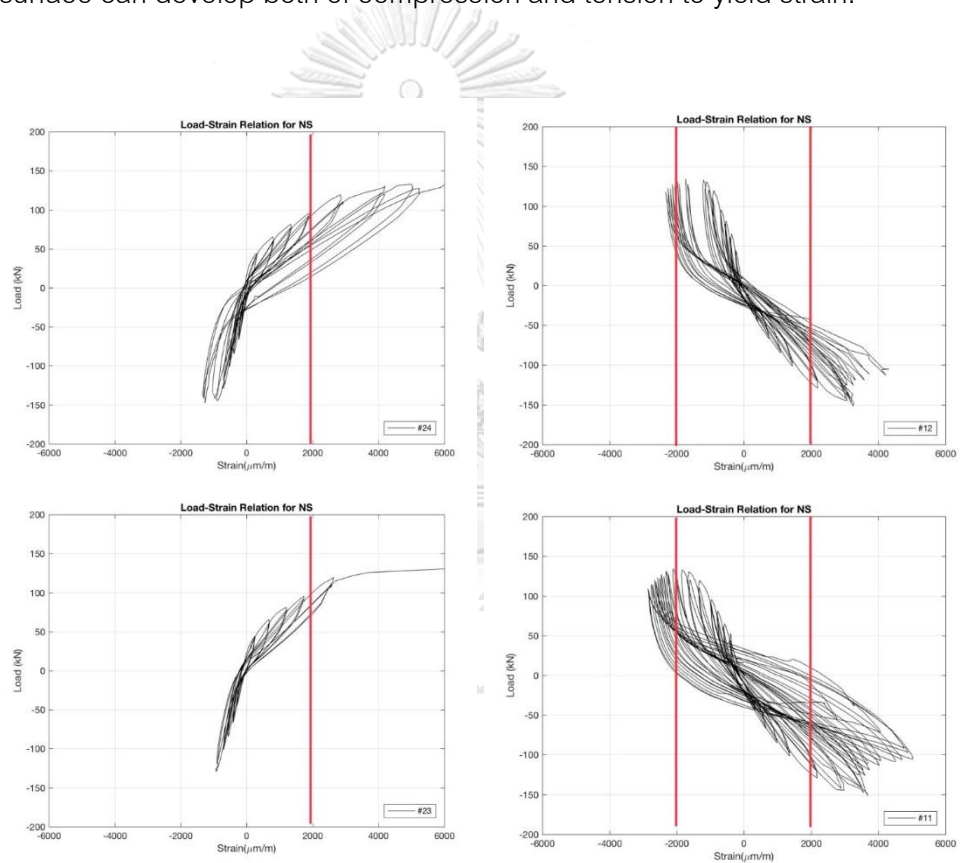


Figure 5.25 Strain in the longitudinal reinforcement of SC2 at level 1 and level 2

#### 5.4.3 Experimental result of specimen SC3

Specimen SC3 has contained all its lap splices with 700mm length in the critical region. Strengthening by using steel collars with spacing 333mm along the column 1100 mm height with the external Volumatic ratio is 0.01755.

##### 5.4.3.1 Progressive damage of specimen SC3

The column specimen SC3 began to crack at the lateral drift of 0.25%. At this stage, few observable cracks after the movement rate reached 0.5% and have a horizontal direction, after that the cracks went toward a 45 degree angle, continuing from the horizontal direction with 1.5%-2% movement rate along the column 1700 mm height. When the movement rates reached 2%-5%, the crack began at the reinforcing steel of 700 mm height and the concrete began to crush around the base of the column onto the height of 400 mm. Then, the column has more cracks and spalling of concrete at the movement rate of 2.5%-3.5% to 700 mm. When the column took repeated force at the movement rate of 4%-5%, the left surface of the column began to crack and more concrete spall until the concrete on all sides of the column peel off to 700 mm. in height. At the same time, the right side of the column has some cracks and peeled off the concrete at the corners to the height of 700 mm, which is a lengthwise extension of reinforced steel. For this sample, the reinforced concrete column has a horizontal displacement at the yield point of 43.9 mm, the highest horizontal movement is 82.7 mm, and the highest lateral force recorded is 137 kN.

Table 5.6 Experimental results specimen SC3

SC2	Load (kN)	Displacement (mm)	% Drift
$P_{max}$	137	61.4	2.79%
$0.8 P_{max}$	109	82.7	3.76%

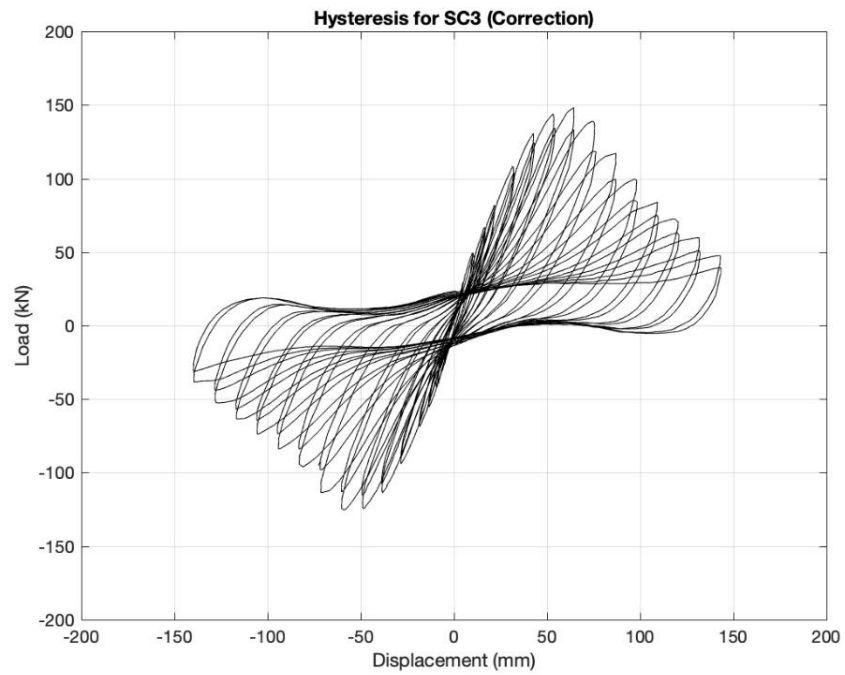


Figure 5.26 Hysteresis of SC3 specimen

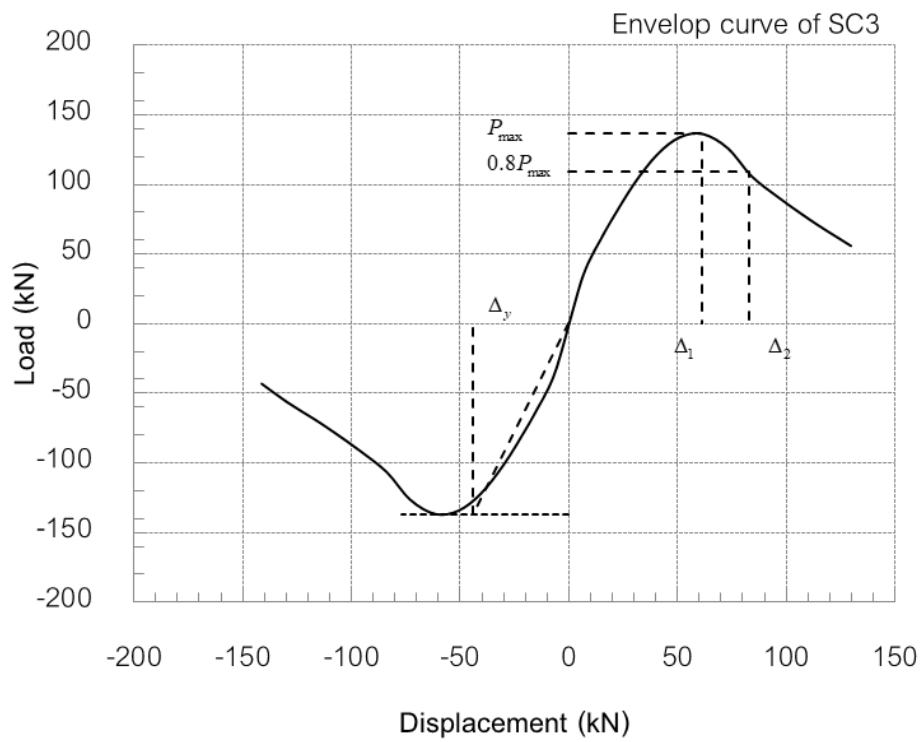


Figure 5.27 Envelop curve of SC3 specimen

#### 5.4.3.2 Appearance failure of specimen SC3

The lap-splice specimen strength by using external steel collars spacing 333 mm was failed by bond slip failure. The crushing of the concrete was observed at the interface of the column base and foundation as shown in Figure 5.28. As a result, the loss of concrete to subject compressive stress leads to the capacity of the lateral load was drop to 80% finally.

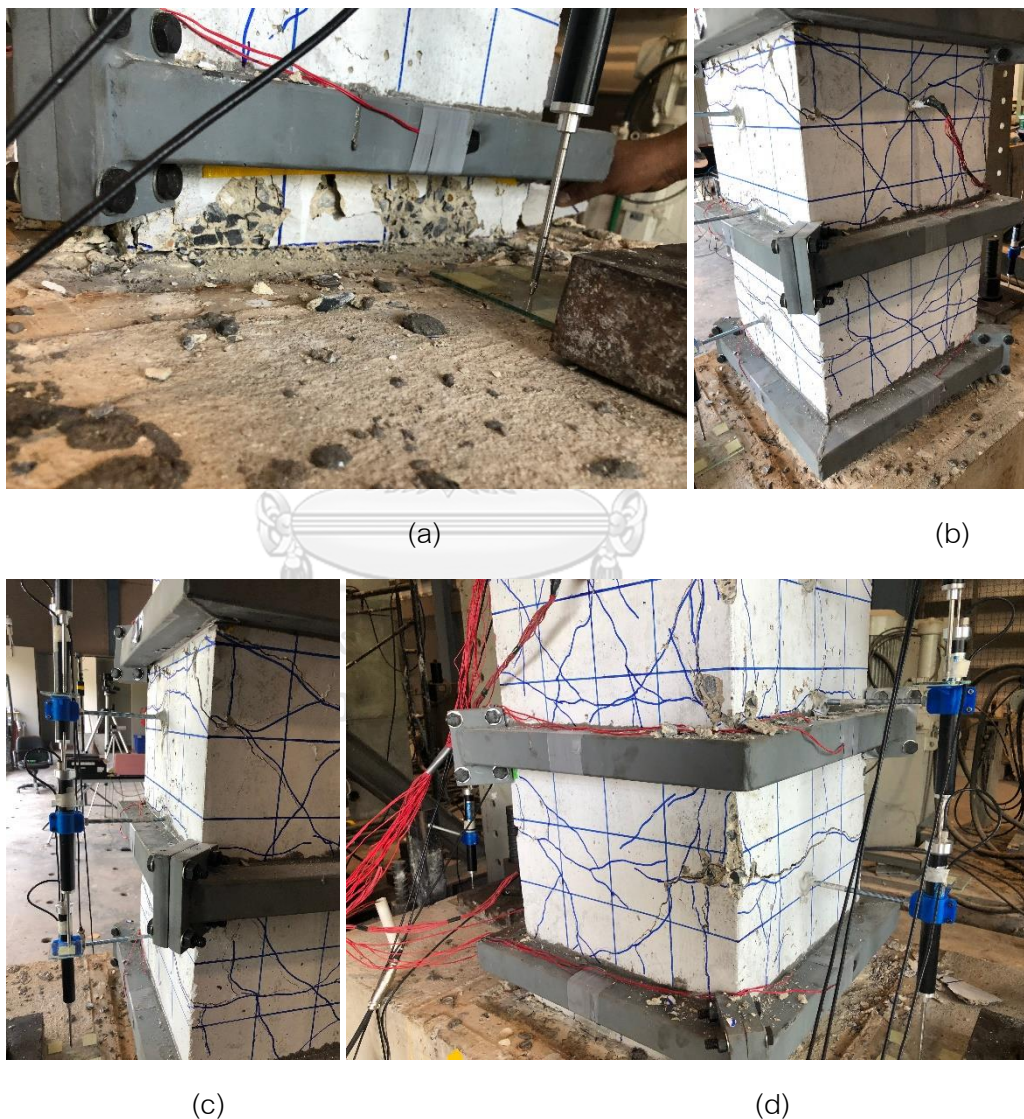
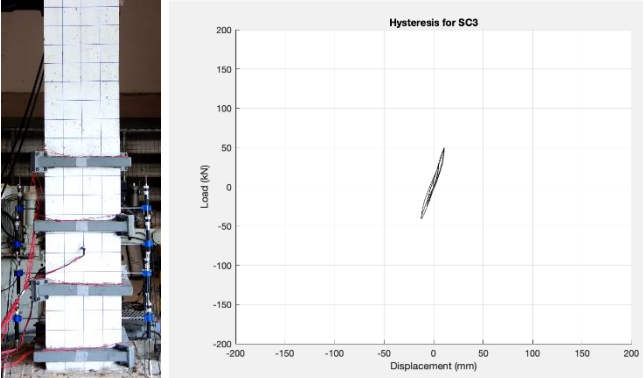
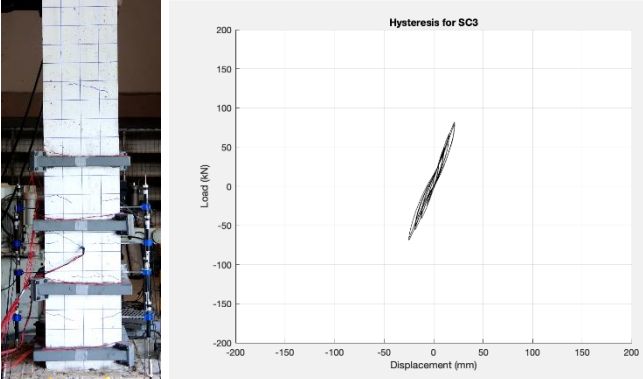
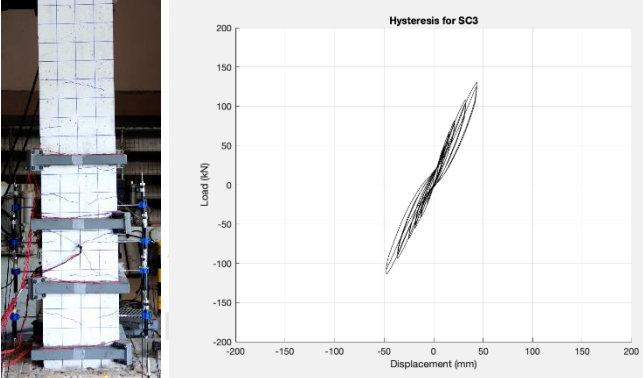
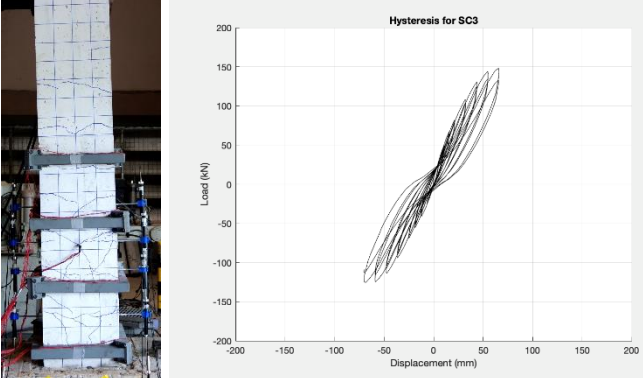
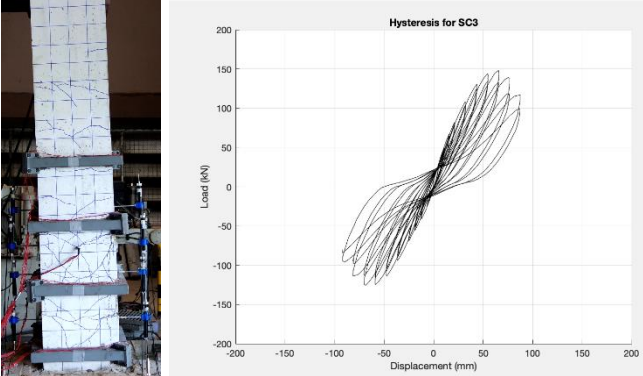
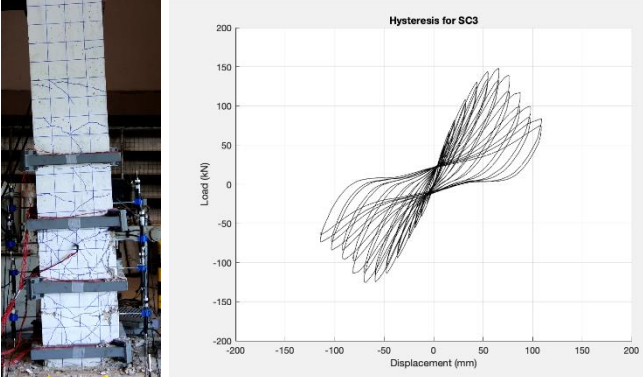
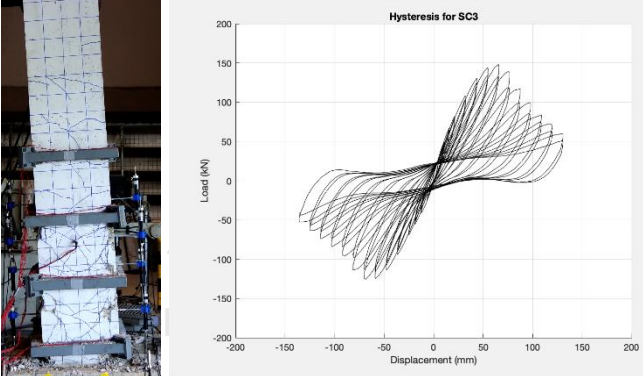
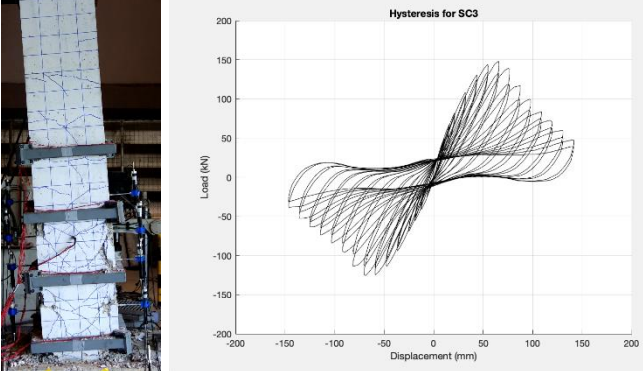


Figure 5.28 Flexural joint failure of strengthening lap-splice column SC3

%Drift	Crack pattern and lateral load-displacement	Appearance damage
0.5%		<p>small number of cracks after the movement rate reached 0.5% and has a horizontal direction</p>
1.0%		<p>Increase number of cracks continuing</p>
2.0%		<p>cracks went toward a 45 degree angle, continuing from the horizontal direction</p>
3.0%		<p>Concrete crushing in the corner of column and cracks went toward a vertical , continuing from 45 degree angle</p>

%Drift	Crack pattern and lateral load-displacement	Appearance damage
4.0%		Concrete spalling along vertical crack
5.0%		Buckling occurs in a longitudinal reinforcing bar between two tie hoops
6.0%		Tie hoop failure by the bar end of tie hoop are open cause the column lost the shear strength reasonable to shear crack happen instantly
7.0%		The second tie hoop are break off cause the column lost the shear strength reasonable fail finally

### 5.4.3.3 Strain in Reinforcing steels of specimen SC3

The strengthening column with steel collars spacing 333 mm shows the result of developing to yield strength. Strain gage #23 and #24 are measure in longitudinal reinforcing bar anchored into the footing and popped up to overlap with the other bar to column top. Place on the corner bar with 50 mm height above footing, shows the longitudinal reinforcement can develop yield strength at the first cycle of 1.0% drift. As shown in Figure 5.29. In contrast, the compression steel doesn't yield. Strain gage #11 and #12 are measures in longitudinal reinforcing bar anchored into the footing below footing surface can develop both of compression and tension to yield strain.

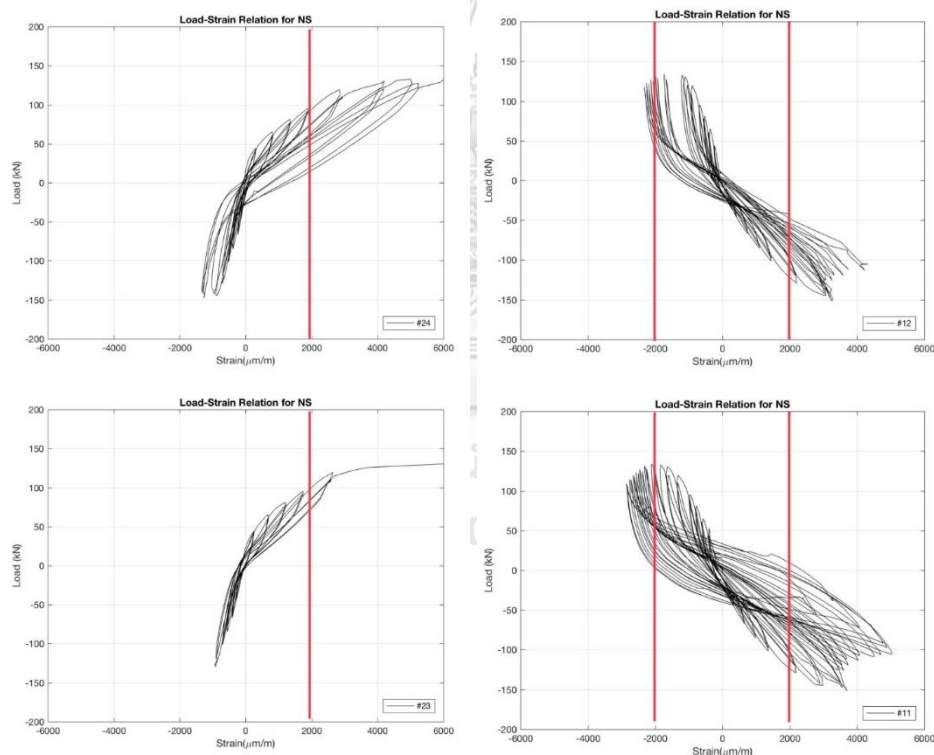


Figure 5.29 Strain in the longitudinal reinforcement of NS at level 1 and level 2



### 5.5 Comparison between column with and without strengthening of steel collars

The following sections will present the comparison of the specimen with and without steel collars in terms of ductility, average curvature, lateral strength degradation and energy dissipated by each specimen.

#### 5.5.1 Displacement ductility

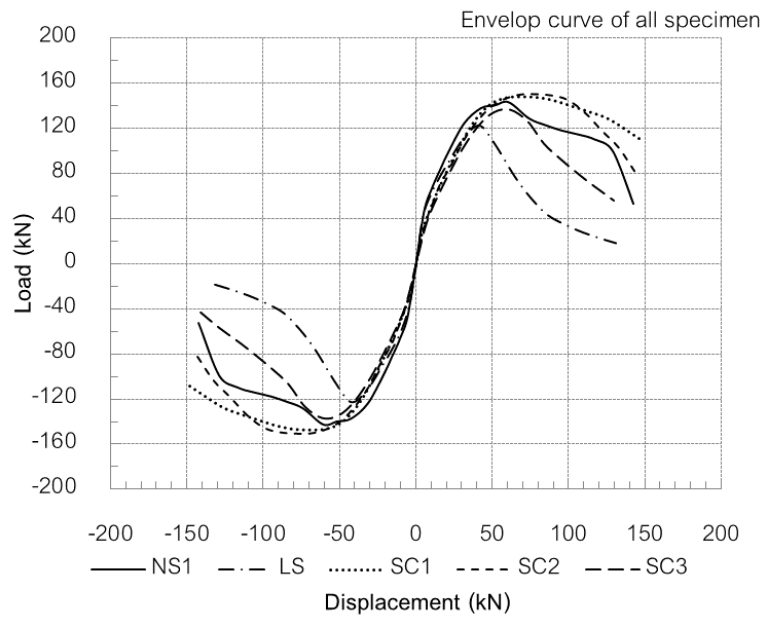


Figure 5.30 Envelop curve of all specimen

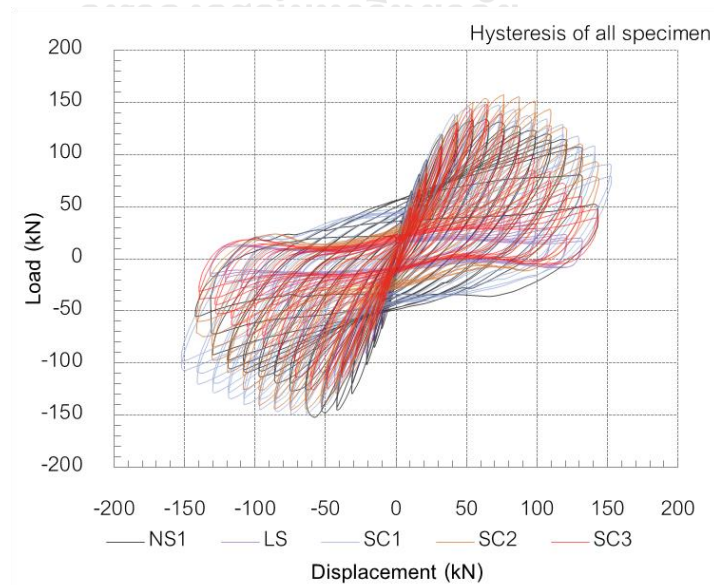


Figure 5.31 Hysteresis of all specimen

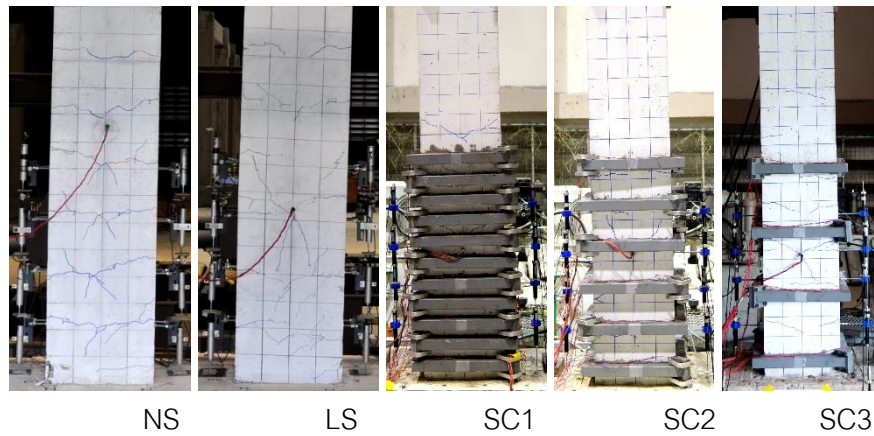


Figure 5.32 Damage state at 2.0% drift.

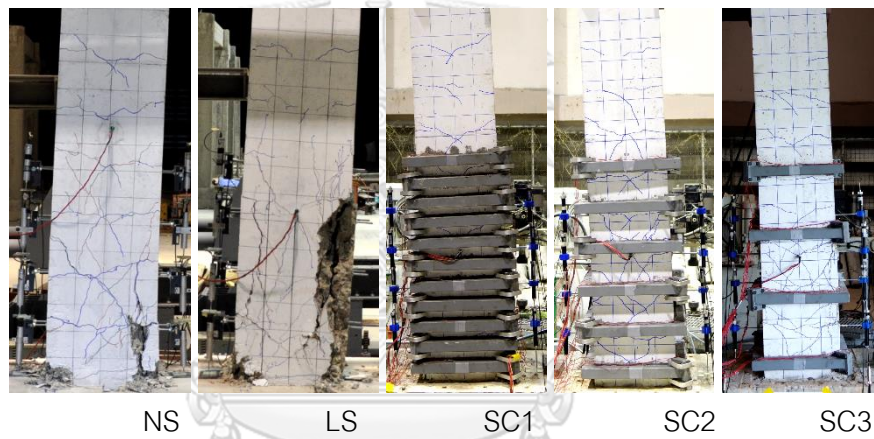


Figure 5.33 Damage state at 4.0% drift.

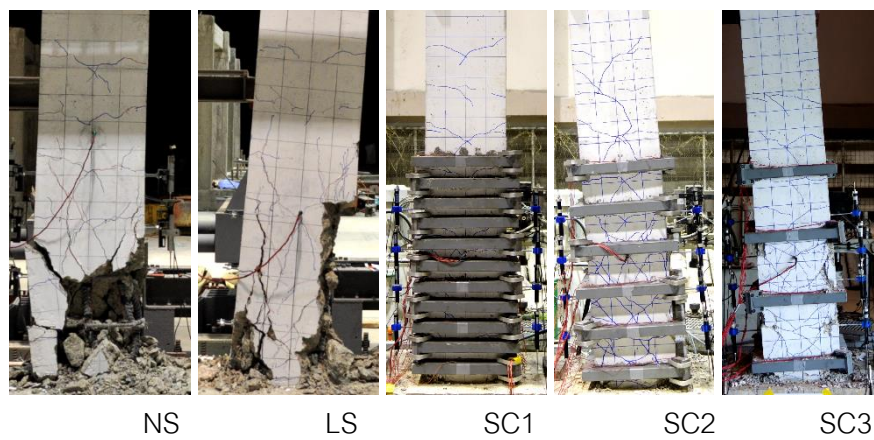


Figure 5.34 Damage state at failure

Table 5.7 Experimental results of lateral load capacity and displacement ductility of all specimen

Specimen	$P_{max}$	Disp@ $P_{max}$	$0.8 P_{max}$	Displ@ $0.8P_{max}$	Drift@ 0.8 $P_{max}$	Disp@75% secant	Ductility
NS	143	60.7	114	109.0	4.95	29.5	3.69
LS	122	41.9	98	55.8	2.54	35.3	1.58
SC1	148	70.3	118	136.8	6.22	39.8	3.43
SC2	151	76.3	121	120.4	5.47	43.6	2.76
SC3	137	61.4	109	82.7	3.76	43.9	1.88

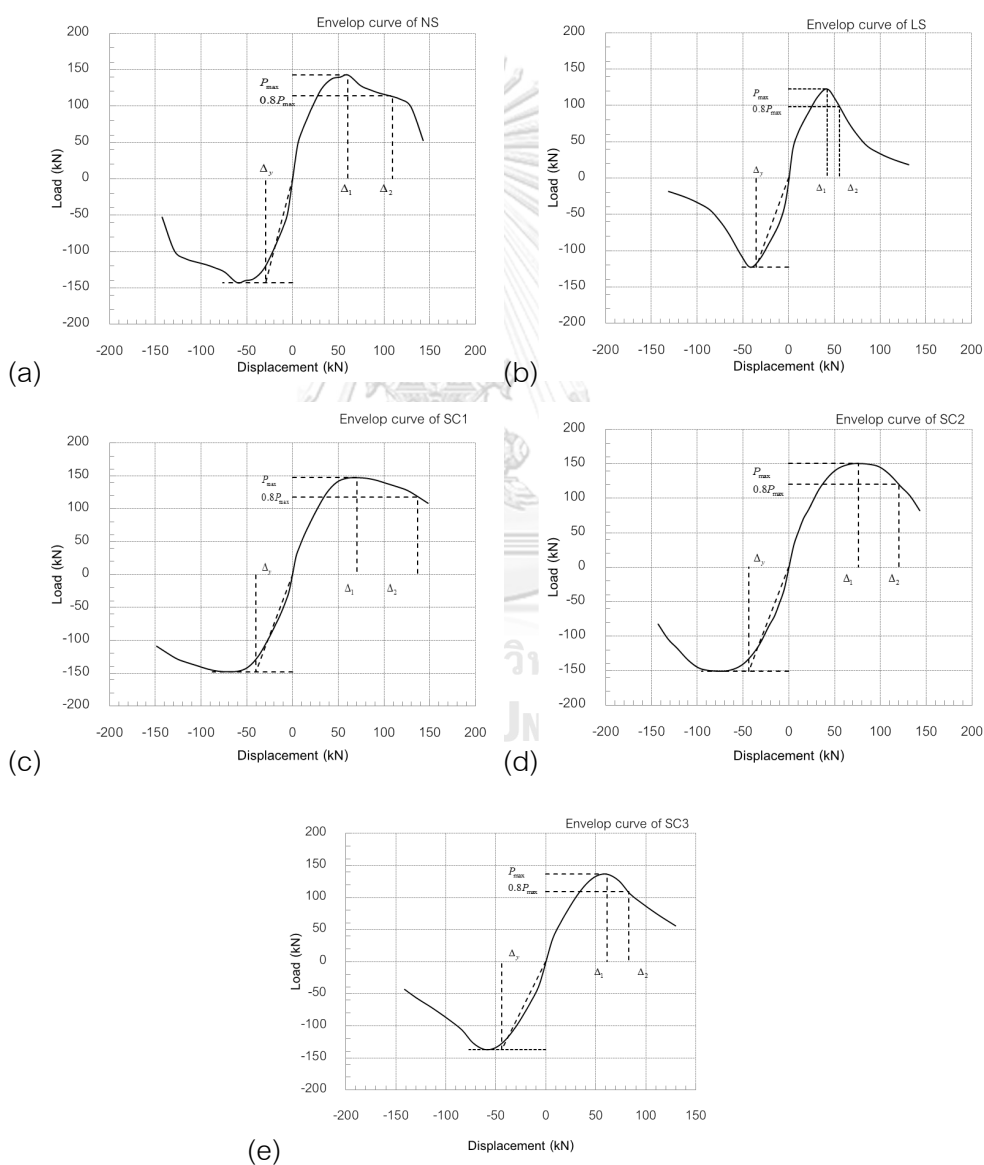


Figure 5.35 Envelop curve of (a) NS, (b) LS, (c) SC1, (d) SC2 and (e) SC3

### 5.5.2 Moment-curvature distribution

For calculation, the curvature of the column was divided into segments. Curvature between any two segments is calculated as the difference between measurements of vertical transducers attached on the sides of each segment divided by the product of the horizontal and vertical dimensions of each segment. The reinforcement detailing of all specimens with the curvature measurement levels are shown in Figure 5.36 to Figure 5.40. Curvature that indicates the bending force distribution to the section of column height. As results are in accordance with the result of displacement ductility for all specimens. The specimen without lap splices (NS) curvature is concentrated in the region of 400 mm where the maximum moment occurred. For the specimen with mechanical splice curvature are close to NS specimen. Different from the rotation of lap-splices specimen (LS) and the strengthen column (SC1, SC2 SC3) is concentrated in the region 200mm above the base for columns. Maximum curvature is concentrated in the region just above the lap-splices due to the crank portion of longitudinal reinforcement. Also, depicting that rotation at that location is higher than at the base after bond failure.

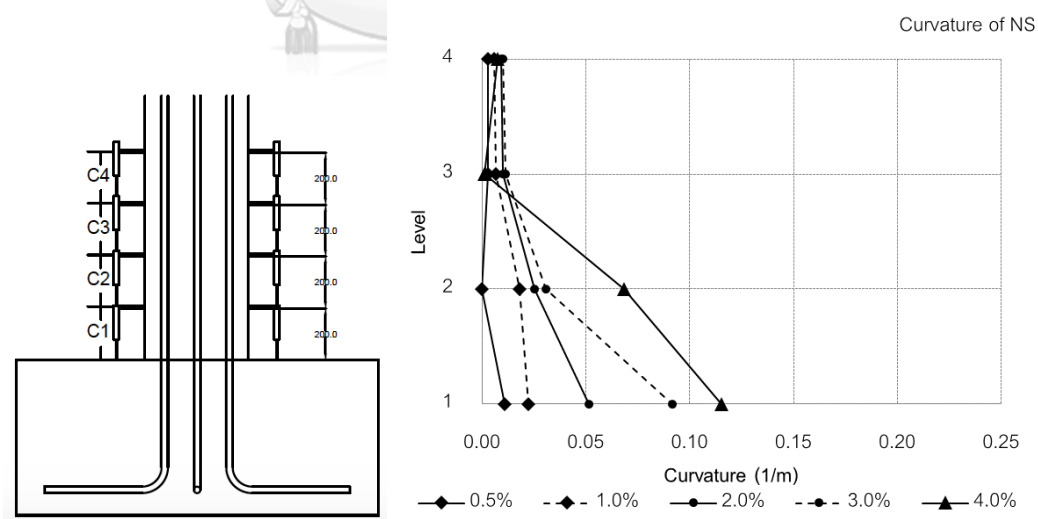


Figure 5.36 Curvature distribution on the specimen NS

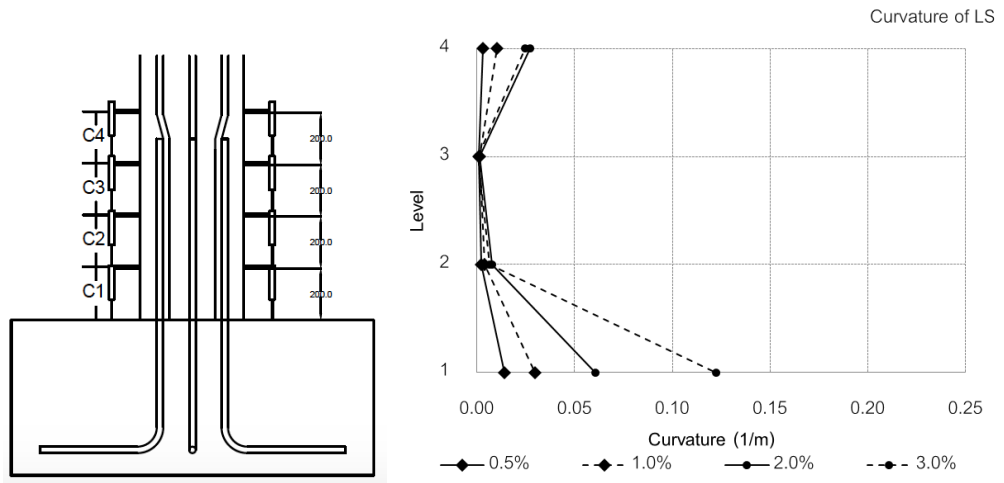


Figure 5.37 Curvature distribution on the specimen LS

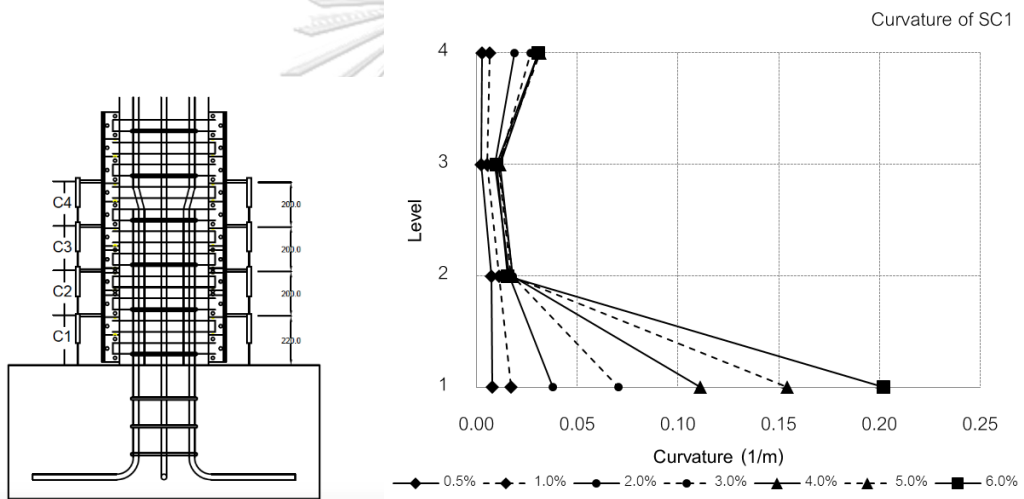


Figure 5.38 Curvature distribution on the specimen SC1

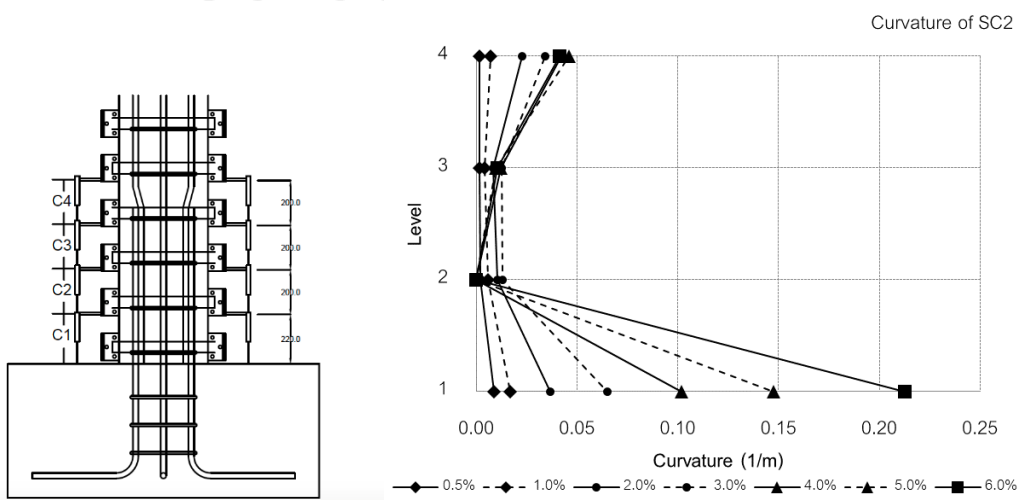


Figure 5.39 Curvature distribution on the specimen SC2

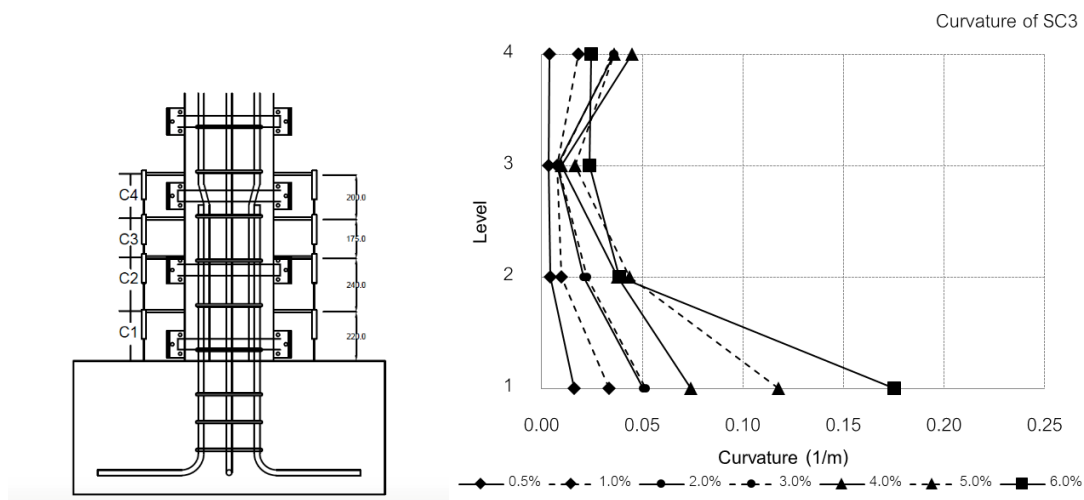


Figure 5.40 Curvature distribution on the specimen SC3

### 5.5.3 Distribution of column section rotation

To understand the column deformation deeply. Rotation is a value that indicates the bending force distribution along with the column height. As results are in accordance with the result of displacement ductility for all specimens. There is an interesting observed that the rotation of lap-splices specimen (LS) is concentrated in the region 200mm above the base for columns. Maximum rotation is concentrated in the region just above the lap-splices due to the crank portion of longitudinal reinforcement. Also, depicting that rotation at that location is higher than at the base after bond failure. One reason for this behavior is that rotation due to yield penetration of the starter bar is far less than the rotation due to lap-splices.

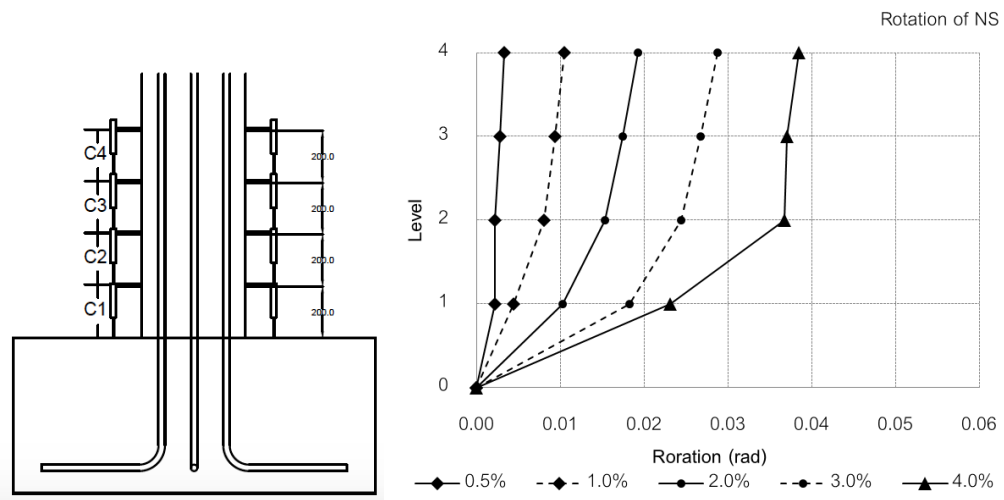


Figure 5.41 Curvature distribution on the specimen NS

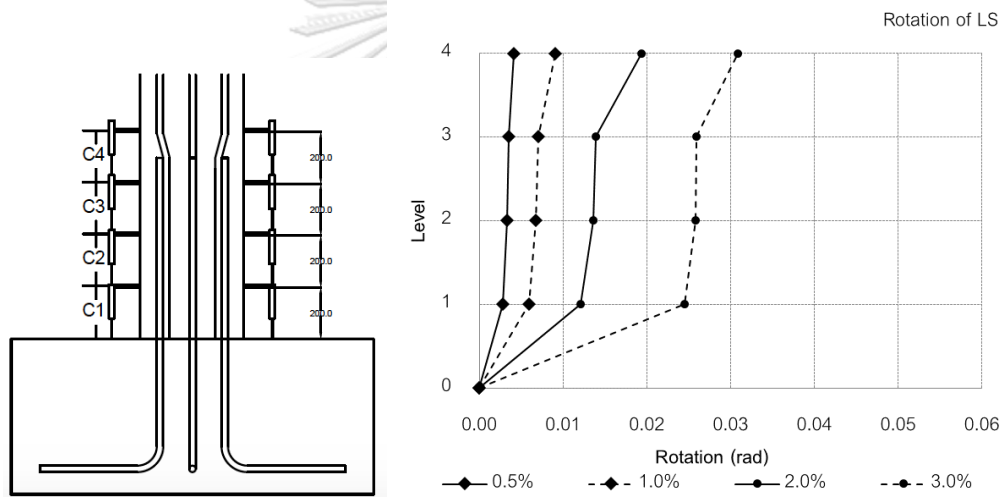


Figure 5.42 Curvature distribution on the specimen LS

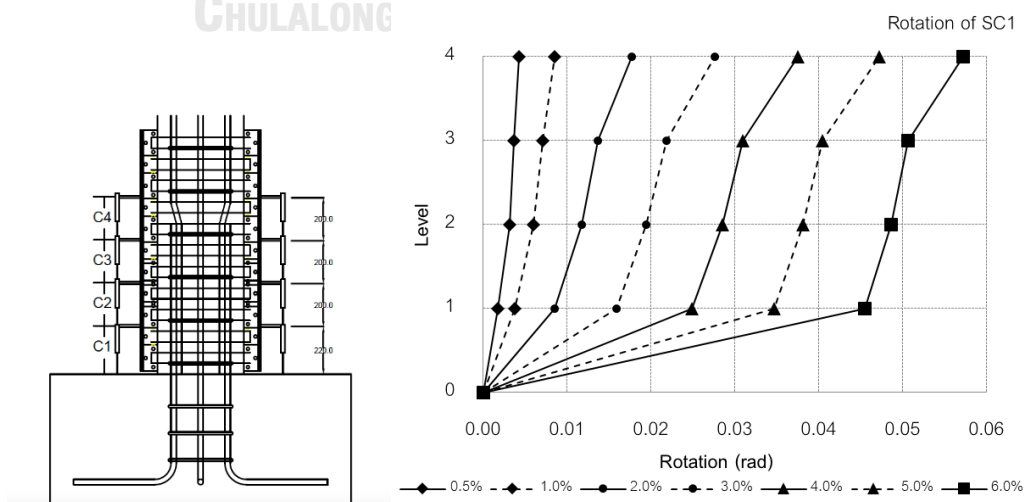


Figure 5.43 Curvature distribution on the specimen SC1

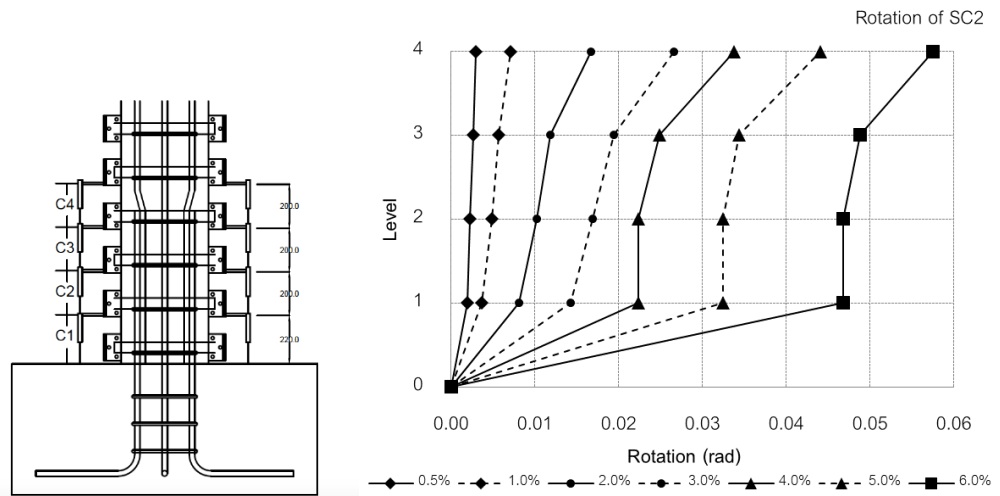


Figure 5.44 Curvature distribution on the specimen SC2

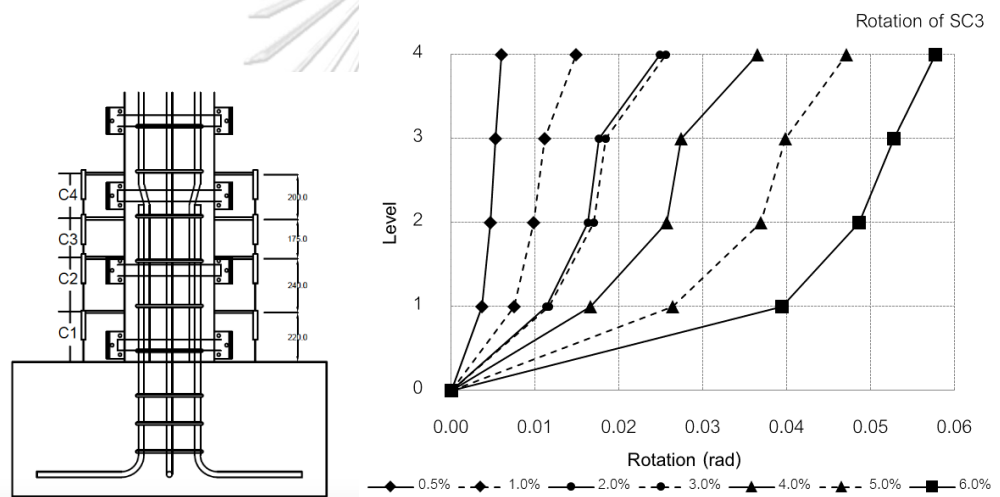


Figure 5.45 Curvature distribution on the specimen SC3



#### 5.5.4 Energy dissipation

The energy dissipation of four specimens is compared in this section. The dissipation energy of their specimens was not entirely different when cycle 2.0% drift. On the other hand, after the 3.0% drift cycle, the energy dissipation trends were clearly different. After 3% drift, the LS and SC3 cannot dissipate the energy anymore because the specimen failed by laps splice failure. But the dissipation of the energy capacity of NS, SC1 and SC22 was 34 kN-m, 25 kN-m and 25 kN-m respectively. The energy dissipation capacity of NS more increased significantly after 3% drift than SC1 and SC2 columns. In a comparison of SC1 had a slightly higher energy dissipation capacity and this can be the effect of the number of steel collars. The cumulative dissipated energy for all specimens is compared in Figure 3.56.

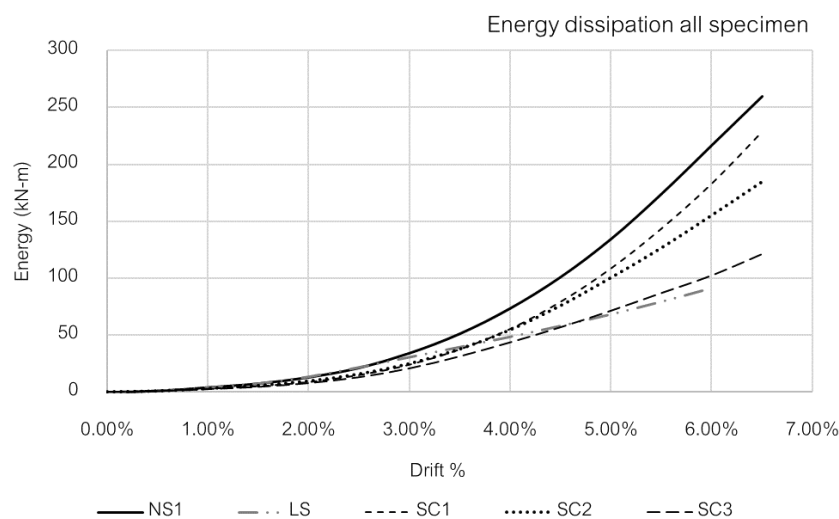


Figure 5.46 Energy dissipation all specimen

Table 5.8 Cumulative energy dissipation of all specimens

Specimen	NS	LS	SC1	SC2	SC3
0.00%	0	0	0	0	0
0.25%	338	235	194	213	169
0.50%	1161	966	763	792	675
0.75%	2432	2189	1704	1730	1463
1.00%	4199	3952	3003	3122	2594
1.50%	7537	7596	5459	5858	4851
2.00%	13028	13528	9391	10046	8414
2.50%	21340	21834	15845	16524	13890
3.00%	34261	30769	25434	25918	22039
3.50%	51330	39664	39079	39011	32948
4.00%	73634	48706	57524	56214	45510
4.50%	101184	58277	81220	77434	59068
5.00%	134642	68500	110759	102042	73691
5.50%	174234	79675	145819	128254	89389
6.00%	217167	91617	184958	156977	106224
6.50%	233470		230498	186211	123943
7.00%			275490		

## 5.6 Discussion of the column with and without external steel collars

- The appearance damage in the plastic hinge region of lap-splice column strengthen with external steel collars has been classified as two types of failure by failing in bond-slip failure. were failed in flexural joint failure. However, there is a slight difference in the matter of damage appearance that the strengthen column did not show the damage clearly, that It is an issue to be concerned as it is not possible to assess the damage appear.
- Data analysis of lateral load-displacement, the ductility was shown the seismic responsibility of all specimens. The lap-splice column strengthens with external steel collars shows the behavior consider with the varies volumatic. How ever the SC2 is suitable to be used due to the convenient installation of an amount not too much and still capable.
- Curvature can explain to the moment distribution of specimen by lap-splice column strengthen with external steel collars were concentrated in the region 200mm above the base of columns the same as lap-splice colum. Difference to non-splice column NS which distributes curvature from fixed support to free end as cantilever column.

## CHAPTER 6

### CONCLUSION

The research studied the behavior of seven RC columns through full-scale testing. The cantilever columns were subjected to a cyclic lateral loading and a constant gravity load. The spliced reinforcement conditions provided in the tested specimen were non splicing (continuous reinforcement), conventional lap splicing, and mechanical splicing. Then, the behavior of lap-spliced RC columns strengthened with external steel collars were investigated. Finally, the lateral load vs displacement relations of the tested specimens were predicted using the proposed numerical model using the fiber model. The findings can be summarized as follows:

#### 6.1 Behavior of RC columns with spliced reinforcement

The research explored the behavior of the tested specimens by comparing the non-spliced column and the columns with lap splices. The used lap splice length was equal to 28 times the diameter of longitudinal reinforcement and all reinforcement was spliced at the same section. The test results indicated that the lateral load capacity of the lap-spliced column decreased by 15% compared to the non-spliced column. The ductility of the specimen with a lap splice decreased by 58% with respect to the specimen without lap splices.

The lateral load capacity of the specimen with mechanical splices is close to that of the non-spliced column. The ductility of the specimen with mechanical splices decreased about 20% comparing to the specimen without lap splices. The use of mechanical splices could prevent the bond-slip failure in the tested specimens.

#### 6.2 Effect of external steel collars on the behavior of lap-spliced columns

The external steel collars were used for strengthening lap-spliced columns. A volumetric ratio of the external steel collars was assigned as the test variable. The volumetric ratio was between 0.017 and 0.048. The test results indicated that the

lateral load capacity of the lap-spliced columns with external steel collars increased 12-23% with respect to the lap-spliced column. The ductilities of the specimens with external steel collars were 20% higher than the lap-spliced specimen.

### 6.3 Numerical modeling for RC columns with spliced reinforcement

An analysis procedure was proposed based on a fiber model. The model included an effect of buckling in longitudinal steels and a stress-strain relationship of lap-spliced steels. The presence of mechanical splices is considered in this model. The lateral load capacities predicted by the proposed model were in a good agreement with test results.



## REFERENCES

- [1] P. Lukkunaprasit *et al.*, "Performance of structures in the Mw 6.1 Mae Lao earthquake in Thailand on May 5, 2014 and implications for future construction," *Journal of Earthquake Engineering*, vol. 20, no. 2, pp. 219-242, 2016.
- [2] M. Melek and J. W. Wallace, "Cyclic behavior of columns with short lap splices," *Structural Journal*, vol. 101, no. 6, pp. 802-811, 2004.
- [3] H. Pam and J. Ho, "Effects of steel lap splice locations on strength and ductility of reinforced concrete columns," *Advances in Structural Engineering*, vol. 13, no. 1, pp. 199-214, 2010.
- [4] T.-H. Kim, B.-S. Kim, Y.-S. Chung, and H. Shin, "Seismic performance assessment of reinforced concrete bridge piers with lap splices," *Engineering Structures*, vol. 28, no. 6, pp. 935-945, 2006.
- [5] Z. B. Haber, M. S. Saiidi, and D. H. Sanders, "Seismic performance of precast columns with mechanically spliced column-footing connections," *ACI Structural Journal*, vol. 111, no. 3, pp. 639-650, 2014.
- [6] M. Ameli, J. E. Parks, D. N. Brown, and C. P. Pantelides, "Seismic evaluation of grouted splice sleeve connections for reinforced precast concrete column-to-cap beam joints in accelerated bridge construction Date: March-April 2015," 2015.
- [7] W. Lloyd, "Qualification of the Bar-Lock Rebar Coupler for Use in Nuclear Safety-Related Applications Mechanical Testing Program and Performance Analysis," *Idaho National Engineering and Environmental Laboratory Materials Department, Report No. INEEL/EXT-02-01387*, 2001.
- [8] D. Hillis and M. Saiidi, "Design, Construction, and Nonlinear Dynamic. Analysis of Three Bridge Bents Used in a Bridge System Test," *Center for Civil Engineering Earthquake Research, Department of Civil and Environmental Engineering, University of Nevada, Reno, Nevada, Report No. CCEER-09-03*, 2009.
- [9] Y. Yang, L. H. Sneed, M. S. Saiidi, and A. Belarbi, "Repair of earthquake-damaged bridge columns with interlocking spirals and fractured bars," Missouri University of

Science and Technology. Center for Transportation ..., 2014.

- [10] D. E. Lehman, S. E. Gookin, A. M. Nacamuli, and J. P. Moehle, "Repair of earthquake-damaged bridge columns," *Structural Journal*, vol. 98, no. 2, pp. 233-242, 2001.
- [11] K. Kawashima, S. Unjoh, and H. Iida, "Seismic inspection and seismic strengthening of reinforced concrete bridge piers with termination of main reinforcement at mid-height," in *Proceedings of the 1st US Japan Workshop on Seismic Retrofit of Bridges, Tsukuba, Japan, 1990*.
- [12] M. N. Priestley, F. Seible, Y. Xiao, and R. Verma, "Steel jacket retrofitting of reinforced concrete bridge columns for enhanced shear strength-part 1: Theoretical considerations and test design," *Structural Journal*, vol. 91, no. 4, pp. 394-405, 1994.
- [13] R. S. Aboutaha, M. D. Engelhardt, J. O. Jirsa, and M. E. Kreger, "Rehabilitation of shear critical concrete columns by use of rectangular steel jackets," *Structural Journal*, vol. 96, no. 1, pp. 68-78, 1999.
- [14] S. Dritsos and K. Pilakoutas, "Composite technique for repair/strengthening of RC members," in *Second international symposium on composite materials and structures. China: Peking University Press, 1992*.
- [15] H. Sezen and J. P. Moehle, "Shear strength model for lightly reinforced concrete columns," *Journal of Structural Engineering*, vol. 130, no. 11, pp. 1692-1703, 2004.
- [16] M. Ohue, H. Morimoto, S. Fujii, and S. Morita, "The behavior of RC short columns failing in splitting bond-shear under dynamic lateral loading," *Transactions of the Japan Concrete Institute*, vol. 7, no. 1, pp. 293-300, 1985.
- [17] F. Esaki, "Reinforcing effect of steel plate hoops on ductility of R/C square columns," in *Proc., 11th World Conf. on Earthquake Engineering, 1996*: Pergamon, Elsevier Science, p. 199.
- [18] Y. Mo and S. Wang, "Seismic behaviour of reinforced concrete columns," *Magazine of Concrete Research*, vol. 52, no. 6, pp. 419-432, 2000.
- [19] A. C. Lynn, J. P. Moehle, S. A. Mahin, and W. T. Holmes, "Seismic evaluation of

- existing reinforced concrete building columns," *Earthquake Spectra*, vol. 12, no. 4, pp. 715-739, 1996.
- [20] M. H. Harajli, "Axial stress–strain relationship for FRP confined circular and rectangular concrete columns," *Cement and Concrete Composites*, vol. 28, no. 10, pp. 938-948, 2006.
- [21] R. Park and T. Paulay, *Reinforced concrete structures*. John Wiley & Sons, 1975.
- [22] M. Tazarv and M. S. Saiidi, "DESIGN AND CONSTRUCTION OF BRIDGE COLUMNS INCORPORATING MECHANICAL BAR SPLICES IN PLASTIC HINGE ZONES," 2015.
- [23] M. S. Saiidi and H. Wang, "Exploratory study of seismic response of concrete columns with shape memory alloys reinforcement," *ACI Materials Journal*, vol. 103, no. 3, p. 436, 2006.
- [24] M. S. Saiidi, M. O'Brien, and M. Sadrossadat-Zadeh, "Cyclic Response of Concrete Bridge Columns Using Superelastic Nitinol and Bendable Concrete," *ACI Structural Journal*, vol. 106, no. 1, 2009.
- [25] S. Varela and M. Saiidi, "Dynamic performance of novel bridge columns with superelastic CuAlMn shape memory alloy and ECC," *International journal of bridge engineering*, vol. 2, no. 3, pp. 29-58, 2014.
- [26] J. C. Chai, H. S. Lee, and S. V. Patankar, "Finite volume method for radiation heat transfer," *Journal of thermophysics and heat transfer*, vol. 8, no. 3, pp. 419-425, 1994.
- [27] K. C. Tsai and M. L. Lin, "Seismic jacketing of RC columns for enhanced axial load carrying performance," *Journal of the Chinese Institute of Engineers*, vol. 25, no. 4, pp. 389-402, 2002.
- [28] M. L. Lin, P. C. Chen, K. C. Tsai, Y. J. Yu, and J. G. Liu, "Seismic steel jacketing of rectangular RC bridge columns for the mitigation of lap-splice failures," *Earthquake Engineering & Structural Dynamics*, vol. 39, no. 15, pp. 1687-1710, 2010.
- [29] E. Choi, Y.-S. Chung, K. Park, and J.-S. Jeon, "Effect of steel wrapping jackets on the bond strength of concrete and the lateral performance of circular RC columns,"



*Engineering Structures*, vol. 48, pp. 43-54, 2013.

- [30] A. Ghobarah, A. Biddah, and M. Mahgoub, "Rehabilitation of reinforced concrete columns using corrugated steel jacketing," *Journal of Earthquake Engineering*, vol. 1, no. 04, pp. 651-673, 1997.
- [31] P. Nagaprasad, D. R. Sahoo, and D. C. Rai, "Seismic strengthening of RC columns using external steel cage," *Earthquake Engineering & Structural Dynamics*, vol. 38, no. 14, pp. 1563-1586, 2009.
- [32] A. C. Masri and S. C. Goel, "Seismic design and testing of an RC slab-column frame strengthened by steel bracing," *Earthquake Spectra*, vol. 12, no. 4, pp. 645-666, 1996.
- [33] M. F. Belal, H. M. Mohamed, and S. A. Morad, "Behavior of reinforced concrete columns strengthened by steel jacket," *HBRC Journal*, vol. 11, no. 2, pp. 201-212, 2015.
- [34] A. Tarabia and H. Albakry, "Strengthening of RC columns by steel angles and strips," *Alexandria Engineering Journal*, vol. 53, no. 3, pp. 615-626, 2014.
- [35] G. Campione, "Strength and ductility of RC columns strengthened with steel angles and battens," *Construction and Building materials*, vol. 35, pp. 800-807, 2012.
- [36] R. Montuori and V. Piluso, "Reinforced concrete columns strengthened with angles and battens subjected to eccentric load," *Engineering Structures*, vol. 31, no. 2, pp. 539-550, 2009.
- [37] M. A. Hussain and R. G. Driver, "Experimental study on the seismic performance of externally confined reinforced concrete columns," in *Proceedings of the 13th World Conference on Earthquake Engineering (WCEE)*. Vancouver, BC, Canada: CANADA, 2004.
- [38] J. Liu, R. G. Driver, and A. S. Lubell, "Experimental Study on Short Concrete Columns with External Steel Collars," *ACI Structural Journal*, vol. 108, no. 3, 2011.
- [39] Y. Xiao and H. Wu, "Retrofit of reinforced concrete columns using partially stiffened steel jackets," *Journal of Structural Engineering*, vol. 129, no. 6, pp. 725-732, 2003.
- [40] D. C. Kent and R. Park, "Flexural members with confined concrete," *Journal of the*

*Structural Division*, 1971.

- [41] J. B. Mander, M. J. Priestley, and R. Park, "Theoretical stress-strain model for confined concrete," *Journal of structural engineering*, vol. 114, no. 8, pp. 1804-1826, 1988.
- [42] J. Hoshikuma, K. Kawashima, K. Nagaya, and A. Taylor, "Stress-strain model for confined reinforced concrete in bridge piers," *Journal of Structural Engineering*, vol. 123, no. 5, pp. 624-633, 1997.
- [43] A. Gomes and J. Appleton, "Nonlinear cyclic stress-strain relationship of reinforcing bars including buckling," *Engineering Structures*, vol. 19, no. 10, pp. 822-826, 1997.
- [44] M. Menegotto and P. Pinto, "Method of Analysis for Cyclically Loaded RC Frames Including Changes in Geometry and Non-elastic Behaviour of Elements Under Combined Normal Force and Bending," in *IABSE Congress Reports of the Working Commission*, 1973, vol. 13.
- [45] F. M. Silvia Mazzoni, Michael H. Scott, Gregory L. Fenves, et al., "Opensees Command Language Manual," 2007.
- [46] P. Kruavit, "Cyclic behavior of reinforced concrete column with mechanical splice," Chulalongkorn University, 2013.
- [47] N. Sheikh and J. Thomas, "Factors influencing food choice among ethnic minority adolescents," *Nutrition & Food Science*, vol. 94, no. 5, pp. 29-35, 1994.
- [48] S. Mau and M. El-Mabsout, "Inelastic buckling of reinforcing bars," *Journal of engineering mechanics*, vol. 115, no. 1, pp. 1-17, 1989.
- [49] G. Monti and C. Nuti, "Nonlinear cyclic behavior of reinforcing bars including buckling," *Journal of Structural Engineering*, vol. 118, no. 12, pp. 3268-3284, 1992.
- [50] O. Bayrak and S. A. Sheikh, "Plastic hinge analysis," *Journal of Structural Engineering*, vol. 127, no. 9, pp. 1092-1100, 2001.
- [51] M. N. Priestley, F. Seible, and G. M. Calvi, *Seismic design and retrofit of bridges*. John Wiley & Sons, 1996.
- [52] X. Huang, "Applicability criteria of fiber-section elements for the modelling of RC

columns subjected to cyclic loading," *University of Toronto*, 2012.

- [53] S. TARIVERDILLOU and A. FARJADI, "CYCLIC RESPONSE OF LAP SPLICED REINFORCED CONCRETE COLUMNS," 2009.
- [54] I. D. Karsan and J. O. Jirsa, "Behavior of concrete under compressive loadings," *Journal of the Structural Division*, 1969.
- [55] X. Huang and O. S. Kwon, "Numerical models of RC elements and their impacts on seismic performance assessment," *Earthquake Engineering & Structural Dynamics*, vol. 44, no. 2, pp. 283-298, 2015.
- [56] M. Saatcioglu and S. R. Razvi, "Strength and ductility of confined concrete," *Journal of Structural Engineering*, vol. 118, no. 6, pp. 1590-1607, 1992.
- [57] A. He, J. Cai, Q.-J. Chen, X. Liu, P. Huang, and X.-L. Tang, "Seismic behaviour of steel-jacket retrofitted reinforced concrete columns with recycled aggregate concrete," *Construction and Building Materials*, vol. 158, pp. 624-639, 2018.
- [58] P. Pudjisuryadi and P. Suprobo, "Performance of square reinforced concrete columns externally confined by steel angle collars under combined axial and lateral load," *Procedia Engineering*, vol. 125, pp. 1043-1049, 2015.
- [59] P. Pudjisuryadi and P. Suprobo, "Axial compressive behavior of square concrete columns externally collared by light structural steel angle sections," Petra Christian University, 2016.

## APPENDIX A

### Bridge parameter

An RC bridge, was chosen to be studied in this research is Standard Drawings for Bridge Construction (2010) from the Department of Rural Roads. Kinds of span length are 10 meters which are located in the middle of the bridge. The roadway width is 10 meters along the bridge. The detail is shown by the following:

- Rectangular reinforced concrete column dimensions 400 × 400 mm in cross section
- Reinforced with 8 longitudinal reinforcements of 25 mm (DB25) nominal diameter and yield strength not lower than 400 Mpa.
- Transverse reinforcement consisted of 12 mm-diameter cage ties and yield strength not lower than 400 Mpa.
- The compressive strength of concrete 28 days is 25 Mpa.

The types of piers in this bridge: the piers that support the pile-bent type with 7 meter height maximum. The bracing beam is placed below the deck with 3 meter height maximum as shown in Figure 0.1. The component of the bridge is calculated to dead load include bridge deck, pier, top beam, bracing beam, pavement and railing are summarize to gravity load of the pier. Axial load in each column are analysis by using SAP2000 program that shows the average of axial load is 30.56 Tons as shown in Figure 0.2

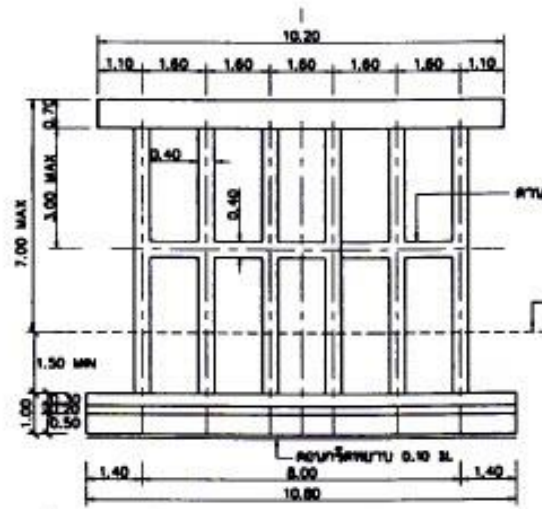


Figure 0.1 Standard Drawings for Bridge Construction (2010) from Department of Rural Roads. Kinds of span length is 10 meters

Table 0.1 Calculate bridge dead load to each column

Column No.	1	2	3	4	5	6	Summary	Average
Axial load (tons)	35.45	28.77	27.45	27.45	28.77	35.45	183.34	30.56

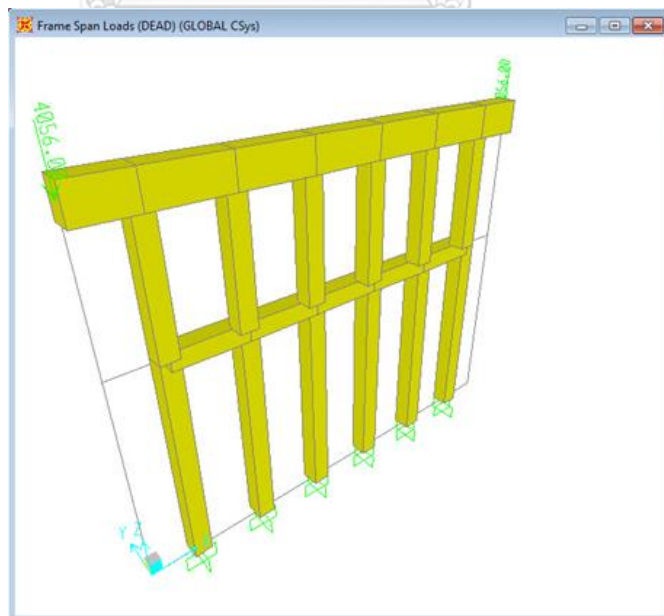
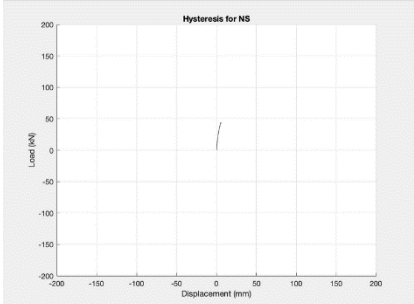

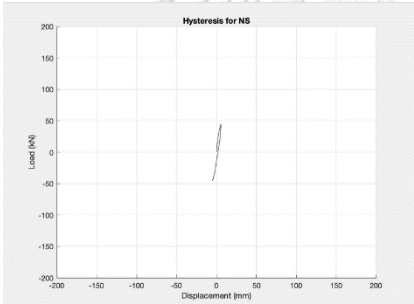

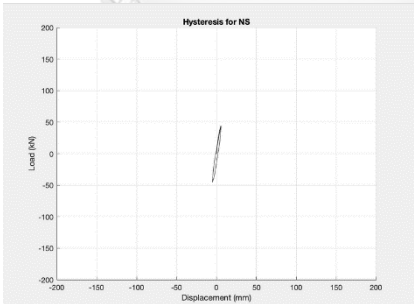

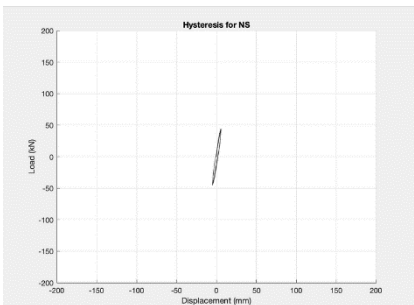



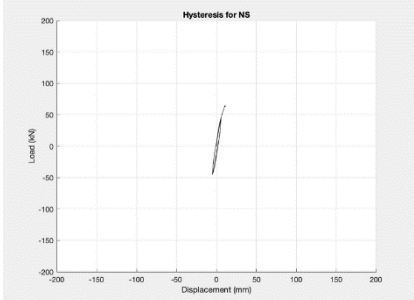

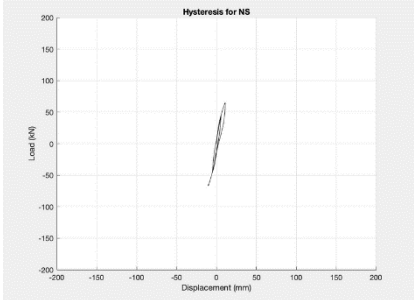

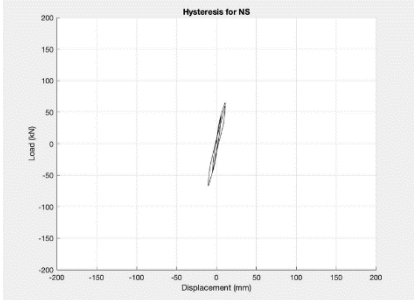

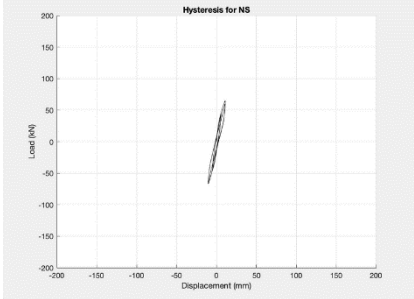

Figure 0.2 Calculate bridge dead load

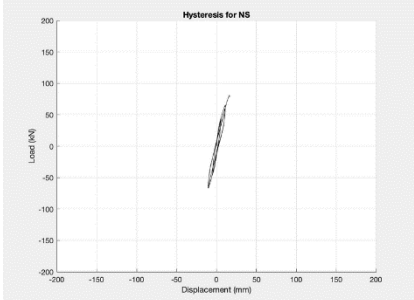

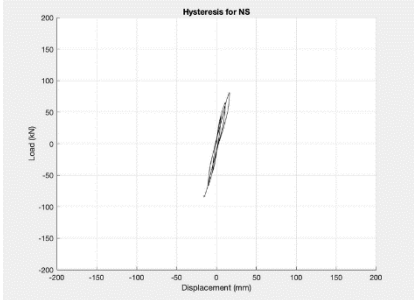

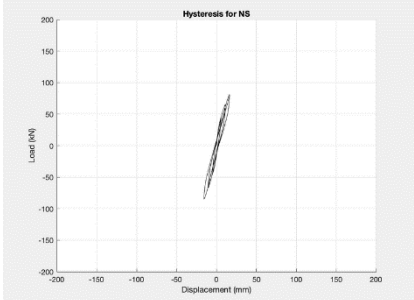

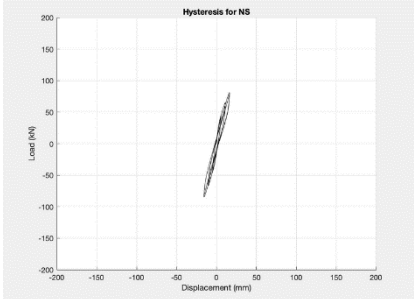

APPENDIX B

Cyclic behavior of NS column specimen

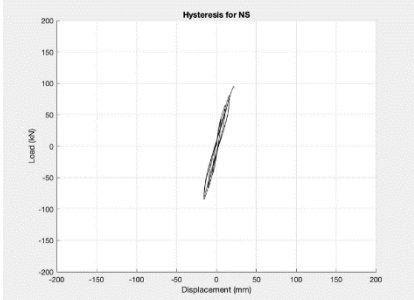

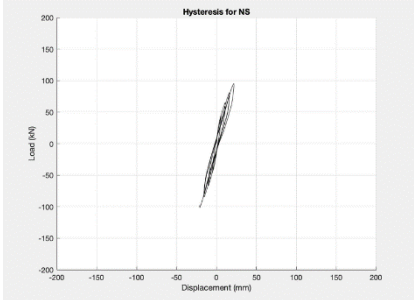

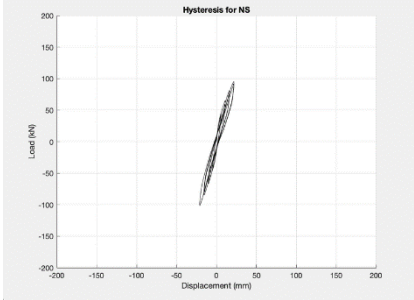

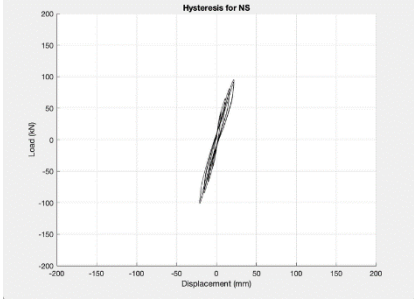

Table 0.1 Cyclic behavior of NS column

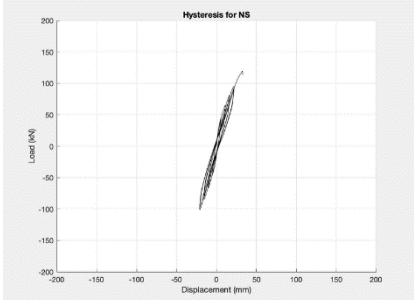

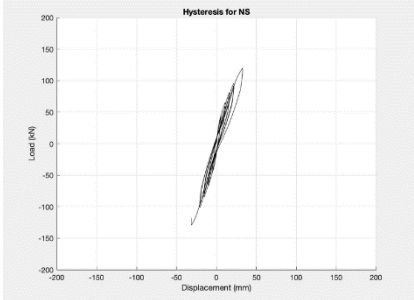

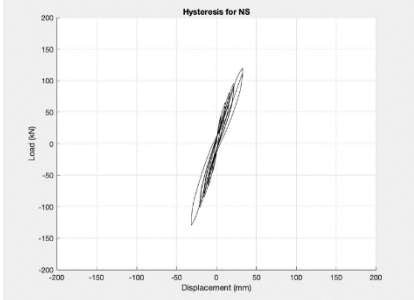

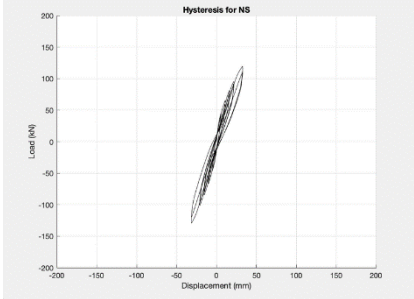

Drift	Cycle	Hysteresis	Damage
0.25 %	+1		
	-1		
	+2		
	-2		

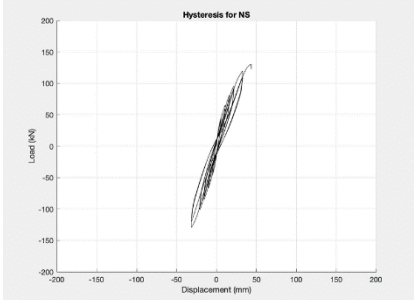

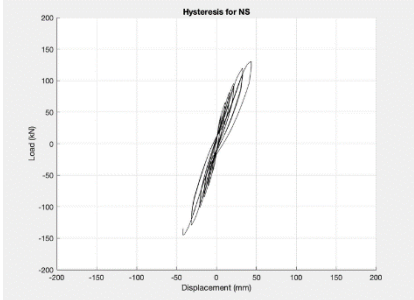

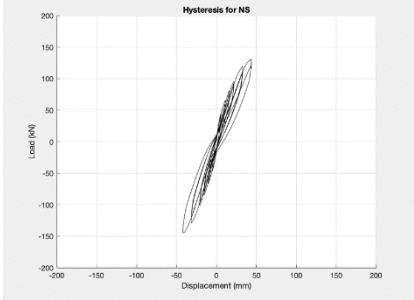

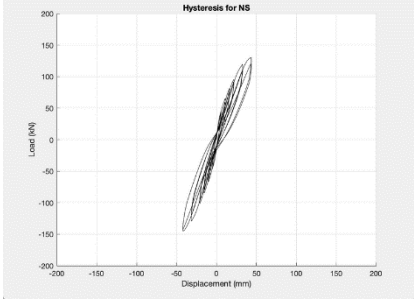

Drift	Cycle	Hysteresis	Damage
0.5%	+1		
	-1		
	+2		
	-2		

Drift	Cycle	Hysteresis	Damage
0.75 %	+1		
	-1		
	+2		
	-2		

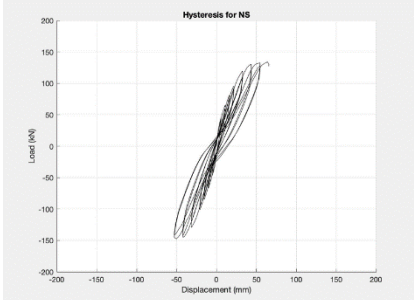

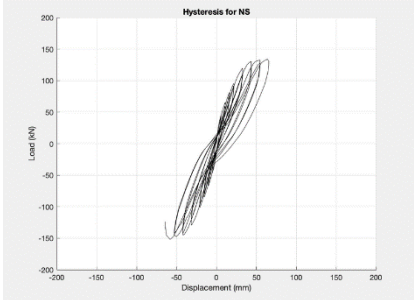

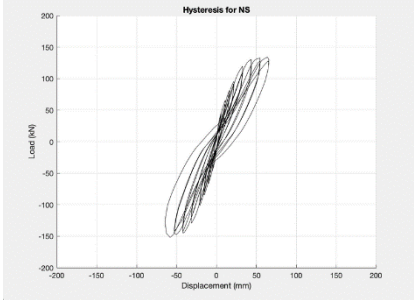
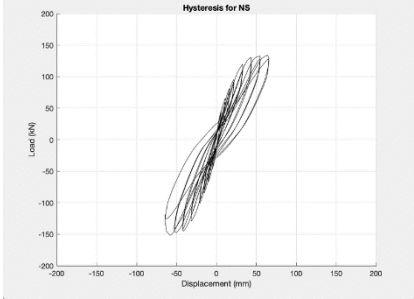



Drift	Cycle	Hysteresis	Damage
1%	+1		
	-1		
	+2		
	-2		

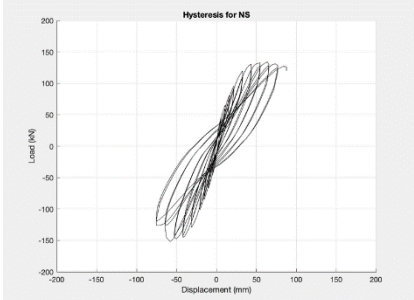

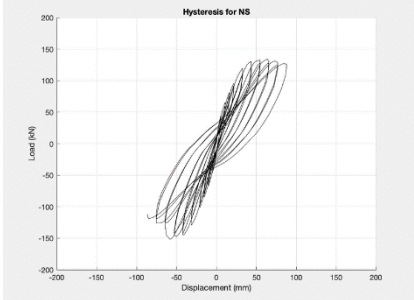

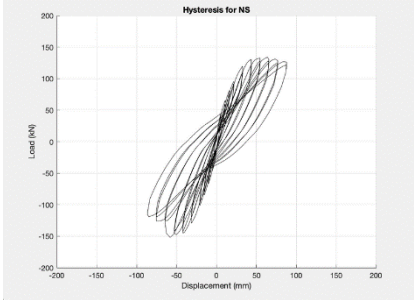

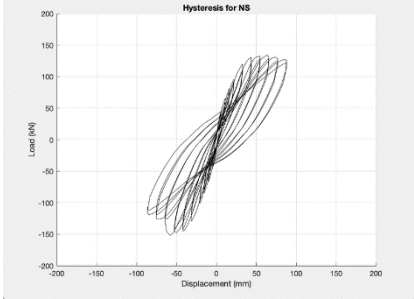

Drift	Cycle	Hysteresis	Damage
1.5%	+1		
	-1		
	+2		
	-2		

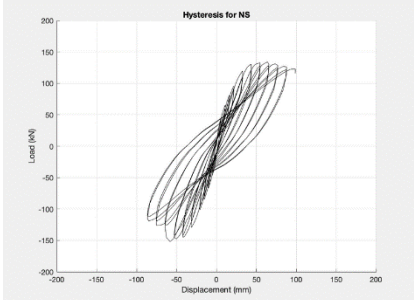

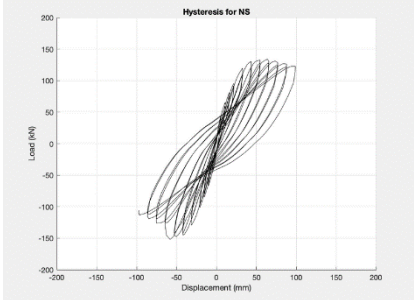

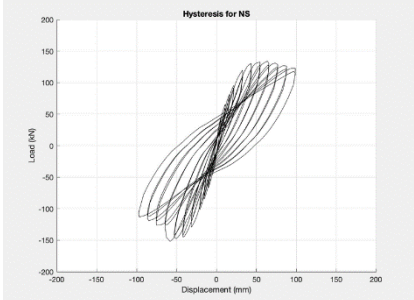

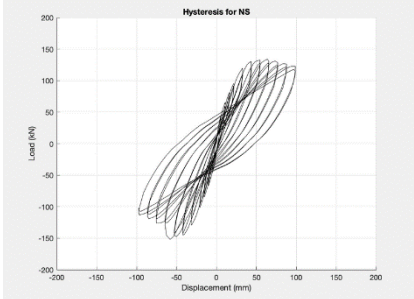

Drift	Cycle	Hysteresis	Damage
2%	+1		
	-1		
	+2		
	-2		

Drift	Cycle	Hysteresis	Damage
2.5%	+1		
	-1		
	+2		
	-2		

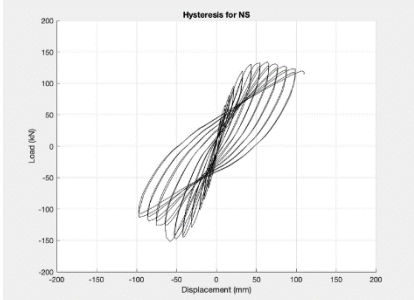

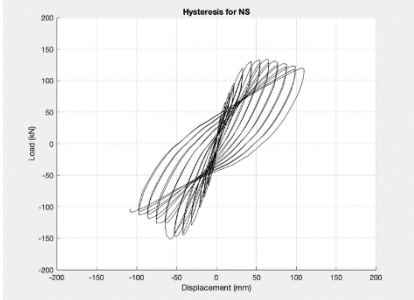

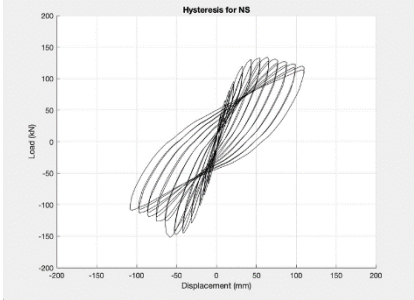

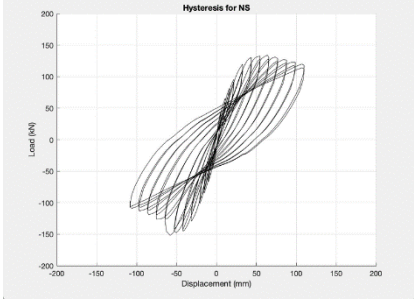

Drift	Cycle	Hysteresis	Damage
3%	+1		
	-1		
	+2		
	-2		

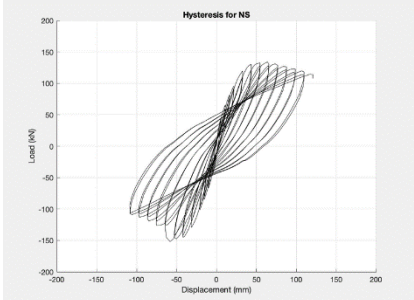

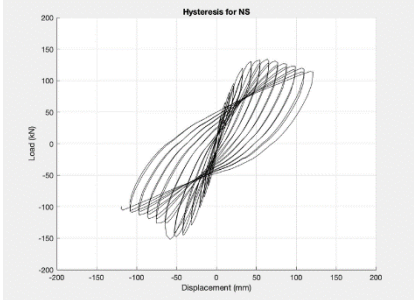

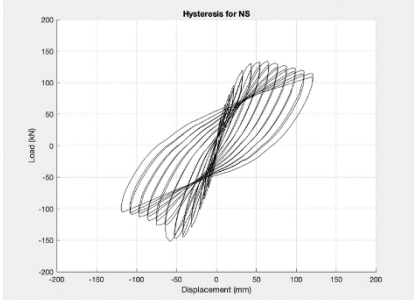

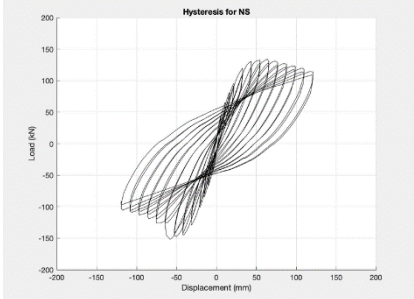

Drift	Cycle	Hysteresis	Damage
3.5%	+1		
	-1		
	+2		
	-2		

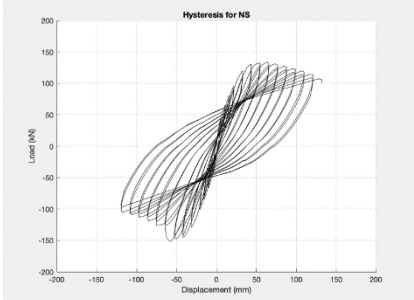

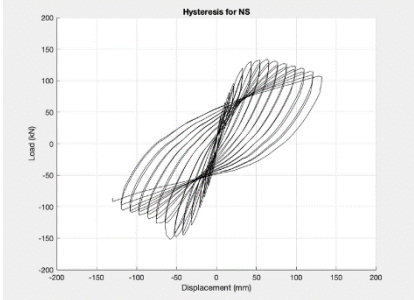

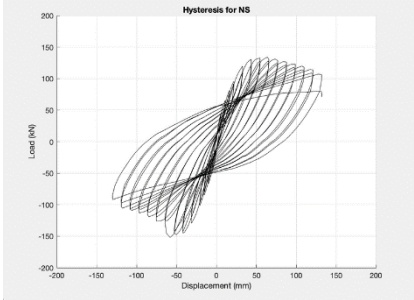

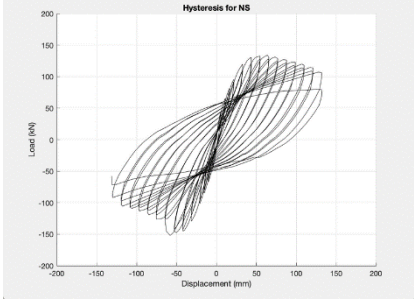

Drift	Cycle	Hysteresis	Damage
4%	+1		
	-1		
	+2		
	-2		

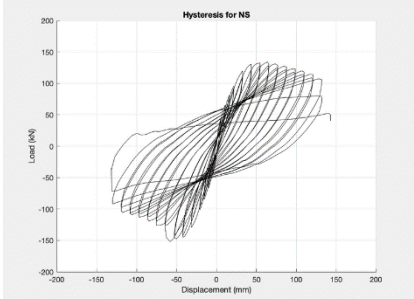

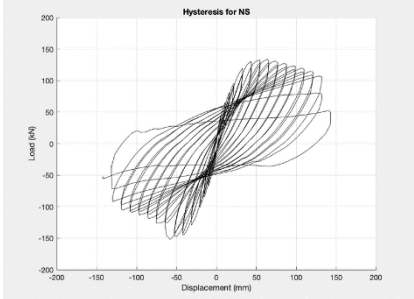

Drift	Cycle	Hysteresis	Damage
4.5%	+1		
	-1		
	+2		
	-2		



Drift	Cycle	Hysteresis	Damage
5%	+1		
	-1		
	+2		
	-2		

Drift	Cycle	Hysteresis	Damage
5.5%	+1		
	-1		
	+2		
	-2		

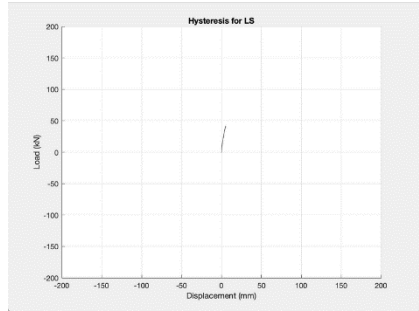

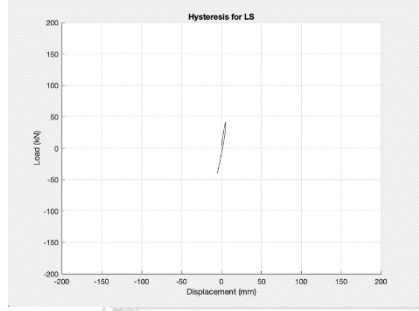

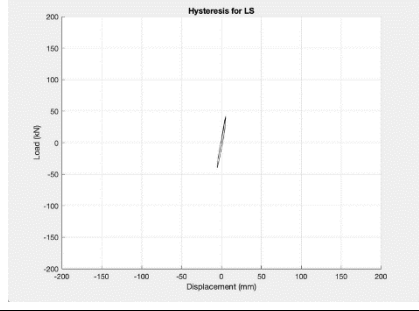

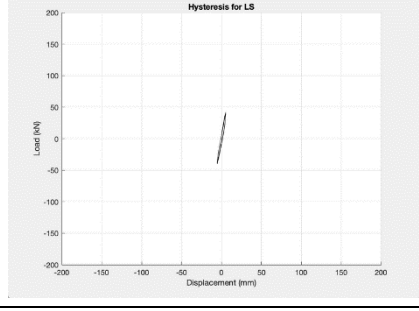

Drift	Cycle	Hysteresis	Damage
6%	+1		
	-1		
	+2		
	-2		

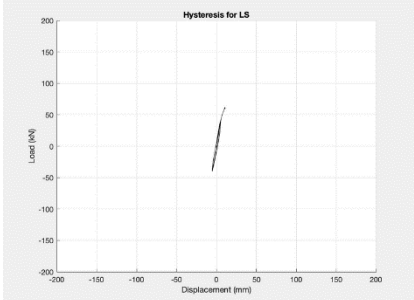

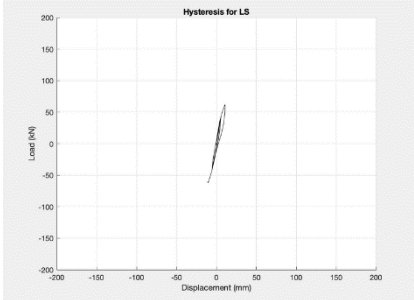

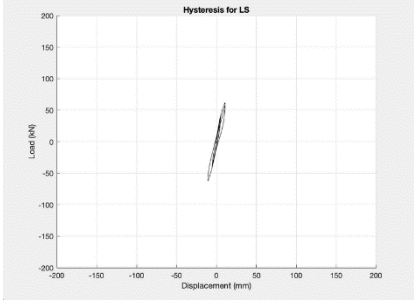

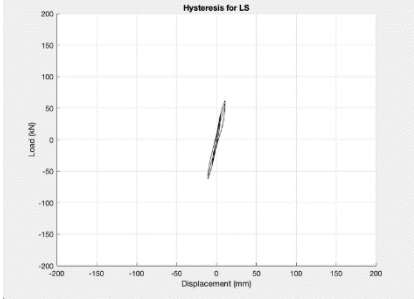

Drift	Cycle	Hysteresis	Damage
6.5%	+1		
	-1		

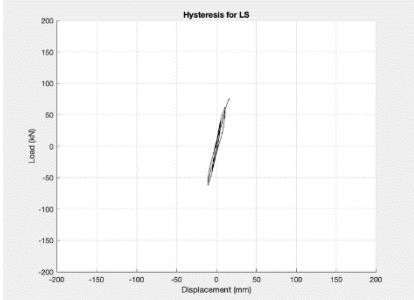

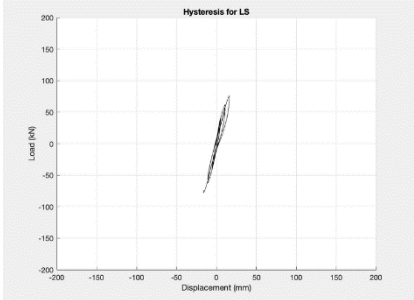

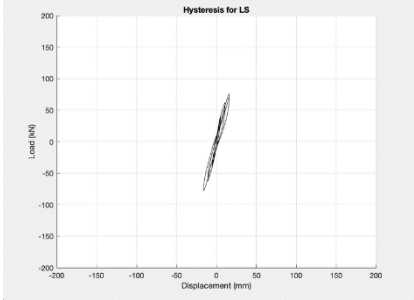

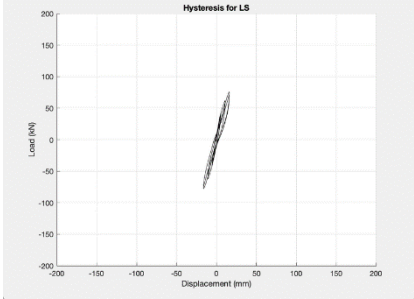
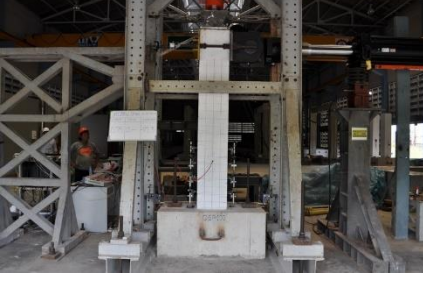
## APPENDIX C

## Cyclic behavior of LS column specimen

Table 0.1 Cyclic behavior of LS column

Drift	Cycle	Hysteresis	Damage
0.25 %	+1		
	-1		
	+2		
	-2		

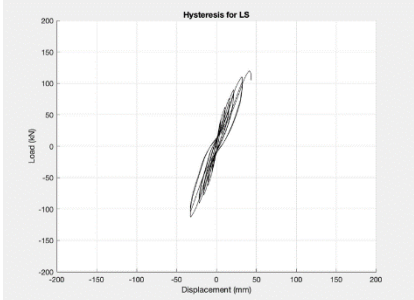

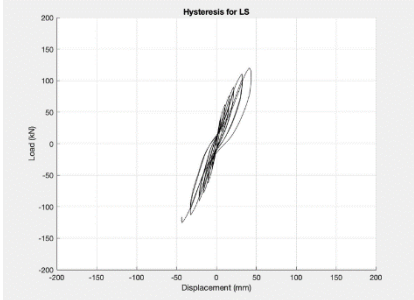

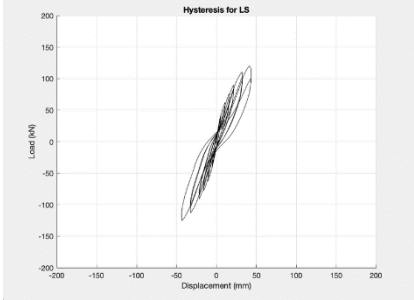

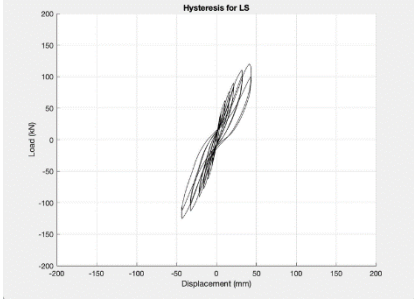

Drift	Cycle	Hysteresis	Damage
0.5%	+1		
	-1		
	+2		
	-2		

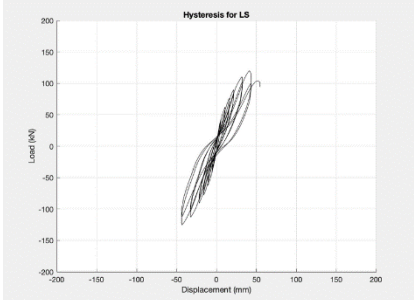

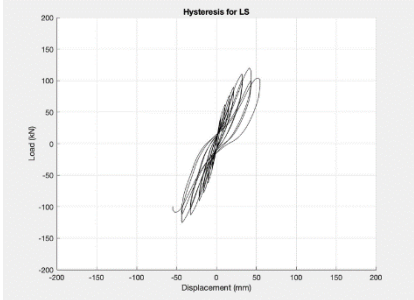

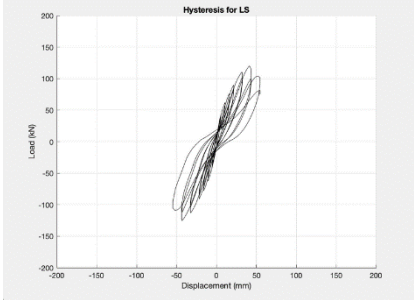

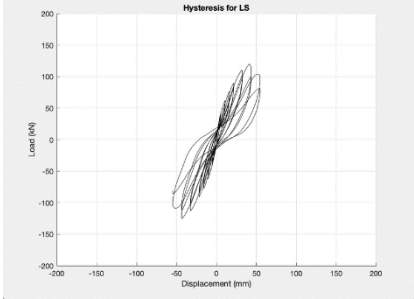

Drift	Cycle	Hysteresis	Damage
0.75 %	+1		
	-1		
	+2		
	-2		

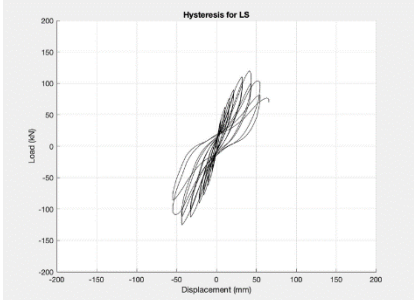

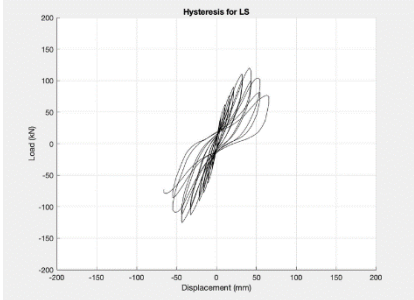

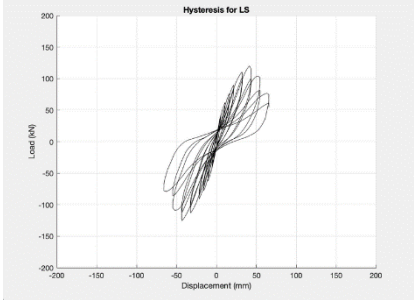

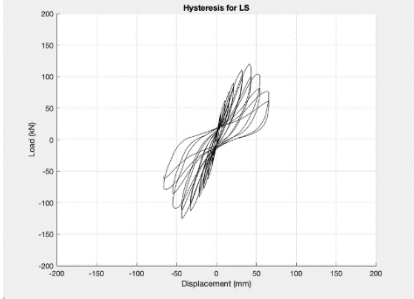

Drift	Cycle	Hysteresis	Damage
1%	+1		
	-1		
	+2		
	-2		

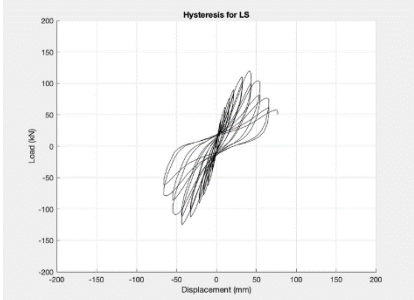

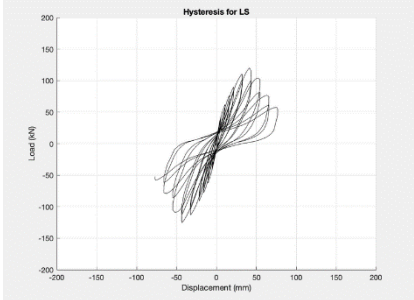

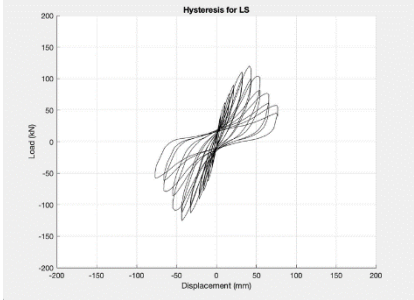

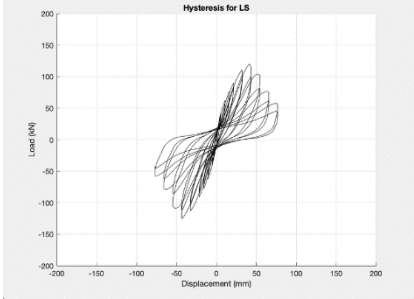



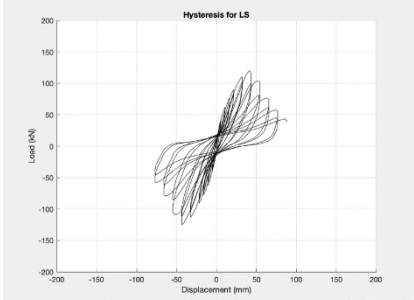

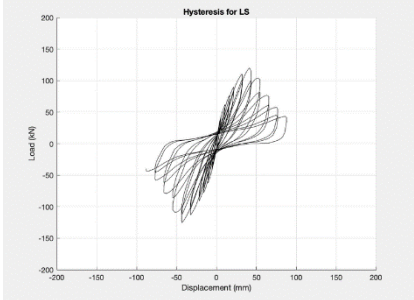

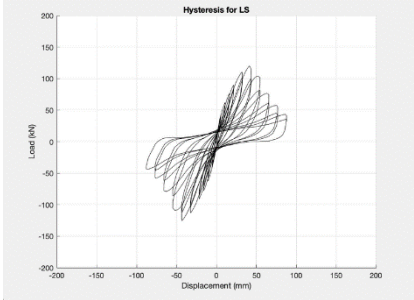

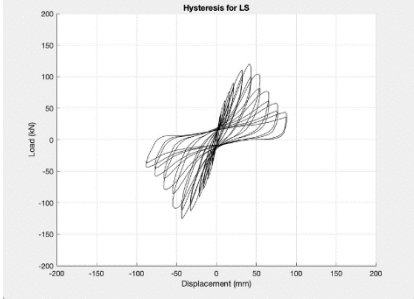

Drift	Cycle	Hysteresis	Damage
1.5%	+1		
	-1		
	+2		
	-2		

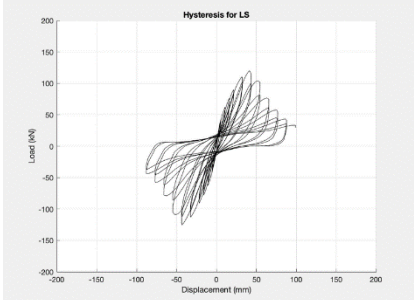

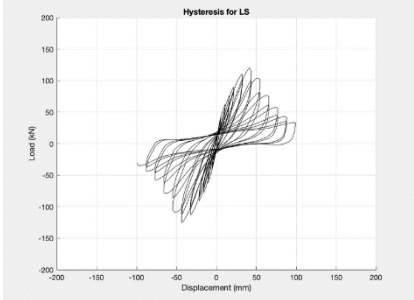

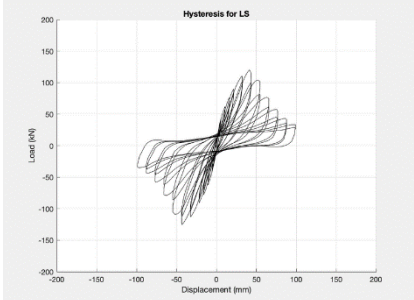

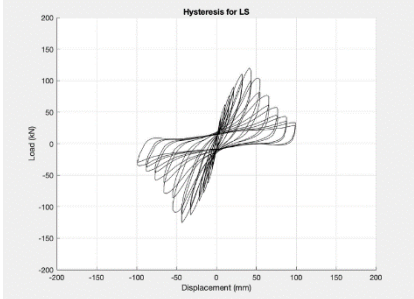

Drift	Cycle	Hysteresis	Damage
2%	+1		
	-1		
	+2		
	-2		

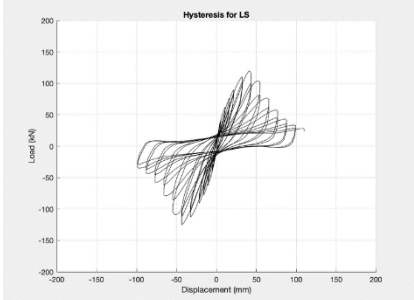

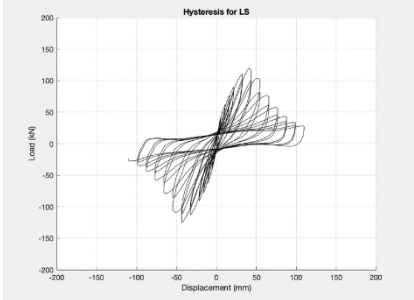

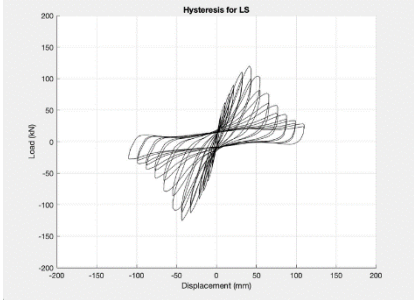

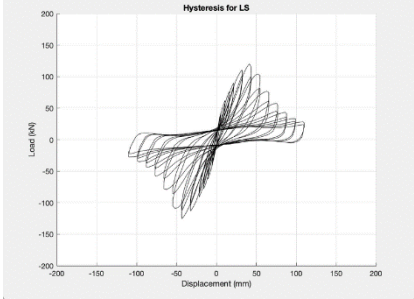

Drift	Cycle	Hysteresis	Damage
2.5%	+1		
	-1		
	+2		
	-2		

Drift	Cycle	Hysteresis	Damage
3%	+1		
	-1		
	+2		
	-2		

Drift	Cycle	Hysteresis	Damage
3.5%	+1		
	-1		
	+2		
	-2		

Drift	Cycle	Hysteresis	Damage
4%	+1		
	-1		
	+2		
	-2		

Drift	Cycle	Hysteresis	Damage
4.5%	+1		
	-1		
	+2		
	-2		

Drift	Cycle	Hysteresis	Damage
5%	+1		
	-1		
	+2		
	-2		



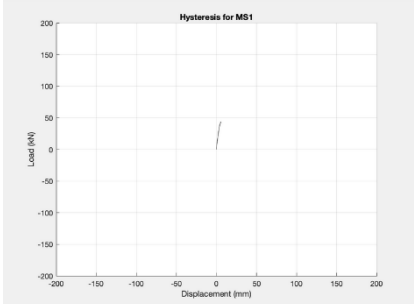

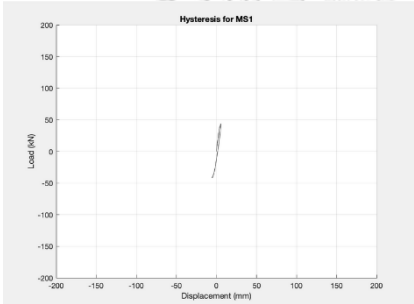

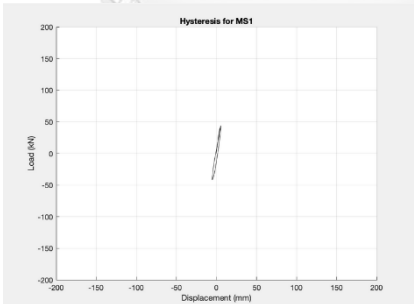

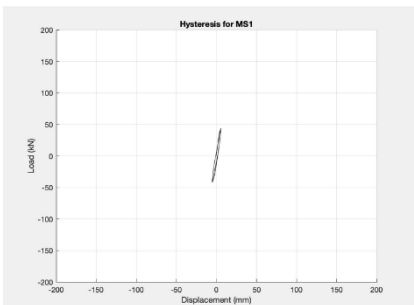

Drift	Cycle	Hysteresis	Damage
5.5%	+1		
	-1		
	+2		
	-2		

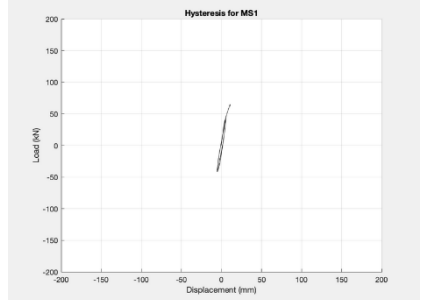

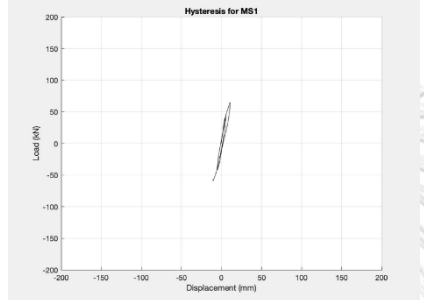

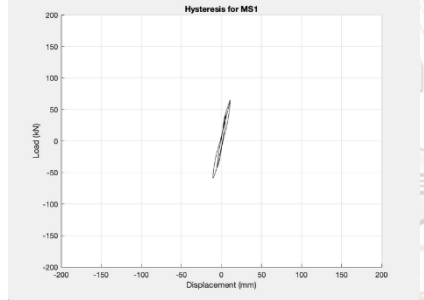

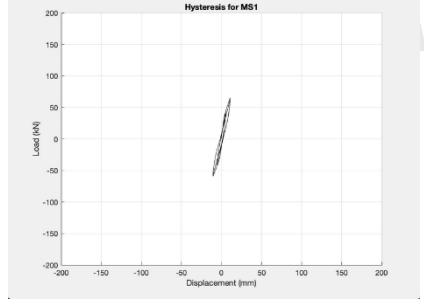

Drift	Cycle	Hysteresis	Damage
6%	+1		
	-1		
	+2		
	-2		

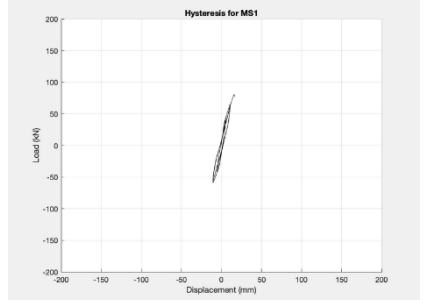

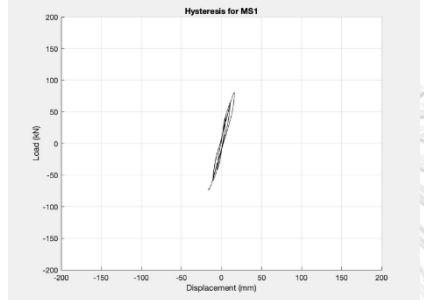

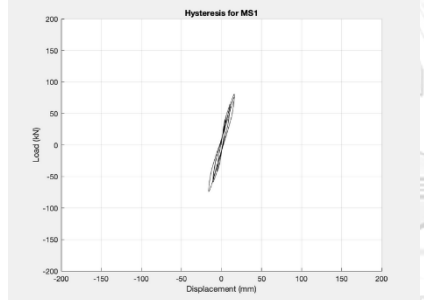

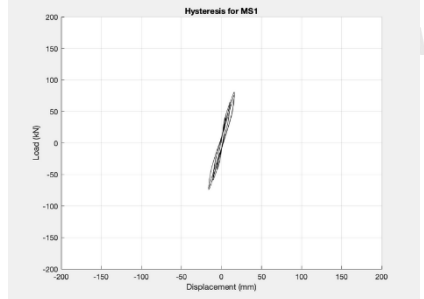

APPENDIX D

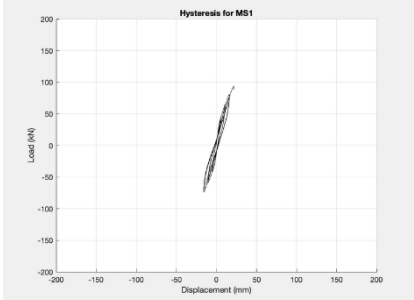

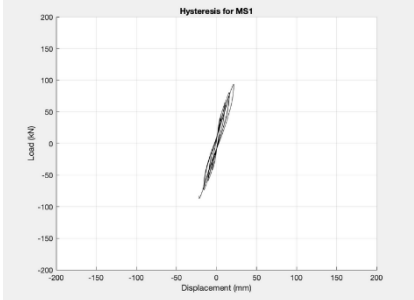

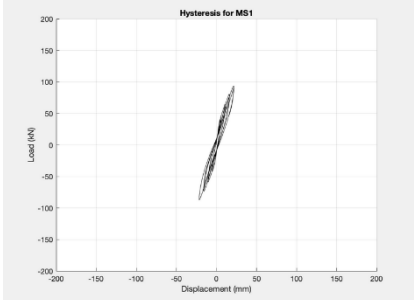

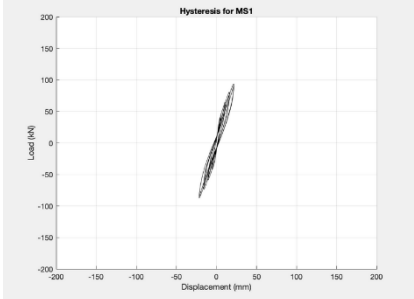

Cyclic behavior of MS1 column specimen

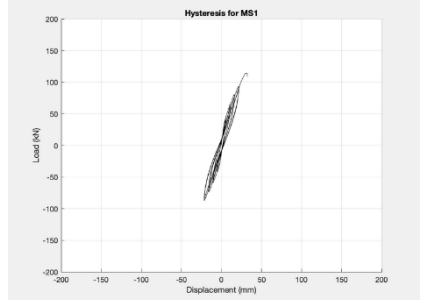

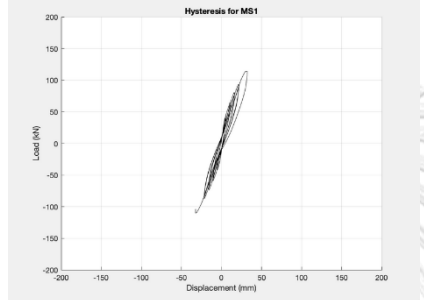

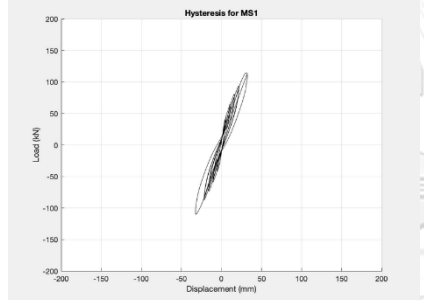

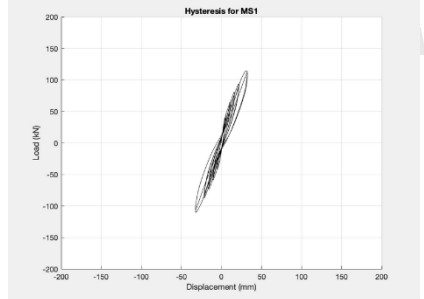

Table 0.1 Cyclic behavior of MS1 column

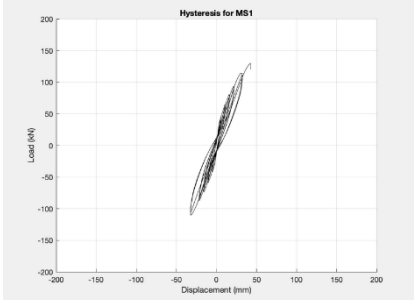

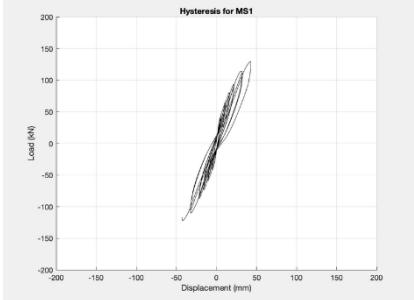

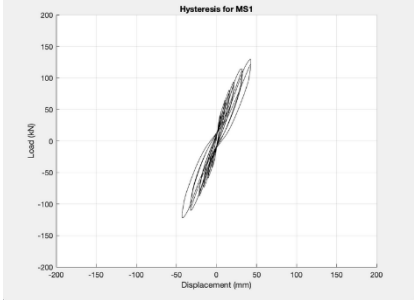

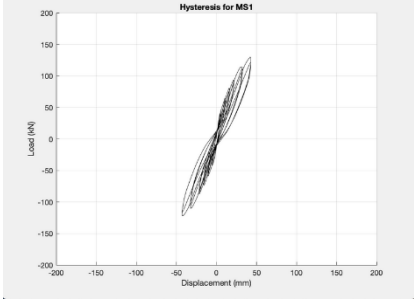

Drift	Cycle	Hysteresis	Damage
0.25 %	+1		
	-1		
	+2		
	-2		

Drift	Cycle	Hysteresis	Damage
0.5%	+1		
	-1		
	+2		
	-2		

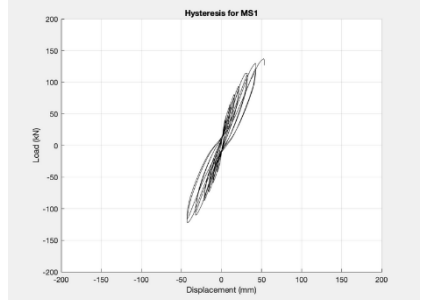

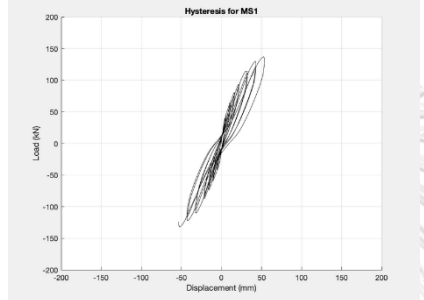

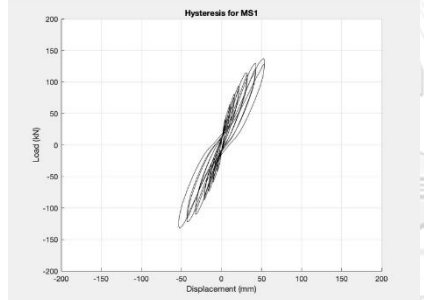

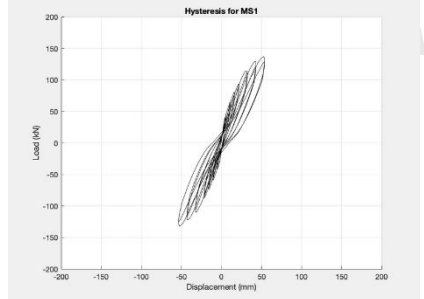

Drift	Cycle	Hysteresis	Damage
0.75 %	+1		
	-1		
	+2		
	-2		

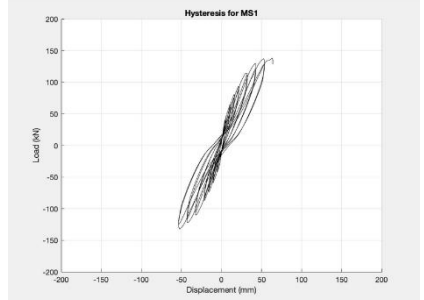

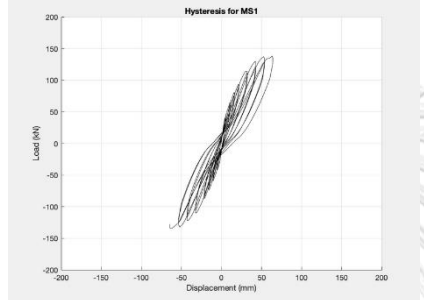

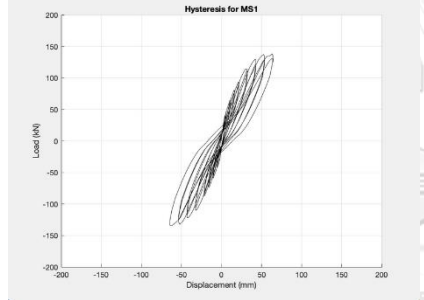

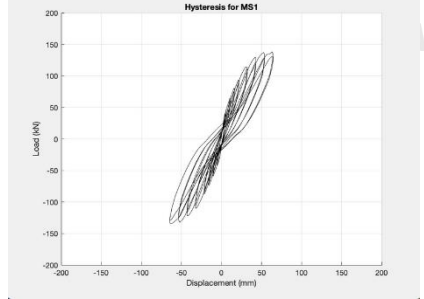
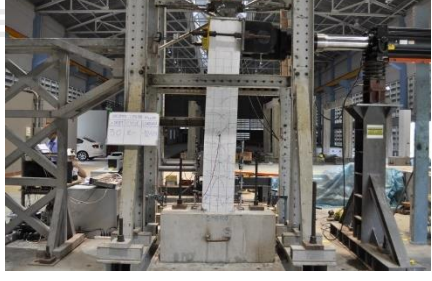
Drift	Cycle	Hysteresis	Damage
1%	+1		
	-1		
	+2		
	-2		

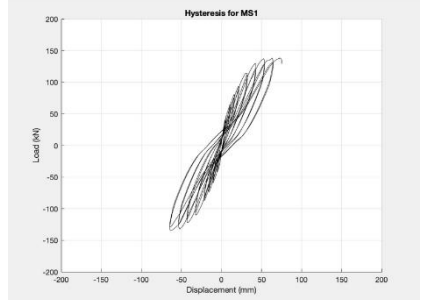

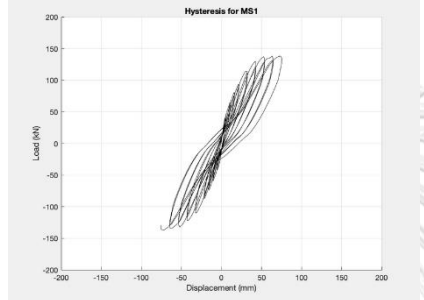

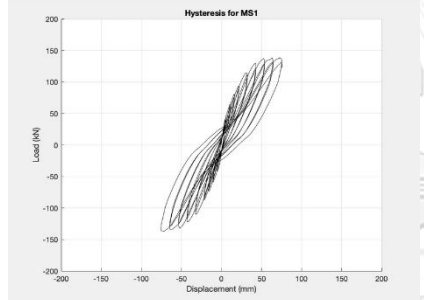

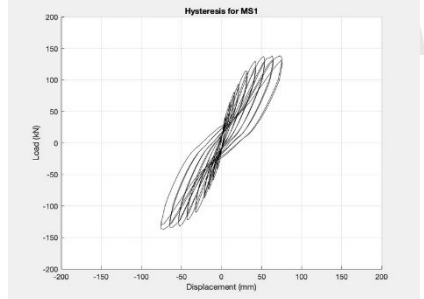

Drift	Cycle	Hysteresis	Damage
1.5%	+1		
	-1		
	+2		
	-2		

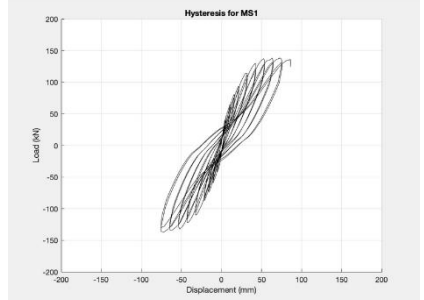

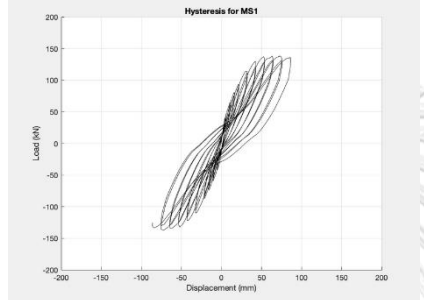

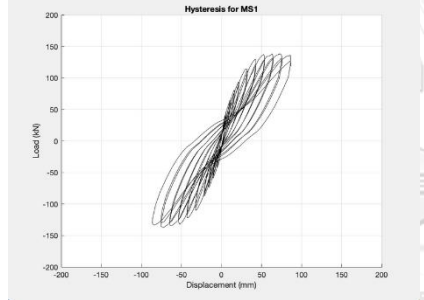

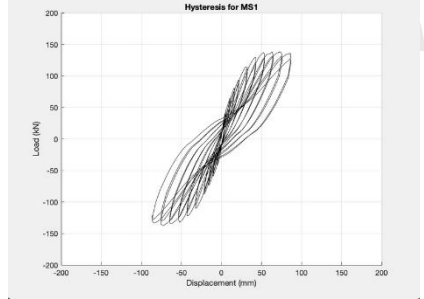

Drift	Cycle	Hysteresis	Damage
2%	+1		
	-1		
	+2		
	-2		

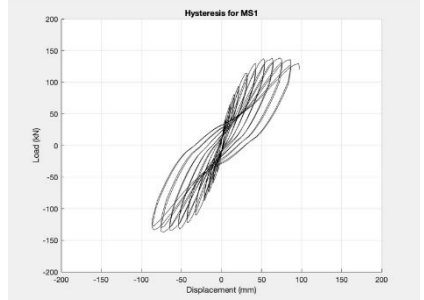

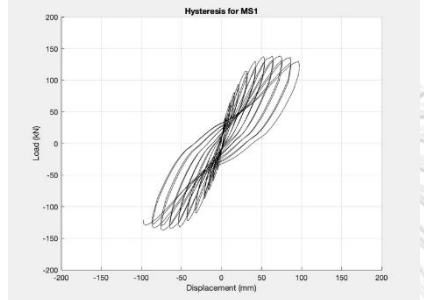

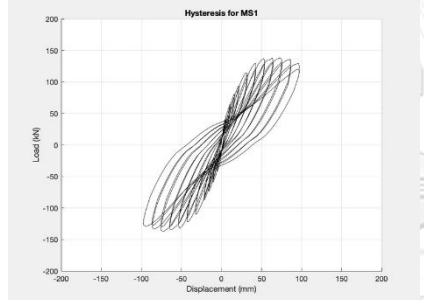

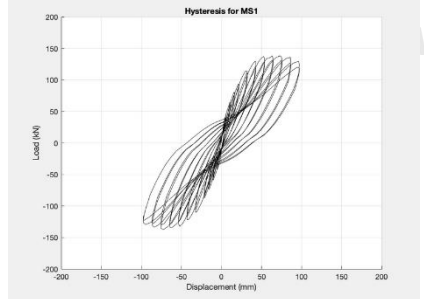



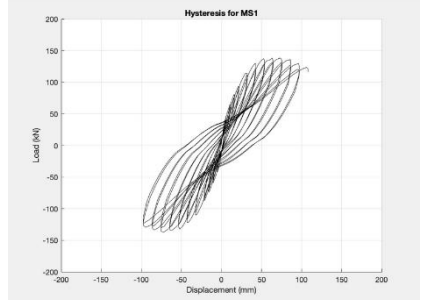

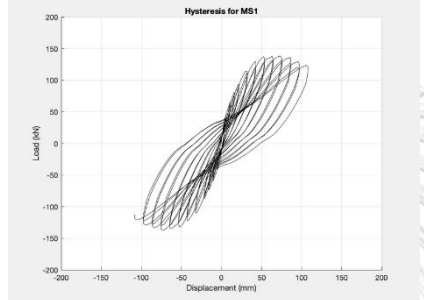

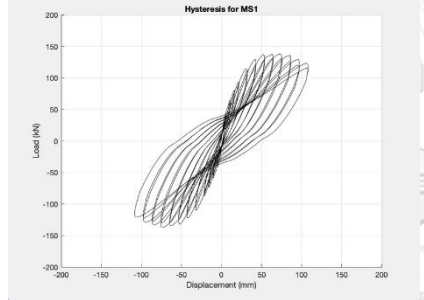

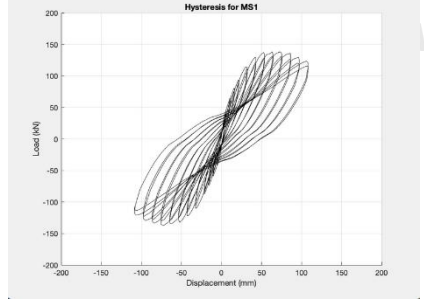

Drift	Cycle	Hysteresis	Damage
2.5%	+1		
	-1		
	+2		
	-2		

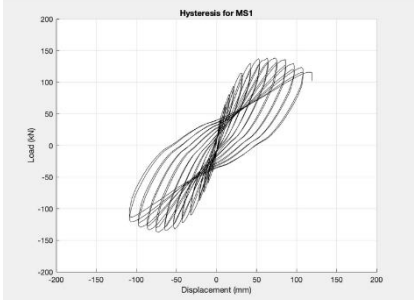

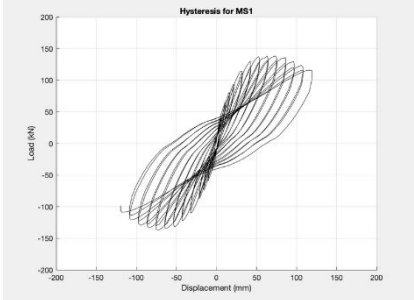

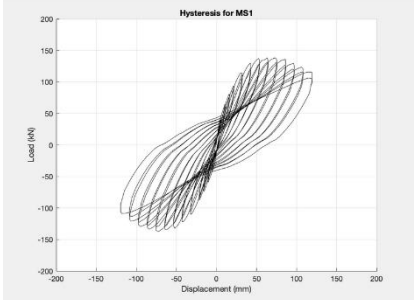

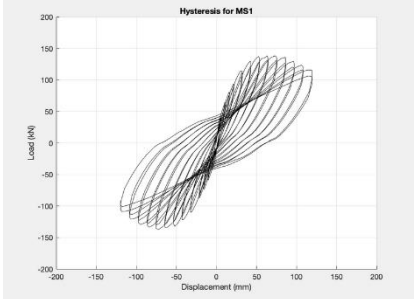

Drift	Cycle	Hysteresis	Damage
3%	+1		
	-1		
	+2		
	-2		

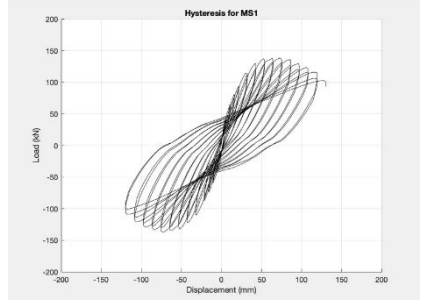

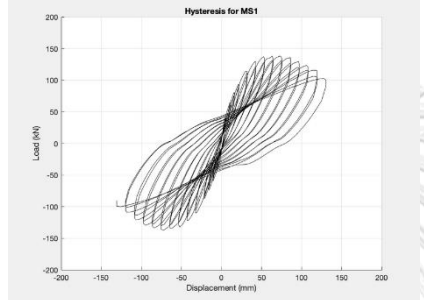

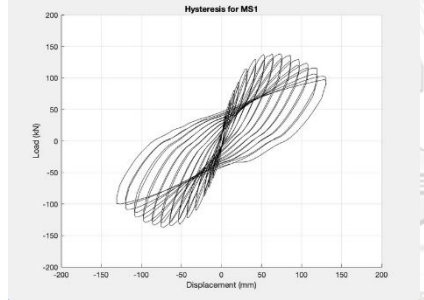

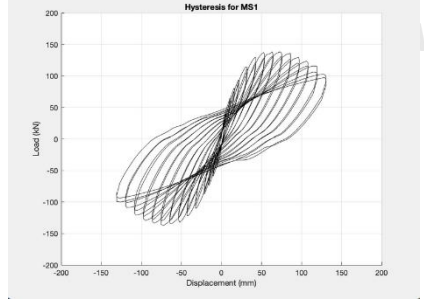

Drift	Cycle	Hysteresis	Damage
3.5%	+1		
	-1		
	+2		
	-2		

Drift	Cycle	Hysteresis	Damage
4%	+1		
	-1		
	+2		
	-2		

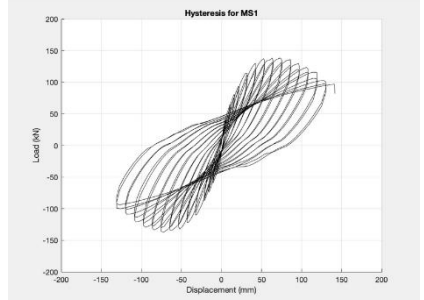

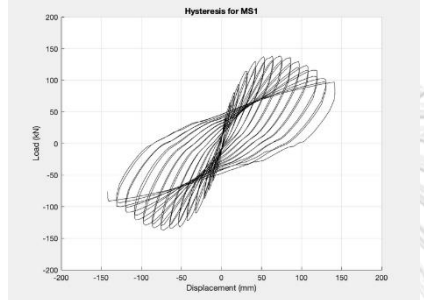

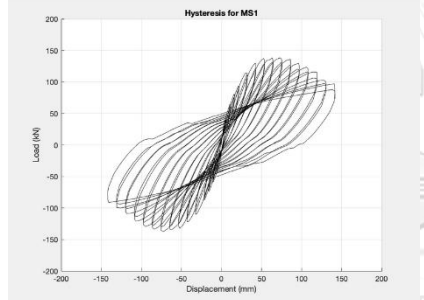

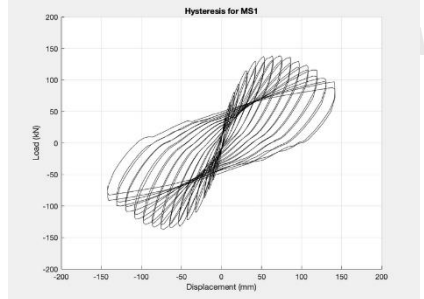

Drift	Cycle	Hysteresis	Damage
4.5%	+1		
	-1		
	+2		
	-2		

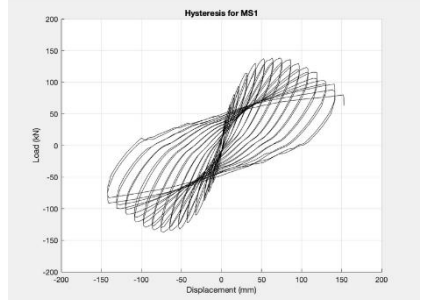

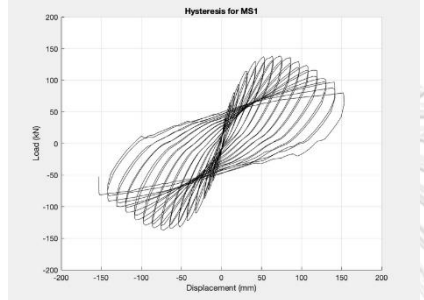

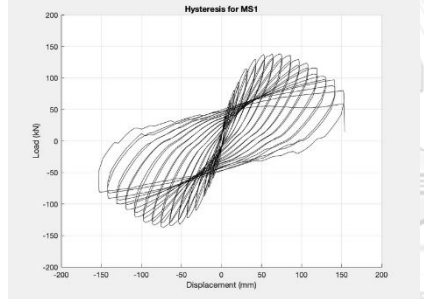

Drift	Cycle	Hysteresis	Damage
5%	+1		
	-1		
	+2		
	-2		

Drift	Cycle	Hysteresis	Damage
5.5%	+1		
	-1		
	+2		
	-2		

Drift	Cycle	Hysteresis	Damage
6%	+1		
	-1		
	+2		
	-2		



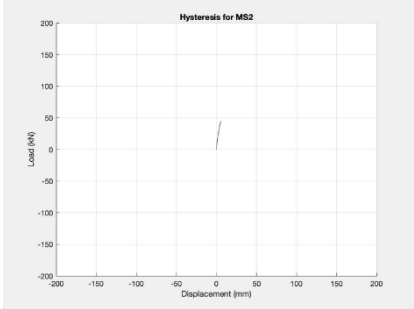

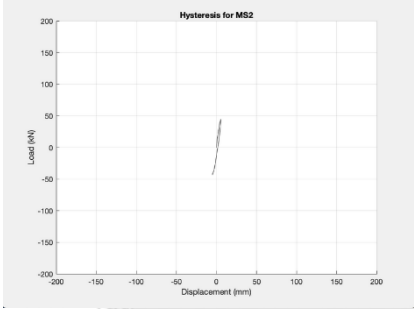

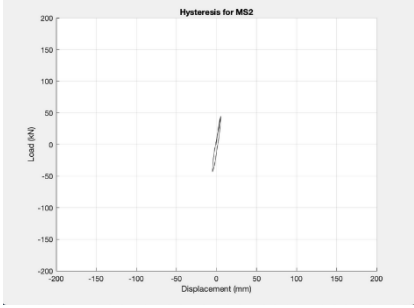

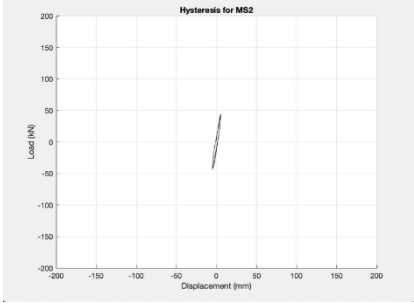

Drift	Cycle	Hysteresis	Damage
6.5%	+1		
	-1		
	+2		
	-2		

Drift	Cycle	Hysteresis	Damage
7%	+1		
	-1		
	+2		

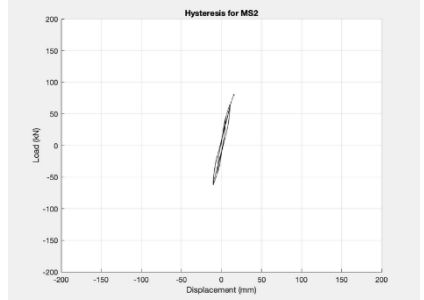

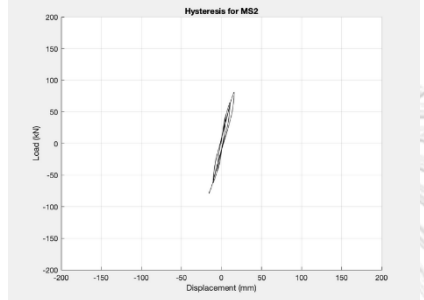

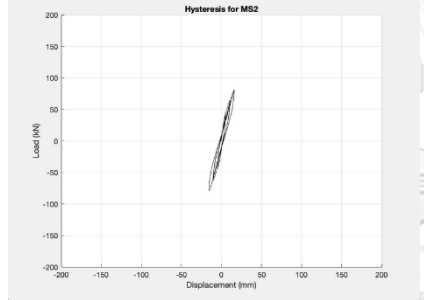

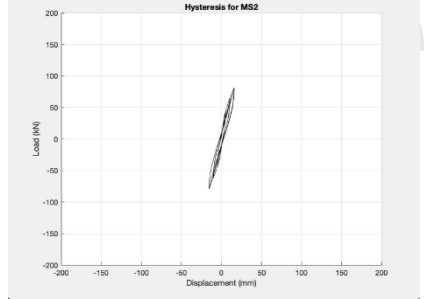

## APPENDIX E

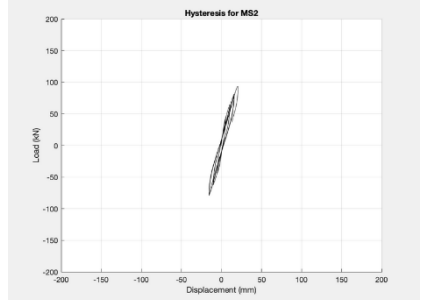

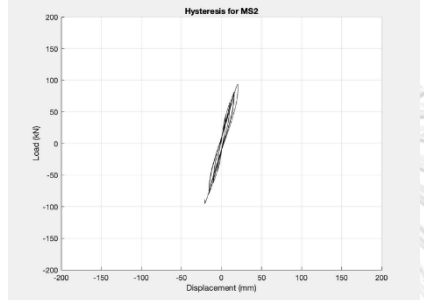

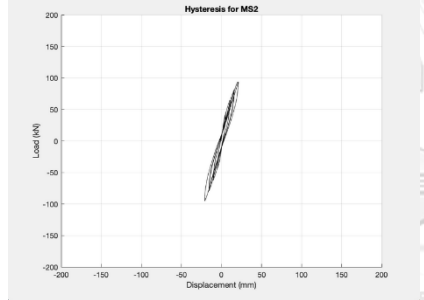

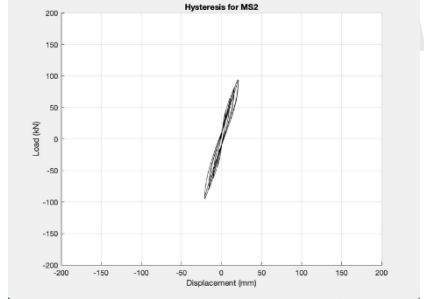

## Cyclic behavior of MS2 column specimen

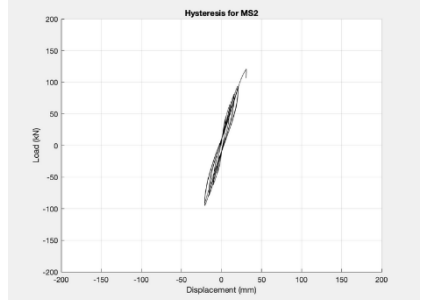

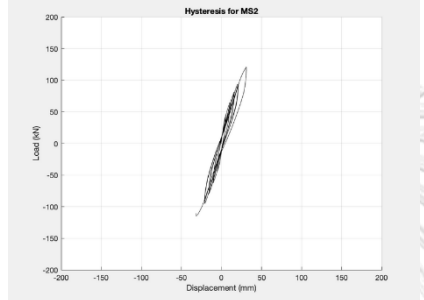

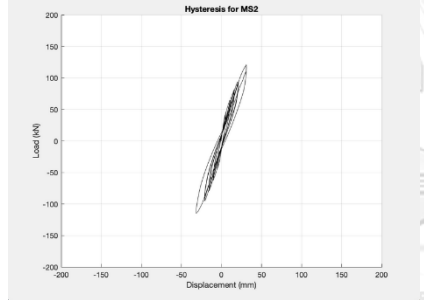

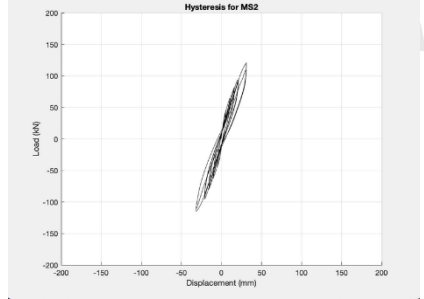

Table 0.1 Cyclic behavior of MS2 column

Drift	Cycle	Hysteresis	Damage
0.25 %	+1		
	-1		
	+2		
	-2		

Drift	Cycle	Hysteresis	Damage
0.5%	+1		
	-1		
	+2		
	-2		

Drift	Cycle	Hysteresis	Damage
0.75 %	+1		
	-1		
	+2		
	-2		

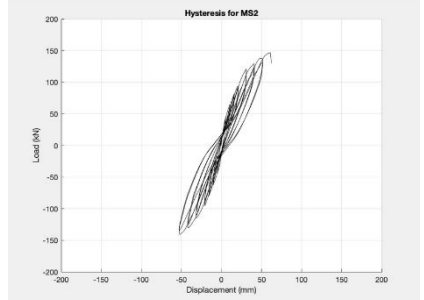

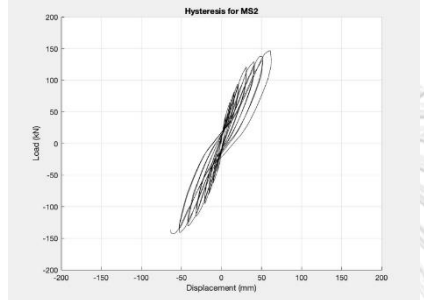

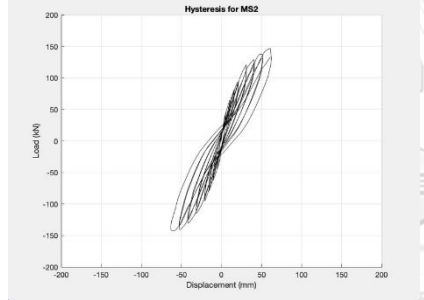

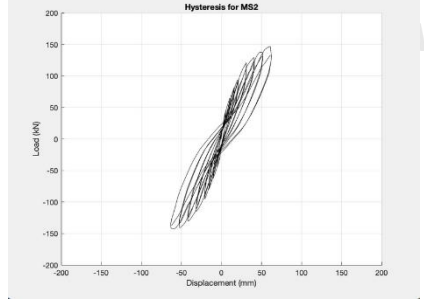

Drift	Cycle	Hysteresis	Damage
1%	+1		
	-1		
	+2		
	-2		

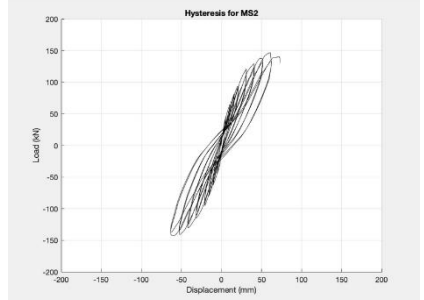

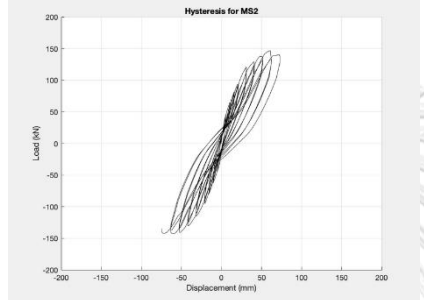

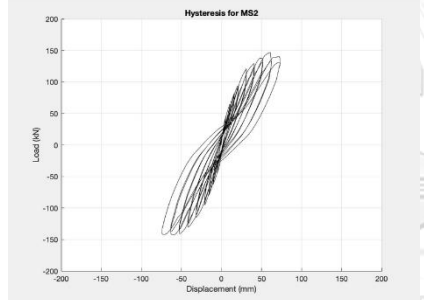

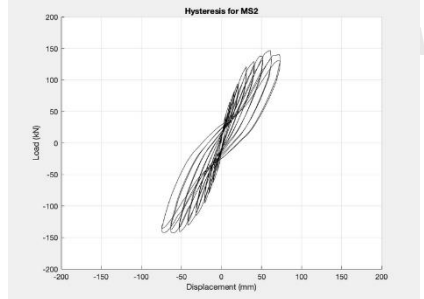

Drift	Cycle	Hysteresis	Damage
1.5%	+1		
	-1		
	+2		
	-2		

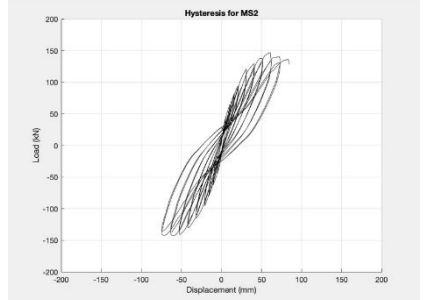

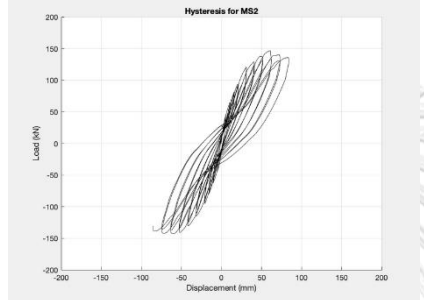

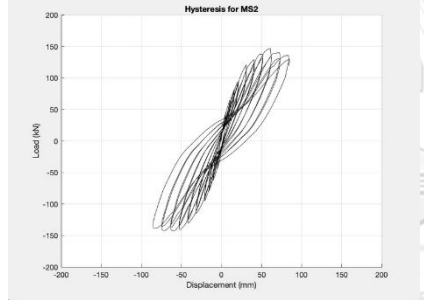

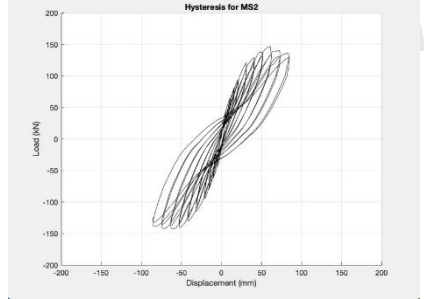

Drift	Cycle	Hysteresis	Damage
2%	+1		
	-1		
	+2		
	-2		

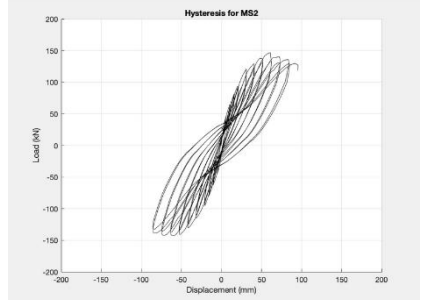

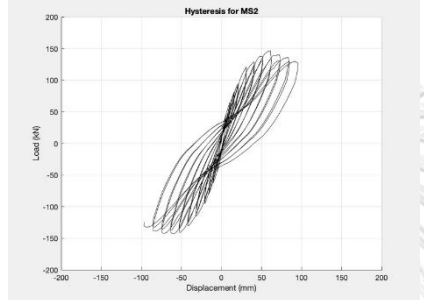

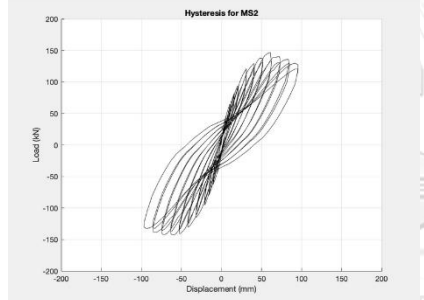

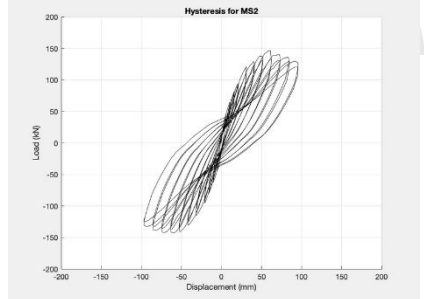



Drift	Cycle	Hysteresis	Damage
2.5%	+1		
	-1		
	+2		
	-2		

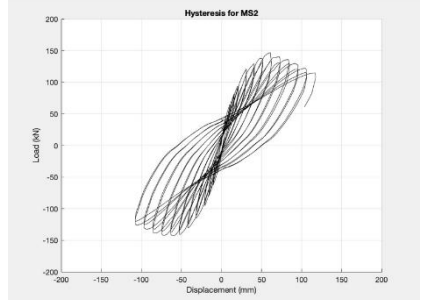

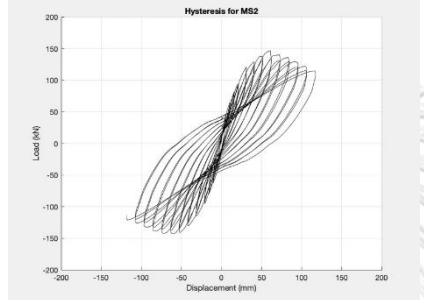

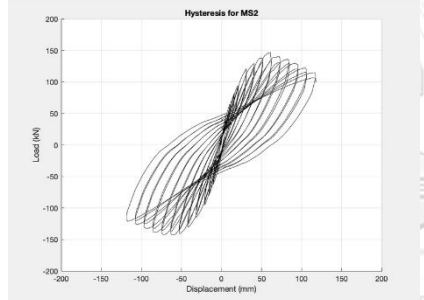

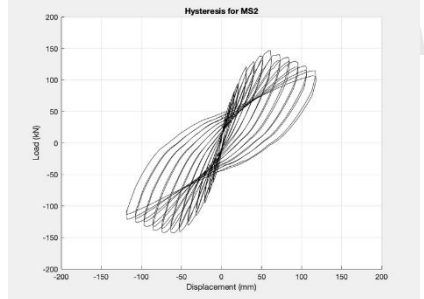

Drift	Cycle	Hysteresis	Damage
3%	+1		
	-1		
	+2		
	-2		

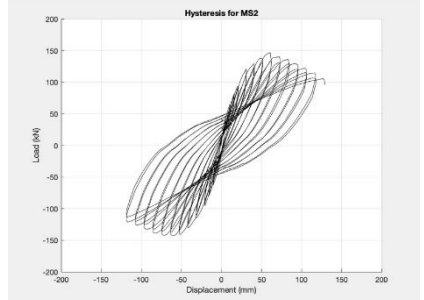

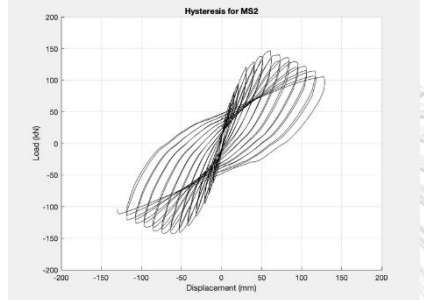

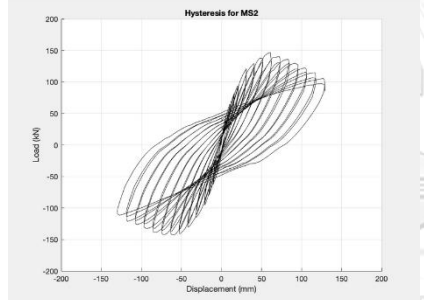

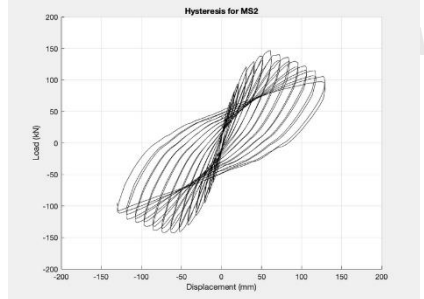

Drift	Cycle	Hysteresis	Damage
3.5%	+1		
	-1		
	+2		
	-2		

Drift	Cycle	Hysteresis	Damage
4%	+1		
	-1		
	+2		
	-2		

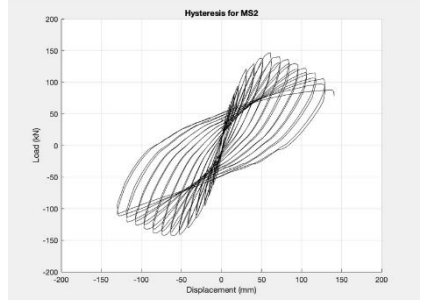

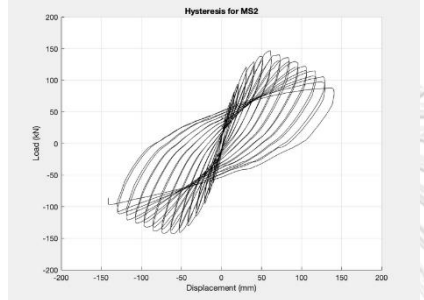

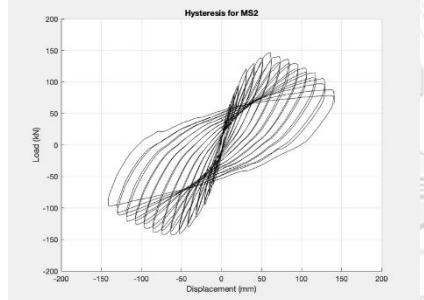

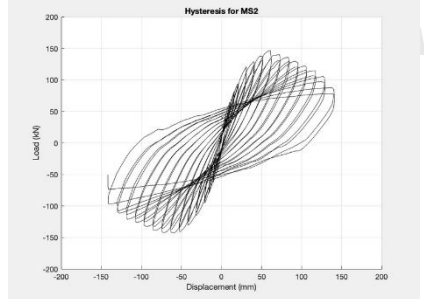

Drift	Cycle	Hysteresis	Damage
4.5%	+1		
	-1		
	+2		
	-2		

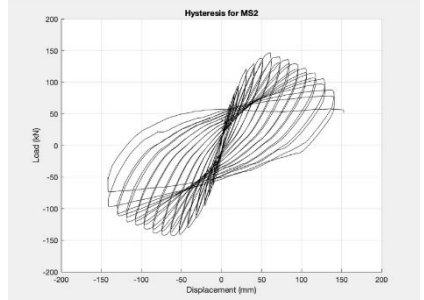

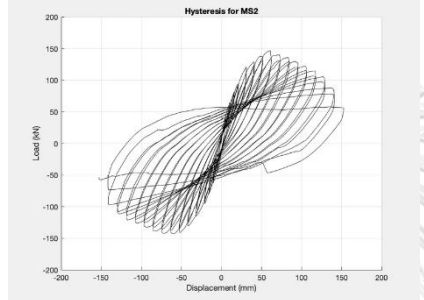

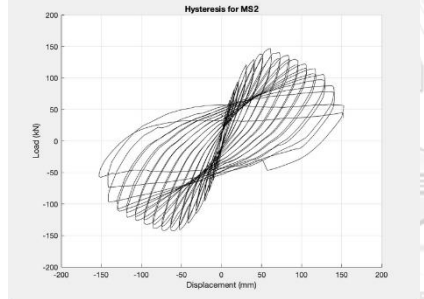

Drift	Cycle	Hysteresis	Damage
5%	+1		
	-1		
	+2		
	-2		

Drift	Cycle	Hysteresis	Damage
5.5%	+1		
	-1		
	+2		
	-2		

Drift	Cycle	Hysteresis	Damage
6%	+1		
	-1		
	+2		
	-2		



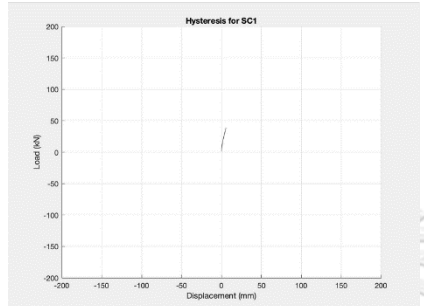

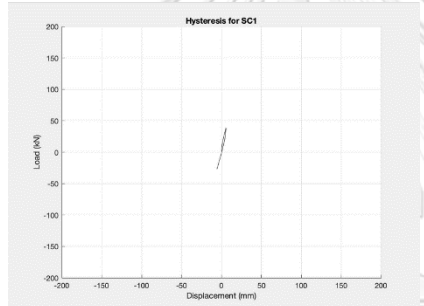

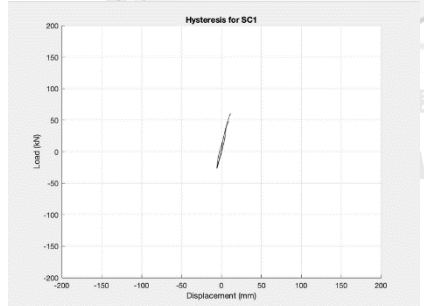

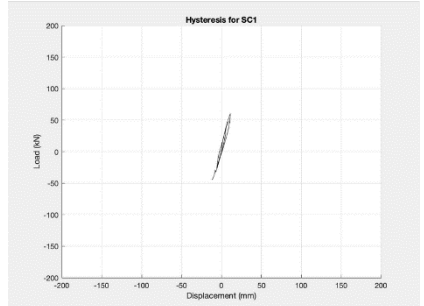

Drift	Cycle	Hysteresis	Damage
6.5%	+1		
	-1		
	+2		
	-2		

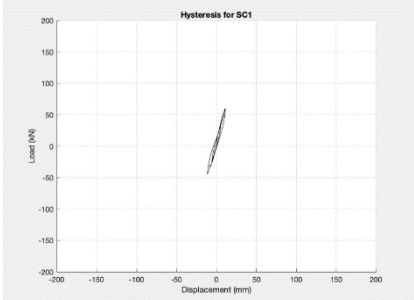

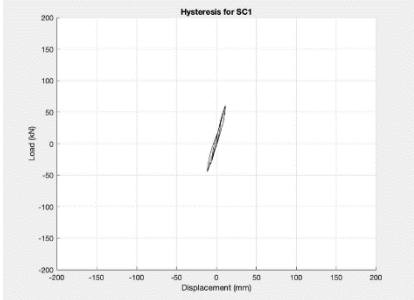

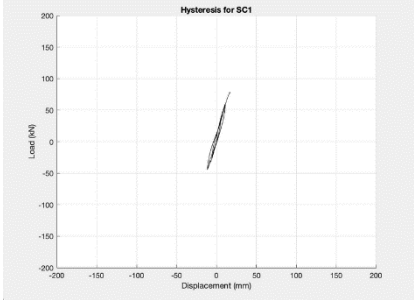

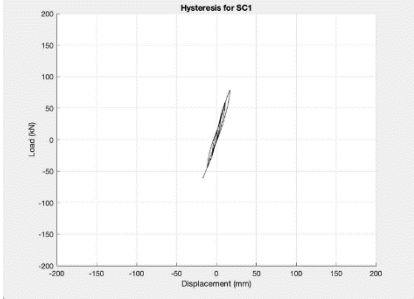

Drift	Cycle	Hysteresis	Damage
7%	+1		
	-1		
	+2		

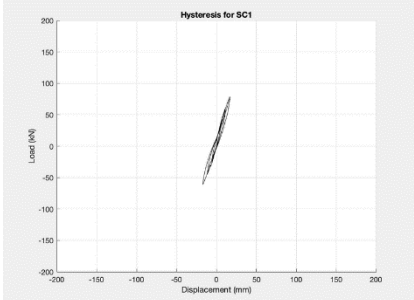

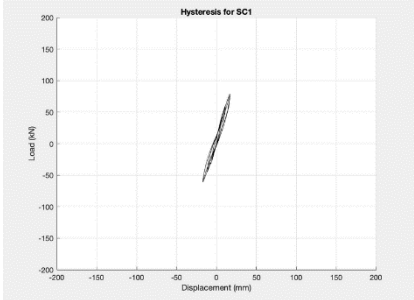

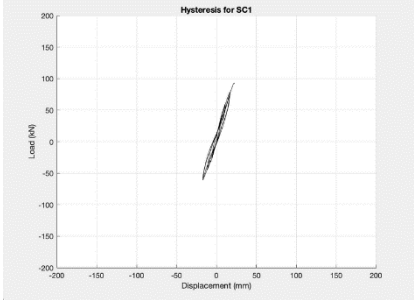

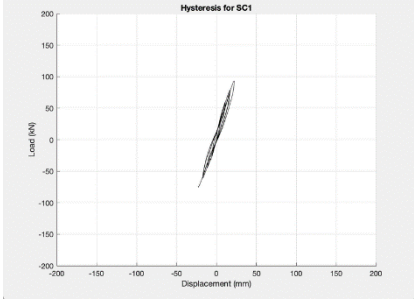

APPENDIX F

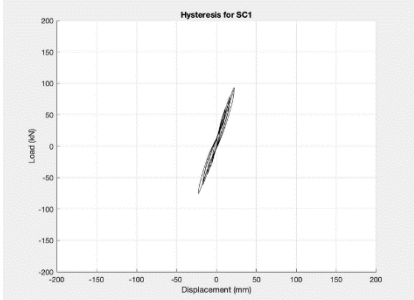

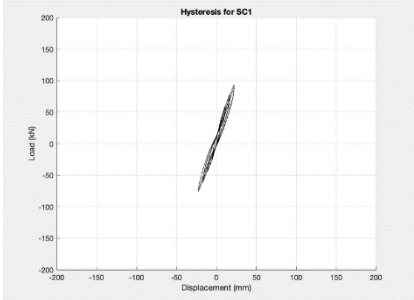

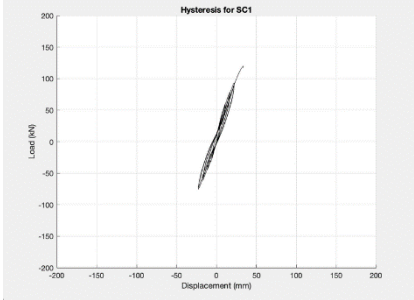
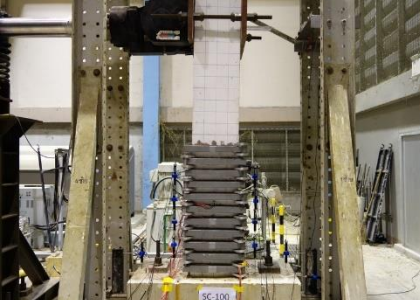
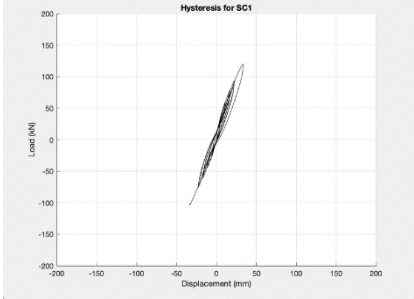

Cyclic behavior of SC1 column specimen

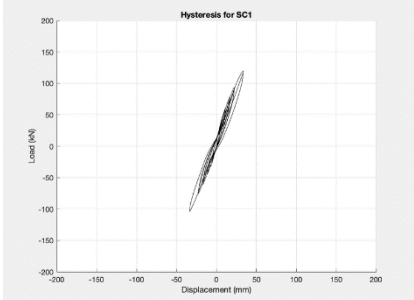

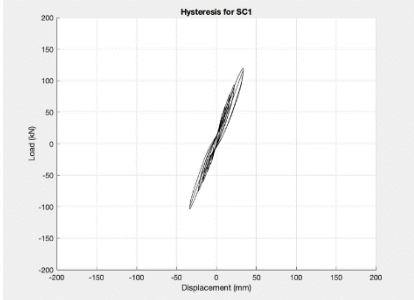

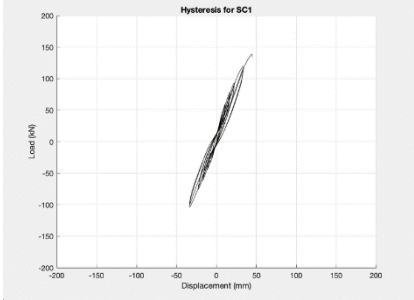

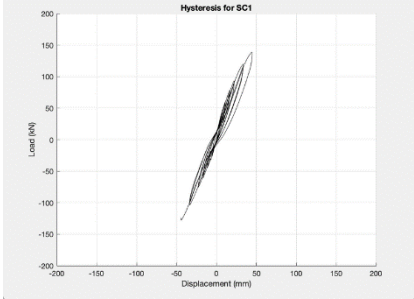

Table 0.1 Cyclic behavior of SC1 column

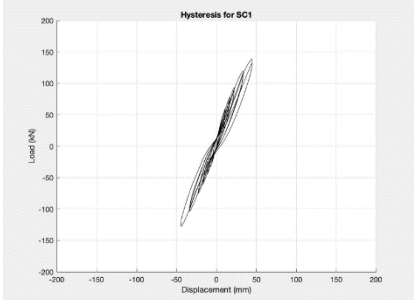

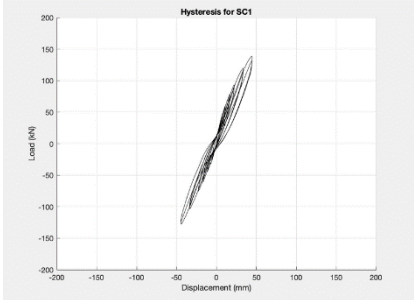

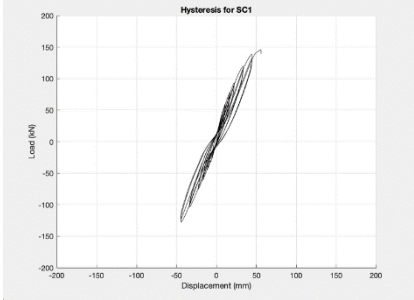
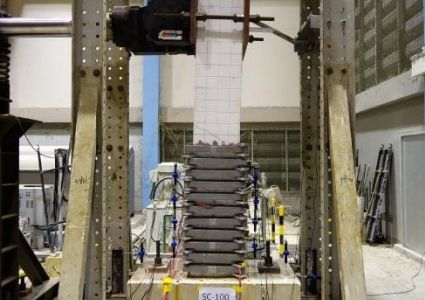
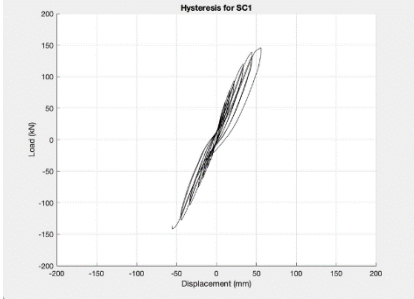

Drift	Cycle	Hysteresis	Damage
0.25 %	+1		
	-1		
	+2		
	-2		

Drift	Cycle	Hysteresis	Damage
0.5%	+1		
	-1		
	+2		
	-2		

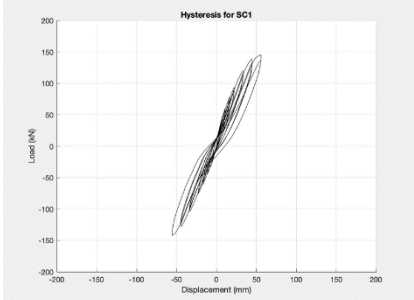

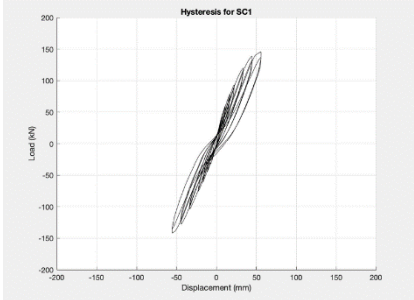

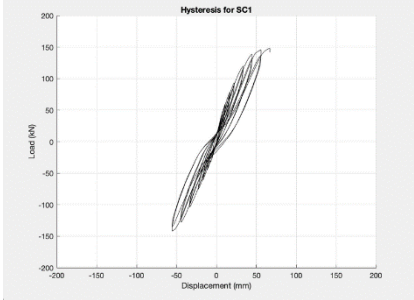

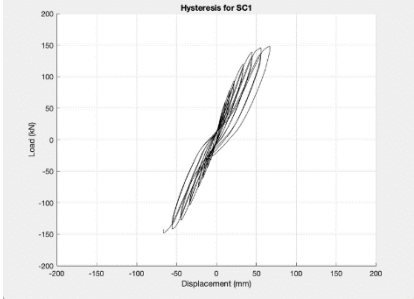

Drift	Cycle	Hysteresis	Damage
0.75 %	+1		
	-1		
	+2		
	-2		

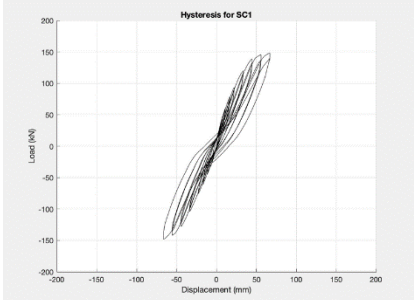

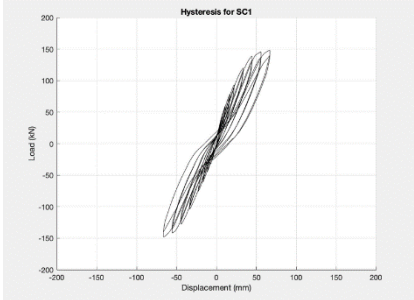

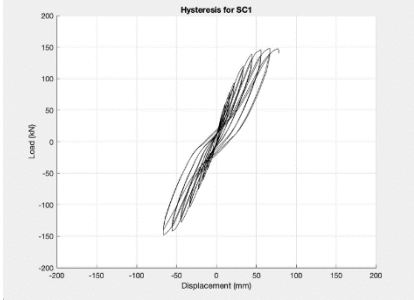

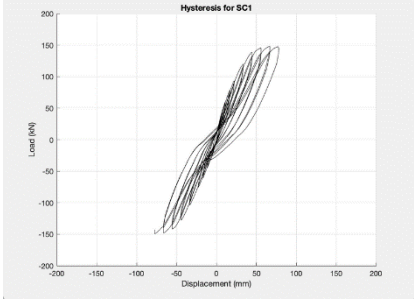
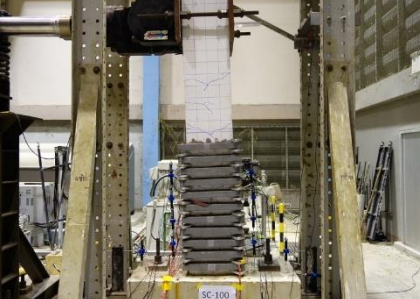
Drift	Cycle	Hysteresis	Damage
1%	+1		
	-1		
	+2		
	-2		

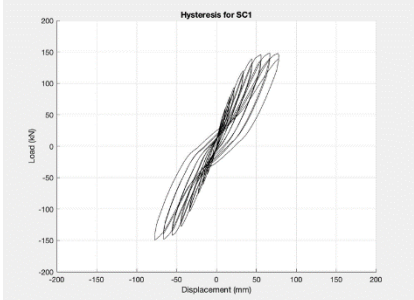

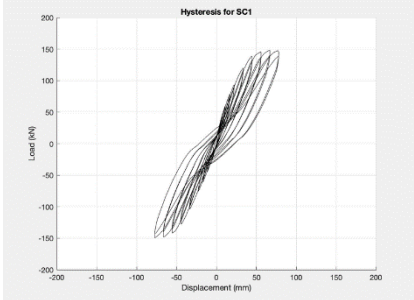

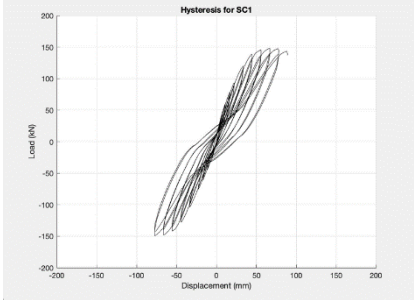

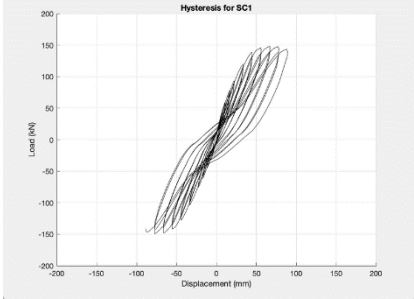

Drift	Cycle	Hysteresis	Damage
1.5%	+1		
	-1		
	+2		
	-2		

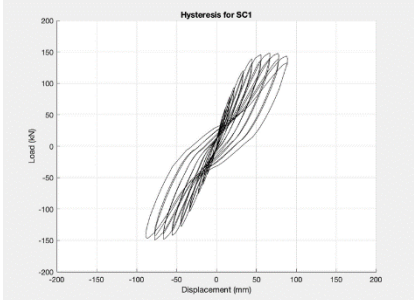

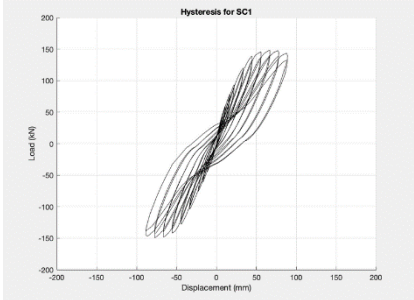

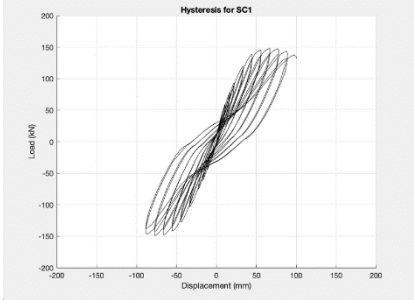

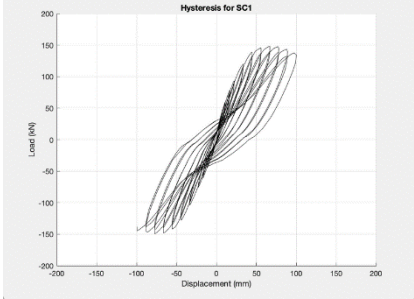

Drift	Cycle	Hysteresis	Damage
2%	+1		
	-1		
	+2		
	-2		

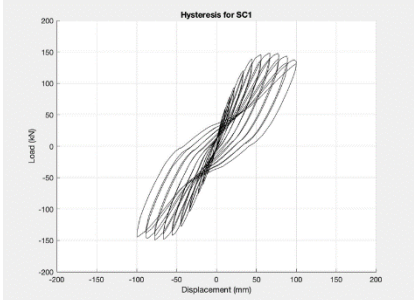

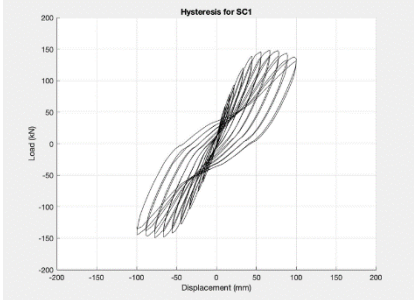

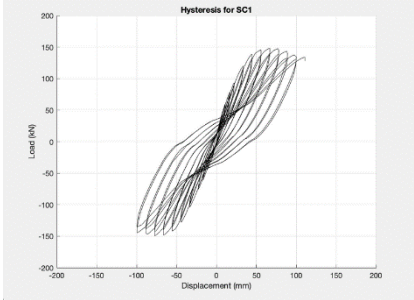

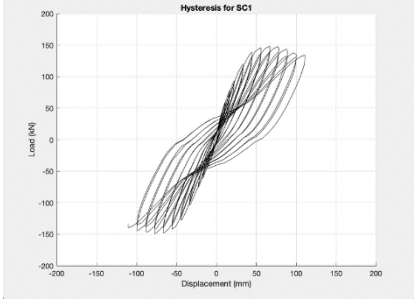



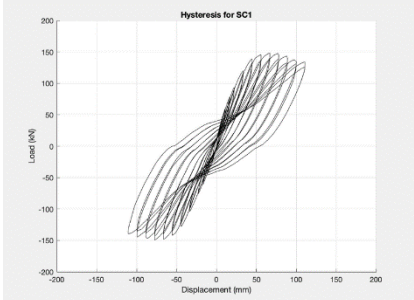

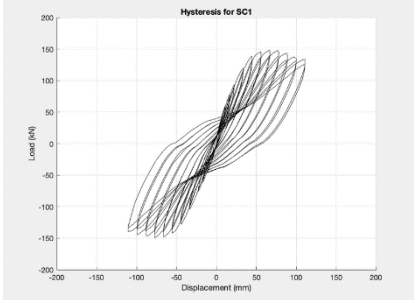

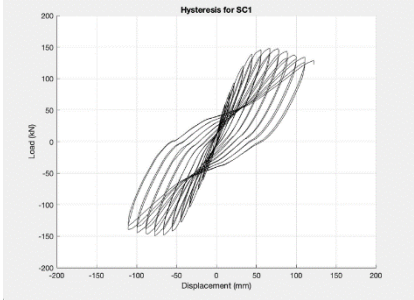

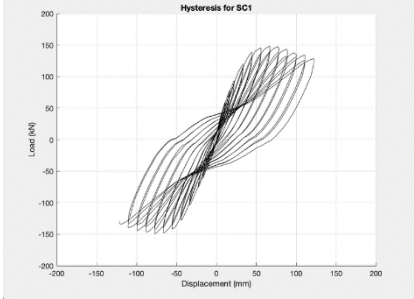
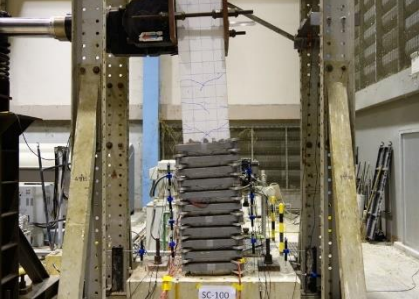
Drift	Cycle	Hysteresis	Damage
2.5%	+1		
	-1		
	+2		
	-2		

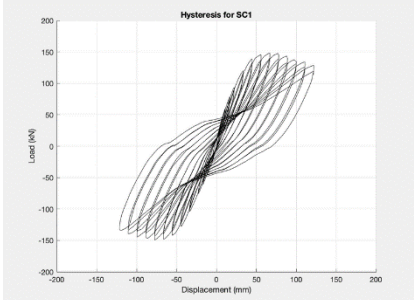

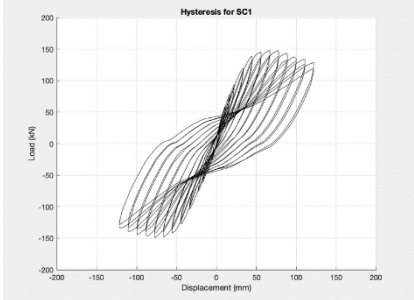
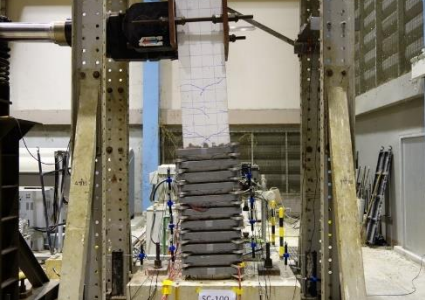
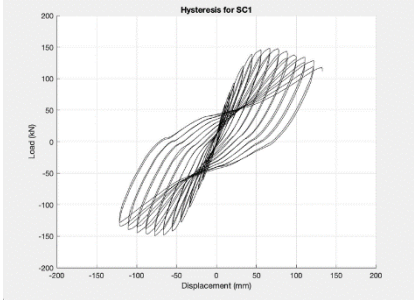

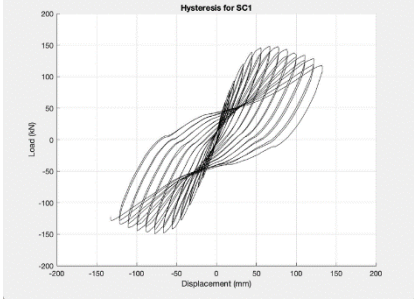
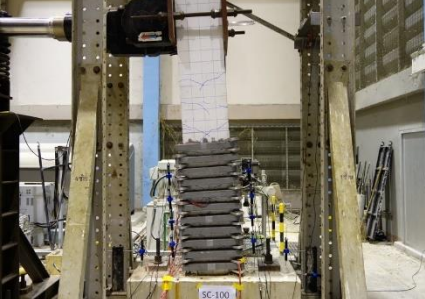
Drift	Cycle	Hysteresis	Damage
3%	+1		
	-1		
	+2		
	-2		

Drift	Cycle	Hysteresis	Damage
3.5%	+1		
	-1		
	+2		
	-2		

Drift	Cycle	Hysteresis	Damage
4%	+1		
	-1		
	+2		
	-2		

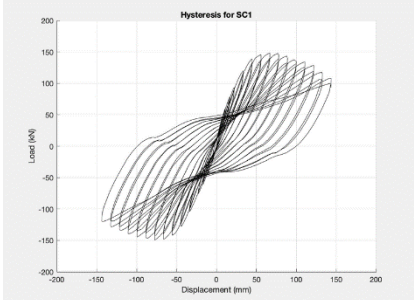

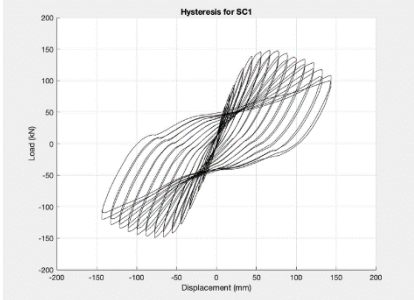

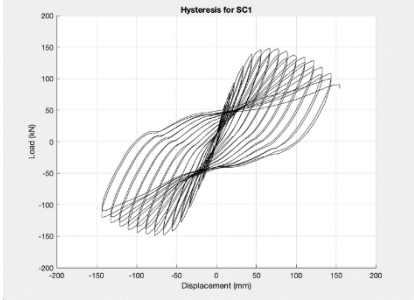

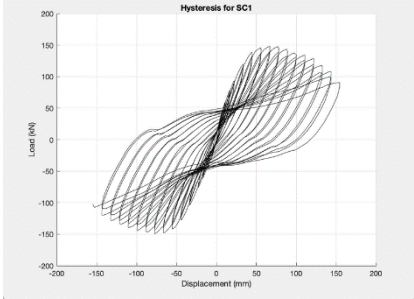
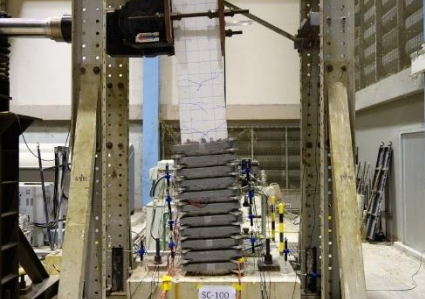
Drift	Cycle	Hysteresis	Damage
4.5%	+1		
	-1		
	+2		
	-2		

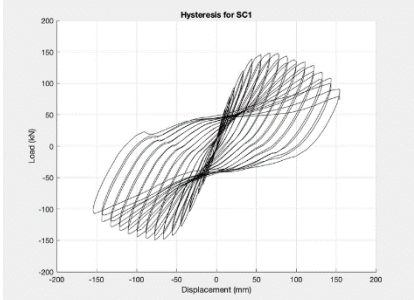

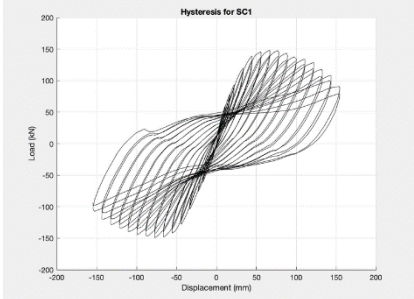
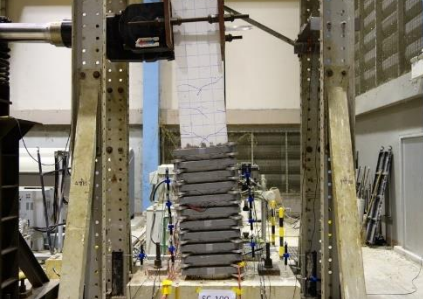
Drift	Cycle	Hysteresis	Damage
5%	+1		
	-1		
	+2		
	-2		

Drift	Cycle	Hysteresis	Damage
5.5%	+1		
	-1		
	+2		
	-2		

Drift	Cycle	Hysteresis	Damage
6%	+1		
	-1		
	+2		
	-2		



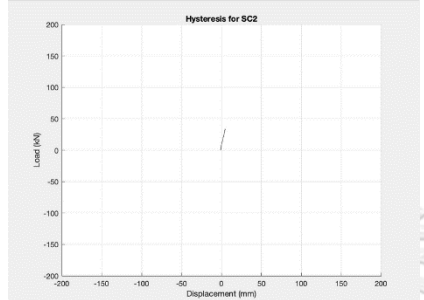

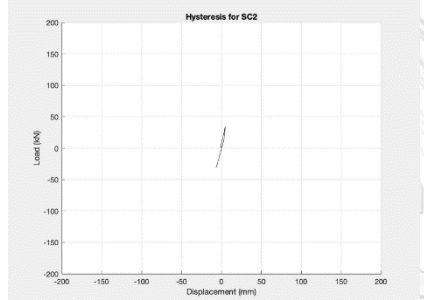

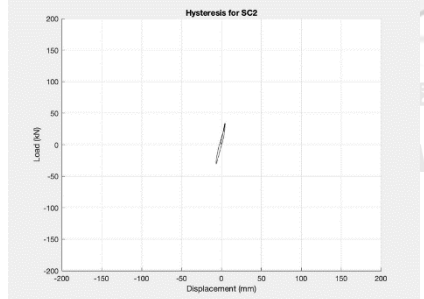

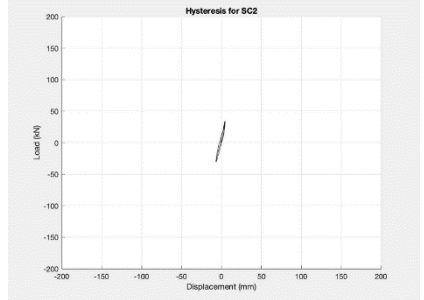

Drift	Cycle	Hysteresis	Damage
6.5%	+1		
	-1		
	+2		
	-2		

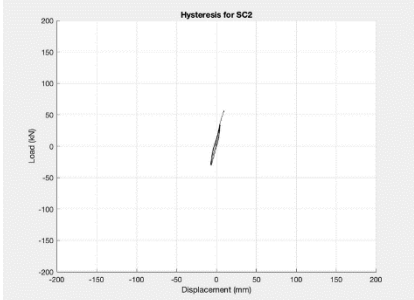

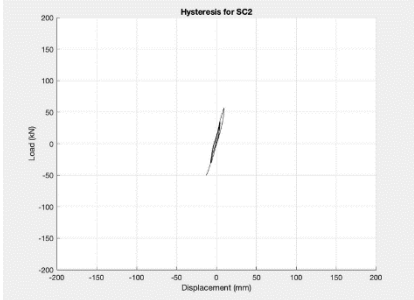
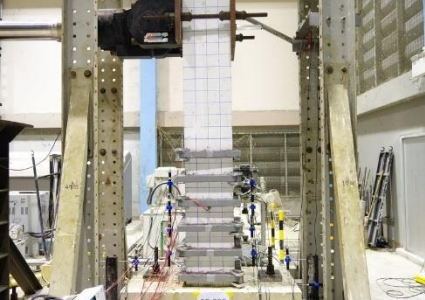
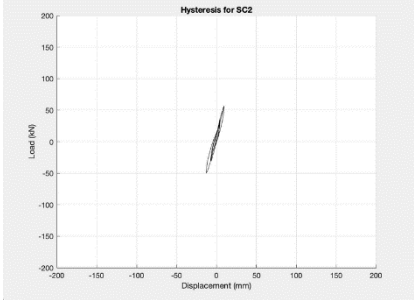
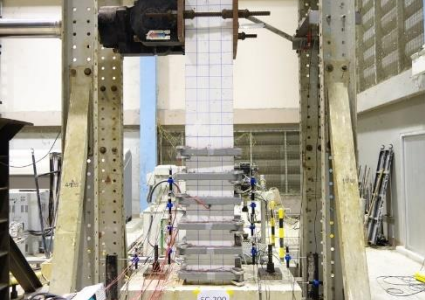
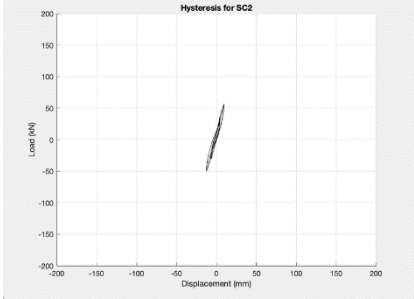
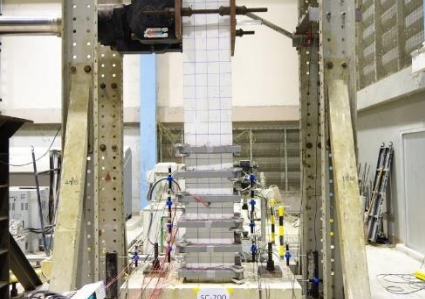
Drift	Cycle	Hysteresis	Damage
7%	+1		
	-1		

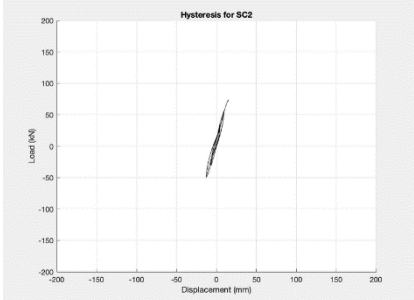
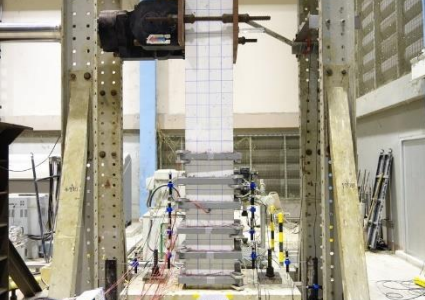
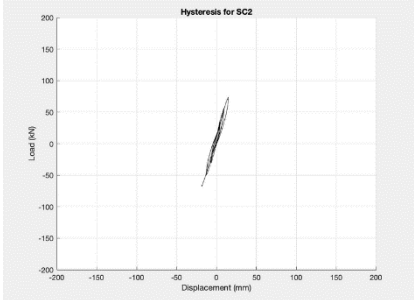
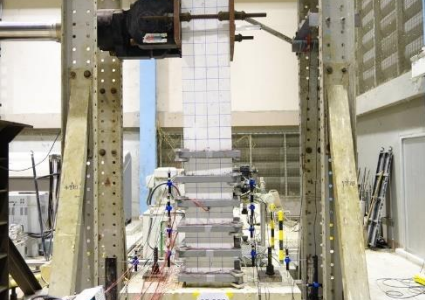
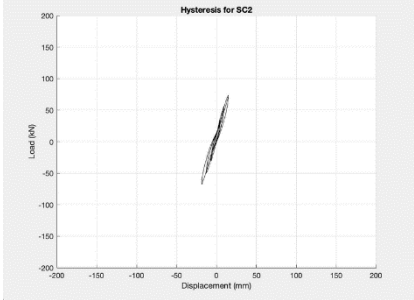

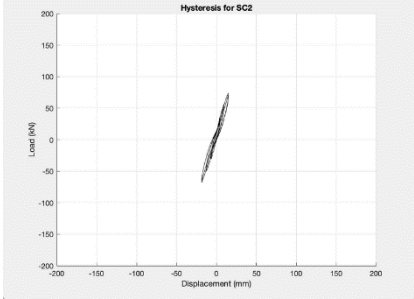
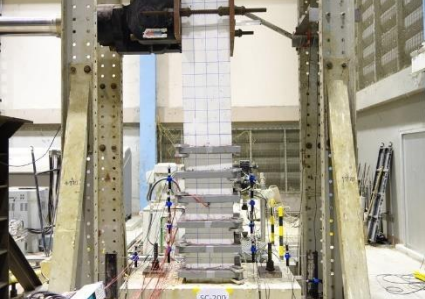
APPENDIX G

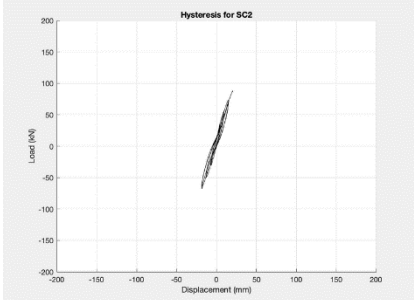

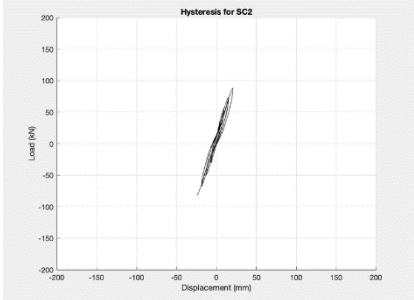
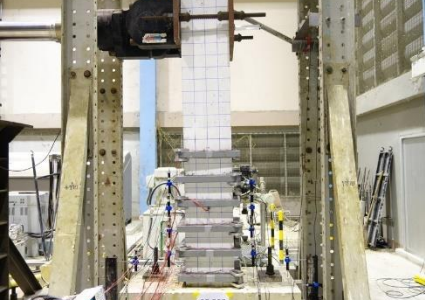
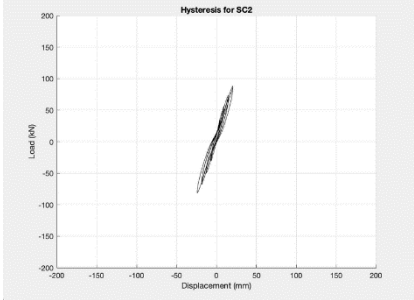
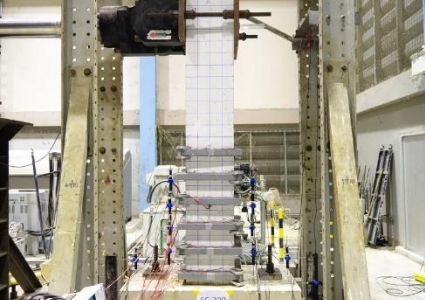
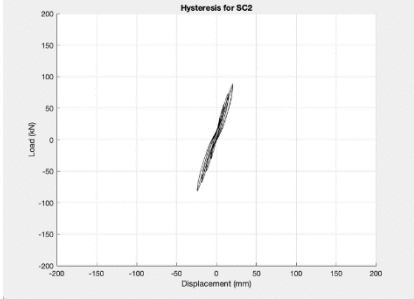
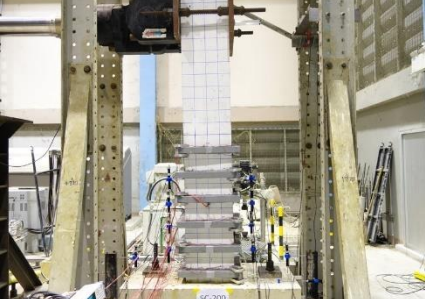
Cyclic behavior of SC2 column specimen

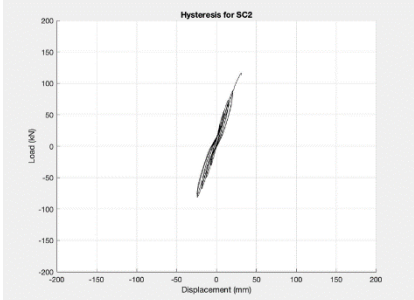

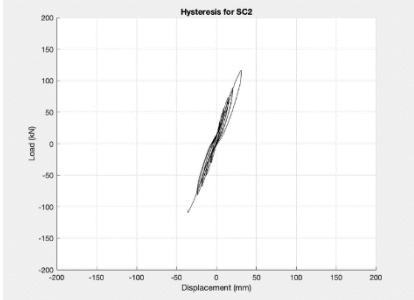

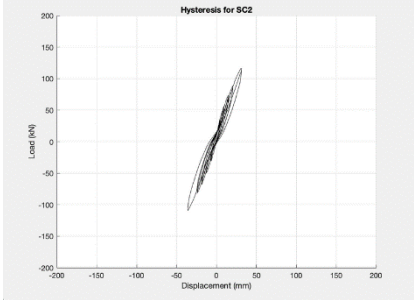

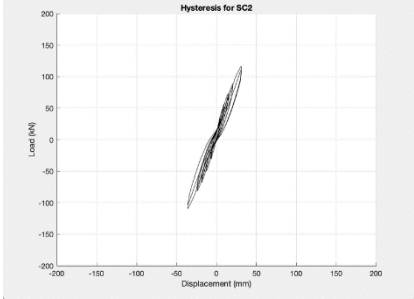
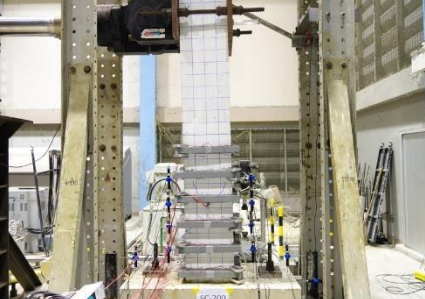
Table 0.1 Cyclic behavior of SC2 column

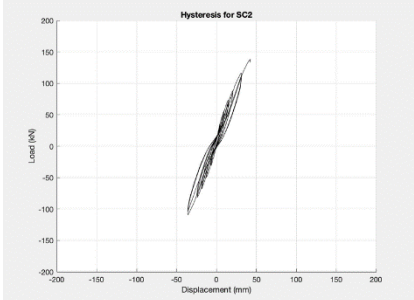

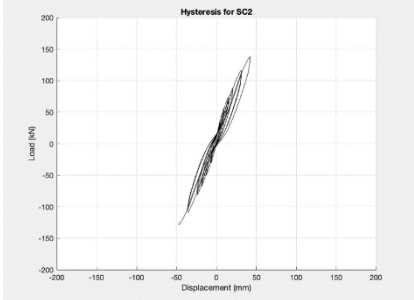
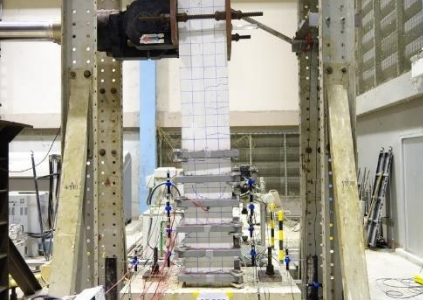
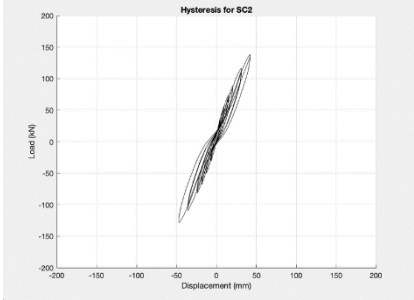

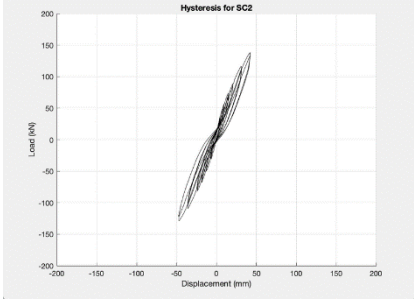
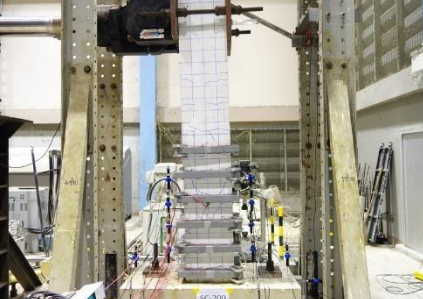
Drift	Cycle	Hysteresis	Damage
0.25 %	+1		
	-1		
	+2		
	-2		

Drift	Cycle	Hysteresis	Damage
0.5%	+1		
	-1		
	+2		
	-2		

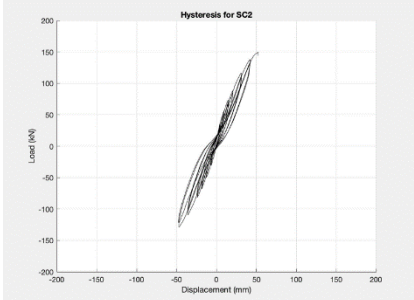

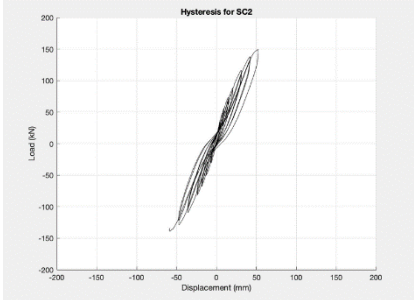

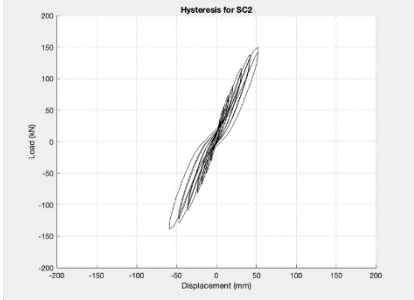

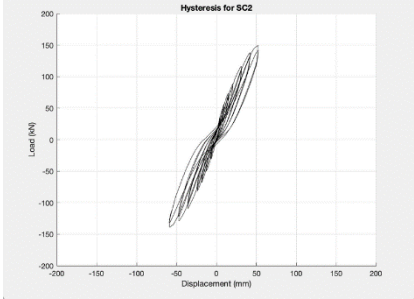
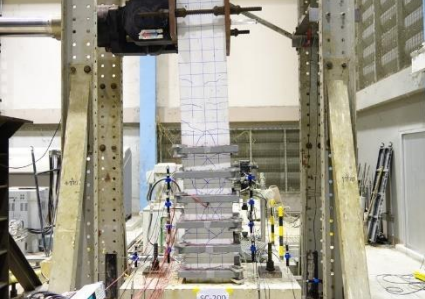
Drift	Cycle	Hysteresis	Damage
0.75 %	+1		
	-1		
	+2		
	-2		

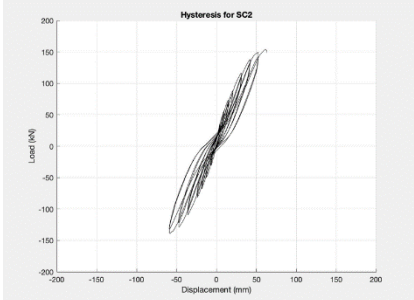

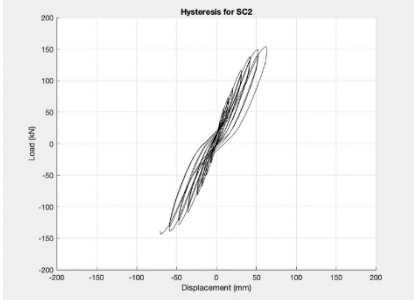
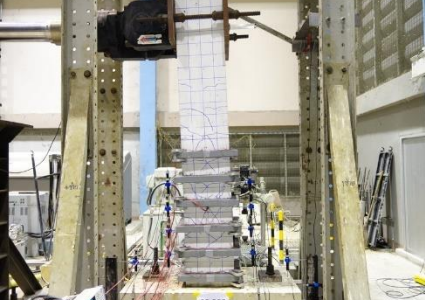
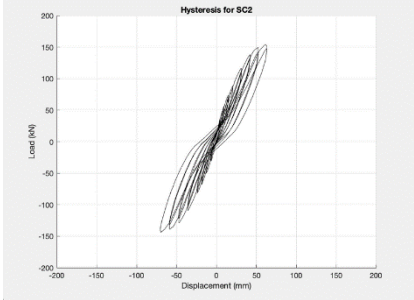
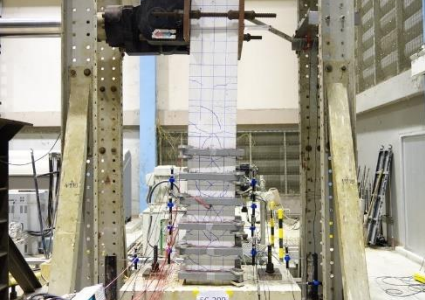
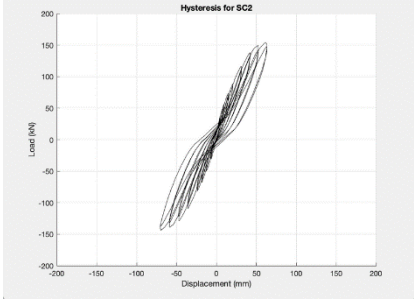
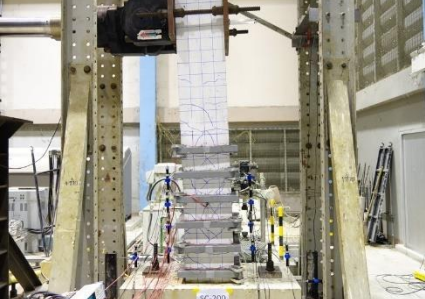
Drift	Cycle	Hysteresis	Damage
1%	+1		
	-1		
	+2		
	-2		

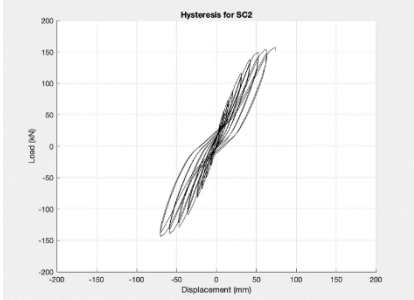
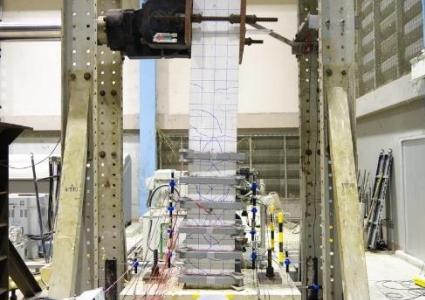
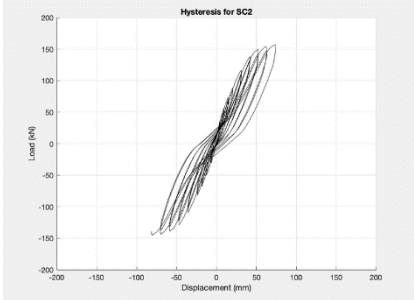
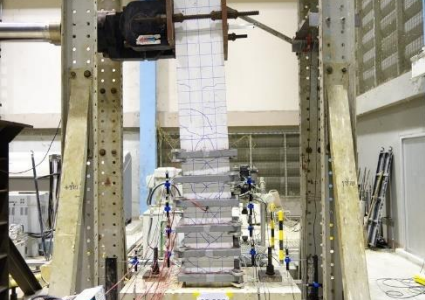
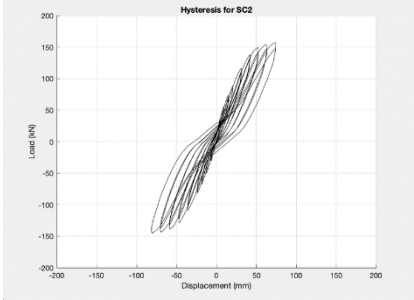

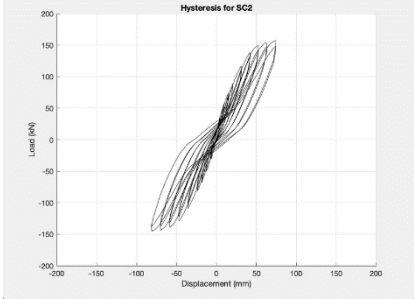

Drift	Cycle	Hysteresis	Damage
1.5%	+1		
	-1		
	+2		
	-2		

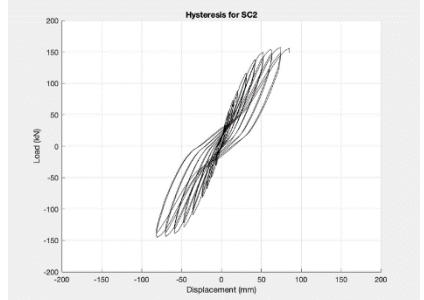

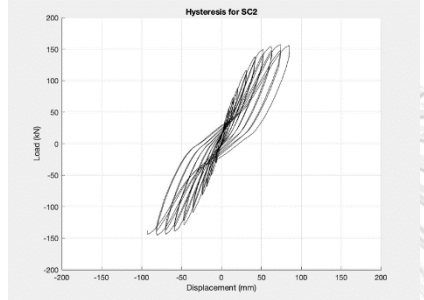

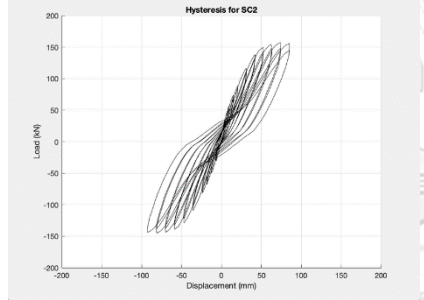

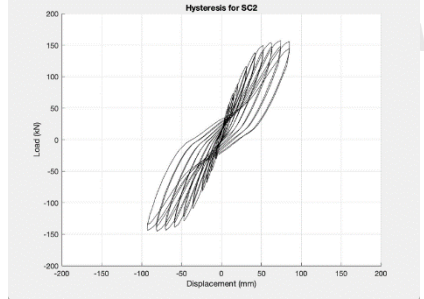
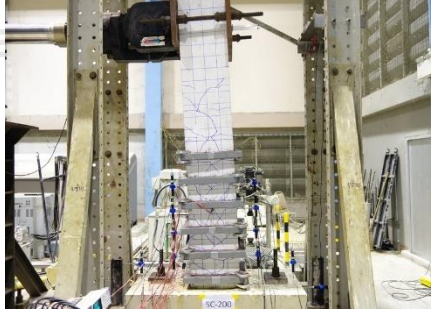
Drift	Cycle	Hysteresis	Damage
2%	+1		
	-1		
	+2		
	-2		

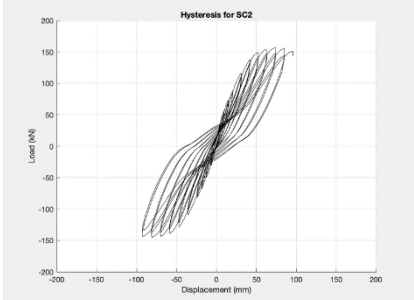

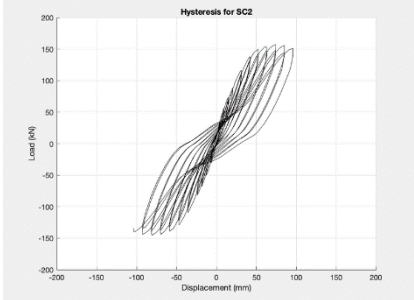

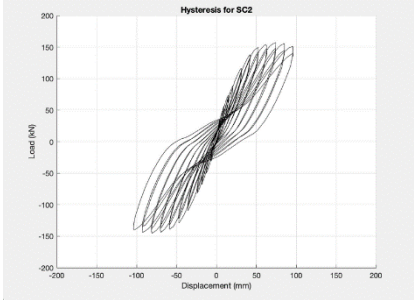

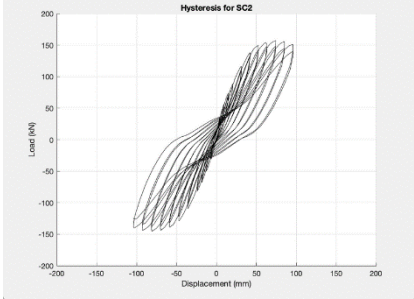
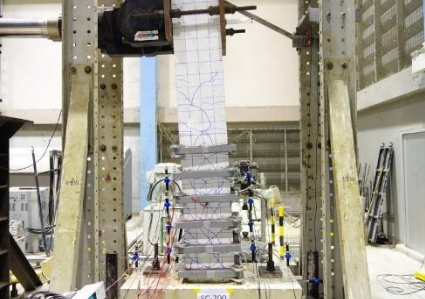


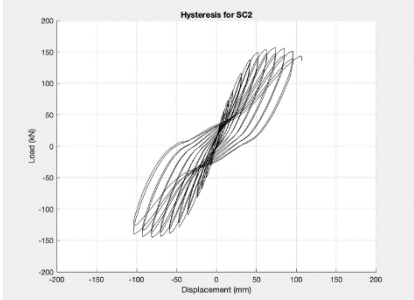
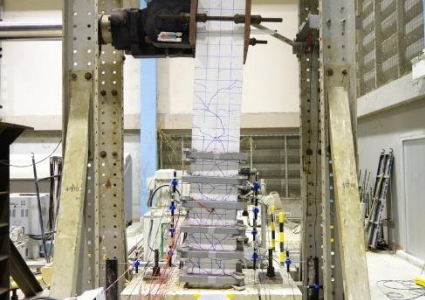
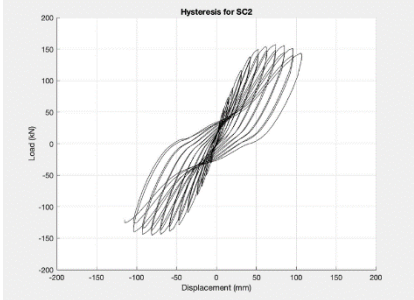

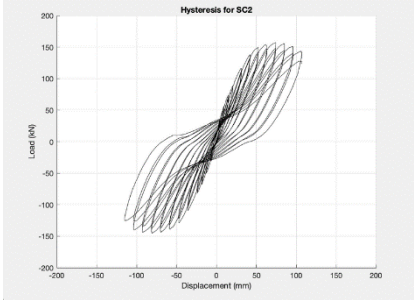
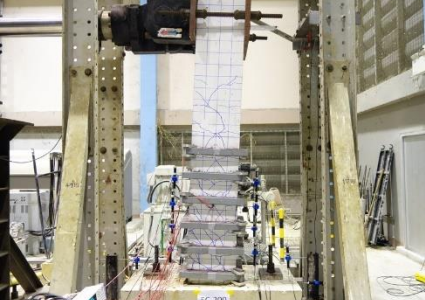
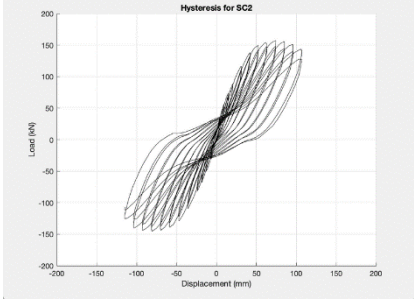
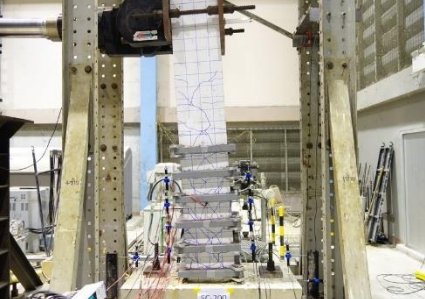
Drift	Cycle	Hysteresis	Damage
2.5%	+1		
	-1		
	+2		
	-2		

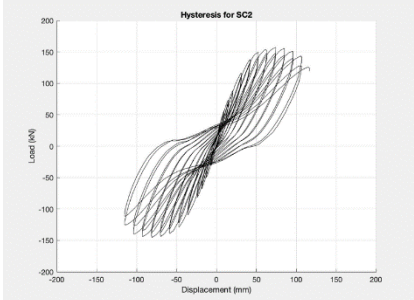
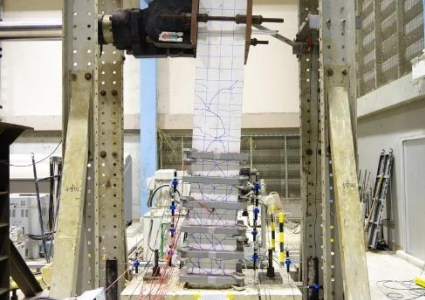
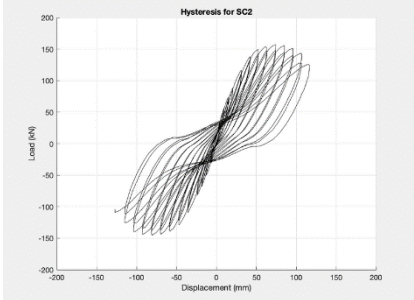

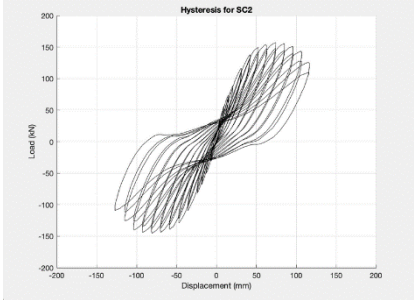
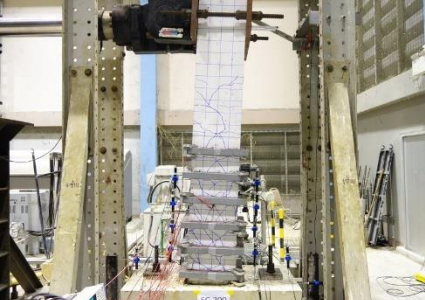
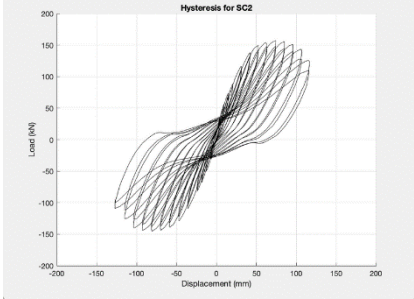

Drift	Cycle	Hysteresis	Damage
3%	+1		
	-1		
	+2		
	-2		

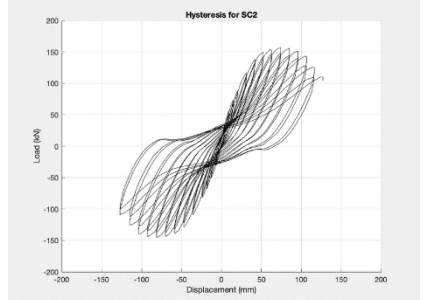

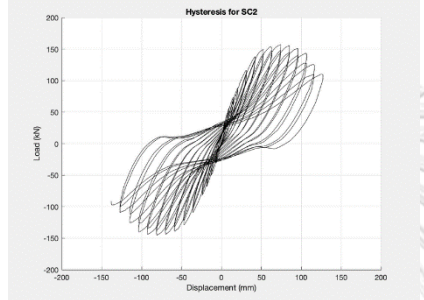

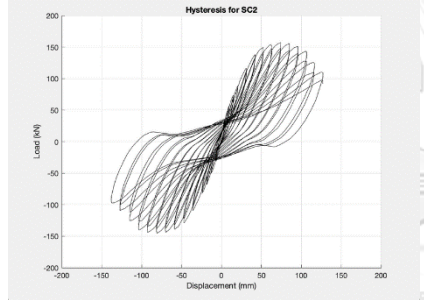

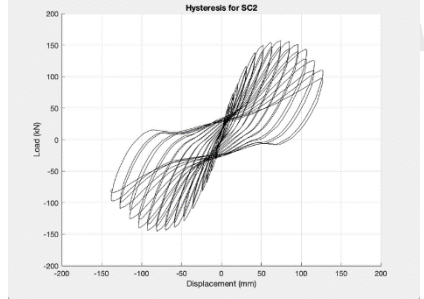
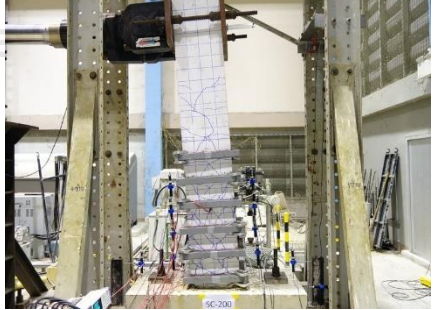
Drift	Cycle	Hysteresis	Damage
3.5%	+1		
	-1		
	+2		
	-2		

Drift	Cycle	Hysteresis	Damage
4%	+1		
	-1		
	+2		
	-2		

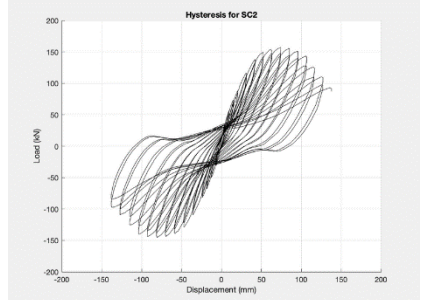

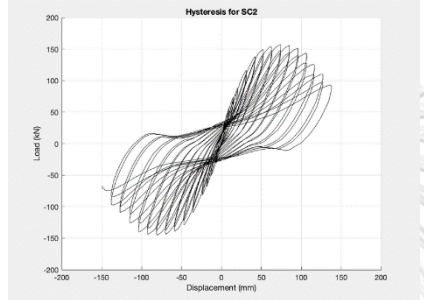

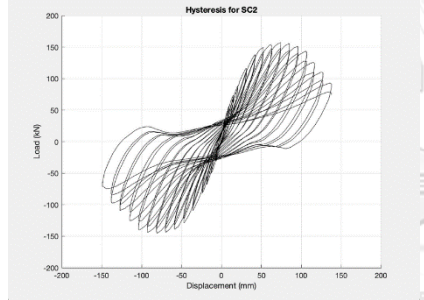

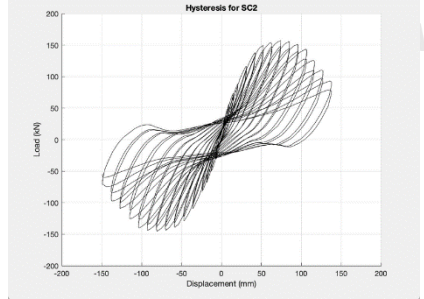
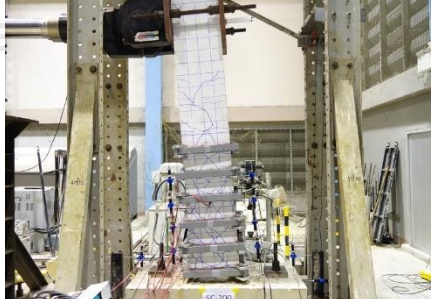
Drift	Cycle	Hysteresis	Damage
4.5%	+1		
	-1		
	+2		
	-2		

Drift	Cycle	Hysteresis	Damage
5%	+1		
	-1		
	+2		
	-2		

Drift	Cycle	Hysteresis	Damage
5.5%	+1		
	-1		
	+2		
	-2		

Drift	Cycle	Hysteresis	Damage
6%	+1		
	-1		
	+2		
	-2		

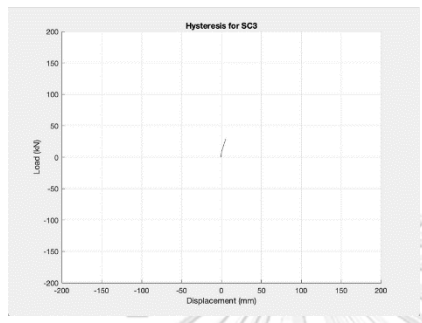

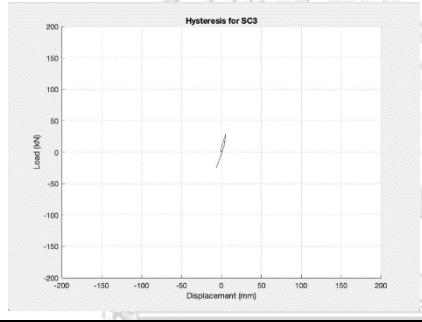

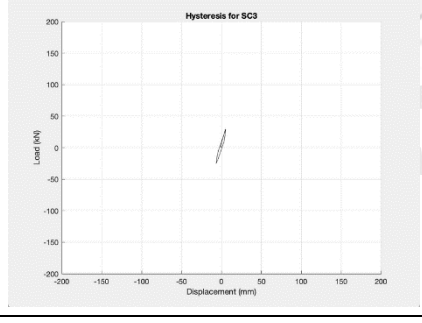
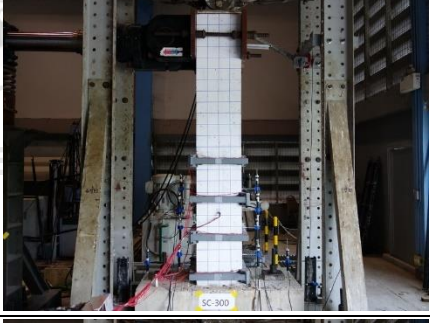
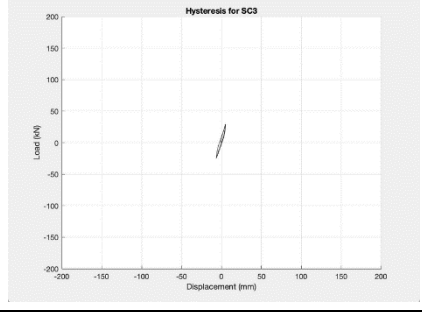
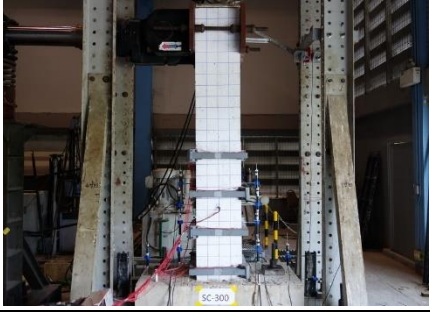


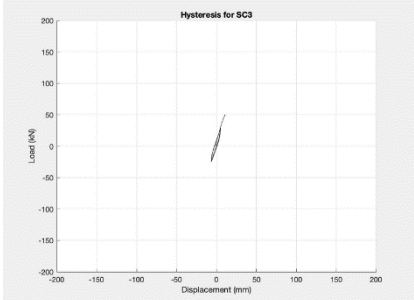
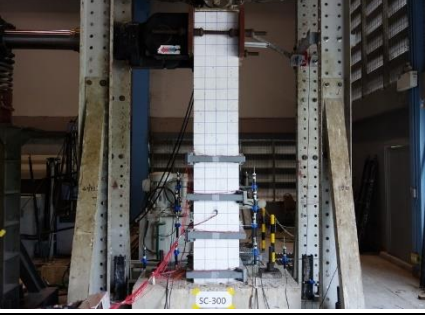
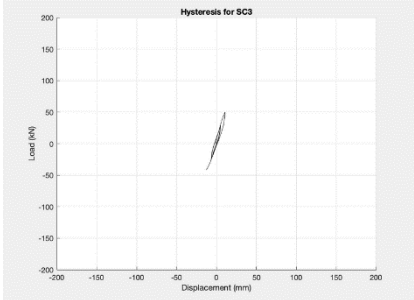
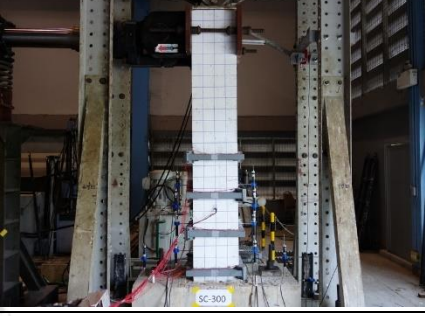
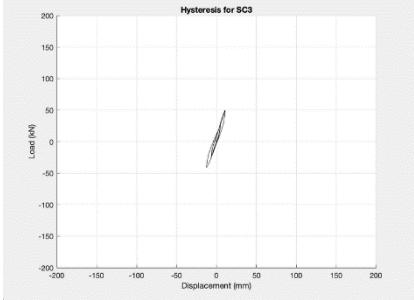
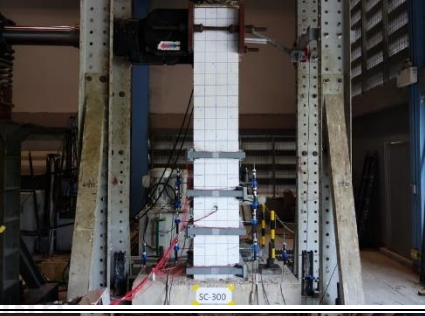
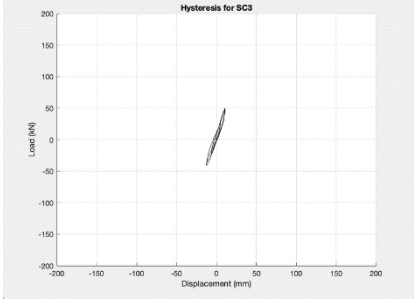
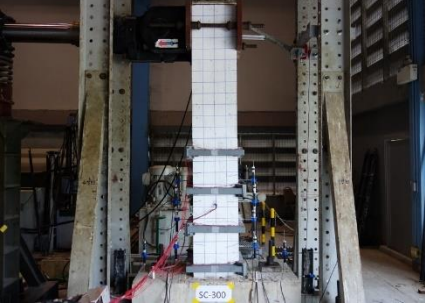
Drift	Cycle	Hysteresis	Damage
6.5%	+1		
	-1		
	+2		
	-2		

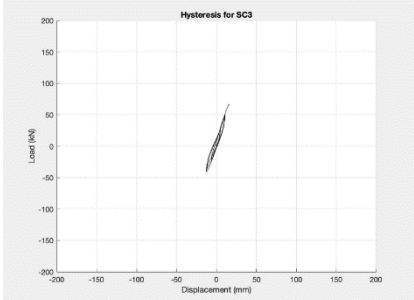
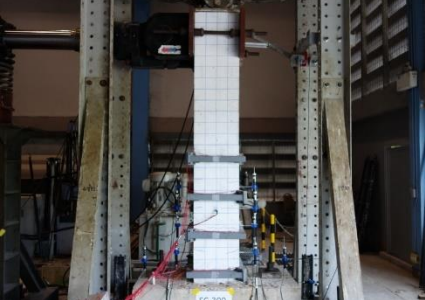
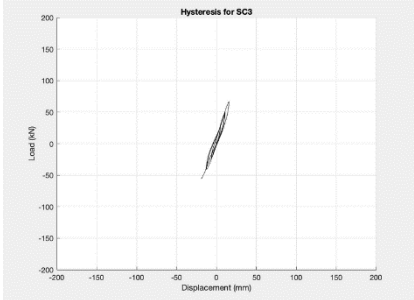
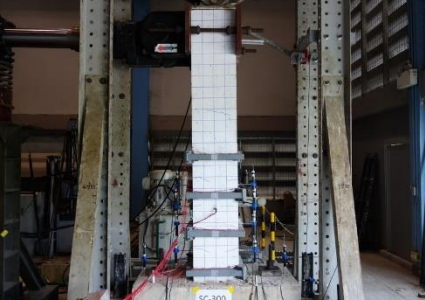
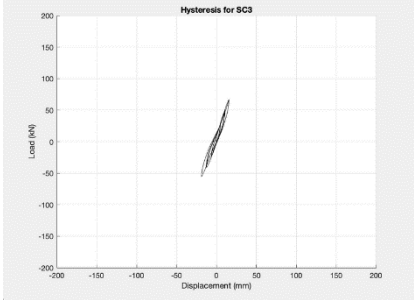
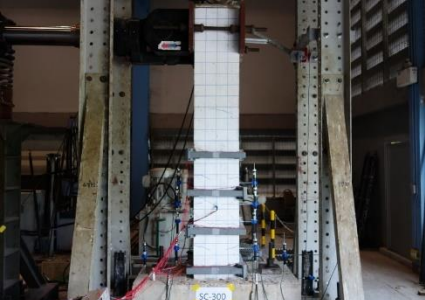
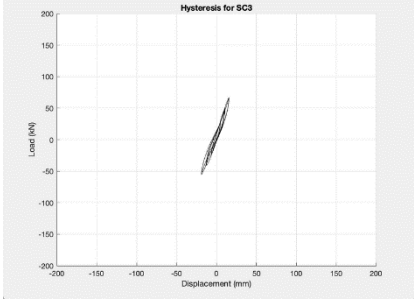
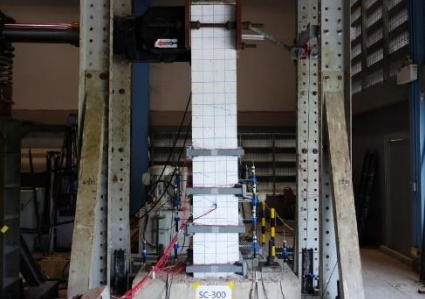
## APPENDIX H

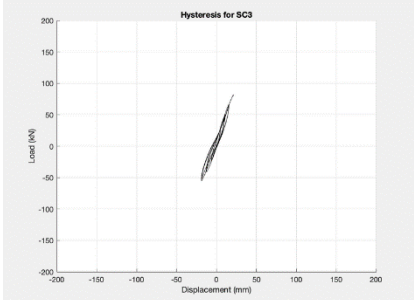
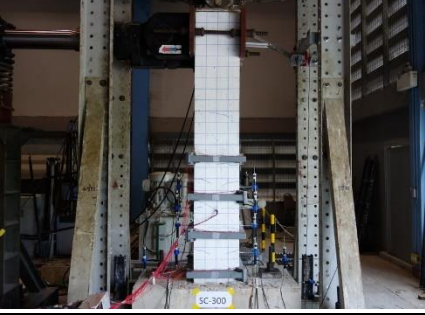
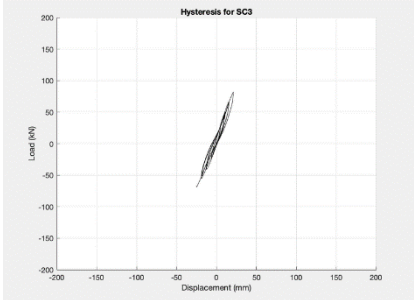
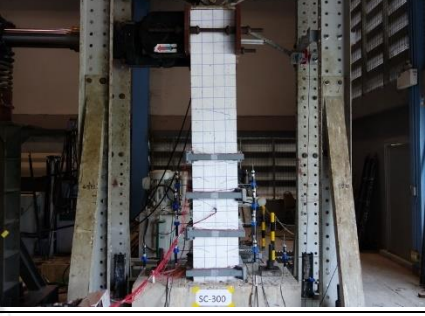
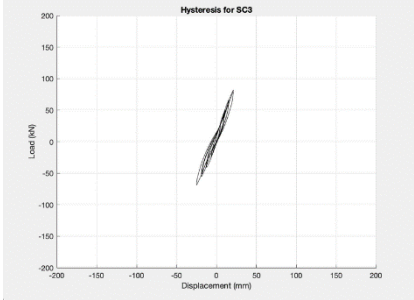
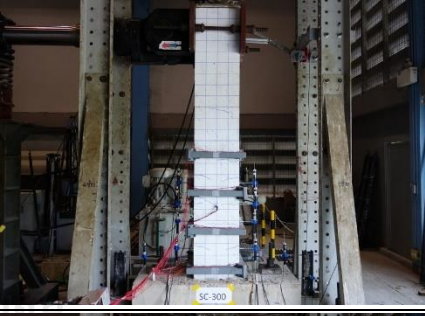
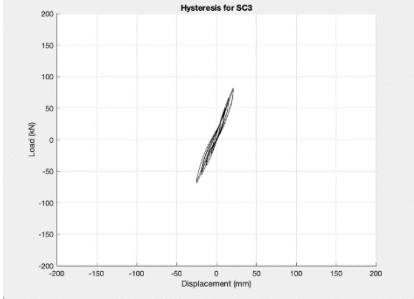
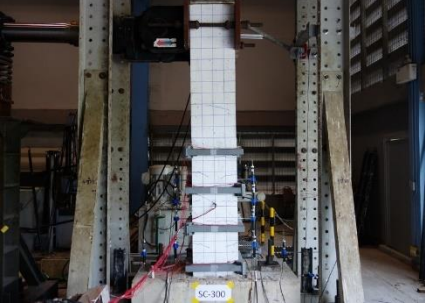
## Cyclic behavior of SC3 column specimen

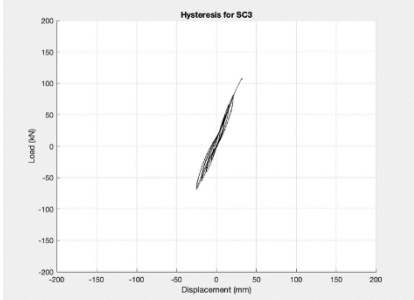

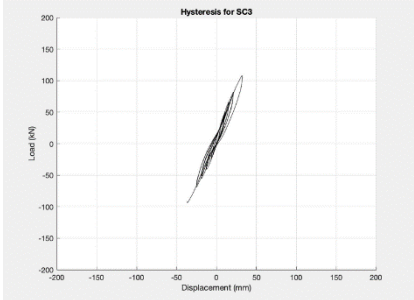
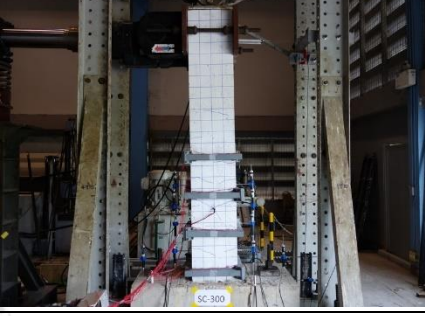
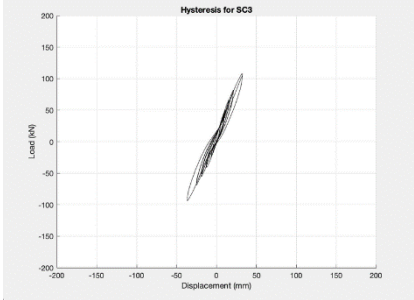
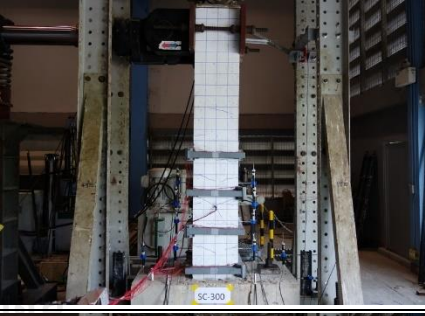
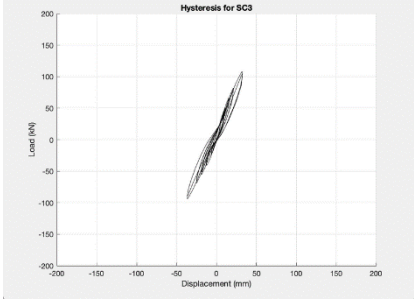
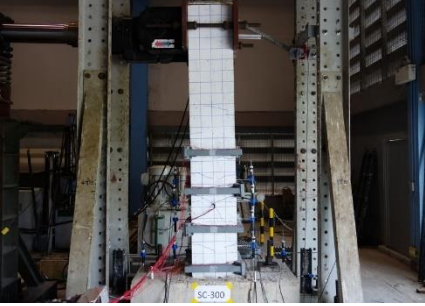
Table 0.1 Cyclic behavior of SC3 column

Drift	Cycle	Hysteresis	Damage
0.25 %	+1		
	-1		
	+2		
	-2		

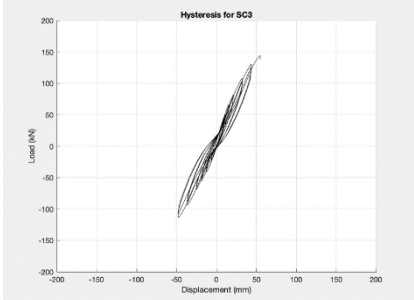

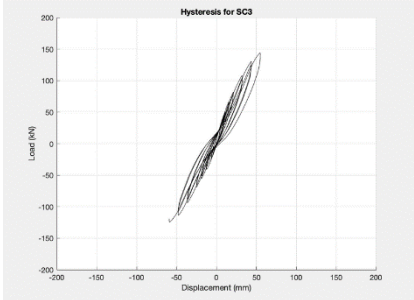

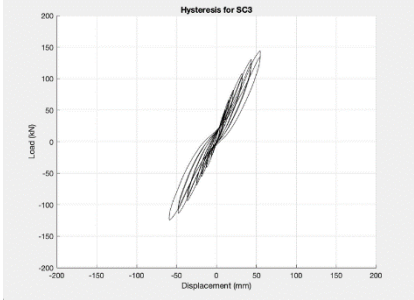
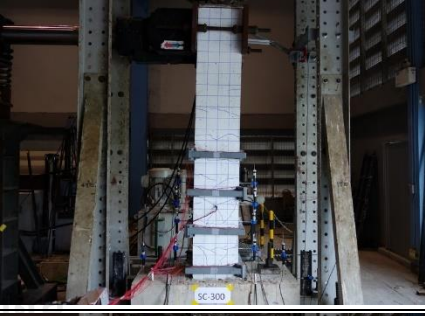
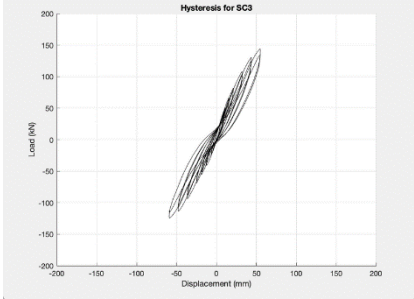
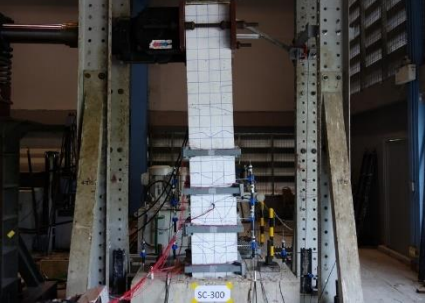
Drift	Cycle	Hysteresis	Damage
0.5%	+1		
	-1		
	+2		
	-2		

Drift	Cycle	Hysteresis	Damage
0.75 %	+1		
	-1		
	+2		
	-2		

Drift	Cycle	Hysteresis	Damage
1%	+1		
	-1		
	+2		
	-2		

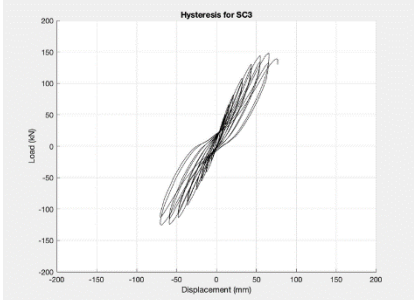

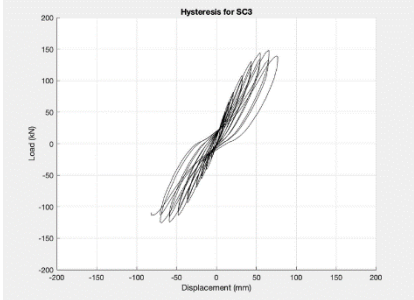

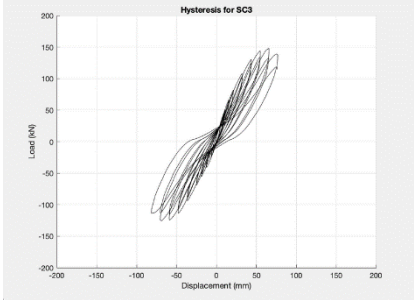
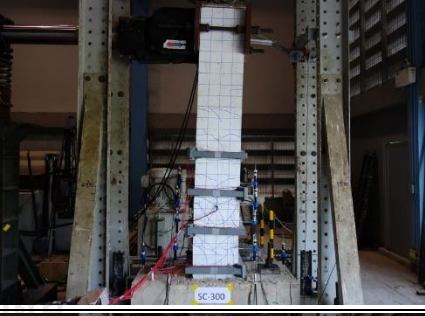
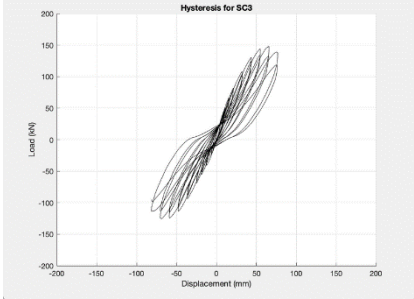
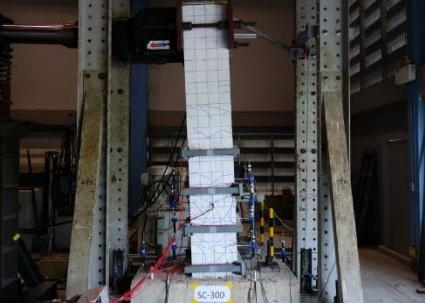
Drift	Cycle	Hysteresis	Damage
1.5%	+1		
	-1		
	+2		
	-2		

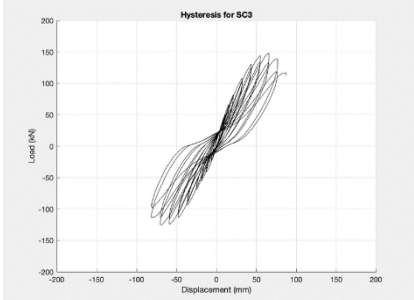

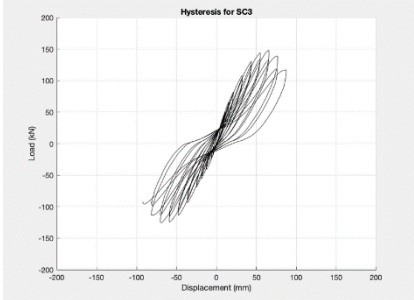

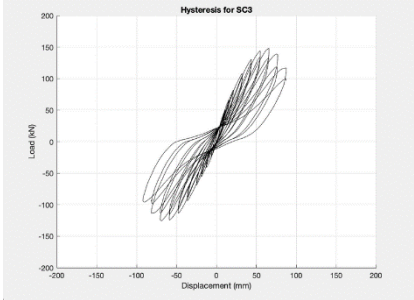

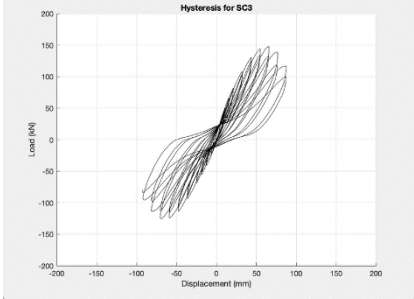
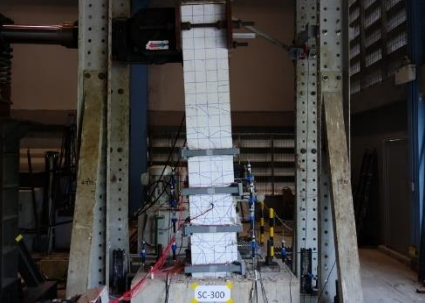
Drift	Cycle	Hysteresis	Damage
2%	+1		
	-1		
	+2		
	-2		

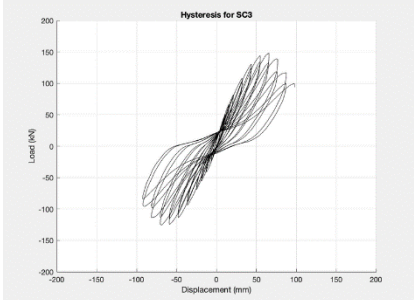

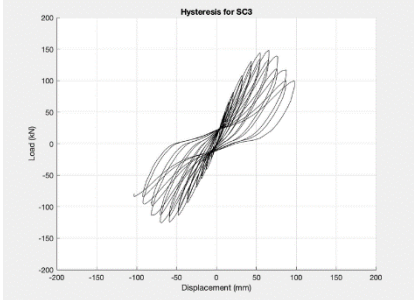

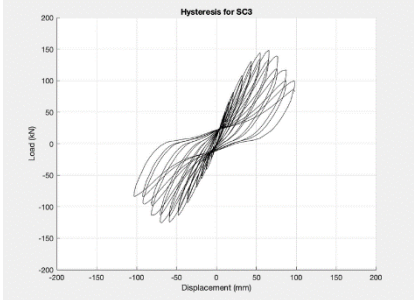

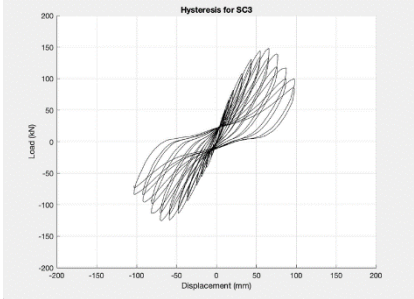
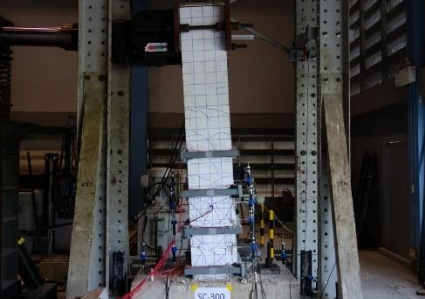
Drift	Cycle	Hysteresis	Damage
2.5%	+1		
	-1		
	+2		
	-2		

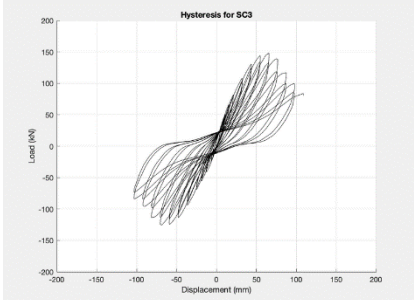
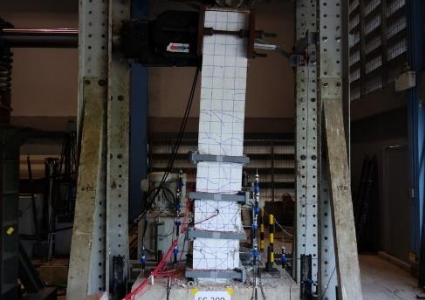
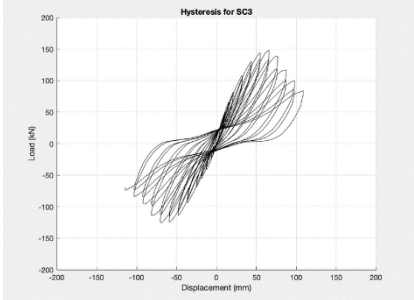

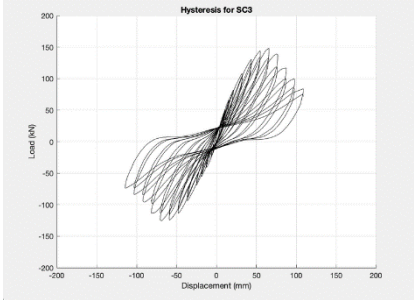

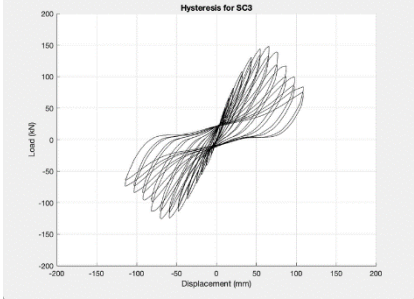



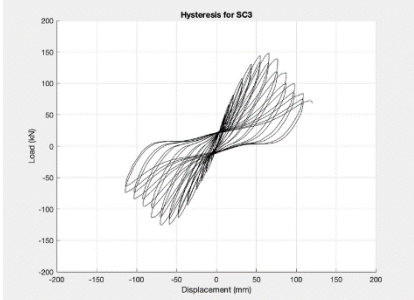
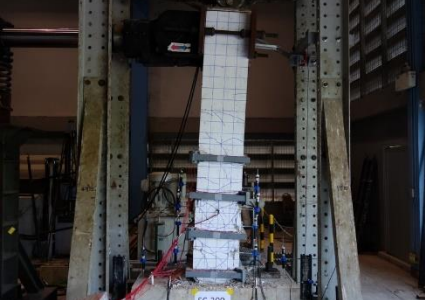
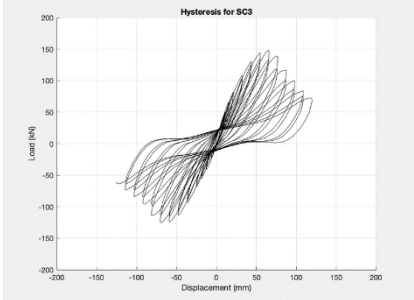

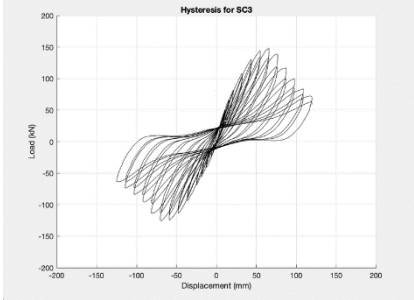

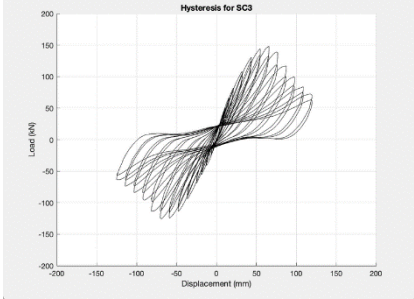

Drift	Cycle	Hysteresis	Damage
3%	+1		
	-1		
	+2		
	-2		

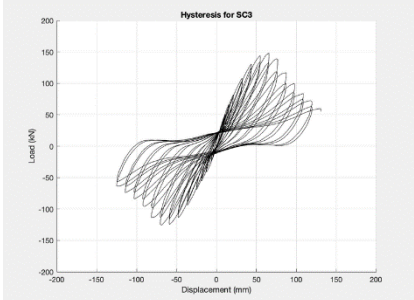
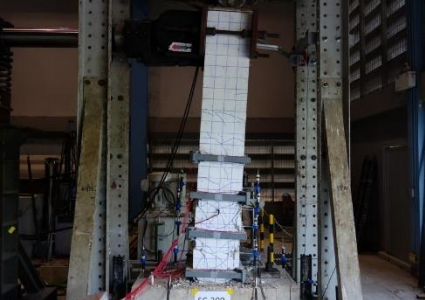
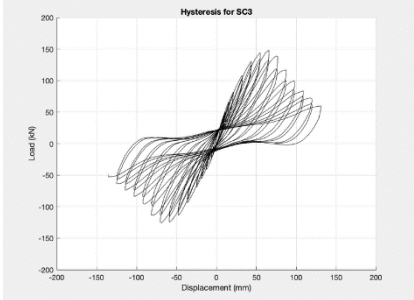

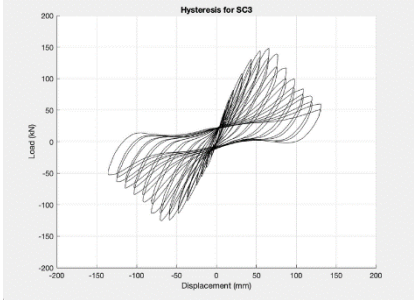

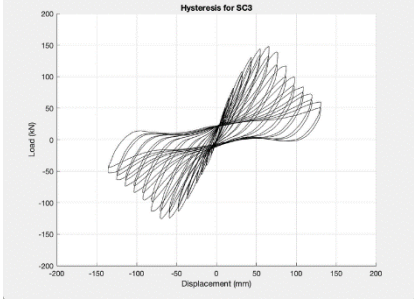

Drift	Cycle	Hysteresis	Damage
3.5%	+1		
	-1		
	+2		
	-2		

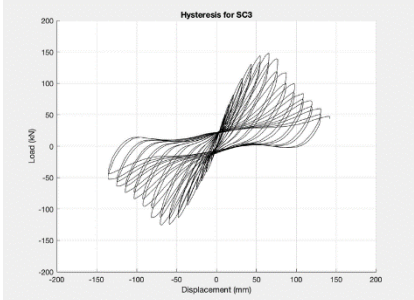
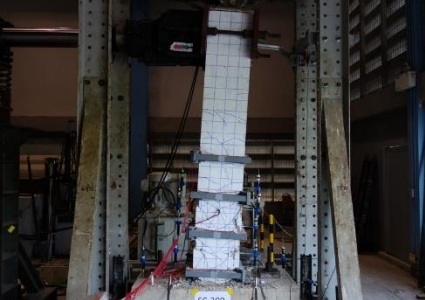
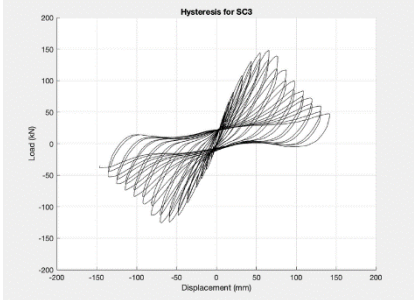

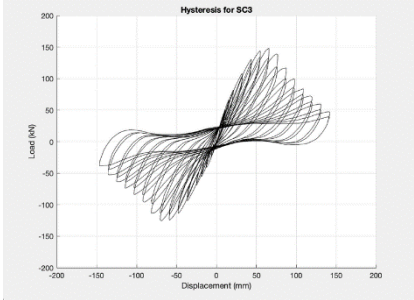

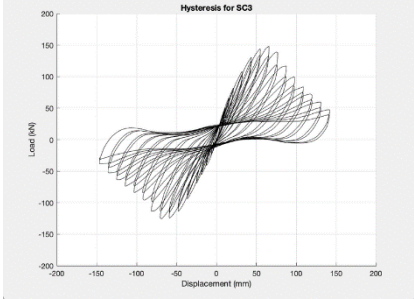

Drift	Cycle	Hysteresis	Damage
4%	+1		
	-1		
	+2		
	-2		

Drift	Cycle	Hysteresis	Damage
4.5%	+1		
	-1		
	+2		
	-2		

Drift	Cycle	Hysteresis	Damage
5%	+1		
	-1		
	+2		
	-2		

Drift	Cycle	Hysteresis	Damage
5.5%	+1		
	-1		
	+2		
	-2		

Drift	Cycle	Hysteresis	Damage
6%	+1		
	-1		
	+2		
	-2		

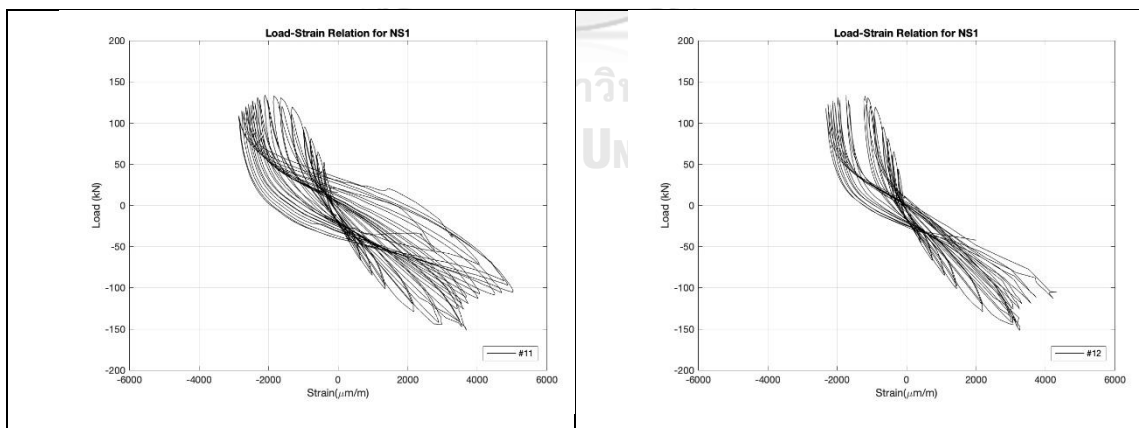
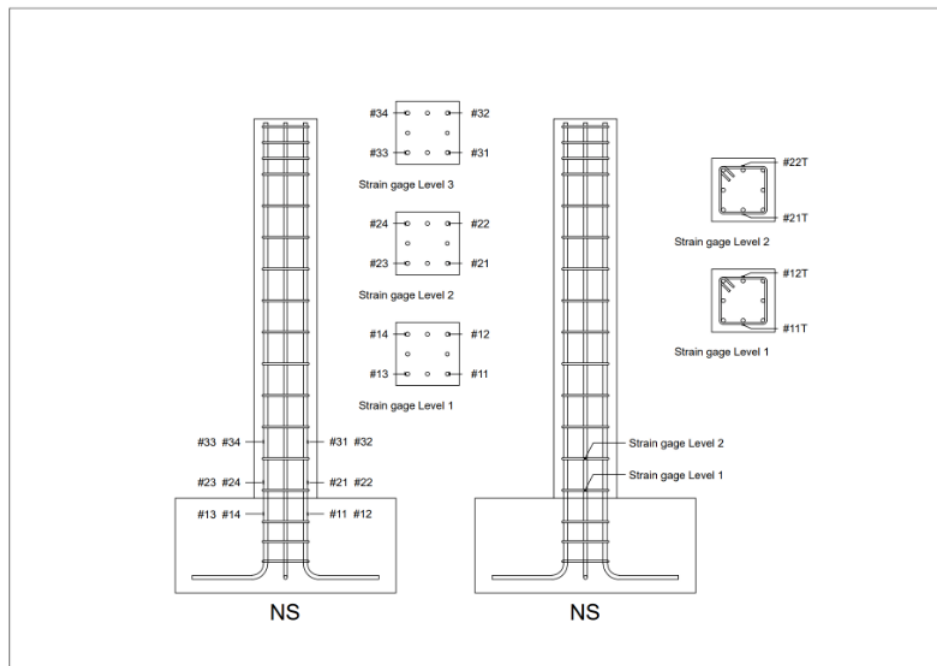
Drift	Cycle	Hysteresis	Damage
6.5%	+1		
	-1		
	+2		
	-2		

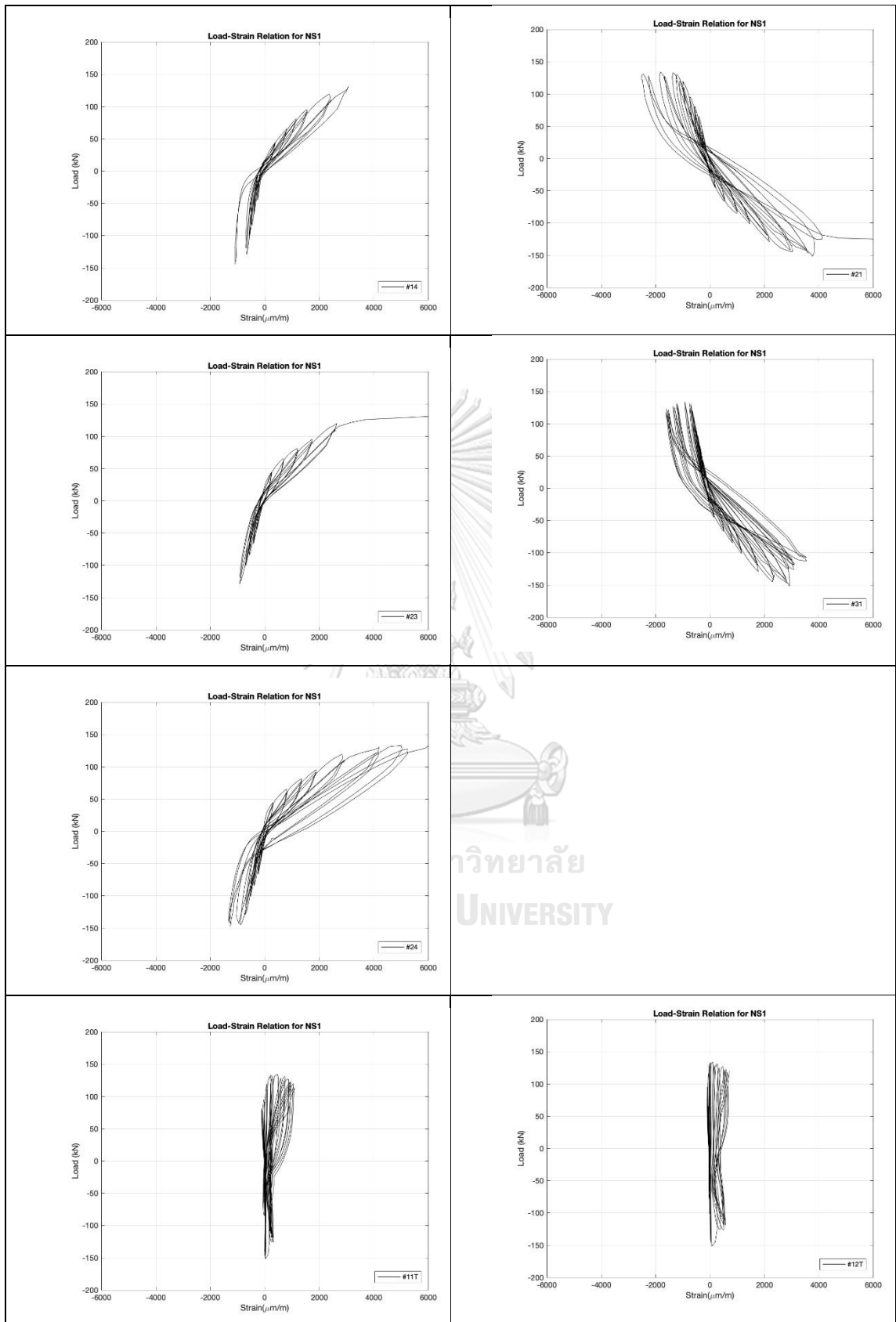


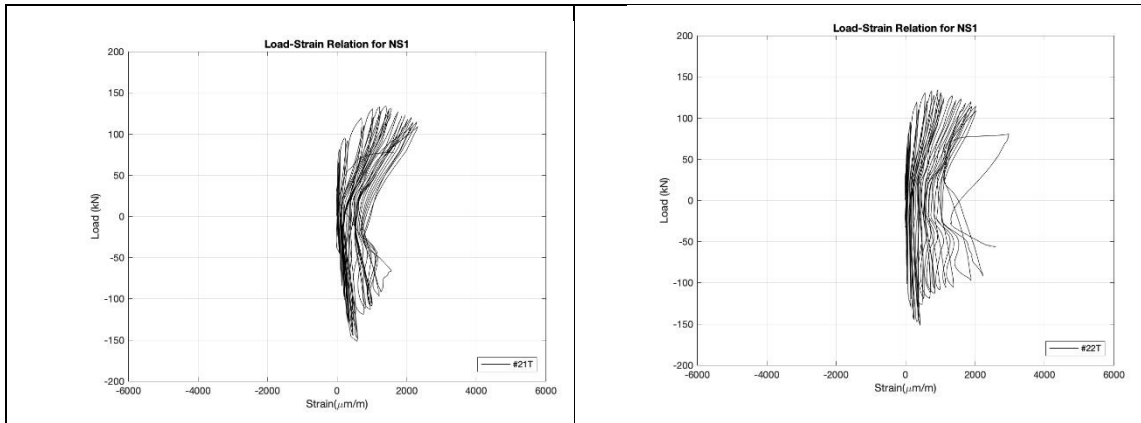
## APPENDIX C

### Strain in steel reinforcement

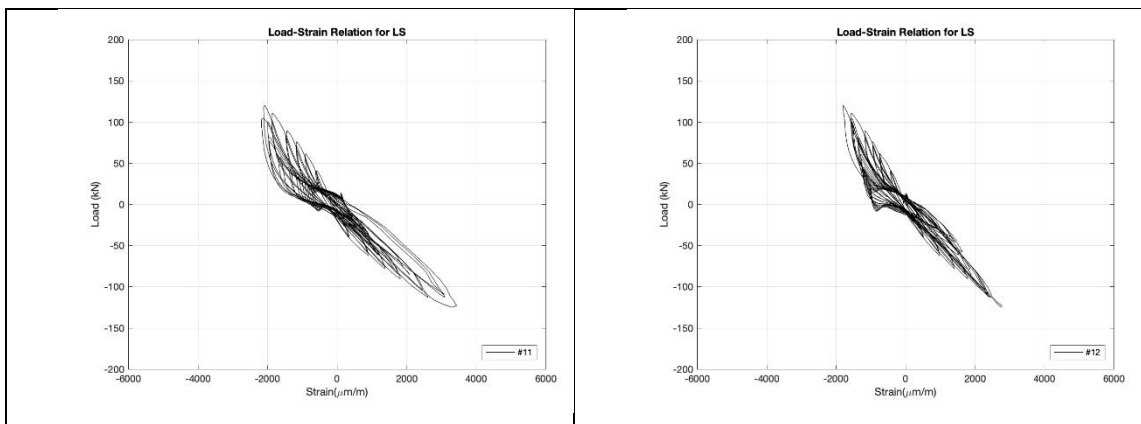
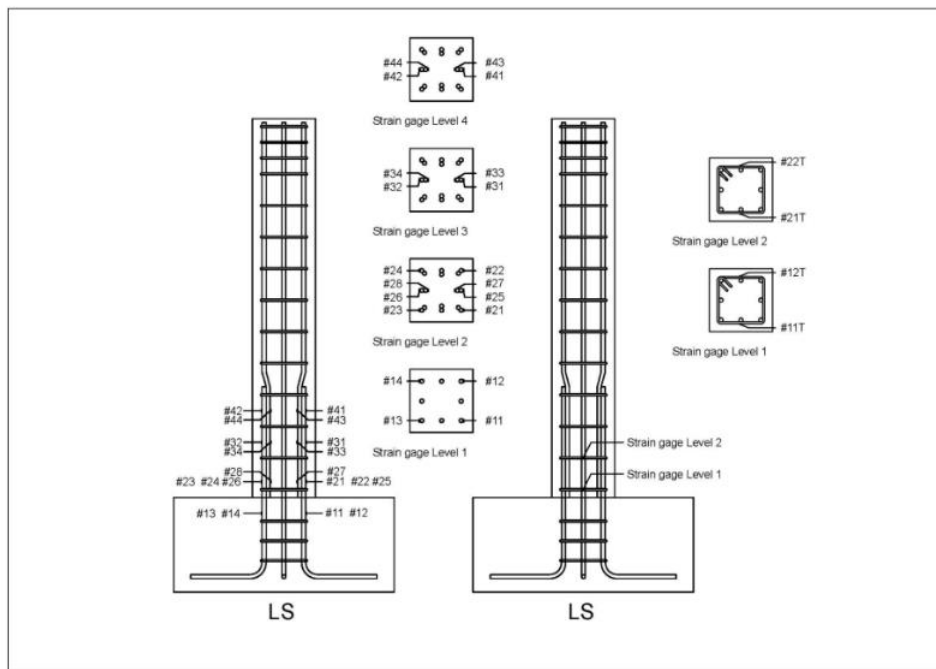
- Strain detailing on reinforcement of NS column

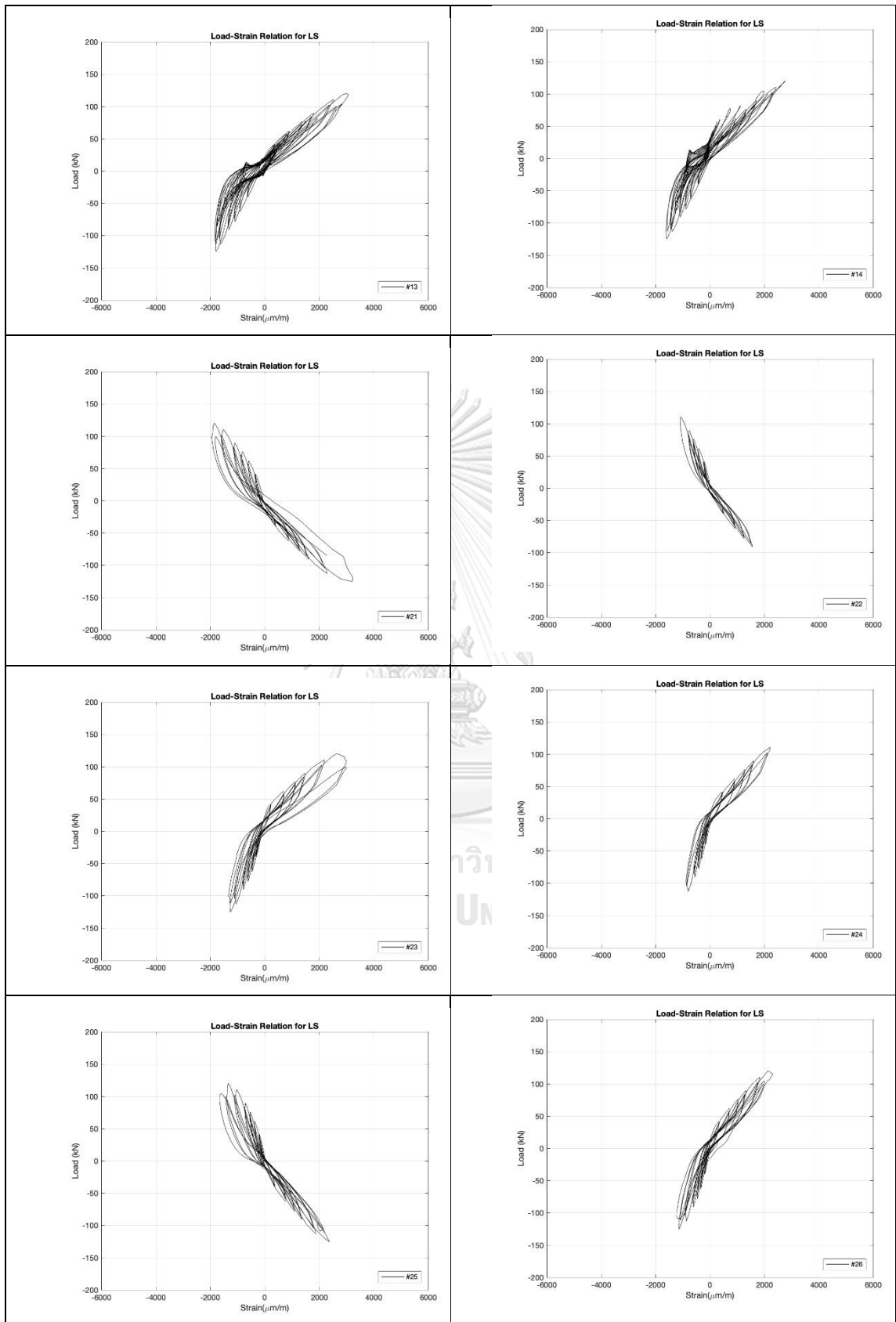


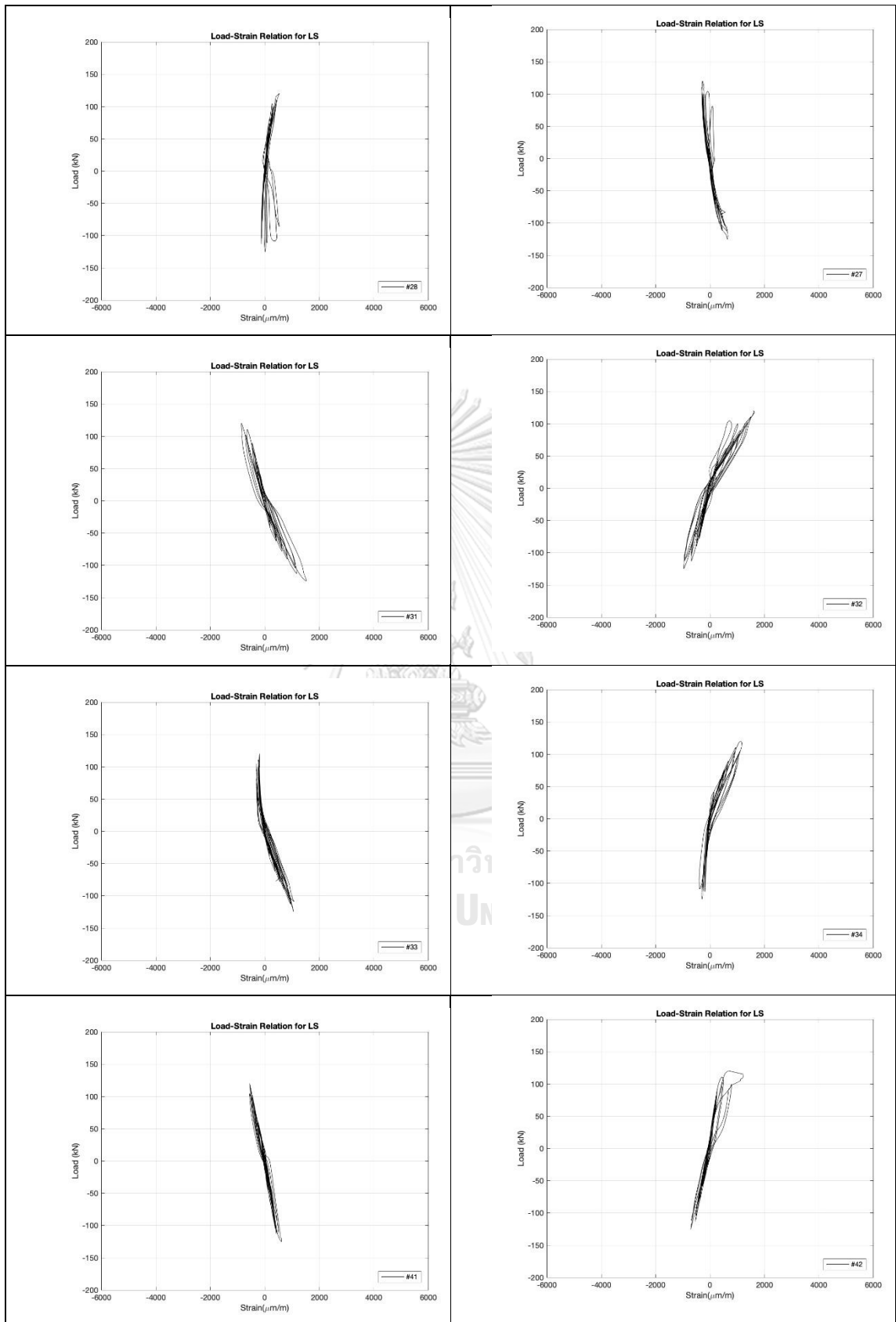


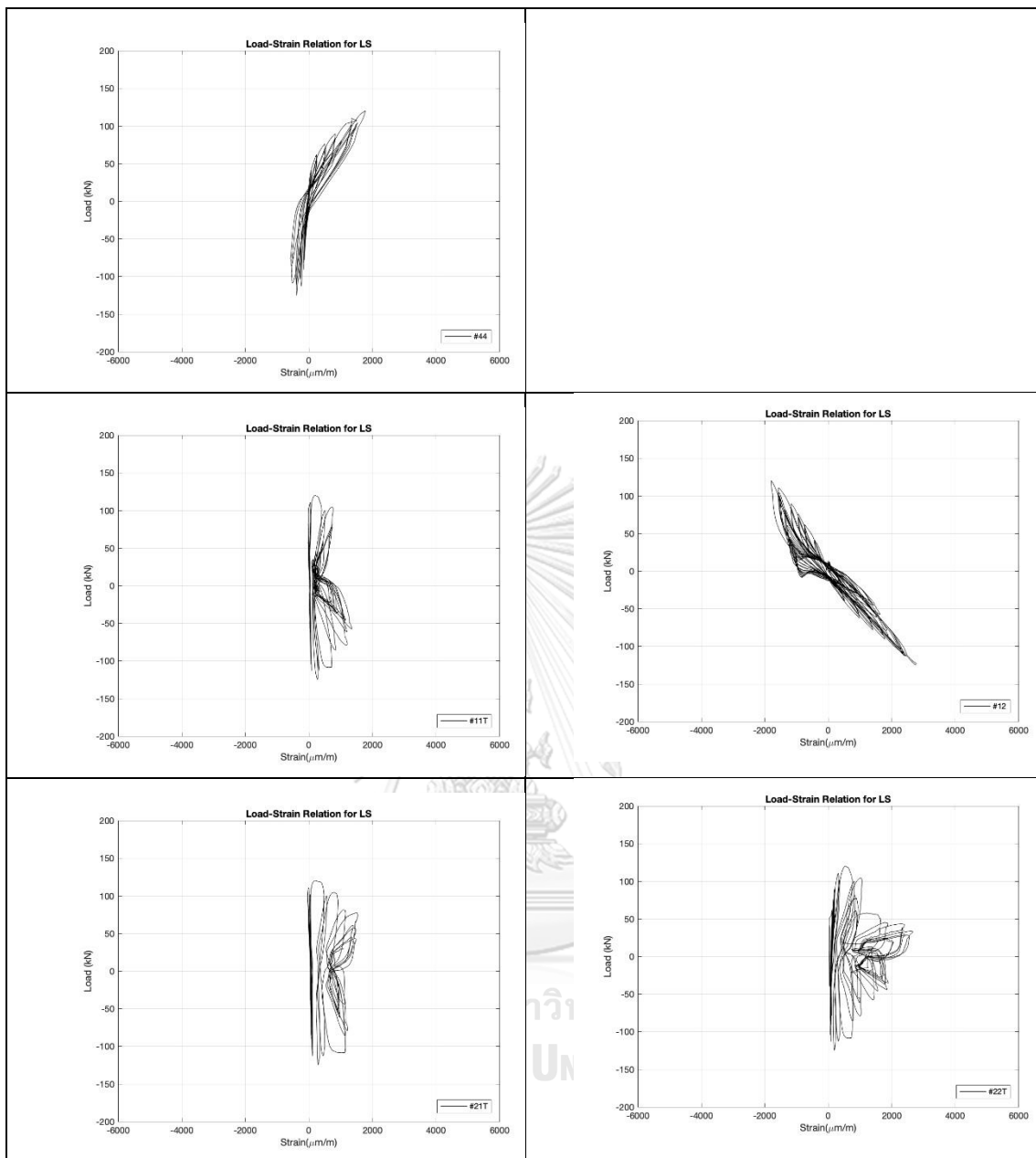


- Strain detailing on reinforcement of LS column

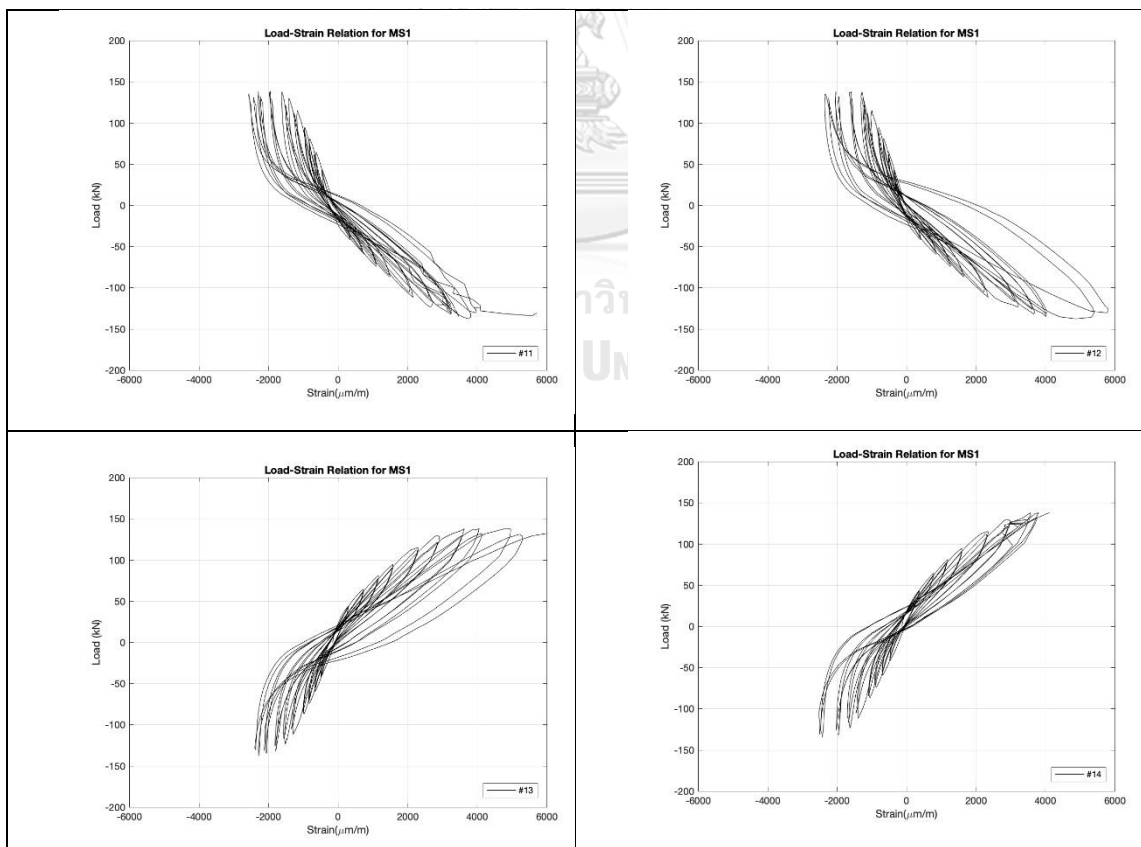
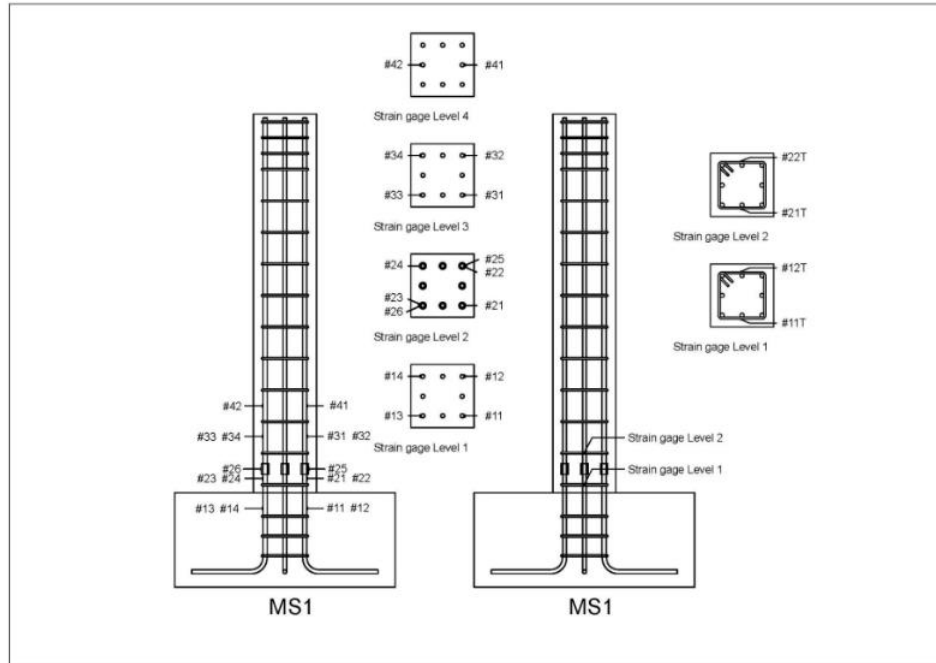


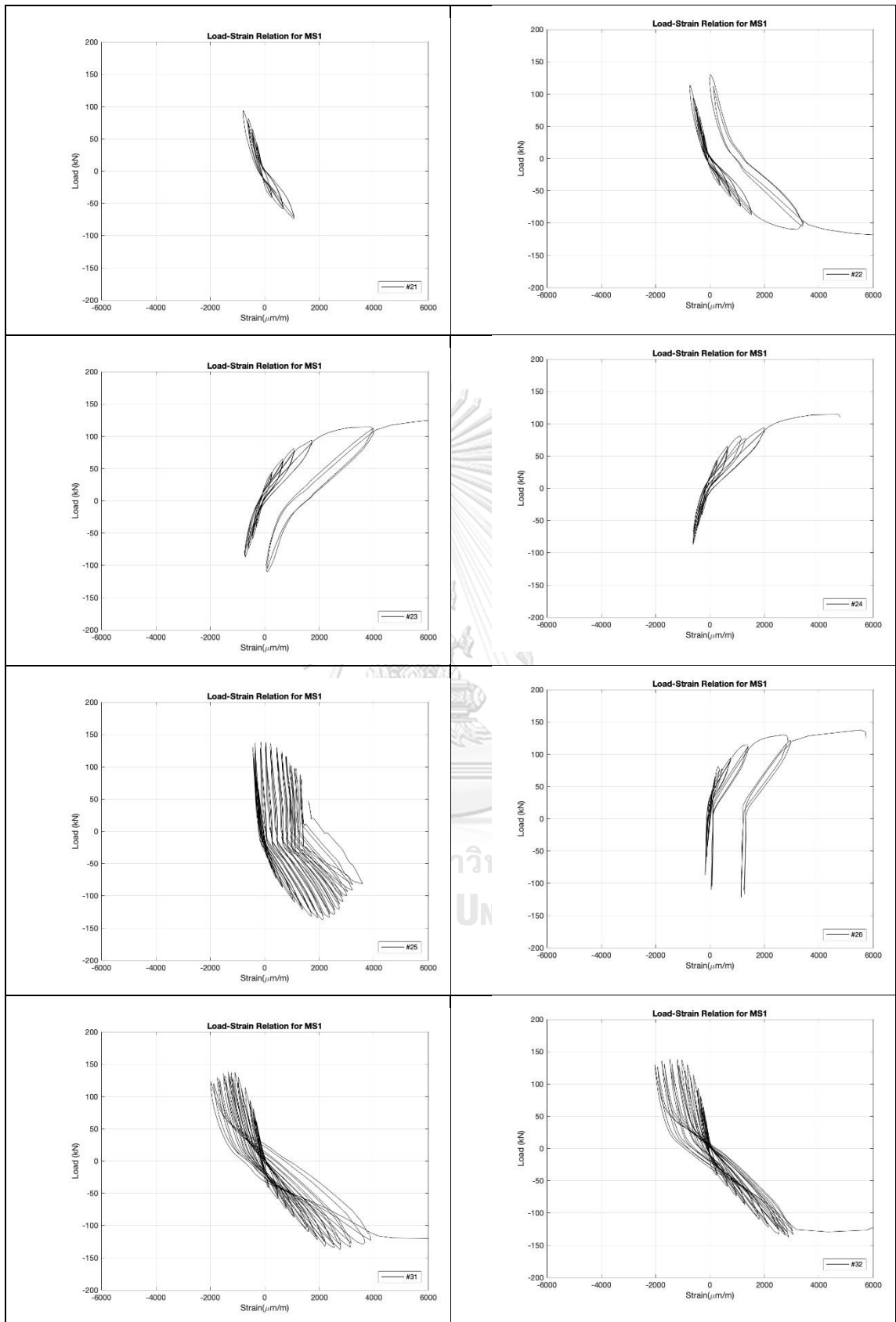




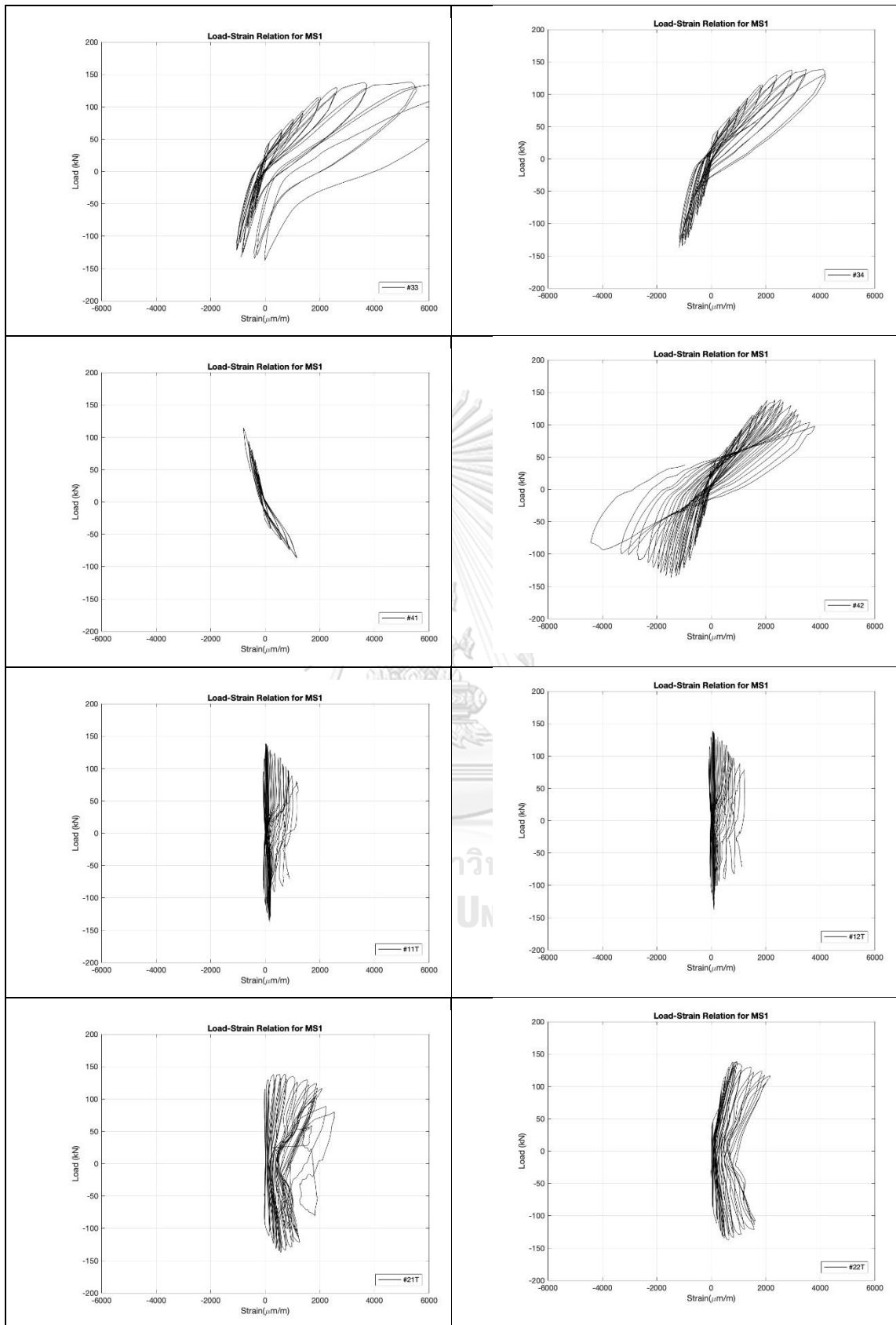


- Strain detailing on reinforcement of MS1 column

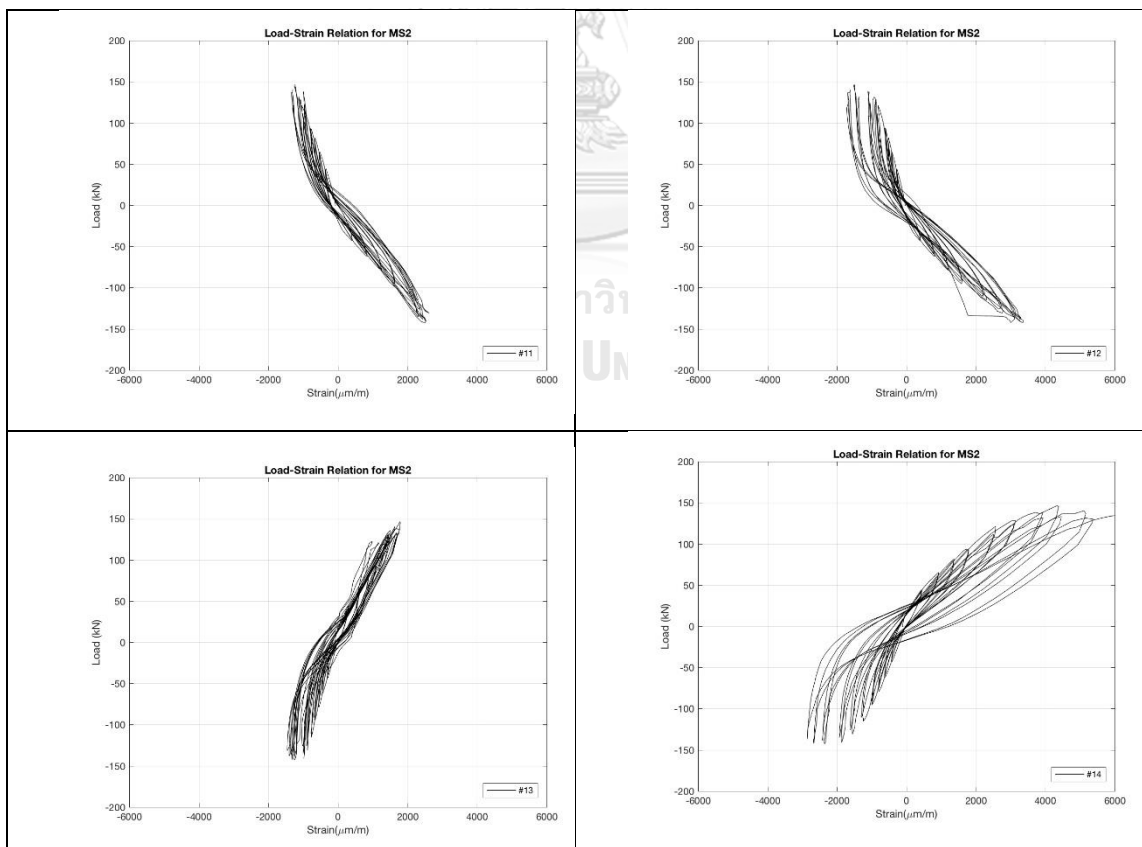
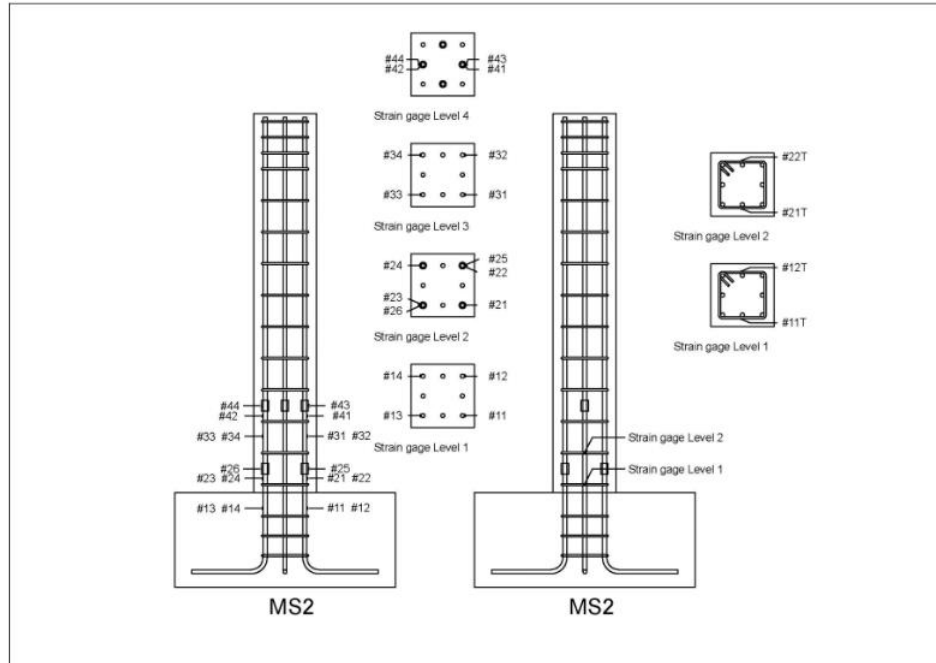


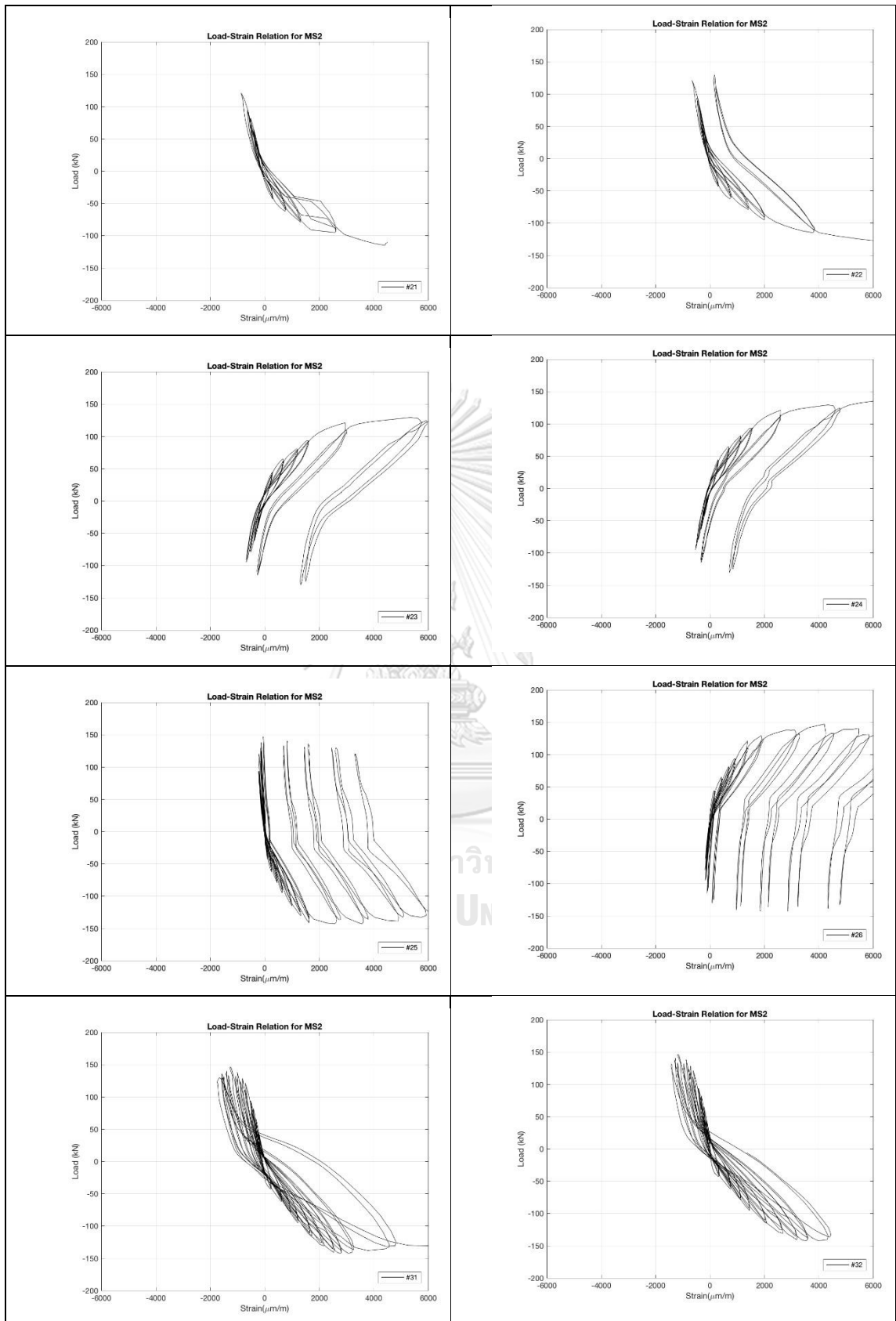


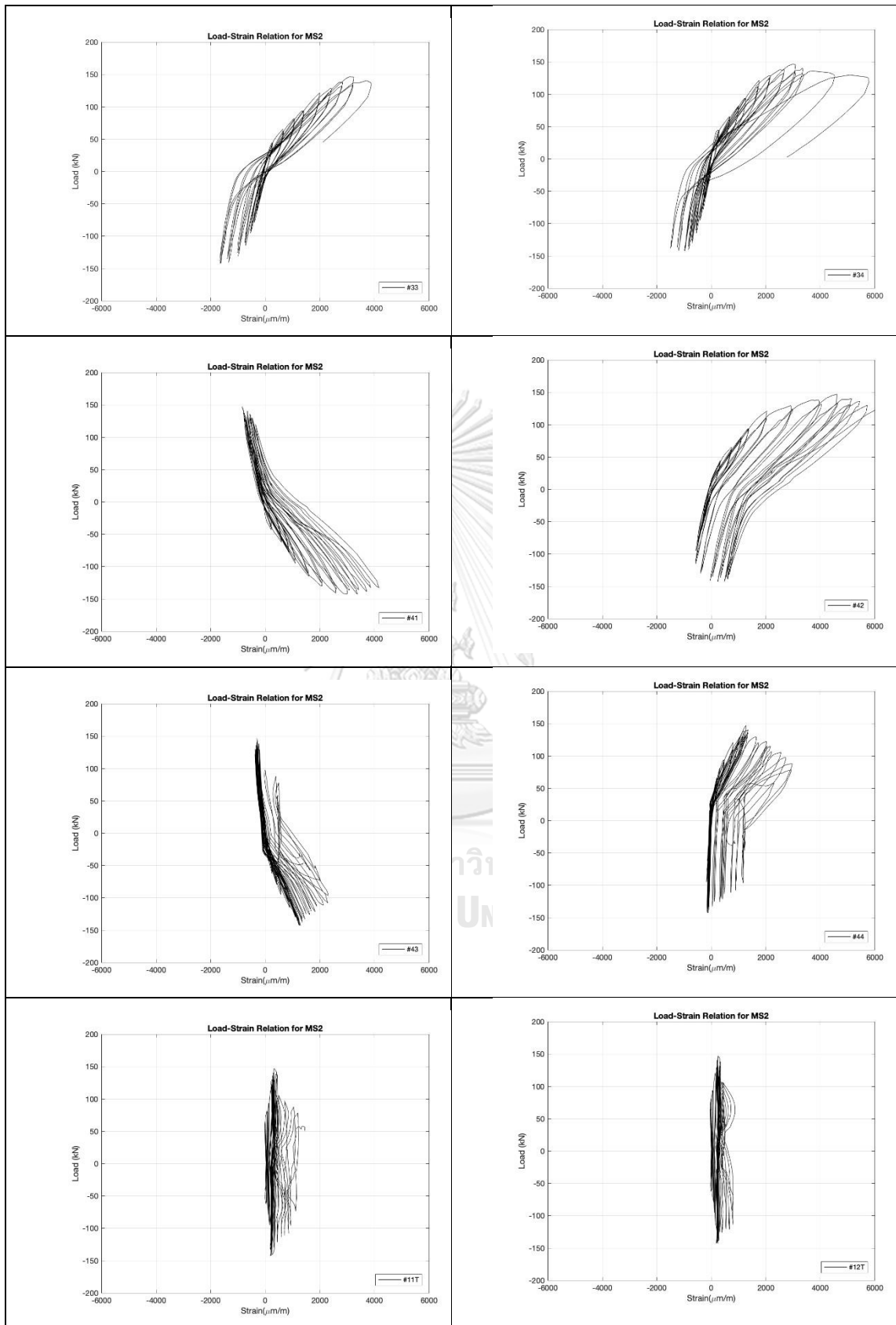


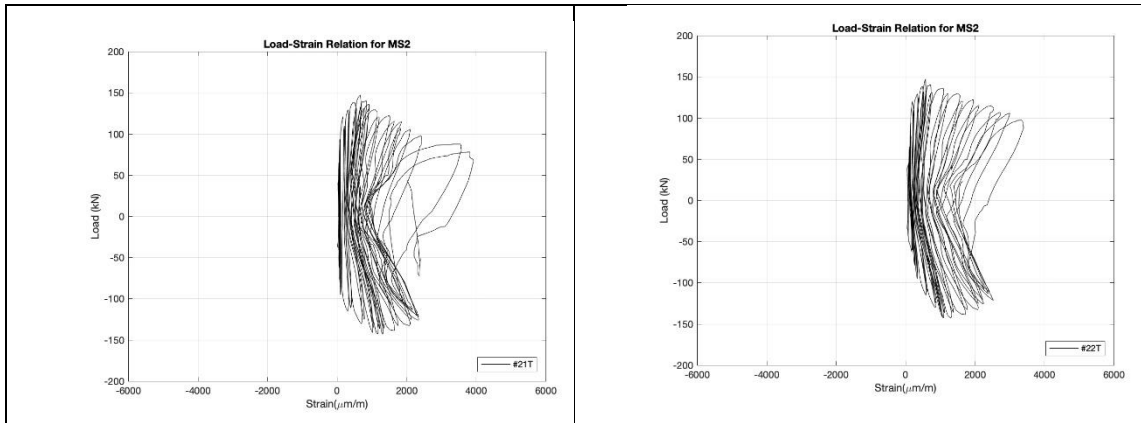


- Strain detailing on reinforcement of MS2 column

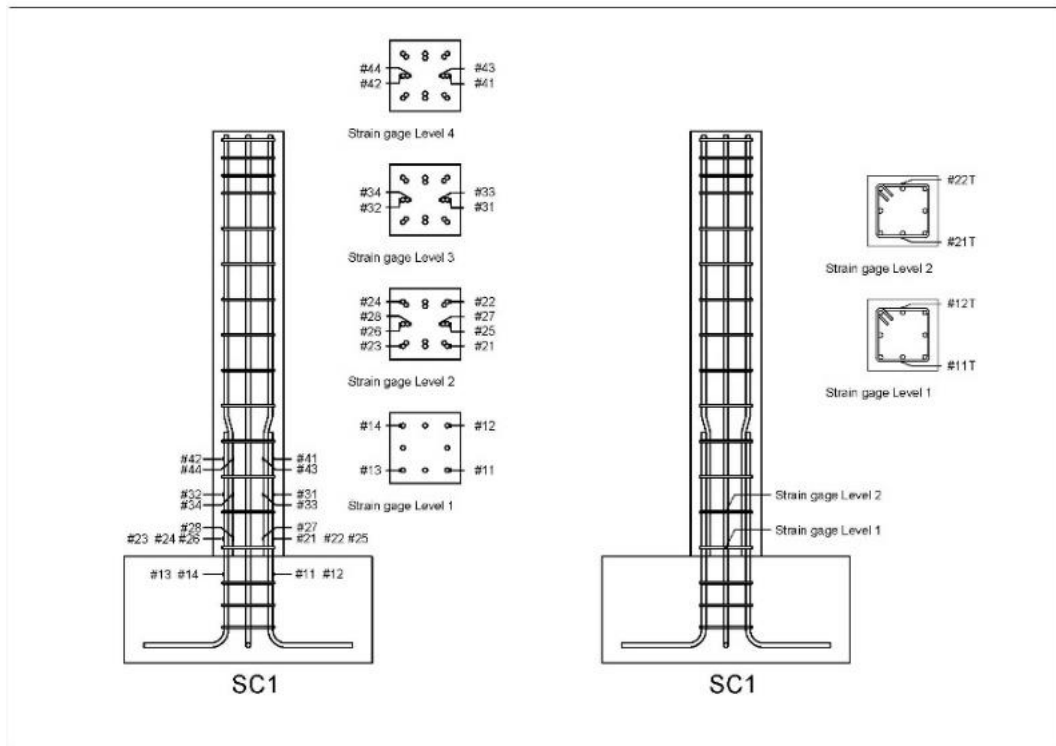


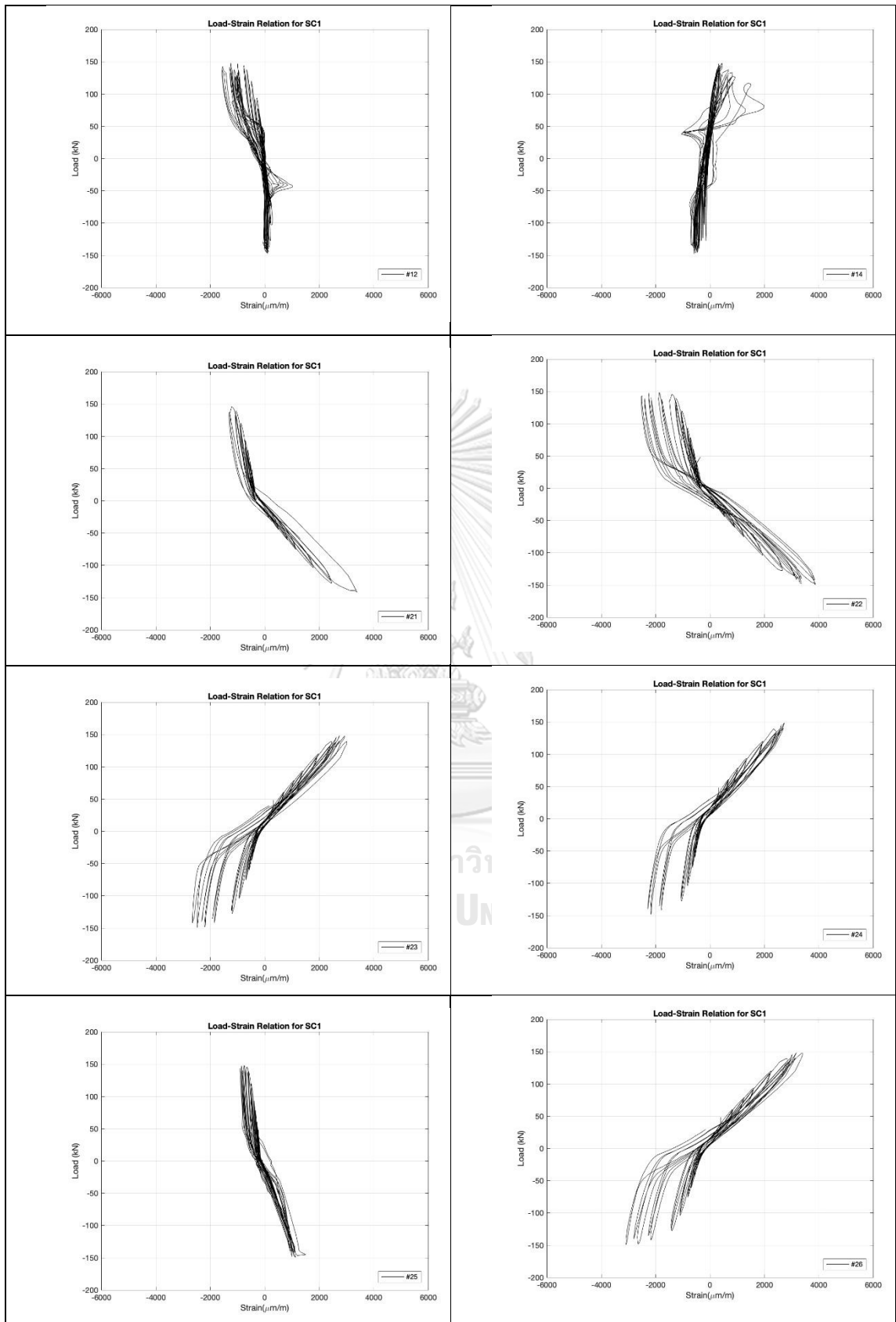


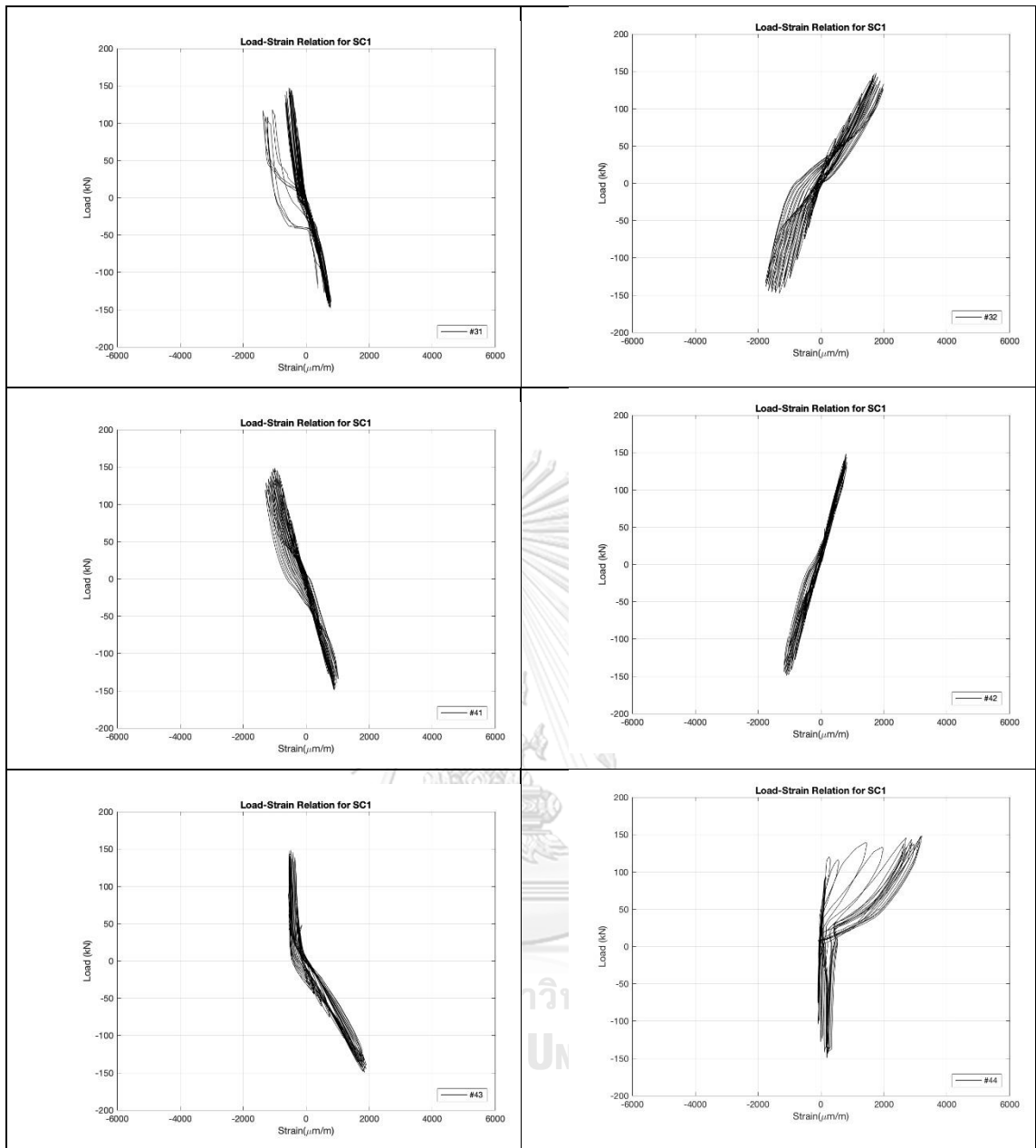


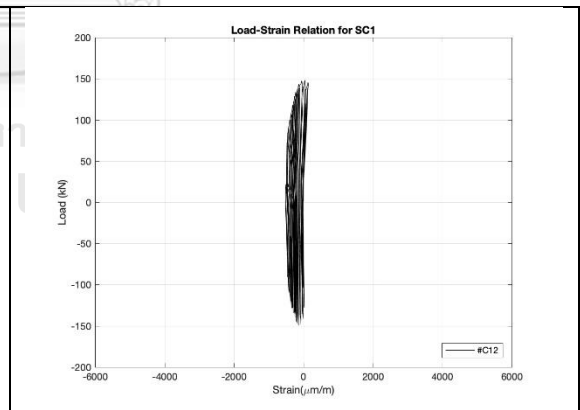
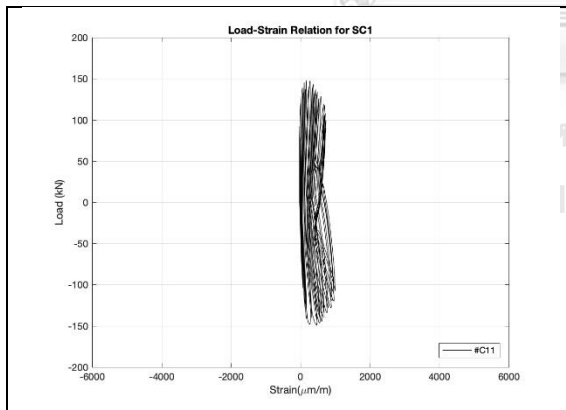
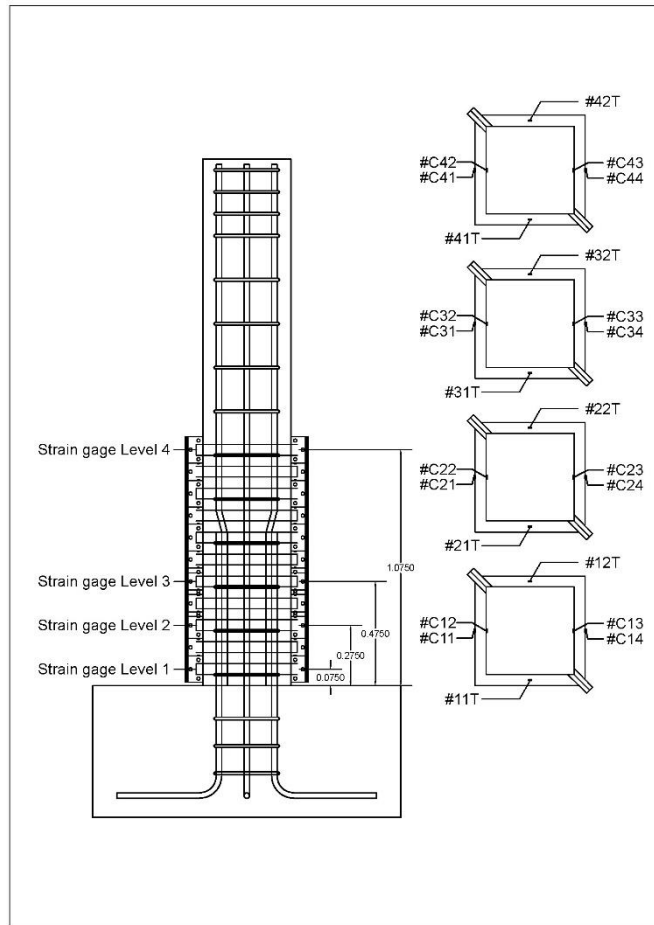


- Strain detailing on reinforcement of SC1 column

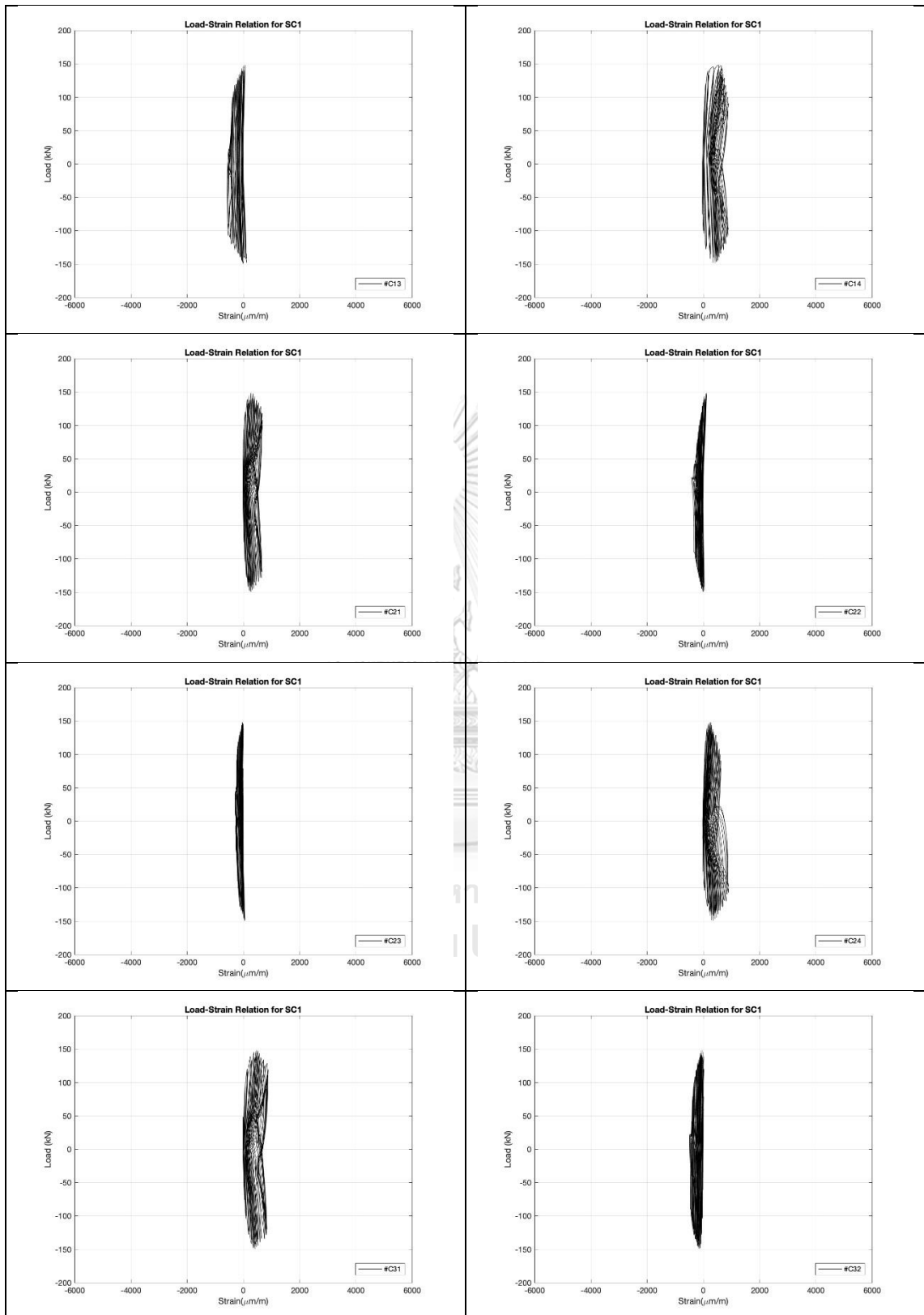


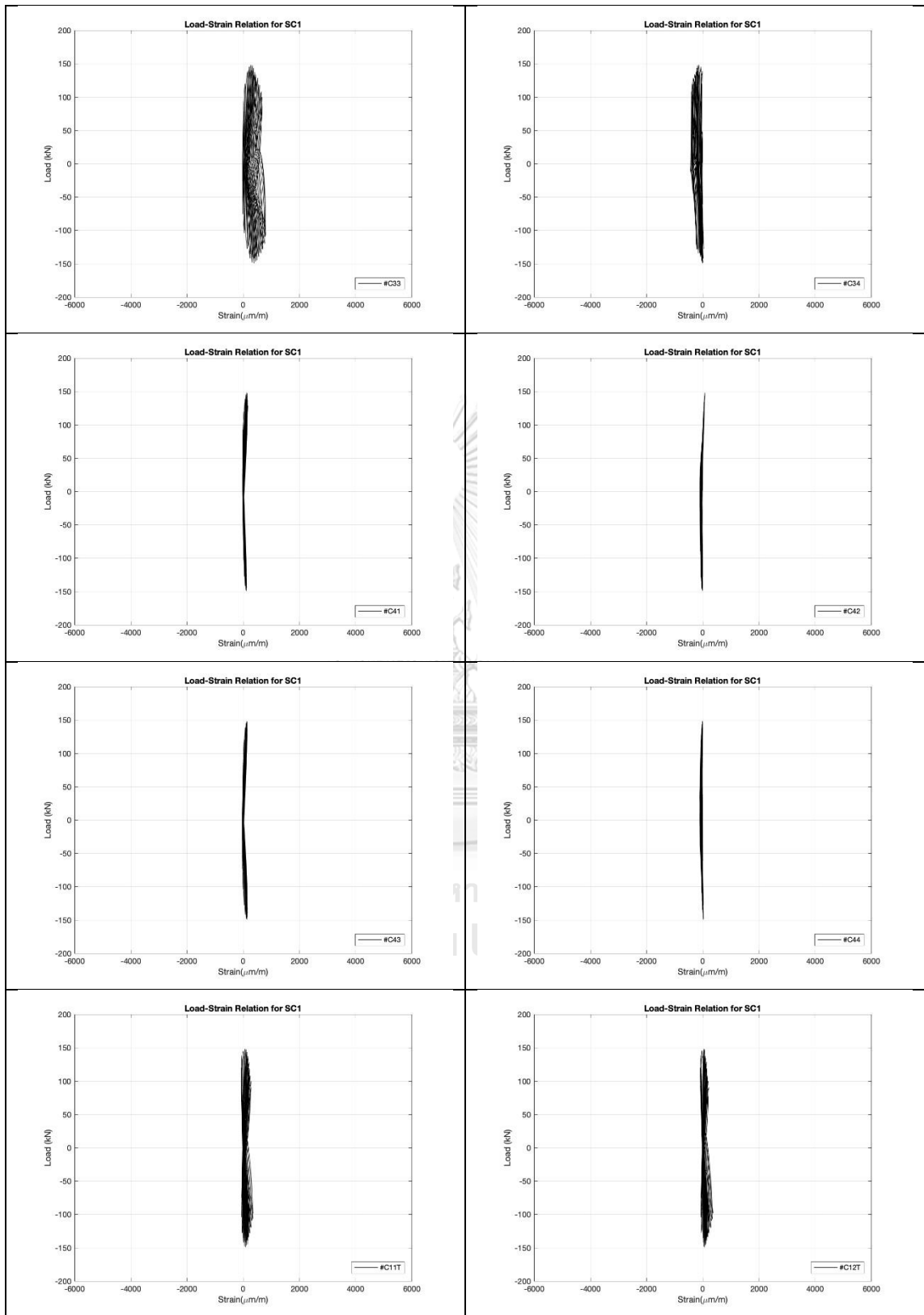


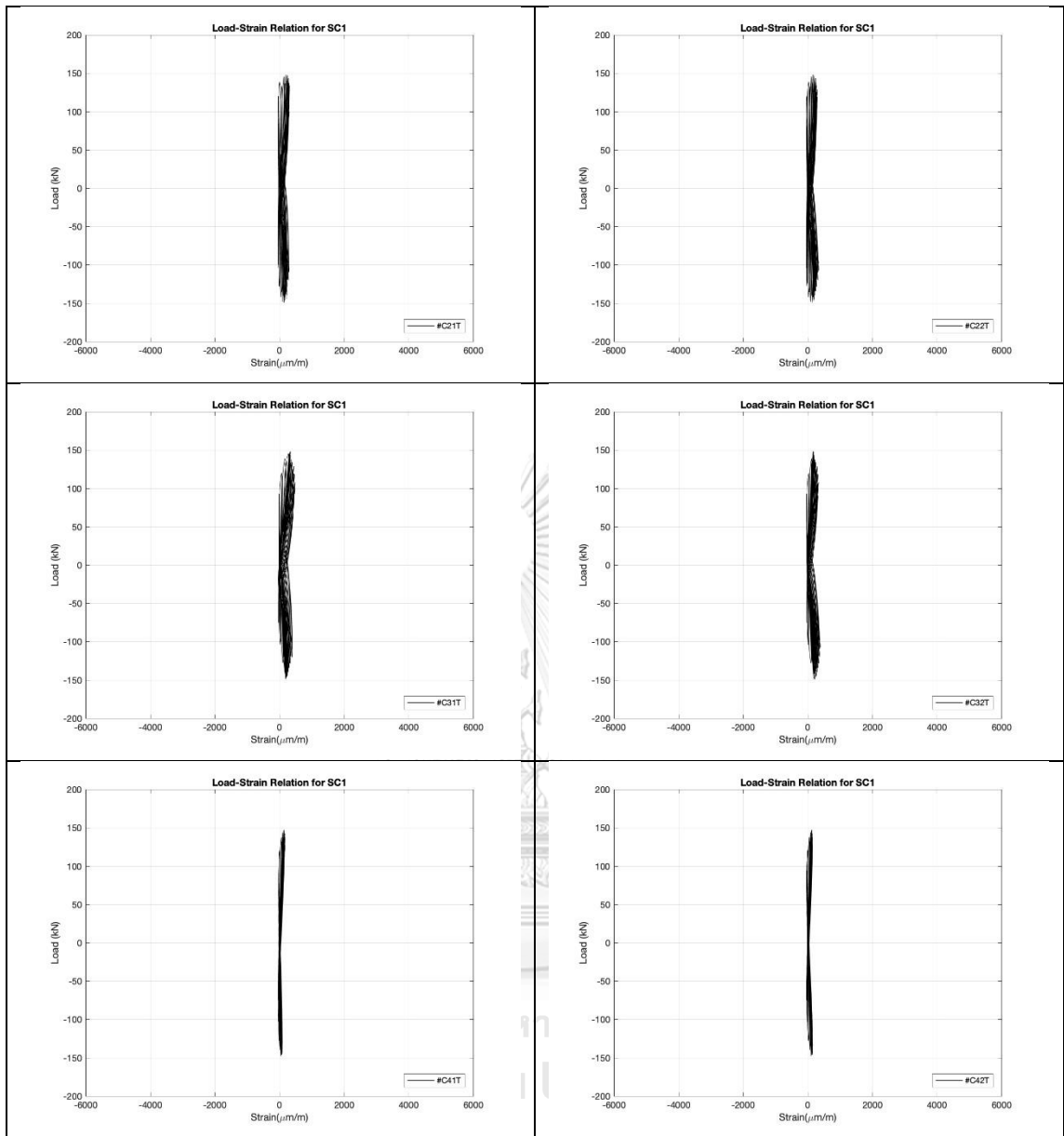




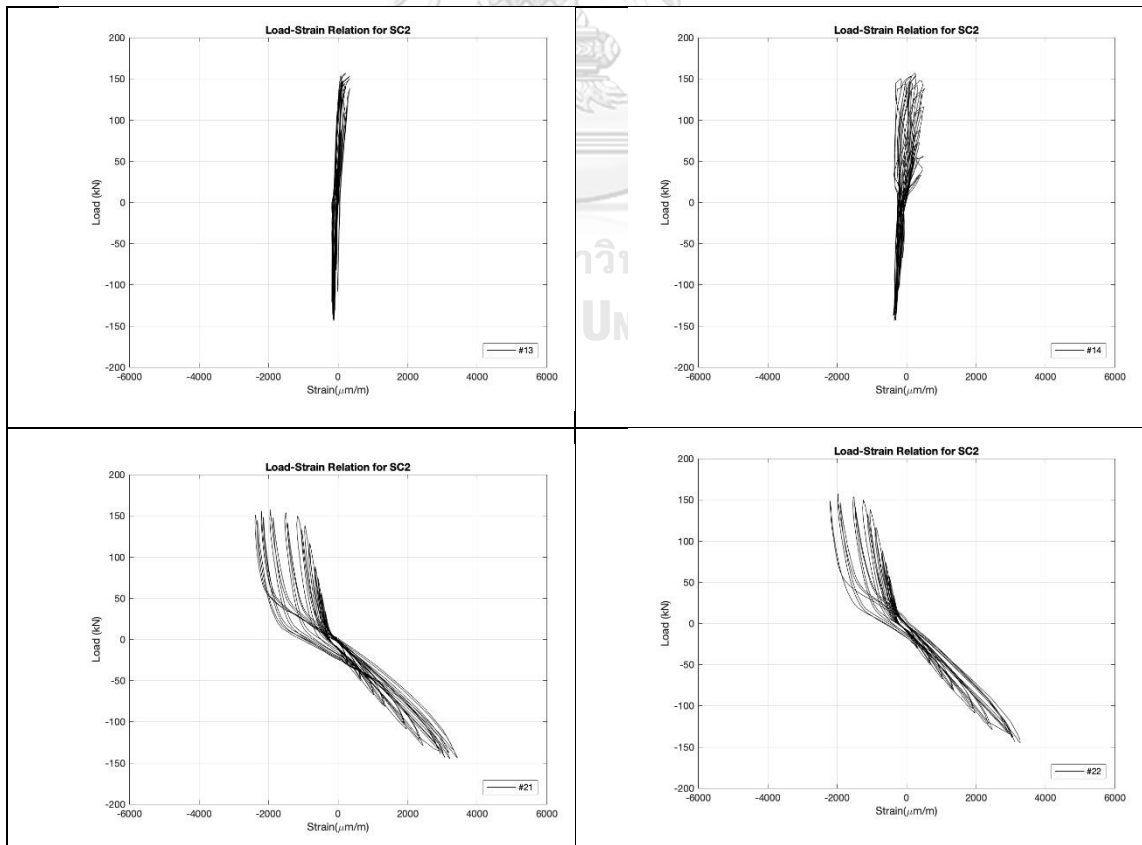
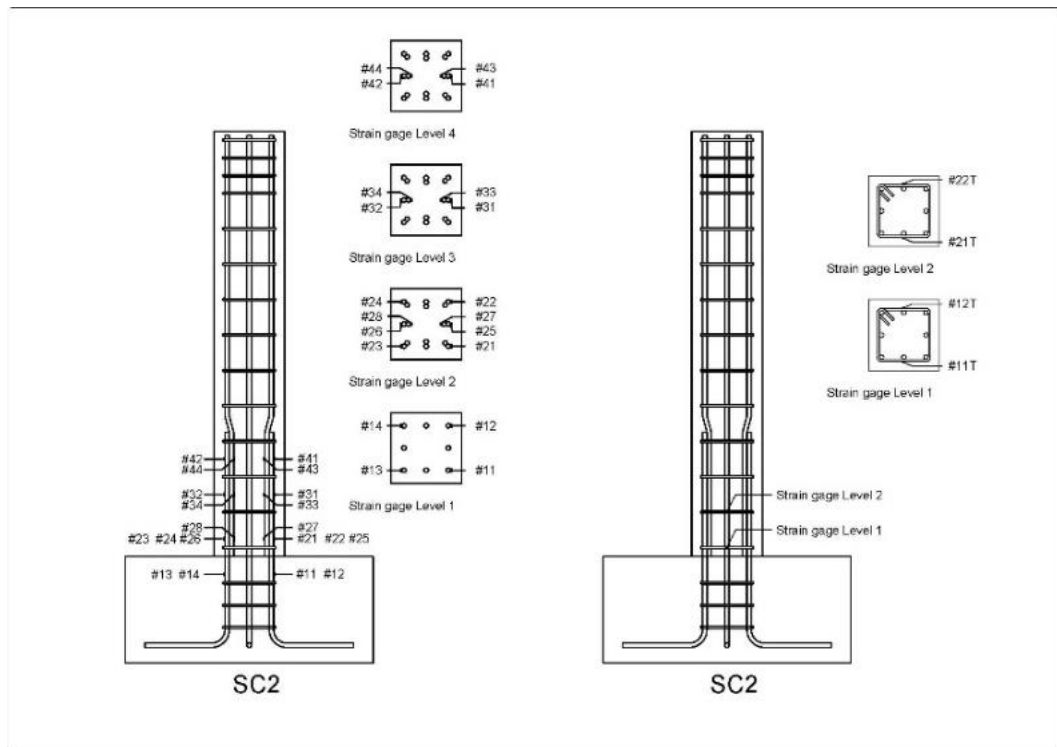


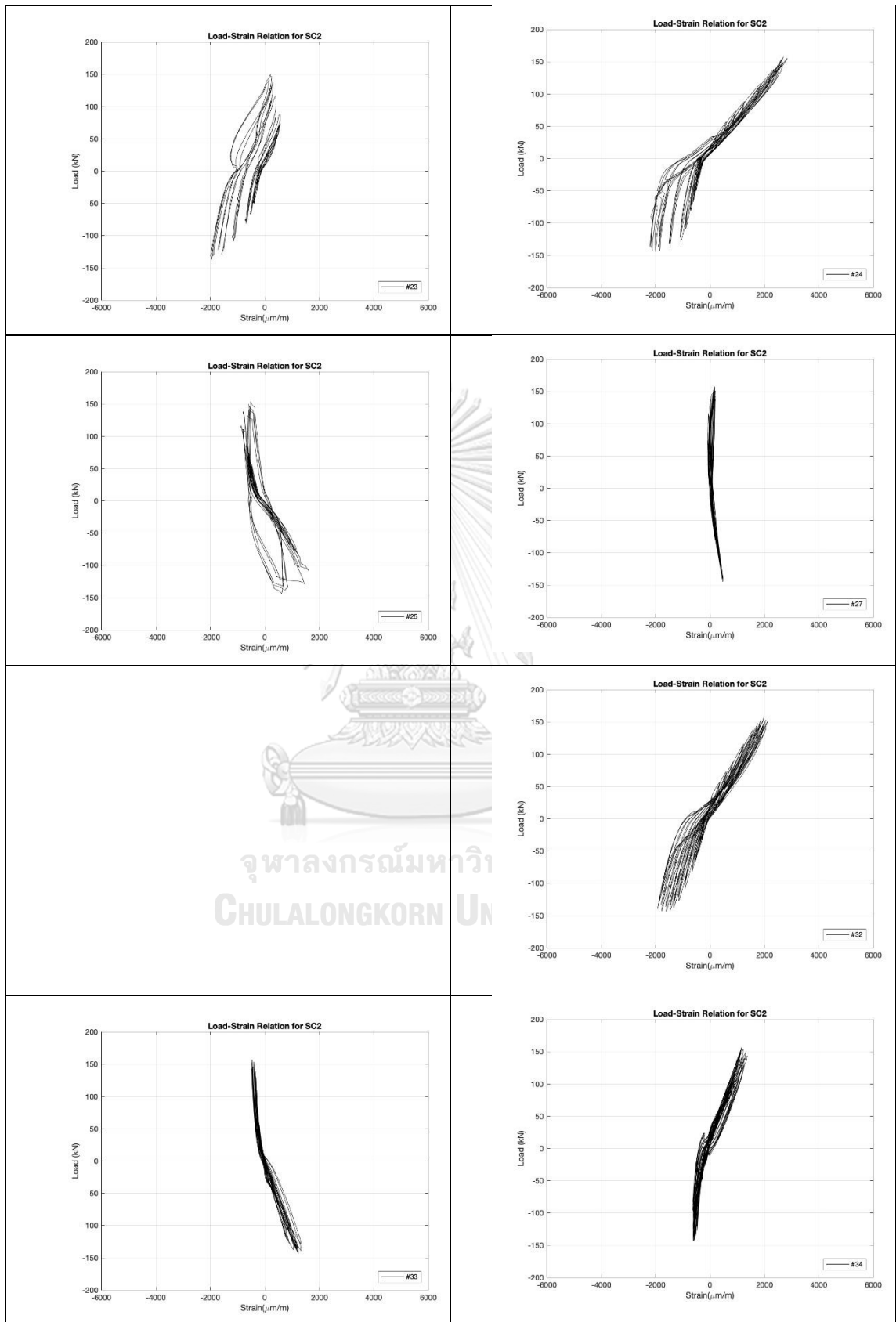


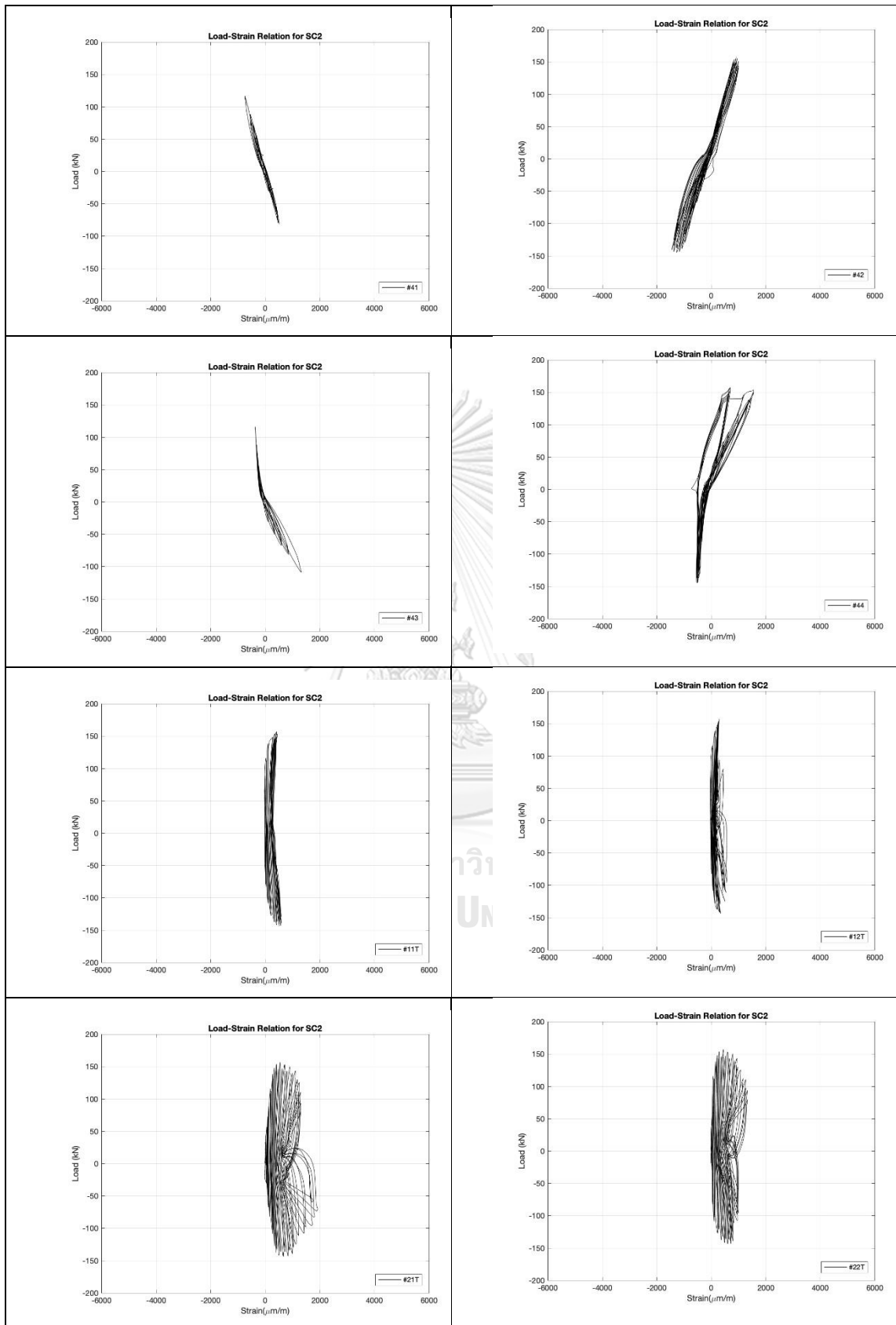


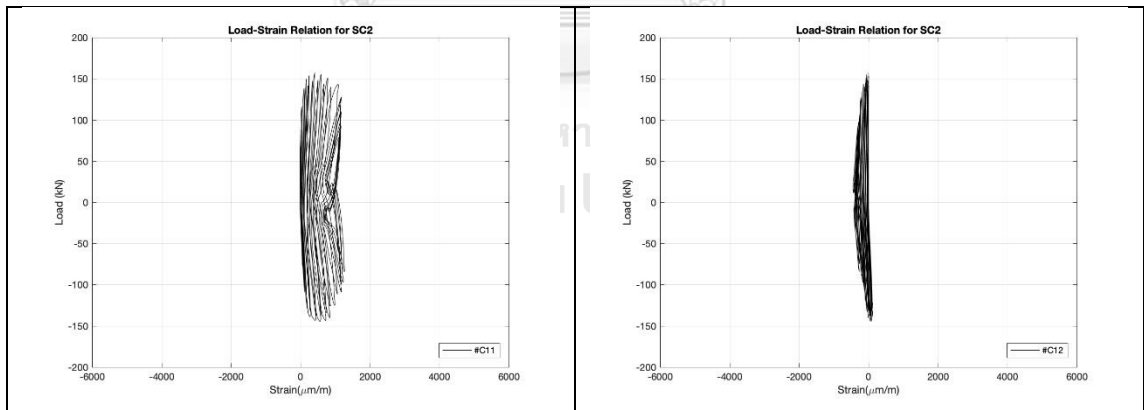
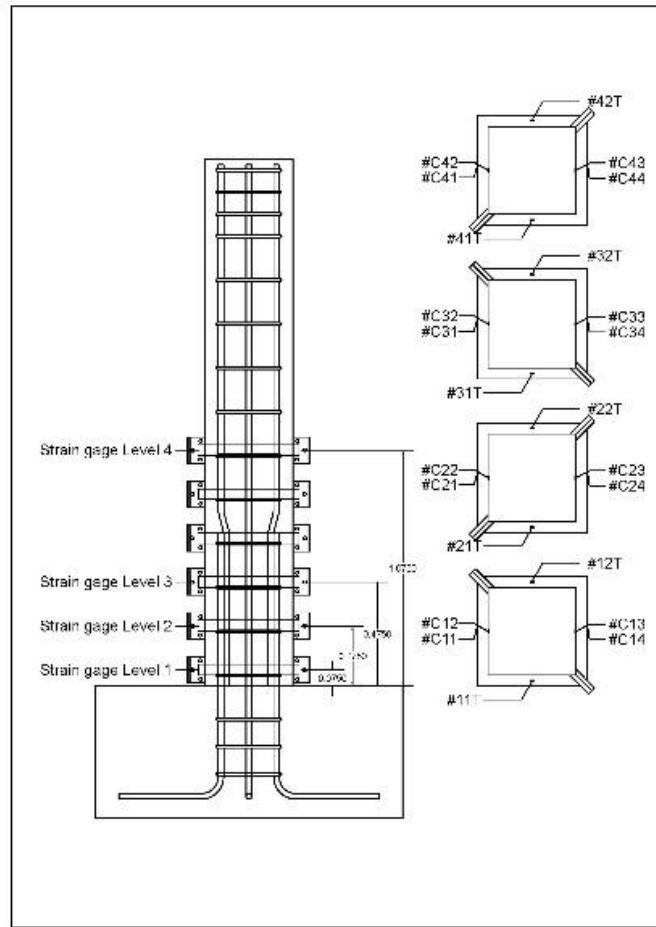


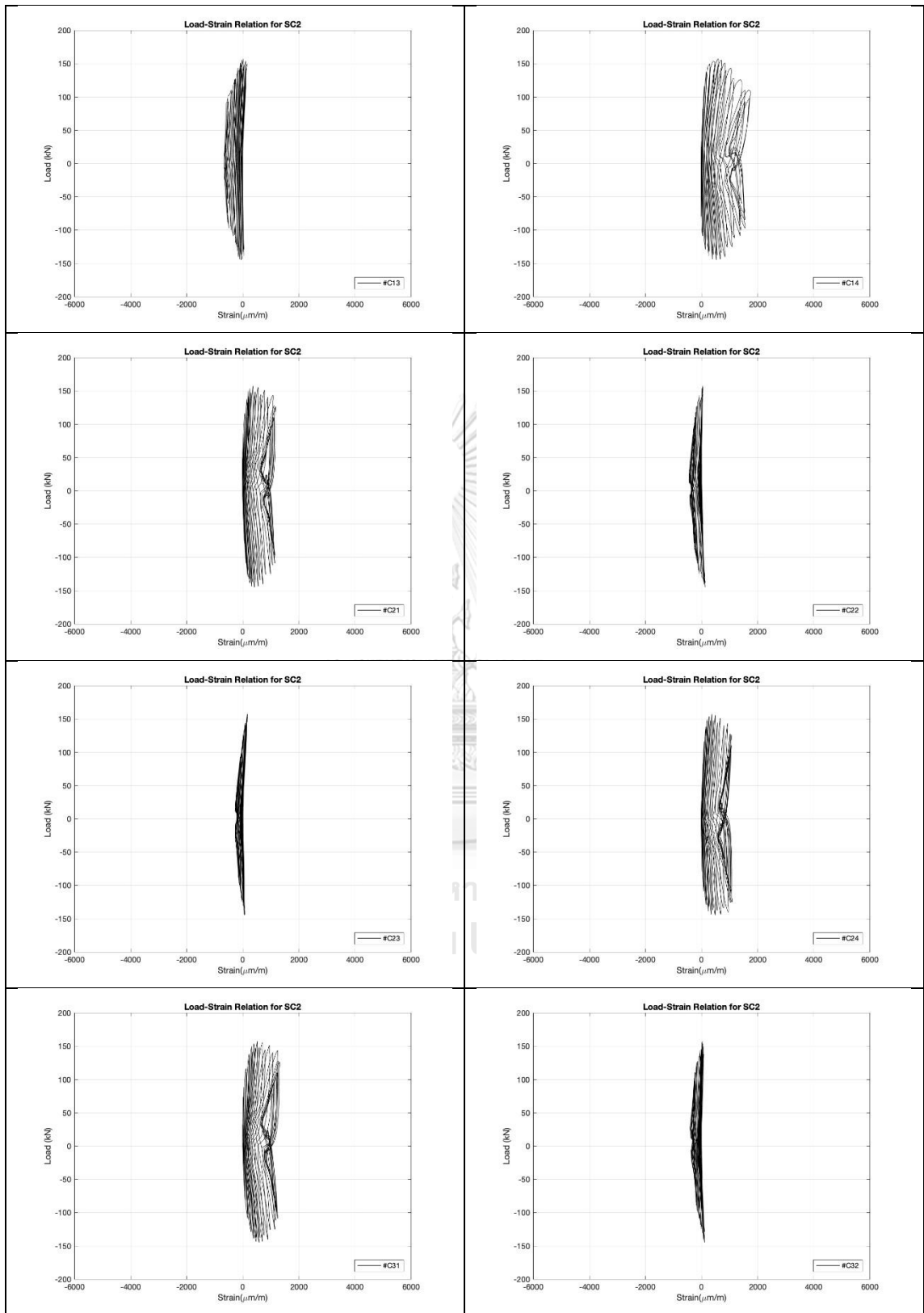
- Strain detailing on reinforcement of SC2 column



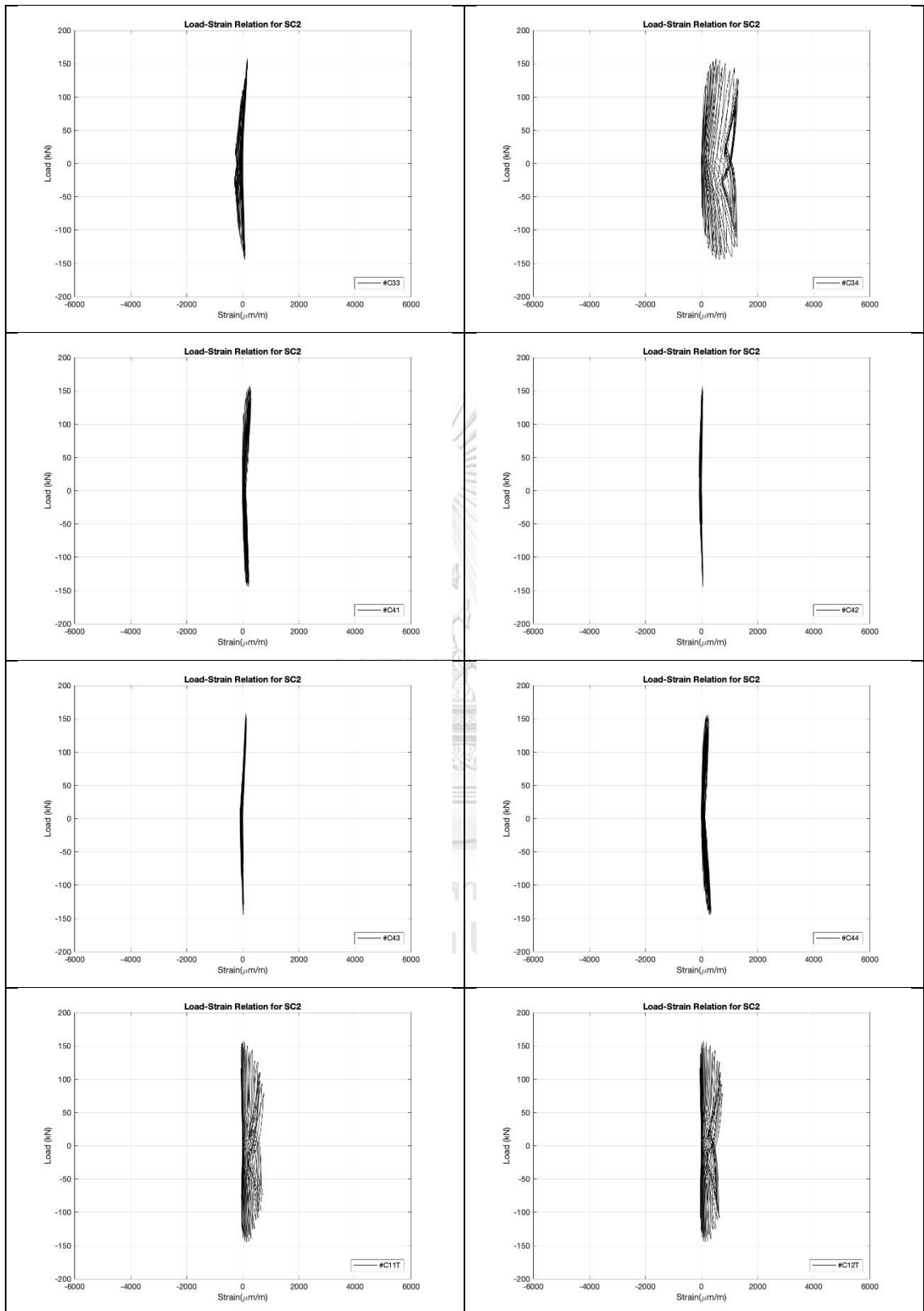


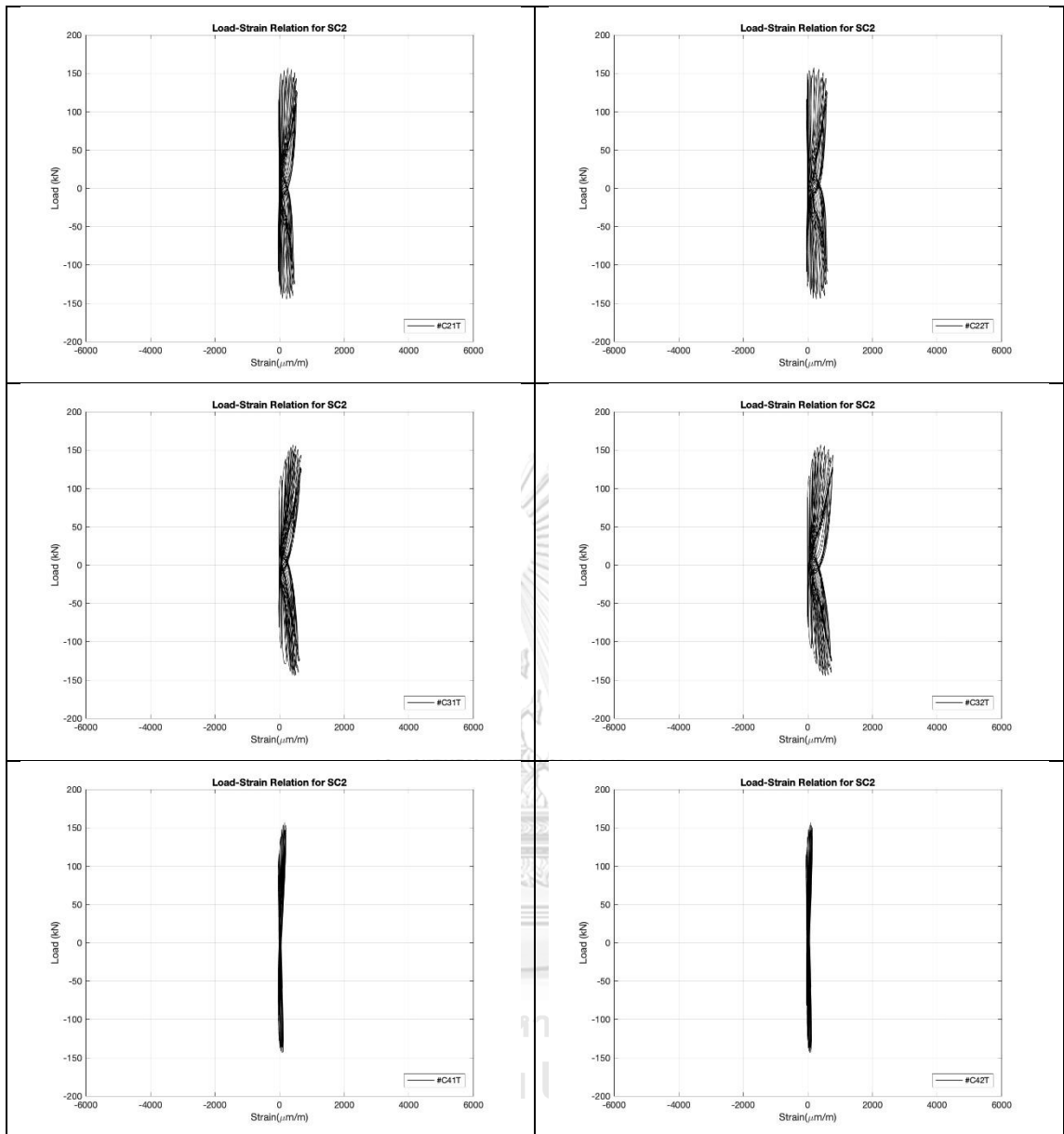




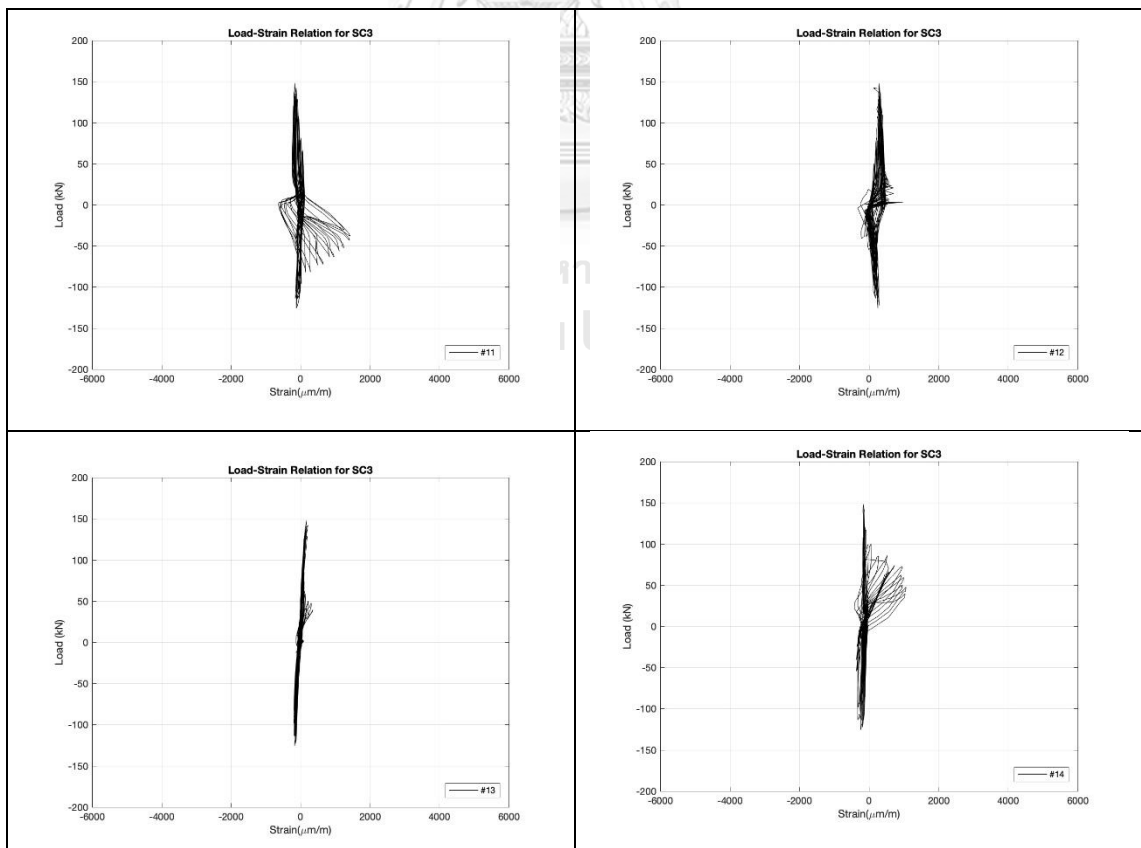
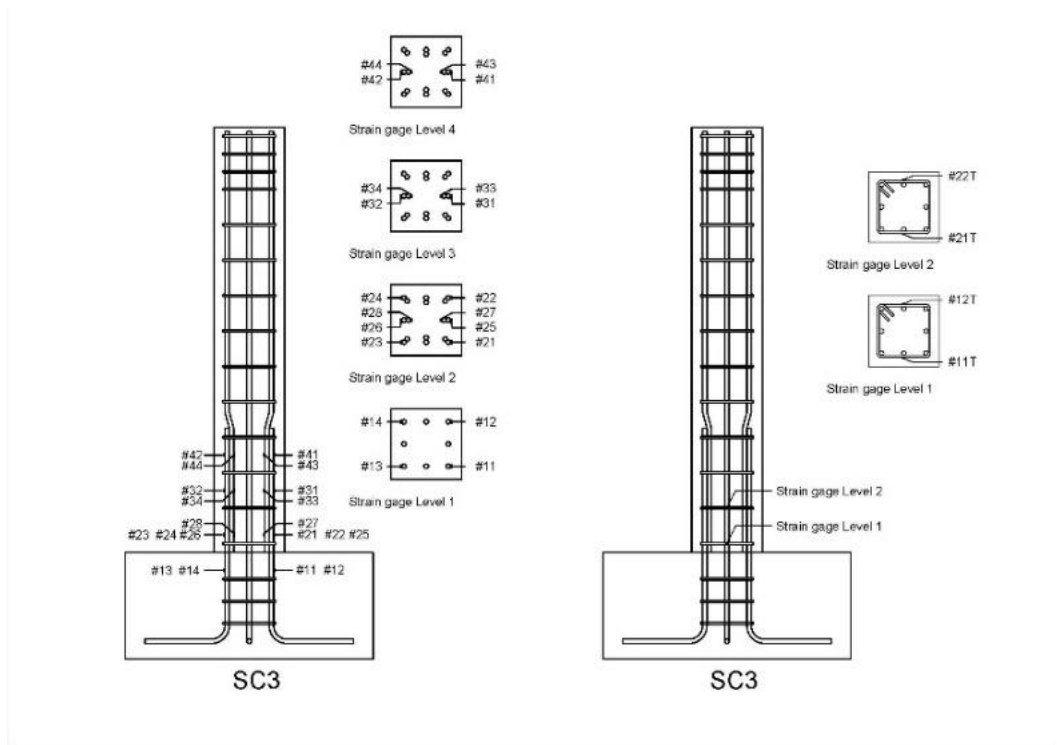


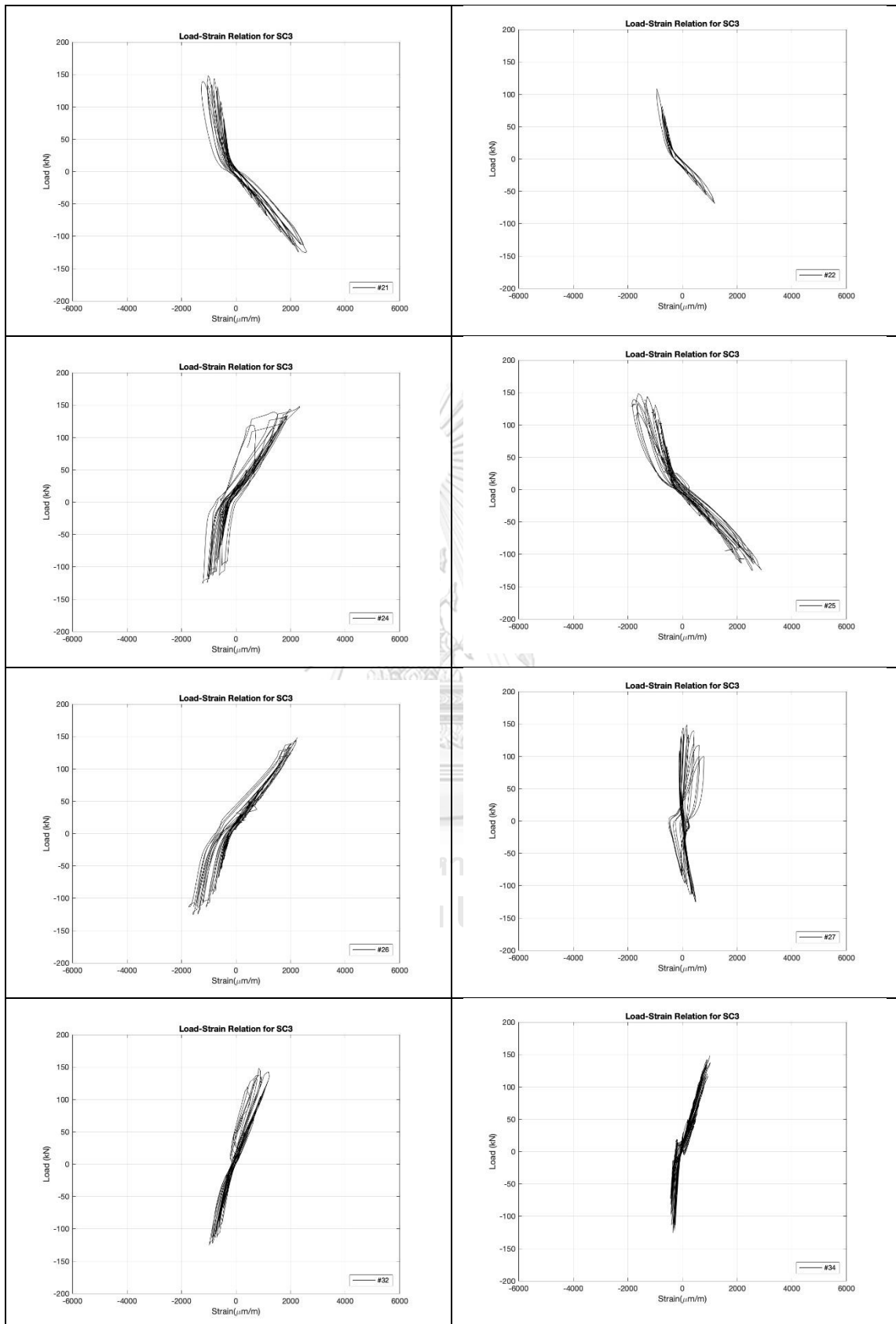


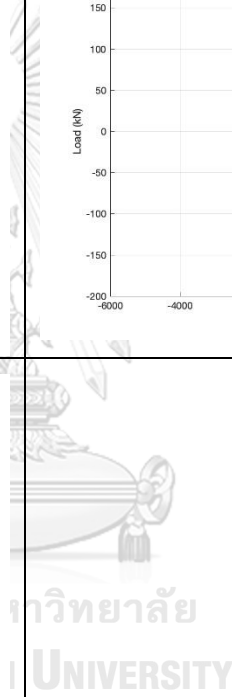
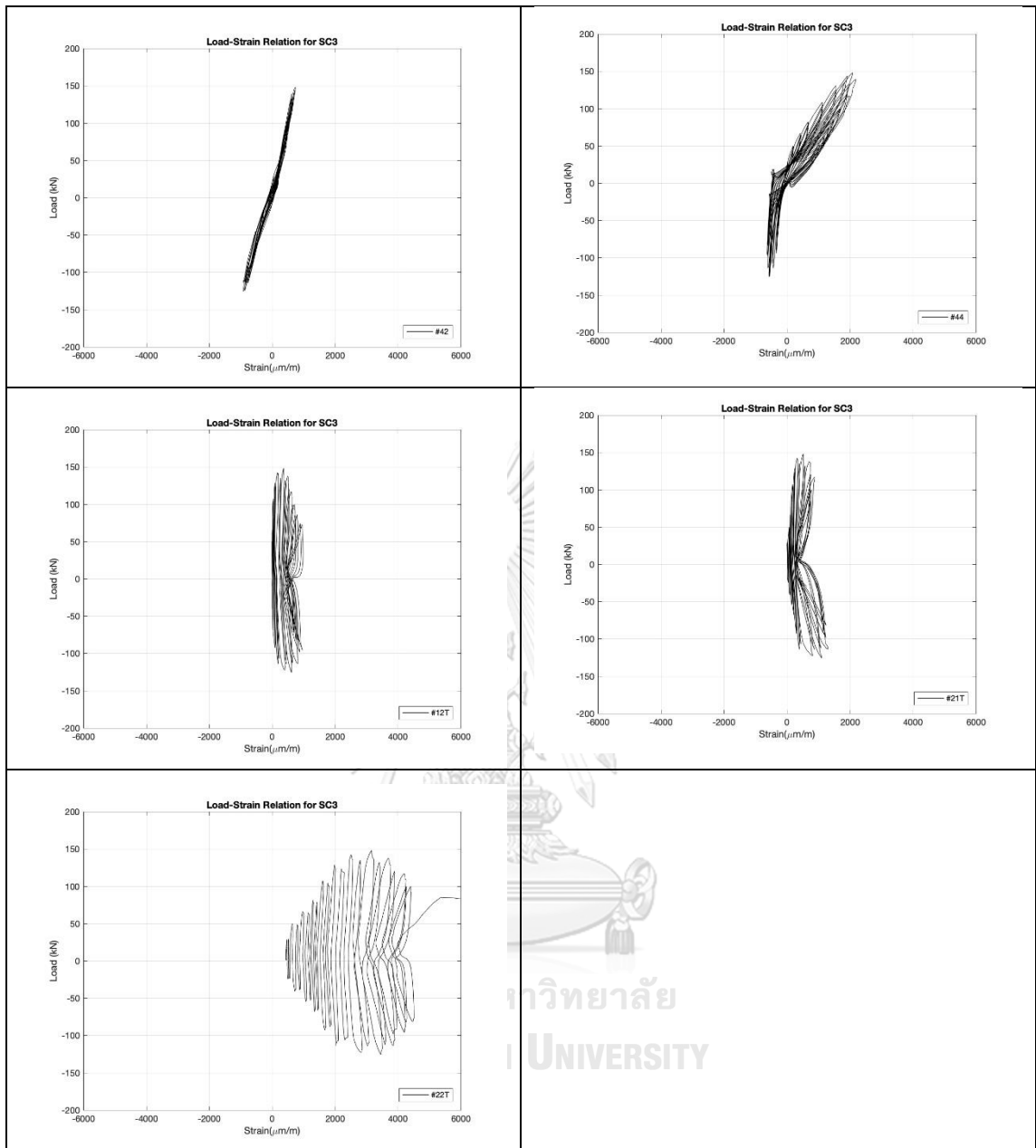


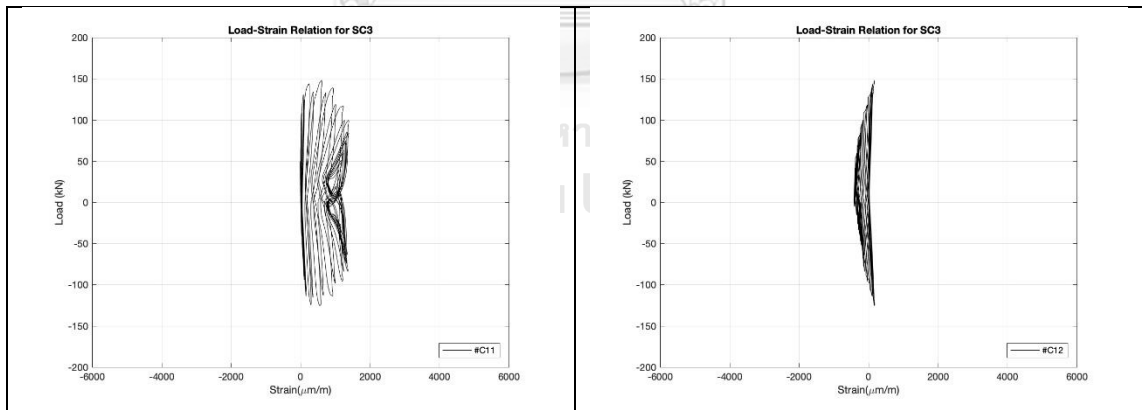
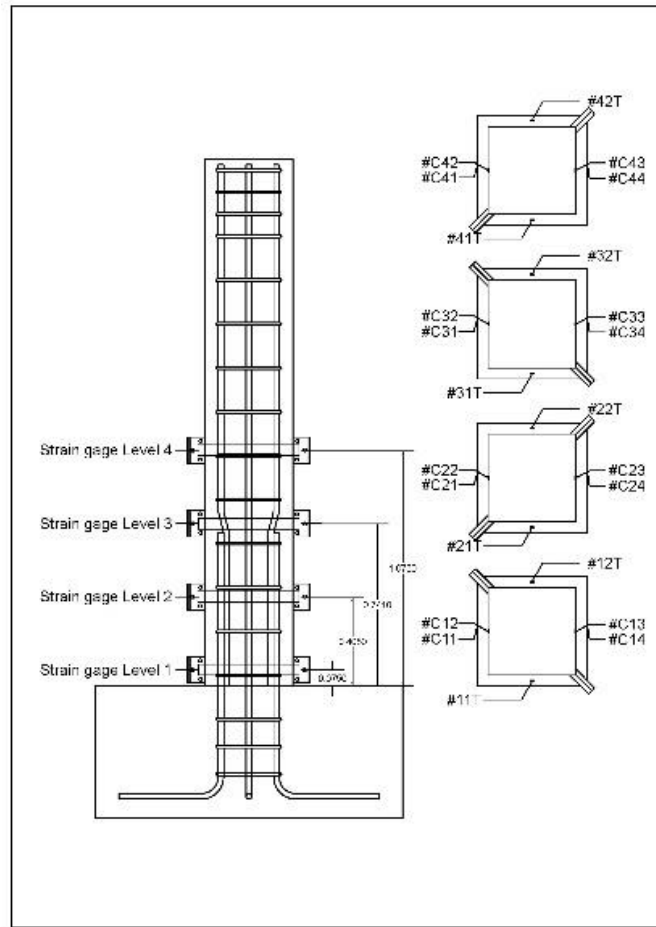


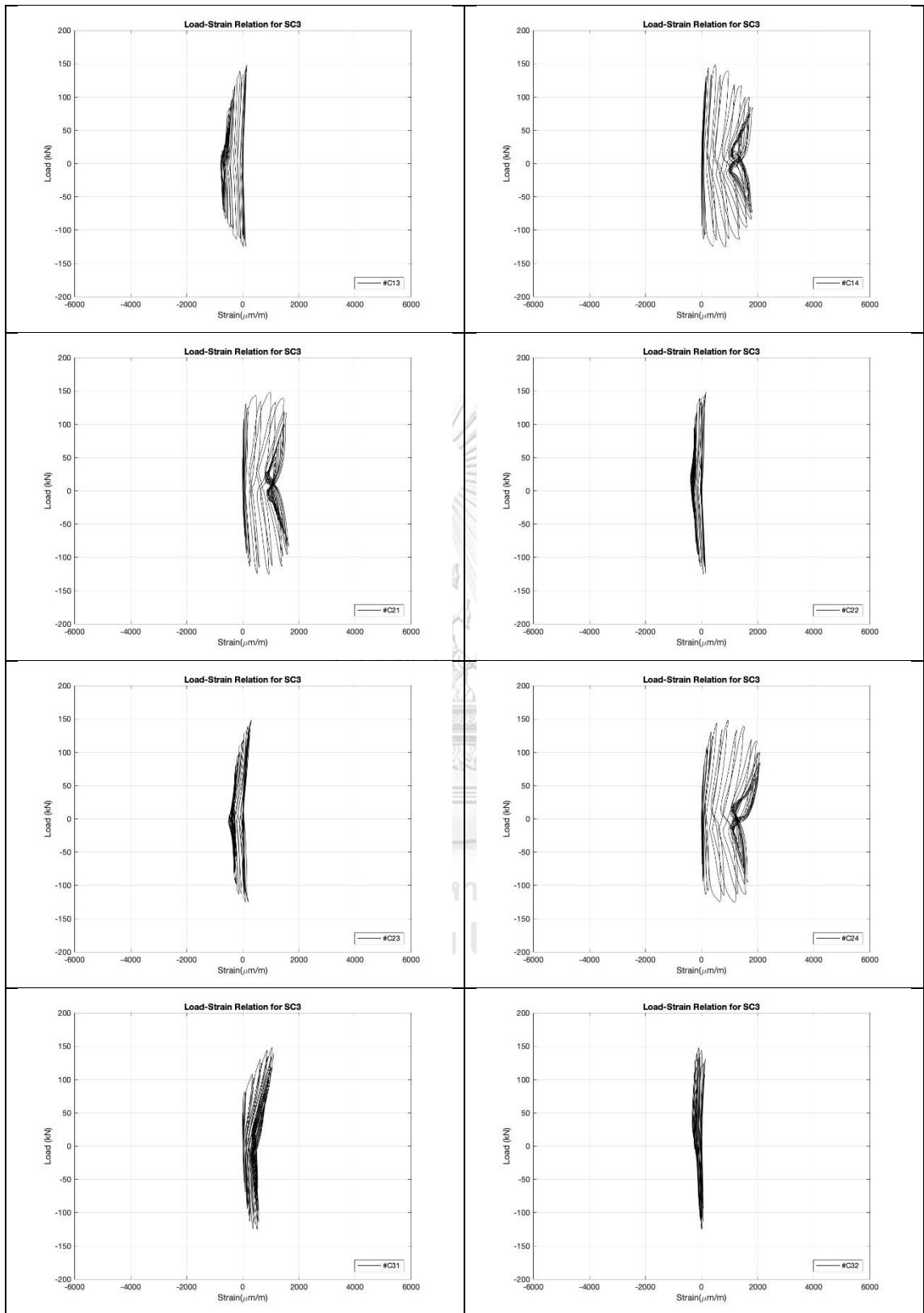
- Strain detailing on reinforcement of SC3 column

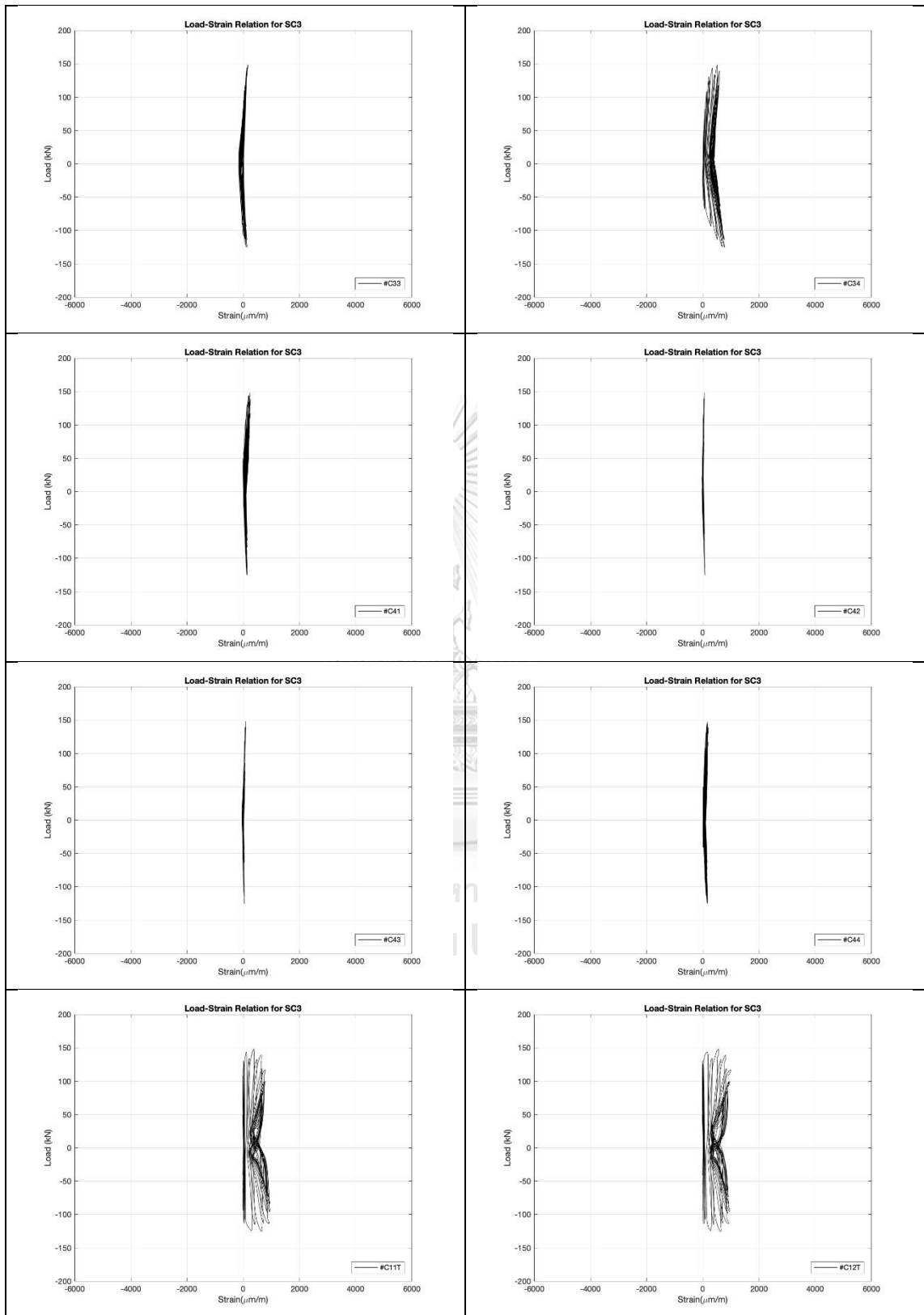




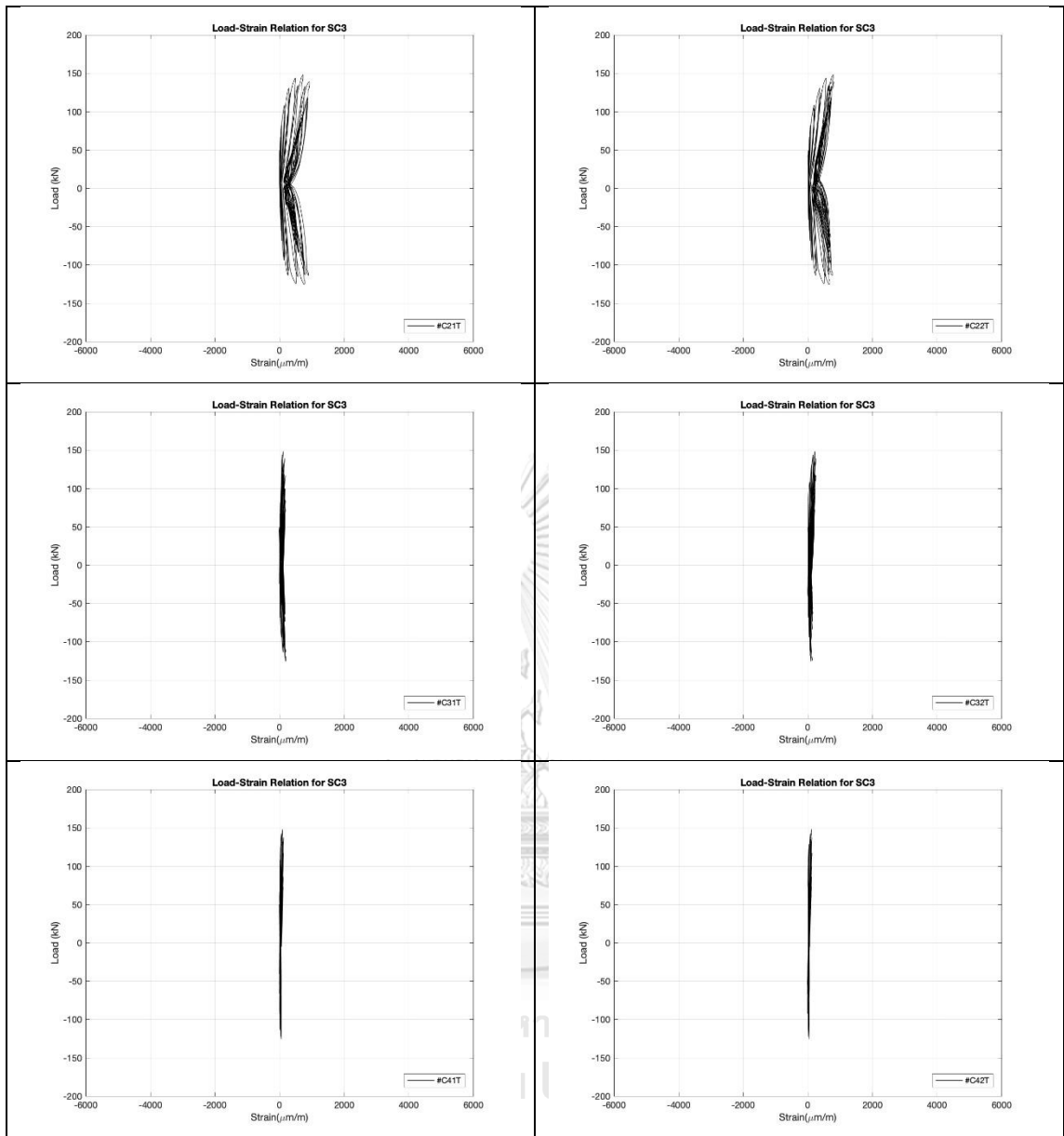












## VITA

NAME Pochara Kruavit

DATE OF BIRTH 8 Oct 1987

PLACE OF BIRTH Petchaboon

INSTITUTIONS ATTENDED B.Eng Faculty Civil of engineering Chiangmai University  
M.Eng Faculty Civil of engineering Chulalongkorn University

HOME ADDRESS 11/2 Nakniwas Rd. Lardprao Bangkok 10230

